Swansea University
Prifysgol Abertawe

On a new variational and computational framework for polyconvex nonlinear continuum mechanics and convex multi-variable nonlinear electro-elasticity

by

Rogelio Ortigosa Martínez

Submitted to the College of Engineering
in partial fulfilment of the requirements for the degree of

Doctor of Philosophy

at

Swansea University

March 30, 2016

DECLARATION

This work has not previously been accepted in substance for any degree and is not being concurrently submitted in candidature for any degree.

Signed .....(candidate)
Date .....

STATEMENT 1

This thesis is the result of my own investigations, except where otherwise stated. When correction services have been used, the extent and nature of the correction is clearly marked in a footnote(s). Other sources are acknowledged by footnotes giving explicit references. A bibliography is appended.

Signed .....(candidate)
Date .....

STATEMENT 2

I hereby give consent for my thesis, if accepted, to be available for photocopying and for inter-library loan, and for the title and summary to be made available to outside organisations.

Signed .....(candidate)
Date .....

Acknowledgements

I would like first of all to express my gratitude to my first supervisor, Dr. Antonio J. Gil, whom I profoundly admire for his dedication, enthusiasm and excellent guidance throughout this time of my life. I have grown both professionally and personally working under his supervision and for that I am indebted to him. I truly consider myself privileged for having the opportunity of working for Dr. Gil.

I also would like to thank Prof. Javier Bonet, my co-supervisor, for his insightful, acute and bright ideas. It has been a pleasure to have the opportunity to work with these two bright academics. I truly consider myself extremely fortunate for having two supervisors of this calibre.

I want to express my gratitude to Dr. Chun Hean Lee for his valuable help and for the numerous and fruitful technical discussions we had during this time. Moreover, I would like to thank my colleague Roman Poya for the interesting scientific discussions that we had and for those which are certainly coming. Special thanks to Dr. Miquel Aguirre, an outstanding researcher and a great person. Many thanks to my colleagues Ossama I.I. Hassan, Emilio García Blanco and Jibran M. Haider. Special thanks to Dr. Aurelio Arranz Carreño for his valuable suggestions and directions which helped improve my coding skills.

I would like to dedicate this work to my wife Cintia, who has lovingly and patiently supported me during this time. I also dedicate this work to my parents to whom I am indebted for their constant support and love. To my brother Pedro Antonio, for all the good and enjoyable times we spend every time I visit him in Spain. Finally but not least, I cannot conclude without making explicit mention to my grandparents, Rogelio and Fuensanta, who visited us in Swansea every single year of my PhD. Thank you for your loving company and for the beautiful and treasured memories from each of your visits.

Abstract

The world of smart materials has experienced a dramatic revolution in the last decades. Electro Active and Magneto Active Materials are some of the most iconic of these, among which, dielectric and magnetostrictive elastomers are becoming extremely popular due to their outstanding actuation capabilities, and in lesser degree, to their energy harvesting capabilities. A clear example illustrating these extraordinary capabilities has been reported in the experimental literature, which has shown unprecedented extreme electrically induced deformations for the most representative dielectric elastomer, namely the acrylic elastomer VHB 4910.

This thesis is focused on the development of well-posed constitutive models for nonlinear electro-elasticity in scenarios characterised by extreme deformations and extreme electric fields. This fundamental objective represents the underlying ingredient for the novel variational and computational frameworks developed hereby in the context of electro-elasticity. Very remarkably, the similarity between the equations in both electro-elasticity and magneto-elasticity, enables the variational and computational frameworks developed to be extended to the latter scenario, characterised by magnetomechanical interactions.

Despite the enormous interest of the experimental and computational scientific community, the definition of suitable constitutive models is still at its early stages for both electro and magneto active materials. In the more specific context of elasticity, considerable effort has been devoted to the definition of polyconvex energy functionals, which entail the most widely accepted constitutive restriction, namely the ellipticity or Legendre-Hadamard condition. This condition, strongly related to the material stability of the constitutive equations, ensures the well-posedness of the governing equations. An extension of the ellipticity condition to the context of nonlinear electro-elasticity and hence, magneto-elasticity, is proposed in this work, ensuring the well-posedness of the equations for the entire range of deformations and electric or magnetic fields.

It is important to emphasise that in this work, the extension of the ellipticity condition to the field of electro-elasticity is exclusively based on material stability considerations. The energy functional encoding the constitutive response of the electro active material is defined according to a novel convex multi-variable representation in terms of an extended set of arguments which ensures material stability. The extended set of arguments, including those characterising the concept of polyconvexity in the more specific scenario of nonlinear elasticity, is further enriched with additional electromechanical entities.

Unfortunately, proof of sequential weak lower semicontinuity of the proposed definition of multi-variable convexity is not provided in this work. This condition, and the additional requirement of appropriate coercivity conditions on the energy functional, would ensure the existence of minimisers. Nevertheless, although of extreme relevance and scientific interest, this topic is not in the scope of the thesis and could be the objective of further research.

Very remarkably, the extension of the condition of ellipticity to the field of electro-elasticity is based on an enrichment of the convex multi-variable nature of the polyconvexity condition in the field of elasticity. Notice that in the latter context, multi-variable convexity is tantamount to polyconvexity of the strain energy. This extension from the field of elasticity is the underlying reason behind the division of this thesis into two main parts. The first part is entirely focused on convex multi-variable (polyconvex) elasticity and the second part, on convex multi-variable electro-elasticity.

Regarding the first part of this thesis, an interesting and novel ingredient has been included. Published in Bonet et al. [1], a new tensor cross product operation and its associated algebra has been introduced enabling an efficient algebraic manipulation of the co-factor and the Jacobian of the deformation gradient tensor, both featuring in the definition of polyconvexity, and their respective derivatives. This algebraic ingredient is the key element which has enabled to propose a novel variational and computational framework in the context of elasticity. Moreover, a new set of variables work conjugate to those intervening in the definition of polyconvexity has been proposed. Based on both sets of extended variables, novel and interesting mixed variational principles, developed to overcome the shortcomings of classical displacement based formulations, are presented in this thesis.

An extension of both variational and computational frameworks developed in the first part of this thesis is carried out in the second part, focused on nonlinear electro-elasticity, whereby the tensor cross product operation aforementioned is of extreme relevance. Based on the new concept of multi-variable convexity in this more general context, new interesting mixed variational principles and their Finite Element computational implementation are presented in this thesis.

Finally, an insightful and physically motivated interpretation of multi-variable convexity is presented in this work, which exploits the connections between the Legendre-Hadamard condition and the hyperbolicity of the dynamic equations. This has been presented both for the particular case of Solid Dynamics and for the more general scenario of electro-magneto-mechanics, the latter being deliberately analysed as it facilitates an straightforward particularisation to either electro-elasticity or magneto-elasticity. This work shows that the convex multi-variable nature of the energy functional must rely on arguments whose differentiation with respect to time yields a first order conservation law.

In reference to this revealing interpretation, a completely novel set of first order hyperbolic conservation laws for all the arguments of multi-variable convexity in both scenarios, namely elasticity and electro-magneto-elasticity, is presented in this thesis. Some of these conservation laws have been presented in recent publications, as those for the purely geometrical arguments of multi-variable convexity, namely the deformation gradient tensor, its co-factor and its Jacobian. Two completely new conservations laws are presented in this thesis for two of the arguments of the extended set in electro-magneto-elasticity.

Very remarkably, and in connection to the pioneering work of Hughes et al. [2]

in the field of Computational Fluid Dynamics, the new concept of multi-variable convexity enables the definition of a generalised convex entropy function which permits a symmetrisation of the set of first order conservation laws in terms of the new associated work (conjugate) variables, presented in this thesis for both elasticity and electro-magneto-elasticity.

Author's publications

Journal publications as a result of this PhD thesis

- J. Bonet, A.J. Gil and **R. Ortigosa**, "A computational framework for polyconvex large strain elasticity", *Computer Methods in Applied Mechanics and Engineering*, Volume 283, 2015, pages 1061-1094, doi: 10.1016/j.cma.2014.10.002.

- J. Bonet, A.J. Gil, C. H. Lee, M. Aguirre and **R. Ortigosa**, "A first order hyperbolic framework for large strain computational solid dynamics. Part I: Total Lagrangian isothermal elasticity", *Computer Methods in Applied Mechanics and Engineering*, Volume 283, 2015, pages 689-732, doi: 10.1016/j.cma.2014.09.024.

- **R. Ortigosa**, A. J. Gil, J. Bonet and C. Hesch, "A computational framework for polyconvex large strain elasticity for geometrically exact beam theory", *Computational mechanics*, 2015, doi: 10.1007/s00466-015-1231-5.

- J. Bonet, A. J. Gil and **R. Ortigosa**, "On a tensor cross product based formulation of large strain solid mechanics", *International Journal of Solid and Structures*, Volume 84, 2016, pages 49-63, doi: 10.1016/j.ijsolstr.2015.12.030.

- **R. Ortigosa** and A. J. Gil, "A new framework for large strain electromechanics based on convex multi-variable strain energies: variational formulation and material characterisation", *Computer Methods in Applied Mechanics and Engineering*, Volume 302, 2016, pages 293-328, doi: 10.1016/j.cma.2015.11.036.

- **R. Ortigosa** and A. J. Gil. "A new framework for large strain electromechanics based on convex multi-variable strain energies: Finite Element discretisation and computational implementation", *Computer Methods in Applied Mechanics and Engineering*, Volume 302, 2016, pages 329-360, doi: 10.1016/j.cma.2015.12.007.

- **R. Ortigosa** and A. J. Gil, "A new framework for large strain electromechanics based on convex multi-variable strain energies: hyperbolicity and conservation laws", *Computer Methods in Applied Mechanics and Engineering*, Volume 309, 2016, pages 202-242, doi: 10.1016/j.cma.2016.05.019.

- A. J. Gil, C. H. Lee, J. Bonet and **R. Ortigosa**, "A first order hyperbolic framework for large strain computational solid dynamics. Part II: Total Lagrangian compressible, nearly incompressible and truly incompressible elasticity", *Computer Methods in Applied Mechanics and Engineering*, Volume 300, 2016, pages 146-181, doi: 10.1016/j.cma.2015.11.010.

- **R. Ortigosa** and A. J. Gil, "A new computational framework for large strain nearly and truly incompressible electromechanics based on convex multi-variable strain energies", *Computer Methods in Applied Mechanics and Engineering*, Volume 310, 2016, pages 297-334, doi: 10.1016/j.cma.2016.06.025.

- **R. Ortigosa** and A. J. Gil, "A computational framework for incompressible electromechanics based on convex multi-variable strain energies for geometrically exact shell theory", *Computer Methods in Applied Mechanics and Engineering*, under review.

Conference publications

- A.J. Gil and **R. Ortigosa**, "A new computational framework for large strain electromechanics. In proceedings of the 7$^{\text{th}}$ European Congress on Computational Methods in Applied Sciences and Engineering, Crete, Greece, June 5-10, 2016.

- A.J. Gil, **R. Ortigosa** and J. Bonet, "A computational framework for polyconvex large strain electromechanics. In Proceedings of the 13$^{\text{th}}$ US National Congress on Computational Mechanics (USNCCM), San Diego, July 27-30, 2015.

- C.H. Lee, A. J. Gil, J. Bonet and **R. Ortigosa**, "A Total Lagrangian hydrocode for linear tetrahedral elements in compressible, nearly incompressible and truly incompressible solid dynamics". In Proceedings of the 13$^{\text{th}}$ US National Congress on Computational Mechanics (USNCCM), San diego, July 27-30, 2015.

- **R. Ortigosa**, A.J. Gil and J. Bonet, "A variational framework for large strain polyconvex dielectric elastomers. In proceedings of the 23$^{\text{rd}}$ UK Association of Computational Mechanics in Engineering (ACME) Conference, Swansea, United Kingdom, April 8-10, 2015.

- C. H. Lee, A. J. Gil, J. Bonet and **R. Ortigosa**, "An entropy-based stabilised Petrov-Galerkin formulation for linear tetrahedral elements in compressible, nearly incompressible and truly incompressible isothermal fast dynamics". In Proceedings of the 23$^{\text{rd}}$ UK Association of Computational Mechanics in Engineering (ACME) Conference, Swasnea, Inited Kigdom, April 8-10, 2015.

- R. Ortigosa, A.J.Gil and J. Bonet, "Polyconvexity in the context of large strain electromechanics. In proceedings of the 6$^{\text{th}}$ International Conference on Computational Methods for coupled problems in science and engineering, Venice, May 18-20, 2015.

- **R. Ortigosa**, A.J.Gil and J. Bonet, "Polyconvexity in the context of large strain electromechanics. In proceedings of the 6$^{\text{th}}$ International Conference on Computational Methods for coupled problems in science and engineering, Venice, May 18-20, 2015.

- R. Palma, A. J. Gil and **R. Ortigosa**, "Finite element analysis of flexo-thermo-piezo-magneto-electricity using Cosserat micropolar mechanics". In

proceedings of the 6th International Conference on Computational Methods for coupled problems in science and engineering, Venice, May 18-20, 2015.

- A.J.Gil, **R. Ortigosa** and J. Bonet, "A computational framework for large strain electromechanics. In proceedings of the 11th World Congress on Computational Mechanics, Barcelona, Spain, July 20-25, 2014.

- **R. Ortigosa**, A.J. Gil and J. Bonet, "A computational framework for large strain electromechanics. In proceedings of the 22nd UK Association of Computational Mechanics in Engineering (ACME) Conference, Exeter, United Kingdom, April 2-4, 2014.

- J. Bonet , **R. Ortigosa** and A.J.Gil, "A new variational formulation for large strain piezoelectric hyperelastic materials. In proceedings of the 5th International Conference on Computational Methods for coupled problems in science and engineering, Ibiza, Spain, June 17-19, 2013.

- **R. Ortigosa**, A.J. Gil and J. Bonet , "A new variational formulation for large strain piezoelectric hyperelastic materials. In proceedings of the International Conference in Computational Mechanics (CM), Durham, United Kingdom, March 25-27, 2013.

- **R. Ortigosa**, A. J. Gil and J. Bonet, "On the development of constitutive laws for large strain hyperelastic piezoelectric materials", In Proceedings of the 8th European Solid Mechanics Conference, Gratz, 9-13 July 2012.

- **R. Ortigosa**, A. J. Gil and J. Bonet, "Nonlinear variational formulation for piezoelectric and dielectric anisotropic materials", In Proceedings of the 20th UK Conference of the Association of Computational Mechanics in Engineering, Manchester, 27-28 March 2012.

Contents

List of Figures

List of Tables

Part I

Preliminaries

Chapter 1

Introduction

1.1 Motivation

The advance over the last decades in existing smart materials and the advent of new ones superseding their predecessors portends a brilliant and encouraging future for these materials and renders a prolific scenario for the development of new interesting and challenging areas of research. The main distinctive feature of each of these materials is their actuation principle. The application of a characteristic stimuli produces a very particular response on these materials. For instance, some of the earliest Electro Active Materials, namely piezoelectric crystals and piezoelectric ceramics, create a distribution of electric potential when subjected to a mechanical excitation. This actuation principle can be reverted due to the non-centrosymmetric internal structure of these materials . Thus, the application of an electric field would lead to a deformation. Alternatively, electrostrictive materials, deprived from a centrosymemtric internal structure, exhibit exclusively one way electro-mechanical coupling, where deformations can be electrically induced.

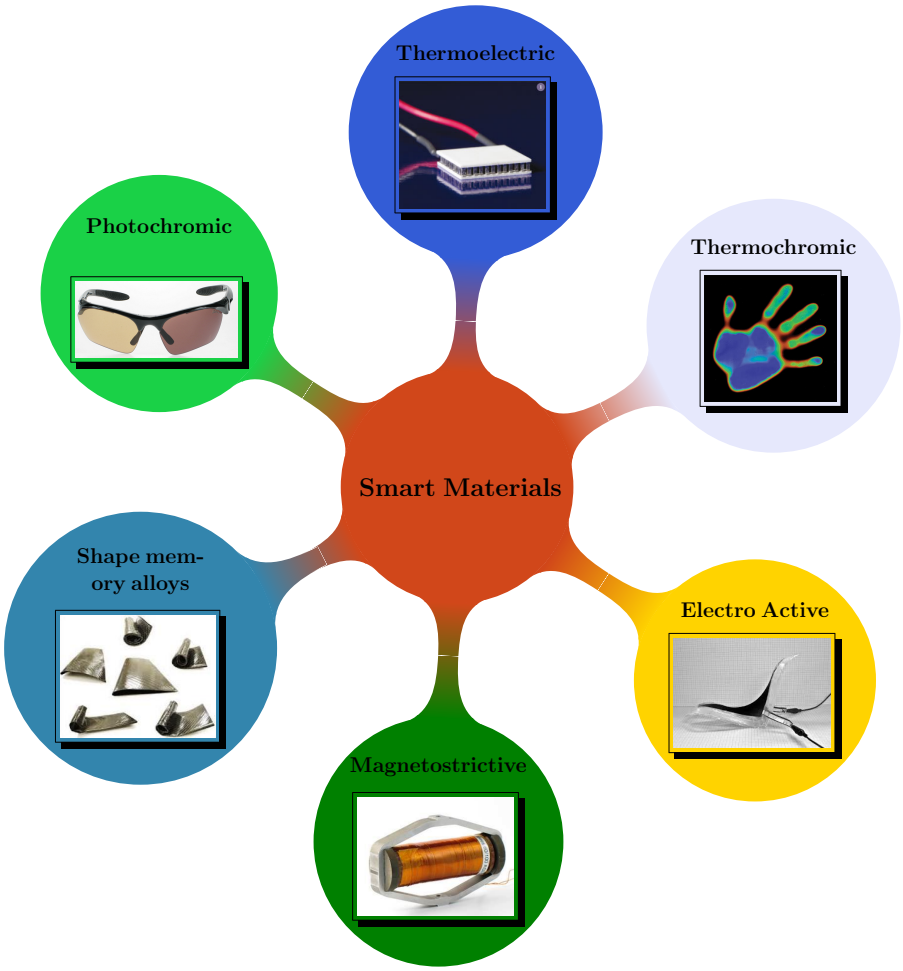

Figure 1.1: Classification and examples of Smart Materials.

Another type of smart materials with potential applications within the field

of artificial actuators is that of magneto-active elastomers [3]. A magnetic inactive matrix of elastomer is enriched with magneto-active particles. Thus, the application of a magnetic field can lead to the deformation of the material. Thermoelectric, photochromic, etc. are additional examples of smart materials where a thermal or photonic stimuli induces a change in the distribution of electric field or in the colour, respectively. A non-exhaustive classification of smart materials is depicted in Figure 1.2.

Among the wide spectrum of smart materials, this thesis is focused on Electro Active Materials. Refer to Figure 1.2 for a brief classification of these materials. The actuator and harvesting capabilities of the earliest of these materials, namely piezoelectric crystals and ceramics, were not very long ago eclipsed by those of Electro Active Polymers (EAP). This heterogeneous group can be subsequently classified into two main subgroups, namely Electronic Electro Active Polymers (EEAP) and Ionic Electro Active Polymers (IEAP) [4]. Within the first subgroup, Dielectric Elastomers (DE) and electrostrictive relaxor ferroelectric polymers or simply Piezoelectric Polymers (PP), have become increasingly relevant. The second subgroup includes ionic gels, Ionic Polymer Metal Composites (IPMC) and carbon nanotubes.

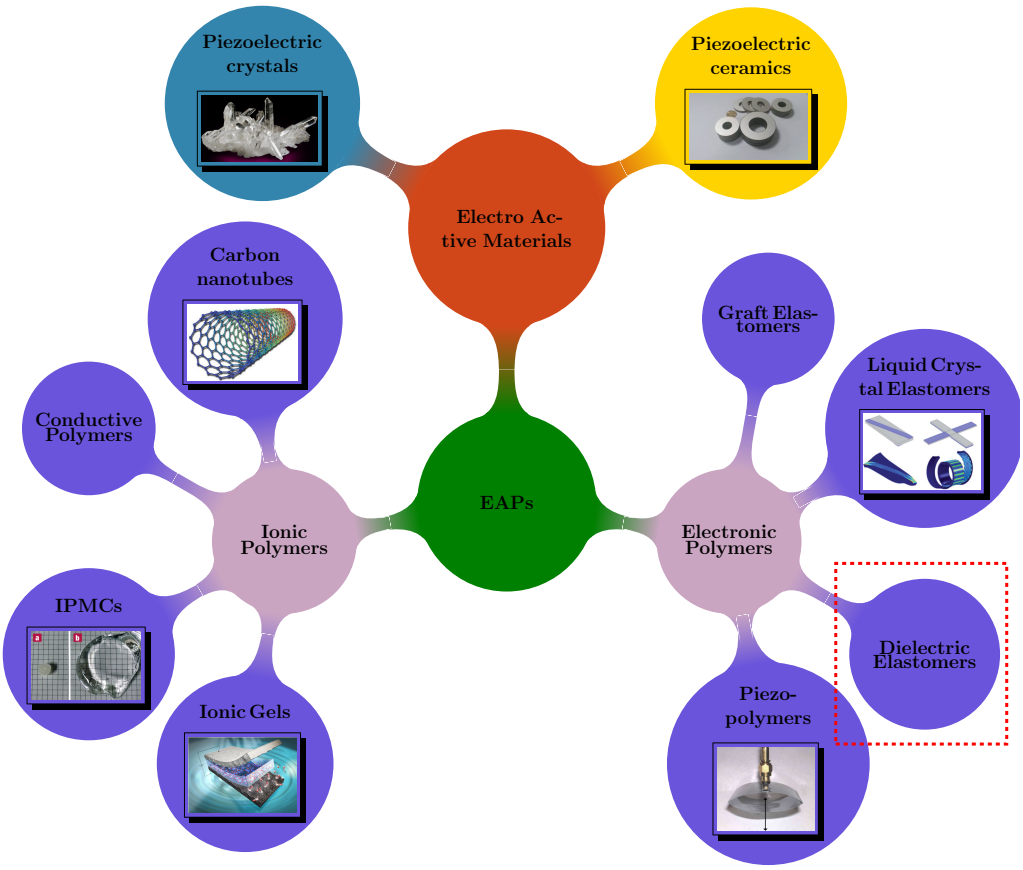

Figure 1.2: Classification of Electro Active Materials. The scope of this thesis is mainly on dielectric elastomers, as indicated by the red dashed line.

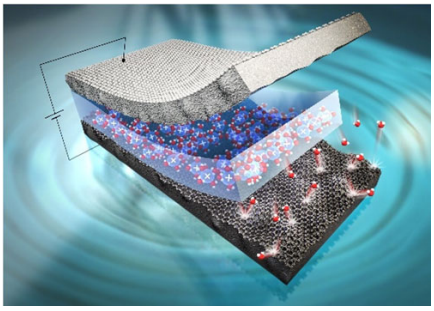

(a)

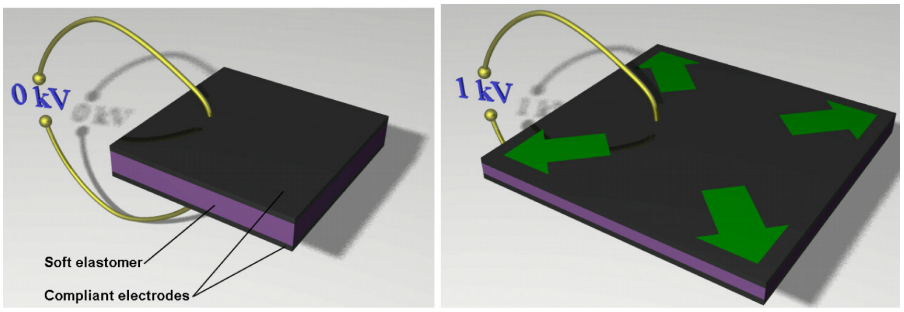

(b)

Figure 1.3: Working principle in ionic and electronic polymers: (a) the application of an electric potential gradient across the material triggers the diffusion of ions, leading to a bending type deformation; (b) the application of an electric field generates electrostatic forces which cause a compression in the direction of application of the electric field.

In this work, only electronic polymers are considered. The main difference between these two subgroups resides in their underlying working principle. Maxwell or Coulomb forces are responsible for the subsequent electrically induced deformations in electronic polymers. On the contrary, the diffusion or mobility of ions is the driving force in ionic polymers [4] (refer to Figure 1.3).

Figure 1.4 displays some interesting examples where electronic polymers are used as actuators. In particular, Figure 1.4(a) shows a realistic application of dielectric elastomers as soft robots. The application of an electric field on the dielectric elastomer produces an artificial rotary joint to bend upwards and downwards, achieving the desired flapping effect. Another example of dielectric elastomers in the field of robotics is shown in Figure 1.4(b). Figure 1.4(c) shows an electroactive polymer propelled airship. The airship, slightly pressurised with Helium, is endowed with a series of electroactive polymer patches located on both opposite sides of the body and tail. The antagonist contraction-expansion of the patches leads to the movement of the airship, which literally swims through air. Figures 1.4(g) and 1.4(h) display an electroactive polymer actuated device at different stages of the deformation. Figure 1.4(i) shows an space antenna which modulates its curvature using piezoelectric actuators. Figure 1.4(k) displays an image of the Boeing MFX-1, equipped with

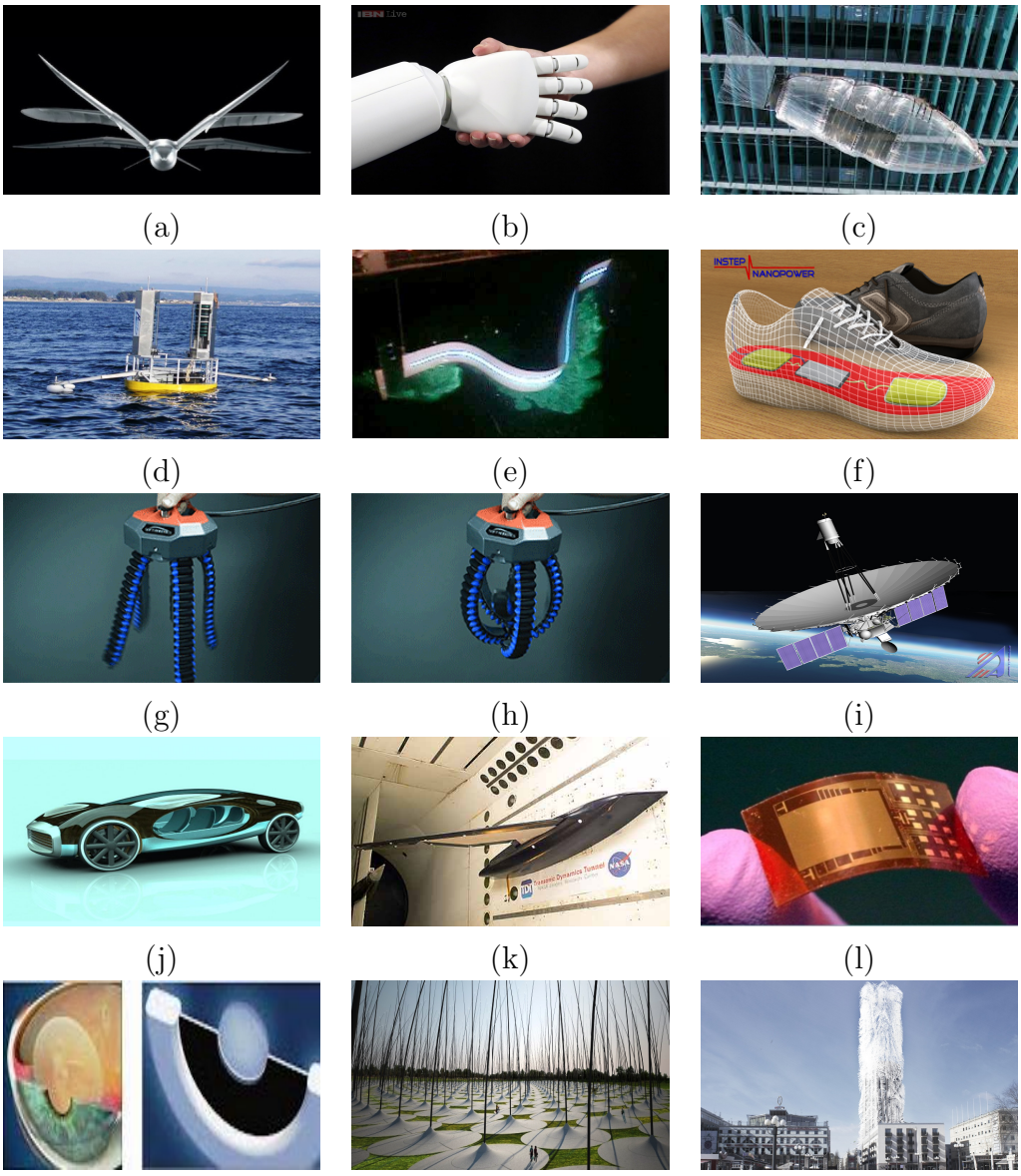

Figure 1.4: Relevant applications of electronic polymers. (a) Dielectric elastomer actuated flapping wing; (b) Dielectric elastomer actuated hand; (c) Dielectric elastomer actuated biomimetic airship; (d) Dielectric elastomer ocean power generator; (e) Piezoelectric eel; (f) Piezoelectric shoe; (g) and (h) Electrically actuated device; (i) Piezoelectric actuated space antenna; (j) Piezoelectric technology incorporated in automobile; (k) Boeing MFX-1: morphing aircraft test at Langley NASA; (l) Piezoelectric nano-harvester; (m) Dielectric elastomer biomimetic lens; (n) Piezoelectric wind farm; (o) Piezoelectric skyscraper.

Figure 1.5: Extreme electrically induced deformations in dielectric elastomers: images corresponding to the experiment carried out by Li et al. Initial (no applied electric field) configuration on the left. Final (after the application of an electric field) configuration on the right.

piezoelectric actuators on carbon fiber skin for morphing purposes. Finally, Figure 1.4(m) shows a dielectric elastomer actuated lense.

Figure 1.4 shows also interesting examples of energy harvesting applications. Figure 1.4(d) clearly illustrates the use of dielectric elastomers for power generation purposes. Figure 1.4(e) shows an interesting military application where piezoelectric eels are used as part of submarine devices in long endurance military missions. Figure 1.4(f) presents a conventional shoe endowed with piezoelectric patches which enable a conversion of the kinetic energy from motion into electric energy. Figure 1.4(j) shows a photovoltaic piezoelectric auto-mobile, equipped with piezoelectric crystals which generate electricity from the surrounding air flow. Figure 1.4(l) displays a extremely flexible piezoelectric nano harvester, able to produce electric energy from the slightest deformation. Figure 1.4(n) displays a planned wind-farm outside Abu Dhabi consisting of a field of 55 meters piezoelectric carbon fibre stalks. Finally, Figure 1.4(o) shows a conceptual design of the Söder Torn, a skyscraper based in Stockholm. Architecture firm Belatchew has proposed to endow this tower with millions of tiny piezoelectric straws.

The present manuscript is mainly focused on dielectric elastomers (as indicated in Figure 1.2). The acrylic elastomer VHB 4910 is the most iconic example. These materials are becoming increasingly attractive due to their outstanding actuation properties [5–8]. A voltage induced area expansion of 1980% on a dielectric elastomer membrane film has been recently reported by Li et al. [9] (refer to Figure 1.5). In this specific case, the electromechanical instability is harnessed as a means for obtaining these electrically induced massive deformations.

For these extreme scenarios, characterised by large deformations and large electric fields, the consideration of appropriate and suitable constitutive models used to represent the constitutive behaviour of these materials is vital, as defective constitutive models can lead to ill-posedness of the governing equations. The objective of this thesis is the development of appropriate constitutive laws complying with the well-posedness of the governing equations for the entire range of deformations and electric fields.

1.2 State of the art

A great effort has been devoted to the development of appropriate constitutive models in the field of nonlinear elasticity [10, 11]. The definition of suitable constitutive restrictions is crucial if physically admissible solutions are expected to occur. Revisiting the well established theory for nonlinear elasticity, an extension to the field of nonlinear electro-elasticity has been carried out in this thesis. This is the underlying reason behind the subdivision of this work into two main parts. The first part focuses on the well established theory for (reversible) nonlinear elasticity from the constitutive, variational and computational standpoints. This enables a well founded extension to the field of nonlinear electro-elasticity, integrated in the second part of this thesis.

1.2.1 Nonlinear elasticity

Large strain elastic and inelastic analysis by finite elements or other computational techniques is now well established for many engineering applications [12–23]. Often elasticity is described by means of a hyperelastic model defined in terms of a stored energy functional which depends on the deformation gradient of the mapping between initial and final configurations [10–12, 24–29]. It has also been shown that for the model to be well defined in a mathematical sense, this dependency with respect to the deformation gradient has to be based upon appropriate convexity criteria [11, 12, 26] which guarantees ellipticity and hence, the well-posedness of the governing equations. Ellipticity has therefore, important physical implications as it guarantees the existence of real wave speeds [30] (Legendre-Hadamard condition) in the material in the vicinity of an equilibrium configuration and it is strongly related to material stability of the constitutive equations.

Different convex restrictions can be considered upon the strain energy complying with the ellipticity condition (refer to the relevant part of Figure 1.6 in the context of elasticity). It is very well known that convexity of the strain energy with respect to the deformation gradient should not be used as a physically admissible constraint as it precludes buckling [27]. Quasiconvexity, introduced by Morrey [31], is an integral inequality which complies with the ellipticity condition and does not preclude buckling. However, the integral nature of this condition makes it cumbersome to prove quasiconvexity for explicit energy functionals. The simplest convexity restriction upon the strain energy which complies with ellipticity and does not exclude buckling effects is polyconvexity. Moreover, polyconvexity automatically verifies sequential weak lower semicontinuity of the strain energy [11, 25, 27, 32] and when endowed with appropriate coercivity or growth conditions, it guarantees the existence of minimisers for the total energy potential in nonlinear elasticity (refer to Figure 1.6).

The strain energy function is polyconvex [27–29, 33–36] if it can be expressed as a convex multi-variable function of the components of the deformation gradient, its

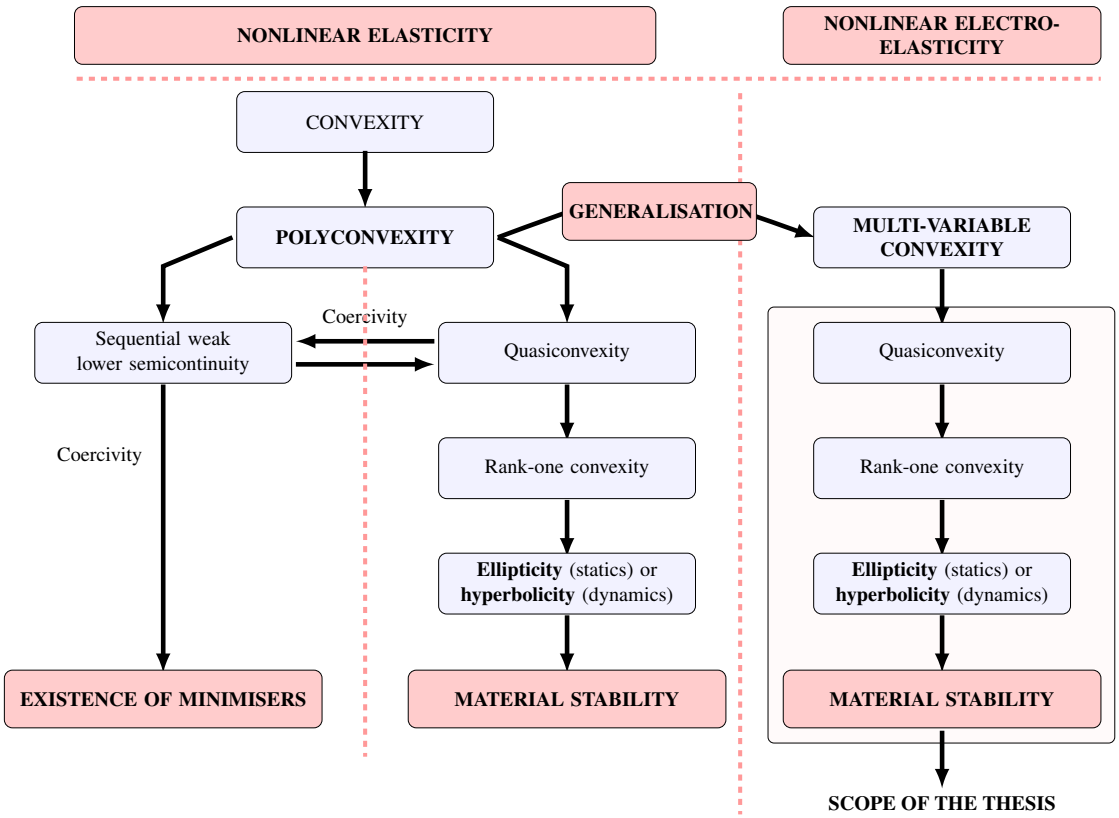

Figure 1.6: Implications of generalised convexity conditions. The shadowed region indicates the field of interest of the present work in the context of electro-elasticity.

determinant and the components of its adjoint or co-factor. Numerous authors have previously incorporated polyconvexity into computational models for both isotropic and non-isotropic materials for a variety of applications [32, 37–41].

From the computational standpoint, several well established reliable techniques can be utilised for the numerical simulation of nonlinear elasticity. The most common of these relies on a Finite Element discretisation of the classical displacement based formulation [12], where only geometry is part of the unknowns of the problem. It is very well known that when low order interpolation spaces are employed, this type of formulations render a series of detrimental deficiencies such us volumetric locking and spurious pressure oscillations in nearly incompressible scenarios [14, 42–45], bending locking in bending dominated scenarios, etc. to name but a few. Alternatively, mixed formulations [12, 40, 42–44, 46–51, 51–58], where not only geometry but also strains and stresses are part of the unknowns of the problem, have been successfully utilised in order to remedy the deficiencies of displacement based formulations.

1.2.2 Nonlinear electro-mechanics

Dielectric elastomers [5–8] possess outstanding capabilities as artificial actuators [5–9] and as energy harvesters and power generators [59].

Despite the widespread interest of the experimental [5–9] and computational scientific community [3, 60–69], the definition of suitable constitutive models for electro-active materials is still at its early stages.

As customary in nonlinear continuum mechanics, the constitutive behaviour of the material is encoded in an energy functional which depends typically upon appropriate strain measures, a Lagrangian electric variable and, if dissipative effects are considered, upon an electromechanical internal variable. Notice that this energy functional is equivalent to the strain energy functional in nonlinear elasticity, now denominated as internal energy [61, 62].

Several authors have proposed alternative representations of the energy functional in terms of electromechanical invariants [61–66]. However, some restrictions need to be imposed on the invariant representation if physically admissible behaviours are expected to occur. Bustamante and Merodio [70] considered classical constitutive inequalities, namely: the Baker-Ericksen inequality, the pressure-compression inequality, the traction-extension inequality and the ordered forces inequality. The objective was to study under what conditions a specific invariant representation of the energy functional for magneto-sensitive elastomers would violate the previous inequalities for very specific deformation scenarios.

As stated in the previous Section, the most well accepted constitutive inequality, which ensures the material stability of the constitutive equations is ellipticity, also known as the Legendre-Hadamard condition [11, 27]. Several authors have also studied under what conditions positive definiteness of the generalised electromechanical acoustic tensor and hence, the Legendre-Hadamard condition is compromised for a specific invariant representation of the energy functional [30, 71, 72]. Recently, a material stability criterion based on an incremental quasi-convexity condition of the energy functional has been introduced by Miehe et al [73].

In nonlinear elasticity, ellipticity is satisfied by polyconvex energy functionals. This thesis, based on a series of publications by the author [74–76], explores an extension of ellipticity to the context of nonlinear electro-elasticity for the entire range of deformations and electric fields.

From the computational standpoint, the scientific community typically resorts to a discretisation of a displacement-electric potential based variational principle via the Finite Element Method [60–69, 77–79]. Bustamante [63] presents alternative variational principles in which the unknown variables are displacements and the Lagrangian electric displacement field and the vector potential. Moreover, the authors in Reference [80] have presented a series of mixed variational principles for electro-elasticity.

1.3 Scope of the thesis

The main scope of this thesis is on the development of well-posed constitutive laws for nonlinear electro-elasticity in scenarios characterised by extreme electrically induced deformations in the presence of high electric fields. With reference to this underlying objective, this work proposes an extension of the concept of polyconvexity to the field of nonlinear electro-elasticity based on a new convex multi-variable definition of the energy functional.

1.3.1 Nonlinear elasticity

Several authors have incorporated the concept of polyconvexity into computational models for a variety of applications [37, 44, 81]. The classical approach consists of ensuring that the stored energy function satisfies the polyconvexity condition first but then proceed towards an evaluation of stresses and elasticity tensors by re-expressing the energy function in terms of the deformation gradient alone. This inevitably leads to the differentiation of inverse functions of the deformation gradient, its transpose or the inverse of the right Cauchy-Green tensor. These derivatives are readily obtained using standard algebra but can lead to lengthy expressions. An alternative approach is explored in this work and has been published in References [44] and [43] recovering the concept of the tensor cross-product originally introduced by de Boer [82] but not previously used in continuum mechanics. This tensor cross product allows for simpler expressions to be obtained for the area and volume maps and their derivatives. The resulting formulas for the elasticity tensors provide useful physical insights by separating positive definite material components from geometrical components.

Remarkably, the convex multi-variable nature of polyconvexity enables a one to one and invertible relationship between the arguments which define polyconvexity and their work conjugates. This invertible relationship enables a complementary energy to be defined exclusively in terms of the work conjugates. This two ingredients are the basis for the development of new Hu-Washizu an Hellinger-Reissner type of mixed variational principles. A Finite Element implementation of these new mixed variational principles is carried out in this work. The robustness and accuracy of the new variational and computational framework is tested and compared against that for the classical displacement-based formulations via a series of challenging numerical examples.

Exploring the strong relationship between the Legendre-Hadamard condition (automatically satisfied by polyconvex functionals) and the hyperbolicity of the governing equations, this work elucidates the underlying physical interpretation of the convex multi-variable dependence of the strain energy upon its arguments, showing that their respective time rates can be expressed as first order conservation laws [43]. Following the work of Bonet et al. [43], a novel set of hyperbolic equations for nonlinear polyconvex elasticity is presented in this thesis, including conservation

laws for the arguments of polyconvexity, namely the deformation gradient tensor, its co-cofactor and its Jacobian. Moreover, the convex multi-variable nature of the polyconvex strain energy enables to define a generalised convex entropy functional which permits a symmetrisation of the first order conservation laws in terms of its work (entropy) conjugates [43].

1.3.2 Nonlinear electro-elasticity

Multi-variable convexity of the strain energy, or equivalently, convexity with respect to the deformation gradient, its co-factor and its determinant, automatically ensures the sequential weak lower semicontinuity [27] of the strain energy in the context of nonlinear elasticity (refer to Figure 1.6). It is therefore possible to assert that multi-variable convexity entails the polyconvexity of the strain energy.

Based on the definition of multi-variable convexity (or polyconvexity) in the context of nonlinear elasticity, this thesis explores an extension of the concept of multi-variable convexity to the context of nonlinear electro-elasticity, motivated by material stability considerations exclusively (refer to Figure 1.6). Therefore, the ultimate objective of this work is to propose an extended definition of multi-variable convexity which ensures the material stability of the constitutive equations in non-linear electro-elasticity. Proof of sequential weak lower semicontinuity of the new extended concept of multi-variable convexity is out of the scope of this thesis. Hence, existence of minimisers, ensured under additional coercivity assumptions (refer to Figure 1.6), are not proved hereby. Consequently, the term polyconvexity must be avoided in this thesis in the context of nonlinear electro-elasticity and only the more appropriate concept of multi-variable convexity should be used instead.

The new concept of multi-variable convexity requires an enrichment of the convex nature of the internal energy with respect to that of the strain energy in nonlinear elasticity. Thus, in addition to the purely geometrical arguments which characterise multi-variable convexity (polyconvexity) in this more specific context, namely the deformation gradient tensor, its co-factor and its Jacobian, additional electromechanical variables will define the extended convex multi-variable set. Crucially, in comparison to the work of other authors [83], this new extended set enables the electromechanical energy of the vacuum to be considered as a degenerate case of multi-variable convexity.

The extended set of variables enables the introduction of a set of work conjugate variables [84]. Multi-variable convexity of the internal energy ensures a one to one and invertible relationship between both sets of variables. In addition, the convex nature of the internal energy enables three additional energy functionals to be defined (at least implicitly) by making appropriate use of the Legendre transform[1].

[1]Two partial Legendre transforms can be obtained by fixing either purely mechanical or purely electrical variables of the extended set. A total Legendre transform of the internal energy would render the third energy functional in terms of the elements of the extended set of work conjugate variables

A series of novel Hu-Washizu type of mixed variational principles, which were initially developed to overcome the shortcomings of more classical displacement based formulations in the context of elasticity, are developed by exploiting the new extended electro-kinematic set and its associated set work conjugate variables. A Finite Element implementation of these new variational principles is carried out.

An additional ingredient of this new convex multi-variable framework for nonlinear electro-elasticity is the new tensor cross product operation developed by Bonet et al. [44, 82], which enables tedious algebra to be remarkably simplified, yielding insightful representations of otherwise complex expressions (i.e. electro-mechanical tangent operators).

The consideration of convex multi-variable internal energy functionals ensures the positive definiteness of the generalised electro-mechanical acoustic tensor [30, 71, 72] and hence, existence of real wave speeds in the material in the vicinity of an equilibrium configuration. In analogy to the analysis carried out in the context of polyconvex elasticity, a completely new set of first order hyperbolic equations is presented in this thesis for convex multi-variable electro-magneto-mechanics, where this further deliberate generalisation (including magnetomechanical interactions) has been used as a detour which elegantly enables a particularisation of the resulting hyperbolic framework to more specific scenarios where only electromechanical (and even magnetomechanical) interactions are considered. Finally, the convex multi-variable nature of the internal energy enables the definition of a generalised convex entropy functional which subsequently permits a novel (in this context) symmetrisation of the system of conservation laws in terms of the entropy conjugates.

1.4 Outline of the thesis

In order to elaborate the objectives indicated in the previous Section, this thesis is organised as follows,

- ***Chapter II*** exploits the algebra of the new tensor cross product operation which greatly facilitates the manipulation of the co-factor and its derivatives. This tensor cross product operation leads to new physically insightful representations for tangent operators of the energy functional, presented in this Chapter both in reference and spatial settings.

  A series of new Hu-Washizu and Hellinger-Reissner types of mixed variational principles are presented in this Chapter. Additionally, mixed variational principles for fully and nearly incompressible scenarios are also presented with the new tensor cross product operation featuring heavily and enabling the simplification of algebraic manipulations.

- ***Chapter III*** presents the Finite Element implementation of the various new mixed variational principles presented in the preceding Chapter. Discretisation of the stationary conditions of these new mixed variational principles and

of their linearisations has been carried out, leading to the definition of the classical residual vectors and stiffness matrices. A static condensation procedure has been presented for the Hellinger-Reissner mixed variational principle, where a particular choice of functional spaces for the different variables satisfying the Ladyzenskaja-Babuška-Brezzi condition has been utilised, the resulting formulation having a comparable computational cost to those of displacement based formulations. Finally, linear continuous interpolation using tetrahedral elements for both displacement and pressure unknowns, stabilised via a Petrov-Galerkin technique for fully incompressible scenarios has been presented in this Chapter.

- ***Chapter IV*** endows the common denominator of both variational and computational frameworks developed in the two preceding Chapters, namely multi-variable convexity (or polyconvexity in this context), with a physical and insightful interpretation. Exploration of the connections between the Legendre-Hadamard condition (satisfied by any polyconvex functional) and the hyperbolicity of the equations for Solid Dynamics enables to assert that the time derivative of each of the arguments defining the multi-variable convexity of the internal must be necessarily expressed as first order conservation laws. A set of first order conservation laws for convex multi-variable (polyconvex) elasticity is presented in this Chapter.

  Finally, symmetrisation of the system of conservation laws in terms of the work (entropy) variables is also presented in this Chapter, facilitated by the definition of a generalised convex entropy functional.

- ***Chapter V*** extends the ideas presented in ***Chapter III*** to the field of electro-elasticity. A new definition of multi-variable convexity is postulated in this Chapter, based upon an extended set of kinetic and electric variables, which entails the well-posedness or ellipticity (hyperbolicity in dynamic scenarios) of the equations for the entire range of deformations and electric fields. New mixed variational principles are presented in this Chapter, where the new tensor cross product operation and its associated algebra feature heavily.

- ***Chapter VI*** presents the Finite Element implementation of the various mixed variational principles presented in the preceding Chapter, which represent a reliable and robust alternative to more classical potential displacement based formulations. Finally, a series of challenging numerical examples are included to show the applicability and robustness of the proposed formulations.

- ***Chapter VII***, extends the ideas presented in Chapter ***Chapter IV*** to the field of nonlinear electro-magneto-mechanics. A new set of conservation laws for all the arguments which determine the multi-variable convexity of the internal energy in electro-magneto-mechanics is presented in this Chapter. Moreover, the existence of a generalised convex entropy functional which leads to

the symmetrisation of the conservation laws in terms of the extended set of entropy variables is presented in this Chapter.

- ***Chapter VIII*** concludes the thesis by summarising its main concluding aspects and key contributions and indicates some suggestions for further research works.

Part II

Polyconvex formulation of nonlinear elasticity

Chapter 2

On a tensor cross product based formulation of large strain solid mechanics

2.1 Introduction

Ellipticity is the most widely accepted constitutive condition in nonlinear elasticity [27,37,38]. As stated in the previous Chapter, this condition has extremely relevant physical implications, since it ensures the existence of travelling plane waves in the material [37]. A special class of energy functionals which satisfy the ellipticity condition is that of polyconvex functionals [27–29,33,85], already mentioned in the previous Chapter.

Multi-variable convexity, or equivalently, polyconvexity (in purely mechanical context) has been incorporated in the field of nonlinear elasticity by several authors [32,37–40,86]. Typically, stresses and elasticity tensors are obtained by re-expressing the polyconvex energy function in terms of the deformation gradient alone, leading to lengthy expressions associated to the differentiation of inverse functions of the deformation gradient, its transpose or the inverse of the right Cauchy-Green tensor. An alternative approach has recently been proposed by Bonet et al. in [44] and [43] based on the definition of a tensor cross-product originally introduced by de Boer [82] but not previously used in continuum mechanics. This tensor cross product allows for simpler expressions for the area and volume maps and their derivatives. The resulting formulas for the elasticity tensors provide useful physical insights by separating positive definite material components from geometrical components.

This Chapter explores the proposed formulation both in the reference setting, using Piola-Kirchhoff stress tensors and in the spatial setting using Kirchhoff and Cauchy stress tensors. Some formulas derived with the tensor cross product formulation are compared against their classical equivalent versions in order to demonstrate the advantages of the proposed methodology. Both isotropic and anisotropic cases are considered. This Chapter illustrates the proposed concepts using the well established model of a Mooney-Rivlin material.

This Chapter is organised as follows. Section 2.2 introduces the novel tensor cross product notation in the context of large strain deformation. Whilst this product had already been proposed by de Boer in [82] (in German), it has not previously been described in the English literature or used in the context of solid mechanics, so most readers will be unfamiliar with it. This product is used to re-express the adjoint of the deformation gradient and its directional derivatives in a novel, simple and convenient manner. Section 2.3 reviews the definition of polyconvex elastic strain energy functions and defines a new set of stress variables conjugate to the main kinematic variables. The relationships between these stress variables and the standard first Piola-Kirchhoff stress tensor are provided. The section also derives complementary strain energy functions in terms of the new conjugate stresses. The algebra is greatly simplified via the tensor cross product. The fourth order elasticity tensors are derived in this section taking advantage of the tensor cross product operation leading to interesting insights into the consequences of convexity. Both compressible and nearly incompressible cases are discussed in the context of Mooney-Rivlin models, although the extension to more general strain energy functions is straight-

forward. Section 2.4 derives similar equations using entirely material tensors such as the right Cauchy-Green tensor and the second Piola-Kirchhoff tensor or spatial tensors such as the Kirchhoff or Cauchy stresses. Expressions for both material and spatial elasticity tensor are given in the context of the new proposed notation. Section 2.5 particularises the above expressions for the case of isotropic and anisotropic materials. A number of mixed and complementary energy variational principles are presented in Section 2.6. Several of these have been used in [44] for the purpose of constructing novel finite element approximations. Finally, Section 2.7 provides some concluding remarks and a summary of the key contributions of this paper. An illustrative diagram of the layout of the present Chapter can be found in Figure 2.1.

2.2 Definitions and notation

2.2.1 Motion and deformation

Let us consider the motion of an elastic body which in its initial or material configuration is defined by a domain V of boundary ∂V with outward unit normal $\boldsymbol{N}$, with boundary ∂V. After the motion, the elastic body occupies a spatial configuration defined by a domain v of boundary ∂v with outward unit normal $\boldsymbol{n}$, with boundary ∂v. The motion of the elastic body V is defined by a pseudo-time t dependent mapping field $\boldsymbol{\phi}$ which links a material particle from material configuration $\boldsymbol{X}$ to spatial configuration $\boldsymbol{x}$ according to $\boldsymbol{x} = \boldsymbol{\phi}(\boldsymbol{X}, t)$, where displacement boundary conditions can be defined as $\boldsymbol{x} = (\boldsymbol{\phi})_{\partial_u V}$ on the boundary $\partial_u V \subset \partial V$, where the notation $(\bullet)_{\partial_u V}$ is used to indicate the *given* value of a variable $\bullet$ on the boundary $\partial_u V$.

The two-point deformation gradient tensor or fibre-map $\boldsymbol{F}$, which relates a fibre of differential length from the material configuration $d\boldsymbol{X}$ to the spatial configuration $d\boldsymbol{x}$, namely $d\boldsymbol{x} = \boldsymbol{F} d\boldsymbol{x}$, is defined as the material gradient $\boldsymbol{\nabla}_0$ of the spatial configuration [10–12, 24–29, 85]

$$\boldsymbol{F} = \boldsymbol{\nabla}_0 \boldsymbol{x} = \frac{\partial \boldsymbol{\phi}(\boldsymbol{X}, t)}{\partial \boldsymbol{X}}. \tag{2.1}$$

In addition, $J = \det \boldsymbol{F}$ represents the Jacobian or volume-map of the deformation, which relates differential volume elements in the material configuration dV and the spatial configuration dv as $dv = JdV$. Finally, the element area vector is mapped from initial $d\boldsymbol{A}$ (colinear with $\boldsymbol{N}$) to final $d\boldsymbol{a}$ (colinear with $\boldsymbol{n}$) configuration by means of the two-point co-factor or adjoint tensor $\boldsymbol{H}$ as $d\boldsymbol{a} = \boldsymbol{H} d\boldsymbol{A}$, which is related to the deformation gradient via the so-called Nanson's rule [12]

$$\boldsymbol{H} = J\boldsymbol{F}^{-T}. \tag{2.2}$$

Clearly, the components of this tensor are the order 2 minors of the deformation gradient and it is often referred to as the co-factor or adjoint tensor. This tensor

Figure 2.1: Chapter layout.

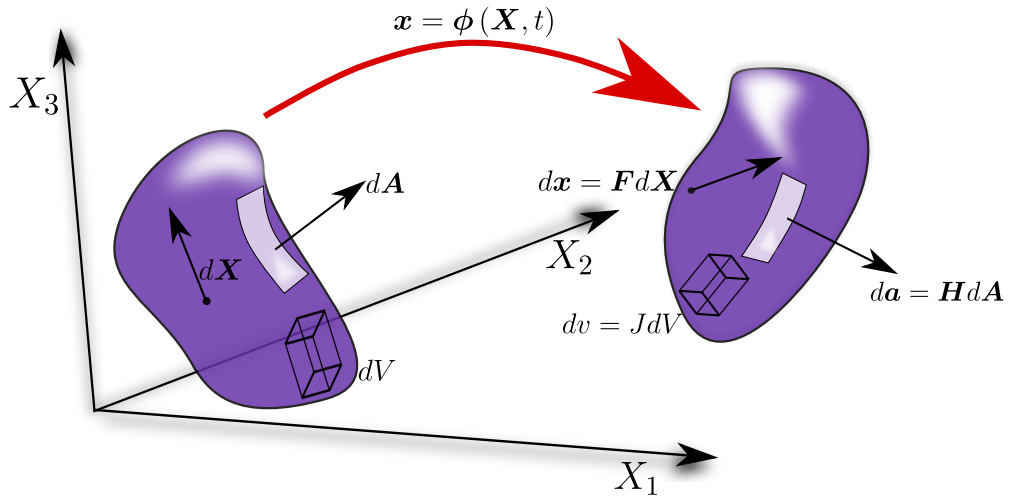

Figure 2.2: Deformation mapping of a continuum and associated kinematics magnitudes: $\boldsymbol{F}, \boldsymbol{H}, J$.

and its derivatives will feature heavily in the formulation that follows as it is a key variable for polyconvex elastic models. Its evaluation and, more importantly, the evaluation of its derivatives using equation (2.2) is not ideal, and a more convenient formula can be derived for three dimensional applications. This relies on the use of a tensor cross product operation, presented for the first time in Reference [82], page 76, but included in 2.2.2 for completeness.

Finally, Figure 2.2 depicts the deformation process as well the three kinematic maps, that is, $\boldsymbol{F}$, $\boldsymbol{H}$ and J. Virtual or linear incremental variations of $\boldsymbol{x}$ will be denoted $\delta\boldsymbol{u}$ and $\boldsymbol{u}$, respectively. It will be assumed that $\boldsymbol{x}$ satisfy appropriate prescribed displacement based boundary conditions in $\partial_u V$, and that $\delta\boldsymbol{u}$ and $\boldsymbol{u}$ will satisfy the equivalent homogeneous conditions in this section of the boundary. Additionally, the body is under the action of certain body forces per unit undeformed volume $\boldsymbol{f}_0$ and traction per unit undeformed area $\boldsymbol{t}_0$ in $\partial_t V$, where $\partial_t V \cup \partial_u V = \partial V$ and $\partial_t V \cap \partial_u V = \emptyset$.

2.2.2 Tensor cross product

The key element of the framework proposed is the extension of the standard vector cross product to define the cross product between second order tensors and between tensors and vectors. This rediscovers the work of de Boer [82] which, to the best knowledge of the authors, does not appear in any English language publication. The original nomenclature in [82] is "Das äuβere Tensorprodukt von Tensoren", which has been translated here as tensor cross product.

The left cross product of a vector $\boldsymbol{v}$ and a second order tensor $\boldsymbol{A}$ to give a second order tensor denoted $\boldsymbol{v} \times \boldsymbol{A}$ is defined so that when applied to a general vector $\boldsymbol{w}$

gives

$$(\boldsymbol{v}\times\boldsymbol{A})\,\boldsymbol{w}=\boldsymbol{v}\times(\boldsymbol{A}\boldsymbol{w})\,;\quad (\boldsymbol{v}\times\boldsymbol{A})_{ij}=\mathcal{E}_{ikl}v_kA_{lj}, \tag{2.3}$$

where $\mathcal{E}_{ijk}$ (or $\mathcal{E}_{IJK}$) symbolises the third order alternating tensor components[1] and the use of repeated indices implies summation, unless otherwise stated. In addition, throughout this thesies, the symbol $(\cdot)$ is used to indicate the scalar product or contraction of a single index $\boldsymbol{a}\cdot\boldsymbol{b}$; the symbol $(:)$ is used to indicate double contraction of two indices $\boldsymbol{A}:\boldsymbol{B}=A_{ij}B_{ij}$; the symbol $(\times)$ is used to indicate the cross product between vectors $[\boldsymbol{a}\otimes\boldsymbol{b}]_i=\mathcal{E}_{ijk}a_jb_k$ and the symbol $(\otimes)$ is used to indicate the outer or dyadic product $[\boldsymbol{a}\otimes\boldsymbol{b}]_{ij}=a_ib_j$.

Note that the notation $\times$ instead of $\times$ is used if the outcome of the operation is a second order tensor rather than a vector. The effect of the above operation is to replace the columns of $\boldsymbol{A}$ by the cross products between $\boldsymbol{v}$ and the original columns of $\boldsymbol{A}$. Similarly, the right cross product of a second order tensor $\boldsymbol{A}$ by a vector $\boldsymbol{v}$ to give a second order tensor denoted $\boldsymbol{A}\times\boldsymbol{v}$ is defined so that for every vector $\boldsymbol{w}$ the following relationship applies

$$(\boldsymbol{A}\times\boldsymbol{v})\,\boldsymbol{w}=\boldsymbol{A}\,(\boldsymbol{v}\times\boldsymbol{w})\,;\quad (\boldsymbol{A}\times\boldsymbol{v})_{ij}=\mathcal{E}_{jkl}A_{ik}v_l. \tag{2.4}$$

The effect is now to replace the rows of $\boldsymbol{A}$ by the cross products of its original rows by $\boldsymbol{v}$. Finally, the cross product of two second order tensors $\boldsymbol{A}$ and $\boldsymbol{B}$ to give a new second order tensor denoted $\boldsymbol{A}\times\boldsymbol{B}$ is defined so that for any arbitrary vectors $\boldsymbol{v}$ and $\boldsymbol{w}$ gives

$$\boldsymbol{v}\cdot(\boldsymbol{A}\times\boldsymbol{B})\,\boldsymbol{w}=(\boldsymbol{v}\times\boldsymbol{A}):(\boldsymbol{B}\times\boldsymbol{w})\,;\quad (\boldsymbol{A}\times\boldsymbol{B})_{ij}=\mathcal{E}_{ikl}\mathcal{E}_{jmn}A_{km}B_{ln}. \tag{2.5}$$

In this paper, the tensor cross product will be mostly applied between two-point tensors. For this purpose, the above definition can be particularised to second order two-point tensors or material tensors as,

$$(\boldsymbol{A}\times\boldsymbol{B})_{iI}=\mathcal{E}_{ijk}\mathcal{E}_{IJK}A_{jJ}B_{kK};\quad (\boldsymbol{A}\times\boldsymbol{B})_{IJ}=\mathcal{E}_{IKL}\mathcal{E}_{JMN}A_{KM}B_{LN}. \tag{2.6}$$

When applied to a second order tensor $\boldsymbol{A}$ and a fourth order tensor $\mathbb{H}$, two possible operations are defined as

$$(\mathbb{H}\times\boldsymbol{A})_{pPiI}=\mathcal{E}_{ijk}\mathcal{E}_{IJK}\mathbb{H}_{pPjJ}A_{kK};\quad (\boldsymbol{A}\times\mathbb{H})_{iIpP}=\mathcal{E}_{ijk}\mathcal{E}_{IJK}A_{jJ}\mathbb{H}_{kKpP}. \tag{2.7}$$

Moreover, the double application of the tensor cross product between a fourth order tensor and two second order tensors is associative, namely

$$\boldsymbol{A}\times\mathbb{H}\times\boldsymbol{B}=(\boldsymbol{A}\times\mathbb{H})\times\boldsymbol{B}=\boldsymbol{A}\times(\mathbb{H}\times\boldsymbol{B})\,. \tag{2.8}$$

Finally, when applied to a second order tensor $\boldsymbol{A}$ and a third order tensors $\mathbb{Q}$, two possible operations are defined as

$$(\mathbb{Q}\times\boldsymbol{A})_{PiI}=\mathcal{E}_{ijk}\mathcal{E}_{IJK}\mathbb{Q}_{PjJ}A_{kK};\quad (\boldsymbol{A}\times\mathbb{Q})_{iIP}=\mathcal{E}_{ijk}\mathcal{E}_{IJK}A_{jJ}\mathbb{H}_{kKP}. \tag{2.9}$$

[1]Lower case indices $\{i,j,k\}$ will be used to represent the spatial configuration whereas capital case indices $\{I,J,K\}$ will be used to represent the material description.

Box 1 shows the practical evaluation of these products. Finally, the cross vector product of two two-point tensors to give a spatial vector is also defined by a cross product operation with respect to the first indices and a contraction with respect to the second set of indices, so that,

$$\boldsymbol{v}\cdot(\boldsymbol{A}\times\boldsymbol{B}) = \boldsymbol{v}\cdot\boldsymbol{\mathcal{E}} : (\boldsymbol{A}\boldsymbol{B}^T) = \mathrm{tr}\left(\boldsymbol{v}\times(\boldsymbol{A}\boldsymbol{B}^T)\right); \qquad (\boldsymbol{A}\times\boldsymbol{B})_i = \mathcal{E}_{ijk}A_{jI}B_{kI}. \tag{2.10}$$

Remark 2.1: It is easy to show using simply algebraic manipulations based on the permutation properties of $\boldsymbol{\mathcal{E}}$ or the fact that $\mathcal{E}_{ijk}\mathcal{E}_{kln} = \delta_{il}\delta_{jn} - \delta_{in}\delta_{jl}$, that the above tensor cross products satisfy the following properties (note that $\boldsymbol{v}$, $\boldsymbol{v}_1$, $\boldsymbol{v}_2$, $\boldsymbol{w}$, $\boldsymbol{w}_1$ and $\boldsymbol{w}_2$ denote arbitrary vectors and $\boldsymbol{A}$, $\boldsymbol{A}_1$, $\boldsymbol{A}_2$, $\boldsymbol{B}$, $\boldsymbol{B}_1$, $\boldsymbol{B}_2$ and $\boldsymbol{C}$ are second order tensors)

$$\boldsymbol{A}\times\boldsymbol{B} = \boldsymbol{B}\times\boldsymbol{A} \tag{2.11}$$

$$(\boldsymbol{A}\times\boldsymbol{B})^T = \boldsymbol{A}^T\times\boldsymbol{B}^T \tag{2.12}$$

$$\boldsymbol{A}\times(\boldsymbol{B}_1+\boldsymbol{B}_2) = \boldsymbol{A}\times\boldsymbol{B}_1 + \boldsymbol{A}\times\boldsymbol{B}_2 \tag{2.13}$$

$$\alpha\,(\boldsymbol{A}\times\boldsymbol{B}) = (\alpha\boldsymbol{A})\times\boldsymbol{B} = \boldsymbol{A}\times(\alpha\boldsymbol{B}) \tag{2.14}$$

$$(\boldsymbol{A}\times\boldsymbol{B}) : \boldsymbol{C} = (\boldsymbol{B}\times\boldsymbol{C}) : \boldsymbol{A} = (\boldsymbol{A}\times\boldsymbol{C}) : \boldsymbol{B} \tag{2.15}$$

$$\boldsymbol{A}\times\boldsymbol{I} = (\mathrm{tr}\boldsymbol{A})\,\boldsymbol{I} - \boldsymbol{A}^T \tag{2.16}$$

$$\boldsymbol{I}\times\boldsymbol{I} = 2\boldsymbol{I} \tag{2.17}$$

$$(\boldsymbol{A}\times\boldsymbol{A}) : \boldsymbol{A} = 6\,\mathrm{det}\boldsymbol{A} \tag{2.18}$$

$$\mathrm{Cof}\boldsymbol{A} = \frac{1}{2}\boldsymbol{A}\times\boldsymbol{A} \tag{2.19}$$

$$(\boldsymbol{v}_1\otimes\boldsymbol{v}_2)\times(\boldsymbol{w}_1\otimes\boldsymbol{w}_2) = (\boldsymbol{v}_1\times\boldsymbol{w}_1)\otimes(\boldsymbol{v}_2\times\boldsymbol{w}_2) \tag{2.20}$$

$$\boldsymbol{v}\times(\boldsymbol{A}\times\boldsymbol{w}) = (\boldsymbol{v}\times\boldsymbol{A})\times\boldsymbol{w} = \boldsymbol{v}\times\boldsymbol{A}\times\boldsymbol{w} \tag{2.21}$$

$$\boldsymbol{A}\times(\boldsymbol{v}\otimes\boldsymbol{w}) = -\boldsymbol{v}\times\boldsymbol{A}\times\boldsymbol{w} \tag{2.22}$$

$$(\boldsymbol{A}\times\boldsymbol{B})\,(\boldsymbol{v}\times\boldsymbol{w}) = (\boldsymbol{A}\boldsymbol{v})\times(\boldsymbol{B}\boldsymbol{w}) + (\boldsymbol{B}\boldsymbol{v})\times(\boldsymbol{A}\boldsymbol{w}) \tag{2.23}$$

$$(\boldsymbol{A}_1\times\boldsymbol{A}_2)\,(\boldsymbol{B}_1\times\boldsymbol{B}_2) = (\boldsymbol{A}_1\boldsymbol{B}_1)\times(\boldsymbol{A}_2\boldsymbol{B}_2) + (\boldsymbol{A}_1\boldsymbol{B}_2)\times(\boldsymbol{A}_2\boldsymbol{B}_1) \tag{2.24}$$

$$(\boldsymbol{A}_1\boldsymbol{B})\times(\boldsymbol{A}_2\boldsymbol{B}) = (\boldsymbol{A}_1\times\boldsymbol{A}_2)\,\mathrm{Cof}\boldsymbol{B} \tag{2.25}$$

Box 1. Enumeration of tensor cross products:

$$[\boldsymbol{v}\times\boldsymbol{A}] = \begin{bmatrix} v_yA_{zx}-v_zA_{yx} & v_yA_{zy}-v_zA_{yy} & v_yA_{zz}-v_zA_{yz} \\ v_zA_{xx}-v_xA_{zx} & v_zA_{xy}-v_xA_{zy} & v_zA_{xz}-v_xA_{zz} \\ v_xA_{yx}-v_yA_{xx} & v_xA_{yy}-v_yA_{xy} & v_xA_{yz}-v_yA_{xz} \end{bmatrix}$$

$$[\boldsymbol{A}\times\boldsymbol{w}] = \begin{bmatrix} A_{xy}v_z-A_{xz}v_y & A_{xz}v_x-A_{xx}v_z & A_{xx}v_y-A_{xy}v_x \\ A_{yy}v_z-A_{yz}v_y & A_{yz}v_x-A_{yx}v_z & A_{yx}v_y-A_{yy}v_x \\ A_{zy}v_z-A_{zz}v_y & A_{zz}v_x-A_{zx}v_z & A_{zx}v_y-A_{zy}v_x \end{bmatrix}$$

$$[\boldsymbol{A}\times\boldsymbol{B}] = \begin{bmatrix} [\boldsymbol{A}\times\boldsymbol{B}]_{xx} & [\boldsymbol{A}\times\boldsymbol{B}]_{xy} & [\boldsymbol{A}\times\boldsymbol{B}]_{xz} \\ [\boldsymbol{A}\times\boldsymbol{B}]_{yx} & [\boldsymbol{A}\times\boldsymbol{B}]_{yy} & [\boldsymbol{A}\times\boldsymbol{B}]_{yz} \\ [\boldsymbol{A}\times\boldsymbol{B}]_{zx} & [\boldsymbol{A}\times\boldsymbol{B}]_{zy} & [\boldsymbol{A}\times\boldsymbol{B}]_{zz} \end{bmatrix}$$

$$\begin{aligned}
[\boldsymbol{A}\times\boldsymbol{B}]_{xx} &= A_{yy}B_{zz}-A_{yz}B_{zy}+A_{zz}B_{yy}-A_{zy}B_{yz} \\
[\boldsymbol{A}\times\boldsymbol{B}]_{xy} &= A_{yz}B_{zx}-A_{yx}B_{zz}+A_{zx}B_{yz}-A_{zz}B_{yx} \\
[\boldsymbol{A}\times\boldsymbol{B}]_{xz} &= A_{yx}B_{zy}-A_{yy}B_{zx}+A_{zy}B_{yx}-A_{zx}B_{yy} \\
[\boldsymbol{A}\times\boldsymbol{B}]_{yx} &= A_{xz}B_{zy}-A_{xy}B_{zz}+A_{zy}B_{xz}-A_{zz}B_{xy} \\
[\boldsymbol{A}\times\boldsymbol{B}]_{yy} &= A_{zz}B_{xx}-A_{zx}B_{xz}+A_{xx}B_{zz}-A_{xz}B_{zx} \\
[\boldsymbol{A}\times\boldsymbol{B}]_{yz} &= A_{zx}B_{xy}-A_{zy}B_{xx}+A_{xy}B_{zx}-A_{xx}B_{zy} \\
[\boldsymbol{A}\times\boldsymbol{B}]_{zx} &= A_{xy}B_{yz}-A_{xz}B_{yy}+A_{yz}B_{xy}-A_{yy}B_{xz} \\
[\boldsymbol{A}\times\boldsymbol{B}]_{zy} &= A_{xz}B_{yx}-A_{xx}B_{yz}+A_{yx}B_{xz}-A_{yz}B_{xx} \\
[\boldsymbol{A}\times\boldsymbol{B}]_{zz} &= A_{xx}B_{yy}-A_{xy}B_{yx}+A_{yy}B_{xx}-A_{yx}B_{xy}
\end{aligned}$$

2.2.3 Alternative expressions for the area and volume maps

Using equation (2.19) it is possible to express the area map tensor $\boldsymbol{H}$ as [1]

$$\boldsymbol{H} = \frac{1}{2}\boldsymbol{F}\times\boldsymbol{F} \tag{2.26}$$

Moreover, the first and second directional derivatives of $\boldsymbol{H}$ with respect to geometry changes are now easily evaluated as

$$D\boldsymbol{H}[\delta\boldsymbol{u}] = \boldsymbol{F}\times D\boldsymbol{F}[\delta\boldsymbol{u}] = \boldsymbol{F}\times\boldsymbol{\nabla}_0\delta\boldsymbol{u} \tag{2.27}$$

$$D^2\boldsymbol{H}[\delta\boldsymbol{u};\boldsymbol{u}] = D\boldsymbol{F}[\boldsymbol{u}]\times D\boldsymbol{F}[\delta\boldsymbol{u}] = \boldsymbol{\nabla}_0\delta\boldsymbol{u}\times\boldsymbol{\nabla}_0\boldsymbol{u} \tag{2.28}$$

Similarly, the derivatives of the volume ratio J are easily expressed with the help of (2.15), (2.18) and the definition of $\boldsymbol{H}$ given by equation (2.26)

$$DJ[\delta\boldsymbol{u}] = \boldsymbol{H}:\boldsymbol{\nabla}_0\delta\boldsymbol{u}; \quad D^2J[\delta\boldsymbol{u};\boldsymbol{u}] = \boldsymbol{F}:(\boldsymbol{\nabla}_0\delta\boldsymbol{u}\times\boldsymbol{\nabla}_0\boldsymbol{u}) \tag{2.29}$$

The above formulas simplify greatly the manipulation of the derivatives of $\boldsymbol{H}$ and J by avoiding differentiating the inverse of the deformation gradient. They will be key to the development of the framework presented below. Alternatively, the classical approach to compute the first directional derivative of $\boldsymbol{H}$ and J [12] is

$$D\boldsymbol{H}\left[\delta\boldsymbol{u}\right] = JG_{\delta\boldsymbol{u}}\boldsymbol{F}^{-T} - J\boldsymbol{G}_{\delta\boldsymbol{u}}\boldsymbol{F}^{-T}, \tag{2.30a}$$

$$DJ\left[\delta\boldsymbol{u}\right] = JG_{\delta\boldsymbol{u}}, \tag{2.30b}$$

where

$$G_{\delta\boldsymbol{u}} = \boldsymbol{F}^{-T} : \boldsymbol{\nabla}_0\delta\boldsymbol{u}; \qquad \boldsymbol{G}_{\delta\boldsymbol{u}} = \boldsymbol{F}^{-T}\left(\boldsymbol{\nabla}_0\delta\boldsymbol{u}\right)^T. \tag{2.31}$$

The second directional derivatives of $\boldsymbol{H}$ and J [12] is

$$\begin{aligned} D^2\boldsymbol{H}\left[\delta\boldsymbol{u};\boldsymbol{u}\right] = {} & J\boldsymbol{G}_{\delta\boldsymbol{u}}\boldsymbol{G}_{\boldsymbol{u}}\boldsymbol{F}^{-T} + J\boldsymbol{G}_{\boldsymbol{u}}\boldsymbol{G}_{\delta\boldsymbol{u}}\boldsymbol{F}^{-T} \\ & - JG_{\delta\boldsymbol{v}}\boldsymbol{G}_{\boldsymbol{u}}\boldsymbol{F}^{-T} - JG_{\boldsymbol{u}}\boldsymbol{G}_{\delta\boldsymbol{u}}\boldsymbol{F}^{-T} \\ & + JG_{\delta\boldsymbol{u}}G_{\boldsymbol{u}}\boldsymbol{F}^{-T} - J\mathrm{tr}\left(\boldsymbol{G}_{\delta\boldsymbol{u}}\boldsymbol{G}_{\boldsymbol{u}}\right)\boldsymbol{F}^{-T}, \end{aligned} \tag{2.32a}$$

$$D^2J\left[\delta\boldsymbol{u};\boldsymbol{u}\right] = JG_{\delta\boldsymbol{u}}G_{\boldsymbol{u}} - J\mathrm{tr}\left(\boldsymbol{G}_{\delta\boldsymbol{u}}\boldsymbol{G}_{\boldsymbol{u}}\right), \tag{2.32b}$$

where

$$G_{\boldsymbol{u}} = \boldsymbol{F}^{-T} : \boldsymbol{\nabla}_0\boldsymbol{u}; \qquad \boldsymbol{G}_{\boldsymbol{u}} = \boldsymbol{F}^{-T}\left(\boldsymbol{\nabla}_0\boldsymbol{u}\right)^T. \tag{2.33}$$

Comparison of (2.27) vs. (2.30a), (2.28) vs. (2.32a), (2.29) vs. (2.30b) and (2.32b) demonstrates very clearly the simplification introduced as a result of using the new tensor cross product algebra.

It is also possible to derive alternative expressions for both $\boldsymbol{H}$ and J. For instance, combining equation (2.26) with equation (2.1) and noting that the derivatives of $\boldsymbol{F}$ are second derivatives of $\boldsymbol{x}$ and therefore symmetric, gives, after simple use of the product rule

$$\boldsymbol{H} = \frac{1}{2}\mathrm{CURL}\left(\boldsymbol{x} \times \boldsymbol{F}\right), \tag{2.34}$$

where the material CURL of a second order two point tensor is defined in the usual fashion by

$$\left(\mathrm{CURL}\boldsymbol{A}\right)_{iI} = \mathcal{E}_{IJK}\frac{\partial A_{iK}}{\partial X_J}. \tag{2.35}$$

It is clear from equation (2.34) that the material divergence of $\boldsymbol{H}$ vanishes, as does the material CURL of $\boldsymbol{F}$, that is

$$\mathrm{DIV}\boldsymbol{H} = \boldsymbol{0}; \qquad \mathrm{CURL}\boldsymbol{F} = \boldsymbol{0}, \tag{2.36}$$

where the material divergence is defined by the contraction

$$\left(\mathrm{DIV}\boldsymbol{A}\right)_i = \frac{\partial A_{iI}}{\partial X_I}. \tag{2.37}$$

Combining equations (2.1) and (2.2b) an alternative equation for J emerges as

$$J = \frac{1}{3}\boldsymbol{H} : \boldsymbol{\nabla}_0\boldsymbol{x} = \frac{1}{3}\mathrm{DIV}\left(\boldsymbol{H}^T\boldsymbol{x}\right). \tag{2.38}$$

2.3 Polyconvex elasticity

2.3.1 The strain energy

Polyconvex energy functionals [27] are a very interesting type of energy functionals which satisfy the ellipticity condition and therefore, the well-posedness of the governing equations in finite strain elasticity for the entire range of deformations [43,86]. Essentially, the strain energy Ψ per unit undeformed volume must be a function of the deformation gradient $\boldsymbol{F}$ via a convex multi-variable function W as

$$\Psi\left(\boldsymbol{\nabla}_0\boldsymbol{x}\right) = W\left(\boldsymbol{F}, \boldsymbol{H}, J\right), \tag{2.39}$$

where W is convex with respect to its 19 variables, namely, J and the 3×3 components of $\boldsymbol{F}$ and $\boldsymbol{H}$. Moreover, invariance with respect to rotations in the material configuration implies that W must be independent of the rotational components of $\boldsymbol{F}$ and $\boldsymbol{H}$. This is typically achieved by ensuring that W depends on $\boldsymbol{F}$ and $\boldsymbol{H}$ via the symmetric tensors $\boldsymbol{C} = \boldsymbol{F}^T\boldsymbol{F}$ and $\boldsymbol{G} = \boldsymbol{H}^T\boldsymbol{H}$, respectively. For example, a general compressible Mooney-Rivlin material can be described by an energy function of the type

$$W_{MR} = \alpha\boldsymbol{F} : \boldsymbol{F} + \beta\boldsymbol{H} : \boldsymbol{H} + f\left(J\right), \tag{2.40}$$

where α and β are positive material parameters and f denotes a convex function of J. It is clear therefore that W_{MR} is convex with respect to all of its variables. The condition of vanishing energy at the initial reference configuration can be established by ensuring that $f\left(1\right) = -\left(3\alpha + 3\beta\right)$ or by adding an appropriate constant to W_{MR}. Doing this, however, has no practical effect on the resulting formulation as this will be driven by derivatives of the strain energy. Appropriate values for α and β and suitable functions f will be found in the sections below.

In the classical manner, the strain energy function W_{MR} (2.40) can also be rewritten in terms of the invariants $\{I_1, I_2, I_3\}$ of the right Cauchy-Green deformation tensor $\boldsymbol{C}$ as

$$\widetilde{\Psi}_{MR}\left(\boldsymbol{C}\right) = \alpha I_1 + \beta I_2 + g\left(I_3\right), \tag{2.41}$$

with

$$I_1 = \mathrm{tr}\,\boldsymbol{C}; \qquad I_2 = \left(\det\boldsymbol{C}\right)\left(\mathrm{tr}\boldsymbol{C}^{-1}\right); \qquad I_3 = \det\boldsymbol{C} \tag{2.42}$$

where g is not necessarily a convex function of the invariant I_3.

Remark 2.2:

A popular constitutive model, which only should be used under small strain scenarios is that of a Saint Venant-Kirchhoff material [12], where the strain energy functional per unit undeformed volume Ψ is defined in terms of the Green-Lagrange strain tensor $\boldsymbol{E}$ as

$$\Psi_{SVK}\left(\boldsymbol{\nabla}_0\boldsymbol{x}\right) = \frac{\lambda}{2}\left(\mathrm{tr}\boldsymbol{E}\right)^2 + \mu\mathrm{tr}\left(\boldsymbol{E}\boldsymbol{E}\right); \qquad \boldsymbol{E} = \frac{1}{2}\left(\boldsymbol{C} - \boldsymbol{I}\right), \tag{2.43}$$

with λ and μ the Lamé coefficients and $\boldsymbol{I}$, the second order identity tensor. Alternatively, Ψ_{SVK} can be expressed in terms of $\boldsymbol{C}$ as

$$\Psi_{SVK}(\boldsymbol{C}) = \frac{\mu}{4}\left(\text{tr}(\boldsymbol{CC}) - 2\text{tr}(\boldsymbol{C}) + 3\right) + \frac{\lambda}{8}\left(\text{tr}(\boldsymbol{C}) - 3\right)^2. \tag{2.44}$$

As shown in [32], it is possible to re-express the term $\text{tr}(\boldsymbol{CC})$ in (2.44) as

$$\text{tr}(\boldsymbol{CC}) = (\boldsymbol{F}:\boldsymbol{F})^2 - 2(\boldsymbol{H}:\boldsymbol{H}). \tag{2.45}$$

Introduction of identity (2.45) into (2.44) enables to rewrite the strain energy functional in terms of $\boldsymbol{F}$ and J as

$$W_{SVK}(\boldsymbol{F},\boldsymbol{H}) = \frac{\mu}{4}\left((\boldsymbol{F}:\boldsymbol{F})^2 - 2(\boldsymbol{F}:\boldsymbol{F}) - 2(\boldsymbol{H}:\boldsymbol{H}) + 3\right) + \frac{\lambda}{8}\left((\boldsymbol{F}:\boldsymbol{F}) - 3\right)^2. \tag{2.46}$$

Equation (2.46) represents a re-expression of the Saint Venant-Kirchhoff model in terms of the fibre and area maps, namely $\boldsymbol{F}$ and $\boldsymbol{H}$. Notice that the above definition of the strain energy is not convex with respect to its two arguments, namely $\{\boldsymbol{F},\boldsymbol{H}\}$. An equivalent and non unique representation of above equation (2.46) in terms of the three kinematic arguments of polyconvexity, namely $\{\boldsymbol{F},\boldsymbol{H},J\}$ can be defined as

$$\hat{W}_{SVK}(\boldsymbol{F},\boldsymbol{H},J) = \frac{\mu}{4}\left((\boldsymbol{F}:\boldsymbol{F})^2 - 2(\boldsymbol{F}:\boldsymbol{F}) - 2J\left(\boldsymbol{H}:\boldsymbol{F}^{-T}\right) + 3\right) + \frac{\lambda}{8}\left((\boldsymbol{F}:\boldsymbol{F}) - 3\right)^2. \tag{2.47}$$

Unfortunately, the strain energy $\hat{W}_{SVK}$ in above equation (2.47) is not convex with respect to its arguments, namely $\{\boldsymbol{F},\boldsymbol{H},J\}$. As expected, it is not possible to obtain a polyconvex representation of the Saint Venant-Kirchhoff constitutive model.

2.3.2 Conjugate stresses and the first Piola-Kirchhoff tensor

The three strain measures $\boldsymbol{F}$, $\boldsymbol{H}$ and J have conjugate stresses $\boldsymbol{\Sigma}_{\boldsymbol{F}}$, $\boldsymbol{\Sigma}_{\boldsymbol{H}}$ and Σ_J defined by

$$\boldsymbol{\Sigma}_{\boldsymbol{F}}(\boldsymbol{F},\boldsymbol{H},J) = \frac{\partial W}{\partial \boldsymbol{F}}; \quad \boldsymbol{\Sigma}_{\boldsymbol{H}}(\boldsymbol{F},\boldsymbol{H},J) = \frac{\partial W}{\partial \boldsymbol{H}}; \quad \Sigma_J(\boldsymbol{F},\boldsymbol{H},J) = \frac{\partial W}{\partial J}. \tag{2.48}$$

For instance, for the case of a Mooney-Rivlin material (refer to (2.40))

$$\boldsymbol{\Sigma}_{\boldsymbol{F}} = 2\alpha\boldsymbol{F}; \qquad \boldsymbol{\Sigma}_{\boldsymbol{H}} = 2\beta\boldsymbol{H}; \quad \Sigma_J = f'(J). \tag{2.49}$$

The set of conjugate stresses defined in equation (2.48) enables the directional derivative of the stain energy to be expressed as

$$DW[\delta\boldsymbol{F},\delta\boldsymbol{H},\delta J] = \boldsymbol{\Sigma}_{\boldsymbol{F}}:\delta\boldsymbol{F} + \boldsymbol{\Sigma}_{\boldsymbol{H}}:\delta\boldsymbol{H} + \Sigma_J\delta J. \tag{2.50}$$

In order to develop a relationship between these conjugate stresses and the more standard first Piola-Kirchhoff stress tensor $\boldsymbol{P}$, recall that

$$D\Psi\left[\delta\boldsymbol{u}\right] = \boldsymbol{P} : \boldsymbol{\nabla}_0\delta\boldsymbol{u}; \quad \boldsymbol{P} = \left.\frac{\partial\Psi\left(\boldsymbol{F}\right)}{\partial\boldsymbol{F}}\right|_{\boldsymbol{F}=\boldsymbol{\nabla}_0\boldsymbol{x}}. \tag{2.51}$$

With the help of the last two equations, the chain rule and equations (2.27) and (2.29a) it is possible to express the virtual internal work as

$$\begin{aligned}\boldsymbol{P} : \boldsymbol{\nabla}_0\delta\boldsymbol{u} &= D\Psi\left[\delta\boldsymbol{u}\right] \\ &= DW\left[D\boldsymbol{F}\left[\delta\boldsymbol{u}\right], D\boldsymbol{H}\left[\delta\boldsymbol{u}\right], DJ\left[\delta\boldsymbol{u}\right]\right] \\ &= \boldsymbol{\Sigma}_{\boldsymbol{F}} : D\boldsymbol{F}\left[\delta\boldsymbol{u}\right] + \boldsymbol{\Sigma}_{\boldsymbol{H}} : D\boldsymbol{H}\left[\delta\boldsymbol{u}\right] + \Sigma_J DJ\left[\delta\boldsymbol{u}\right] \\ &= \boldsymbol{\Sigma}_{\boldsymbol{F}} : \boldsymbol{\nabla}_0\delta\boldsymbol{u} + \boldsymbol{\Sigma}_{\boldsymbol{H}} : \left(\boldsymbol{F} \times \boldsymbol{\nabla}_0\delta\boldsymbol{u}\right) + \Sigma_J\left(\boldsymbol{H} : \boldsymbol{\nabla}_0\delta\boldsymbol{u}\right) \\ &= \left(\boldsymbol{\Sigma}_{\boldsymbol{F}} + \boldsymbol{\Sigma}_{\boldsymbol{H}} \times \boldsymbol{F} + \Sigma_J\boldsymbol{H}\right) : \boldsymbol{\nabla}_0\delta\boldsymbol{u},\end{aligned} \tag{2.52}$$

which leads to the evaluation of the first Piola-Kirchhoff tensor as

$$\boldsymbol{P} = \boldsymbol{\Sigma}_{\boldsymbol{F}} + \boldsymbol{\Sigma}_{\boldsymbol{H}} \times \boldsymbol{F} + \Sigma_J\boldsymbol{H}. \tag{2.53}$$

For instance, for the simple compressible Mooney-Rivlin material, the first Piola-Kirchhoff stress tensor is expressed as

$$\boldsymbol{P} = 2\alpha\boldsymbol{F} + 2\beta\boldsymbol{H} \times \boldsymbol{F} + f'\left(J\right)\boldsymbol{H}. \tag{2.54}$$

The condition of a stress-free initial configuration, where $\boldsymbol{F} = \boldsymbol{H} = \boldsymbol{I}$ and $J = 1$, together with property (2.17) of the tensor cross product, leads to the following constraint on the material parameters α, β and $f\left(J\right)$

$$f'\left(1\right) = -2\alpha - 4\beta. \tag{2.55}$$

Alternatively, for the strain energy in equation (2.41), the associated second Piola-Kirchhoff $\boldsymbol{S}$ can be obtained in the classical sense $\left(\boldsymbol{S} = 2\frac{\partial\widetilde{\Psi}(\boldsymbol{C})}{\partial\boldsymbol{C}}\right)$ [12] as

$$\boldsymbol{S} = 2\alpha\boldsymbol{I} + 2\beta I_3\left[\left(\operatorname{tr}\boldsymbol{C}^{-1}\right)\boldsymbol{C}^{-1} - \boldsymbol{C}^{-1}\boldsymbol{C}^{-1}\right] + 2g'(I_3)I_3\boldsymbol{C}^{-1}. \tag{2.56}$$

Finally, the first Piola-Kirchhoff stress tensor can now be obtained via the classical push forward operation, $\boldsymbol{P} = \boldsymbol{F}\boldsymbol{S}$

$$\boldsymbol{P} = 2\alpha\boldsymbol{F} + 2\beta I_3\left[\left(\operatorname{tr}\boldsymbol{C}^{-1}\right)\boldsymbol{F}^{-T} - \boldsymbol{F}^{-T}\boldsymbol{C}^{-1}\right] + 2g'(I_3)I_3\boldsymbol{F}^{-T}, \tag{2.57}$$

which leads to a lengthier expression in comparison with (2.54).

2.3.3 Complementary energy

The convexity of the function $W\left(\boldsymbol{F}, \boldsymbol{H}, J\right)$ with respect to its variables ensures that the relationship between $\{\boldsymbol{F}, \boldsymbol{H}, J\}$ and $\{\boldsymbol{\Sigma}_{\boldsymbol{F}}, \boldsymbol{\Sigma}_{\boldsymbol{H}}, \Sigma_J\}$ is one to one and invertible. Using the reverse relationships, it is therefore possible to define a convex complementary energy function by means of a Legendre transform as

$$\Upsilon\left(\boldsymbol{\Sigma}_{\boldsymbol{F}}, \boldsymbol{\Sigma}_{\boldsymbol{H}}, \Sigma_J\right) = \boldsymbol{\Sigma}_{\boldsymbol{F}} : \boldsymbol{F} + \boldsymbol{\Sigma}_{\boldsymbol{H}} : \boldsymbol{H} + \Sigma_J J - W\left(\boldsymbol{F}, \boldsymbol{H}, J\right), \tag{2.58}$$

so that the reverse constitutive equations are derived as

$$\boldsymbol{F} = \frac{\partial \Upsilon}{\partial \boldsymbol{\Sigma}_{\boldsymbol{F}}}; \qquad \boldsymbol{H} = \frac{\partial \Upsilon}{\partial \boldsymbol{\Sigma}_{\boldsymbol{H}}}; \qquad J = \frac{\partial \Upsilon}{\partial \Sigma_J}. \tag{2.59}$$

For instance, in the particular case of a Mooney-Rivlin material, the complementary energy adopts the following expression

$$\Upsilon_{MR}\left(\boldsymbol{\Sigma}_{\boldsymbol{F}}, \boldsymbol{\Sigma}_{\boldsymbol{H}}, \Sigma_J\right) = \frac{1}{4\alpha}\boldsymbol{\Sigma}_{\boldsymbol{F}} : \boldsymbol{\Sigma}_{\boldsymbol{F}} + \frac{1}{4\beta}\boldsymbol{\Sigma}_{\boldsymbol{H}} : \boldsymbol{\Sigma}_{\boldsymbol{H}} + g\left(\Sigma_J\right), \tag{2.60}$$

where the complementary function g is defined by the Legendre transform

$$g\left(\Sigma_J\right) = \Sigma_J J\left(\Sigma_J\right) - f\left(J\left(\Sigma_J\right)\right) \tag{2.61}$$

and the relationship $J\left(\Sigma_J\right)$ is obtained inverting equation (2.49c), that is, $J\left(f'\left(x\right)\right) = x$. Note that if either α or β is zero, the corresponding term in the complementary energy also vanishes. For instance, the case $\beta = 0$ corresponds to a compressible neo-Hookean material, for which

$$\Upsilon_{NH}\left(\boldsymbol{\Sigma}_{\boldsymbol{F}}, J\right) = \frac{1}{4\alpha}\boldsymbol{\Sigma}_{\boldsymbol{F}} : \boldsymbol{\Sigma}_{\boldsymbol{F}} + g\left(\Sigma_J\right); \quad \boldsymbol{\Sigma}_{\boldsymbol{H}} = \boldsymbol{0}. \tag{2.62}$$

Remark 2.3: The complementary energy defined above does not coincide with the more traditional definition of complementary energy $\Psi^*(\boldsymbol{P}) = \boldsymbol{P} : \boldsymbol{F} - \Psi(\boldsymbol{F})$. It is in fact easy to show that

$$\begin{aligned} \boldsymbol{P} : \boldsymbol{F} &= \left(\boldsymbol{\Sigma}_{\boldsymbol{F}} + \boldsymbol{\Sigma}_{\boldsymbol{H}} \times \boldsymbol{F} + \Sigma_J \boldsymbol{H}\right) : \boldsymbol{F} \\ &= \boldsymbol{\Sigma}_{\boldsymbol{F}} : \boldsymbol{F} + \boldsymbol{\Sigma}_{\boldsymbol{H}} : \left(\boldsymbol{F} \times \boldsymbol{F}\right) + \Sigma_J \boldsymbol{H} : \boldsymbol{F} \\ &= \boldsymbol{\Sigma}_{\boldsymbol{F}} : \boldsymbol{F} + 2\boldsymbol{\Sigma}_{\boldsymbol{H}} : \boldsymbol{H} + 3\Sigma_J J \\ &\neq \boldsymbol{\Sigma}_{\boldsymbol{F}} : \boldsymbol{F} + \boldsymbol{\Sigma}_{\boldsymbol{H}} : \boldsymbol{H} + \Sigma_J J, \end{aligned} \tag{2.63}$$

and therefore $\Upsilon(\boldsymbol{\Sigma}_{\boldsymbol{F}}, \boldsymbol{\Sigma}_{\boldsymbol{H}}, \Sigma_J) \neq \Psi^*(\boldsymbol{P})$. Note that only in the exceptional cases where this relation is invertible, it is possible to carry out the Legendre transform in order to obtain $\Psi^*(\boldsymbol{P})$ (see [87] and [88]).

Remark 2.4: In the case of thermoelasticity, the strain energy is also a convex function of the entropy η, and the temperature θ is given by,

$$\theta = \frac{\partial W(\boldsymbol{F}, \boldsymbol{H}, J, \eta)}{\partial \eta} \tag{2.64}$$

and the complementary energy function which will now depend on the temperature can be interpreted as a generalised Gibbs energy function defined as

$$\Upsilon\left(\boldsymbol{\Sigma}_{\boldsymbol{F}}, \boldsymbol{\Sigma}_{\boldsymbol{H}}, \Sigma_J, \theta\right) = \boldsymbol{\Sigma}_{\boldsymbol{F}} : \boldsymbol{F} + \boldsymbol{\Sigma}_{\boldsymbol{H}} : \boldsymbol{H} + \Sigma_J J + \eta\theta - W\left(\boldsymbol{F}, \boldsymbol{H}, J, \eta\right). \tag{2.65}$$

2.3.4 Stress based compatibility conditions and equilibrium

In linear elasticity it is well known that the stress tensor field must satisfy a set of differential compatibility conditions usually known as Beltrami-Mitchell equations [89]. These conditions ensure that the stress tensor can be derived from a displacement field. In the large strain case, it is also possible to derive a set of relationships that the above conjugate stresses have to satisfy in order to ensure that they correspond to an actual deformation process, that there exist a mapping $\boldsymbol{x} = \boldsymbol{\phi}(\boldsymbol{X})$ such that

$$\frac{\partial \Upsilon}{\partial \boldsymbol{\Sigma_F}} = \boldsymbol{\nabla}_0 \boldsymbol{x}; \qquad \frac{\partial \Upsilon}{\partial \boldsymbol{\Sigma_H}} = \frac{1}{2} \boldsymbol{\nabla}_0 \boldsymbol{x} \times \boldsymbol{\nabla}_0 \boldsymbol{x}; \qquad \frac{\partial \Upsilon}{\partial \Sigma_J} = \det\left(\boldsymbol{\nabla}_0 \boldsymbol{x}\right). \tag{2.66}$$

These conditions can be enforced directly in the context of a mixed computational formulation using appropriate variational principles as described in [44]. Alternatively, an equivalent set of constraints for the conjugate stresses can be derived as

$$\begin{aligned} \mathrm{CURL}\left(\frac{\partial \Upsilon}{\partial \boldsymbol{\Sigma_F}}\right) &= \boldsymbol{0}; \\ 2\frac{\partial \Upsilon}{\partial \boldsymbol{\Sigma_H}} - \left(\frac{\partial \Upsilon}{\partial \boldsymbol{\Sigma_F}} \times \frac{\partial \Upsilon}{\partial \boldsymbol{\Sigma_F}}\right) &= \boldsymbol{0}; \\ 3\frac{\partial \Upsilon}{\partial \Sigma_J} - \left(\frac{\partial \Upsilon}{\partial \boldsymbol{\Sigma_F}} : \frac{\partial \Upsilon}{\partial \boldsymbol{\Sigma_H}}\right) &= 0. \end{aligned} \tag{2.67}$$

These constraints together with the equilibrium equation provide a full set of equations for the augmented set of stresses $\boldsymbol{\Sigma_F}$, $\boldsymbol{\Sigma_H}$, Σ_J. Equilibrium can be enforced in the conventional manner in a Lagrangian setting by means of the divergence of the first Piola-Kirchhoff tensor as [12]

$$\boldsymbol{f}_0 + \mathrm{DIV}\, \boldsymbol{P} = \boldsymbol{0}. \tag{2.68}$$

Simple algebra using equation (2.53) and the vector cross product defined by equation (2.10) gives an expression in terms of the conjugate stresses as

$$\boldsymbol{f}_0 + \mathrm{DIV}\, \boldsymbol{\Sigma_F} + (\mathrm{CURL}\, \boldsymbol{\Sigma_H}) \times \frac{\partial \Upsilon}{\partial \boldsymbol{\Sigma_F}} + \boldsymbol{\nabla}_0 \Sigma_J : \frac{\partial \Upsilon}{\partial \boldsymbol{\Sigma_H}} = \boldsymbol{0}. \tag{2.69}$$

This differential equilibrium equation must be complemented by appropriate boundary conditions. Traction boundary conditions on $\partial_t V$ imply

$$\boldsymbol{P}\boldsymbol{N} = \boldsymbol{\Sigma_F}\boldsymbol{N} + (\boldsymbol{\Sigma_H} \times \frac{\partial \Upsilon}{\partial \boldsymbol{F}})\boldsymbol{N} + \Sigma_J \frac{\partial \Upsilon}{\partial \boldsymbol{H}} N = \boldsymbol{t}_0. \tag{2.70}$$

2.3.5 Tangent elasticity operator

A tangent elasticity operator will be required in order to ensure quadratic convergence of a Newton-Raphson type of solution process. This is typically evaluated in terms of a fourth order tangent elasticity tensor defined by

$$D^2\Psi\left[\delta \boldsymbol{u}; \boldsymbol{u}\right] = \boldsymbol{\nabla}_0 \delta \boldsymbol{u} : D\boldsymbol{P}\left[\boldsymbol{u}\right] = \boldsymbol{\nabla}_0 \delta \boldsymbol{u} : \boldsymbol{\mathcal{C}} : \boldsymbol{\nabla}_0 \boldsymbol{u}; \quad \boldsymbol{\mathcal{C}} = \frac{\partial \boldsymbol{P}}{\partial \boldsymbol{F}} = \frac{\partial^2 \Psi}{\partial \boldsymbol{F} \partial \boldsymbol{F}}. \tag{2.71}$$

Use of equation (2.53), following a chain rule derivation similar to that of equation (2.52) and making use of equations (2.27) and (2.28) for the derivatives of $\boldsymbol{H}$, yields after simple algebra

$$\begin{aligned} D^2\Psi\left[\delta\boldsymbol{u};\boldsymbol{u}\right] &= \boldsymbol{\nabla}_0\delta\boldsymbol{u} : D\boldsymbol{P}\left[\boldsymbol{u}\right] \\ &= \boldsymbol{\nabla}_0\delta\boldsymbol{u} : D\boldsymbol{\Sigma}_{\boldsymbol{F}}\left[\boldsymbol{u}\right] + \left(\boldsymbol{\nabla}_0\delta\boldsymbol{u}\times\boldsymbol{F}\right) : D\boldsymbol{\Sigma}_{\boldsymbol{H}}\left[\boldsymbol{u}\right] + \left(\boldsymbol{\nabla}_0\delta\boldsymbol{u} : \boldsymbol{H}\right) D\Sigma_J\left[\boldsymbol{u}\right] \\ &+ \left(\boldsymbol{\Sigma}_{\boldsymbol{H}} + \Sigma_J\boldsymbol{F}\right) : \left(\boldsymbol{\nabla}_0\delta\boldsymbol{u}\times\boldsymbol{\nabla}_0\boldsymbol{u}\right). \end{aligned} \tag{2.72}$$

In general, conjugate stresses $\{\boldsymbol{\Sigma}_{\boldsymbol{F}}, \boldsymbol{\Sigma}_{\boldsymbol{H}}, \Sigma_J\}$ will be functions of the strain variables $\{\boldsymbol{F}, \boldsymbol{H}, J\}$ and the resulting tangent operator can be written as

$$\begin{aligned} D^2\Psi\left[\delta\boldsymbol{u};\boldsymbol{u}\right] = \left[\left(\boldsymbol{\nabla}_0\delta\boldsymbol{u}\right) : \ \ \left(\boldsymbol{\nabla}_0\delta\boldsymbol{u}\times\boldsymbol{F}\right) : \ \ \left(\boldsymbol{\nabla}_0\delta\boldsymbol{u} : \boldsymbol{H}\right)\right]\left[\mathbb{H}_W\right]\begin{bmatrix} : \left(\boldsymbol{\nabla}_0\boldsymbol{u}\right) \\ : \left(\boldsymbol{\nabla}_0\boldsymbol{u}\times\boldsymbol{F}\right) \\ \left(\boldsymbol{\nabla}_0\boldsymbol{u} : \boldsymbol{H}\right)\end{bmatrix} \\ + \left(\boldsymbol{\Sigma}_{\boldsymbol{H}} + \Sigma_J\boldsymbol{F}\right) : \left(\boldsymbol{\nabla}_0\delta\boldsymbol{u}\times\boldsymbol{\nabla}_0\boldsymbol{u}\right), \end{aligned} \tag{2.73}$$

where the Hessian operator $\mathbb{H}_W$ denotes the symmetric positive definite operator containing the second derivatives of $W\left(\boldsymbol{F}, \boldsymbol{H}, J\right)$

$$\left[\mathbb{H}_W\right] = \begin{bmatrix} W_{\boldsymbol{FF}} & W_{\boldsymbol{FH}} & W_{\boldsymbol{F}J} \\ W_{\boldsymbol{HF}} & W_{\boldsymbol{HH}} & W_{\boldsymbol{H}J} \\ W_{J\boldsymbol{F}} & W_{J\boldsymbol{H}} & W_{JJ} \end{bmatrix}, \tag{2.74}$$

where $W_{\boldsymbol{AB}}$ denotes $\frac{\partial W^2}{\partial\boldsymbol{A}\partial\boldsymbol{B}}$. Note that the first term in equation (2.73) is necessarily positive for $\delta\boldsymbol{u} = \boldsymbol{u}$ and therefore buckling can only be induced by the "initial stress" term $\left(\boldsymbol{\Sigma}_{\boldsymbol{H}} + \Sigma_J\boldsymbol{F}\right) : \left(\boldsymbol{\nabla}_0\delta\boldsymbol{u}\times\boldsymbol{\nabla}_0\boldsymbol{u}\right)$. In effect, the above expression for the elasticity tensor separates the material dependencies or physics of the problem (encapsulated in the Hessian tensor) from the geometry dependencies included via the initial stress term.

Comparison of both equations (2.71) and (2.73) enables, by considering the different tensor cross operations in equations (2.7), to obtain an equivalent representation of the elasticity tensor $\boldsymbol{\mathcal{C}}$ (2.71) in terms of the components of the Hessian operator $\left[\mathbb{H}_W\right]$ (2.74) as

$$\begin{aligned} \boldsymbol{\mathcal{C}} = W_{\boldsymbol{FF}} + \boldsymbol{F}\times\left(W_{\boldsymbol{HH}}\times\boldsymbol{F}\right) + W_{JJ}\boldsymbol{H}\otimes\boldsymbol{H} + 2(W_{\boldsymbol{FH}}\times\boldsymbol{F})^{\mathrm{sym}} \\ + 2(W_{\boldsymbol{F}J}\otimes\boldsymbol{H})^{\mathrm{sym}} + 2((\boldsymbol{F}\times W_{\boldsymbol{H}J})\otimes\boldsymbol{H})^{\mathrm{sym}} + \boldsymbol{\mathcal{A}}, \end{aligned} \tag{2.75}$$

with the fourth order tensor $\boldsymbol{\mathcal{A}}$ defined as

$$\mathcal{A}_{iIjJ} = \mathcal{E}_{ijp}\mathcal{E}_{IJP}\left(\boldsymbol{\Sigma}_{\boldsymbol{H}} + \Sigma_J\boldsymbol{\Sigma}_{\boldsymbol{H}}\right)_{pP}. \tag{2.76}$$

Moreover, for any fourth order tensor $\boldsymbol{\mathcal{T}}$ included in equation (2.75), the symmetrised tensor $\boldsymbol{\mathcal{T}}^{\mathrm{sym}}$ is defined as $\mathcal{T}^{\mathrm{sym}}_{iIjJ} = \frac{1}{2}\left(\mathcal{T}_{iIjJ} + \mathcal{T}_{iJjI}\right)$.

Remark 2.5: Equation (2.73) makes it easy to highlight the relationship between polyconvexity and ellipticity. Ellipticity is equivalent to rank-one convexity and requires that the double contraction of the elasticity tensor by an arbitrary rank-one tensor $\boldsymbol{v} \otimes \boldsymbol{V}$ should be positive, that is,

$$(\boldsymbol{v} \otimes \boldsymbol{V}) : \boldsymbol{\mathcal{C}} : (\boldsymbol{v} \otimes \boldsymbol{V}) > 0. \tag{2.77}$$

Taking $\boldsymbol{\nabla}_0 \delta \boldsymbol{u} = \boldsymbol{\nabla}_0 \boldsymbol{u} = \boldsymbol{v} \otimes \boldsymbol{V}$ in equation (2.73) makes the initial stress term vanish since,

$$\boldsymbol{\nabla}_0 \delta \boldsymbol{u} \boldsymbol{\times} \boldsymbol{\nabla}_0 \boldsymbol{u} = (\boldsymbol{v} \otimes \boldsymbol{V}) \boldsymbol{\times} (\boldsymbol{v} \otimes \boldsymbol{V}) = (\boldsymbol{v} \times \boldsymbol{v}) \otimes (\boldsymbol{V} \times \boldsymbol{V}) = \boldsymbol{0}. \tag{2.78}$$

This leaves only the contribution from the first positive definite term in equation (2.73). It is therefore easy to note that polyconvexity implies ellipticity [11].

It is helpful to consider the simple case of the compressible Mooney-Rivlin material defined in (2.40) for which the off-diagonal terms of the Hessian operator vanish and the tangent elastic operator becomes

$$\begin{aligned} D^2\Psi_{MR}\left[\delta \boldsymbol{u}; \boldsymbol{u}\right] = {} & 2\alpha \boldsymbol{\nabla}_0 \delta \boldsymbol{u} : \boldsymbol{\nabla}_0 \boldsymbol{u} + 2\beta \left(\boldsymbol{\nabla}_0 \delta \boldsymbol{u} \boldsymbol{\times} \boldsymbol{F}\right) : \left(\boldsymbol{\nabla}_0 \boldsymbol{u} \boldsymbol{\times} \boldsymbol{F}\right) \\ & + f''\left(J\right) \left(\boldsymbol{\nabla}_0 \delta \boldsymbol{u} : \boldsymbol{H}\right) \left(\boldsymbol{\nabla}_0 \boldsymbol{u} : \boldsymbol{H}\right) + \left(\boldsymbol{\Sigma}_{\boldsymbol{H}} + \Sigma_J \boldsymbol{F}\right) : \left(\boldsymbol{\nabla}_0 \delta \boldsymbol{u} \boldsymbol{\times} \boldsymbol{\nabla}_0 \boldsymbol{u}\right). \end{aligned} \tag{2.79}$$

It is now possible to derive appropriate values for the material parameters α, β and the function $f\left(J\right)$ by ensuring that at the reference configuration the above operator coincides with the classic linear elasticity operator, which is typically expressed in terms of the Lamé coefficients $\{\lambda, \mu\}$ as

$$D^2\Psi_{LIN}\left[\delta \boldsymbol{u}; \boldsymbol{u}\right] = \lambda \left(\boldsymbol{\nabla}_0 \delta \boldsymbol{u} : \boldsymbol{I}\right) \left(\boldsymbol{\nabla}_0 \boldsymbol{u} : \boldsymbol{I}\right) + \mu \left(\boldsymbol{\nabla}_0 \delta \boldsymbol{u} : \boldsymbol{\nabla}_0 \boldsymbol{u} + \left(\boldsymbol{\nabla}_0 \delta \boldsymbol{u}\right)^T : \boldsymbol{\nabla}_0 \boldsymbol{u}\right). \tag{2.80}$$

Substituting $\boldsymbol{F} = \boldsymbol{H} = \boldsymbol{I}$; $J = 1$ into equation (2.79), making repeated use of property (2.16) for the tensor cross product and taking into account the zero initial stress condition (2.55), gives after lengthy but simple algebra

$$\begin{aligned} D^2\Psi_{MR}\left[\delta \boldsymbol{u}; \boldsymbol{u}\right]\big|_{\boldsymbol{I}} = {} & \left(2\alpha + 2\beta\right) \left(\boldsymbol{\nabla}_0 \delta \boldsymbol{u} : \boldsymbol{\nabla}_0 \boldsymbol{u} + \left(\boldsymbol{\nabla}_0 \delta \boldsymbol{u}\right)^T : \boldsymbol{\nabla}_0 \boldsymbol{u}\right) \\ & + \left(f''\left(1\right) - 2\alpha\right) \left(\boldsymbol{\nabla}_0 \delta \boldsymbol{u} : \boldsymbol{I}\right) \left(\boldsymbol{\nabla}_0 \boldsymbol{u} : \boldsymbol{I}\right). \end{aligned} \tag{2.81}$$

Identifying coefficients leads to the condition relating α, β to μ

$$\alpha + \beta = \frac{\mu}{2}, \tag{2.82}$$

and the condition for the second derivative of f at the origin

$$f''\left(1\right) = \lambda + 2\alpha. \tag{2.83}$$

A commonly used expression for f that satisfies these requirements is

$$f(J) = -4\beta J - 2\alpha \ln J + \frac{\lambda}{2\varepsilon^2}\left(J^{\varepsilon} + J^{-\varepsilon}\right); \quad \varepsilon \geq 1. \tag{2.84}$$

For this particular constitutive model, it is easy to observe that the above Hessian operator $[\mathbb{H}_W]$ (2.74) is positive definite, i.e,

$$[\mathbb{H}_W] = \begin{bmatrix} 2\alpha\boldsymbol{\mathcal{I}} & \mathbf{0} & \mathbf{0} \\ \mathbf{0} & 2\beta\boldsymbol{\mathcal{I}} & \mathbf{0} \\ \mathbf{0} & \mathbf{0} & f''(J) \end{bmatrix}, \tag{2.85}$$

where $\boldsymbol{\mathcal{I}}$ denotes the fourth order identity tensor $\mathcal{I}_{iIjJ} = \delta_{ij}\delta_{IJ}$. Notice that positive definiteness of the above Hessian operator in (2.85) is subjected to convexity of the function $f(J)$, which is the case of the expression in equation (2.84).

2.3.6 A modified Mooney-Rivlin material model

It is interesting to observe that the strain energy expressed in terms of the full set of kinematic variables $\boldsymbol{F}$, $\boldsymbol{H}$ and J is not a unique function. That is, the same physical strain energy $\Psi(\boldsymbol{F})$ can be expressed by a set of different functions $W(\boldsymbol{F}, \boldsymbol{H}, J)$. For instance, the addition of multiples of the function $\boldsymbol{F} : \boldsymbol{H} - 3J$, which vanishes for kinematically compatible variables, has no effect on the actual physical strain energy described and therefore,

$$\Psi(\boldsymbol{F}) = W(\boldsymbol{F}, \boldsymbol{H}, J) + \xi(\boldsymbol{F} : \boldsymbol{H} - 3J) = W_{\xi}(\boldsymbol{F}, \boldsymbol{H}, J), \tag{2.86}$$

where ξ can be an arbitrary constant provided that the resulting function W_{ξ} is still convex in its variables. For instance, in the case of Mooney-Rivlin materials (see (2.40)), it is easy to show that convexity is still maintained for values of ξ such that $\alpha\beta \geq \frac{\xi^2}{4}$. Is is easy to show that the addition of the above term does no alter the first Piola Kirchhoff stress tensor but leads to modified conjugate stresses as

$$\boldsymbol{\Sigma}^{\xi}_{\boldsymbol{F}} = \boldsymbol{\Sigma}_{\boldsymbol{F}} + \xi\boldsymbol{H}; \quad \boldsymbol{\Sigma}^{\xi}_{\boldsymbol{H}} = \boldsymbol{\Sigma}_{\boldsymbol{H}} + \xi\boldsymbol{F}; \quad \Sigma^{\xi}_{J} = \Sigma_{J} - 3\xi. \tag{2.87}$$

It is now possible to adjust the value of ξ so that some or all the conjugate stresses at the initial configuration vanish. As an interesting example, consider the case of a Mooney-Rivlin material for which $\alpha = \beta = \mu/4$. Choosing $\xi = -\mu/2$ leads to the following polyconvex strain energy function

$$W^{\xi}_{MR}(\boldsymbol{F}, \boldsymbol{H}, J) = \frac{\mu}{4}(\boldsymbol{F} - \boldsymbol{H}) : (\boldsymbol{F} - \boldsymbol{H}) + \frac{\mu}{2}(J - \ln J) + \frac{\lambda}{2\epsilon^2}\left(J^{\epsilon} + J^{-\epsilon}\right). \tag{2.88}$$

It is easy to show that all the conjugate stresses in this model vanish at the initial configuration. In addition, the term $(\boldsymbol{F} - \boldsymbol{H})$ has a clear physical interpretation as distortion given that when applied to a reference vector, it measures the difference between the mapped fibre and area vectors.

2.3.7 Nearly incompressible Mooney-Rivlin material

Very often it is convenient or even necessary to separate the distortional component from the volumetric response of the material. This is invariably the case when attempting to model either nearly-incompressible or truly incompressible solids. Typically, this is achieved by separating the strain energy into isochoric and volumetric components, $\hat{\Psi}$ and U, respectively, as [90]

$$\Psi\left(\boldsymbol{\nabla}_0\boldsymbol{x}\right) = \hat{\Psi}\left(\boldsymbol{\nabla}_0\boldsymbol{x}\right) + U\left(\det\boldsymbol{\nabla}_0\boldsymbol{x}\right); \quad \hat{\Psi}\left(\boldsymbol{\nabla}_0\boldsymbol{x}\right) = \Psi\left(\left(\det\boldsymbol{\nabla}_0\boldsymbol{x}\right)^{-1/3}\boldsymbol{\nabla}_0\boldsymbol{x}\right). \tag{2.89}$$

The first term in this energy expression leads to the deviatoric component of the Piola-Kirchhoff tensor and the derivative of the function U accounts for the pressure p. In the context of polyconvex elasticity, it is also possible to construct a similar decomposition in the form

$$W\left(\boldsymbol{F},\boldsymbol{H},J\right) = \hat{W}\left(\boldsymbol{F},\boldsymbol{H},J\right) + U\left(J\right). \tag{2.90}$$

For the purpose of deriving the conditions that need to be satisfied in order to ensure that the U-term alone accounts for the pressure p, it is necessary to restrict the derivation to the exact continuum context, where geometrically compatibility conditions are enforced exactly. Recall first that the pressure itself is obtained from the first Piola-Kirchhoff tensor via the contraction

$$p = \frac{1}{3}J^{-1}\boldsymbol{P} : \boldsymbol{F}. \tag{2.91}$$

Note that the sign convention used above is positive pressure in tension, negative in compression. Substituting the relationship between the Piola-Kirchhoff stress tensor and the conjugate stresses given by equation (2.53), yields a relationship between the pressure and the conjugate stresses as

$$\begin{aligned} p &= \frac{1}{3}J^{-1}\left(\boldsymbol{\Sigma}_{\boldsymbol{F}} + \boldsymbol{\Sigma}_{\boldsymbol{H}} \boldsymbol{\times} \boldsymbol{F} + \Sigma_J\boldsymbol{H}\right) : \boldsymbol{F} \\ &= \frac{1}{3}J^{-1}\left(\boldsymbol{\Sigma}_{\boldsymbol{F}} : \boldsymbol{F} + 2\boldsymbol{\Sigma}_{\boldsymbol{H}} : \boldsymbol{H} + 3\Sigma_J J\right), \end{aligned} \tag{2.92}$$

where property (2.18) has been made use of. Substituting the constitutive relationships (2.48) and decomposition (2.90) into this equation for the pressure gives

$$p = \frac{1}{3}J^{-1}\left(\frac{\partial\hat{W}}{\partial\boldsymbol{F}} : \boldsymbol{F} + 2\frac{\partial\hat{W}}{\partial\boldsymbol{H}} : \boldsymbol{H} + 3J\frac{\partial\hat{W}}{\partial J}\right) + U'\left(J\right). \tag{2.93}$$

Therefore the condition that $\hat{W}$ needs to satisfy in order to ensure a correct decomposition into volumetric and deviatoric components is

$$\frac{\partial\hat{W}}{\partial\boldsymbol{F}} : \boldsymbol{F} + 2\frac{\partial\hat{W}}{\partial\boldsymbol{H}} : \boldsymbol{H} + 3J\frac{\partial\hat{W}}{\partial J} = 0. \tag{2.94}$$

In order to fulfil this requirement, it is sufficient for $\hat{W}$ to satisfy the following mixed homogeneous condition (refer to [12], page 168)

$$\hat{W}\left(\alpha\boldsymbol{F}, \alpha^2\boldsymbol{H}, \alpha^3 J\right) = \hat{W}\left(\boldsymbol{F}, \boldsymbol{H}, J\right). \tag{2.95}$$

Differentiating this equation with respect to α at $\alpha = 1$, quickly leads to condition (2.94). A simple way to ensure that this requirement is satisfied would be to construct $\hat{W}$ in terms of the isochoric components of $\boldsymbol{F}$ and $\boldsymbol{H}$

$$\hat{W}\left(\boldsymbol{F}, \boldsymbol{H}\right) = W\left(\hat{\boldsymbol{F}}, \hat{\boldsymbol{H}}, 1\right), \tag{2.96}$$

where the isochoric components could be defined in the usual fashion [12] as

$$\hat{\boldsymbol{F}} = \left(\det\boldsymbol{F}\right)^{-1/3}\boldsymbol{F}; \qquad \hat{\boldsymbol{H}} = \left(\det\boldsymbol{H}\right)^{-1/3}\boldsymbol{H}. \tag{2.97}$$

Unfortunately, the resulting strain energy function constructed in this manner will not be convex with respect to $\boldsymbol{F}$ and $\boldsymbol{H}$. Alternative expressions can be derived by re-defining the isochoric components of $\boldsymbol{F}$ and $\boldsymbol{H}$ as

$$\hat{\boldsymbol{F}} = J^{-1/3}\boldsymbol{F}; \qquad \hat{\boldsymbol{H}} = J^{-2/3}\boldsymbol{H}. \tag{2.98}$$

Or, alternatively, noting that $\boldsymbol{F} : \boldsymbol{H} = 3J$ (refer to property (2.18))

$$\hat{\boldsymbol{F}} = \left(\frac{1}{3}\boldsymbol{F} : \boldsymbol{H}\right)^{-1/3}\boldsymbol{F}; \qquad \hat{\boldsymbol{H}} = \left(\frac{1}{3}\boldsymbol{F} : \boldsymbol{H}\right)^{-2/3}\boldsymbol{H}. \tag{2.99}$$

For instance, in the case of the Mooney-Rivlin material, an equivalent polyconvex isochoric energy function is obtained as [40]

$$\hat{W}\left(\boldsymbol{F}, \boldsymbol{H}, J\right) = \eta J^{-2/3}\left(\boldsymbol{F} : \boldsymbol{F}\right) + \gamma J^{-2}\left(\boldsymbol{H} : \boldsymbol{H}\right)^{3/2}, \tag{2.100}$$

where η and γ are two positive material parameters of a similar nature to parameters α and β appearing in equation (2.40). The most commonly used expression for the volumetric strain energy component $U\left(J\right)$ is given by

$$U\left(J\right) = \frac{1}{2}\kappa\left(J-1\right)^2. \tag{2.101}$$

Note that the dependency of the isochoric strain energy function $\hat{W}$ with respect to J implies that the pressure p and the conjugate stress Σ_J are not identical. They are in fact related by

$$\Sigma_J = \hat{\Sigma}_J + p; \quad \hat{\Sigma}_J = \frac{\partial\hat{W}}{\partial J}; \quad p = U'(J). \tag{2.102}$$

Finally, the tangent elastic operator of this nearly incompressible model can be derived in a manner similar to equation (2.73) to give

$$\begin{aligned} D^2\Psi\left[\delta\boldsymbol{u}; \boldsymbol{u}\right] &= D^2\hat{\Psi}\left[\delta\boldsymbol{u}; \boldsymbol{u}\right] + U''\left(\boldsymbol{\nabla}_0\delta\boldsymbol{u} : \boldsymbol{H}\right)\left(\boldsymbol{\nabla}_0\boldsymbol{u} : \boldsymbol{H}\right) \\ D^2\hat{\Psi}\left[\delta\boldsymbol{u}; \boldsymbol{u}\right] &= \left[\left(\boldsymbol{\nabla}_0\delta\boldsymbol{u}\right) : \quad \left(\boldsymbol{\nabla}_0\delta\boldsymbol{u} \times \boldsymbol{F}\right) : \quad \left(\boldsymbol{\nabla}_0\delta\boldsymbol{u} : \boldsymbol{H}\right)\right]\left[\mathbb{H}_{\hat{W}}\right]\begin{bmatrix} : \left(\boldsymbol{\nabla}_0\boldsymbol{u}\right) \\ : \left(\boldsymbol{\nabla}_0\boldsymbol{u} \times \boldsymbol{F}\right) \\ \left(\boldsymbol{\nabla}_0\boldsymbol{u} : \boldsymbol{H}\right) \end{bmatrix} \\ &\quad + \left(\boldsymbol{\Sigma}_{\boldsymbol{H}} + \Sigma_J\boldsymbol{F}\right) : \left(\boldsymbol{\nabla}_0\delta\boldsymbol{u} \times \boldsymbol{\nabla}_0\boldsymbol{u}\right). \end{aligned} \tag{2.103}$$

For the nearly incompressible model described in equation (2.100), the Hessian operator $[\mathbb{H}_{\hat{W}}]$ in (2.103) adopts a slightly more convoluted expression than that for the compressible Mooney-Rivlin model (with Hessian operator defined in equation (2.85))

$$[\mathbb{H}_{\hat{W}}] = \begin{bmatrix} 2\eta J^{-2/3}\boldsymbol{\mathcal{I}} & \mathbf{0} & -\frac{4}{3}\eta J^{-5/3}\boldsymbol{F} \\ \mathbf{0} & 3\gamma J^{-2}\left(II_{\boldsymbol{H}}^{-1/2}\boldsymbol{\mathcal{H}} + II_{\boldsymbol{H}}^{1/2}\boldsymbol{\mathcal{I}}\right) & -6\gamma J^{-3} II_{\boldsymbol{H}}\boldsymbol{H} \\ -\frac{4}{3}\eta J^{-5/3}\boldsymbol{F} & -6\gamma J^{-3} II_{\boldsymbol{H}}\boldsymbol{H} & \frac{10}{9}\eta J^{-8/3} II_{\boldsymbol{F}} + 6\gamma J^{-4} II_{\boldsymbol{H}}^{3/2} \end{bmatrix}, \tag{2.104}$$

with the fourth order tensor $\boldsymbol{\mathcal{H}}$ defined as $\boldsymbol{\mathcal{H}} = \boldsymbol{H}\otimes\boldsymbol{H}$ and $II_{(\bullet)}$ denotes the squared of the L_2 norm of the entity $(\bullet)$, that is $II_{\boldsymbol{F}} = \boldsymbol{F} : \boldsymbol{F}$.

2.4 Material and Spatial Descriptions

2.4.1 The Second Piola-Kirchhoff tensor

The formulation developed so far has been expressed in terms of the main kinematic variables $\boldsymbol{F}$, $\boldsymbol{H}$ and J. However, material frame indifference implies that the dependency of the strain energy with respect to $\boldsymbol{F}$, $\boldsymbol{H}$ must be via the right Cauchy-Green tensor $\boldsymbol{C} = \boldsymbol{F}^T\boldsymbol{F}$ and its cofactor $\boldsymbol{G} = \boldsymbol{H}^T\boldsymbol{H} = \frac{1}{2}\boldsymbol{C}\times\boldsymbol{C}$. It is therefore possible to express the strain energy as a function of these symmetric tensors as

$$\Psi\left(\boldsymbol{\nabla}_0\boldsymbol{x}\right) = \tilde{W}\left(\boldsymbol{C}, \boldsymbol{G}, C\right) \tag{2.105}$$

where, for consistency, $C = \det\boldsymbol{C} = J^2$ is being used instead of J as the variable describing the volumetric change. Note, however, that the function $\tilde{W}$ need not to be strictly convex with respect to its variables. For instance, in the case of a Mooney-Rivlin material, $\tilde{W}$ is linear with respect to both $\boldsymbol{C}$ and $\boldsymbol{G}$ as,

$$\tilde{W}_{MR}\left(\boldsymbol{C}, \boldsymbol{G}, C\right) = \alpha\boldsymbol{C} : \boldsymbol{I} + \beta\boldsymbol{G} : \boldsymbol{I} + \tilde{f}\left(C\right); \quad \tilde{f}\left(C\right) = f\left(\sqrt{C}\right). \tag{2.106}$$

Using the work conjugacy expression between the second Piola-Kirchhoff $\boldsymbol{S}$ and the right Cauchy-Green tensor $\boldsymbol{C}$ given by

$$D\Psi\left[\delta\boldsymbol{v}\right] = \boldsymbol{S} : \frac{1}{2}D\boldsymbol{C}\left[\delta\boldsymbol{v}\right]; \quad \boldsymbol{S} = 2\frac{\partial\Psi\left(\boldsymbol{C}\right)}{\partial\boldsymbol{C}}\bigg|_{\boldsymbol{C}=(\boldsymbol{\nabla}_0\boldsymbol{x})^T(\boldsymbol{\nabla}_0\boldsymbol{x})}, \tag{2.107}$$

and defining the conjugate stresses to $\boldsymbol{C}$, $\boldsymbol{G}$ and C as

$$\boldsymbol{\Sigma}_{\boldsymbol{C}} = 2\frac{\partial\tilde{W}}{\partial\boldsymbol{C}}; \qquad \boldsymbol{\Sigma}_{\boldsymbol{G}} = 2\frac{\partial\tilde{W}}{\partial\boldsymbol{G}}; \qquad \Sigma_C = 2\frac{\partial\tilde{W}}{\partial C}, \tag{2.108}$$

enables an expression for the second Piola-Kirchhoff tensor to be derived using the same steps employed in equation (2.52) for the derivation of the first Piola-Kirchhoff tensor to give

$$\boldsymbol{S} = \boldsymbol{\Sigma}_{\boldsymbol{C}} + \boldsymbol{\Sigma}_{\boldsymbol{G}}\times\boldsymbol{C} + \Sigma_C\boldsymbol{G}. \tag{2.109}$$

For the particular case of a Mooney-Rivlin material this expression becomes

$$\boldsymbol{S} = 2\alpha \boldsymbol{I} + 2\beta \boldsymbol{I} \times \boldsymbol{C} + \tilde{f}'(C)\, \boldsymbol{G}. \tag{2.110}$$

Note that using the chain rule to relate derivatives with respect to $\boldsymbol{F}$, $\boldsymbol{H}$ and J to derivatives with respect to $\boldsymbol{C}$, $\boldsymbol{G}$ and C it is possible to establish the relationships

$$\boldsymbol{\Sigma}_{\boldsymbol{F}} = \boldsymbol{F}\boldsymbol{\Sigma}_{\boldsymbol{C}}; \qquad \boldsymbol{\Sigma}_{\boldsymbol{H}} = \boldsymbol{H}\boldsymbol{\Sigma}_{\boldsymbol{G}}; \qquad \Sigma_J = J\Sigma_C. \tag{2.111}$$

2.4.2 The material elasticity tensor

It is also possible to derive the total Lagrangian elasticity tensor in terms of the Hessian matrix of $\tilde{W}$ following similar steps to those employed in previous sections. For this purpose, note first that the Lagrangian elasticity tensor $\boldsymbol{\mathcal{C}}_M$ is usually defined via the second directional derivative of the strain energy expressed in terms of the right Cauchy-Green tensor as

$$\begin{aligned} D^2\Psi(\boldsymbol{C})[\delta\boldsymbol{v};\delta\boldsymbol{u}] &= \frac{1}{2}D\boldsymbol{C}[\delta\boldsymbol{v}] : \boldsymbol{\mathcal{C}}_M : \frac{1}{2}D\boldsymbol{C}[\boldsymbol{u}] + \boldsymbol{S} : \frac{1}{2}D^2\boldsymbol{C}[\delta\boldsymbol{v};\boldsymbol{u}] \\ &= \left(\boldsymbol{F}^T\boldsymbol{\nabla}_0\delta\boldsymbol{v}\right) : 2\frac{\partial \boldsymbol{S}}{\partial \boldsymbol{C}} : \left(\boldsymbol{F}^T\boldsymbol{\nabla}_0\boldsymbol{u}\right) + \boldsymbol{S} : \left[(\boldsymbol{\nabla}_0\delta\boldsymbol{v})^T(\boldsymbol{\nabla}_0\boldsymbol{u})\right]. \end{aligned} \tag{2.112}$$

Note that due to the symmetry of both $\boldsymbol{S}$ and $\boldsymbol{C}$, it is only necessary to consider one of the two terms making up the differential of the right Cauchy-Green tensor. The first term in the above equation can be related to the Hessian of the strain energy functional $\tilde{W}$ using similar steps to those employed above to derive equation (2.73). Similar algebra eventually leads to

$$\begin{aligned} D^2\Psi\left[\delta\boldsymbol{v};\boldsymbol{u}\right] = \left[\delta\boldsymbol{C} : \;\; \delta\boldsymbol{G} : \;\; \delta C\right]\left[\mathbb{H}_{\tilde{W}}\right]\begin{bmatrix} : \Delta\boldsymbol{C} \\ : \Delta\boldsymbol{G} \\ \Delta C \end{bmatrix} + \boldsymbol{S} : \left[(\boldsymbol{\nabla}_0\delta\boldsymbol{v})^T(\boldsymbol{\nabla}_0\boldsymbol{u})\right] \\ + \left(\boldsymbol{\Sigma}_{\boldsymbol{G}} + \Sigma_C\boldsymbol{C}\right) : \left[(\boldsymbol{F}^T\boldsymbol{\nabla}_0\delta\boldsymbol{v}) \times (\boldsymbol{F}^T\boldsymbol{\nabla}_0\boldsymbol{u})\right], \end{aligned} \tag{2.113}$$

where the derivatives of $\boldsymbol{C}$, $\boldsymbol{G}$ and C are

$$\delta\boldsymbol{C} = \boldsymbol{F}^T\boldsymbol{\nabla}_0\delta\boldsymbol{v}; \quad \delta\boldsymbol{G} = \boldsymbol{C} \times (\boldsymbol{F}^T\boldsymbol{\nabla}_0\delta\boldsymbol{v}); \quad \delta C = \boldsymbol{G} : (\boldsymbol{F}^T\boldsymbol{\nabla}_0\delta\boldsymbol{v}) \tag{2.114}$$

and similarly,

$$\Delta\boldsymbol{C} = \boldsymbol{F}^T\boldsymbol{\nabla}_0\boldsymbol{u}; \quad \Delta\boldsymbol{G} = \boldsymbol{C} \times (\boldsymbol{F}^T\boldsymbol{\nabla}_0\boldsymbol{u}); \quad \Delta C = \boldsymbol{G} : (\boldsymbol{F}^T\boldsymbol{\nabla}_0\boldsymbol{u}). \tag{2.115}$$

Note that since these expressions multiply symmetric tensors only one component of these derivatives, rather than the full symmetric expression, has been used. Note also that for the Mooney-Rivlin material model most of the terms of the Hessian matrix vanish, namely

$$\left[\mathbb{H}_{\tilde{W}_{MR}}\right] = \begin{bmatrix} \boldsymbol{0} & \boldsymbol{0} & \boldsymbol{0} \\ \boldsymbol{0} & \boldsymbol{0} & \boldsymbol{0} \\ \boldsymbol{0} & \boldsymbol{0} & \tilde{f}''(C) \end{bmatrix}. \tag{2.116}$$

In the classical manner, it is possible to obtain the Lagrangian elasticity tensor $\boldsymbol{\mathcal{C}}_M$ [12] via differentiation of equation (2.56) as

$$\begin{aligned}\boldsymbol{\mathcal{C}}_M = &\left[4\beta I_3 \mathrm{tr}\,\boldsymbol{C}^{-1} + 4g''(I_3)I_3^2 + 4g'(I_3)I_3\right]\boldsymbol{C}^{-1}\otimes\boldsymbol{C}^{-1}\\ &- 4\beta I_3\left[\boldsymbol{C}^{-1}\otimes\left(\boldsymbol{C}^{-1}\boldsymbol{C}^{-1}\right) + \left(\boldsymbol{C}^{-1}\boldsymbol{C}^{-1}\right)\otimes\boldsymbol{C}^{-1}\right]\\ &- 4\left[\beta\mathrm{tr}\,\boldsymbol{C}^{-1} + g'(I_3)\right]I_3\boldsymbol{\mathcal{I}} - 4\beta I_3\boldsymbol{\mathcal{J}},\end{aligned} \tag{2.117}$$

where

$$\boldsymbol{\mathcal{I}} = -\frac{\partial \boldsymbol{C}^{-1}}{\partial \boldsymbol{C}}; \qquad \boldsymbol{\mathcal{J}} = \frac{\partial\left(\boldsymbol{C}^{-1}\boldsymbol{C}^{-1}\right)}{\partial \boldsymbol{C}}, \tag{2.118}$$

with components

$$\left(\boldsymbol{\mathcal{I}}\right)_{IJKL} = \frac{1}{2}\left[\left(\boldsymbol{C}\right)^{-1}_{IK}\left(\boldsymbol{C}\right)^{-1}_{JL} + \left(\boldsymbol{C}\right)^{-1}_{IL}\left(\boldsymbol{C}\right)^{-1}_{JK}\right], \tag{2.119}$$

and

$$\begin{aligned}\left(\boldsymbol{\mathcal{J}}\right)_{IJKL} = -\frac{1}{2}&\left[\left(\boldsymbol{C}^{-1}\boldsymbol{C}^{-1}\right)_{IK}\left(\boldsymbol{C}\right)^{-1}_{JL} + \left(\boldsymbol{C}^{-1}\boldsymbol{C}^{-1}\right)_{IL}\left(\boldsymbol{C}\right)^{-1}_{JK}\right.\\ &\left.+\left(\boldsymbol{C}\right)^{-1}_{IK}\left(\boldsymbol{C}^{-1}\boldsymbol{C}^{-1}\right)_{JL} + \left(\boldsymbol{C}\right)^{-1}_{IL}\left(\boldsymbol{C}^{-1}\boldsymbol{C}^{-1}\right)_{JK}\right].\end{aligned} \tag{2.120}$$

2.4.3 The Kirchhoff and Cauchy stress tensors

In addition to the first and second Piola-Kirchhoff stresses, it is necessary to derive expressions for the Cauchy and Kirchhoff stresses as often these tensors are needed in order to express plasticity models or simply to display solution results. Such expressions can be relatively easily derived from the standard relationship between these tensors [12]

$$J\boldsymbol{\sigma} = \boldsymbol{\tau} = \boldsymbol{P}\boldsymbol{F}^T. \tag{2.121}$$

Substituting equation (2.53) for the first Piola-Kirchhoff tensor and recalling that $\boldsymbol{H}\boldsymbol{F}^T = J\boldsymbol{I}$ gives,

$$J\boldsymbol{\sigma} = \boldsymbol{\tau} = \boldsymbol{\Sigma}_{\boldsymbol{F}}\boldsymbol{F}^T + \left(\boldsymbol{\Sigma}_{\boldsymbol{H}} \times \boldsymbol{F}\right)\boldsymbol{F}^T + J\Sigma_J\boldsymbol{I}. \tag{2.122}$$

The middle term in this expression can be transformed with the help of property (2.25) of the tensor cross product by taking $\boldsymbol{B} := \boldsymbol{F}$, $\boldsymbol{A}_1 := J^{-1}\boldsymbol{\Sigma}_{\boldsymbol{H}}\boldsymbol{H}^T$ and $\boldsymbol{A}_2 := \boldsymbol{I}$ as follows,

$$\left(\boldsymbol{A}_1\boldsymbol{B}\right) \times \left(\boldsymbol{A}_2\boldsymbol{B}\right) = \left(J^{-1}\boldsymbol{\Sigma}_{\boldsymbol{H}}\boldsymbol{H}^T\boldsymbol{F}\right) \times \boldsymbol{F} = \boldsymbol{\Sigma}_{\boldsymbol{H}} \times \boldsymbol{F}; \tag{2.123a}$$

$$\left(\boldsymbol{A}_1 \times \boldsymbol{A}_2\right)\mathrm{Cof}\boldsymbol{B} = \left[\left(J^{-1}\boldsymbol{\Sigma}_{\boldsymbol{H}}\boldsymbol{H}^T\right) \times \boldsymbol{I}\right]\boldsymbol{H} = \left[\left(\boldsymbol{\Sigma}_{\boldsymbol{H}}\boldsymbol{H}^T\right) \times \boldsymbol{I}\right]\boldsymbol{F}^{-T}, \tag{2.123b}$$

where equation (2.2) has been used for the last step in both equations (2.123a)-(2.123b). Multiplication by $\boldsymbol{F}^T$ on (2.123a)-(2.123b) renders

$$\left(\boldsymbol{\Sigma}_{\boldsymbol{H}} \times \boldsymbol{F}\right)\boldsymbol{F}^T = \left(\boldsymbol{\Sigma}_{\boldsymbol{H}}\boldsymbol{H}^T\right) \times \boldsymbol{I}, \tag{2.124}$$

thus giving an expression for the Kirchhoff stresses as

$$J\boldsymbol{\sigma} = \boldsymbol{\tau} = \boldsymbol{\Sigma}_{\boldsymbol{F}}\boldsymbol{F}^T + \left(\boldsymbol{\Sigma}_{\boldsymbol{H}}\boldsymbol{H}^T\right) \times \boldsymbol{I} + J\Sigma_J\boldsymbol{I}, \tag{2.125}$$

or introducing the notation

$$\boldsymbol{\tau_F} = \boldsymbol{\Sigma_F}\boldsymbol{F}^T = \boldsymbol{F}\boldsymbol{\Sigma_C}\boldsymbol{F}^T; \quad \boldsymbol{\tau_H} = \boldsymbol{\Sigma_H}\boldsymbol{H}^T = \boldsymbol{H}\boldsymbol{\Sigma_G}\boldsymbol{H}^T; \quad \tau_J = J\Sigma_J = J^2\Sigma_C, \tag{2.126}$$

gives,

$$J\boldsymbol{\sigma} = \boldsymbol{\tau} = \boldsymbol{\tau_F} + \boldsymbol{\tau_H} \boldsymbol{\times} \boldsymbol{I} + \tau_J \boldsymbol{I}. \tag{2.127}$$

For the particular case of the Mooney-Rivlin model under consideration, the above equations lead after simple algebra to

$$J\boldsymbol{\sigma} = \boldsymbol{\tau} = 2\alpha\, \boldsymbol{b} + 2\beta\, \boldsymbol{g} \boldsymbol{\times} \boldsymbol{I} + Jf'(J)\boldsymbol{I}; \quad \boldsymbol{b} = \boldsymbol{F}\boldsymbol{F}^T; \quad \boldsymbol{g} = \boldsymbol{H}\boldsymbol{H}^T. \tag{2.128}$$

Alternatively, in the standard manner [12], post-multiplication of equation (2.57) by $\boldsymbol{F}^T$ leads to the following expression for the Kirchhoff stress tensor as

$$\boldsymbol{\tau} = 2\alpha\boldsymbol{b} + 2\beta\left[I_3\left(\operatorname{tr}\boldsymbol{b}^{-1}\right)\boldsymbol{I} - I_3\boldsymbol{b}^{-1}\right] + 2g'(I_3)I_3\boldsymbol{I}. \tag{2.129}$$

2.4.4 The spatial elasticity tensor

In the context of a spatial description, it is usually necessary to derive a spatial or Eulerian elasticity tensor which relates the second derivative of the strain energy to the spatial gradients of virtual velocities and displacements. For this purpose, equation (2.73) for the tangent elasticity operator is transformed with the help of the chain rule, which provides a relationship between material and spatial gradients, namely $\boldsymbol{\nabla}_0\boldsymbol{a} = (\boldsymbol{\nabla}\boldsymbol{a})\boldsymbol{F}$ for any field $\boldsymbol{a}$, and the repeated use of property (2.25). After simple algebra this leads to

$$\begin{aligned} D^2\Psi\left[\delta\boldsymbol{v};\boldsymbol{u}\right] &= \left[(\boldsymbol{\nabla}\delta\boldsymbol{v})\,\boldsymbol{F} : \ (\boldsymbol{\nabla}\delta\boldsymbol{v}\boldsymbol{\times}\boldsymbol{I})\,\boldsymbol{H} : \ (\boldsymbol{\nabla}\delta\boldsymbol{v} : \boldsymbol{I})\,J\right]\left[\mathbb{H}_W\right]\begin{bmatrix} :(\boldsymbol{\nabla}\boldsymbol{u})\,\boldsymbol{F} \\ :(\boldsymbol{\nabla}\boldsymbol{u}\boldsymbol{\times}\boldsymbol{I})\,\boldsymbol{H} \\ (\boldsymbol{\nabla}\boldsymbol{u} : \boldsymbol{I})\,J \end{bmatrix} \\ &\quad + (\boldsymbol{\Sigma_H} + \Sigma_J\boldsymbol{F}) : \left[(\boldsymbol{\nabla}\delta\boldsymbol{v}\boldsymbol{\times}\boldsymbol{\nabla}\boldsymbol{u})\,\boldsymbol{H}\right] \\ &= \left[(\boldsymbol{\nabla}\delta\boldsymbol{v}) : \ (\boldsymbol{\nabla}\delta\boldsymbol{v}\boldsymbol{\times}\boldsymbol{I}) : \ \operatorname{div}\delta\boldsymbol{v}\right]\boldsymbol{\phi}_*\left[\mathbb{H}_W\right]\begin{bmatrix} :(\boldsymbol{\nabla}\boldsymbol{u}) \\ :(\boldsymbol{\nabla}\boldsymbol{u}\boldsymbol{\times}\boldsymbol{I}) \\ \operatorname{div}\boldsymbol{u} \end{bmatrix} \\ &\quad + (\boldsymbol{\tau_H} + \tau_J\boldsymbol{I}) : (\boldsymbol{\nabla}\delta\boldsymbol{v}\boldsymbol{\times}\boldsymbol{\nabla}\boldsymbol{u})\,, \end{aligned} \tag{2.130}$$

where $\boldsymbol{\phi}_*[\mathbb{H}_W]$ denotes the appropriate push forward of the components of the Hessian operator with either $\boldsymbol{F}$, $\boldsymbol{H}$ or J. Specifically, in component form, this operator is defined for a generic material as

$$\boldsymbol{\phi}_*[\mathbb{H}_W] = \begin{bmatrix} F_{jI}\frac{\partial^2 W}{\partial F_{iI}\partial F_{kJ}}F_{lJ} & F_{jI}\frac{\partial^2 W}{\partial F_{iI}\partial H_{kJ}}H_{lJ} & F_{jI}\frac{\partial^2 W}{\partial F_{iI}\partial J}J \\ H_{jI}\frac{\partial^2 W}{\partial H_{iI}\partial F_{kJ}}F_{lJ} & H_{jI}\frac{\partial^2 W}{\partial H_{jI}\partial H_{kJ}}H_{lJ} & H_{jI}\frac{\partial^2 W}{\partial H_{iI}\partial J}J \\ J\frac{\partial^2 W}{\partial J\partial F_{kJ}}F_{lJ} & J\frac{\partial^2 W}{\partial J\partial H_{kJ}}H_{lJ} & J\frac{\partial^2 W}{\partial J\partial J}J, \end{bmatrix}, \tag{2.131}$$

which for the particular case of Mooney-Rivlin becomes

$$\boldsymbol{\phi}_*[\mathbb{H}_W] = \begin{bmatrix} 2\alpha b_{jl}\delta_{ik} & 0 & 0 \\ 0 & 2\beta g_{jl}\delta_{ik} & 0 \\ 0 & 0 & J^2 f''(J) \end{bmatrix}. \tag{2.132}$$

Substituting this expression into equation (2.130) gives after simple algebra

$$\begin{aligned} D^2\Psi_{MR}\left[\delta\boldsymbol{v};\boldsymbol{u}\right] = {} & 2\alpha\left(\boldsymbol{\nabla}\delta\boldsymbol{v}\right)\boldsymbol{b} : \boldsymbol{\nabla}\boldsymbol{u} + 2\beta\left(\boldsymbol{\nabla}\delta\boldsymbol{v}\boldsymbol{\times}\boldsymbol{I}\right)\boldsymbol{g} : \left(\boldsymbol{\nabla}\boldsymbol{u}\boldsymbol{\times}\boldsymbol{I}\right) \\ & + f''\left(J\right)J^2\,\mathrm{div}\delta\boldsymbol{v}\,\mathrm{div}\boldsymbol{u} + \left(\boldsymbol{\tau}_{\boldsymbol{H}} + \tau_J\boldsymbol{I}\right) : \left(\boldsymbol{\nabla}\delta\boldsymbol{v}\boldsymbol{\times}\boldsymbol{\nabla}\boldsymbol{u}\right). \end{aligned} \tag{2.133}$$

2.5 Isotropic and anisotropic elasticity

2.5.1 Isotropic elasticity

In the particular case of isotropic elasticity, the expression for the energy density functional $\Psi = \Psi(\boldsymbol{\nabla}_0\boldsymbol{x})$ can be established through the invariants I_1, I_2 and I_3 of the right Cauchy-Green strain tensor $\boldsymbol{C}$ (2.42). An alternative set of equations for the above invariants, more suitable in the case of a isotropic polyconvex energy functional, is given by

$$I_1 = \boldsymbol{F} : \boldsymbol{F}; \qquad I_2 = \boldsymbol{H} : \boldsymbol{H}; \qquad I_3 = J^2, \tag{2.134}$$

leading to a representation of the energy density functional as

$$\Psi(\boldsymbol{\nabla}_0\boldsymbol{x}) = W(\boldsymbol{F},\boldsymbol{H},J) = w(I_1,I_2,I_3). \tag{2.135}$$

In order to obtain simple expressions for the first Piola-Kirchhoff and elasticity tensors directly in terms of the derivatives of the function w rather than W, note that the first and second derivatives of the invariants are given by

$$\begin{aligned} DI_1[\delta\boldsymbol{u}] &= 2\boldsymbol{F} : \boldsymbol{\nabla}_0\delta\boldsymbol{u}; && (2.136)\\ DI_2[\delta\boldsymbol{u}] &= 2(\boldsymbol{F}\boldsymbol{\times}\boldsymbol{H}) : \boldsymbol{\nabla}_0\delta\boldsymbol{u}; && (2.137)\\ DI_3[\delta\boldsymbol{u}] &= 2J\boldsymbol{H} : \boldsymbol{\nabla}_0\delta\boldsymbol{u}; && (2.138)\\ D^2I_1[\delta\boldsymbol{u};\boldsymbol{u}] &= 2\boldsymbol{\nabla}_0\delta\boldsymbol{u} : \boldsymbol{\nabla}_0\boldsymbol{u}; && (2.139)\\ D^2I_2[\delta\boldsymbol{u};\boldsymbol{u}] &= 2(\boldsymbol{F}\boldsymbol{\times}\boldsymbol{\nabla}_0\delta\boldsymbol{u}) : (\boldsymbol{F}\boldsymbol{\times}\boldsymbol{\nabla}_0\boldsymbol{u}) + 2\boldsymbol{H} : (\boldsymbol{\nabla}_0\delta\boldsymbol{u}\boldsymbol{\times}\boldsymbol{\nabla}_0\boldsymbol{u}); && (2.140)\\ D^2I_3[\delta\boldsymbol{u};\boldsymbol{u}] &= 2(\boldsymbol{H} : \boldsymbol{\nabla}_0\delta\boldsymbol{u})(\boldsymbol{H} : \boldsymbol{\nabla}_0\boldsymbol{u}) + 2J\boldsymbol{F} : (\boldsymbol{\nabla}_0\delta\boldsymbol{u}\boldsymbol{\times}\boldsymbol{\nabla}_0\boldsymbol{u}). && (2.141) \end{aligned}$$

The first Piola-Kirchhoff tensor can be derived either using directly the first three equations above which enable the internal virtual work to be written as

$$\boldsymbol{P} : \boldsymbol{\nabla}_0\delta\boldsymbol{u} = [\mathbb{D}_w]\begin{bmatrix} 2\boldsymbol{F} : \boldsymbol{\nabla}_0\delta\boldsymbol{u} \\ 2(\boldsymbol{F}\boldsymbol{\times}\boldsymbol{H}) : \boldsymbol{\nabla}_0\delta\boldsymbol{u} \\ 2J\boldsymbol{H} : \boldsymbol{\nabla}_0\delta\boldsymbol{u} \end{bmatrix}; \quad [\mathbb{D}_w] = \left[\frac{\partial w}{\partial I_1}, \frac{\partial w}{\partial I_2}, \frac{\partial w}{\partial I_3}\right], \tag{2.142}$$

thereby leading to

$$\boldsymbol{P} = 2\frac{\partial w}{\partial I_1}\boldsymbol{F} + 2\frac{\partial w}{\partial I_2}\boldsymbol{H} \times \boldsymbol{F} + 2\frac{\partial w}{\partial I_3}J\boldsymbol{H}. \tag{2.143}$$

Alternatively, it is also possible to obtain the same equation for the first Piola-Kirchhoff stress tensor via the work conjugate stresses $\boldsymbol{\Sigma}_{\boldsymbol{F}}$, $\boldsymbol{\Sigma}_{\boldsymbol{H}}$ and Σ_J and using the chain rule to give

$$\boldsymbol{\Sigma}_{\boldsymbol{F}} = 2\frac{\partial w}{\partial I_1}\boldsymbol{F}; \qquad \boldsymbol{\Sigma}_{\boldsymbol{H}} = 2\frac{\partial w}{\partial I_2}\boldsymbol{H}; \qquad \Sigma_J = 2\frac{\partial w}{\partial I_3}J. \tag{2.144}$$

Introducing these equations into equation (2.53) leads immediately to equation (2.143). The tangent elasticity operator can be formulated by differentiating again equation (2.142), which after simple algebra using the second derivatives of the invariants given above leads to

$$\begin{aligned} D^2\Psi\left[\delta\boldsymbol{u};\boldsymbol{u}\right] = &\begin{bmatrix} 2\boldsymbol{F} : \boldsymbol{\nabla}_0\delta\boldsymbol{u} \\ 2(\boldsymbol{F}\times\boldsymbol{H}) : \boldsymbol{\nabla}_0\delta\boldsymbol{u} \\ 2J\boldsymbol{H} : \boldsymbol{\nabla}_0\delta\boldsymbol{u} \end{bmatrix}^T [\mathbb{H}_w] \begin{bmatrix} 2\boldsymbol{F} : \boldsymbol{\nabla}_0\boldsymbol{u} \\ 2(\boldsymbol{F}\times\boldsymbol{H}) : \boldsymbol{\nabla}_0\boldsymbol{u} \\ 2J\boldsymbol{H} : \boldsymbol{\nabla}_0\boldsymbol{u} \end{bmatrix} \\ &+ [\mathbb{D}_w] \begin{bmatrix} 2\boldsymbol{\nabla}_0\delta\boldsymbol{u} : \boldsymbol{\nabla}_0\boldsymbol{u} \\ 2(\boldsymbol{F}\times\boldsymbol{\nabla}_0\delta\boldsymbol{u}) : (\boldsymbol{F}\times\boldsymbol{\nabla}_0\boldsymbol{u}) \\ 2(\boldsymbol{H} : \boldsymbol{\nabla}_0\delta\boldsymbol{u})(\boldsymbol{H} : \boldsymbol{\nabla}_0\boldsymbol{u}) \end{bmatrix} \\ &+ [\mathbb{D}_w] \begin{bmatrix} 0 \\ 2\boldsymbol{H} : (\boldsymbol{\nabla}_0\delta\boldsymbol{u}\times\boldsymbol{\nabla}_0\boldsymbol{u}) \\ 2J\boldsymbol{F} : (\boldsymbol{\nabla}_0\delta\boldsymbol{u}\times\boldsymbol{\nabla}_0\boldsymbol{u}) \end{bmatrix}, \end{aligned} \tag{2.145}$$

with

$$[\mathbb{H}_w] = \begin{bmatrix} \frac{\partial^2 w}{\partial I_1 \partial I_1} & \frac{\partial^2 w}{\partial I_1 \partial I_2} & \frac{\partial^2 w}{\partial I_1 \partial I_3} \\ \frac{\partial^2 w}{\partial I_2 \partial I_1} & \frac{\partial^2 w}{\partial I_2 \partial I_2} & \frac{\partial^2 w}{\partial I_2 \partial I_3} \\ \frac{\partial^2 w}{\partial I_3 \partial I_1} & \frac{\partial^2 w}{\partial I_3 \partial I_2} & \frac{\partial^2 w}{\partial I_3 \partial I_3} \end{bmatrix}. \tag{2.146}$$

Note that the sum of the first two terms needs to be positive for materials with a polyconvex strain energy function, as the last term represents the geometrical term depicted in equation (2.73).

2.5.2 Anisotropic elasticity

It is possible to derive similar expressions for the strain energy to those in Section 2.5.1 for anisotropic materials by extending the range of invariants taken into account. As part of the well known *Open problems* [28], Ball laid out the challenge of deriving polyconvex invariant representations of the strain energy $\Psi(\boldsymbol{F})$ fully characterising the functional basis of complex anisotropic material symmetry groups. Schröder et al. [37–39] successfully and elegantly accomplished this challenge for the

triclinic, monoclinic, hexagonal and rhombic crystal symmetry groups by introducing a linear tangent map $\boldsymbol{L}$ mapping the cartesian base vectors $\{\boldsymbol{E}_1, \boldsymbol{E}_2, \boldsymbol{E}_3\}$ onto crystallographic motivated base vectors $\{\boldsymbol{a}_1, \boldsymbol{a}_2, \boldsymbol{a}_3\}$.

The generic expression for the tangent mapping $\boldsymbol{L}$ in terms of the lengths of the crystallographic motivated base vectors $\{\boldsymbol{a}_1, \boldsymbol{a}_2, \boldsymbol{a}_3\}$, namely $\{a, b, c\}$, respectively and in terms of the angles $\{\alpha, \beta, \gamma\}$ between the basis $\{\boldsymbol{E}_1, \boldsymbol{E}_2, \boldsymbol{E}_3\}$ and $\{\boldsymbol{a}_1, \boldsymbol{a}_2, \boldsymbol{a}_3\}$ (refer to Figure 2.3) is defined as [38]

$$\boldsymbol{L} = \begin{bmatrix} a & b\cos\gamma & c\cos\gamma \\ 0 & b\sin\gamma & \frac{c(\cos\alpha - \cos\beta\cos\gamma)}{\sin\gamma} \\ 0 & 0 & L_{33} \end{bmatrix}; \qquad \boldsymbol{a}_i = \boldsymbol{L}\boldsymbol{E}_i. \tag{2.147}$$

where the coefficient L_{33} in above equation (2.147) is defined as

$$L_{33} = \frac{c\sqrt{1 + 2\cos\alpha\cos\beta\cos\gamma - (\cos^2\alpha + \cos^2\beta + \cos^2\gamma)}}{\sin\gamma}. \tag{2.148}$$

For instance, for the rhombic material symmetry group, the expression of the tangent map $\boldsymbol{L}$ is [38]

$$\boldsymbol{L}_{rh} = \begin{bmatrix} a & 0 & 0 \\ 0 & b & 0 \\ 0 & 0 & c \end{bmatrix}. \tag{2.149}$$

The expression of $\boldsymbol{L}$ for the seven crystal symmetry groups can be found in Reference [38]. With the help of this second order tensor $\boldsymbol{L}$, Schröder et al. [37,37,38] introduced a positive definite metric tensor $\boldsymbol{Q}$ defined as

$$\boldsymbol{Q} = \boldsymbol{L}\boldsymbol{L}^T. \tag{2.150}$$

The symmetric positive definite nature of this tensor proved extremely convenient for the derivation of anisotropic invariants convex with respect to the deformation gradient tensor $\boldsymbol{F}$ or with respect the co-factor $\boldsymbol{H}$ [32, 37–40].

However, a representation of the strain energy in terms of this crystallographic motivated structural tensor is not sufficient for the complete characterisation of the functional basis of trigonal, tetragonal and cubic material symmetry groups. For these more complex anisotropies, Schröder et al. [39] introduced a crystallographic motivated positive definite fourth order tensor $\boldsymbol{\mathcal{Q}}$ defined in terms of the crystallographic base vectors $\{\boldsymbol{a}_1, \boldsymbol{a}_2, \boldsymbol{a}_3\}$ as

$$\boldsymbol{\mathcal{Q}} = \sum_{i=1}^{3} \boldsymbol{a}_i \otimes \boldsymbol{a}_i \otimes \boldsymbol{a}_i \otimes \boldsymbol{a}_i. \tag{2.151}$$

Notice that these vectors, namely $\{\boldsymbol{a}_1, \boldsymbol{a}_2, \boldsymbol{a}_3\}$ are generally defined in terms of their respective lengths, namely $\{a, b, c\}$, respectively and in terms of the angles $\{\alpha, \beta, \gamma\}$ between the basis $\{\boldsymbol{E}_1, \boldsymbol{E}_2, \boldsymbol{E}_3\}$ and $\{\boldsymbol{a}_1, \boldsymbol{a}_2, \boldsymbol{a}_3\}$ (refer to Figure 2.3). For

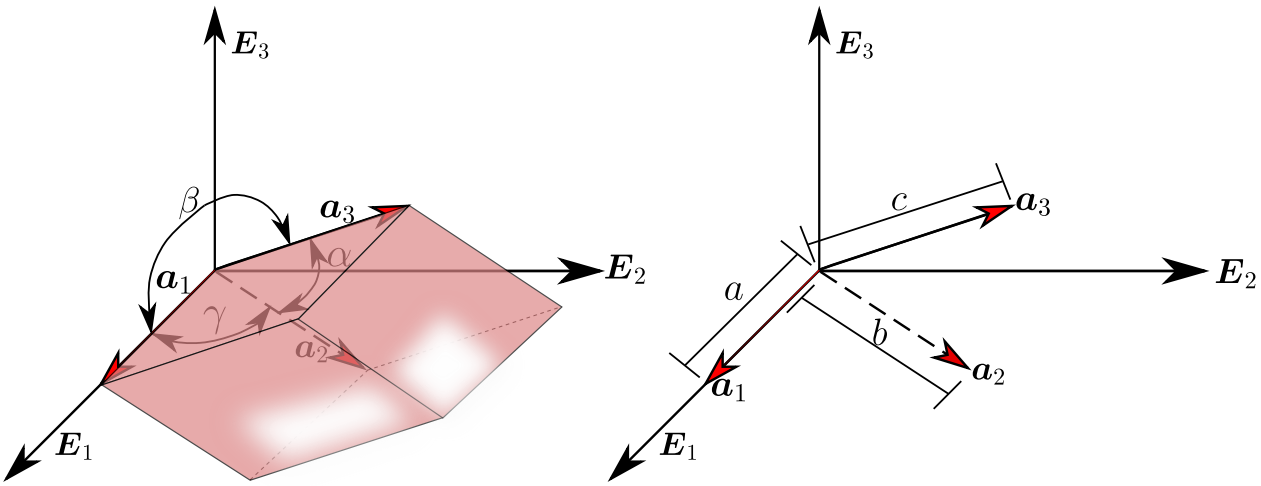

Figure 2.3: Relation between the cartesian vectors $\{\boldsymbol{E}_1, \boldsymbol{E}_2, \boldsymbol{E}_3\}$ and the crystallographic motivated base vectors $\{\boldsymbol{a}_1, \boldsymbol{a}_2, \boldsymbol{a}_3\}$ for a generic crystal lattice.

instance, for the tetragonal symmetry group (where $\alpha = \beta = \gamma = \pi/2$), the crystallographic base vectors are defined as

$$\boldsymbol{a}_1 = a\boldsymbol{E}_1; \qquad \boldsymbol{a}_2 = a\boldsymbol{E}_2; \qquad \boldsymbol{a}_3 = c\boldsymbol{E}_3, \tag{2.152}$$

which yields the following definition for $\boldsymbol{\mathcal{Q}}_{\text{tet}}$ (with the subscript *tet* emphasising the tetragonal material symmetry group) for this material symmetry group,

$$\boldsymbol{\mathcal{Q}}_{\text{tet}} = a^4 \left(\boldsymbol{E}_1 \otimes \boldsymbol{E}_1 \otimes \boldsymbol{E}_1 \otimes \boldsymbol{E}_1 + \boldsymbol{E}_2 \otimes \boldsymbol{E}_2 \otimes \boldsymbol{E}_2 \otimes \boldsymbol{E}_2\right) + c^4 \boldsymbol{E}_3 \otimes \boldsymbol{E}_3 \otimes \boldsymbol{E}_3 \otimes \boldsymbol{E}_3. \tag{2.153}$$

Triclinic, Monoclinic, Hexagonal and Rhombic symmetry groups

Following the work of Schröder et al. [37,38], a complete (polyconvex) representation of the functional basis for triclinic, monoclinic, hexagonal and rhombic symmetry groups can be obtained by extending the arguments of the strain energy, namely

$$\Psi\left(\boldsymbol{F}\right) = W\left(\boldsymbol{F}, \boldsymbol{H}, J\right) = w_{\text{TMHR}}\left(I_1, I_2, I_3, I_4, I_5\right), \tag{2.154}$$

where $w_{\text{TMHR}}\left(I_1, I_2, I_3, I_4, I_5\right)$[2] must be convex with respect to its 5 variables, namely I_1 $(2.134)_a$, I_2 $(2.134)_b$, I_3 $(2.134)_c$, I_4 and I_5. The two additional invariants, namely I_4 and I_5, are anisotropic functions defined as [37,38]

$$I_4 = \text{tr}\left(\boldsymbol{CQ}\right) = \boldsymbol{FL} : \boldsymbol{FL}; \qquad I_5 = \text{tr}\left(\boldsymbol{GQ}\right) = \boldsymbol{HL} : \boldsymbol{HL}, \tag{2.155}$$

with the positive definite second order tensor $\boldsymbol{Q}$ defined in (2.150).

[2]The subscript TMHR has been used to indicate that a complete representation of the functional basis of the Triclinic, Monoclinic, Hexagonal and Rhombic symmetry groups is obtained by following this definition of the strain energy.

Remark 2.6: An example of particular interest in many bioengineering applications is that of transversely isotropic materials [91], [92], typically characterised by a preferred direction $\boldsymbol{N}$, expressed in the reference configuration. For this type of anisotropy, the metric tensor $\boldsymbol{Q}_{\text{hex}}$ is the same as that for the hexagonal symmetry group (the subscript *hex* emphasises the hexagonal anisotropy of this tensor), namely

$$\boldsymbol{Q}_{\text{hex}} = \alpha\left(\boldsymbol{I} - \boldsymbol{N}\otimes\boldsymbol{N}\right) + \beta\boldsymbol{N}\otimes\boldsymbol{N} = \alpha\boldsymbol{I} + (\beta-\alpha)\,\boldsymbol{N}\otimes\boldsymbol{N}; \quad \beta \geq \alpha, \tag{2.156}$$

where the condition $\beta \geq \alpha$ is used to enforce the positive definiteness of the metric tensor $\boldsymbol{Q}_{\text{hex}}$ and hence, convexity of the invariants I_4 and I_5 with respect to $\boldsymbol{F}$ and $\boldsymbol{H}$, respectively.

The first and second derivatives of these two new invariants can be obtained using standard algebra and the properties of the tensor cross product to give

$$\begin{aligned}
DI_4[\delta\boldsymbol{u}] &= 2\boldsymbol{F}\boldsymbol{Q} : \boldsymbol{\nabla}_0\delta\boldsymbol{u}; && (2.157)\\
DI_5[\delta\boldsymbol{u}] &= 2\left[\boldsymbol{F}\times(\boldsymbol{H}\boldsymbol{Q})\right] : \boldsymbol{\nabla}_0\delta\boldsymbol{u}; && (2.158)\\
D^2I_4[\delta\boldsymbol{u};\boldsymbol{u}] &= 2(\boldsymbol{\nabla}_0\delta\boldsymbol{u})\boldsymbol{Q} : (\boldsymbol{\nabla}_0\boldsymbol{u}); && (2.159)\\
D^2I_5[\delta\boldsymbol{u};\boldsymbol{u}] &= 2(\boldsymbol{F}\times\boldsymbol{\nabla}_0\delta\boldsymbol{u})\boldsymbol{Q} : (\boldsymbol{F}\times\boldsymbol{\nabla}_0\boldsymbol{u}) && (2.160)\\
&+ 2(\boldsymbol{H}\boldsymbol{Q}) : (\boldsymbol{\nabla}_0\delta\boldsymbol{u}\times\boldsymbol{\nabla}_0\boldsymbol{u}). && (2.161)
\end{aligned}$$

The above expressions enable the internal virtual energy to be expressed in terms of the vector $[\mathbb{D}_{w_{\text{TMHR}}}]$ containing the derivatives of $w_{\text{TMHR}}(I_1, I_2, I_3, I_4, I_5)$ with respect to the 5 invariants as

$$\boldsymbol{P} : \boldsymbol{\nabla}_0\delta\boldsymbol{u} = [\mathbb{D}_{w_{\text{TMHR}}}]\begin{bmatrix} 2\boldsymbol{F} : \boldsymbol{\nabla}_0\delta\boldsymbol{u} \\ 2(\boldsymbol{F}\times\boldsymbol{H}) : \boldsymbol{\nabla}_0\delta\boldsymbol{u} \\ 2J\boldsymbol{H} : \boldsymbol{\nabla}_0\delta\boldsymbol{u} \\ 2(\boldsymbol{F}\boldsymbol{Q}) : \boldsymbol{\nabla}_0\delta\boldsymbol{u} \\ 2\left[\boldsymbol{F}\times(\boldsymbol{H}\boldsymbol{Q})\right] : \boldsymbol{\nabla}_0\delta\boldsymbol{u} \end{bmatrix}, \tag{2.162}$$

and therefore the first Piola-Kirchhoff tensor emerges as

$$\boldsymbol{P} = 2\frac{\partial w}{\partial I_1}\boldsymbol{F} + 2\frac{\partial w}{\partial I_2}\boldsymbol{H}\times\boldsymbol{F} + 2\frac{\partial w}{\partial I_3}J\boldsymbol{H} + 2\frac{\partial w}{\partial I_4}(\boldsymbol{F}\boldsymbol{Q}) + 2\frac{\partial w}{\partial I_5}(\boldsymbol{H}\boldsymbol{Q})\times\boldsymbol{F}. \tag{2.163}$$

Finally, the tangent elastic operator can be expressed in terms of the 5×5 Hessian matrix of the function $[\mathbb{H}_{w_{\text{TMHR}}}]$ using the second derivatives of the two new

invariants given in equations (2.160) and (2.161). After simple algebra, this leads to

$$
\begin{aligned}
D^2\Psi\left[\delta\boldsymbol{u};\boldsymbol{u}\right] = &\begin{bmatrix} 2\boldsymbol{F}:\boldsymbol{\nabla}_0\delta\boldsymbol{u} \\ 2(\boldsymbol{F}\times\boldsymbol{H}):\boldsymbol{\nabla}_0\delta\boldsymbol{u} \\ 2J\boldsymbol{H}:\boldsymbol{\nabla}_0\delta\boldsymbol{u} \\ 2(\boldsymbol{F}\boldsymbol{Q}):\boldsymbol{\nabla}_0\delta\boldsymbol{u} \\ 2\left[\boldsymbol{F}\times(\boldsymbol{H}\boldsymbol{Q})\right]:\boldsymbol{\nabla}_0\delta\boldsymbol{u} \end{bmatrix}^T [\mathbb{H}_{w_{\mathrm{TMHR}}}] \begin{bmatrix} 2\boldsymbol{F}:\boldsymbol{\nabla}_0\boldsymbol{u} \\ 2(\boldsymbol{F}\times\boldsymbol{H}):\boldsymbol{\nabla}_0\boldsymbol{u} \\ 2J\boldsymbol{H}:\boldsymbol{\nabla}_0\boldsymbol{u} \\ 2(\boldsymbol{F}\boldsymbol{Q}):\boldsymbol{\nabla}_0\boldsymbol{u} \\ 2\left[\boldsymbol{F}\times(\boldsymbol{H}\boldsymbol{Q})\right]:\boldsymbol{\nabla}_0\boldsymbol{u} \end{bmatrix} \\
&+ [\mathbb{D}_{w_{\mathrm{TMHR}}}] \begin{bmatrix} 2\boldsymbol{\nabla}_0\delta\boldsymbol{u}:\boldsymbol{\nabla}_0\boldsymbol{u} \\ 2(\boldsymbol{F}\times\boldsymbol{\nabla}_0\delta\boldsymbol{u}):(\boldsymbol{F}\times\boldsymbol{\nabla}_0\boldsymbol{u}) \\ 2(\boldsymbol{H}:\boldsymbol{\nabla}_0\delta\boldsymbol{u})(\boldsymbol{H}:\boldsymbol{\nabla}_0\boldsymbol{u}) \\ 2(\boldsymbol{\nabla}_0\delta\boldsymbol{u})\boldsymbol{Q}:(\boldsymbol{\nabla}_0\boldsymbol{u}) \\ 2(\boldsymbol{F}\times\boldsymbol{\nabla}_0\delta\boldsymbol{u})\boldsymbol{Q}:(\boldsymbol{F}\times\boldsymbol{\nabla}_0\boldsymbol{u}) \end{bmatrix} \\
&+ [\mathbb{D}_{w_{\mathrm{TMHR}}}] \begin{bmatrix} 0 \\ 2\boldsymbol{H}:(\boldsymbol{\nabla}_0\delta\boldsymbol{u}\times\boldsymbol{\nabla}_0\boldsymbol{u}) \\ 2J\boldsymbol{F}:(\boldsymbol{\nabla}_0\delta\boldsymbol{u}\times\boldsymbol{\nabla}_0\boldsymbol{u}) \\ 0 \\ 2(\boldsymbol{H}\boldsymbol{Q}):(\boldsymbol{\nabla}_0\delta\boldsymbol{u}\times\boldsymbol{\nabla}_0\boldsymbol{u}) \end{bmatrix},
\end{aligned}
\tag{2.164}
$$

where as in equation (2.145), the sum of the two first terms in above equation (2.164) is positive definite for polyconvex materials and only the third term (geometrically based) can induce buckling.

Trigonal, Tetragonal and Cubic symmetry groups

A polyconvex representation of the internal energy as that in equation (2.154) in terms of I_4 and I_5 (2.155) is not sufficient to fully characterise the functional basis of the trigonal, tetragonal and cubic symmetry groups. The underlying anisotropy of these material symmetry groups can be fully characterised by the following definition of the strain energy $\Psi(\boldsymbol{F})$ as [39]

$$
\Psi\left(\boldsymbol{F}\right) = W\left(\boldsymbol{F},\boldsymbol{H},J\right) = w_{\mathrm{TTC}}\left(I_1,I_2,I_3,I_4^\star,I_5^\star,I_6^\star\right), \tag{2.165}
$$

with $w_{\mathrm{TTC}}\left(I_1,I_2,I_3,I_4^\star,I_5^\star,I_6^\star\right)$[3] convex with respect to its 6 variables, namely I_1 $(2.134)_a$, I_2 $(2.134)_b$, I_3 $(2.134)_c$, $I_4^\star$, $I_5^\star$ and $I_6^\star$. The three additional invariants, namely $I_4^\star$, $I_5^\star$ and $I_6^\star$, are anisotropic functions defined as [39]

$$
I_4^\star = \left(\boldsymbol{C}:\boldsymbol{\mathcal{Q}}:\boldsymbol{I}\right); \quad I_5^\star = \left(\boldsymbol{G}:\boldsymbol{\mathcal{Q}}:\boldsymbol{I}\right); \quad I_6^\star = \left(\boldsymbol{C}:\boldsymbol{\mathcal{Q}}:\boldsymbol{C}\right), \tag{2.166}
$$

with the symmetric positive definite fourth order tensor $\boldsymbol{\mathcal{Q}}$ defined in equation (2.151). The first and second derivative of $I_4^\star$ and $I_5^\star$ in above equation (2.166) adopt the same expressions as those for I_4 $(2.155)_a$ and I_5 $(2.155)_b$ in equation

[3]The subscript TTC has been used to indicate that a complete representation of the functional basis of the Trigonal, Tetragonal and Cubic symmetry groups is obtained by following this definition of the strain energy.

(2.157) by simply replacing the metric tensor $\boldsymbol{Q}$ with the second order tensor $\boldsymbol{Q}^\star$, defined as $\boldsymbol{Q}^\star = \boldsymbol{\mathcal{Q}} : \boldsymbol{I}$. The first and second derivatives of $I_6^\star$ can be obtained as

$$
\begin{aligned}
DI_6{}^\star[\delta\boldsymbol{u}] &= 4\boldsymbol{F}\boldsymbol{Q}^\star : \boldsymbol{\nabla}_0\delta\boldsymbol{u}; && (2.167)\\
D^2I_6{}^\star[\delta\boldsymbol{u};\boldsymbol{u}] &= 4\boldsymbol{\nabla}_0\delta\boldsymbol{u}\boldsymbol{Q}^\star : \boldsymbol{\nabla}_0\boldsymbol{u} + 8\boldsymbol{\nabla}_0\delta\boldsymbol{u} : \boldsymbol{\mathcal{C}}^\star : \boldsymbol{\nabla}_0\boldsymbol{u}, && (2.168)
\end{aligned}
$$

with $\mathcal{C}^\star_{iIjJ} = F_{iN}\mathcal{Q}_{NIJP}F_{jP}$. The above expressions enable the internal virtual energy to be expressed in terms of the vector $[\mathbb{D}_{w_{\mathrm{TTC}}}]$ containing the derivatives of $w_{\mathrm{TTC}}(I_1, I_2, I_3, I_4^\star, I_5^\star, I_6^\star)$ with respect to the 6 invariants as

$$
\boldsymbol{P} : \boldsymbol{\nabla}_0\delta\boldsymbol{u} = [\mathbb{D}_{w_{\mathrm{TTC}}}]
\begin{bmatrix}
2\boldsymbol{F} : \boldsymbol{\nabla}_0\delta\boldsymbol{u}\\
2(\boldsymbol{F}\times\boldsymbol{H}) : \boldsymbol{\nabla}_0\delta\boldsymbol{u}\\
2J\boldsymbol{H} : \boldsymbol{\nabla}_0\delta\boldsymbol{u}\\
2(\boldsymbol{F}\boldsymbol{Q}) : \boldsymbol{\nabla}_0\delta\boldsymbol{u}\\
2\left[\boldsymbol{F}\times(\boldsymbol{H}\boldsymbol{Q})\right] : \boldsymbol{\nabla}_0\delta\boldsymbol{u}\\
4\boldsymbol{F}\boldsymbol{Q}^\star : \boldsymbol{\nabla}_0\delta\boldsymbol{u}
\end{bmatrix}, \tag{2.169}
$$

and therefore the first Piola-Kirchhoff tensor emerges as

$$
\begin{aligned}
\boldsymbol{P} = {} & 2\frac{\partial w}{\partial I_1}\boldsymbol{F} + 2\frac{\partial w}{\partial I_2}\boldsymbol{H}\times\boldsymbol{F} + 2\frac{\partial w}{\partial I_3}J\boldsymbol{H}\\
& + 2\frac{\partial w}{\partial I_4}(\boldsymbol{F}\boldsymbol{Q}) + 2\frac{\partial w}{\partial I_5}(\boldsymbol{H}\boldsymbol{Q})\times\boldsymbol{F} + 4\frac{\partial w}{\partial I_6}\boldsymbol{F}\boldsymbol{Q}^\star.
\end{aligned} \tag{2.170}
$$

Finally, the tangent elastic operator can be expressed in terms of the 6×6 Hessian matrix of the function $[\mathbb{H}_{w_{\mathrm{TTC}}}]$ as

$$
\begin{aligned}
D^2\Psi\left[\delta\boldsymbol{u};\boldsymbol{u}\right] = {} & \begin{bmatrix}
2\boldsymbol{F} : \boldsymbol{\nabla}_0\delta\boldsymbol{u}\\
2(\boldsymbol{F}\times\boldsymbol{H}) : \boldsymbol{\nabla}_0\delta\boldsymbol{u}\\
2J\boldsymbol{H} : \boldsymbol{\nabla}_0\delta\boldsymbol{u}\\
2(\boldsymbol{F}\boldsymbol{Q}) : \boldsymbol{\nabla}_0\delta\boldsymbol{u}\\
2\left[\boldsymbol{F}\times(\boldsymbol{H}\boldsymbol{Q})\right] : \boldsymbol{\nabla}_0\delta\boldsymbol{u}\\
4\boldsymbol{F}\boldsymbol{Q}^\star
\end{bmatrix}^T
[\mathbb{H}_{w_{\mathrm{TTC}}}]
\begin{bmatrix}
2\boldsymbol{F} : \boldsymbol{\nabla}_0\boldsymbol{u}\\
2(\boldsymbol{F}\times\boldsymbol{H}) : \boldsymbol{\nabla}_0\boldsymbol{u}\\
2J\boldsymbol{H} : \boldsymbol{\nabla}_0\boldsymbol{u}\\
2(\boldsymbol{F}\boldsymbol{Q}) : \boldsymbol{\nabla}_0\boldsymbol{u}\\
2\left[\boldsymbol{F}\times(\boldsymbol{H}\boldsymbol{Q})\right] : \boldsymbol{\nabla}_0\boldsymbol{u}\\
4\boldsymbol{F}\boldsymbol{Q}^\star
\end{bmatrix}\\
& + [\mathbb{D}_{w_{\mathrm{TTC}}}]
\begin{bmatrix}
2\boldsymbol{\nabla}_0\delta\boldsymbol{u} : \boldsymbol{\nabla}_0\boldsymbol{u}\\
2(\boldsymbol{F}\times\boldsymbol{\nabla}_0\delta\boldsymbol{u}) : (\boldsymbol{F}\times\boldsymbol{\nabla}_0\boldsymbol{u})\\
2(\boldsymbol{H} : \boldsymbol{\nabla}_0\delta\boldsymbol{u})(\boldsymbol{H} : \boldsymbol{\nabla}_0\boldsymbol{u})\\
2(\boldsymbol{\nabla}_0\delta\boldsymbol{u})\boldsymbol{Q} : (\boldsymbol{\nabla}_0\boldsymbol{u})\\
2(\boldsymbol{F}\times\boldsymbol{\nabla}_0\delta\boldsymbol{u})\boldsymbol{Q} : (\boldsymbol{F}\times\boldsymbol{\nabla}_0\boldsymbol{u})\\
4\left(\boldsymbol{F}\boldsymbol{Q}^\star : \boldsymbol{\nabla}_0\delta\boldsymbol{u}\right) + 8\boldsymbol{\nabla}_0\delta\boldsymbol{u} : \boldsymbol{\mathcal{C}}^\star : \boldsymbol{\nabla}_0\boldsymbol{u}
\end{bmatrix}\\
& + [\mathbb{D}_{w_{\mathrm{TTC}}}]
\begin{bmatrix}
0\\
2\boldsymbol{H} : (\boldsymbol{\nabla}_0\delta\boldsymbol{u}\times\boldsymbol{\nabla}_0\boldsymbol{u})\\
2J\boldsymbol{F} : (\boldsymbol{\nabla}_0\delta\boldsymbol{u}\times\boldsymbol{\nabla}_0\boldsymbol{u})\\
0\\
2(\boldsymbol{H}\boldsymbol{Q}) : (\boldsymbol{\nabla}_0\delta\boldsymbol{u}\times\boldsymbol{\nabla}_0\boldsymbol{u})\\
0
\end{bmatrix}.
\end{aligned} \tag{2.171}
$$

As in equations (2.145) and (2.164), the sum of the two first terms in above equation (2.164) is positive definite for polyconvex materials and only the third term (geometrically based) can induce buckling.

2.6 Variational formulations

This section shows how the proposed tensor cross product algebra can facilitate the formulation of various mixed variational formulations [48, 49] in order to establish the static equilibrium and compatibility equations. The section starts reviewing the standard displacement based variational principle. This provides a useful background for comparison with mixed and complementary energy variational principles presented later in the section.

2.6.1 Standard displacement based variational principle

The solution of large strain elastic problems is often expressed by means of the total energy minimisation variational principle as

$$\Pi(\boldsymbol{x}^*) = \inf_{\boldsymbol{x}\in\mathcal{X}} \left\{ \int_V \Psi\left(\boldsymbol{\nabla}_0\boldsymbol{x}\right)\, dV - \int_V \boldsymbol{f}_0\cdot\boldsymbol{x}\, dV - \int_{\partial_t V} \boldsymbol{t}_0\cdot\boldsymbol{x}\, dA, \right\}, \tag{2.172}$$

where $\boldsymbol{x}^*$ denotes the exact solution and $\mathcal{X}$ the appropriate Sobolev space of functions satisfying the relevant displacement boundary conditions. The strain energy function in this potential can be replaced by the convex function $W(\boldsymbol{F}_{\boldsymbol{x}}, \boldsymbol{H}_{\boldsymbol{x}}, J_{\boldsymbol{x}})$, where the geometrically compatible strain measures are defined by

$$\boldsymbol{F}_{\boldsymbol{x}} \equiv \boldsymbol{\nabla}_0\boldsymbol{x}; \qquad \boldsymbol{H}_{\boldsymbol{x}} \equiv \frac{1}{2}\boldsymbol{\nabla}_0\boldsymbol{x} \times \boldsymbol{\nabla}_0\boldsymbol{x}; \qquad J_{\boldsymbol{x}} \equiv \det\boldsymbol{\nabla}_0\boldsymbol{x}. \tag{2.173}$$

The stationary condition of this functional leads to the principle of virtual work (or power), commonly written as

$$D\Pi\left[\delta\boldsymbol{u}\right] = \int_V \boldsymbol{P}_{\boldsymbol{x}} : \boldsymbol{\nabla}_0\delta\boldsymbol{u}\, dV - \int_V \boldsymbol{f}_0\cdot\delta\boldsymbol{u}\, dV - \int_{\partial_t V} \boldsymbol{t}_0\cdot\delta\boldsymbol{u}\, dA = 0; \quad \forall\delta\boldsymbol{u}\in\mathcal{X}_0. \tag{2.174}$$

In this expression, the first Piola-Kirchhoff tensor $\boldsymbol{P}_{\boldsymbol{x}}$ is evaluated in the standard fashion using equation (2.53) in terms of the gradient of the deformation $\boldsymbol{\nabla}_0\boldsymbol{x}$ as

$$\boldsymbol{P}_{\boldsymbol{x}} = \boldsymbol{\Sigma}^{\boldsymbol{x}}_{\boldsymbol{F}} + \boldsymbol{\Sigma}^{\boldsymbol{x}}_{\boldsymbol{H}} \times \boldsymbol{F}_{\boldsymbol{x}} + \Sigma^{\boldsymbol{x}}_{J}\boldsymbol{H}_{\boldsymbol{x}}, \tag{2.175}$$

where the superscript $\boldsymbol{x}$ in the above stresses indicates that they are evaluated in terms of the geometric deformation gradient as

$$\begin{aligned} \boldsymbol{\Sigma}^{\boldsymbol{x}}_{\boldsymbol{F}} &= \boldsymbol{\Sigma}_{\boldsymbol{F}}\left(\boldsymbol{F}_{\boldsymbol{x}}, \boldsymbol{H}_{\boldsymbol{x}}, J_{\boldsymbol{x}}\right); \\ \boldsymbol{\Sigma}^{\boldsymbol{x}}_{\boldsymbol{H}} &= \boldsymbol{\Sigma}_{\boldsymbol{H}}\left(\boldsymbol{F}_{\boldsymbol{x}}, \boldsymbol{H}_{\boldsymbol{x}}, J_{\boldsymbol{x}}\right); \\ \Sigma^{\boldsymbol{x}}_{J} &= \Sigma_{J}\left(\boldsymbol{F}_{\boldsymbol{x}}, \boldsymbol{H}_{\boldsymbol{x}}, J_{\boldsymbol{x}}\right). \end{aligned} \tag{2.176}$$

An iterative Newton-Raphson process to converge towards the solution is usually established by solving a linearised system for the increment $\boldsymbol{u}$ as

$$D^2\Pi\left[\delta\boldsymbol{u};\boldsymbol{u}\right] = -D\Pi\left(\boldsymbol{x}_k\right)\left[\delta\boldsymbol{u}\right]; \quad \boldsymbol{x}_{k+1} = \boldsymbol{x}_k + \boldsymbol{u}, \tag{2.177}$$

where, in the absence of follower forces, the second derivative of the total energy functional is given by

$$D^2\Pi\left[\delta\boldsymbol{u};\boldsymbol{u}\right] = \int_V D^2\Psi\left[\boldsymbol{\nabla}_0\delta\boldsymbol{u}, \boldsymbol{\nabla}_0\boldsymbol{u}\right]\, dV. \tag{2.178}$$

The tangent operator is evaluated using equation (2.73), taking $\boldsymbol{F} = \boldsymbol{\nabla}_0\boldsymbol{x}$, $\boldsymbol{H} = \frac{1}{2}\boldsymbol{\nabla}_0\boldsymbol{x} \times \boldsymbol{\nabla}_0\boldsymbol{x}$ and $J = \det\boldsymbol{\nabla}_0\boldsymbol{x}$.

2.6.2 Mixed Variational Principle

An equivalent but alternative expression for the total energy variational principle can be written in terms of the geometry and strain variables as a constrained minimisation problem in the form

$$\Pi(\boldsymbol{x}^*) = \inf_{\substack{\boldsymbol{x},\,\boldsymbol{F},\,\boldsymbol{H},\,J,\,\text{s.t.}\\ \boldsymbol{F}=\boldsymbol{F}_x,\\ \boldsymbol{H}=\boldsymbol{H}_x,\\ J=J_x}} \left\{ \int_V W\left(\boldsymbol{F},\boldsymbol{H},J\right)\, dV - \int_V \boldsymbol{f}_0\cdot\boldsymbol{x}\, dV - \int_{\partial_t V} \boldsymbol{t}_0\cdot\boldsymbol{x}\, dA \right\}. \tag{2.179}$$

Using a standard Lagrange multiplier approach to enforce the compatibility constraints gives the following augmented mixed variational principle

$$\begin{aligned}\Pi_M(\boldsymbol{x}^*,\boldsymbol{F}^*,\boldsymbol{H}^*,J^*,\boldsymbol{\Sigma_F}^*,\boldsymbol{\Sigma}_{\boldsymbol{H}}^*,\Sigma_J^*) = \inf_{\boldsymbol{x},\boldsymbol{F},\boldsymbol{H},J} \Bigg\{ \sup_{\boldsymbol{\Sigma_F},\boldsymbol{\Sigma_H},\Sigma_J} \Bigg\{ \int_V W(\boldsymbol{F},\boldsymbol{H},J)\, dV \\ + \int_V \boldsymbol{\Sigma_F} : (\boldsymbol{F}_{\boldsymbol{x}} - \boldsymbol{F})\, dV + \int_V \boldsymbol{\Sigma_H} : (\boldsymbol{H}_{\boldsymbol{x}} - \boldsymbol{H})\, dV + \int_V \Sigma_J(J_{\boldsymbol{x}} - J)\, dV \\ - \int_V \boldsymbol{f}_0\cdot\boldsymbol{x}\, dV - \int_{\partial_t V} \boldsymbol{t}_0\cdot\boldsymbol{x}\, dA \Bigg\}\Bigg\}.\end{aligned} \tag{2.180}$$

This expression belongs to the general class of Hu-Washizu type of mixed variational principles [93] which have been widely used for the development of enhanced finite element formulations [12]. Note that the stress variables $\{\boldsymbol{\Sigma_F}, \boldsymbol{\Sigma_H}, \Sigma_J\}$ in this expression, at this stage, are simply Lagrange multipliers and are as yet unconnected to the strain variables. Both stress and strain variables belong to appropriate Sobolev function spaces, which generally require simple piecewise continuity and are unrestricted on the boundaries.

The stationary condition of the above augmented Lagrangian with respect to the first variable enforces equilibrium in the form of the principle of virtual work as

$$D_1\Pi_M\left[\delta\boldsymbol{u}\right] = \int\limits_V \boldsymbol{P}_M : \boldsymbol{\nabla}_0\delta\boldsymbol{u}\, dV - \int\limits_V \boldsymbol{f}_0\cdot\delta\boldsymbol{u}\, dV - \int\limits_{\partial_t V} \boldsymbol{t}_0\cdot\delta\boldsymbol{u}\, dA = 0, \tag{2.181}$$

where the first Piola-Kirchhoff stress now emerges as

$$\boldsymbol{P}_M = \boldsymbol{\Sigma}_{\boldsymbol{F}} + \boldsymbol{\Sigma}_{\boldsymbol{H}} \times \boldsymbol{F}_{\boldsymbol{x}} + \Sigma_J \boldsymbol{H}_{\boldsymbol{x}}. \tag{2.182}$$

The stationary conditions with respect to the three strain variables enforce the constitute relationships between the stresses and the derivatives of the strain energy in a weak form

$$\begin{aligned} D_{2,3,4}\Pi_M\left[\delta\boldsymbol{F},\delta\boldsymbol{H},\delta J\right] = &\int\limits_V \left(\frac{\partial W}{\partial \boldsymbol{F}} - \boldsymbol{\Sigma}_{\boldsymbol{F}}\right) : \delta\boldsymbol{F}\, dV + \int\limits_V \left(\frac{\partial W}{\partial \boldsymbol{H}} - \boldsymbol{\Sigma}_{\boldsymbol{H}}\right) : \delta\boldsymbol{H}\, dV \\ &+ \int\limits_V \left(\frac{\partial W}{\partial J} - \Sigma_J\right)\delta J\, dV = 0. \end{aligned} \tag{2.183}$$

Finally, the stationary conditions with respect to the stress variables enforce the geometric compatibility conditions between strains and geometry

$$\begin{aligned} D_{5,6,7}\Pi_M\left[\delta\boldsymbol{\Sigma}_{\boldsymbol{F}},\delta\boldsymbol{\Sigma}_{\boldsymbol{H}},\delta\Sigma_J\right] = &\int\limits_V \delta\boldsymbol{\Sigma}_{\boldsymbol{F}} : \left(\boldsymbol{F}_{\boldsymbol{x}} - \boldsymbol{F}\right)\, dV + \int\limits_V \delta\boldsymbol{\Sigma}_{\boldsymbol{H}} : \left(\boldsymbol{H}_{\boldsymbol{x}} - \boldsymbol{H}\right)\, dV \\ &+ \int\limits_V \delta\Sigma_J \left(J_{\boldsymbol{x}} - J\right)\, dV. \end{aligned} \tag{2.184}$$

In order to complete the formulation, it is necessary to develop a Newton-Raphson iterative process and the appropriate tangent operators. For this purpose, note first that a process equivalent to equation (2.177) for the extended set of variables is established by first solving a linear system for the increments of this set of variables $\{\boldsymbol{u}, \Delta\boldsymbol{F}, \Delta\boldsymbol{H}, \Delta J, \Delta\boldsymbol{\Sigma}_{\boldsymbol{F}}, \Delta\boldsymbol{\Sigma}_{\boldsymbol{H}}, \Delta\Sigma_J\}$ as

$$\begin{aligned} &D^2_{1\ldots7;1\ldots7}\Pi_M\left[\delta\boldsymbol{u},\delta\boldsymbol{F},\delta\boldsymbol{H},\delta J,\delta\boldsymbol{\Sigma}_{\boldsymbol{F}},\delta\boldsymbol{\Sigma}_{\boldsymbol{H}},\delta\Sigma_J;\boldsymbol{u},\Delta\boldsymbol{F},\Delta\boldsymbol{H},\Delta J,\Delta\boldsymbol{\Sigma}_{\boldsymbol{F}},\Delta\boldsymbol{\Sigma}_{\boldsymbol{H}},\Delta\Sigma_J\right] = \\ &- D_{1\ldots7}\Pi_M\left[\delta\boldsymbol{u},\delta\boldsymbol{F},\delta\boldsymbol{H},\delta J,\delta\boldsymbol{\Sigma}_{\boldsymbol{F}},\delta\boldsymbol{\Sigma}_{\boldsymbol{H}},\delta\Sigma_J\right]; \quad \forall\delta\boldsymbol{u},\delta\boldsymbol{F},\delta\boldsymbol{H}\delta J,\delta\boldsymbol{\Sigma}_{\boldsymbol{F}},\delta\boldsymbol{\Sigma}_{\boldsymbol{H}},\delta\Sigma_J. \end{aligned} \tag{2.185}$$

This is followed by the incremental updates

$$\begin{aligned} &\boldsymbol{x}_{k+1} = \boldsymbol{x}_k + \boldsymbol{u}; \quad \boldsymbol{F}_{k+1} = \boldsymbol{F}_k + \Delta\boldsymbol{F}; \quad \boldsymbol{H}_{k+1} = \boldsymbol{H}_k + \Delta\boldsymbol{H}; \quad J_{k+1} = J_k + \Delta J; \\ &\boldsymbol{\Sigma}^{k+1}_{\boldsymbol{F}} = \boldsymbol{\Sigma}^{k}_{\boldsymbol{F}} + \Delta\boldsymbol{\Sigma}_{\boldsymbol{F}}; \quad \boldsymbol{\Sigma}^{k+1}_{\boldsymbol{H}} = \boldsymbol{\Sigma}^{k}_{\boldsymbol{H}} + \Delta\boldsymbol{\Sigma}_{\boldsymbol{H}}; \quad \Sigma^{k+1}_{J} = \Sigma^{k}_{J} + \Delta\Sigma_J. \end{aligned} \tag{2.186}$$

The second derivatives that make up the linear operator in equation (2.185) can be derived with relative ease component by component. For instance, the second derivative with respect to the geometry, is obtained differentiating again the principle

of virtual work (2.181) with the help of equation (2.182) to give the initial stress component of the tangent operator as

$$D^2_{1;1}\Pi_M\left[\delta\boldsymbol{u};\boldsymbol{u}\right] = \int\limits_V \left(\boldsymbol{\Sigma_H} + \Sigma_J \boldsymbol{F_x}\right) : \left(\boldsymbol{\nabla}_0\delta\boldsymbol{u} \times \boldsymbol{\nabla}_0\boldsymbol{u}\right)\, dV. \tag{2.187}$$

The terms involving second derivatives with respect to the strain variables emerge from the Hessian of the strain energy function $W\left(\boldsymbol{F},\boldsymbol{H},J\right)$ as

$$D^2_{2,3,4;2,3,4}\Pi_M\left[\delta\boldsymbol{F},\delta\boldsymbol{H},\delta J;\Delta\boldsymbol{F},\Delta\boldsymbol{H},\Delta J\right] = \int\limits_V \left[\delta\boldsymbol{F}:\ \ \delta\boldsymbol{H}:\ \ \delta J\right]\left[\mathbb{H}_W\right]\begin{bmatrix}:\Delta\boldsymbol{F}\\:\Delta\boldsymbol{H}\\ \Delta J\end{bmatrix} dV. \tag{2.188}$$

The second derivative with respect to stresses vanishes as the functional is linear with respect to the stress tensors. There are, however, a number of cross derivative terms that do not vanish. These are the cross derivatives with respect to strains and stresses and their symmetric counterpart, which are easily derived from either equation (2.183) or (2.184) to give

$$\begin{aligned} D^2_{2,3,4;5,6,7}\Pi_M\left[\delta\boldsymbol{F},\delta\boldsymbol{H},\delta J;\Delta\boldsymbol{\Sigma_F},\Delta\boldsymbol{\Sigma_H},\Delta\Sigma_J\right] &= -\int\limits_V \left(\delta\boldsymbol{F}:\Delta\boldsymbol{\Sigma_F} + \delta\boldsymbol{H}:\Delta\boldsymbol{\Sigma_H} + \delta J\Delta\Sigma_J\right)\, dV \\ D^2_{5,6,7;2,3,4}\Pi_M\left[\delta\boldsymbol{\Sigma_F},\delta\boldsymbol{\Sigma_H},\delta\Sigma_J;\Delta\boldsymbol{F},\Delta\boldsymbol{H},\Delta J\right] &= -\int\limits_V \left(\delta\boldsymbol{\Sigma_F}:\Delta\boldsymbol{F} + \delta\boldsymbol{\Sigma_H}:\Delta\boldsymbol{H} + \delta\Sigma_J\Delta J\right)\, dV. \end{aligned} \tag{2.189}$$

And the cross derivatives with respect to geometry and stresses, which emerge after some simple algebra from equations (2.181), (2.182) and (2.184) as (refer to equations (2.27) and (2.29))

$$\begin{aligned} D^2_{1;5,6,7}\Pi_M\left[\delta\boldsymbol{u};\Delta\boldsymbol{\Sigma_F},\Delta\boldsymbol{\Sigma_H},\Delta\Sigma_J\right] = \int\limits_V \big[&\boldsymbol{\nabla}_0\delta\boldsymbol{u}:\Delta\boldsymbol{\Sigma_F} + \boldsymbol{F_x}:\left(\boldsymbol{\nabla}_0\delta\boldsymbol{u}\times\Delta\boldsymbol{\Sigma_H}\right) \\ &+ \Delta\Sigma_J\boldsymbol{H_x}:\boldsymbol{\nabla}_0\delta\boldsymbol{u}\big]\, dV; \end{aligned} \tag{2.190}$$

$$\begin{aligned} D^2_{5,6,7;1}\Pi_M\left[\delta\boldsymbol{\Sigma_F},\delta\boldsymbol{\Sigma_H},\delta\Sigma_J;\boldsymbol{u}\right] = \int\limits_V \big[&\boldsymbol{\nabla}_0\boldsymbol{u}:\delta\boldsymbol{\Sigma_F} + \boldsymbol{F_x}:\left(\boldsymbol{\nabla}_0\boldsymbol{u}\times\delta\boldsymbol{\Sigma_H}\right) \\ &+ \delta\Sigma_J\boldsymbol{H_x}:\boldsymbol{\nabla}_0\boldsymbol{u}\big]\, dV. \end{aligned} \tag{2.191}$$

The set of equations derived in this section enables the use of arbitrary discretisation spaces for each of the problem variables. This level of flexibility may be useful but it is costly given the large number of unknowns generated in the process. An alternative approach that significantly reduces the number of problem variables is presented in the next section.

2.6.3 Mixed Complementary Energy Principle

In order to derive a variational principle in terms of the complementary energy, recall first the mixed variational principle (2.180) with a different ordering of terms

$$\begin{aligned}\Pi_M(\boldsymbol{x}^*, \boldsymbol{F}^*, \boldsymbol{H}^*, J^*, \boldsymbol{\Sigma_F}^*, \boldsymbol{\Sigma}_{\boldsymbol{H}}^*, \Sigma_J^*) = \inf_{\boldsymbol{x},\boldsymbol{F},\boldsymbol{H},J} \Bigg\{ \sup_{\boldsymbol{\Sigma_F},\boldsymbol{\Sigma_H},\Sigma_J} \{ \\ - \int_V \left[\boldsymbol{\Sigma_F} : \boldsymbol{F} + \boldsymbol{\Sigma_H} : \boldsymbol{H} + \Sigma_J J - W(\boldsymbol{F}, \boldsymbol{H}, J)\right] dV - \int_V \boldsymbol{f}_0 \cdot \boldsymbol{x}\, dV - \int_{\partial_t V} \boldsymbol{t}_0 \cdot \boldsymbol{x}\, dA \\ + \int_V \boldsymbol{\Sigma_F} : \boldsymbol{F}_{\boldsymbol{x}}\, dV + \int_V \boldsymbol{\Sigma_H} : \boldsymbol{H}_{\boldsymbol{x}}\, dV + \int_V \Sigma_J J_{\boldsymbol{x}}\, dV \Bigg\} \Bigg\}.\end{aligned} \tag{2.192}$$

Comparing the term in square brackets in the first integral with the definition of the complementary energy given by equation (2.58), enables a mixed complementary variational principle to be established as[4]

$$\begin{aligned}\Pi_C(\boldsymbol{x}^*, \boldsymbol{\Sigma_F}^*, \boldsymbol{\Sigma}_{\boldsymbol{H}}^*, \Sigma_J^*) = \inf_{\boldsymbol{x}} \Bigg\{ \sup_{\boldsymbol{\Sigma_F},\boldsymbol{\Sigma_H},\Sigma_J} \Bigg\{ - \int_V \Upsilon\left(\boldsymbol{\Sigma_F}, \boldsymbol{\Sigma_H}, \Sigma_J\right) dV \\ + \int_V \boldsymbol{\Sigma_F} : \boldsymbol{F}_{\boldsymbol{x}}\, dV + \int_V \boldsymbol{\Sigma_H} : \boldsymbol{H}_{\boldsymbol{x}}\, dV + \int_V \Sigma_J J_{\boldsymbol{x}}\, dV - \int_V \boldsymbol{f}_0 \cdot \boldsymbol{x}\, dV - \int_{\partial_t V} \boldsymbol{t}_0 \cdot \boldsymbol{x}\, dA \Bigg\} \Bigg\}.\end{aligned} \tag{2.193}$$

This represents a Hellinger-Reissner type of variational principle [12]. The stationary condition of this principle with respect to its first variable, the geometry, enforces equilibrium in a manner identical to equations (2.181) and (2.182), that is,

$$\begin{aligned}D_1\Pi_C\left[\delta\boldsymbol{u}\right] = D_1\Pi_M\left[\delta\boldsymbol{u}\right] = \int_V \boldsymbol{P}_M : \boldsymbol{\nabla}_0 \delta\boldsymbol{u}\, dV - \int_V \boldsymbol{f}_0 \cdot \delta\boldsymbol{u}\, dV - \int_{\partial_t V} \boldsymbol{t}_0 \cdot \delta\boldsymbol{u}\, dA = 0 \\ \boldsymbol{P}_C = \boldsymbol{P}_M = \boldsymbol{\Sigma_F} + \boldsymbol{\Sigma_H} \boldsymbol{\times} \boldsymbol{F}_{\boldsymbol{x}} + \Sigma_J \boldsymbol{H}_{\boldsymbol{x}}.\end{aligned} \tag{2.194}$$

Similarly, the stationary conditions with respect to stresses, enforce the geometric compatibility conditions, now expressed as,

$$\begin{aligned}D_{2,3,4}\Pi_C\left[\delta\boldsymbol{\Sigma_F}, \delta\boldsymbol{\Sigma_H}, \delta\Sigma_J\right] = \int_V \delta\boldsymbol{\Sigma_F} : \left(\boldsymbol{F}_{\boldsymbol{x}} - \frac{\partial \Upsilon}{\partial \boldsymbol{\Sigma_F}}\right) dV \\ + \int_V \delta\boldsymbol{\Sigma_H} : \left(\boldsymbol{H}_{\boldsymbol{x}} - \frac{\partial \Upsilon}{\partial \boldsymbol{\Sigma_H}}\right) dV \\ + \int_V \delta\Sigma_J \left(J_{\boldsymbol{x}} - \frac{\partial \Upsilon}{\partial \Sigma_J}\right) dV.\end{aligned} \tag{2.195}$$

[4]Note that this step relies on the strong duality property of the mixed functional which allows the order of the inf and sup operations with respect to strains and stresses to be swapped. This is the case here given the convexity of the strain energy function.

The second derivatives of the complementary energy functional required for a Newton-Raphson process are mostly the same as those derived in the previous section for the mixed variational principle. In particular, the following terms are identical, namely

$$\begin{aligned} D^2_{1;1}\Pi_C\left[\delta\boldsymbol{u};\boldsymbol{u}\right] =& D^2_{1;1}\Pi_M\left[\delta\boldsymbol{u};\boldsymbol{u}\right]; \\ D^2_{2,3,4;1}\Pi_C\left[\delta\boldsymbol{\Sigma_F},\delta\boldsymbol{\Sigma_H},\delta\Sigma_J;\boldsymbol{u}\right] =& D^2_{5,6,7;1}\Pi_M\left[\delta\boldsymbol{\Sigma_F},\delta\boldsymbol{\Sigma_H},\delta\Sigma_J;\boldsymbol{u}\right]; \\ D^2_{1;2,3,4}\Pi_C\left[\delta\boldsymbol{u};\Delta\boldsymbol{\Sigma_F},\Delta\boldsymbol{\Sigma_H},\Delta\Sigma_J\right] =& D^2_{1;5,6,7}\Pi_M\left[\delta\boldsymbol{u};\Delta\boldsymbol{\Sigma_F},\Delta\boldsymbol{\Sigma_H},\Delta\Sigma_J\right]. \end{aligned} \tag{2.196}$$

A new term, however, emerges when taking the second derivatives with respect to stresses, leading to a constitutive expression similar to equation (2.188) but now involving the second derivative of the complementary energy function. This term can be evaluated by differentiating again equation (2.195)

$$\begin{aligned} &D^2_{2,3,4;2,3,4}\Pi_C\left[\delta\boldsymbol{\Sigma_F},\delta\boldsymbol{\Sigma_H},\delta\Sigma_J;\Delta\boldsymbol{\Sigma_F},\Delta\boldsymbol{\Sigma_H},\Delta\Sigma_J\right] = \\ &\quad -\int_V \left[\delta\boldsymbol{\Sigma_F}:\ \ \delta\boldsymbol{\Sigma_H}:\ \ \delta\Sigma_J\right]\left[\mathbb{H}_\Upsilon\right]\begin{bmatrix}:\Delta\boldsymbol{\Sigma_F}\\:\Delta\boldsymbol{\Sigma_H}\\ \Delta\Sigma_J\end{bmatrix} dV. \end{aligned} \tag{2.197}$$

Where $[\mathbb{H}_\Upsilon]$ denotes the Hessian operator of the complementary energy function. Note that this component is clearly negative on account of the variational principle involving a maximisation with respect to stresses. It is possible to change this sign by simply changing the overall sign of the principle (2.193). This would also change the sign of $D^2_{1;1}\Pi_C\left[\delta\boldsymbol{u};\boldsymbol{u}\right]$ but this term is neither positive nor negative since it contains tensor cross products of the gradient of $\delta\boldsymbol{u}$ and $\boldsymbol{u}$. For practical purposes, however, this will not be necessary, as the stress variables will typically be eliminated locally in each finite element. What is essential is that the Hessian matrix is invertible, which is ensured by the convexity of the function Υ.

2.6.4 Variational principles for incompressible and nearly incompressible models

Many applications of practical importance rely on the decomposition of the strain energy into isochoric and volumetric components. For such cases, it is possible to modify the variational formulations above in such a way that different approaches are used for the isochoric and volumetric components. In particular, it is often useful to follow a standard displacement based formulation for the isochoric component and a mixed approach for the volumetric terms [13]. In the present framework, this leads

to the following hybrid mixed variational principle

$$\begin{aligned}\hat{\Pi}_M(\boldsymbol{x}^*, J^*, p^*) = \inf_{\boldsymbol{x},J}\Bigg\{\sup_p\Bigg\{&\int_V \hat{W}\left(\boldsymbol{F}_{\boldsymbol{x}}, \boldsymbol{H}_{\boldsymbol{x}}, J_{\boldsymbol{x}}\right)\, dV \\ &+ \int_V U\left(J\right)\, dV + \int_V p\left(J_{\boldsymbol{x}} - J\right)\, dV \\ &- \int_V \boldsymbol{f}_0 \cdot \boldsymbol{x}\, dV - \int_{\partial_t V} \boldsymbol{t}_0 \cdot \boldsymbol{x}\, dA\Bigg\}\Bigg\},\end{aligned} \tag{2.198}$$

where $\hat{W}$ and U are the isochoric and volumetric components of the strain energy defined in Section 2.3.7. Note that, in general $\hat{W}$, will be a direct function of the volume ratio. This volume ratio is expressed differently in the two terms making up the strain energy: it is directly evaluated from the geometry in the isochoric strain energy, whereas it is expressed as an independent variable J in the volumetric component. The third integral term above enforces the compatibility between these two measures. The particular case of full incompressibility can be obtained by simply taking $J = 1$ in the above expression to give

$$\begin{aligned}\hat{\Pi}^I_M(\boldsymbol{x}^*, p^*) = \inf_{\boldsymbol{x},J}\Bigg\{\sup_p\Bigg\{&\int_V \hat{W}\left(\boldsymbol{F}_{\boldsymbol{x}}, \boldsymbol{H}_{\boldsymbol{x}}, J_{\boldsymbol{x}}\right)\, dV + \int_V p\left(J_{\boldsymbol{x}} - 1\right)\, dV \\ &- \int_V \boldsymbol{f}_0 \cdot \boldsymbol{x}\, dV - \int_{\partial_t V} \boldsymbol{t}_0 \cdot \boldsymbol{x}\, dA\Bigg\}\Bigg\}.\end{aligned} \tag{2.199}$$

The stationary conditions of these hybrid functionals are evaluated in the same fashion as above. For instance, the first derivative with respect to geometry gives the principle of virtual work as

$$\begin{aligned}D_1\hat{\Pi}_M\left[\delta\boldsymbol{u}\right] = D_1\hat{\Pi}^I_M\left[\delta\boldsymbol{u}\right] = &\int_V \boldsymbol{P}_I : \boldsymbol{\nabla}_0\delta\boldsymbol{u}\, dV - \int_V \boldsymbol{f}_0 \cdot \delta\boldsymbol{u}\, dV \\ &- \int_{\partial_t V} \boldsymbol{t}_0 \cdot \delta\boldsymbol{u}\, dA = 0,\end{aligned} \tag{2.200}$$

where the first Piola-Kirchoff stress tensor is now evaluated as

$$\boldsymbol{P}_I = \boldsymbol{\Sigma}^{\boldsymbol{x}}_{\boldsymbol{F}} + \boldsymbol{\Sigma}^{\boldsymbol{x}}_{\boldsymbol{H}} \times \boldsymbol{F}_{\boldsymbol{x}} + \Sigma_J \boldsymbol{H}_{\boldsymbol{x}}; \quad \Sigma_J = \hat{\Sigma}^{\boldsymbol{x}}_J + p \tag{2.201}$$

and the last term in (2.201) indicates that the volumetric conjugate stress includes a component due to the independent variable p as well as a contribution due to the isochoric strain energy function as

$$\hat{\Sigma^{\boldsymbol{x}}_J} = \frac{\partial \hat{W}\left(\boldsymbol{F}_{\boldsymbol{x}}, \boldsymbol{H}_{\boldsymbol{x}}, J_{\boldsymbol{x}}\right)}{\partial J_{\boldsymbol{x}}}. \tag{2.202}$$

The first derivative with respect to J enforces the volumetric component of the constitutive model as

$$D_2\hat{\Pi}_M\left[\delta J\right] = \int_V \left(U'(J) - p\right)\delta J\, dV = 0. \tag{2.203}$$

Finally, the stationary condition with respect to the pressure enforces geometric compatibility between J and $J_{\boldsymbol{x}} = \det\boldsymbol{\nabla}_0\boldsymbol{x}$ as

$$\begin{aligned} D_3\hat{\Pi}_M\left[\delta p\right] &= \int_V \left(J_{\boldsymbol{x}} - J\right)\delta p\, dV = 0; \\ D_2\hat{\Pi}^I_M\left[\delta p\right] &= \int_V \left(J_{\boldsymbol{x}} - 1\right)\delta p\, dV = 0. \end{aligned} \tag{2.204}$$

The evaluation of second derivatives required for a Newton-Raphson process proceeds along the same lines as in the previous sections. For instance, the second derivative with respect to geometry contains the isochoric tangent operator as given by equation (2.103)

$$D^2_{1;1}\hat{\Pi}_M\left[\delta\boldsymbol{u};\boldsymbol{u}\right] = D^2_{1;1}\hat{\Pi}^I_M\left[\delta\boldsymbol{u};\boldsymbol{u}\right] = \int_V D^2\Psi\left[\delta\boldsymbol{u};\boldsymbol{u}\right]\, dV. \tag{2.205}$$

The second derivative with respect to J is evaluated from equation (2.203)

$$D^2_{2;2}\hat{\Pi}_M\left[\delta J;\Delta J\right] = \int_V U''\delta J\Delta J\, dV. \tag{2.206}$$

There are also cross derivative terms different from zero. For instance, the cross derivative with respect to J and p is

$$D^2_{2;3}\hat{\Pi}_M\left[\delta J;\Delta p\right] = -\int_V \Delta p\delta J\, dV; \quad D^2_{3;2}\hat{\Pi}_M\left[\delta p;\Delta J\right] = -\int_V \delta p\Delta J\, dV. \tag{2.207}$$

Finally, the cross derivative terms between pressure and geometry are (refer to equation (2.29))

$$\begin{aligned} D^2_{1;3}\hat{\Pi}_M\left[\delta\boldsymbol{u};\Delta p\right] &= D^2_{1;2}\hat{\Pi}^I_M\left[\delta\boldsymbol{u};\Delta p\right] = \int_V \left(\boldsymbol{H}_x : \boldsymbol{\nabla}_0\delta\boldsymbol{u}\right)\Delta p\, dV; \\ D^2_{3;1}\hat{\Pi}_M\left[\delta p;\boldsymbol{u}\right] &= D^2_{2;1}\hat{\Pi}^I_M\left[\delta p;\boldsymbol{u}\right] = \int_V \delta p\left(\boldsymbol{H}_x : \boldsymbol{\nabla}_0\boldsymbol{u}\right)\, dV. \end{aligned} \tag{2.208}$$

2.6.5 Alternative mixed variational principles

The enforcement of the geometrical compatibility constraints in the mixed principles presented above can be formulated in a variety of forms. For instance, the constraint

for the area map $\boldsymbol{H}$ can be expressed directly in terms of $\boldsymbol{\nabla}_0\boldsymbol{x}$ or indirectly in terms of $\boldsymbol{F}$. Similarly, J can be related to $\det \boldsymbol{F}$ or to $\frac{1}{3}\boldsymbol{H} : \boldsymbol{F}$ or even to $\frac{1}{3}\boldsymbol{H} : \boldsymbol{\nabla}_0\boldsymbol{x}$. In this way alternative variational principles may be constructed. As an example of the resulting type of functional consider the expression

$$\begin{aligned}\tilde{\Pi}_M(\boldsymbol{x}^*, \boldsymbol{F}^*, \boldsymbol{H}^*, J^*, \boldsymbol{\Gamma}_{\boldsymbol{F}}^*, \boldsymbol{\Gamma}_{\boldsymbol{H}}^*, \Gamma_J^*) = \inf_{\boldsymbol{x},\boldsymbol{F},\boldsymbol{H},J} \Bigg\{ \sup_{\boldsymbol{\Gamma}_{\boldsymbol{F}},\boldsymbol{\Gamma}_{\boldsymbol{H}},\Gamma_J} \Bigg\{ \int_V W(\boldsymbol{F}, \boldsymbol{H}, J)\, dV \\ + \int_V \boldsymbol{\Gamma}_{\boldsymbol{F}} : (\boldsymbol{\nabla}_0\boldsymbol{x} - \boldsymbol{F})\, dV \\ + \int_V \boldsymbol{\Gamma}_{\boldsymbol{H}} : (\tfrac{1}{2}\boldsymbol{F} \times \boldsymbol{\nabla}_0\boldsymbol{x} - \boldsymbol{H})\, dV \\ + \int_V \Gamma_J(\tfrac{1}{3}\boldsymbol{H} : \boldsymbol{\nabla}_0\boldsymbol{x} - J)\, dV \\ - \int_V \boldsymbol{f}_0 \cdot \boldsymbol{x}\, dV - \int_{\partial_t V} \boldsymbol{t}_0 \cdot \boldsymbol{x}\, dA \Bigg\} \Bigg\}.\end{aligned} \tag{2.209}$$

Note that the stress variables $\{\boldsymbol{\Gamma}_{\boldsymbol{F}}, \boldsymbol{\Gamma}_{\boldsymbol{H}}, \Gamma_J\}$ in this expression are simply Lagrange multipliers and will generally not coincide with the conjugate stresses $\{\boldsymbol{\Sigma}_{\boldsymbol{F}}, \boldsymbol{\Sigma}_{\boldsymbol{H}}, \Sigma_J\}$ as shown below. The stationary condition of the above Lagrangian with respect to the first variable enforces equilibrium in the form of the principle of virtual work as

$$D_1\tilde{\Pi}_M\,[\delta\boldsymbol{u}] = \int_V \tilde{\boldsymbol{P}}_M : \boldsymbol{\nabla}_0\delta\boldsymbol{u}\, dV - \int_V \boldsymbol{f}_0 \cdot \delta\boldsymbol{u}\, dV - \int_{\partial_t V} \boldsymbol{t}_0 \cdot \delta\boldsymbol{u}\, dA = 0, \tag{2.210}$$

where the first Piola-Kirchhoff stress now emerges as:

$$\tilde{\boldsymbol{P}}_M = \boldsymbol{\Gamma}_{\boldsymbol{F}} + \tfrac{1}{2}\boldsymbol{\Gamma}_{\boldsymbol{H}} \times \boldsymbol{F} + \tfrac{1}{3}\Gamma_J\boldsymbol{H}. \tag{2.211}$$

The stationary conditions with respect to the three strain variables enforce the constitute relationships between the stress multipliers and the derivatives of the strain energy in a weak form

$$\begin{aligned}D_{2,3,4}\tilde{\Pi}_M\,[\delta\boldsymbol{F}, \delta\boldsymbol{H}, \delta J] = \int_V \left(\frac{\partial W}{\partial \boldsymbol{F}} - \boldsymbol{\Gamma}_{\boldsymbol{F}} + \tfrac{1}{2}\boldsymbol{\Gamma}_{\boldsymbol{H}} \times \boldsymbol{\nabla}_0\boldsymbol{x}\right) : \delta\boldsymbol{F}\, dV \\ + \int_V \left(\frac{\partial W}{\partial \boldsymbol{H}} - \boldsymbol{\Gamma}_{\boldsymbol{H}} + \tfrac{1}{3}\Gamma_J\boldsymbol{\nabla}_0\boldsymbol{x}\right) : \delta\boldsymbol{H}\, dV \\ + \int_V \left(\frac{\partial W}{\partial J} - \Gamma_J\right) \delta J\, dV = 0.\end{aligned} \tag{2.212}$$

Note that for sufficiently rich function spaces the above equation gives relation-

ships between the stress Lagrange multipliers and the conjugate stresses as

$$\Gamma_J = \Sigma_J; \quad \Sigma_J = \frac{\partial W}{\partial J}; \tag{2.213}$$

$$\boldsymbol{\Gamma_H} = \boldsymbol{\Sigma_H} + \tfrac{1}{3}\Sigma_J \boldsymbol{\nabla}_0 \boldsymbol{x}; \quad \boldsymbol{\Sigma_H} = \frac{\partial W}{\partial \boldsymbol{H}}; \tag{2.214}$$

$$\boldsymbol{\Gamma_F} = \boldsymbol{\Sigma_F} + \tfrac{1}{2}\boldsymbol{\Sigma_H} \times \boldsymbol{\nabla}_0 \boldsymbol{x} + \tfrac{1}{6}\Sigma_J \, \boldsymbol{\nabla}_0 \boldsymbol{x} \times \boldsymbol{\nabla}_0 \boldsymbol{x}; \quad \boldsymbol{\Sigma_F} = \frac{\partial W}{\partial \boldsymbol{F}}. \tag{2.215}$$

Substituting these relationships into equation (2.211) gives a hybrid relationship for the first Piola-Kirchhoff stress tensor as

$$\tilde{\boldsymbol{P}}_M = \boldsymbol{\Gamma_F} + \boldsymbol{\Sigma_H} \times \bar{\boldsymbol{F}} + \Sigma_J \bar{\boldsymbol{H}}. \tag{2.216}$$

where the average fibre and area maps are:

$$\bar{\boldsymbol{F}} = \tfrac{1}{2}(\boldsymbol{F} + \boldsymbol{\nabla}_0 \boldsymbol{x}); \tag{2.217}$$

$$\bar{\boldsymbol{H}} = \tfrac{1}{3}(\boldsymbol{H} + \boldsymbol{\nabla}_0 \boldsymbol{x} \times \bar{\boldsymbol{F}}). \tag{2.218}$$

Finally, the stationary conditions with respect to the stress variables enforce the geometric compatibility conditions between strains and geometry

$$\begin{aligned} D_{5,6,7}\tilde{\Pi}_M \left[\delta\boldsymbol{\Sigma_F}, \delta\boldsymbol{\Sigma_H}, \delta\Sigma_J\right] = & \int_V \delta\boldsymbol{\Sigma_F} : \left(\boldsymbol{\nabla}_0 \boldsymbol{x} - \boldsymbol{F}\right) \, dV \\ & + \int_V \delta\boldsymbol{\Gamma_H} : \left(\tfrac{1}{2}\boldsymbol{F} \times \boldsymbol{\nabla}_0 \boldsymbol{x} - \boldsymbol{H}\right) \, dV \\ & + \int_V \delta\Gamma_J \left(\tfrac{1}{3}\boldsymbol{H} : \boldsymbol{\nabla}_0 \boldsymbol{x} - J\right) \, dV. \end{aligned} \tag{2.219}$$

2.7 Concluding remarks

This Chapter presents a novel approach for the formulation of polyconvex large strain elasticity based on the simplified algebra associated to the tensor cross product, originally presented by de Boer [82] and recently re-introduced by Bonet et al. in [1, 43, 44]. Five key novel contributions are included in the present Chapter. First, the use of the tensor cross product and its properties to define the area map, its derivatives and the derivatives of the volume map, which leads to much simpler algebra than that in the conventional approach followed in large strain elasticity. Second, the definition of stresses $\{\boldsymbol{\Sigma_F}, \boldsymbol{\Sigma_H}, \Sigma_J\}$ conjugate to the main extended kinematic variable set $\{\boldsymbol{F}, \boldsymbol{H}, J\}$, which are elegantly related to the classical stress tensors, and the introduction of a convex complementary strain energy functional in terms of this new set of conjugate stresses. Third, the derivation of compatibility and equilibrium equations for the conjugate set of stresses. Fourth, the development of a new set of formulae for material and spatial elasticity tensor in a manner that

clearly separates physical components from geometrical dependencies. Fifth, the application of the proposed methodology for isotropic and anisotropic constitutive models where the strain energy can be expressed as functions of a set of invariants. Sixth, the development of a series of mixed and complementary variational principles which enforce equilibrium in the form of a principle of virtual work together with the geometric compatibility constraints in a weak form.

Chapter 3

Polyconvex elasticity. Computational implementation

3.1 Introduction

This Chapter presents the Finite Element implementation of some of the most relevant mixed variational principles for compressible and fully incompressible scenarios introduced in Section 2.6, suitable for the simulation of large strain polyconvex elasticity. In particular, the discretisation of the first and second directional derivatives for the Hu-Washizu mixed variational principle in Section 2.6.2 will be presented hereby, leading to the classical definition of residual vectors and stiffness matrices. Similar expressions for the residual vectors and stiffness matrices for the Hellinger-Reissner variational principle presented in Section 2.6.3 will also be obtained.

For both Hu-Washizu and Hellinger-Reissner mixed variational principles, a specific choice of functional spaces complying with the Ladyzenskaja-Babuška-Brezzi (LBB) condition [94, 95] has been used, where discontinuous functional spaces have been used for the interpolation of the kinematic strains $\{\boldsymbol{F}, \boldsymbol{H}, J\}$ and for their respective work conjugates, namely $\{\boldsymbol{\Sigma_J}, \boldsymbol{\Sigma_H}, \Sigma_J\}$. This discontinuity across elements of the aforementioned variables enables a static condensation procedure to be carried out for the variables involved, leading to a formulation comparable to a displacement based formulation in terms of the computational cost. The static condensation procedure for the Hellinger-Reissner formulation will be presented in the present Chapter. Similar steps can be followed for the Hu-Washizu variational principle, which will not be presented hereby.

For the fully incompressible formulation presented in Section 2.6.4, linear tetrahedral elements have been used for the interpolation of both displacements and the pressure fields. It is well known that this choice of interpolation spaces does not satisfy the LBB condition [45, 96]. A Petrov-Galerkin type of stabilisation has been pursued for the circumvention of the LBB condition.

The objective of this Chapter is to show the robustness of the proposed mixed formulations and their superiority with respect to classical displacement-based formulations. The later are well known to suffer from deficiencies such as volumetric locking in nearly incompressible scenarios [14, 43, 45], spurious pressure oscillations, bending locking [42], etc. to name a few. A series of challenging numerical examples will be presented in this Chapter in order to illustrate the benefits of the proposed mixed variational formulations.

This Chapter is organised as follows. Section 3.2 shows the Finite Element implementation of the Hu-Washizu and Hellinger-Reissner variational principles presented in Sections 2.6.2 and 2.6.3. Moreover, it presents the Finite Element implementation of a stabilised linear tetrahedral Finite Element formulation for the fully incompressible formulation presented in Section 2.6.4. A number of benchmark examples are used in Section 3.3 in order to demonstrate the validity and convergence characteristics of the formulation proposed. Finally, Section 3.4 provides some concluding remarks and a summary of the key contributions of this chapter. An illustrative diagram of the layout of the present Chapter can be found in Figure 3.1.

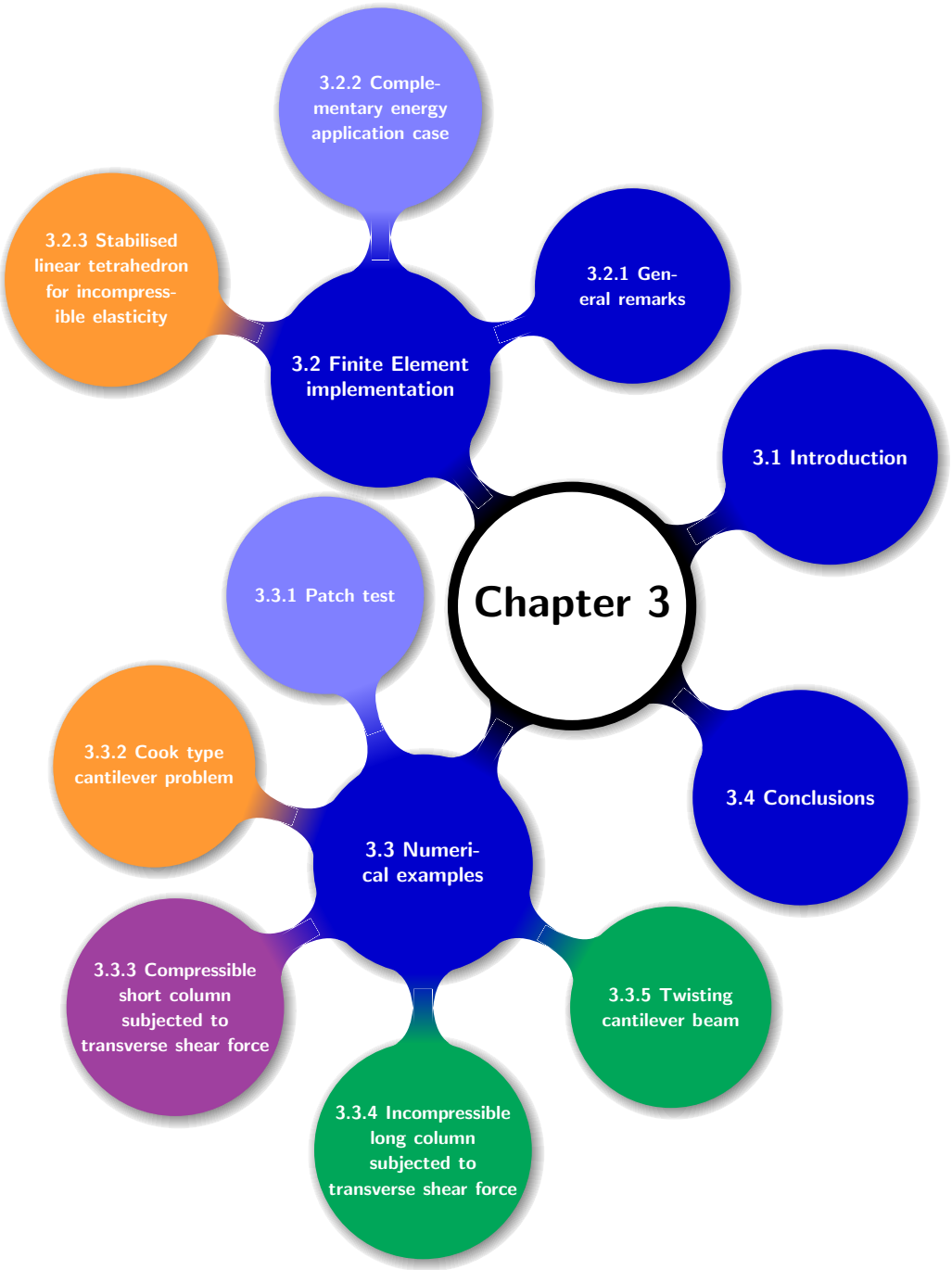

Figure 3.1: Chapter layout.

3.2 Finite Element implementation

The objective of this Section is to present the Finite Element framework associated to some relevant mixed variational principles presented in Section 2.6. In particular, the Hu-Washizu, Hellinger-Reissner and the mixed variational principles for nearly and trully incompressible scenarios presented in Sections 2.6.2, 2.6.3 and 2.6.4, respectively, will be considered in this Section.

3.2.1 General remarks

The implementation of the various variational principles described in Chapter 2 and more specifically, in Section 2.6 is based on a finite element partition of the domain into a set of elements. Inside each element the problem variables are interpolated in terms of a set of shape functions N_a as

$$\boldsymbol{x} = \sum_{a=1}^{n_x} \boldsymbol{x}_a N_a^{\boldsymbol{x}}; \quad \boldsymbol{F} = \sum_{a=1}^{n_F} \boldsymbol{F}_a N_a^{\boldsymbol{F}}; \quad ...; \quad \boldsymbol{\Sigma}_{\boldsymbol{F}} = \sum_{a=1}^{n_{\Sigma_F}} \boldsymbol{\Sigma}_{\boldsymbol{F}a} N_a^{\boldsymbol{\Sigma}_{\boldsymbol{F}}}; \quad ..., \tag{3.1}$$

where a denotes the nodes or other degrees of freedom used in the interpolation of the above variables. In general, different interpolations can (and are often) used to describe different variables. However, the same interpolation space will invariably be used for strain-stress conjugate pairs; that is, $N_a^{\boldsymbol{F}} = N_a^{\boldsymbol{\Sigma}_{\boldsymbol{F}}}$, etc. The virtual and incremental equivalents of the variables are also interpolated using the same spaces as

$$\delta\boldsymbol{u} = \sum_{a=1}^{n_x} \delta\boldsymbol{v}_a N_a^{\boldsymbol{x}}; \quad \delta\boldsymbol{F} = \sum_{a=1}^{n_F} \delta\boldsymbol{F}_a N_a^{\boldsymbol{F}}; \quad ...; \quad \delta\boldsymbol{\Sigma}_{\boldsymbol{F}} = \sum_{a=1}^{n_F} \delta\boldsymbol{\Sigma}_{\boldsymbol{F}}^{\boldsymbol{a}} N_a^{\boldsymbol{\Sigma}_{\boldsymbol{F}}}; \tag{3.2}$$

$$\boldsymbol{u} = \sum_{a=1}^{n_x} \boldsymbol{u}_a N_a^{\boldsymbol{x}}; \quad \Delta\boldsymbol{F} = \sum_{a=1}^{n_F} \Delta\boldsymbol{F}_a N_a^{\boldsymbol{F}}; \quad ...; \quad \Delta\boldsymbol{\Sigma}_{\boldsymbol{F}} = \sum_{a=1}^{n_F} \Delta\boldsymbol{\Sigma}_{\boldsymbol{F}}^{\boldsymbol{a}} N_a^{\boldsymbol{\Sigma}_{\boldsymbol{F}}}. \tag{3.3}$$

Finite element equations are derived by simply substituting the above expressions into the functional expressions provided in Section 2.6. In many cases this is a rather standard process and leads to well established equations. For instance, substituting the above interpolation for the virtual displacement $\delta\boldsymbol{u}$ into any of the virtual work statements given by equations (2.174), (2.181), (2.194) or (2.200) leads to the standard definition of the residual forces as

$$D_1\Pi\left[\delta\boldsymbol{u}\right] = \sum_a \boldsymbol{R}_{\boldsymbol{x}}^a \cdot \delta\boldsymbol{u}; \quad \boldsymbol{R}_{\boldsymbol{x}}^a = \int_V \boldsymbol{P}\boldsymbol{\nabla}_0 N_a^{\boldsymbol{x}}\, dV - \int_V \boldsymbol{f}_0 N_a^{\boldsymbol{x}}\, dV - \int_{\partial_t V} \boldsymbol{t}_0 N_a^{\boldsymbol{x}}\, dA, \tag{3.4}$$

where the Piola-Kirchhoff stress above will be evaluated in accordance with each of the formulations presented in Section 2.6. Similar expressions for other residual terms can be easily derived. For instance, the geometric compatibility residuals

emerge from the discretisation of equations (2.184) or (2.195) as

$$\begin{gathered}\boldsymbol{R}^a_{\boldsymbol{\Sigma_F}} = \int_V (\boldsymbol{F}_x - \boldsymbol{F})\, N^{\boldsymbol{F}}_a \, dV; \quad \boldsymbol{R}^a_{\boldsymbol{\Sigma_H}} = \int_V (\boldsymbol{H}_x - \boldsymbol{H})\, N^{\boldsymbol{H}}_a \, dV; \\ \boldsymbol{R}^a_{\Sigma_J} = \int_V (J_x - J)\, N^J_a \, dV.\end{gathered} \tag{3.5}$$

Very similar equations emerge in the case of the mixed potential for the constitutive equation residuals

$$\begin{gathered}\boldsymbol{R}^a_{\boldsymbol{F}} = \int_V \left(\frac{\partial W}{\partial \boldsymbol{F}} - \boldsymbol{\Sigma_F}\right) N^{\boldsymbol{F}}_a \, dV; \quad \boldsymbol{R}^a_{\boldsymbol{H}} = \int_V \left(\frac{\partial W}{\partial \boldsymbol{H}} - \boldsymbol{\Sigma_H}\right) N^{\boldsymbol{H}}_a \, dV; \\ \boldsymbol{R}^a_J = \int_V \left(\frac{\partial W}{\partial J} - \Sigma_J\right) N^J_a \, dV.\end{gathered} \tag{3.6}$$

In order to complete the finite element formulation it is necessary to derive equations for the components of the tangent matrix by discretising the tangent operators defined in the previous section. For the case of the mixed variational principle Π_M (2.180), the resulting matrix operator can be represented as

$$D^2\Pi_M\left[\delta\boldsymbol{u}, \delta\boldsymbol{D}, \delta\boldsymbol{\Sigma}; \boldsymbol{u}, \Delta\boldsymbol{D}, \Delta\boldsymbol{\Sigma}\right] = \begin{bmatrix}\delta\boldsymbol{u} & \delta\boldsymbol{D} & \delta\boldsymbol{\Sigma}\end{bmatrix} \begin{bmatrix}\boldsymbol{K_{xx}} & \boldsymbol{0} & \boldsymbol{K_{x\Sigma}} \\ \boldsymbol{0} & \boldsymbol{K_{DD}} & \boldsymbol{K_{D\Sigma}} \\ \boldsymbol{K_{\Sigma x}} & \boldsymbol{K_{\Sigma D}} & \boldsymbol{0}\end{bmatrix} \begin{bmatrix}\boldsymbol{u} \\ \Delta\boldsymbol{D} \\ \Delta\boldsymbol{\Sigma}\end{bmatrix}, \tag{3.7}$$

where $\boldsymbol{D} = \{\boldsymbol{F}_a, \boldsymbol{H}_a, J_a\}$ denotes the set of strain variables and $\boldsymbol{\Sigma} = \{\boldsymbol{\Sigma_{F}}a, \boldsymbol{\Sigma_{H}}a, \Sigma_{J}a\}$ denotes the set of stress conjugate variables. Alternatively, for the case of a mixed complementary energy functional Π_C in (2.193), the matrix operator for the complementary energy functional yields

$$D^2\Pi_C\left[\delta\boldsymbol{u}, \delta\boldsymbol{\Sigma}; \boldsymbol{u}, \Delta\boldsymbol{\Sigma}\right] = \begin{bmatrix}\delta\boldsymbol{u} & \delta\boldsymbol{\Sigma}\end{bmatrix} \begin{bmatrix}\boldsymbol{K_{xx}} & \boldsymbol{K_{x\Sigma}} \\ \boldsymbol{K_{\Sigma x}} & \boldsymbol{K_{\Sigma\Sigma}}\end{bmatrix} \begin{bmatrix}\boldsymbol{u} \\ \Delta\boldsymbol{\Sigma}\end{bmatrix}. \tag{3.8}$$

Some of the terms in the above matrices are very straightforward to obtain. For instance the term $\boldsymbol{K_{D\Sigma}}$ relating stresses and strains in equation (6.37) follows from the discretisation of the corresponding tangent operator component given in equation (2.189) as

$$\boldsymbol{K}^{ab}_{\boldsymbol{D\Sigma}} = -\int_V \begin{bmatrix}N^{\boldsymbol{F}}_a N^{\boldsymbol{F}}_b \boldsymbol{\mathcal{I}} & \boldsymbol{0} & \boldsymbol{0} \\ \boldsymbol{0} & N^{\boldsymbol{H}}_a N^{\boldsymbol{H}}_b \boldsymbol{\mathcal{I}} & \boldsymbol{0} \\ \boldsymbol{0} & \boldsymbol{0} & N^J_a N^J_b \boldsymbol{\mathcal{I}}\end{bmatrix} dV, \tag{3.9}$$

The diagonal components of the tangent matrices (6.37) and (3.8) associated with strains or stresses, $\boldsymbol{K_{DD}}$ and $\boldsymbol{K_{\Sigma\Sigma}}$ respectively, can be obtained from the discretisation of the corresponding Hessian term in the tangent operator. For instance, the

strain term becomes

$$\boldsymbol{K}^{ab}_{\boldsymbol{DD}} = \int_V \begin{bmatrix} N^{\boldsymbol{F}}_a N^{\boldsymbol{F}}_b W_{\boldsymbol{FF}} & N^{\boldsymbol{F}}_a N^{\boldsymbol{H}}_b W_{\boldsymbol{FH}} & N^{\boldsymbol{F}}_a N^{J}_b W_{\boldsymbol{F}J} \\ N^{\boldsymbol{H}}_a N^{\boldsymbol{F}}_b H_{\boldsymbol{HF}} & N^{\boldsymbol{H}}_a N^{\boldsymbol{H}}_b H_{\boldsymbol{HH}} & N^{\boldsymbol{H}}_a N^{J}_b H_{\boldsymbol{H}J} \\ N^{J}_a N^{\boldsymbol{F}}_b H_{J\boldsymbol{F}} & N^{J}_a N^{\boldsymbol{H}}_b H_{J\boldsymbol{H}} & N^{J}_a N^{J}_b H_{JJ} \end{bmatrix} dV, \tag{3.10}$$

and the corresponding tangent stress term

$$\boldsymbol{K}^{ab}_{\boldsymbol{\Sigma\Sigma}} = -\int_V \begin{bmatrix} N^{\boldsymbol{F}}_a N^{\boldsymbol{F}}_b \Upsilon_{\boldsymbol{\Sigma_F\Sigma_F}} & N^{\boldsymbol{F}}_a N^{\boldsymbol{H}}_b \Upsilon_{\boldsymbol{\Sigma_F\Sigma_H}} & N^{\boldsymbol{F}}_a N^{J}_b \Upsilon_{\boldsymbol{\Sigma_F}\Sigma_J} \\ N^{\boldsymbol{H}}_a N^{\boldsymbol{F}}_b \Upsilon_{\boldsymbol{\Sigma_H\Sigma_F}} & N^{\boldsymbol{H}}_a N^{\boldsymbol{H}}_b \Upsilon_{\boldsymbol{\Sigma_H\Sigma_H}} & N^{\boldsymbol{H}}_a N^{J}_b \Upsilon_{\boldsymbol{\Sigma_H}\Sigma_J} \\ N^{J}_a N^{\boldsymbol{F}}_b \Upsilon_{\Sigma_J\boldsymbol{\Sigma_F}} & N^{J}_a N^{\boldsymbol{H}}_b \Upsilon_{\Sigma_J\boldsymbol{\Sigma_H}} & N^{J}_a N^{J}_b \Upsilon_{\Sigma_J\Sigma_J} \end{bmatrix} dV. \tag{3.11}$$

The final two terms of the tangent matrix involve derivatives with respect to geometry and require more careful analysis. Consider first the top diagonal component $\boldsymbol{K}_{\boldsymbol{xx}}$. This term emerges from the discretisation of the initial stress component of the tangent operator defined in equation (2.187). After discretisation and some simple algebra using property (2.20) of the tensor cross product, the component relating nodes a, b of this operator becomes

$$\begin{aligned} D^2_{1,1}\Pi_M\left[\delta\boldsymbol{u}_a N^{\boldsymbol{x}}_a; \boldsymbol{u}_b N^{\boldsymbol{x}}_b\right] &= \int_V \left(\boldsymbol{\Sigma_H} + \Sigma_J \boldsymbol{F_x}\right) : \left[\left(\delta\boldsymbol{u}_a \otimes \boldsymbol{\nabla}_0 N^{\boldsymbol{x}}_a\right) \boldsymbol{\times} \left(\boldsymbol{u}_b \otimes \boldsymbol{\nabla}_0 N^{\boldsymbol{x}}_b\right)\right] dV \\ &= \int_V \left(\boldsymbol{\Sigma_H} + \Sigma_J \boldsymbol{F_x}\right) : \left[\left(\delta\boldsymbol{u}_a \times \boldsymbol{u}_b\right) \otimes \left(\boldsymbol{\nabla}_0 N^{\boldsymbol{x}}_a \times \boldsymbol{\nabla}_0 N^{\boldsymbol{x}}_b\right)\right] dV \\ &= \left(\delta\boldsymbol{u}_a \times \boldsymbol{u}_b\right) \cdot \int_V \left(\boldsymbol{\Sigma_H} + \Sigma_J \boldsymbol{F_x}\right) \left(\boldsymbol{\nabla}_0 N^{\boldsymbol{x}}_a \times \boldsymbol{\nabla}_0 N^{\boldsymbol{x}}_b\right) dV \\ &= \left(\delta\boldsymbol{u}_a \times \boldsymbol{u}_b\right) \cdot \boldsymbol{k}^{ab}_{\boldsymbol{xx}} = \delta\boldsymbol{u}_a \cdot \boldsymbol{K}^{ab}_{\boldsymbol{xx}} \boldsymbol{u}_b, \end{aligned} \tag{3.12}$$

with initial stress vector $\boldsymbol{k}^{ab}_{\boldsymbol{xx}}$ and equivalent skew symmetric matrix $\boldsymbol{K}^{ab}_{\boldsymbol{xx}}$

$$\begin{aligned} \boldsymbol{k}^{ab}_{\boldsymbol{xx}} &= \int_V \left(\boldsymbol{\Sigma_H} + \Sigma_J \boldsymbol{F_x}\right) \left(\boldsymbol{\nabla}_0 N^{\boldsymbol{x}}_a \times \boldsymbol{\nabla}_0 N^{\boldsymbol{x}}_b\right) dV; \\ \left[\boldsymbol{K}^{ab}_{\boldsymbol{xx}}\right]_{ij} &= \mathcal{E}_{ijk} \left[\boldsymbol{k}^{ab}_{\boldsymbol{xx}}\right]_k. \end{aligned} \tag{3.13}$$

Similar derivations starting from equation (2.190) yield the final component relating geometry changes to stress changes $\boldsymbol{K}_{\boldsymbol{x\Sigma}}$. For clarity, however, the terms relating to each one of the conjugate stresses is derived individually. The first term relating geometry to conjugate stress $\boldsymbol{\Sigma_F}$ is obtained as

$$\begin{aligned} D^2_{\boldsymbol{x};\boldsymbol{\Sigma_F}}\Pi_M\left[\delta\boldsymbol{u}_a N^{\boldsymbol{x}}_a; \Delta\boldsymbol{\Sigma}^b_{\boldsymbol{F}} N^{\boldsymbol{F}}_b\right] &= \int_V \left(\delta\boldsymbol{u}_a \otimes \boldsymbol{\nabla}_0 N^{\boldsymbol{x}}_a\right) : \Delta\boldsymbol{\Sigma}^b_{\boldsymbol{F}} N^{\boldsymbol{F}}_b \, dV \\ &= \delta\boldsymbol{u}_a \cdot \left[\int_V \left(\boldsymbol{I} \otimes \boldsymbol{\nabla}_0 N^{\boldsymbol{x}}_a\right) N^{\boldsymbol{F}}_b \, dV\right] : \Delta\boldsymbol{\Sigma}^b_{\boldsymbol{F}} \\ &= \delta\boldsymbol{u}_a \cdot \boldsymbol{\mathcal{K}}^{ab}_{\boldsymbol{x\Sigma_F}} : \Delta\boldsymbol{\Sigma}^b_{\boldsymbol{F}}, \end{aligned} \tag{3.14}$$

where the third order tensor $\boldsymbol{\mathcal{K}}^{ab}_{\boldsymbol{x}\boldsymbol{\Sigma}_{\boldsymbol{F}}}$ is

$$\boldsymbol{\mathcal{K}}^{ab}_{\boldsymbol{x}\boldsymbol{\Sigma}_{\boldsymbol{F}}} = \int_V (\boldsymbol{I} \otimes \boldsymbol{\nabla}_0 N^{\boldsymbol{x}}_a)\, N^{\boldsymbol{F}}_b \, dV. \tag{3.15}$$

The third term relating geometry to conjugate stress Σ_J is obtained as

$$\begin{aligned} D^2_{\boldsymbol{x};\Sigma_J}\Pi_M \left[\delta\boldsymbol{u}_a N^{\boldsymbol{x}}_a; \Delta\Sigma^b_J N^J_b\right] =& \int_V \Delta\Sigma^b_J N^J_b \boldsymbol{H}_{\boldsymbol{x}} : (\delta\boldsymbol{u}_a \otimes \boldsymbol{\nabla}_0 N^{\boldsymbol{x}}_a)\, dV \\ =& \delta\boldsymbol{u}_a \cdot \left[\int_V N^J_b \boldsymbol{H}_{\boldsymbol{x}} \boldsymbol{\nabla}_0 N^{\boldsymbol{x}}_a \, dV\right] \Delta\Sigma^b_J \\ =& \delta\boldsymbol{u}_a \cdot \boldsymbol{k}^{ab}_{\boldsymbol{x}\Sigma_J} \Delta\Sigma^b_J, \end{aligned} \tag{3.16}$$

where the vector $\boldsymbol{k}^{ab}_{\boldsymbol{x}\Sigma_J}$ is

$$\boldsymbol{k}^{ab}_{\boldsymbol{x}\Sigma_J} = \int_V N^J_b \boldsymbol{H}_{\boldsymbol{x}} \boldsymbol{\nabla}_0 N^{\boldsymbol{x}}_a \, dV. \tag{3.17}$$

Finally, the term relating geometry to changes in $\boldsymbol{\Sigma}_{\boldsymbol{H}}$ is

$$\begin{aligned} D^2_{\boldsymbol{x};\boldsymbol{\Sigma}_{\boldsymbol{H}}}\Pi_M \left[\delta\boldsymbol{u}_a N^{\boldsymbol{x}}_a; \Delta\boldsymbol{\Sigma}^b_{\boldsymbol{H}} N^{\boldsymbol{H}}_b\right] =& \int_V [\boldsymbol{F}_{\boldsymbol{x}} \boldsymbol{\times} (\delta\boldsymbol{u}_a \otimes \boldsymbol{\nabla}_0 N^{\boldsymbol{x}}_a)] : \Delta\boldsymbol{\Sigma}^b_{\boldsymbol{H}} N^{\boldsymbol{H}}_b \, dV \\ =& -\delta\boldsymbol{u}_a \boldsymbol{\times} \left[\int_V (\boldsymbol{F}_{\boldsymbol{x}} \boldsymbol{\times} \boldsymbol{\nabla}_0 N^{\boldsymbol{x}}_a)\, N^{\boldsymbol{H}}_b \, dV\right] : \Delta\boldsymbol{\Sigma}^b_{\boldsymbol{H}} \\ =& \delta\boldsymbol{u}_a \cdot \boldsymbol{\mathcal{K}}^{ab}_{\boldsymbol{x}\boldsymbol{\Sigma}_{\boldsymbol{H}}} : \Delta\boldsymbol{\Sigma}^b_{\boldsymbol{H}}, \end{aligned} \tag{3.18}$$

where property (2.22) has been made use of, leading to

$$\left[\boldsymbol{\mathcal{K}}^{ab}_{\boldsymbol{x}\boldsymbol{\Sigma}_{\boldsymbol{H}}}\right]_{ijI} = \mathcal{E}_{ijk} \left[\int_V (\boldsymbol{F}_{\boldsymbol{x}} \boldsymbol{\times} \boldsymbol{\nabla}_0 N^{\boldsymbol{x}}_a)\, N^{\boldsymbol{H}}_b \, dV\right]_{kI}, \tag{3.19}$$

where equation (2.3) has been used.

3.2.2 Complementary energy application case

The equations provided above can be implemented using a variety of finite element spaces. Of course, not all choices will lead to effective or valid finite element formulations. Moreover, the cost of implementation of mixed formulation may be significantly higher than that of standard displacement based approaches given the number of additional unknowns created. However, careful analysis of the continuity required for each of the variables, shows that only displacements need to be continuous across elements. Stress and strain variables can actually be discretised

independently on each element of the mesh. This enables a static condensation process to be carried out before assembly of the global tangent matrix. In order to illustrate this process and as an example of the complementary energy formulation proposed, this section describes a choice of interpolation functions that permits such a condensation. In particular, a quadratic tetrahedron element is proposed for the geometry discretisation, with linear element by element interpolations for the stresses conjugate to the deformation gradient and its co-factor and a constant interpolation for the stress conjugate to the Jacobian (refer to Figure 3.2). The resulting element is very similar to that proposed in reference [40]. These authors propose instead a formulation in terms of the Lagrangian variables $\{\boldsymbol{C}, \boldsymbol{G}, C\}$ (refer to Section 2.4.1) and their respective work conjugates, namely $\{\boldsymbol{\Sigma_C}, \boldsymbol{\Sigma_G}, \Sigma_C\}$, where the variables $\{\boldsymbol{C}, \boldsymbol{\Sigma_C}\}$ are not treated as independent variables, but obtained from the geometry, namely $\boldsymbol{C} = \boldsymbol{C_x}$ and also from other independent variables, namely $\boldsymbol{\Sigma_C} = \boldsymbol{\Sigma_C}(\boldsymbol{C_x}, \boldsymbol{G}, C)$ (with $\{\boldsymbol{G}, C\}$ and their associated work conjugates being treated as independent variables).

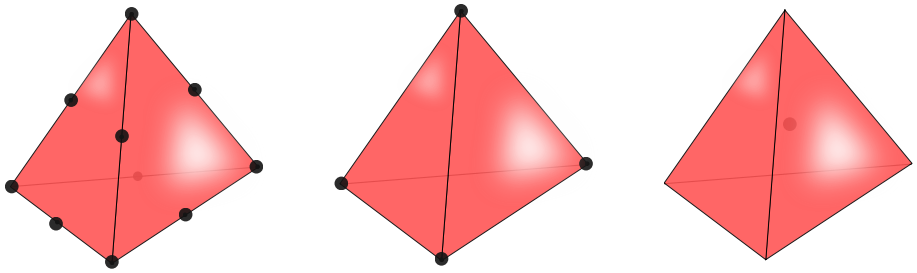

Figure 3.2: Finite Element interpolation for the Hu-Washizu mixed variational principle in Section 2.6.2 and for the Hellinger-Reissner mixed variational principle in Section 2.6.3. From left fo rigth: continuous quadratic interpolation for displacements; linear discontinuous interpolation for $\{\boldsymbol{F}, \boldsymbol{H}\}$ and $\{\boldsymbol{\Sigma_F}, \boldsymbol{\Sigma_H}\}$; constant interpolation for J and Σ_J.

The resulting formulation is obtained by applying the set of equations derived in the previous section with shape functions $N_a^{\boldsymbol{x}}$ $(a = 1, ..., 10)$ that are quadratic and continuous across elements, $N_a^{\boldsymbol{F}} = N_a^{\boldsymbol{H}}$ $(a = 1, ..., 4)$ linear and discontinuous across elements and N_a^J $(a = 1)$ constant and discontinuous across elements. The fact that the shape functions associated with stresses are discontinuous across elements allows for the elimination of stress unknowns inside each element to take place. In order to illustrate this, for a given element the system of equations to be solved can be written as

$$\begin{bmatrix} \boldsymbol{K}^e_{\boldsymbol{xx}} & \boldsymbol{K}^e_{\boldsymbol{x\Sigma}} \\ \boldsymbol{K}^e_{\boldsymbol{\Sigma x}} & \boldsymbol{K}^e_{\boldsymbol{\Sigma\Sigma}} \end{bmatrix} \begin{bmatrix} \boldsymbol{u}^e \\ \Delta\boldsymbol{\Sigma}^e \end{bmatrix} = - \begin{bmatrix} \boldsymbol{R}^e_{\boldsymbol{x}} \\ \boldsymbol{R}^e_{\boldsymbol{\Sigma}} \end{bmatrix}. \tag{3.20}$$

The second row of equations enables the stress increments to be expressed in terms of displacements as

$$\Delta\boldsymbol{\Sigma}^e = - \left[\boldsymbol{K}^e_{\boldsymbol{\Sigma\Sigma}}\right]^{-1} \left(\boldsymbol{K}^e_{\boldsymbol{\Sigma x}} \boldsymbol{u}^e + \boldsymbol{R}^e_{\boldsymbol{\Sigma}}\right). \tag{3.21}$$

Substituting this relationship into the first row of equation (3.20) gives an augmented set of equations for the displacement vector

$$\begin{aligned} \bar{\boldsymbol{K}}^e_{\boldsymbol{x}\boldsymbol{x}} \boldsymbol{u}^e &= -\,\bar{\boldsymbol{R}}^e_{\boldsymbol{x}}; \\ \bar{\boldsymbol{K}}^e_{\boldsymbol{x}\boldsymbol{x}} = \boldsymbol{K}^e_{\boldsymbol{x}\boldsymbol{x}} - \boldsymbol{K}^e_{\boldsymbol{x}\boldsymbol{\Sigma}} \left[\boldsymbol{K}^e_{\boldsymbol{\Sigma}\boldsymbol{\Sigma}}\right]^{-1} \boldsymbol{K}^e_{\boldsymbol{\Sigma}\boldsymbol{x}}; &\quad \bar{\boldsymbol{R}}^e_{\boldsymbol{x}} = \boldsymbol{R}^e_{\boldsymbol{x}} - \boldsymbol{K}^e_{\boldsymbol{x}\boldsymbol{\Sigma}} \left[\boldsymbol{K}^e_{\boldsymbol{\Sigma}\boldsymbol{\Sigma}}\right]^{-1} \boldsymbol{R}^e_{\boldsymbol{\Sigma}} \end{aligned}. \tag{3.22}$$

This augmented stiffness matrix and residual vector can now be assembled into a global system in the usual finite element manner.

3.2.3 Stabilised linear tetrahedron for incompressible elasticity

As a final case study of the application of the present framework, a linear tetrahedron for modelling full incompressible elasticity is described. This will also serve as an example of the introduction of a Petrov-Galerkin type of stabilisation to a mixed formulation in which the discretisation spaces do not satisfy the LBB condition. In the proposed formulation, both the geometry and pressure are discretised using linear tetrahedral elements in terms of the same standard shape functions N_a as

$$\boldsymbol{x} = \sum_{a=1}^{4} \boldsymbol{x}_a N_a; \quad p = \sum_{a=1}^{4} p_a N_a. \tag{3.23}$$

Note that in this case the pressure is continuous across elements and therefore cannot be eliminated locally. This adds to the number of global degrees of freedom but the resulting tetrahedron will be capable of simulating incompressible deformations without locking [97]. Unfortunately, it is well know that an incompressible mixed formulation with linear displacements and linear pressures on tetrahedral element spaces does not satisfy the necessary LBB condition and leads to unstable solutions [14]. The classical solution to this problem is to introduce a Petrov-Galerkin stabilisation [58, 84, 97, 98]. This is done by defining the stabilised virtual pressure and velocity as

$$\delta p^{st} = \delta p - \tau_p \left(\boldsymbol{H}_{\boldsymbol{x}} : \boldsymbol{\nabla}_0 \delta \boldsymbol{u}\right); \tag{3.24a}$$

$$\delta \boldsymbol{u}^{st} = \delta \boldsymbol{u} - \tau_{\boldsymbol{v}} \left(\boldsymbol{H}_{\boldsymbol{x}} \boldsymbol{\nabla}_0 \delta p\right). \tag{3.24b}$$

Note that in the usual Petrov-Galerkin manner, the term in parenthesis in (3.24a) is the derivative of the constraint equation $\det \boldsymbol{\nabla}_0 \boldsymbol{x} = 1$ and that τ_p has the same units as an elastic constant. The stabilised term in (3.24b) is defined following [84], namely $\tau_{\boldsymbol{v}} = \frac{\alpha h^2}{2\mu}$, where μ is an elastic constant, h is the mesh size and α is a non-dimensional stabilisation parameter. Substituting expression (3.24a) into the constraint equation (2.204) leads to an additional term in the principle of virtual work (2.200) as

$$D_1 \hat{\Pi}^{st}_M \left[\delta \boldsymbol{u}\right] = \int_V \boldsymbol{P}_{st} : \boldsymbol{\nabla}_0 \delta \boldsymbol{u} \, dV - \int_V \boldsymbol{f}_0 \cdot \delta \boldsymbol{u} \, dV - \int_{\partial_t V} \boldsymbol{t}_0 \cdot \delta \boldsymbol{u} \, dA = 0, \tag{3.25}$$

where the stabilised first Piola-Kirchhoff tensor is

$$\boldsymbol{P}_{st} = \boldsymbol{\Sigma}^{\boldsymbol{x}}_{\boldsymbol{F}} + \boldsymbol{\Sigma}^{\boldsymbol{x}}_{\boldsymbol{H}} \times \boldsymbol{F}_{\boldsymbol{x}} + \Sigma^{st}_{J} \boldsymbol{H}_{\boldsymbol{x}}; \quad \Sigma^{st}_{J} = \hat{\Sigma}^{\boldsymbol{x}}_{J} + p + \tau_p \left(J_{\boldsymbol{x}} - 1 \right). \tag{3.26}$$

Substituting equation (3.24b) into the principle of virtual work (2.200) leads to an additional term in the constraint equation (2.204) (after grouping all terms multiplying δp),

$$D_2 \hat{\Pi}^{st}_{M} \left[\delta p \right] = \int_V \delta p \left(J_{\boldsymbol{x}} - 1 \right) \, dV - \int_V \tau_{\boldsymbol{v}} \left(\boldsymbol{H}_{\boldsymbol{x}} \boldsymbol{\nabla}_0 \delta p \right) \cdot \left(\boldsymbol{H}_{\boldsymbol{x}} \boldsymbol{\nabla}_0 p \right) \, dV. \tag{3.27}$$

Clearly, as the mesh is refined and the enforcement of the volumetric constraint is improved, the stabilisation terms in (3.26) and (3.27) will tend to zero. Introducing the discretisation equations for the geometry and pressure gives the equilibrium and constraints residuals as

$$\boldsymbol{R}^a_{\boldsymbol{x}} = \int_V \boldsymbol{P}_{st} \boldsymbol{\nabla}_0 N_a \, dV - \int_V \boldsymbol{f}_0 N^{\boldsymbol{x}}_a \, dV - \int_{\partial_t V} \boldsymbol{t}_0 N^{\boldsymbol{x}}_a \, dA; \tag{3.28a}$$

$$R^a_p = \int_V \left(J_{\boldsymbol{x}} - 1 \right) N_a \, dv - \int_V \tau_{\boldsymbol{v}} \left(\boldsymbol{H}_{\boldsymbol{x}} \boldsymbol{\nabla}_0 N_a \right) \cdot \left(\boldsymbol{H}_{\boldsymbol{x}} \boldsymbol{\nabla}_0 p \right) \, dV. \tag{3.28b}$$

The system of liner equations to be solved at each Newton-Raphson iteration is now expressed globally as

$$\begin{bmatrix} \boldsymbol{K}^{st}_{\boldsymbol{xx}} & \boldsymbol{k}_{\boldsymbol{x}p} \\ \boldsymbol{k}^{st}_{p\boldsymbol{x}} & \boldsymbol{k}^{st}_{pp} \end{bmatrix} \begin{bmatrix} \boldsymbol{u} \\ \Delta \boldsymbol{p} \end{bmatrix} = - \begin{bmatrix} \boldsymbol{R}_{\boldsymbol{x}} \\ \boldsymbol{R}_p \end{bmatrix}. \tag{3.29}$$

The off-diagonal term $\boldsymbol{k}_{\boldsymbol{x}p}$ of (3.29) is in fact identical to that obtained in the previous section relating the volumetric stress and geometry via equation (3.17), that is

$$\boldsymbol{k}^{ab}_{\boldsymbol{x}p} = \int_V N_b \boldsymbol{H}_{\boldsymbol{x}} \boldsymbol{\nabla}_0 N_a \, dV. \tag{3.30}$$

The diagonal component $\boldsymbol{K}^{st}_{\boldsymbol{xx}}$ in the above tangent matrix can be broken down into three terms: a constitutive component due to the Hessian of the isochoric strain energy $\hat{W}$, an initial stress term similar to that derived in equation (3.13) plus a contribution from geometric derivative of the stabilisation term $\tau_p \left(J_{\boldsymbol{x}} - 1 \right)$, that is

$$\boldsymbol{K}^{st}_{\boldsymbol{xx}} = \left(\boldsymbol{K}_{\hat{W}} + \boldsymbol{K}_0 + \boldsymbol{K}_{\tau_p} \right). \tag{3.31}$$

The stabilisation component is easily evaluated for equations (3.25) and (3.26)

as

$$\begin{aligned}\delta\boldsymbol{u}_a \cdot \boldsymbol{K}^{ab}_{\tau_p}\boldsymbol{u}_b &= \int_V \tau_p \left[\boldsymbol{H}_{\boldsymbol{x}} : (\delta\boldsymbol{u}_a \otimes \boldsymbol{\nabla}_0 N_a)\right] DJ_{\boldsymbol{x}}\left[\boldsymbol{u}_b N_b\right]\, dV \\ &= \int_V \tau_p \left[\boldsymbol{H}_{\boldsymbol{x}} : (\delta\boldsymbol{u}_a \otimes \boldsymbol{\nabla}_0 N_a)\right]\left[\boldsymbol{H}_{\boldsymbol{x}} : (\boldsymbol{u}_b \otimes \boldsymbol{\nabla}_0 N_b)\right]\, dV \\ &= \int_V \tau_p \left(\delta\boldsymbol{u}_a \cdot \boldsymbol{H}_{\boldsymbol{x}}\boldsymbol{\nabla}_0 N_a\right)\left(\boldsymbol{u}_b \cdot \boldsymbol{H}_{\boldsymbol{x}}\boldsymbol{\nabla}_0 N_b\right)\, dV \\ &= \delta\boldsymbol{u}_a \cdot \left[\int_V \tau_p \left(\boldsymbol{H}_{\boldsymbol{x}}\boldsymbol{\nabla}_0 N_a\right) \otimes \left(\boldsymbol{H}_{\boldsymbol{x}}\boldsymbol{\nabla}_0 N_b\right)\, dV\right]\boldsymbol{u}_b,\end{aligned} \tag{3.32}$$

where equation (2.29) has been made use of, leading to

$$\boldsymbol{K}^{ab}_{\tau_p} = \int_V \tau_p \left(\boldsymbol{H}_{\boldsymbol{x}}\boldsymbol{\nabla}_0 N_a\right) \otimes \left(\boldsymbol{H}_{\boldsymbol{x}}\boldsymbol{\nabla}_0 N_b\right)\, dV. \tag{3.33}$$

The initial stress component is given by equation (3.13) with a volumetric stress component that includes the additional stabilisation term, that is

$$\begin{aligned}\boldsymbol{k}^{ab}_0 &= \int_V \left(\boldsymbol{\Sigma}_{\boldsymbol{H}} + \Sigma_J \boldsymbol{F}_x\right)\left(\boldsymbol{\nabla}_0 N_a \times \boldsymbol{\nabla}_0 N_b\right)\, dV; \\ \left[\boldsymbol{K}^{ab}_0\right]_{ij} &= \mathcal{E}_{ijk}\left[\boldsymbol{k}^{ab}_0\right]_k.\end{aligned} \tag{3.34}$$

Finally, the constitutive component is given by the Hessian of the isochoric strain energy as

$$\delta\boldsymbol{u}_a \cdot \boldsymbol{K}^{ab}_{\hat{W}}\boldsymbol{u}_b = \int_V \left[D\boldsymbol{F}_{\boldsymbol{x}}\left[\delta\boldsymbol{u}_a N_a\right] : \quad D\boldsymbol{H}_{\boldsymbol{x}}\left[\delta\boldsymbol{u}_a N_a\right] : \quad DJ_{\boldsymbol{x}}\left[\delta\boldsymbol{u}_a N_a\right]\right]\left[\mathbb{H}_{\hat{W}}\right]\begin{bmatrix} : D\boldsymbol{F}_{\boldsymbol{x}}\left[\boldsymbol{u}_b N_b\right] \\ : D\boldsymbol{H}_{\boldsymbol{x}}\left[\boldsymbol{u}_b N_b\right] \\ DJ_{\boldsymbol{x}}\left[\boldsymbol{u}_b N_b\right]\end{bmatrix} dV. \tag{3.35}$$

The off-diagonal term $\boldsymbol{k}^{st}_{p\boldsymbol{x}}$ in (3.29) can be broken down into three terms stemming from the linearisation of the right hand side of equation (3.27) with respect to the geometry, that is

$$\boldsymbol{k}^{st}_{p\boldsymbol{x}} = \boldsymbol{k}_J - \boldsymbol{k}_{\boldsymbol{H}_1} - \boldsymbol{k}_{\boldsymbol{H}_2}, \tag{3.36}$$

where

$$\delta p_a \boldsymbol{k}^{ab}_J \cdot \boldsymbol{u}_b = \int_V \delta p_a N_a DJ_{\boldsymbol{x}}\left[\boldsymbol{u}_b N_b\right] dV = \delta p_a \left[\int_V N_a \boldsymbol{H}_{\boldsymbol{x}}\boldsymbol{\nabla}_0 N_b\, dV\right]\boldsymbol{u}_b, \tag{3.37}$$

which gives

$$\boldsymbol{k}^{ab}_J = \int_V N_a \boldsymbol{H}_{\boldsymbol{x}}\boldsymbol{\nabla}_0 N_b\, dV. \tag{3.38}$$

Computation of the directional derivative of the second term on the right hand side of equation (3.27) is split into two terms, corresponding to the liearisation of each of the cofactor terms $\boldsymbol{H}_{\boldsymbol{x}}$ featuring in the integrand. The first term (with the help of properties (2.11) and (2.15)) yields

$$\begin{aligned}
\delta p_a \boldsymbol{k}^{ab}_{\boldsymbol{H}_1} \cdot \boldsymbol{u}_b &= \delta p_a \int_V \tau_{\boldsymbol{v}} \left(\boldsymbol{H}_{\boldsymbol{x}} \boldsymbol{\nabla}_0 N_a\right) \cdot \left(D\boldsymbol{H}_{\boldsymbol{x}} \left[\boldsymbol{u}_b N_b\right] \boldsymbol{\nabla}_0 p\right) \, dV \\
&= \delta p_a \int_V \tau_{\boldsymbol{v}} \left(\boldsymbol{H}_{\boldsymbol{x}} \boldsymbol{\nabla}_0 N_a\right) \cdot \left[\left(\boldsymbol{F}_{\boldsymbol{x}} \times \left(\boldsymbol{u}_b \otimes \boldsymbol{\nabla}_0 N_b\right)\right) \boldsymbol{\nabla}_0 p\right] \, dV \\
&= \delta p_a \int_V \tau_{\boldsymbol{v}} \left[\left(\boldsymbol{H}_{\boldsymbol{x}} \boldsymbol{\nabla}_0 N_a \otimes \boldsymbol{\nabla}_0 p\right) \times \boldsymbol{F}_{\boldsymbol{x}}\right] : \left(\boldsymbol{u}_b \otimes \boldsymbol{\nabla}_0 N_b\right) \, dV \\
&= \delta p_a \left[\int_V \tau_{\boldsymbol{v}} \left[\left(\boldsymbol{H}_{\boldsymbol{x}} \boldsymbol{\nabla}_0 N_a \otimes \boldsymbol{\nabla}_0 p\right) \times \boldsymbol{F}_{\boldsymbol{x}}\right] \boldsymbol{\nabla}_0 N_b \, dV\right] \cdot \boldsymbol{u}_b,
\end{aligned} \tag{3.39}$$

which gives

$$\boldsymbol{k}^{ab}_{\boldsymbol{H}_1} = \int_V \tau_{\boldsymbol{v}} \left[\left(\boldsymbol{H}_{\boldsymbol{x}} \boldsymbol{\nabla}_0 N_a \otimes \boldsymbol{\nabla}_0 p\right) \times \boldsymbol{F}_{\boldsymbol{x}}\right] \boldsymbol{\nabla}_0 N_b \, dV. \tag{3.40}$$

Analogously, the second term yields

$$\boldsymbol{k}^{ab}_{\boldsymbol{H}_2} = \int_V \tau_{\boldsymbol{v}} \left[\left(\boldsymbol{H}_{\boldsymbol{x}} \boldsymbol{\nabla}_0 p \otimes \boldsymbol{\nabla}_0 N_a\right) \times \boldsymbol{F}_{\boldsymbol{x}}\right] \boldsymbol{\nabla}_0 N_b \, dV. \tag{3.41}$$

Finally, the diagonal term $\boldsymbol{k}^{st}_{pp}$ is given as,

$$k^{st,ab}_{pp} = -\int_V \tau_{\boldsymbol{v}} \left(\boldsymbol{H}_{\boldsymbol{x}} \boldsymbol{\nabla}_0 N_a\right) \cdot \left(\boldsymbol{H}_{\boldsymbol{x}} \boldsymbol{\nabla}_0 N_b\right) \, dV. \tag{3.42}$$

3.3 Numerical examples

The objective of this section is to present a series of numerical examples in order to prove the robustness, accuracy and applicability of the computational framework presented above. Numerical results dealing with both compressible and incompressible polyconvex constitutive models will be presented.

For the compressible case, four different formulations are presented: i) a standard displacement $\{\boldsymbol{x}\}$ based formulation as described in Section 2.6.1, hereby denoted as **DF**; ii) a seven field $\{\boldsymbol{x}, \boldsymbol{F}, \boldsymbol{H}, J, \boldsymbol{\Sigma}_{\boldsymbol{F}}, \boldsymbol{\Sigma}_{\boldsymbol{H}}, \Sigma_J\}$ mixed formulation as described in Section 2.6.2, denoted as **M7F**; iii) a four field $\{\boldsymbol{x}, \boldsymbol{\Sigma}_{\boldsymbol{F}}, \boldsymbol{\Sigma}_{\boldsymbol{H}}, \Sigma_J\}$ mixed formulation based on the complementary energy principle described in Section 2.6.3, denoted by **MCF** and iv) an alternative five field $\{\boldsymbol{x}, \boldsymbol{H}, J, \boldsymbol{\Sigma}_{\boldsymbol{H}}, \Sigma_J\}$ mixed formulation, denoted as **M5F**. In this last case, the deformation gradient is enforced to coincide strongly with the material gradient of the spatial coordinates, namely $\boldsymbol{F} = \boldsymbol{\nabla}_0 \boldsymbol{x}$.

All of the numerical results presented correspond to the following selection of functional spaces: continuous quadratic interpolation of the displacement field (geometry) $\boldsymbol{x}$, piecewise linear interpolation of the strain and stress fields $\boldsymbol{F}$, $\boldsymbol{H}$, $\boldsymbol{\Sigma}_{\boldsymbol{F}}$ and $\boldsymbol{\Sigma}_{\boldsymbol{H}}$ and piecewise constant interpolation of the Jacobian J and its associated stress conjugate Σ_J. With these functional spaces, the three mixed formulations **M7F**, **MCF** and **M5F** will render identical results. Essentially, this is due to a combination of factors. For instance, the fact that the interpolation space for $\boldsymbol{F}$ coincides with the space of the material gradient of $\boldsymbol{x}$. In addition, the fact that in a Mooney-Rivlin material, the main kinematic variables $\boldsymbol{F}$ and $\boldsymbol{H}$ are linearly proportional to the conjugate stresses $\boldsymbol{\Sigma}_{\boldsymbol{F}}$ and $\boldsymbol{\Sigma}_{\boldsymbol{H}}$, respectively, implies that interpolating kinematic variables or stresses, as in the case of using complementary energy, will lead to the same results. This would not be the case if these relationships were heavily nonlinear.

For the incompressible case, a two field $\{\boldsymbol{x}, p\}$ mixed formulation is employed, as described in Section 2.6.4. In this case, two interpolations will be compared. First, a P1-P1 linear continuous interpolation for both displacement and pressure fields (e.g. with the help of stabilisation) and, second, a P2-P0 continuous quadratic interpolation for the displacement field and piecewise constant interpolation for the pressure field (e.g. without stabilisation). From the post-processing standpoint, the numerical results in terms of stresses will be reported for the Cauchy stress components $\boldsymbol{\sigma}$ and the hydrostatic pressure p (e.g. $p = \frac{1}{3}\boldsymbol{\sigma} : \boldsymbol{I}$). It is important to emphasise that their evaluation is carried out via equation (2.122).

3.3.1 Patch test

The first numerical example includes a standard three dimensional patch test in order to assess the correctness of the computational implementation. This problem was already presented in [40]. Two different polyconvex compressible constitutive models are considered. The first polyconvex model is a standard Mooney-Rivlin model, based on equation (2.40), as follows

$$W_s\left(\boldsymbol{F}, \boldsymbol{H}, J\right) = \alpha_s\left(\boldsymbol{F} : \boldsymbol{F}\right) + \beta_s\left(\boldsymbol{H} : \boldsymbol{H}\right) + f_s(J) \tag{3.43a}$$

$$f_s(J) = -4\beta_s \ln J - 2\alpha_s \ln J + \frac{\lambda_s}{2\varepsilon_s^2}\left(J^{\varepsilon_s} - J^{-\varepsilon_s}\right), \tag{3.43b}$$

where α_s, β_s, λ_s and ε_s are user defined material parameters given by

$$\alpha_s = 126kPa, \quad \beta_s = 252kPa, \quad \lambda_s = 81512kPa, \quad \varepsilon_s = 20. \tag{3.44}$$

A second polyconvex constitutive model, based on that presented in [40], is defined as follows,

$$W_q\left(\boldsymbol{F}, \boldsymbol{H}, J\right) = \alpha_q\left(\boldsymbol{F} : \boldsymbol{F}\right)^2 + \beta_q\left(\boldsymbol{H} : \boldsymbol{H}\right)^2 + f_q(J) \tag{3.45a}$$

$$f_q(J) = -24\beta_q \ln J - 12\alpha_q \ln J + \frac{\lambda_q}{2\varepsilon_q^2}\left(J^{\varepsilon_q} - J^{-\varepsilon_q}\right), \tag{3.45b}$$

where α_q, β_q, λ_q and ε_q are user defined material parameters. Note that for this second polyconvex model W_q, $\boldsymbol{F}$ and $\boldsymbol{H}$ can be expressed in terms of their respective conjugate stresses $\boldsymbol{\Sigma_F}$ and $\boldsymbol{\Sigma_H}$, respectively, as

$$\boldsymbol{F} = \left(\frac{1}{4\alpha_q(\boldsymbol{\Sigma_F} : \boldsymbol{\Sigma_F})}\right)^{1/3} \boldsymbol{\Sigma_F}; \qquad \boldsymbol{H} = \left(\frac{1}{4\beta_q\,(\boldsymbol{\Sigma_H} : \boldsymbol{\Sigma_H})}\right)^{1/3} \boldsymbol{\Sigma_H}. \tag{3.46a}$$

Above equations (3.46) enable the explicit computation of the strain variables in terms of their stress conjugates without having to resort to a numerical solution via a Newton-Raphson nonlinear solver. This will be of interest when using the complementary energy mixed formulation **MCF**. On the contrary, the Jacobian J can only be obtained in terms of its conjugate stress Σ_J after solving numerically above equations (3.43b) and (3.45b). The material parameters used for this constitutive model are taken as

$$\alpha_q = 21kPa, \quad \beta_q = 42kPa, \quad \lambda_q = 8000kPa, \quad \varepsilon_q = 20. \tag{3.47}$$

For both constitutive models W_s and W_q, the linear elasticity constitutive operator in the reference configuration renders the same material parameters, namely shear modulus $\mu = 756kPa$ and Poisson's ratio $\nu = 0.49546$. A homogeneous deformation mapping is defined through a stretch $\Delta L/L = 0.5$ in the OX direction, applied to a cubic shape domain of side L, as depicted in Figure 6.2. To achieve this deformation, non-zero normal Dirichlet boundary conditions are applied on the boundary faces perpendicular to the OX axis and zero normal Dirichlet boundary conditions are defined on two adjacent faces perpendicular to the OY and OZ axes. Zero Neumann boundary conditions are defined everywhere else.

The domain is discretised using two different meshes of $(2 \times 2 \times 2)\times 6$ tetrahedral elements. First, a structured mesh is shown in Figure 6.2(a) and, second, a distorted mesh is shown in Figure 6.2(b) (as presented in reference [40]) where the interior node is displaced randomly. The objective of this example is to demonstrate that the same solution is obtained for both meshes.

As expected, hence passing the patch test, for the three mixed formulations defined above, namely **M7F**, **MCF** and **M5F**, the results are identical for both meshes (the only numerical difference due to machine accuracy). Recall that for the **M5F** formulation, the deformation gradient is enforced to coincide strongly with the material gradient of the spatial coordinates. A resulting Cauchy stress component of $\sigma_{xx} = 929.9kPa$ is obtained for the model W_s and a value of $\sigma_{xx} = 1,087.4kPa$ is obtained for the model W_q, which is identical to that reported in reference [40]. The homogeneous deformation gradient tensors for both constitutive models, $\boldsymbol{F}_{W_s}$ and $\boldsymbol{F}_{W_q}$, are

$$\boldsymbol{F}_{W_s} = \begin{bmatrix} 1.5 & 0 & 0 \\ 0 & 0.8161 & 0 \\ 0 & 0 & 0.8161 \end{bmatrix}; \quad \boldsymbol{F}_{W_q} = \begin{bmatrix} 1.5 & 0 & 0 \\ 0 & 0.8170 & 0 \\ 0 & 0 & 0.8170 \end{bmatrix}. \tag{3.48}$$

For completeness, the quadratic convergence of the Newton-Raphson algorithm is displayed in Figure 3.4.

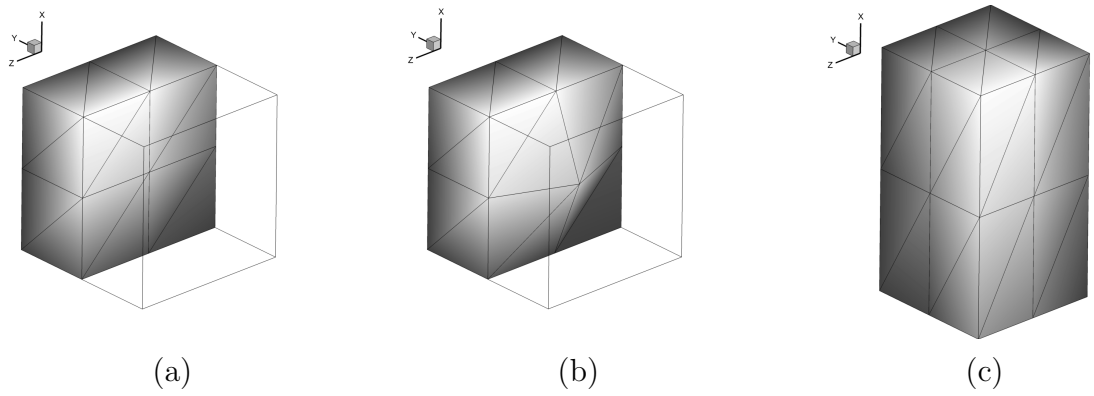

Figure 3.3: Three dimensional patch test. (a) View of half undistorted mesh in the reference configuration. (b) View of half distorted mesh in the reference configuration. (c) Example of deformed geometry after stretching of $\Delta L/L = 0.5$ in the OX direction for a Mooney-Rivlin model W_s defined in (3.43) with parameters defined in ((3.44)).

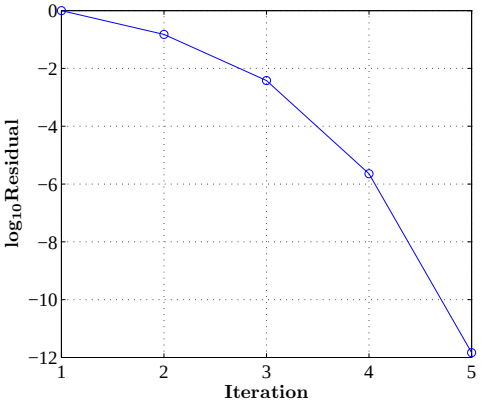

Figure 3.4: Three dimensional patch test. Quadratic convergence of the Newton-Raphson linearisation procedure.

3.3.2 Cook type cantilever problem.

In this section, we analyse the same problem presented in [40] where a Cook type cantilever problem of thickness $t = 10m$ is analysed. The geometry of the problem is shown in Figure 3.5(a) where, as it can be observed, the cantilever is clamped on its left end and subjected to an upwards parabolic shear force distribution applied on its right end of maximum value $\tau_{max} = 16kPa$. Note that this force is not considered to be a follower-load during the deformation process. The problem is analysed with two polyconvex compressible constitutive models. The first polyconvex model is given by a Mooney-Rivlin material defined as

$$W_p\left(\boldsymbol{F},\boldsymbol{H},J\right) = \alpha_p\left(\boldsymbol{F}:\boldsymbol{F}\right) + \beta_p\left(\boldsymbol{H}:\boldsymbol{H}\right) + f_p(J) \tag{3.49a}$$

$$f_p(J) = -4\beta_p \ln J - 2\alpha_p \ln J + \frac{\lambda_p}{2}\left(J-1\right)^2, \tag{3.49b}$$

where the material parameters are chosen as

$$\alpha_p = 126kPa, \quad \beta_p = 252kPa, \quad \lambda_p = 81512kPa. \tag{3.50}$$

The second polyconvex model, W_q, is identical to that presented in (3.45) with material parameters those in (3.47). This renders for both W_p and W_q models an identical linear elasticity operator in the reference state defined by a shear modulus $\mu = 756kPa$ and a Poisson's ratio $\nu = 0.49546$. The nearly incompressible nature of the material will emphasise the differences between the **DF** formulation and the alternative mixed formulations, particularly in terms of stresses. Notice that in the case of the polyconvex model defined by W_p, the stress conjugate Σ_J to the Jacobian J is obtained as

$$\Sigma_J = -\frac{2\left(\alpha_p + 2\beta_p\right)}{J} + \lambda_p\left(J-1\right). \tag{3.51}$$

Notice also that this simple expression enables, without the need to employ a Newton-Raphson procedure, to express directly the Jacobian J in terms of its conjugate stress Σ_J as follows

$$J = \frac{\left(\lambda_p + \Sigma_J\right) + \sqrt{\left(\lambda_p + \Sigma_J\right)^2 + 8\lambda_p\left(\alpha_p + 2\beta_p\right)}}{2\lambda_p}, \text{ if } \lambda_p > 0; \tag{3.52a}$$

$$J = -\frac{2\left(\alpha_p + 2\beta_p\right)}{\Sigma_J}, \text{ if } \lambda_p = 0. \tag{3.52b}$$

These expressions are particularly useful when using the complementary energy formulation **MCF**. Three discretisations are considered, namely coarse, medium and fine, comprised of $(7\times7\times5)\times6$, $(10\times10\times6)\times6$ and $(14\times14\times5)\times6$ tetrahedral elements, respectively. The fine mesh is displayed, as an example, in all of the numerical results presented in Figures 3.5(c)-(d) and thereafter. For completeness, Table 6.4 displays the discretisation details for each of the meshes employed. Notice how the number of degrees of freedom associated to the strain/stress variables is

Mesh	Elems.	Dofs. $\boldsymbol{x}$	Dofs. $\boldsymbol{F}, \boldsymbol{H}, \boldsymbol{\Sigma_F}, \boldsymbol{\Sigma_H}$	Dofs. J, Σ_J
Coarse	1,470	$2,475 \times 3$	$1,470 \times 4 \times 9$	$1,470 \times 1$
Medium	3,600	$5,730 \times 3$	$3,600 \times 4 \times 9$	$3,600 \times 1$
Fine	5,880	$9,251 \times 3$	$5,880 \times 4 \times 9$	$5,880 \times 1$

Table 3.1: Cook type cantilever problem. Mesh discretisation details. Column 2: number of tetrahedral elements (Elems.). Column 3: number of degrees of freedom (Dofs.) associated to the spatial coordinates $\boldsymbol{x}$. Column 4: number of degrees of freedom (Dofs.) associated to the strain/stress fields $\boldsymbol{F}, \boldsymbol{H}, \boldsymbol{\Sigma_F}, \boldsymbol{\Sigma_H}$. Column 5: number of degrees of freedom (Dofs.) associated to the strain/stress fields J, Σ_J.

proportional to the number of tetrahedral elements of the mesh. As stated in previous sections, these degrees of freedom are condensed out at an element level, not increasing then the size of the resulting discrete system of equations.

For the three discretisations and the two constitutive models above described, the four implementations **DF**, **M7F**, **MCF** and **M5F** where analysed. For instance, Figure 3.5(b) displays the stress field σ_{xx} for the fine discretisation and the constitutive model W_q by using the various mixed formulations (i.e. the three implementations render identical results).

Figures 3.5(c)-(d) display the contour plot of σ_{xx} using the constitutive model W_p and the fine discretisation. Results are presented comparing the mixed formulations, which render identical results (see Figure 3.5(c)) versus the **DF** formulation (see Figure 3.5(d)).

A more detailed comparison is established in Tables 6.5 and 3.3, where results obtained with the four formulations, namely the three mixed formulations and the **DF** formulation are displayed. Results are presented for both stresses and displacements sampled at points A, B and C (as presented in Reference [40]). As can be noticed, the **DF** implementation underestimates the displacements obtained with the alternative mixed formulations. It can be seen how the **DF** implementation converges from below whereas the alternative mixed formulations converge from above. In addition,the results obtained with the constitutive model W_q match very well those presented in Reference [40].

As expected (e.g nearly incompressible material), regarding the stresses, the differences are more significant, specially for the W_q constitutive model. The higher nonlinearity of the W_q model with respect to the W_p model highlights the differences between both formulations. Whereas the results for the **DF** formulation do not seem to converge with clear pressure oscillations, the results for the alternative mixed formulations show a very defined convergence pattern. The results obtained with the constitutive model W_q match very well those presented in Reference [40].

Finally, it is important to mention that the equivalence between the **MCF** formulation and the other mixed formulations can be badly affected with the choice

	W_p model			W_q model		
	Fine	Medium	Coarse	Fine	Medium	Coarse
σ_{xx}^A	-103.12	-105.31	-106.64	-114.36	-117.63	-116.46
σ_{xx}^B	120.35	121.98	118.17	171.37	172.83	166.76
σ_{yy}^A	-113.89	-116.18	-117.27	-147.38	-150.96	-148.07
σ_{yy}^B	196.49	197.99	194.78	366.43	365.96	364.85
u_x^C	-20.76	-20.78	-20.81	-20.32	-20.30	-20.25
u_y^C	18.93	18.95	18.98	18.66	18.66	18.66
u_z^C	0.010	0.016	0.036	-0.001	-0.0005	0.007

Table 3.2: Cook type cantilever problem. Stress components (kPa) and displacements (m) at points A, B and C as displayed in Figure 3.5(b). Results are obtained using the mixed formulations. Coarse, medium and fine discretisations of $(7 \times 7 \times 5) \times 6$, $(10 \times 10 \times 6) \times 6$ and $(14 \times 14 \times 5) \times 6$ tetrahedral elements, respectively. W_p model (columns 2 to 4) defined in (3.49) with parameters given in (3.50). W_q model (columns 5 to 7) defined in (3.45) with material parameters in (3.47).

of the parameter ε_q used in equation (3.45) (ε_s in equation (3.43)). The higher the coefficient ε_q (ε_s) the stricter the error tolerance must be when solving numerically equation (3.45b) (or equation (3.43b)) via the Newton-Raphson nonlinear solver. Otherwise, small variations in the Jacobian J can introduce significant changes in the conjugate stress Σ_J and make the **MCF** formulation to yield different results to those of the **M7F** and **M5F** formulations.

3.3.3 Compressible short column subjected to transverse shear force.

In this example, a short column of squared cross sectional area is analysed when subjected to large deformations, as depicted in Figure 3.6(a). The height of the column is $h = 5m$ and the size of the square defining the cross section is $a = 1m$. The column is clamped at its bottom end and it is subjected at the top end to a shear stress distribution parabolic in the OY direction and constant in the OX direction, of maximum value $\tau_{max} = 76kPa$. Note that this force is not considered to be a follower-load during the deformation process.

The objective of this example is to demonstrate the p-order of accuracy of the different mixed formulations, as a function of the chosen finite element approximation spaces. For this purpose, the column is initially discretised with $(2 \times 2 \times 10) \times 6$ tetrahedral elements (see Figure 3.6(b)) and, subsequently, h-refinement is carried out generating a total of four discretisations. As a closed form solution is not available for this problem, the finest mesh is used to generate numerically the so-called

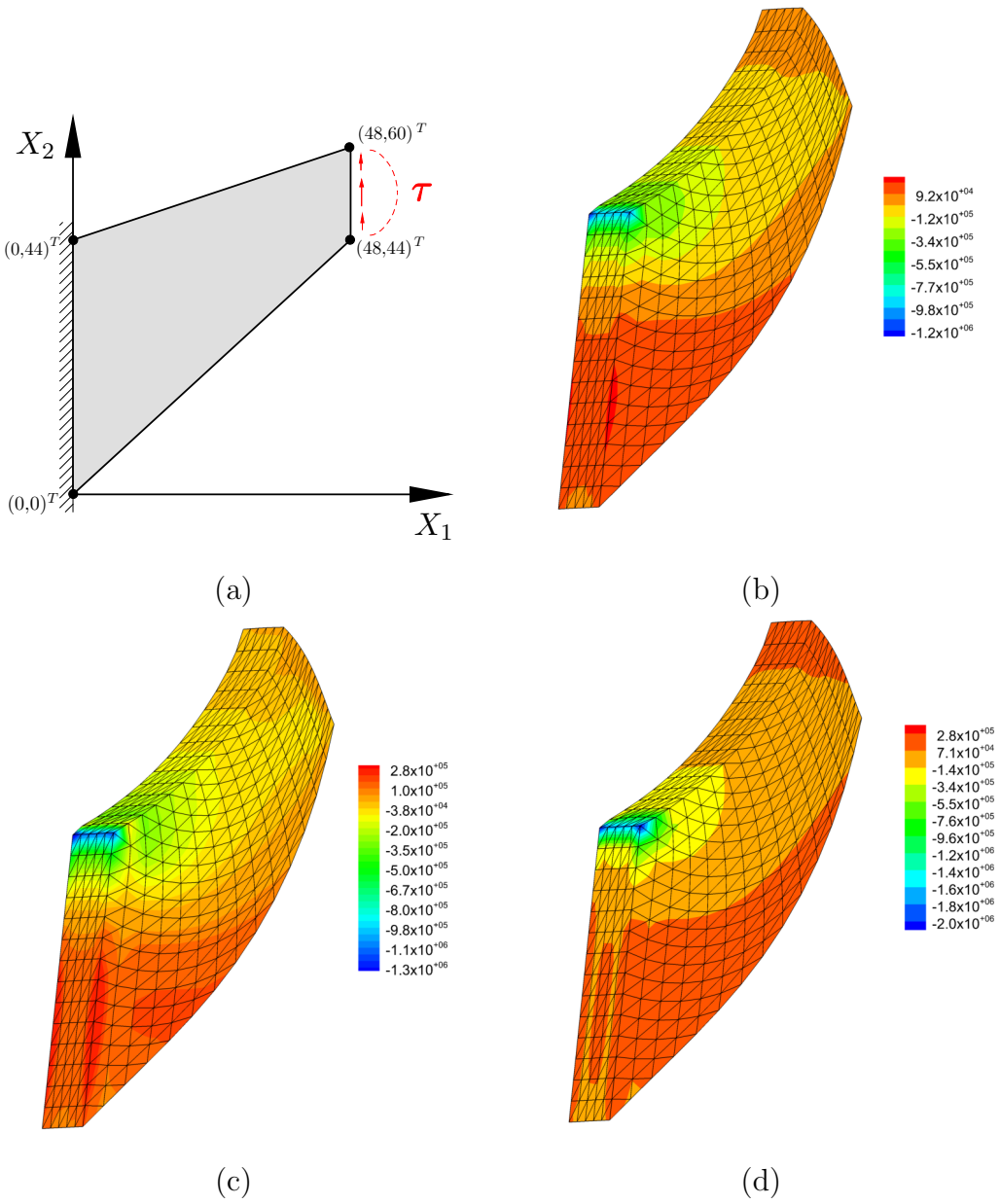

Figure 3.5: Cook type cantilever problem. (a) Geometry of the problem and boundary conditions. (b) Contour plot of stress field $\sigma_{xx}(Pa)$ for the polyconvex model W_q defined in (3.45) with material parameters in (3.47). Mixed formulations. (c) Contour plot of stress field $\sigma_{xx}(Pa)$ for the polyconvex model W_p defined in (3.49) with material parameters given in (3.50). Mixed formulations. (d) Contour plot of stress field $\sigma_{xx}(Pa)$ for the polyconvex model W_p defined in (3.49) with material parameters given in (3.50). **DF** formulation. Representation of the finest discretisation employed with $(14 \times 14 \times 5) \times 6$ tetrahedral elements.

	W_p model			W_q model		
	Fine	Medium	Coarse	Fine	Medium	Coarse
σ_{xx}^A	-94.40	-75.28	-189.83	-98.39	-79.41	-192.31
σ_{xx}^B	232.99	305.44	88.03	238.37	310.57	94.58
σ_{yy}^A	-134.17	-114.81	-223.26	-132.36	-115.06	-221.94
σ_{yy}^B	419.31	485.52	279.44	426.22	492.28	286.87
u_x^C	-20.55	-20.43	-20.21	-20.20	-20.00	-19.86
u_y^C	18.83	18.80	18.74	18.60	18.57	18.51
u_z^C	-0.060	-0.086	-0.143	-0.061	-0.087	-0.143

Table 3.3: Cook type cantilever problem. Stress components (kPa) and displacements (m) at points A, B and C as displayed in Figure 3.5(b). Results obtained using the **DF** formulation. Coarse, medium and fine discretisations of $(7 \times 7 \times 5) \times 6$, $(10 \times 10 \times 6) \times 6$ and $(14 \times 14 \times 5) \times 6$ tetrahedral elements, respectively. W_p model (columns 2 to 4) defined in (3.49) with parameters given in (3.50). W_q model (columns 5 to 7) defined in (3.45) with material parameters in (3.47).

"benchmark" solution (for each mixed formulation) for comparison purposes. The error between the benchmark solution and the other discretisations is measured in the L^2 norm for all the unknown variables. The constitutive model is a compressible Mooney-Rivlin type material defined by an energy function W_c as

$$W_c\left(\boldsymbol{F}, \boldsymbol{H}, J\right) = \alpha_c\left(\boldsymbol{F} : \boldsymbol{F}\right) + \beta_c\left(\boldsymbol{H} : \boldsymbol{H}\right) + f_c(J) \tag{3.53a}$$

$$f_c(J) = -4\beta_c \ln J - 2\alpha_c \ln J, \tag{3.53b}$$

where the material parameters are chosen as

$$\alpha_c = 47.25kPa; \quad \beta_c = 141.75kPa. \tag{3.54}$$

The selection of these material parameters yield a linear elasticity constitutive operator in the origin defined by a shear modulus $\mu = 378kPa$ and a Poisson's ratio $\nu = 0.3$. Let us define for a tensor (e.g. scalar, vector or second order) field, the L^2 norm as

$$\|\boldsymbol{\zeta}\|_{L^2} = \left[\int_V \left(\boldsymbol{\zeta} : \boldsymbol{\zeta}\right)\, dV\right]^{1/2}, \tag{3.55}$$

associated with the magnitude of the tensor field $\boldsymbol{\zeta}$. In our case, $\boldsymbol{\zeta}$ can be any of the kinematic or kinetic unknowns, namely $\boldsymbol{x}$, $\boldsymbol{F}$, $\boldsymbol{H}$, J, $\boldsymbol{\Sigma}_{\boldsymbol{F}}$, $\boldsymbol{\Sigma}_{\boldsymbol{H}}$ and Σ_J. This enables the definition of the following error norm $\|\boldsymbol{\zeta}_i - \boldsymbol{\zeta}_b\|_{L^2} / \|\boldsymbol{\zeta}_b\|_{L^2}$, where $\boldsymbol{\zeta}_b$ stands for the benchmark solution and $\boldsymbol{\zeta}_i$ the solution of the i-th mesh, with $i = 1, \ldots, (b-1)$. This can then be used to assess the convergence of the algorithm under h-refinement.

Figure 3.7 displays the contour plot distribution of the stress σ_{xx} for different stages of the deformation. The results presented are identical for all of the mixed

formulations. As can be observed, the stress distribution is smooth (absence of pressure modes) and the deformation does not show any locking in its deformation pattern.

Figure 3.8 shows the order of accuracy of the different unknown variables for the mixed formulations (all yielding identical convergence pattern). Figure 3.8(a) displays the convergence of the kinematic variables $\boldsymbol{x}$, $\boldsymbol{F}$, $\boldsymbol{H}$ and J whereas Figure 3.8(b) displays the convergence of the kinetic variables $\boldsymbol{\Sigma}_{\boldsymbol{F}}$, $\boldsymbol{\Sigma}_{\boldsymbol{H}}$ and Σ_J. As expected, the convergence observed is $p+1$ in all the variables.

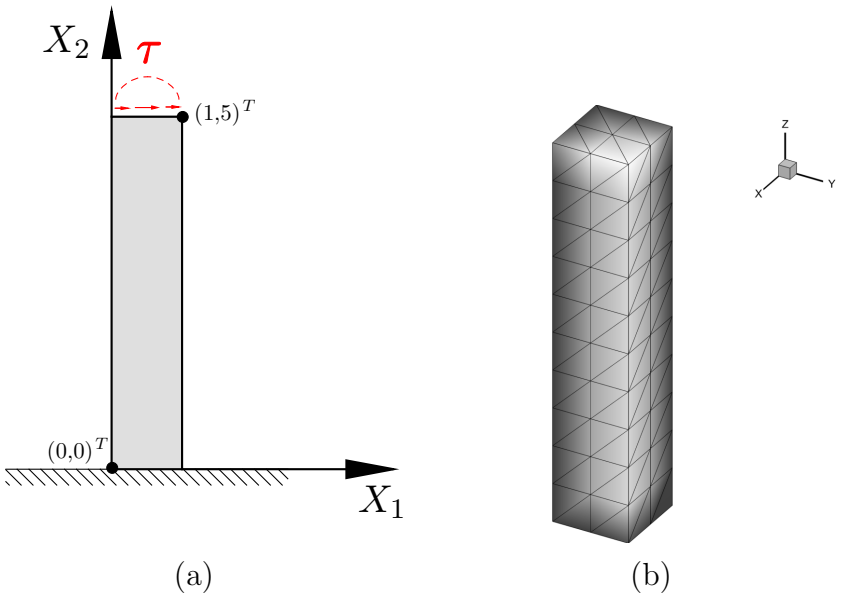

Figure 3.6: Compressible short column of height $h = 5m$ and squared cross section defined by its size $a = 1m$. (a) Boundary conditions: clamped bottom end and parabolic stress distribution at the top end. Axes OX_1 and OX_2 coincide with oy and oz in (b), respectively. (b) Example of finite element discretisation: coarsest mesh with $(2 \times 2 \times 10) \times 6$ tetrahedral elements.

3.3.4 Incompressible long column subjected to transverse shear force.

A very similar example to that presented in the previous section is analysed. In this case, a longer column of height $h = 10m$ of squared cross sectional area is analysed when subjected to large deformations. As in the previous section, the size of the square defining the cross section remains $a = 1m$. The column is clamped at its bottom end and subjected to a parabolic (only in the OY direction) shear stress distribution at the top end of maximum value $\tau_{max} = 14.4kPa$. Note that this force is not considered to be a follower-load during the deformation process. The constitutive model is taken as incompressible Mooney-Rivlin defined via a polyconvex isochoric

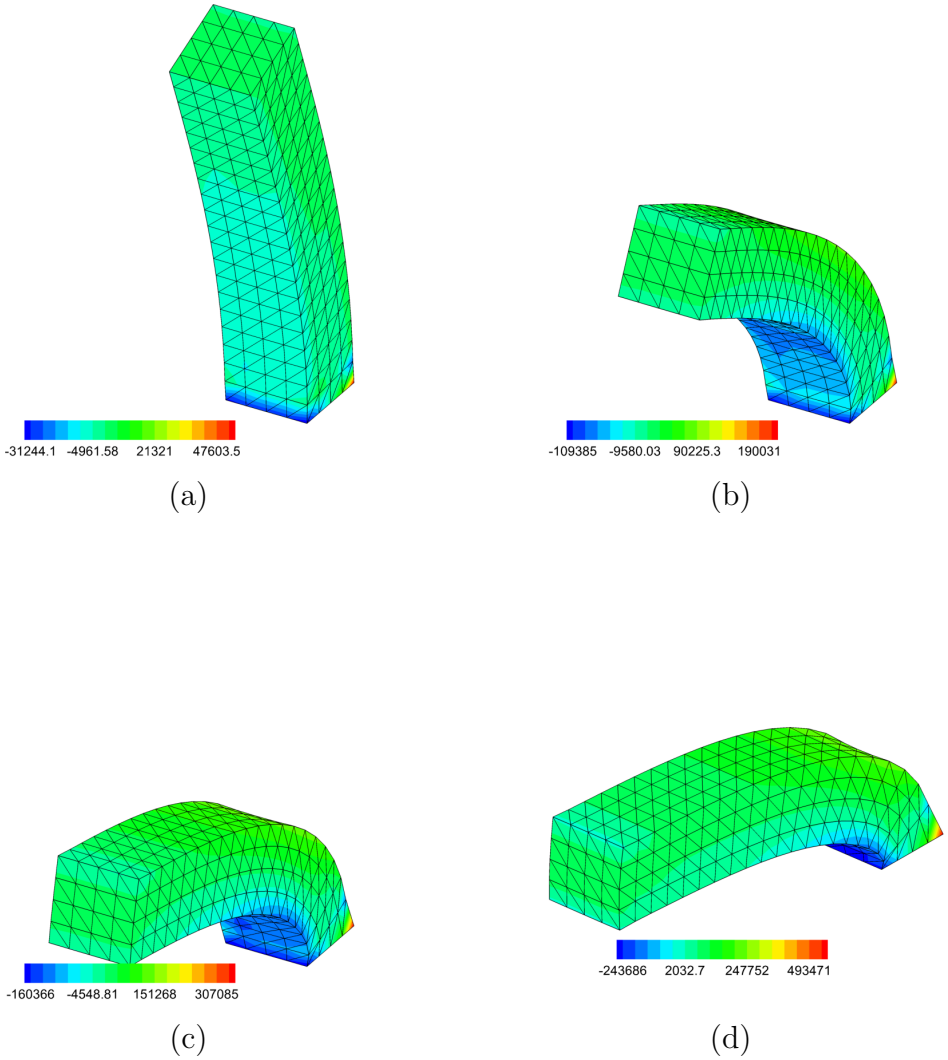

Figure 3.7: Contour plot of the stress $\sigma_{xx}(Pa)$ distribution for the compressible short column example using a mixed formulation. Results after application of an incremental loading of (a) 5% (b) 25% (c) 50% and (d) 100% of the total external shear stress $\tau = \tau_{max}$. Mooney-Rivlin model W_p defined in (3.49) with material parameters given in (3.54). Results shown for a discretisation of $(4 \times 4 \times 20) \times 6$ tetrahedral elements $(3,321 \times 3$ degrees of freedom associated to the spatial coordinates $\boldsymbol{x})$.

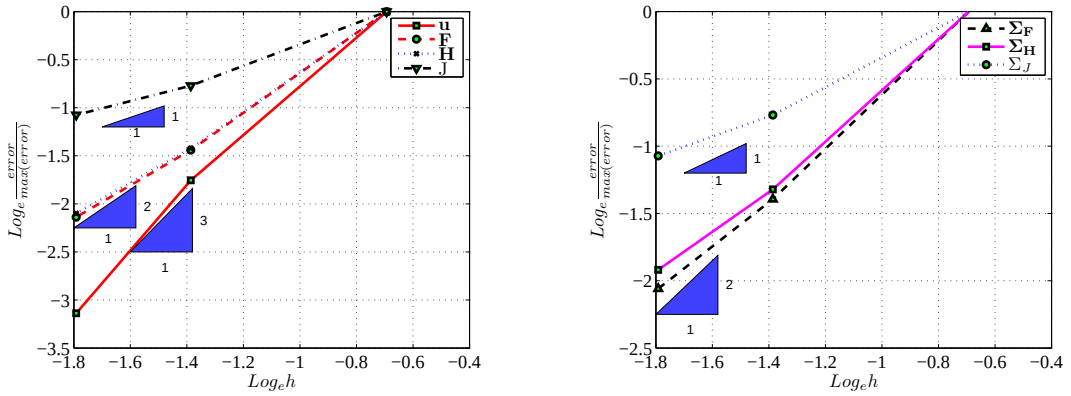

(a) (b)

Figure 3.8: Compressible short column example: order of accuracy of different strain and stress magnitudes for the mixed formulations. (a) Order of accuracy of the kinematic variables $\boldsymbol{x}$, $\boldsymbol{F}$, $\boldsymbol{H}$ and J. (b) Order of accuracy of the kinetic variables $\boldsymbol{\Sigma_F}$, $\boldsymbol{\Sigma_H}$ and Σ_J. Mooney-Rivlin model W_p defined in (3.49) with material parameters given in (3.54).

energy function $\hat{W}_i$ defined as

$$\hat{W}_i\left(\boldsymbol{F},\boldsymbol{H},J\right)=\nu_i J^{-2/3}\left(\boldsymbol{F}:\boldsymbol{F}\right)+\gamma_i J^{-2}\left(\boldsymbol{H}:\boldsymbol{H}\right)^{3/2}, \tag{3.56}$$

where the material parameters are chosen as

$$\nu_i=189kPa,\quad \gamma_i=72.75kPa. \tag{3.57}$$

The selection of these material parameters yield a linear elasticity constitutive operator in the origin defined by shear modulus $\mu=756kPa$ and Poisson's ratio $\nu=0.5$. The objective of this example is to demonstrate the behaviour of the stabilisation technique as presented in Section 3.2.3. For this purpose, two interpolation techniques will be considered: first, a P1-P1 linear continuous interpolation for both displacement and pressure fields (e.g. with the help of stabilisation) and, second, a P2-P0 continuous quadratic interpolation for the displacement field and piecewise constant interpolation for the pressure field (e.g. without stabilisation).

For the P1-P1 interpolation, an unstructured mesh of 17,575 tetrahedral elements is used ($3,859\times 3$ degrees of freedom associated to the spatial coordinates $\boldsymbol{x}$) (refer to Figures 3.9(a)-(c)) and for the P2-P0 interpolation, an unstructured mesh of 3,962 tetrahedral elements is used ($6,675\times 3$ degrees of freedom associated to the spatial coordinates $\boldsymbol{x}$) (refer to Figures 3.9(d)). Notice that a very fine P2-P0 discretisation has been chosen in order to adequately benchmark the solution obtained with the alternative stabilised P1-P1 formulation.

Figure 3.9 displays the contour plot distribution of the hydrostatic pressure. The solution by using the non-stabilised P2-P0 implementation is displayed in the subfigure (d) whereas sub-figures (a) to (c) present the results for the stabilised P1-P1

implementation, with stabilisation parameter $\alpha = 0.1, 0.2, 0.5$, respectively. In all of the P1-P1 analyses, stabilisation coefficient $\tau_p = 0$ was employed.

The results show an excellent agreement between the non-stabilised P2-P0 formulation (see Figure 3.9(d)) and the stabilised P1-P1 formulation when using $\alpha = 0.2$ (see Figure 3.9(b)). Larger values of the stabilisation parameter α lead to stiffer solutions (i.e. volumetric and shear locking) and viceversa. It is also clear that for the stabilised P1-P1 implementation, smooth distributions of stresses are obtained, removing possible spurious pressure oscillations.

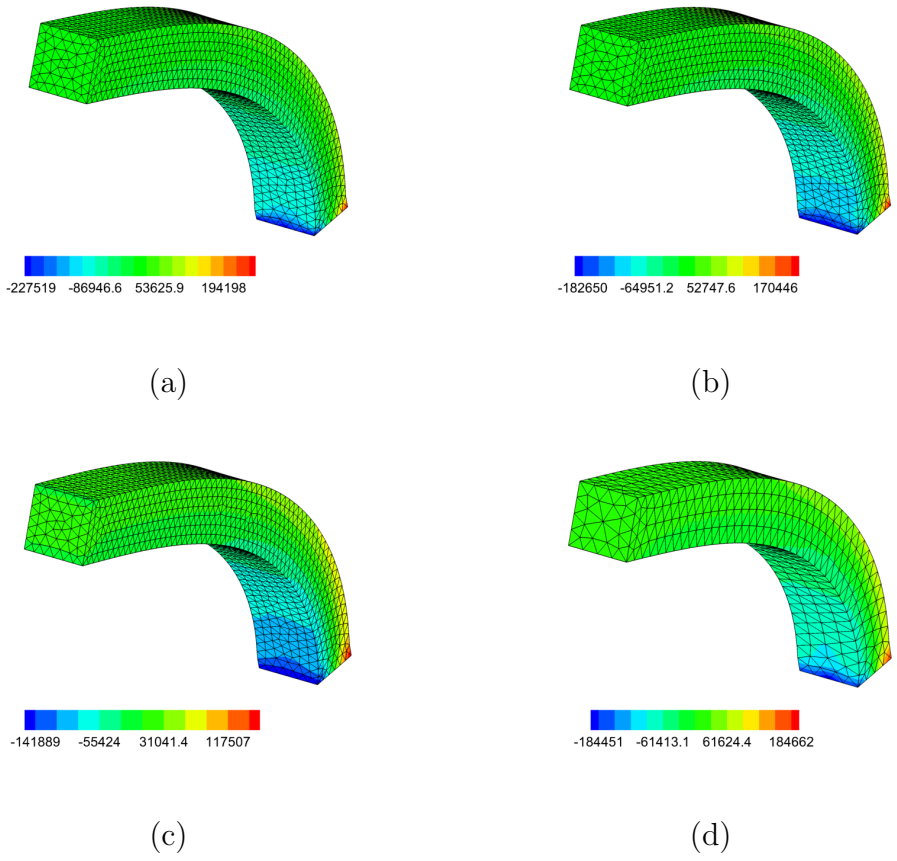

Figure 3.9: Contour plot of the hydrostatic pressure distribution $p(kPa)$ for the incompressible long column example. (a) Stabilised P1-P1 formulation with $\tau_p = 0$ and $\alpha = 0.1$. (b) Stabilised P1-P1 formulation with $\tau_p = 0$ and $\alpha = 0.2$. (c) Stabilised P1-P1 formulation with $\tau_p = 0$ and $\alpha = 0.5$. (d) Non-stabilised P2-P0 formulation. Incompressible Mooney-Rivlin model $\hat{W}_i$ defined in (3.56) with material parameters given in (3.57). Results shown in (a) to (c) are for a discretisation of 17,575 tetrahedral elements ($3,859 \times 3$ degrees of freedom associated to the spatial coordinates $\boldsymbol{x}$). Results shown in (d) are for a discretisation of 3,962 tetrahedral elements ($6,675 \times 3$ degrees of freedom associated to the spatial coordinates $\boldsymbol{x}$).

3.3.5 Twisting cantilever beam

The last example includes the twisting of a cantilever beam of length $L = 6m$ and a squared cross sectional area of side $a = 1m$. The beam is clamped at its left end and subjected to a torsion on its right end. This example is included to demonstrate the robustness of the mixed formulations. The torsion at the right end is generated through Dirichlet boundary conditions as follows

$$(\boldsymbol{I} - \boldsymbol{E}_Y \otimes \boldsymbol{E}_Y)\, \boldsymbol{x} = \theta \boldsymbol{E}_Y \times \boldsymbol{X}, \tag{3.58}$$

where $\boldsymbol{E}_Y$ is the unit vector normal to the cross section in the reference configuration, $\boldsymbol{X}$ are the initial coordinates, θ is the angle of rotation and $\boldsymbol{x}$ are the final coordinates. As can be observed, the section is not restricted to in-plane torsion and zero Neumann boundary conditions are imposed normal to the cross sectional area. A similar example has been presented by the authors in previous references [58,97].

The geometry and boundary conditions for the problem are depicted in Figure 3.10(a). The constitutive model is a compressible Mooney-Rivlin defined by an energy function W_u defined by

$$W_u\left(\boldsymbol{F}, \boldsymbol{H}, J\right) = \alpha_u\left(\boldsymbol{F} : \boldsymbol{F}\right) + \beta_u\left(\boldsymbol{H} : \boldsymbol{H}\right) + f_u(J) \tag{3.59a}$$

$$f_u(J) = -4\beta_u \ln J - 2\alpha_u \ln J, \tag{3.59b}$$

where the material parameters are chosen as

$$\alpha_u = 9.0kPa; \quad \beta_u = 9.0kPa. \tag{3.60}$$

The selection of these material parameters yield a linear elasticity constitutive operator in the origin defined by shear modulus $\mu = 36kPa$ and Poisson's ratio $\nu = 0.25$. The analysis is carried out with a finite element discretisation comprised of 2,304 tetrahedral elements ($4,009 \times 3$ degrees of freedom associated to the spatial coordinates $\boldsymbol{x}$).

Figure 3.11 displays the contour plot distribution of the stresses σ_{xy} (see Figure 3.11(a) and 3.11(b)) and σ_{yy} (see Figure 3.11(c) and 3.11(d)). Results displayed in Figures 3.11(b) and 3.11(d) are obtained by using the **DF** implementation whereas results in Figures 3.11(a) and 3.11(c) are obtained by using the alternative mixed formulations, namely **M7F**, **MCF** and **M5F**, all yielding identical results.

As can observed, important differences in terms of stresses can be observed between the **DF** formulation and the alternative mixed formulations. This deformation pattern is very demanding for the **DF** formulation and improved results would require h-refinement. It is important to emphasise that the results are similar in terms of deformation as the problem is displacement driven by the boundary conditions.

The extreme deformation undertaken by the beam leads to a buckled configuration that can be observed in Figure 3.12, where the out-of-plane configuration can be clearly observed along with the hydrostatic pressure distribution, where negative values (compressive areas) can be identified. Finally, for completeness, different results concerning some of the components of the kinematic variables $\boldsymbol{F}$, $\boldsymbol{H}$ and J

are shown in Figure 3.13. It is possible to observe the smooth distribution of the different fields.

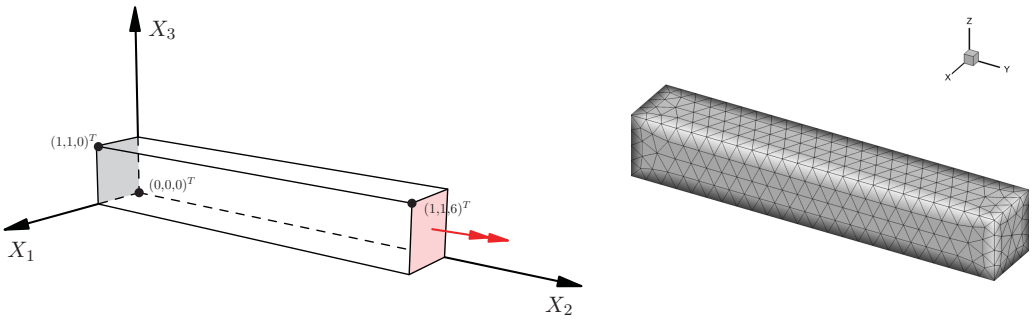

(a) (b)

Figure 3.10: Twisting cantilever beam problem of length $h = 6m$ and squared cross section defined by its size $a = 1m$. (a) Boundary conditions: clamped left end and twisting rotation applied at the right end. Axes OX_1, OX_2 and OX_3 coincide with ox, oy and oz in (b), respectively. (b) Example of finite element discretisation: 2,304 tetrahedral elements ($4,009 \times 3$ degrees of freedom associated to the spatial coordinates $\boldsymbol{x}$).

3.4 Concluding remarks

This Chapter has provided a novel approach to formulate large polyconvex large strain elasticity in the computational context. Two main novelties are included in the chapter. First, the computational Finite Element implementation of several of the mixed variational principles presented in Chapter 2 has been presented. Of special interest in the context of polyconvexity are the new Hu-Washizu and Hellinger-Reissner mixed variational principles Π_M and Π_C defined in the previous Chapter in equations (2.180) and (2.193). The residual vectors and stiffness matrices associated to the aforementioned variational principles, arising after standard Finite Element discretisation, have been presented. Second, the introduction of a stabilised Petrov-Galerking discretisation for the mixed variational principle Π_I in equation (2.199) for full incompressibility, whose Finite Element computational implementation has also been included.

Very remarkably, the new computational framework emerging after Finite Element discretisation of the various mixed variational frameworks presented in Chapter 2 relies heavily on the use of a new tensor cross product introduced in Reference [82] and rediscovered in [44], which proves to greatly facilitate the manipulations of expressions involving the co-factor of the deformation gradients and specially, its derivatives. Finally, a series of challenging numerical examples have been included in the present Chapter in order to illustrate the superiority of the proposed mixed

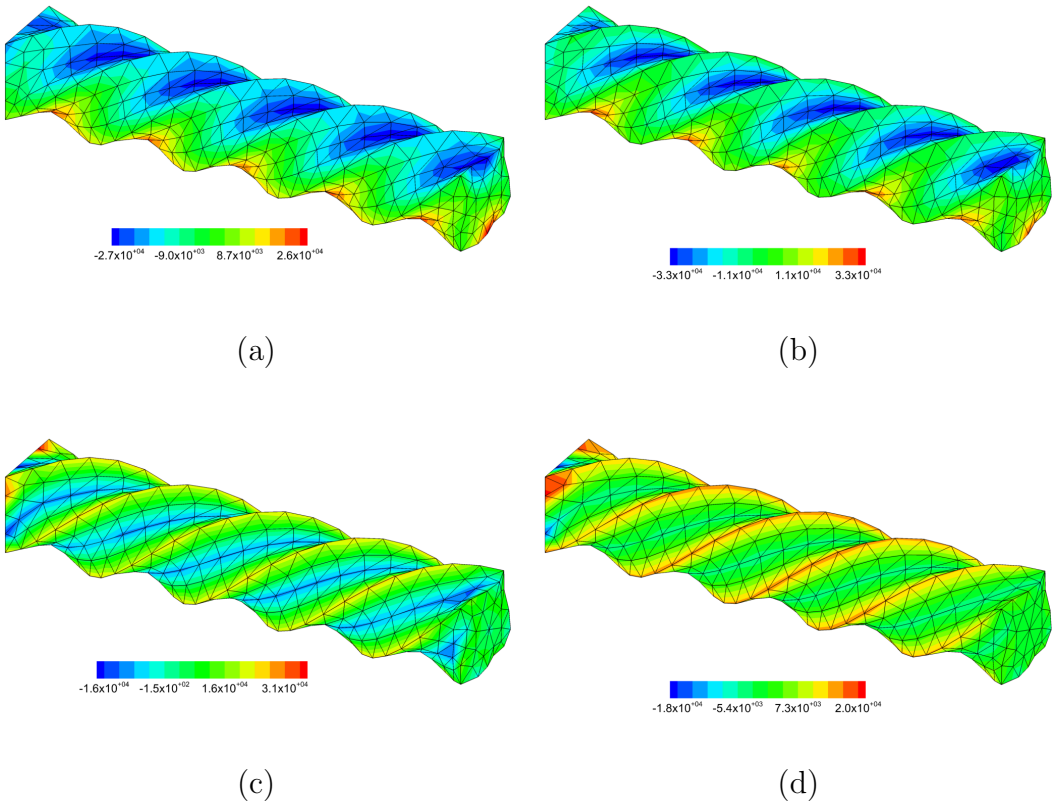

Figure 3.11: Contour plot of the stress $\sigma_{xy}(Pa)$ ((a) and (b)) and $\sigma_{yy}(Pa)$ ((c) and (d)) distribution for the twisting cantilever beam example. Results obtained with the **DF** formulation ((b) and (d)) and alternative mixed formulations ((a) and (c)). Mooney-Rivlin model W_u defined in (3.59) with material parameters given in (3.60). Results shown for a discretisation of 2,304 tetrahedral elements ($4,009 \times 3$ degrees of freedom associated to the spatial coordinates $\boldsymbol{x}$).

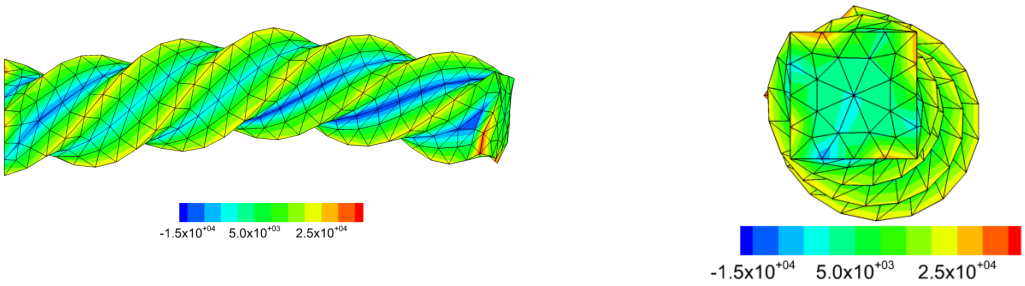

Figure 3.12: Lateral and plan view of the contour plot of the hydrostatic pressure distribution $p(Pa)$ for the twisting cantilever beam example. Results obtained with the alternative mixed formulations. Mooney-Rivlin model W_u defined in (3.59) with material parameters given in (3.60). Results shown for a discretisation of 2,304 tetrahedral elements ($4,009 \times 3$ degrees of freedom associated to the spatial coordinates $\boldsymbol{x}$).

formulations, which clearly overcome the typical drawbacks associated the the classical displacement-based formulations.

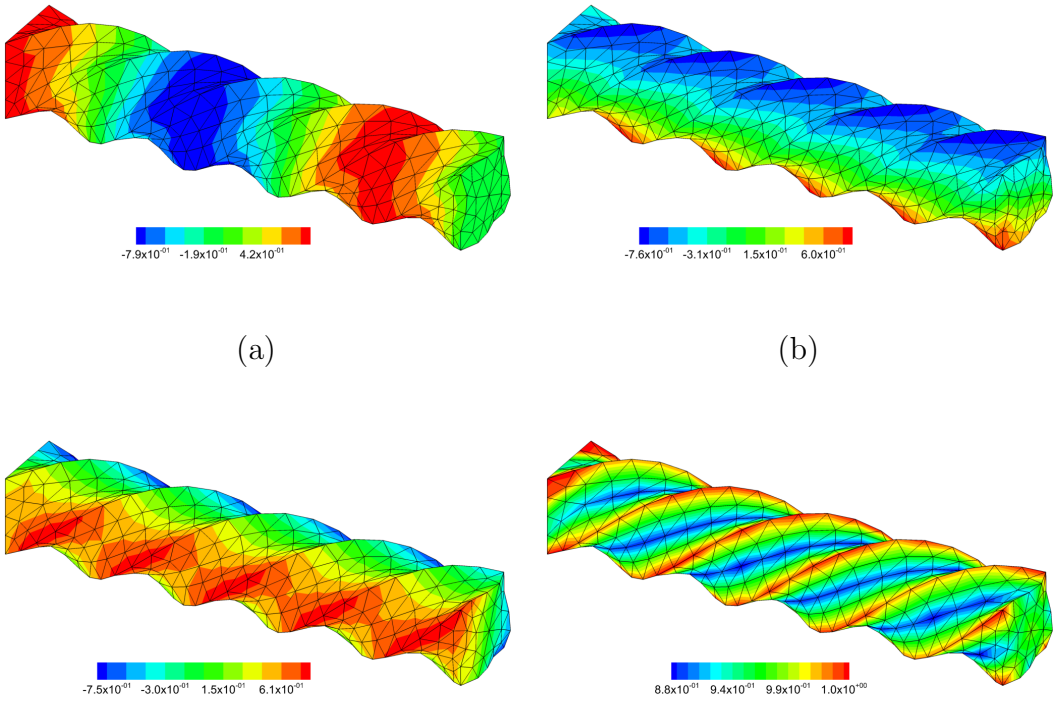

Figure 3.13: Contour plot of the distribution of the components (a) F_{11}, (b) F_{12}, (c) F_{32}, (d) J, for the twisting cantilever beam example. Results obtained with the alternative mixed formulations. Mooney-Rivlin model W_u defined in (3.59) with material parameters given in (3.60). Results shown for a discretisation of 2,304 tetrahedral elements ($4,009 \times 3$ degrees of freedom associated to the spatial coordinates $\boldsymbol{x}$).

Chapter 4

First order hyperbolic framework for polyconvex solid dynamics

4.1 Introduction

Chapter 2 has presented a novel approach for the formulation of polyconvex large strain elasticity. Chapter 3 has presented a new computational framework emerging after Finite Element discretisation of the various new mixed variational principles introduced in Chapter 2, some of those of special interest within the context of polyconvex elasticity, as the Hu-Washizu and the Hellinger-Reissner variational principles described in Section 2.6.2 and 2.6.3, respectively.

Polyconvexity is the most well accepted constitutive restriction [11, 27, 32]. This condition implies the Legendre-Hadamard condition, which entails the existence of travelling waves in the material in the neighbourhood of a stationary point. Crucially, this condition is strongly related to material stability and the development of areas with localised deformations where ellipticity and therefore, well-posedness of the governing no longer hold [86]. The physical implications of polyconvexity (Legendre-Hadamard condition) are therefore of extreme relevance. From the mathematical standpoint, the convex multi-variable nature of the strain energy with respect to the fibre, area and volume maps, namely the deformation gradient tensor, its co-factor and its Jacobian might not be very intuitive. However, it should not be surprising that existence of travelling wave speeds, intimately related to the hyperbolicity of the dynamic equations, is satisfied by a polyconvex definition of the strain energy, for which the time rate of their arguments can be expressed as a first order conservation law. This Chapter explores the hyperbolic nature of the first order hyperbolic equations in polyconvex elasticity, consisting of conservation of linear momentum and a set of geometrical conservation laws for the arguments of polyconvexity.

The authors in References [43, 57] have presented a robust an accurate Stream-Upwind-Petrov-Galerkin (SUPG) computational framework for the solution of computational solid dynamics based on the system of first order hyperbolic conservation laws for nonlinear elasticity. In this framework, closer to that for computational fluid dynamics than the classical techniques for the simulation of solid dynamics (where the equations of motion are expressed in terms of a second order hyperbolic equation) the conservation variables for the first order hyperbolic system of equations are linear momentum and the arguments defining polyconvexity, namely the deformation gradient tensor, its co-factor and its Jacobian.

Alternatively, a computational framework for Solid Dynamics can be naturally derived from the mixed variational principles presented in Section 2.6. In particular, the associated Lagrangian functional and its corresponding action integral [11] for the Hu-Washizu and Hellinger-Reissner mixed variational principles in Section 2.6.2 and 2.6.3 respectively, are presented in this Chapter. The stationary point of the action integral yields a weak variational statement for conservation of linear momentum analogous to that obtained from its homologous total energy potential in the static case (Section 2.6) subjected to a series of compatibility and constitutive-based restrictions. The resulting equations adopt the structure of a second order

hyperbolic equation subjected to a series of constraints, more in line with the more classical approach followed in the traditional Solid Dynamics community [14].

Polyconvexity of the internal energy guarantees the relationship between the set $\{\boldsymbol{F}, \boldsymbol{H}, J\}$ and its associated set of work or entropy conjugates, namely $\{\boldsymbol{\Sigma}_{\boldsymbol{F}}, \boldsymbol{\Sigma}_{\boldsymbol{H}}, \Sigma_J\}$ to be one to one and invertible. Crucially, and in line with the pioneering work of Hughes *et al.* [2] in the context of Computational Fluid Dynamics, the consideration of polyconvex energy functionals in the context of Computational Solid Dynamics, enables the definition of a generalised convex entropy function. This enables the transformation of the system of conservation laws into a symmetric set of hyperbolic equations in terms of the entropy conjugates, namely $\{\boldsymbol{\Sigma}_{\boldsymbol{F}}, \boldsymbol{\Sigma}_{\boldsymbol{H}}, \Sigma_J\}$. The authors in Reference [43] have also presented a SUPG computational framework for the solution of Computational polyconvex Solid Dynamics based on a system of first order hyperbolic equations in terms of the entropy conjugates, namely $\{\boldsymbol{\Sigma}_{\boldsymbol{F}}, \boldsymbol{\Sigma}_{\boldsymbol{H}}, \Sigma_J\}$. The symmetrisation of the equations for Computational polyconvex Solid Dynamics are presented in this Chapter. This Chapter presents the relationship between polyconvexity of the strain energy and positive definiteness of the so called acoustic tensor [11, 86], emerging in the analysis of the eigen-structure of the equations for polyconvex Solid Dynamics. An explicit derivation for the wave speeds for a (polyconvex) Mooney-Rivlin and a (non-polyconvex) Saint Venant-Kirchhoff constitutive models is presented in this Chapter, illustrating the existence of travelling wave speeds for the entire range of deformations for the Mooney-Rivlin model and the development of material instabilities for the Saint Venant-Kirchhoff model for those ranges of deformations with associated non real wave speeds.

Finally, a challenging numerical example is included in this Chapter in order to better illustrate the behaviour of the Mooney-Rivlin and Saint Venant-Kirchhoff constitutive models in dynamic scenarios. Although the Saint Venant-Kirchhoff model should only be used in small strain scenarios, it is considered in this Section in order to graphically illustrate the implications of loss of material stability from the simulation standpoint.

This Chapter is organised as follows. Section 4.2 presents the set of conservation laws in Computational polyconvex Solid Dynamics, including the geometrical conservation laws for the strain measures $\{\boldsymbol{F}, \boldsymbol{H}, J\}$. Section 4.3 studies the eigenvalue structure of the equations for polyconvex Solid Dynamics. Section 4.4 introduces the generalised convex entropy function for polyconvex elasticity presents the conservation laws for polyconvex Solid Dynamics in terms of the entropy conjugates $\{\boldsymbol{\Sigma}_{\boldsymbol{F}}, \boldsymbol{\Sigma}_{\boldsymbol{H}}, \Sigma_J\}$. Section 4.5 presents the associated Lagrangian functionals and corresponding action integrals for the Hu-Washizu and Hellinger-Reissner mixed variational principles in Section 2.6, extending the application of those two formulations to dynamic scenarios. Finally, Section 4.6 includes some relevant theoretical and numerical examples and Section 4.7 provides some concluding remarks. An illustrative diagram containing the layout of the present Chapter has been included in Figure 4.1.

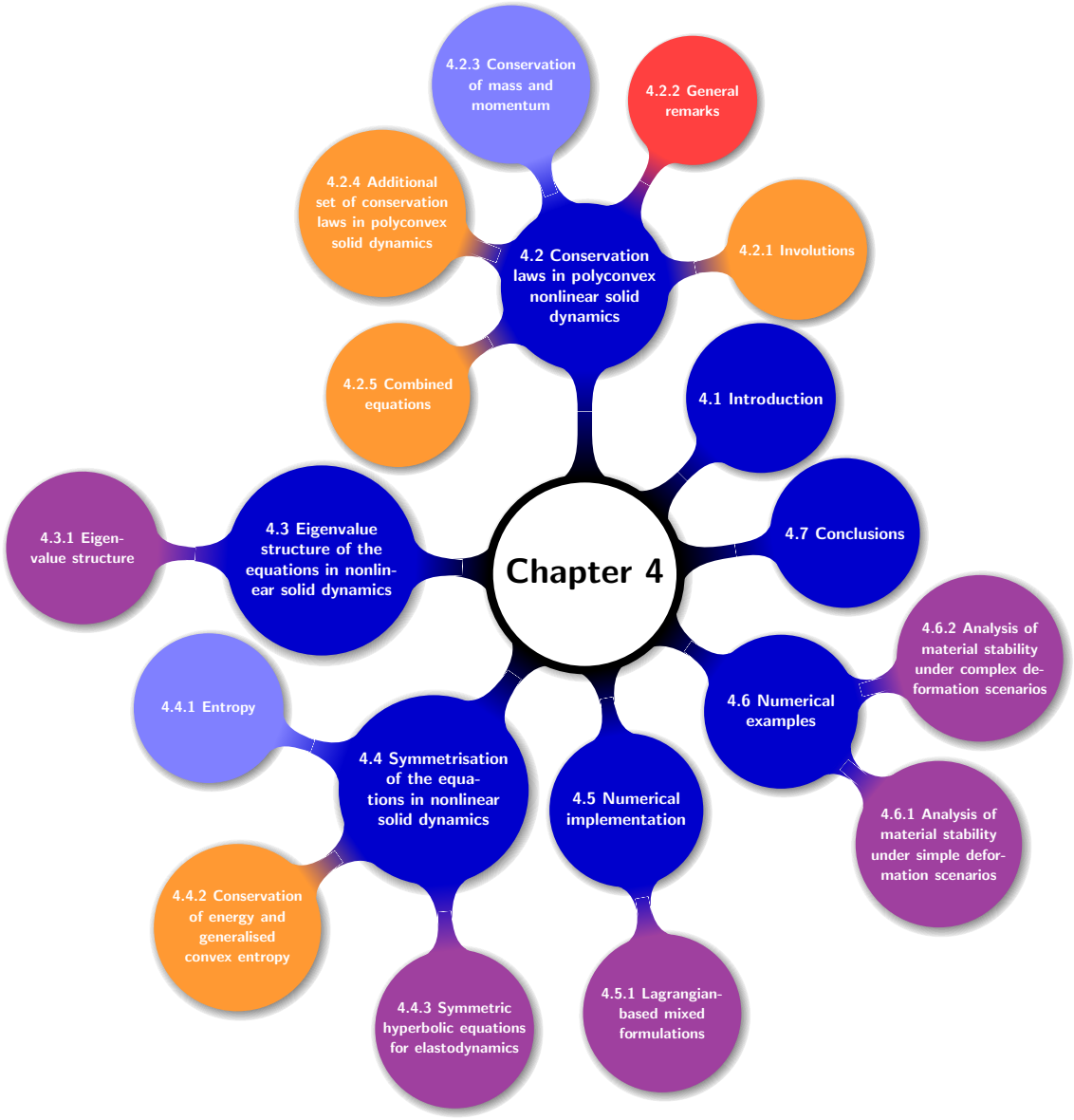

Figure 4.1: Chapter layout.

4.2 Conservation laws in polyconvex nonlinear solid dynamics

The objective of this Section is to present the equations for Computational Solid Dynamics as a set of first order hyperbolic equations including that for conservation of linear momentum and a series of geometrically-based conservation laws for the arguments which define polyconvexity, namely $\{\boldsymbol{F}, \boldsymbol{H}, J\}$. The entire set of conservation laws is presented in this Section.

4.2.1 Involutions

Before presenting the system of hyperbolic equations for polyconvex elasticity, let us consider the motion of the elastic body described in Section 2.2. As stated in equations (2.36), the deformation gradient tensor $\boldsymbol{F}$ and its co-factor $\boldsymbol{H}$ must satisfy certain compatibility conditions, namely

$$\text{CURL}\boldsymbol{F} = \boldsymbol{0}; \qquad \text{DIV}\boldsymbol{H} = \boldsymbol{0}. \tag{4.1}$$

These conditions are such that they are satisfied under exact integration provided they are satisfied by the initial conditions. They are not necessary to close the system of hyperbolic equations that will be presented in the forthcoming Sections. These compatibility equations are therefore called involutions as opposed to constraints. However, not consideration of these involutions might lead to catastrophic results from the numerical standpoint. In particular, spurious modes might arise after long time integrations, destroying the accuracy of the numerical solution. Figure 4.2 illustrates the evolution of a elastic body from the reference configuration to two different configurations at different time stages satisfying the involutions in equation (4.1).

Very crucially, these involutions will be extremely relevant as they will be fundamental for the derivation of conservation laws for both the co-factor and the Jacobian.

4.2.2 General remarks

The aim of this section is, following the work in Reference [44], to express the equations of nonlinear elasticity in the form of a set of global conservation laws for a set of conservation variables $\boldsymbol{\mathcal{U}} = [\mathcal{U}_\alpha]$ with fluxes $\boldsymbol{\mathcal{F}} = [\mathcal{F}_{\alpha I}]$ and source term $\boldsymbol{\mathcal{S}} = [\mathcal{S}_\alpha]$, where $\alpha = 1, \dots, n$ represents the set of unknowns and $I = 1, 2, 3$ the reference coordinates. Global conservation laws are generally expressed as

$$\frac{d}{dt}\int_V \boldsymbol{\mathcal{U}}\, dV + \int_{\partial V} \boldsymbol{\mathcal{F}}\, d\boldsymbol{A} = \int_V \boldsymbol{\mathcal{S}}\, dV. \tag{4.2}$$

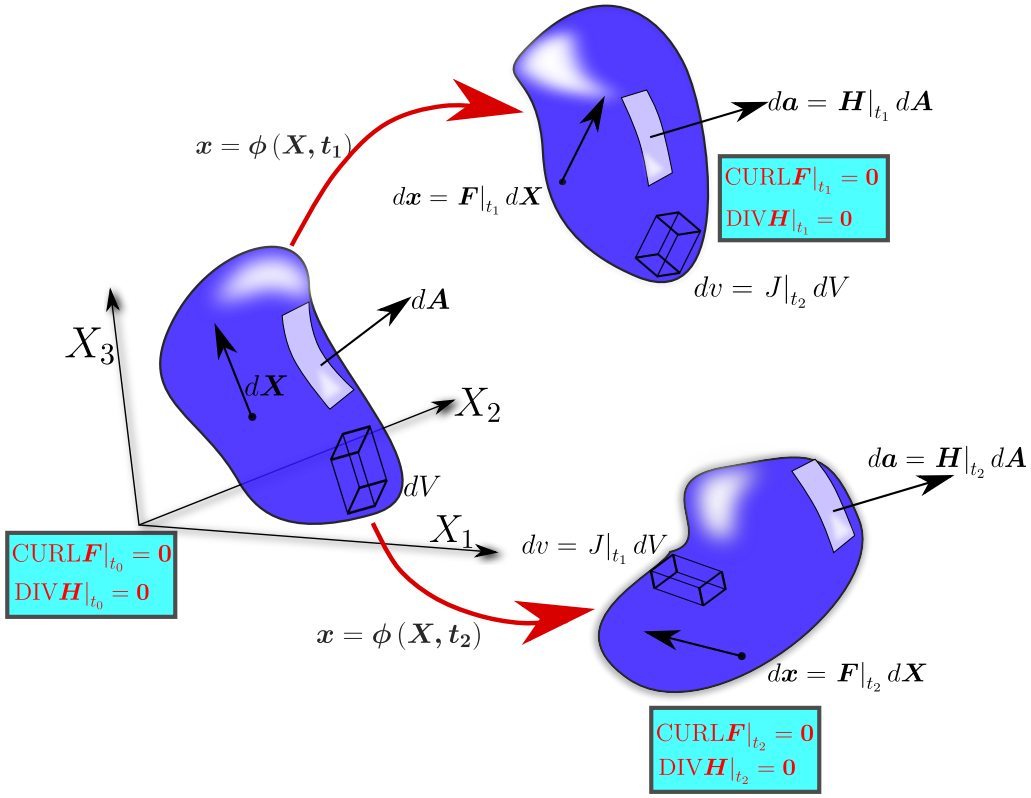

Figure 4.2: Evolution of the continuum from its reference configuration ($t = t_0$) to two different instants $t = t_1$ and $t = t_2$. Satisfaction of the associated involutions at every instant of the deformation. Evolution of the infinitesimal fibre, area and volume elements.

For smooth functions, this integral expression is equivalent to the set of first order differential equations

$$\frac{\partial \boldsymbol{\mathcal{U}}}{\partial t} + \mathrm{DIV}\boldsymbol{\mathcal{F}} = \boldsymbol{\mathcal{S}}. \tag{4.3}$$

In addition, for discontinuous solutions the integral conservation law also leads to the following jump conditions across a discontinuity surface with normal $\boldsymbol{N}$ moving with speed U [99–101]

$$U\left[\!\left[\boldsymbol{\mathcal{U}}\right]\!\right] = \left[\!\left[\boldsymbol{\mathcal{F}}\right]\!\right]\boldsymbol{N} \tag{4.4}$$

where the notation $\left[\!\left[\phi\right]\!\right] = (\phi_+ - \phi_-)$ is used to denote the jump of a variable across a moving discontinuity surface. It is often convenient to express equation (4.3) in the quasi-linear form

$$\frac{\partial \boldsymbol{\mathcal{U}}}{\partial t} + \boldsymbol{\mathcal{A}}_I \frac{\partial \boldsymbol{\mathcal{U}}}{\partial X_I} = \boldsymbol{\mathcal{S}}; \qquad \boldsymbol{\mathcal{A}}_I = [\mathcal{A}_{\alpha\beta}]_I = \frac{\partial \boldsymbol{\mathcal{F}}_I}{\partial \boldsymbol{\mathcal{U}}}, \tag{4.5}$$

where $\boldsymbol{\mathcal{F}}_I$ denotes the columns of the flux matrix and, in general, the square $n \times n$ matrices $\boldsymbol{\mathcal{A}}_I$ (with $\alpha, \beta = 1, \ldots, n$) will not be symmetric. Alternatively, the flux matrix $\boldsymbol{\mathcal{F}}$ defined in (4.3) can be expressed as

$$\boldsymbol{\mathcal{F}} = \boldsymbol{\mathcal{F}}_I \otimes \boldsymbol{E}_I; \qquad \boldsymbol{E}_1 = \begin{bmatrix} 1 \\ 0 \\ 0 \end{bmatrix}; \qquad \boldsymbol{E}_2 = \begin{bmatrix} 0 \\ 1 \\ 0 \end{bmatrix}; \qquad \boldsymbol{E}_3 = \begin{bmatrix} 0 \\ 0 \\ 1 \end{bmatrix}. \tag{4.6}$$

4.2.3 Conservation of mass and momentum

The conservation of mass in a Lagrangian setting is simply stated by

$$\frac{d}{dt}\int_V \rho_0 \, dV = 0. \tag{4.7}$$

This simply implies that the initial density of the material ρ_0 is constant and therefore does not need to be considered as part of the vector of problem unknowns $\boldsymbol{\mathcal{U}}$. Global conservation of linear momentum $\boldsymbol{p} = \rho_0 \boldsymbol{v}$ is established for any arbitrary Lagrangian volume V as

$$\frac{d}{dt}\int_V \boldsymbol{p} \, dV = \int_{\partial V} \boldsymbol{t}_0 \, dA + \int_V \boldsymbol{f}_0 \, dV, \tag{4.8}$$

Assuming the existence of a first Piola-Kirchhoff stress tensor $\boldsymbol{P}$ such that the traction vector associated with the initial area with normal $\boldsymbol{N}$ is $\boldsymbol{t}_0 = \boldsymbol{P}\boldsymbol{N}$, the equivalent local equilibrium equation and jump condition can be written as

$$\frac{\partial \boldsymbol{p}}{\partial t} - \mathbf{DIV}\boldsymbol{P} = \boldsymbol{f}_0; \qquad U\left[\!\left[\boldsymbol{p}\right]\!\right] = -\left[\!\left[\boldsymbol{P}\right]\!\right]\boldsymbol{N}. \tag{4.9}$$

4.2.4 Additional set of conservation laws in polyconvex solid dynamics

The objective of this section is to present the conservation laws associated to three new conservation variables which close the system of conservation laws for polyconvex Solid Dynamics [43].

Conservation of deformation gradient

A conservation law for the deformation gradient tensor can be derived considering its definition in equation (2.1). Differentiation of this equation with respect to time yields

$$\frac{\partial \boldsymbol{F}}{\partial t} = \boldsymbol{\nabla}_0 \boldsymbol{v} = \frac{1}{\rho_0} \boldsymbol{\nabla}_0 \boldsymbol{p}. \tag{4.10}$$

Integration of above equation (4.10) over the undeformed volume V and application of the divergence theorem leads to the following global conservation law for $\boldsymbol{F}$ as

$$\frac{d}{dt} \int_V \boldsymbol{F} \, dV = \int_V \frac{1}{\rho_0} \boldsymbol{\nabla}_0 \boldsymbol{p} \, dV = \int_{\partial V} \frac{1}{\rho_0} \boldsymbol{p} \otimes \, d\boldsymbol{A}. \tag{4.11}$$

Finally, the corresponding local differential equation and jump condition to that in equation (4.11) is

$$\frac{\partial \boldsymbol{F}}{\partial t} - \mathrm{DIV} \left(\frac{1}{\rho_0} \boldsymbol{p} \otimes \boldsymbol{I} \right) = \boldsymbol{0}; \qquad U \left[\!\!\left[\boldsymbol{F} \right]\!\!\right] = - \left[\!\!\left[\frac{1}{\rho_0} \boldsymbol{p} \right]\!\!\right] \otimes \boldsymbol{N}. \tag{4.12}$$

Conservation of area map

A conservation law for the co-factor or area map can be derived considering its definition in equation (2.26). Differentiation of this equation with respect to time yields

$$\frac{\partial \boldsymbol{H}}{\partial t} = \boldsymbol{F} \times \frac{1}{\rho_0} \boldsymbol{\nabla}_0 \boldsymbol{p}. \tag{4.13}$$

Integration of above equation (4.13) over the undeformed volume V and application of chain rule and the divergence theorem results in

$$\frac{d}{dt} \int_V \boldsymbol{H} \, dV = \int_{\partial V} \boldsymbol{F} \times \left(\frac{1}{\rho_0} \boldsymbol{p} \otimes d\boldsymbol{A} \right) - \int_V \frac{1}{\rho_0} \boldsymbol{p} \times \mathrm{CURL} \boldsymbol{F} \, dV. \tag{4.14}$$

Consideration of the curl-free condition for the deformation gradient tensor in equation $(2.36)_b$ enables above equation (4.14) to be finally written as a global conservation law as

$$\frac{d}{dt} \int_V \boldsymbol{H} \, dV = \int_{\partial V} \boldsymbol{F} \times \left(\frac{1}{\rho_0} \boldsymbol{p} \otimes d\boldsymbol{A} \right). \tag{4.15}$$

Finally, the corresponding local differential equation and jump condition to that in equation (4.15) is

$$\frac{\partial \boldsymbol{H}}{\partial t} - \mathrm{CURL} \left(\frac{1}{\rho_0} \boldsymbol{p} \times \boldsymbol{F} \right) = \boldsymbol{0}; \qquad U \left[\!\!\left[\boldsymbol{H} \right]\!\!\right] = - \boldsymbol{F} \times \left[\!\!\left[\frac{1}{\rho_0} \boldsymbol{p} \right]\!\!\right] \otimes \boldsymbol{N}. \tag{4.16}$$

Conservation of volume map

A conservation law for the Jacobian of the deformation gradient or volume map can be derived considering its definition in equation (2.38), namely $J = \frac{1}{3}(\boldsymbol{H} : \boldsymbol{F})$. Differentiation of this equation with respect to time yields

$$\frac{\partial J}{\partial t} = \boldsymbol{H} : \frac{1}{\rho_0}\boldsymbol{\nabla}_0 \boldsymbol{p}. \tag{4.17}$$

Integration of above equation (4.17) over the undeformed volume V and application of chain rule and the divergence theorem results in

$$\frac{d}{dt}\int_V J\, dV = \int_{\partial V} \boldsymbol{H} : \left(\frac{1}{\rho_0}\boldsymbol{p} \otimes d\boldsymbol{A}\right) - \int_V \frac{1}{\rho_0}\boldsymbol{p} \cdot \mathrm{DIV}\boldsymbol{H}\, dV. \tag{4.18}$$

Consideration of the divergence-free condition for the deformation gradient tensor in equation $(2.36)_a$ enables above equation (4.18) to be finally written as a global conservation law as

$$\frac{d}{dt}\int_V J\, dV = \int_{\partial V} \boldsymbol{H} : \left(\frac{1}{\rho_0}\boldsymbol{p} \otimes d\boldsymbol{A}\right). \tag{4.19}$$

Finally, the corresponding local differential equation and jump condition to that in equation (4.19) is

$$\frac{\partial J}{\partial t} - \mathrm{DIV}\left(\frac{1}{\rho_0}\boldsymbol{p}\right) = 0; \qquad U\left[\!\left[J\right]\!\right] = -\boldsymbol{H} : \left(\left[\!\left[\frac{1}{\boldsymbol{H}^T\rho_0}\boldsymbol{p}\right]\!\right] \otimes \boldsymbol{N}\right). \tag{4.20}$$

4.2.5 Combined equations

Combining the results of the various sections above, a full set of first order conservation laws (4.3) can be established with vector of variables $\boldsymbol{\mathcal{U}}$, vector of fluxes $\boldsymbol{\mathcal{F}}_I$ and vector if source terms $\boldsymbol{\mathcal{S}}$ given by

$$\boldsymbol{\mathcal{U}} = \begin{bmatrix} \boldsymbol{p} \\ \boldsymbol{F} \\ \boldsymbol{H} \\ J \end{bmatrix}; \qquad \boldsymbol{\mathcal{F}}_I = -\begin{bmatrix} \boldsymbol{P}\boldsymbol{E}_I \\ \frac{1}{\rho_0}\boldsymbol{p} \otimes \boldsymbol{E}_I \\ \boldsymbol{F} \times \left(\frac{1}{\rho_0}\boldsymbol{p} \otimes \boldsymbol{E}_I\right) \\ \boldsymbol{H} : \left(\frac{1}{\rho_0}\boldsymbol{p} \otimes \boldsymbol{E}_I\right) \end{bmatrix}; \qquad \boldsymbol{\mathcal{S}} = \begin{bmatrix} \boldsymbol{f}_0 \\ \boldsymbol{0} \\ \boldsymbol{0} \\ 0 \end{bmatrix}, \tag{4.21}$$

where the components of the flux vector $\boldsymbol{\mathcal{F}}_I$ are defined as

$$\begin{aligned} \boldsymbol{\mathcal{F}}_I^{\boldsymbol{p}} &= -\boldsymbol{P}\boldsymbol{E}_I; & \boldsymbol{\mathcal{F}}_I^{\boldsymbol{F}} &= -\frac{1}{\rho_0}\boldsymbol{p} \otimes \boldsymbol{E}_I; \\ \boldsymbol{\mathcal{F}}_I^{\boldsymbol{H}} &= -\boldsymbol{F} \times \left(\frac{1}{\rho_0}\boldsymbol{p} \otimes \boldsymbol{E}_I\right); & \boldsymbol{\mathcal{F}}_I^{J} &= -\boldsymbol{H} : \left(\frac{1}{\rho_0}\boldsymbol{p} \otimes \boldsymbol{E}_I\right), \end{aligned} \tag{4.22}$$

where $\boldsymbol{P}$ defined as in equation (2.53) and (2.48). Let us recall the quasilinear form for the system of hyperbolic equations with vector of variables $\boldsymbol{\mathcal{U}}$, vector of fluxes $\boldsymbol{\mathcal{F}}_I$ and vector of source terms $\boldsymbol{\mathcal{S}}$ in (4.21), that is

$$\frac{\partial \boldsymbol{\mathcal{U}}}{\partial t} + \underbrace{\boldsymbol{\mathcal{A}}_I \frac{\partial \boldsymbol{\mathcal{U}}}{\partial X_I}}_{\alpha^\star} = \boldsymbol{\mathcal{S}}, \tag{4.23}$$

where the 'non-trivial' second term on the left-hand side of above equation (4.23), namely $\alpha^\star$ can be expressed as

$$\alpha^\star = -\underbrace{\left[\begin{array}{c:c} \mathbf{0}_{3\times 3} & \\ \frac{\partial \boldsymbol{\mathcal{F}}_I^{\boldsymbol{F}}}{\partial \boldsymbol{p}} & \\ \frac{\partial \boldsymbol{\mathcal{F}}_I^{\boldsymbol{H}}}{\partial \boldsymbol{p}} & \widetilde{\boldsymbol{W}_I} \\ \frac{\partial \boldsymbol{\mathcal{F}}_I^{J}}{\partial \boldsymbol{p}} & \end{array}\right]}_{\boldsymbol{\mathcal{A}}_I} \frac{\partial}{\partial X_I} \left[\begin{array}{c} \cdot \boldsymbol{p} \\ : \boldsymbol{F} \\ : \boldsymbol{H} \\ J \end{array}\right], \tag{4.24}$$

where the entries in the first column of above matrix $\boldsymbol{\mathcal{A}}_I$ can be written in indicial notation as

$$\left[\frac{\partial \boldsymbol{\mathcal{F}}_I^{\boldsymbol{F}}}{\partial \boldsymbol{p}}\right]_{iKk} = \frac{1}{\rho_0}\delta_{ik}\delta_{IK}; \qquad \left[\frac{\partial \boldsymbol{\mathcal{F}}_I^{\boldsymbol{H}}}{\partial \boldsymbol{p}}\right]_{iKk} = \frac{1}{\rho_0}\mathcal{E}_{imk}\mathcal{E}_{KMI}F_{mM}; \qquad \left[\frac{\partial \boldsymbol{\mathcal{F}}_I^{J}}{\partial \boldsymbol{p}}\right]_{i} = \frac{1}{\rho_0}H_{iI} \tag{4.25}$$

In addition, the inner products $(\cdot)$ and $(:)$ appearing in the vector of conservation variables in (4.24) represent standard contraction of repeated indices. Moreover, the expression for the matrix $\widetilde{\boldsymbol{W}_I}$ (4.24) is

$$\widetilde{\boldsymbol{W}_I} = \left[\begin{array}{ccc} \widetilde{\boldsymbol{P}_{\boldsymbol{F}}}\boldsymbol{E}_I & \widetilde{\boldsymbol{P}_{\boldsymbol{H}}}\boldsymbol{E}_I & \widetilde{\boldsymbol{P}_J}\boldsymbol{E}_I \\ \mathbf{0}_{3\times3\times3\times3} & \mathbf{0}_{3\times3\times3\times3} & \mathbf{0}_{3\times3} \\ \mathbf{0}_{3\times3\times3\times3} & \mathbf{0}_{3\times3\times3\times3} & \mathbf{0}_{3\times3} \\ \mathbf{0}_{3\times3} & \mathbf{0}_{3\times3} & 0 \end{array}\right], \tag{4.26}$$

with

$$\begin{aligned} \widetilde{\boldsymbol{P}_{\boldsymbol{F}}} &= W_{\boldsymbol{F}\boldsymbol{F}} + \boldsymbol{F} \times W_{\boldsymbol{H}\boldsymbol{F}} + \boldsymbol{H} \otimes W_{J\boldsymbol{F}}; \\ \widetilde{\boldsymbol{P}_{\boldsymbol{H}}} &= W_{\boldsymbol{F}\boldsymbol{H}} + \boldsymbol{F} \times W_{\boldsymbol{H}\boldsymbol{H}} + \boldsymbol{H} \otimes W_{J\boldsymbol{H}}; \\ \widetilde{\boldsymbol{P}_J} &= W_{\boldsymbol{F}J} + \boldsymbol{F} \times W_{\boldsymbol{H}J} + \boldsymbol{H} W_{JJ} + W_{\boldsymbol{d}J} \otimes \boldsymbol{D}_0 + W_{\boldsymbol{b}J} \otimes \boldsymbol{B}_0. \end{aligned} \tag{4.27}$$

4.3 Eigenvalue structure of the equations in nonlinear solid dynamics

The objective of this Section is to analyse the eigenvalue structure of the combined set of conservation laws for polyconvex Solid Dynamics in equation (4.21).

4.3.1 Eigenvalue structure. The acoustic tensor

The eigenvalues or wave speeds and corresponding eigenvectors of the system of conservation laws in equation (4.21) can be determined by identifying possible plane wave solutions (in the absence of source terms) of the type

$$\boldsymbol{\mathcal{U}} = \phi(\boldsymbol{X}\cdot\boldsymbol{N} - c_\alpha t)\bar{\boldsymbol{\mathcal{U}}}_\alpha = \phi(\boldsymbol{X}\cdot\boldsymbol{N} - c_\alpha t)\left[\begin{array}{c} \bar{\boldsymbol{p}}_\alpha \\ \bar{\boldsymbol{F}}_\alpha \\ \bar{\boldsymbol{H}}_\alpha \\ \bar{J}_\alpha \end{array}\right], \tag{4.28}$$

where c_α are the wave speeds corresponding to the eigenmode $\bar{\boldsymbol{\mathcal{U}}}_\alpha$ and $\boldsymbol{N}$, the normalised direction of propagation. The above expression for the reduced set of conservation variables leads to an eigenvalue problem (refer to equation (4.5)) given by

$$\boldsymbol{\mathcal{A}}_{\boldsymbol{N}}\bar{\boldsymbol{\mathcal{U}}}_\alpha = c_\alpha\bar{\boldsymbol{\mathcal{U}}}_\alpha; \qquad \boldsymbol{\mathcal{A}}_{\boldsymbol{N}} = \boldsymbol{\mathcal{A}}_I N_I. \tag{4.29}$$

Particularisation of the local conservation equation for the deformation gradient tensor $\boldsymbol{F}$ $(4.12)_a$ to plane wave solutions of the type described in equation (4.28) yields (refer to Figure 4.3)

$$-c_\alpha\bar{\boldsymbol{F}}_\alpha\phi' - \frac{1}{\rho_0}\bar{\boldsymbol{p}}_\alpha\otimes\boldsymbol{N}\phi' = \boldsymbol{0} \Rightarrow \bar{\boldsymbol{F}}_\alpha = \bar{\boldsymbol{f}}_\alpha\otimes\boldsymbol{N}, \tag{4.30}$$

where $\bar{\boldsymbol{f}}_\alpha = -\frac{1}{c_\alpha\rho_0}\bar{\boldsymbol{p}}_\alpha$. Moreover, substitution of the above plane wave-like solutions (4.28) in conjunction with (4.30) into equations (4.16) and (4.20) yields

$$\bar{\boldsymbol{H}}_\alpha = \boldsymbol{F}\boldsymbol{\times}\left(\bar{\boldsymbol{f}}_\alpha\otimes\boldsymbol{N}\right); \qquad \bar{J}_\alpha = \boldsymbol{H}:\left(\bar{\boldsymbol{f}}_\alpha\otimes\boldsymbol{N}\right). \tag{4.31}$$

The expressions in above equations (4.30) and (4.31), where $\bar{\boldsymbol{F}}_\alpha$, $\bar{\boldsymbol{H}}_\alpha$ and $\bar{J}_\alpha$ have been expressed in terms of the eigenmode $\bar{\boldsymbol{f}}_\alpha$ enable to re-write and reduced the eigenvalue problem in (4.28) to

$$c_\alpha\bar{\boldsymbol{\mathcal{U}}}^\star_\alpha = \boldsymbol{\mathcal{A}}^\star_{\boldsymbol{N}}\bar{\boldsymbol{\mathcal{U}}}^\star_\alpha, \tag{4.32}$$

in terms of the reduced set of eigenvectors $\bar{\boldsymbol{\mathcal{U}}}^\star_\alpha$ and the reduced Jacobian matrix $\boldsymbol{\mathcal{A}}_{\boldsymbol{N}}{}^\star$ defined as

$$\bar{\boldsymbol{\mathcal{U}}}^\star_\alpha = \begin{bmatrix}\bar{\boldsymbol{p}}_\alpha\\ \bar{\boldsymbol{f}}_\alpha\end{bmatrix}; \qquad \boldsymbol{\mathcal{A}}^\star_{\boldsymbol{N}} = -\begin{bmatrix}\boldsymbol{0} & \boldsymbol{\mathcal{C}}_{\boldsymbol{NN}}\\ \frac{1}{\rho_0}\boldsymbol{I} & \boldsymbol{0}\end{bmatrix} \tag{4.33}$$

with $\boldsymbol{\mathcal{C}}_{\boldsymbol{NN}}$ in above equation (4.33) denoting the classical acoustic tensor [30, 86], defined as

$$\mathcal{C}_{NNij} = \mathcal{C}_{iIjJ}N_IN_J, \tag{4.34}$$

with $\boldsymbol{\mathcal{C}}$ defined in terms of the components of the Hessian operator $[\mathbb{H}_W]$ (2.74) in equation (4.33). Careful analysis of the matrix $\boldsymbol{\mathcal{A}}^\star_{\boldsymbol{N}}$ in above equation (4.33) enables to identify the following multiplicative decomposition of $\boldsymbol{\mathcal{A}}^\star_{\boldsymbol{N}}$ as

$$\boldsymbol{\mathcal{A}}^\star_{\boldsymbol{N}} = -\boldsymbol{S}\boldsymbol{U}, \tag{4.35}$$

where the second orders tensor $\boldsymbol{S}$ and $\boldsymbol{U}$ in above equation (4.35) are defined as

$$\boldsymbol{S} = \begin{bmatrix}\boldsymbol{0} & \boldsymbol{I}\\ \boldsymbol{I} & \boldsymbol{0}\end{bmatrix}; \qquad \boldsymbol{U} = \begin{bmatrix}\frac{1}{\rho_0}\boldsymbol{I} & \boldsymbol{0}_{3\times3}\\ \boldsymbol{0}_{3\times3} & \boldsymbol{\mathcal{C}}_{\boldsymbol{NN}}\end{bmatrix}, \tag{4.36}$$

Following a fundamental theorem in the theory of hyperbolic equations, summarised in Appendix F for completeness, given the symmetric nature of $\boldsymbol{S}$ $(4.36)_a$, a sufficient condition for the existence of real eigenvalues for the above Jacobian matrix $\boldsymbol{\mathcal{A}}^\star_{\boldsymbol{N}}$ (refer to (4.33) and (4.35)) would be the symmetric positive definiteness of

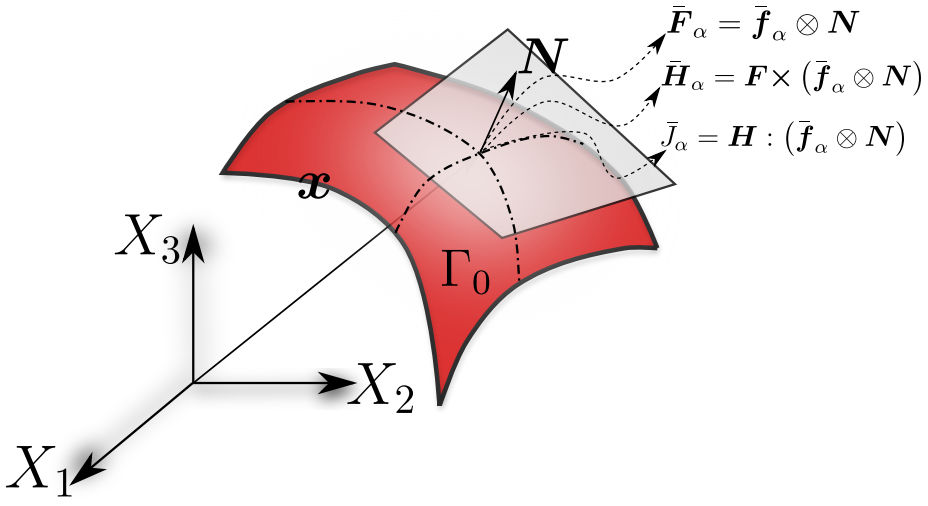

Figure 4.3: Eigenmodes $\bar{\boldsymbol{F}}_\alpha$, $\bar{\boldsymbol{H}}_\alpha$ and $\bar{J}_\alpha$ at a discontinuity surface Γ_0 perpendicular to the vector of propagation $\boldsymbol{N}$.

$\boldsymbol{U}$ $(4.36)_b$ and hence, of $\boldsymbol{\mathcal{C}_{NN}}$ (4.34). Moreover, positive definiteness of the acoustic tensor $\boldsymbol{\mathcal{C}_{NN}}$ can be shown by noticing the following relationship between $\boldsymbol{\mathcal{C}_{NN}}$ and the Hessian operator $[\mathbb{H}_W]$ (recall *Remark 2.5* with $\boldsymbol{v} = \bar{\boldsymbol{f}}_\alpha$ and $\boldsymbol{V} = \boldsymbol{N}$), namely

$$\bar{\boldsymbol{f}}_\alpha \cdot \boldsymbol{\mathcal{C}_{NN}} \bar{\boldsymbol{f}}_\alpha = \begin{bmatrix} \bar{\boldsymbol{F}}_\alpha \\ \bar{\boldsymbol{H}}_\alpha \\ \bar{J}_\alpha \end{bmatrix}^T [\mathbb{H}_W] \begin{bmatrix} \bar{\boldsymbol{F}}_\alpha \\ \bar{\boldsymbol{H}}_\alpha \\ \bar{J}_\alpha \end{bmatrix} > 0. \tag{4.37}$$

As can be seen, the positive definiteness of the acoustic tensor $\boldsymbol{\mathcal{C}_{NN}}$ is implied by the positive definiteness of the extended Hessian operator $[\mathbb{H}_W]$, always satisfied by polyconvex energy functionals (2.39).

Finally, substitution of the expression for the eigenmode $\bar{\boldsymbol{f}}_\alpha$, namely $\bar{\boldsymbol{f}}_\alpha = -\frac{1}{c_\alpha \rho_0} \boldsymbol{p}_\alpha$ in the eigenvalue problem $\boldsymbol{\mathcal{A}}^\star_{\boldsymbol{N}} \bar{\boldsymbol{\mathcal{U}}}^\star_\alpha = c_\alpha \bar{\boldsymbol{\mathcal{U}}}^\star_\alpha$ leads to the final eigenvalue problem associated to a single second order hyperbolic equation defined as

$$\left(\rho_0 c_\alpha^2 \boldsymbol{I} - \boldsymbol{\mathcal{C}_{NN}}\right) \bar{\boldsymbol{p}}_\alpha = \boldsymbol{0}. \tag{4.38}$$

4.4 Symmetrisation of the equations in nonlinear solid dynamics

For completeness, the objective of this Section is to show that, polyconvexity of the internal energy enables the introduction of a generalised convex entropy function which in turn, guarantees the symmetrisation of the system of conservation laws [2, 102] in equation (4.21).

4.4.1 Entropy

Quasi-linear first order hyperbolic systems can be symmetrised with an appropriate change of variables [98], if there exists a convex generalised entropy function $S(\boldsymbol{\mathcal{U}})$ and corresponding entropy flux $\boldsymbol{\Lambda}(\boldsymbol{\mathcal{U}})$ such that in the absence of source terms and for all admissible solutions

$$\frac{\partial S}{\partial t} + \mathrm{DIV}\boldsymbol{\Lambda} \geq 0. \tag{4.39}$$

The above inequality becomes an equality for smooth solutions in the absence of dissipative effects such as viscosity or heat flow. It is now possible to define a new set of conjugate entropy variables $\boldsymbol{\mathcal{V}} = \frac{\partial S}{\partial \boldsymbol{\mathcal{U}}}$ for which the conservation laws (4.5) become

$$\boldsymbol{\mathcal{A}}_0 \frac{\partial \boldsymbol{\mathcal{V}}}{\partial t} + \tilde{\boldsymbol{\mathcal{A}}}_I \frac{\partial \boldsymbol{\mathcal{V}}}{\partial X_I} = \boldsymbol{\mathcal{S}}. \tag{4.40}$$

The symmetric system matrices $\boldsymbol{\mathcal{A}}_0$ and $\tilde{\boldsymbol{\mathcal{A}}}_I$ are

$$\boldsymbol{\mathcal{A}}_0 = \frac{\partial \boldsymbol{\mathcal{U}}}{\partial \boldsymbol{\mathcal{V}}} = \left[\frac{\partial^2 S}{\partial \boldsymbol{\mathcal{U}} \partial \boldsymbol{\mathcal{U}}}\right]^{-1}; \qquad \tilde{\boldsymbol{\mathcal{A}}}_I = \boldsymbol{\mathcal{A}}_I \boldsymbol{\mathcal{A}}_0 = \tilde{\boldsymbol{\mathcal{A}}}_I^T, \tag{4.41}$$

and the entropy flux Λ_I satisfies

$$\frac{\partial \Lambda_I}{\partial \boldsymbol{\mathcal{U}}} = \boldsymbol{\mathcal{V}}^T \boldsymbol{\mathcal{A}}_I. \tag{4.42}$$

Consideration of the symmetry of the matrix $\hat{\boldsymbol{\mathcal{A}}}_I$ enables to re-write the above conjugate set of equations for the entropy variables as

$$\frac{\partial \boldsymbol{\mathcal{V}}}{\partial t} + \boldsymbol{\mathcal{A}}_I^T \frac{\partial \boldsymbol{\mathcal{V}}}{\partial X_I} = \boldsymbol{\mathcal{A}}_0^{-1} \boldsymbol{\mathcal{S}}. \tag{4.43}$$

4.4.2 Conservation of energy and generalised convex entropy

In order to derive a suitable generalised entropy and entropy flux functions for nonlinear elasticity, let us consider the following convex entropy function defined as

$$S(\boldsymbol{p}, \boldsymbol{F}, \boldsymbol{H}, J) = \frac{1}{2\rho_0} \boldsymbol{p} \cdot \boldsymbol{p} + W(\boldsymbol{F}, \boldsymbol{H}, J) \tag{4.44}$$

which clearly represents the kinetic and internal energy per unit undeformed volume. The corresponding flux vector is defined as

$$\boldsymbol{\Lambda} = -\frac{1}{\rho_0} \boldsymbol{P}^T \boldsymbol{p}, \tag{4.45}$$

In order to prove this, note first that the conjugate entropy variables are given by the derivatives of S as,

$$\boldsymbol{\mathcal{V}} = \frac{\partial S}{\partial \boldsymbol{\mathcal{U}}} = \begin{bmatrix} \boldsymbol{v} \\ \boldsymbol{\Sigma}_{\boldsymbol{F}} \\ \boldsymbol{\Sigma}_{\boldsymbol{H}} \\ \Sigma_J \end{bmatrix}. \tag{4.46}$$

Multiplying each of the conservation laws (4.21) by the corresponding conjugate variables (4.46), and using the involution equations (4.1) for the deformation gradient and its co-factor gives

$$\begin{aligned}\dot{S} &= \boldsymbol{v}\cdot\dot{\boldsymbol{p}} + \boldsymbol{\Sigma_F}:\dot{\boldsymbol{F}} + \boldsymbol{\Sigma_H}:\dot{\boldsymbol{H}} + \Sigma_J\dot{J}\\ &= \boldsymbol{v}\cdot\mathrm{DIV}\boldsymbol{P} + \boldsymbol{v}\cdot\boldsymbol{f}_0 + \boldsymbol{\Sigma_F}:\boldsymbol{\nabla}_0\boldsymbol{v} + \boldsymbol{\Sigma_H}:\mathrm{CURL}\left(\boldsymbol{v}\times\boldsymbol{F}\right) + \Sigma_J\mathrm{DIV}\left(\boldsymbol{H}^T\boldsymbol{v}\right)\\ &= \boldsymbol{v}\cdot\mathrm{DIV}\boldsymbol{P} + \boldsymbol{v}\cdot\boldsymbol{f}_0 + \left(\boldsymbol{\Sigma_F} + \boldsymbol{\Sigma_H}\times\boldsymbol{F} + \Sigma_J\boldsymbol{H}\right):\boldsymbol{\nabla}_0\boldsymbol{v}\\ &= \boldsymbol{v}\cdot\mathrm{DIV}\boldsymbol{P} + \boldsymbol{v}\cdot\boldsymbol{f}_0 + \boldsymbol{P}:\boldsymbol{\nabla}_0\boldsymbol{v}\\ &= \mathrm{DIV}\left(\boldsymbol{P}^T\boldsymbol{v}\right) + \boldsymbol{v}\cdot\boldsymbol{f}_0.\end{aligned} \tag{4.47}$$

Notice that the statement in above equation (7.79) is in fact a simplified version of the energy conservation law, or first law of thermodynamics, which, in the absence of the heat sources is globally stated as

$$\frac{d}{dt}\int_V E\,dV = \int_{\partial V}\boldsymbol{t}_0\cdot\boldsymbol{v}\,dA + \int_V \boldsymbol{f}_0\cdot\boldsymbol{v}\,dV, \tag{4.48}$$

where E denotes the total energy per unit undeformed volume. The local version of this equation gives,

$$\frac{\partial E}{\partial t} - \mathrm{DIV}\left(\boldsymbol{P}^T\boldsymbol{v}\right) = \boldsymbol{f}_0\cdot\boldsymbol{v}. \tag{4.49}$$

It is therefore clear that for the reversible scenarios under consideration of smooth solutions (i.e. in the absence of physical shocks), the generalised entropy is simply the total energy per unit undeformed volume, that is, $S = E$, coinciding with the notion of Hamiltonian per unit of undeformed volume.

4.4.3 Symmetric hyperbolic equations for elastodynamics

With the definition of the conjugate entropy variables given above (4.46), it is now possible to derive a symmetric quasi-linear system for these variables. In order to do this, let us consider first the linear momentum equation. This equation can now be transformed making use of the involution equations for $\boldsymbol{F}$ and $\boldsymbol{H}$ in (2.36), yielding

$$\rho_0\frac{\partial\boldsymbol{v}}{\partial t} - \mathrm{DIV}\boldsymbol{\Sigma_F} + \boldsymbol{F_\Sigma}\times\mathrm{CURL}\boldsymbol{\Sigma_H} - \boldsymbol{H_\Sigma}\boldsymbol{\nabla}_0\Sigma_J = \boldsymbol{f}_0, \tag{4.50}$$

which represents the conservation of linear momentum and

$$\left[\mathbb{H}_W\right]^{-1}\frac{\partial}{\partial t}\begin{bmatrix}\boldsymbol{\Sigma_F}\\ \boldsymbol{\Sigma_H}\\ \Sigma_J\end{bmatrix} - \begin{bmatrix}\boldsymbol{\nabla}_0\boldsymbol{v}\\ \boldsymbol{F}_\Sigma\times\boldsymbol{\nabla}_0\boldsymbol{v}\\ \boldsymbol{H_\Sigma}:\boldsymbol{\nabla}_0\boldsymbol{v}\end{bmatrix} = \boldsymbol{0}, \tag{4.51}$$

which represents the remaining set of conservation laws. Notice in above equations (4.50) and (4.51) that the notations $\boldsymbol{F}_\Sigma$ and $\boldsymbol{H}_\Sigma$ have been used here to explicitly indicate that these variables are no being evaluated from the conjugate variables in (4.46) using the reverse constitutive relationships, namely

$$\begin{aligned}\boldsymbol{F_\Sigma} &= \boldsymbol{F}\left(\boldsymbol{\Sigma_F},\boldsymbol{\Sigma_H},\Sigma_J\right);\\ \boldsymbol{H_\Sigma} &= \boldsymbol{H}\left(\boldsymbol{\Sigma_F},\boldsymbol{\Sigma_H},\Sigma_J\right).\end{aligned} \tag{4.52}$$

The symmetric nature of this system is more easily appreciated combining the above set of equations (4.50) and (4.51) to give

$$\boldsymbol{\mathcal{A}}_0 \frac{\partial \boldsymbol{\mathcal{V}}}{\partial t} + \underbrace{\tilde{\boldsymbol{\mathcal{A}}}_I \frac{\partial \boldsymbol{\mathcal{V}}}{\partial X_I}}_{\beta^\star} = \boldsymbol{\mathcal{S}}, \tag{4.53}$$

where matrix $\boldsymbol{\mathcal{A}}_0$ in above equation (4.53) is defined as

$$\boldsymbol{\mathcal{A}}_0 = \begin{bmatrix} \rho_0 \boldsymbol{I} & \boldsymbol{0} \\ \boldsymbol{0} & [\mathbb{H}_W]^{-1} \end{bmatrix}, \tag{4.54}$$

with $\mathbb{H}_W$ defined in equation (2.74). It is therefore certain that the matrix $\boldsymbol{\mathcal{A}}_0$ is symmetric positive definite provided that the strain energy is polyconvex. Finally, the second term on the left-hand side of (4.53), namely $\beta^\star$ can be expanded in indicial notation as

$$\beta^\star = - \underbrace{\begin{bmatrix} \boldsymbol{0} & \delta_{ik}\delta_{KI} & \mathcal{E}_{ijk}\mathcal{E}_{IJK}F_{jJ} & H_{iI} \\ & \boldsymbol{0} & \boldsymbol{0} & \boldsymbol{0} \\ & & \boldsymbol{0} & \boldsymbol{0} \\ & & & 0 \end{bmatrix}}_{\tilde{\boldsymbol{\mathcal{A}}}_I} \frac{\partial}{\partial X_I} \begin{bmatrix} v_k \\ [\boldsymbol{\Sigma}_{\boldsymbol{F}}]_{kK} \\ [\boldsymbol{\Sigma}_{\boldsymbol{H}}]_{kK} \\ \Sigma_J \end{bmatrix}. \tag{4.55}$$

The symmetrisation displayed in (4.55) confirms once again the existence of real waves (e.g. legendre-Hadamard condition) and opens up very interesting possibilities to use stabilised based formulations, as in [2] in the context of Computational Fluid Dynamics and in line with those published in References [42, 43, 57, 103–105] in the context of nonlinear elasticity.

4.5 Numerical implementation

In Section 2.6, a series of mixed variational principles for the solution of polyconvex large strain elasticity for static scenarios and their computational implementation in Chapter 3 were presented. Moreover, a series of numerical examples were presented in Section 3.3, proving these mixed variational principles very convenient from the computational standpoint as the typical inherent deficiencies associated to the classical displacement based formulation can be remedied by these more advanced mixed formulations. The objective of this Section is to study the possible application of these mixed variational principles in the context of dynamic scenarios.

4.5.1 Lagrangian-based mixed formulations

A natural extension of the mixed variational formulations presented in Section 2.6 to dynamic scenarios can be obtained via the definition of the Lagrangian functional [11] and its associated action integral L defined as

$$L\left(\boldsymbol{\phi}, \dot{\boldsymbol{\phi}}\right) = \int_V \mathcal{L}\left(\boldsymbol{\phi}, \dot{\boldsymbol{\phi}}, \boldsymbol{\nabla}_0 \boldsymbol{\phi}\right) \, dV - \int_{\partial V} \mathcal{U}_{\boldsymbol{t}_0} \, dA, \tag{4.56}$$

where the variables $\boldsymbol{\phi}$ denote the so called fields [11]. For the particular case of a displacement based formulation, the field variable coincides with the mapping $\boldsymbol{x}(\boldsymbol{X}, t)$ and the Lagrangian associated to elasto-dynamics is defined as

$$\mathcal{L}(\boldsymbol{x}, \boldsymbol{v}, \boldsymbol{F}_{\boldsymbol{x}}) = \mathcal{K} - \Psi(\boldsymbol{F}_{\boldsymbol{x}}) - \mathcal{U}_{\boldsymbol{f}_0}, \tag{4.57}$$

with the kinetic energy and the energy potential due to conservative volumetric forces per unit undeformed volume $\boldsymbol{f}_0$ defined as

$$\mathcal{K} = \frac{\rho_0}{2}\boldsymbol{v}\cdot\boldsymbol{v}; \qquad \mathcal{U}_{\boldsymbol{f}_0} = -\boldsymbol{f}_0\cdot\boldsymbol{x}. \tag{4.58}$$

Moreover, the boundary term in above equation (4.56) corresponds to the energy potential due to conservative forces per unit undeformed area $\boldsymbol{t}_0$ defined as

$$\mathcal{U}_{\boldsymbol{t}_0} = -\boldsymbol{t}_0\cdot\boldsymbol{x}. \tag{4.59}$$

The solution to the equations of nonlinear elasto-dynamics can then be obtained at the stationary condition of the above action integral, namely $\delta L = 0$, with the directional derivative of the action integral defined as

$$\delta L = \int_V \frac{\partial}{\partial t}\frac{\partial \mathcal{L}}{\partial \dot{\boldsymbol{\phi}}}\cdot\delta\boldsymbol{\phi}\, dV - \int_V \frac{\partial \mathcal{L}}{\partial \boldsymbol{\phi}}\cdot\delta\boldsymbol{\phi}\, dV - \int_V \frac{\partial \mathcal{L}}{\partial \boldsymbol{\nabla}_0\boldsymbol{\phi}}\cdot\boldsymbol{\nabla}_0\delta\boldsymbol{\phi}\, dV. \tag{4.60}$$

For the mixed variational principles Π_M and Π_C presented in Sections 2.6.2 and 2.6.3, respectively, two action integrals L_M and L_C with associated fields are defined as

$$\boldsymbol{\phi}_M = \{\boldsymbol{x}, \boldsymbol{F}, \boldsymbol{H}, J, \boldsymbol{\Sigma}_{\boldsymbol{F}}, \boldsymbol{\Sigma}_{\boldsymbol{H}}, \Sigma_J\}; \qquad \boldsymbol{\phi}_C = \{\boldsymbol{x}, \boldsymbol{\Sigma}_{\boldsymbol{F}}, \boldsymbol{\Sigma}_{\boldsymbol{H}}, \Sigma_J\}. \tag{4.61}$$

and with Lagrangian functionals $\mathcal{L}_M$ and $\mathcal{L}_C$ defined as

$$\begin{aligned}
\mathcal{L}_M\left(\boldsymbol{\phi}, \dot{\boldsymbol{\phi}}\right) &= \mathcal{K} - W(\boldsymbol{F}, \boldsymbol{H}, J) - \boldsymbol{\Sigma}_{\boldsymbol{F}} : (\boldsymbol{F}_{\boldsymbol{x}} - \boldsymbol{F}) - \boldsymbol{\Sigma}_{\boldsymbol{H}} : (\boldsymbol{H}_{\boldsymbol{x}} - \boldsymbol{H}) \\
&\quad - \Sigma_J (J_{\boldsymbol{x}} - J) - \mathcal{U}_{\boldsymbol{f}_0}; \\
\mathcal{L}_C\left(\boldsymbol{\phi}, \dot{\boldsymbol{\phi}}\right) &= \mathcal{K} - \Upsilon(\boldsymbol{\Sigma}_{\boldsymbol{F}}, \boldsymbol{\Sigma}_{\boldsymbol{H}}, \Sigma_J) - \boldsymbol{\Sigma}_{\boldsymbol{F}} : \boldsymbol{F}_{\boldsymbol{x}} - \boldsymbol{\Sigma}_{\boldsymbol{H}} : \boldsymbol{H}_{\boldsymbol{x}} - \Sigma_J J_{\boldsymbol{x}} - \mathcal{U}_{\boldsymbol{f}_0}.
\end{aligned} \tag{4.62}$$

The stationary conditions for the action integral L_M (refer to equation (4.60)) with associated fields $\boldsymbol{\phi}_M$ in $(4.61)_a$ yield,

$$\begin{aligned}
&\int_V \rho_0 \frac{\partial \boldsymbol{v}}{\partial t}\cdot\delta\boldsymbol{u}\, dV + \int_V \boldsymbol{P}_M : \boldsymbol{\nabla}_0\delta\boldsymbol{u}\, dV - \int_{\partial V} \boldsymbol{t}_0\cdot\delta\boldsymbol{u}\, dA - \int_V \boldsymbol{f}_0\cdot\delta\boldsymbol{u}\, dV = 0; \\
&\int_V \delta\boldsymbol{\Sigma}_{\boldsymbol{\mathcal{D}}} : (\boldsymbol{\mathcal{D}}_{\boldsymbol{x}} - \boldsymbol{\mathcal{D}})\, dV = 0; \\
&\int_V \delta\boldsymbol{\mathcal{D}} : \left(\frac{\partial W}{\partial \boldsymbol{\mathcal{D}}} - \boldsymbol{\Sigma}_{\boldsymbol{\mathcal{D}}}\right) dV = 0,
\end{aligned} \tag{4.63}$$

with $\boldsymbol{P}_M$ defined as in equation (2.182) and where the following compact notation has been used in above equation (4.63)

$$\begin{aligned}
\boldsymbol{\mathcal{D}} &= \{\boldsymbol{F}, \boldsymbol{H}, J\}; & \boldsymbol{\Sigma}_{\boldsymbol{\mathcal{D}}} &= \{\boldsymbol{\Sigma}_{\boldsymbol{F}}, \boldsymbol{\Sigma}_{\boldsymbol{H}}, \Sigma_J\}; \\
\delta\boldsymbol{\mathcal{D}} &= \{\delta\boldsymbol{F}, \delta\boldsymbol{H}, \delta J\}; & \delta\boldsymbol{\Sigma}_{\boldsymbol{\mathcal{D}}} &= \{\delta\boldsymbol{\Sigma}_{\boldsymbol{F}}, \delta\boldsymbol{\Sigma}_{\boldsymbol{H}}, \delta\Sigma_J\}.
\end{aligned} \tag{4.64}$$

Notice that the stationary conditions for the action integral in above equation (4.63) are in fact almost identical to the directional derivatives of the total energy functional Π_M, the only difference being the inertial term in equation $(4.63)_a$. Similarly, the stationary conditions for the action integral L_C (refer to equation (4.60)) with associated fields $\boldsymbol{\phi}_C$ in $(4.61)_b$ yield

$$\begin{aligned}
&\int_V \rho_0 \frac{\partial \boldsymbol{v}}{\partial t} \cdot \delta \boldsymbol{x}\, dV + \int_V \boldsymbol{P}_C : \boldsymbol{\nabla}_0 \delta \boldsymbol{x}\, dV - \int_{\partial V} \boldsymbol{t}_0 \cdot \delta \boldsymbol{x}\, dA - \int_V \boldsymbol{f}_0 \cdot \delta \boldsymbol{x}\, dV = 0; \\
&\int_V \delta \boldsymbol{\Sigma}_{\boldsymbol{\mathcal{D}}} : \left(\boldsymbol{\mathcal{D}}_{\boldsymbol{x}} - \frac{\partial \Upsilon}{\partial \boldsymbol{\Sigma}_{\boldsymbol{\mathcal{D}}}} \right) dV = 0.
\end{aligned} \tag{4.65}$$

Alternatively to the mixed variational principles L_M and L_C (refer to equations (4.62) and (4.61)) presented in this Section, the authors in References [43, 57] have presented a computational framework for the system of first order conservation laws in terms of both conservation (refer to equation (4.21)) and entropy (refer to equation (4.51)) variables. Very remarkable, the interpolation of all the unknown variables (either the conservation variables $\boldsymbol{\mathcal{U}}$ (4.21) or its entropy conjugates $\boldsymbol{\mathcal{V}}$ (7.78)) in this framework is based upon linear tetrahedral elements, where a Stream-Upwind-Petrov-Galerkin (SUPG) stabilisation technique enables to circumvent detrimental features such as locking and spurious oscillations.

A comparison of the performance between the (implicit) Lagrangian-based formulations presented in this Section (where the same choice of LBB compliant interpolation spaces as those described in Section 3.3 has been utilised) and that for the (explicit) stabilised formulation presented in References [43, 57] has been included in References [43, 57], showing a good agreement between both formulations.

4.6 Numerical examples

In this Section, the comparison of the polyconvex Mooney-Rivlin and the Saint Venant-Kirchhoff (non-polyconvex) constitutive models presented in equations (2.40) and (2.46) is carried out. First, an explicit derivation of the speed of propagation of shear and pressure waves in the material is obtained for both materials. Finally, a challenging numerical simulation is included where the comparison of the response between both constitutive models in dynamic scenarios is carried out.

4.6.1 Analysis of material stability under simple deformation scenarios

The simple strain energy for the polyconvex Mooney-Rivlin introduced in equation (2.40) and that for the (non-polyconvex) Saint Venant-Kirchhoff constitutive model in (2.46) is considered in this Section. The acoustic tensor $\boldsymbol{\mathcal{C}}_{\boldsymbol{NN}}$ for both constitutive

models can be obtained according to equation (4.34) and (2.75), yielding

$$\begin{aligned}\boldsymbol{\mathcal{C}}_{\boldsymbol{NN}M-R} &= 2\mu_1\boldsymbol{I} + 2\mu_2\left[(\boldsymbol{FN}\otimes\boldsymbol{FN}) - (\boldsymbol{FN}\cdot\boldsymbol{FN})\boldsymbol{I} - \boldsymbol{FF}^T + (\boldsymbol{F}:\boldsymbol{F})\boldsymbol{I}\right] \\ &\quad + f''(J)\,(\boldsymbol{HN}\otimes\boldsymbol{HN})\,; \\ \boldsymbol{\mathcal{C}}_{\boldsymbol{NN}S-V} &= 2\left(\mu+\frac{\lambda}{2}\right)\boldsymbol{I} - \mu\left[(\boldsymbol{FN}\otimes\boldsymbol{FN}) - (\boldsymbol{FN}\cdot\boldsymbol{FN})\boldsymbol{I} - \boldsymbol{FF}^T + (\boldsymbol{F}:\boldsymbol{F})\boldsymbol{I}\right],\end{aligned} \tag{4.66}$$

where after repeated use of the identity $\mathcal{E}_{ijk}\mathcal{E}_{kln} = \delta_{il}\delta_{jn} - \delta_{in}\delta_{jl}$, the following identity has been made use in above equation (4.66)

$$(\boldsymbol{F}\times\boldsymbol{\mathcal{I}}\times\boldsymbol{F})_{iIjJ} = \mathcal{I}_{iIjJ}II_{\boldsymbol{F}} - \delta_{ij}C_{IJ} - b_{ij}\delta_{IJ} + F_{iI}F_{jJ}. \tag{4.67}$$

The eigenvalues of the generalised acoustic tensor $\boldsymbol{\mathcal{C}}_{\boldsymbol{NN}}$ in above equation (4.66) depend on the propagation vector $\boldsymbol{N}$. We restrict our analysis to the simplified scenario where the propagation vector is a principal direction of the deformation. In this case, let the eigenvalues of the deformation $\{\lambda_1, \lambda_2, \lambda_3\}$ be associated to the (unitary) principal directions in the deformed and undeformed configurations, denoted as $\{\boldsymbol{t}_1, \boldsymbol{t}_2, \boldsymbol{n}\}$ and $\{\boldsymbol{T}_1, \boldsymbol{T}_2, \boldsymbol{N}\}$[1]. In that case, the following relations are easy to verify

$$\begin{aligned}\boldsymbol{F}\boldsymbol{T}_\alpha &= \lambda_\alpha\boldsymbol{t}_\alpha; & \boldsymbol{F}^T\boldsymbol{t}_\alpha &= \lambda_\alpha\boldsymbol{T}_\alpha; \\ \boldsymbol{F}\boldsymbol{N} &= \lambda_3\boldsymbol{n}; & \boldsymbol{F}^T\boldsymbol{n} &= \lambda_3\boldsymbol{N}; \\ \boldsymbol{H}\boldsymbol{T}_\alpha &= \frac{J}{\lambda_\alpha}\boldsymbol{t}_\alpha; & \boldsymbol{H}^T\boldsymbol{t}_\alpha &= \frac{J}{\lambda_\alpha}\boldsymbol{T}_\alpha; \\ \boldsymbol{H}\boldsymbol{N} &= \frac{J}{\lambda_3}\boldsymbol{n}; & \boldsymbol{H}^T\boldsymbol{n} &= \frac{J}{\lambda_3}\boldsymbol{N}.\end{aligned} \tag{4.68}$$

Introduction of the different identities in equation (4.68) into equation (4.66) for the specialised scenario considered yields the following expression for the acoustic tensor $\boldsymbol{\mathcal{C}}_{\boldsymbol{NN}}$

$$\begin{aligned}\boldsymbol{\mathcal{C}}_{\boldsymbol{NN}M-R} &= 2\mu_1\boldsymbol{I} + 2\mu_2\left(\left(\lambda_1^2+\lambda_2^2\right)\boldsymbol{I} - \boldsymbol{\Lambda}_T\right) + f''(J)\left(\frac{J}{\lambda_3}\right)^2\boldsymbol{n}\otimes\boldsymbol{n}; \\ \boldsymbol{\mathcal{C}}_{\boldsymbol{NN}S-V} &= 2\left(\mu+\frac{\lambda}{2}\right)\lambda_3^2\boldsymbol{n}\otimes\boldsymbol{n} + g\boldsymbol{I} - \mu\left(\left(\lambda_1^2+\lambda_2^2\right)\boldsymbol{I} - \boldsymbol{\Lambda}_T\right).\end{aligned} \tag{4.69}$$

where the rank two tensor $\boldsymbol{\Lambda}_T$ in above equation (4.69) is defined as

$$\boldsymbol{\Lambda}_T = \lambda_1^2\boldsymbol{t}_1\otimes\boldsymbol{t}_1 + \lambda_2^2\boldsymbol{t}_2\otimes\boldsymbol{t}_2. \tag{4.70}$$

The wave speeds then can be obtained by solving the following equation (refer to equation (4.38))

$$\rho_0 c_\alpha^2 = \bar{\boldsymbol{p}}_\alpha\cdot\boldsymbol{\mathcal{C}}_{\boldsymbol{NN}}\bar{\boldsymbol{p}}_\alpha. \tag{4.71}$$

[1]The deformation gradient tensor is decomposed as $\boldsymbol{F} = \lambda_1\boldsymbol{t}_1\otimes\boldsymbol{T}_1 + \lambda_2\boldsymbol{t}_2\otimes\boldsymbol{T}_2 + \lambda_3\boldsymbol{n}\otimes\boldsymbol{N}$ [12].

Combination of equation (4.71) and the expression for $\boldsymbol{\mathcal{C}_{NN}}$ in (4.69) finally yields

$$\begin{aligned}\rho_0 c^2_{\alpha M-R} &= 2\mu_1 + 2\mu_2\left(\left(\lambda_1^2+\lambda_2^2\right) - \bar{\boldsymbol{p}}_\alpha\cdot\boldsymbol{\Lambda}_T\bar{\boldsymbol{p}}_\alpha\right) + f''(J)\left(\frac{J}{\lambda_3}\right)^2\left(\bar{\boldsymbol{p}}_\alpha\cdot\boldsymbol{n}\right)^2;\\ \rho_0 c^2_{\alpha S-V} &= 2\left(\mu+\frac{\lambda}{2}\right)\lambda_3^2\left(\bar{\boldsymbol{p}}_\alpha\cdot\boldsymbol{n}\right)^2 + g - \mu\left(\left(\lambda_1^2+\lambda_2^2\right) - \bar{\boldsymbol{p}}_\alpha\cdot\boldsymbol{\Lambda}_T\bar{\boldsymbol{p}}_\alpha\right).\end{aligned} \tag{4.72}$$

The first set of eigenvalues corresponding to $p-$waves for both constitutive models is obtained by taking $\bar{\boldsymbol{p}}_\alpha = \boldsymbol{n}$ to give

$$\begin{aligned}c_{1,2\,M-R} &= \pm\sqrt{\frac{2\mu_1 + 2\mu_2\left(\lambda_1^2+\lambda_2^2\right) + f''(J)\left(\frac{J}{\lambda_3}\right)^2}{\rho_0}};\\ c_{1,2\,S-V} &= \pm\sqrt{\frac{\mu\left(3\lambda_3^2-1\right) + \frac{\lambda}{2}\left(\lambda_1^2+\lambda_2^2+3\lambda_3^2-3\right)}{\rho_0}}.\end{aligned} \tag{4.73}$$

The next four eigenvalues correspond to shear waves where the vibration takes place on the propagation plane. The corresponding velocity vectors are orthogonal to $\boldsymbol{n}$ and in the directions of the unit eigenvectors $\{\boldsymbol{t}_1, \boldsymbol{t}_2\}$ of the rank-two tensor $\boldsymbol{\Lambda}_T$. Particularisation of equation (4.72) to the case of shear waves gives

$$\begin{aligned}c_{3,4\,M-R} &= \pm\sqrt{\frac{2\mu_1 + 2\mu_2\lambda_2^2}{\rho_0}}; \qquad c_{3,4\,S-V} = \pm\sqrt{\frac{\mu\left(\lambda_1^2+\lambda_3^2-1\right) + \frac{\lambda}{2}\left(II_{\boldsymbol{F}}-3\right)}{\rho_0}};\\ c_{5,6\,M-R} &= \pm\sqrt{\frac{2\mu_1 + 2\mu_2\lambda_1^2}{\rho_0}}; \qquad c_{5,6\,S-V} = \pm\sqrt{\frac{\mu\left(\lambda_2^2+\lambda_3^2-1\right) + \frac{\lambda}{2}\left(II_{\boldsymbol{F}}-3\right)}{\rho_0}}.\end{aligned} \tag{4.74}$$

Analysis of material stability

The Legendre-Hadamard condition is strongly related to the material stability of the constitutive equations [86]. The objective of this Section is to analyse the material stability of both the Mooney-Rivlin and the Saint Venant-Kirchhoff constitutive models, for which the eigenvalue structure of the system of conservation laws in nonlinear elasticity was analysed in the previous section. In particular, the experimental set up depicted in Figure 4.4 where an incompressible membrane subjected to a biaxial stretch equal in both directions OX_1 and OX_2 is considered. For this particular experimental set up, the deformation gradient tensor depends exclusively on the stretch λ as

$$\boldsymbol{F} = \begin{bmatrix}\lambda & 0 & 0\\ 0 & \lambda & 0\\ 0 & 0 & 1/\lambda^2\end{bmatrix}. \tag{4.75}$$

Figure 4.5 depicts the evolution of the shear and pressure waves in equations (4.73) and (4.74), respectively for both Mooney-Rivlin and Saint Venant-Kirchhoff

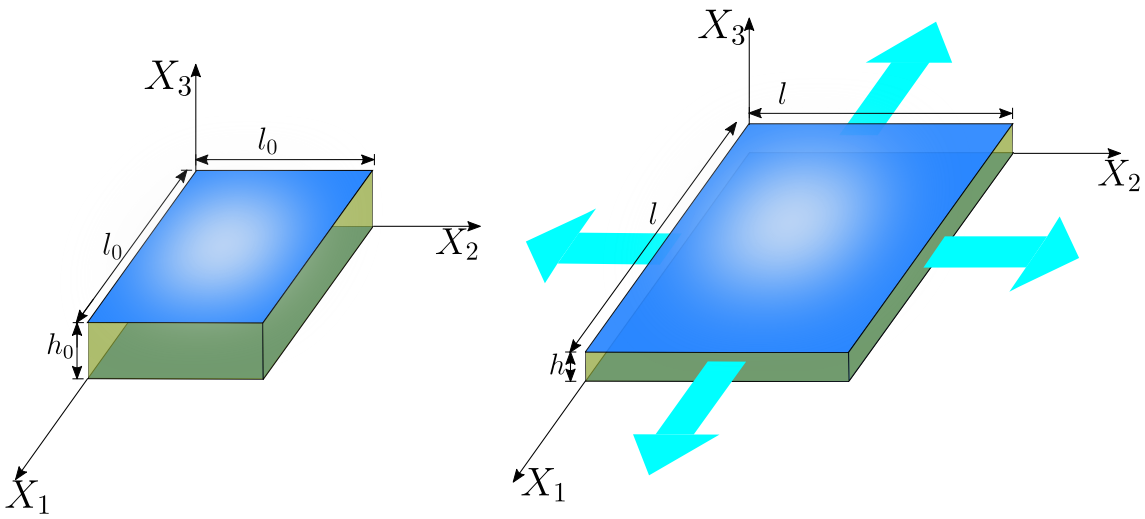

Figure 4.4: Experimental set up. The application of a uniform stretch identical in both directions parallel to the axis OX_1 and OX_2 of a membrane of initial length and thickness l_0 and h_0 respectively, leads to a uniform axial expansion equal in directions parallel to the OX_1 and OX_2 and final thickness $h = 1/\lambda h_0^2$, with λ the stretch in the membrane.

constitutive models (notice that for this particular experimental set up $c_{3,4} = c_{5,6}$) as the stretch in the material (refer to Figure 4.4) is modified within the range $0.95 \leq \lambda \leq 1.2$.

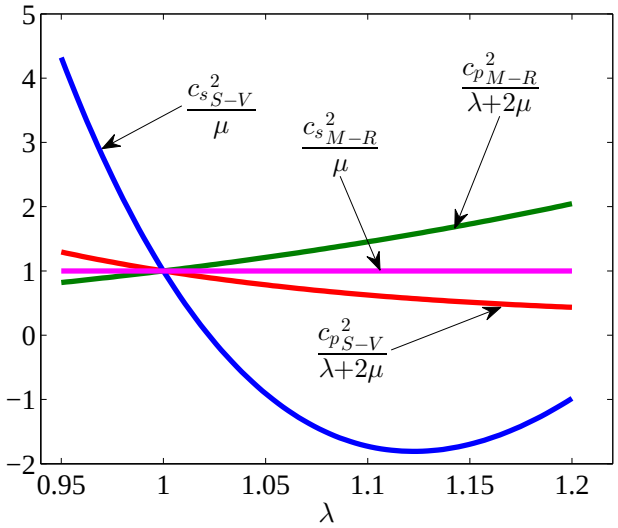

Figure 4.5: Experimental set up. Evolution of pressure and shear waves for both Mooney-Rivlin (polyconvex) and Saint Venant (non-polyconvex) constitutive models in equations (2.40) and (2.46). Subindexes $S-V$ and $M-R$ have been used for easier association with the Saint Venant and Mooney-Rivlin models.

As expected, the pressure and shear waves for this particular experimental set up are always real (c_p^2 and c_s^2 are positive) for the Mooney-Rivlin constitutive model. On the contrary, the shear waves for the Saint Venant-Kirchhoff constitutive model become imaginary (c_s^2 is negative), indicating that material instabilities in the form of shear bands might arise beyond the relatively low value of the critical value of the stretch of $\lambda = 1.035$. Beyond this situation, the Legendre-Hadamard condition no longer holds as the system of conservation laws in equation (4.21), its hyperbolic nature and the governing equations become ill-posed.

4.6.2 Analysis of material stability under complex deformation scenarios

The objective of this Section is to analyse the behaviour of both the Mooney-Rivlin in (2.40) and the Saint Venant-Kirchhoff in (2.46) constitutive models with special emphasis on the material stability of the model under more complex scenarios than the simple experimental set up described in the previous Section (refer to Figure 4.4).

Moreover, a more general situation where the acoustic information does not propagate in the direction of a principal direction of deformation will be considered, where the relations in equation (4.68) are no longer applicable. Under these conditions, an explicit derivation of the critical direction of propagation and value of the deformation for which material instabilities might arise would be a cumbersome task. Alternatively, information regarding material stability for an arbitrary direction of propagation $\boldsymbol{N}$ and for any stage of the deformation can easily be inferred from the acoustic tensor $\boldsymbol{\mathcal{C}_{NN}}$ (refer to equations (4.34) and (2.75)). Loss of material stability is typically associated to loss of positive definiteness of the acoustic tensor [86]. Therefore, a sufficient condition for material instability (refer to Reference [86]) is

$$\begin{aligned} &\mathcal{C} = \min\left(\mathcal{C}_1, \mathcal{C}_2, \mathcal{C}_3\right) \leq 0; && \mathcal{C}_1 = \left(\boldsymbol{\mathcal{C}_{NN}}\right)_{11}; \\ &\mathcal{C}_2 = \left(\boldsymbol{\mathcal{C}_{NN}}\right)_{11}\left(\boldsymbol{\mathcal{C}_{NN}}\right)_{22} - \left(\boldsymbol{\mathcal{C}_{NN}}\right)_{12}\left(\boldsymbol{\mathcal{C}_{NN}}\right)_{21}; && \mathcal{C}_3 = \det\left(\boldsymbol{\mathcal{C}_{NN}}\right). \end{aligned} \tag{4.76}$$

The material stability of both Mooney-Rivlin (2.40) and Saint Venant-Kirchhoff (2.46) constitutive models is studied in the following challenging example, included in References [43,57]. A column with geometry depicted in Figure 4.6(a) subjected to an initial angular velocity $\boldsymbol{\Omega}$ is considered. The initial angular velocity is compatible with the boundary conditions and adopts the following expression

$$\boldsymbol{\Omega}(Z) = \boldsymbol{\Omega}_0 \sin\left(\frac{\pi Z}{2L}\right), \tag{4.77}$$

where the length of the column in the material configuration is $L = 6\,m$ and with $\Omega_0 = 100\,rad/s$ (refer to Figure 4.6(b)). The Young's modulus and Poisson's ratio of the column are $E = 210\,GPa$ and $\nu = 0.3$, respectively. The Hu-Washizu mixed variational principle in equations $(4.62)_a$ and (4.63) has been considered, where a

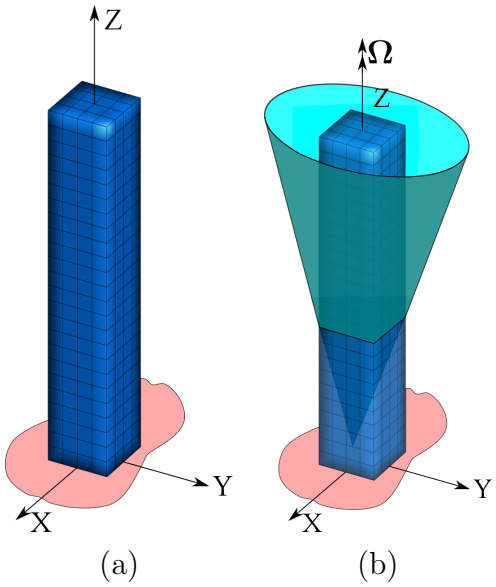

Figure 4.6: Geometry and boundary conditions for twisting column example

generalised α-method [14] time integrator has been used. The same interpolation spaces as those described in Section 3.3 have been considered.

Figure 7.10 shows the pressure contour plot corresponding to different time steps for the Saint Venant-Kirchhoff constitutive model. It is interesting to observe that for $t = 0.098\,s$, pressure oscillations start to occur in the base of the column. On the contrary, a smooth pressure distribution is obtained for the same time step for the Mooney-Rivlin constitutive model, as illustrated in Figure 7.11.

An analysis of material stability for both Saint-Venant and Mooney-Rivlin constitutive models is carried out Figure 4.9 and 4.10 respectively. The value of the material stability indicator $\mathcal{C}$ (4.76) is displayed for different time steps for a point of the domain corresponding to the material coordinates $\boldsymbol{X} = \begin{bmatrix} 0 & 0 & 0 \end{bmatrix}^T$ in terms of the direction vector $\boldsymbol{N}$, spherically parametrised as [86]

$$\boldsymbol{N} = \begin{bmatrix} \cos\alpha \sin\beta \\ \sin\alpha \sin\beta \\ \cos\beta \end{bmatrix}. \tag{4.78}$$

As it can be observed from Figure 4.9, the variable $\mathcal{C}$ (4.76) attains negative values at $t = 0.041\,s$ for the Saint Venant-Kirchhoff constitutive model, indicating the existence of areas prone to strain localisation and shear bands. On the contrary, positive values of $\mathcal{C}$ are obtained for the Mooney-Rivlin constitutive model throughout the simulation, as expected. Finally, Figure 4.11 displays the contour plot of the Jacobian variable (in the Hu-Washizu mixed variational principle, the Jacobian is considered as an independent variable). A region with a very localised deformation is highlighted in this Figure, where loss of ellipticity and subsequent ill-posedness of the governing equations [11,86] pollute the numerical solution, confirming the detri-

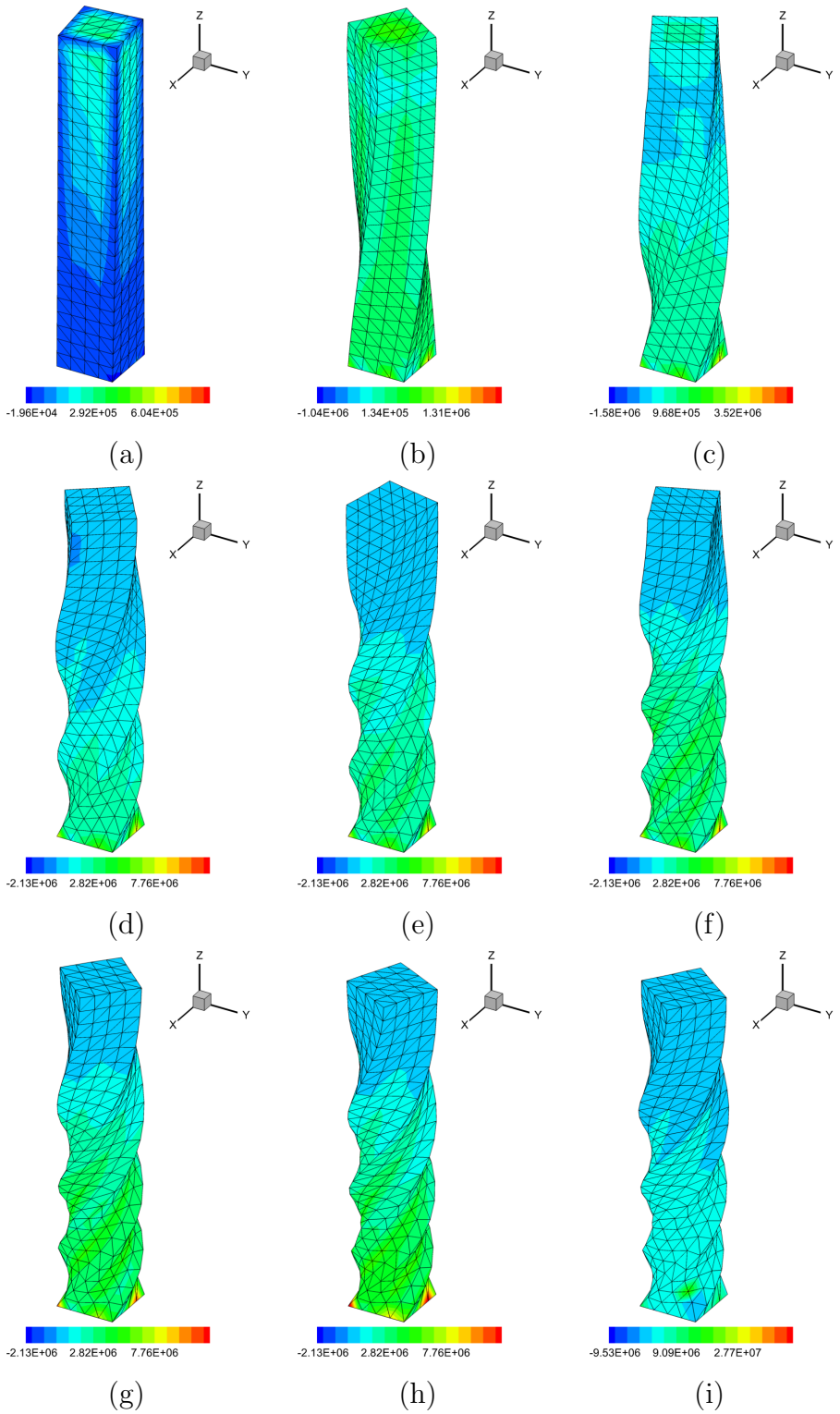

Figure 4.7: Twisting column: contour pressure distribution for the Saint Venant-Kirchhoff constitutive model at different time steps: a) $t = 0.001\,s$; b) $t = 0.01\,s$; c) $t = 0.021\,s$; d) $t = 0.041\,s$; e) $t = 0.051\,s$; f) $t = 0.061\,s$; g) $t = 0.071\,s$; h) $t = 0.088\,s$; i) $t = 0.098\,s$. Material properties of $E = 210\,GPa$, $\nu = 0.3$ and $\rho = 1100\,Kg/m^3$. Hu-Washizu variational principle in equation (4.63). Generalised α-method with $\rho_\infty = 1$ and $\Delta t = 2 \times 10^{-4}\,s$.

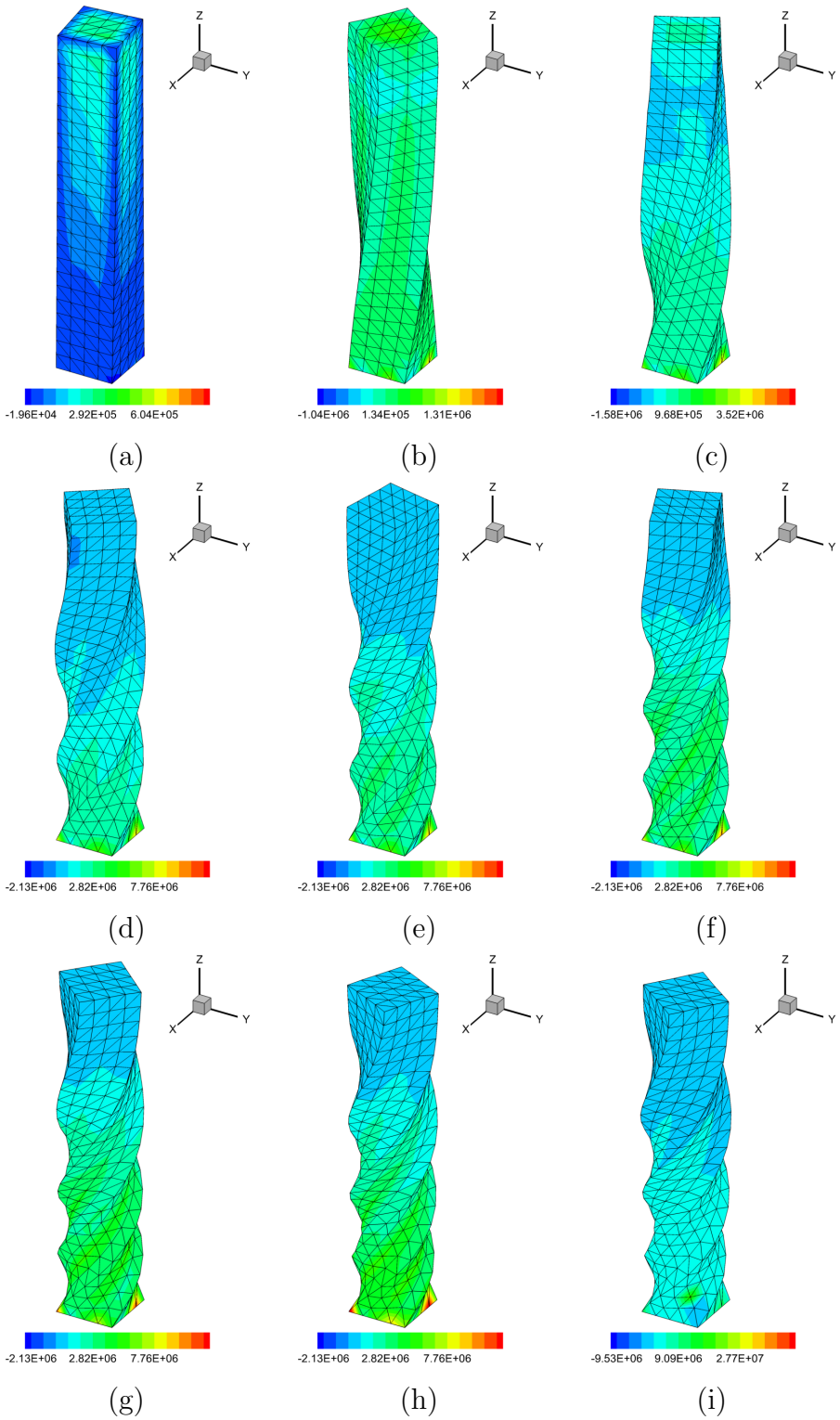

Figure 4.8: Twisting column: contour pressure distribution for the Mooney-Rivlin constitutive model at different time steps: a) $t = 0.001\,s$; b) $t = 0.01\,s$; c) $t = 0.021\,s$; d) $t = 0.041\,s$; e) $t = 0.051\,s$; f) $t = 0.061\,s$; g) $t = 0.071\,s$; h) $t = 0.088\,s$; i) $t = 0.098\,s$. Material properties of $E = 210\,GPa$, $\nu = 0.3$ and $\rho = 1100\,Kg/m^3$. Hu-Washizu variational principle in equation (4.63). Generalised α-method with $\rho_\infty = 1$ and $\Delta t = 2 \times 10^{-4}\,s$.

mental characteristics of the non-polyconvex Saint Venant-Kirchhoff constitutive model.

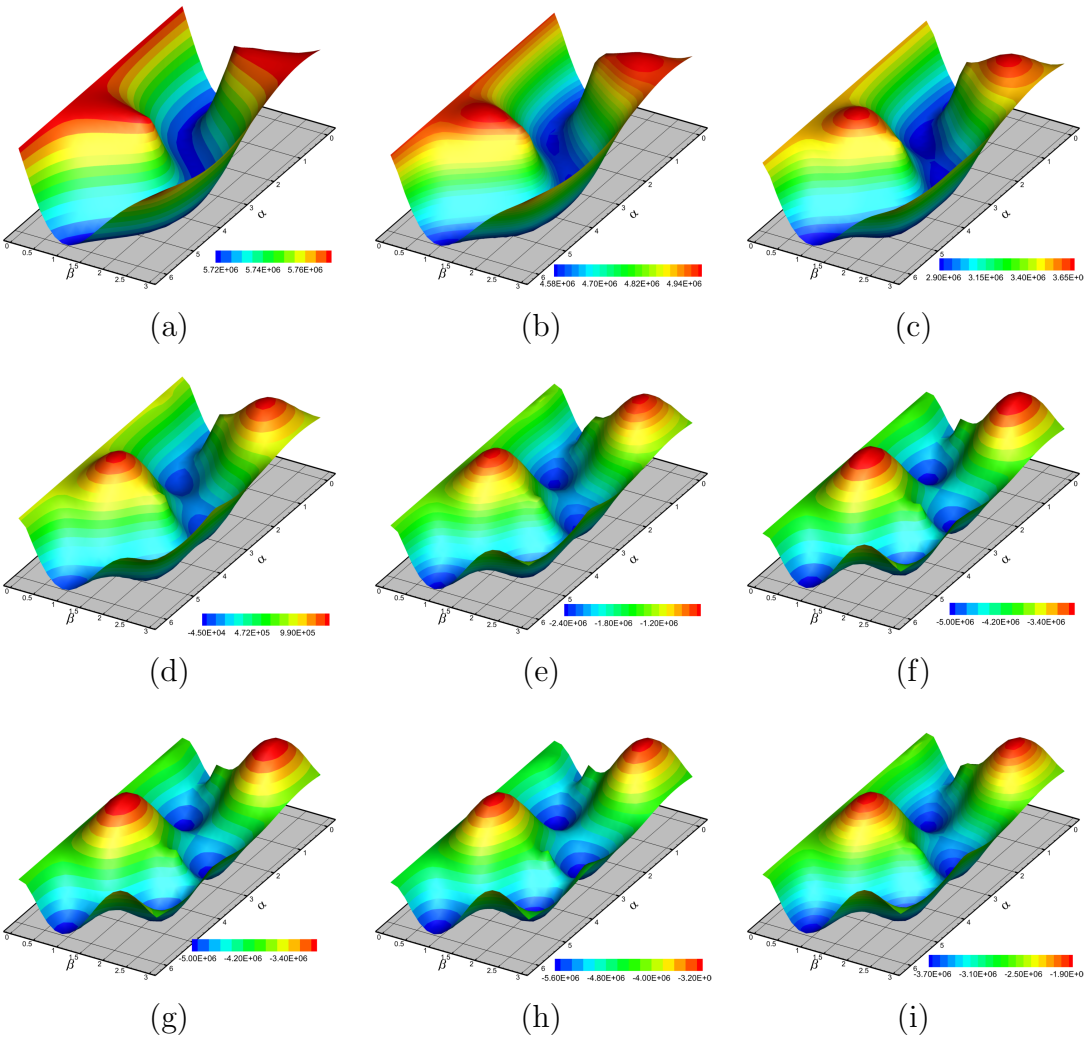

Figure 4.9: Twisting column: distribution of the stability indicator $\mathcal{C}$ (4.76) at the material coordinates $\boldsymbol{X} = [0\ 0\ 0]^T$ in terms of the angles α and β which spherically parametrise the propagation vector $\boldsymbol{N}$ according to equation (4.78). Saint Venant-Kirchhoff constitutive model. Snapshots corresponding to: a) $t = 0.001\,s$; b) $t = 0.01\,s$; c) $t = 0.021\,s$; d) $t = 0.041\,s$; e) $t = 0.051\,s$; f) $t = 0.061\,s$; g) $t = 0.071\,s$; h) $t = 0.088\,s$; i) $t = 0.098\,s$. Material properties of $E = 210\,GPa$, $\nu = 0.3$ and $\rho = 1100\,Kg/m^3$. Hu-Washizu variational principle in equation (4.63). Generalised α-method with $\rho_\infty = 1$ and $\Delta t = 2 \times 10^{-4}\,s$.

4.7 Concluding remarks

This Chapter provides an insightful physical interpretation of polyconvexity. Consideration of the strong relationship between the Legendre-Hadamard condition (au-

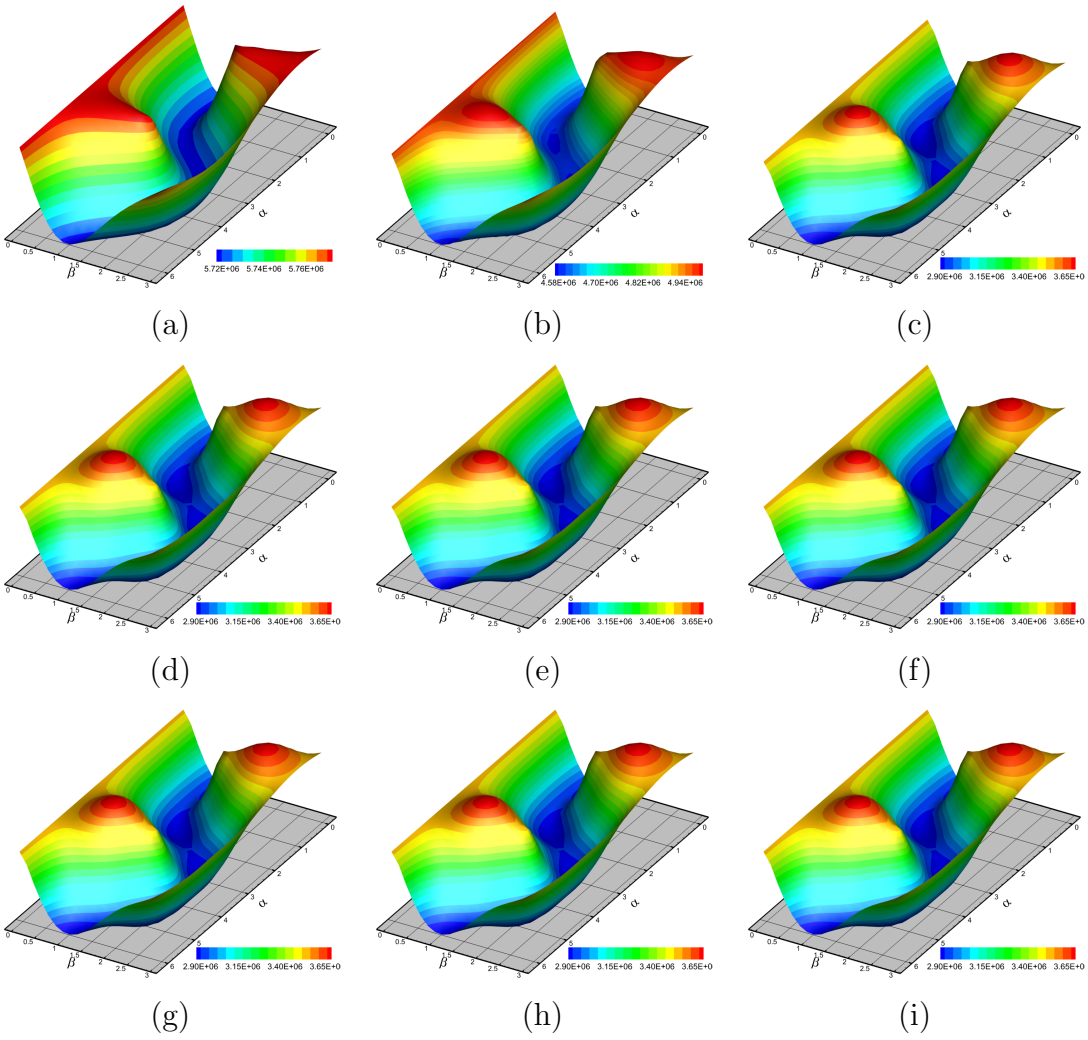

Figure 4.10: Twisting column: distribution of the stability indicator $\mathcal{C}$ (4.76) at the material coordinates $\boldsymbol{X} = [0\ 0\ 0]^T$ in terms of the angles α and β which spherically parametrise the propagation vector $\boldsymbol{N}$ according to equation (4.78). Mooney-Rivlin constitutive model. Snapshots corresponding to: a) $t = 0.001\,s$; b) $t = 0.01\,s$; c) $t = 0.021\,s$; d) $t = 0.041\,s$; e) $t = 0.051\,s$; f) $t = 0.061\,s$; g) $t = 0.071\,s$; h) $t = 0.088\,s$; i) $t = 0.098\,s$. Material properties of $E = 210\,GPa$, $\nu = 0.3$ and $\rho = 1100\,Kg/m^3$. Hu-Washizu variational principle in equation (4.63). Generalised α-method with $\rho_\infty = 1$ and $\Delta t = 2 \times 10^{-4}\,s$.

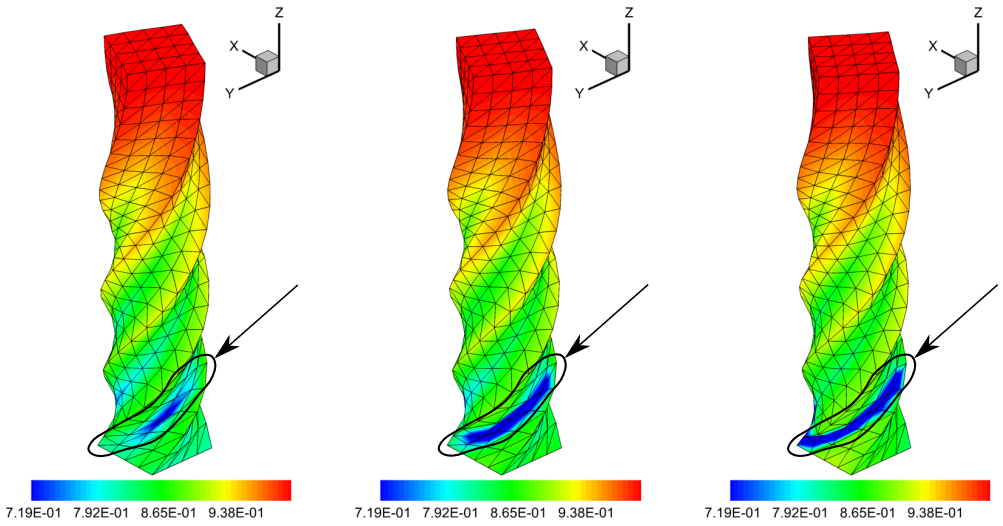

Figure 4.11: Twisting column: contour plot for the Jacobian variable J for the Saint Venant-Kirchhoff constitutive model at different snapshots: a) $t = 0.086\,s$; b) $t = 0.94\,s$; c) $t = 0.98\,s$. Material properties of $E = 210\,GPa$, $\nu = 0.3$ and $\rho = 1100\,Kg/m^3$. Hu-Washizu variational principle in equation (4.63). Generalised α-method with $\rho_\infty = 1$ and $\Delta t = 2 \times 10^{-4}\,s$. Development of strain localisation area.

tomatically satisfied by polyconvex functionals) and hyperbolicity of the equations in Solid Dynamics, enables a more intuitive justification for the convex multi-variable nature of the strain energy with respect to the fibre, area and volume maps. In essence, hyperbolicity of the equations of Solid Dynamics is guaranteed provided that the time rate of these three mappings, and in general, of any argument of the strain energy, can be expressed as a first order hyperbolic equation.

Moreover, the one to one and invertible relationship between the extended set of variables defining polyconvexity and its associated set of entropy variables has facilitated the definition of a generalised convex entropy function and its associated flux. This invertible relationship has enabled a symmetrisation of the set of first order hyperbolic equations for Solid Dynamics in terms of the entropy variables.

The aforementioned relevant aspects are the fundamental ingredients for the robust and accurate computational framework developed by [43, 57], where a set of first order conservation laws in terms of both conservation and entropy variables are considered and addressed numerically via a stabilised SUPG formulation, where linear tetrahedral elements are successfully and accurately utilised. An alternative formulation, based on the definition of the action integral of the Hu-Washizu and Hellinger-Reissner mixed variational principles introduced in Section 2.6 and enabling a natural extension of these mixed variational principles to dynamics scenarios, has been presented in this Chapter.

Finally, a material stability analysis of both the (non-polyconvex) Saint Venant-Kirchhoff and the polyconvex Mooney-Rivlin, introduced in equations (2.46) and (2.40), has been carried out in this Chapter. A study of the possible loss of positive definiteness of the acoustic tensor (refer to equations (4.34) and (2.75)), emanating from the eigenvalue structure of the system of hyperbolic equations (4.21) has been carried out for a simplified experimental set up, described in Figure 4.4 and for a more challenging numerical simulation, described in Figure (4.6).

Part III

Convex multi-variable formulation of nonlinear electro-elasticity

Chapter 5

General formulation of convex multi-variable electromechanics

5.1 Introduction

Following the recent work by Gil and Ortigosa [76], a new convex multi-variable variational framework for the analysis of Electro Active Polymers (EAP) in the context of reversible nonlinear electro-elasticity is presented in this Chapter. These materials, specially dielectric elastomers, are characterised by displaying extremely large deformations when exposed to a high electric field.

Gil and Ortigosa [74–76] extended the concept of polyconvexity to the field of nonlinear electro-elasticity based on a new convex multi-variable definition of the energy functional. As already indicated in the introductory Chapter of this work, it is important to emphasise that, in contrast to the three previous Chapters of this work, strictly focused on nonlinear elasticity, the use of the term polyconvexity will be explicitly avoided in this work in the context of electro-elasticity, which represents the underlying topic for the three forthcoming Chapters. The more appropriate term multi-variable convexity will be used instead. The underlying technical reason behind this alternative nomenclature is well founded and resides in the fact that sequentially weak lower semicontinuity and the coercivity of the new concept of multi-variable convexity, both necessary to prove existence of minimisers [27, 85], has not been proved yet. However, the scope of this thesis is not on the existence of minimisers but on the material stability of the constitutive equations, the latter being satisfied by convex multi-variable energy functionals.

In this Chapter, a new definition of the electro-mechanical internal energy (the analogous to the strain energy in the context of elasticity) is introduced expressed as a convex multi-variable [27] function of a new extended set of electro-mechanical arguments. A new electro-kinematic variable set is introduced including the deformation gradient $\boldsymbol{F}$, its co-factor $\boldsymbol{H}$, its Jacobian J, the Lagrangian electric displacement field $\boldsymbol{D}_0$ and an additional spatial or Eulerian vector $\boldsymbol{d}$ computed as the product between the deformation gradient tensor and the Lagrangian electric displacement field. Crucially, this new definition of the internal energy enables the most accepted constitutive inequality, namely ellipticity, to be extended to the entire range of deformations and electric fields and, in addition, to incorporate the electromechanical energy of the vacuum as a degenerate case of multi-variable convexity.

The extended set of variables $\{\boldsymbol{F}, \boldsymbol{H}, J, \boldsymbol{D}_0, \boldsymbol{d}\}$ enables the introduction of another new set of work conjugate variables $\{\boldsymbol{\Sigma}_{\boldsymbol{F}}, \boldsymbol{\Sigma}_{\boldsymbol{H}}, \Sigma_J, \boldsymbol{\Sigma}_{\boldsymbol{D}_0}, \boldsymbol{\Sigma}_{\boldsymbol{d}}\}$ [84]. Multi-variable convexity of the internal energy guarantees that the relationship between both sets of variables is one to one and invertible. In addition, multi-variable convexity of the internal energy enables three additional energy functionals to be defined (at least implicitly) by making appropriate use of the Legendre transform[1].

The new extended set of electro-kinematic variables associated to the proposed

[1]Two partial Legendre transforms can be obtained by fixing either purely mechanical or purely electrical variables of the extended set. A total Legendre transform of the internal energy would render the third energy functional in terms of the elements of the extended set of work conjugate variables.

definition of multi-variable convexity and their work conjugates enable new mixed variational principles to be defined. The present Chapter presents extended Hu-Washizu type of variational principles [12,40,46–51,51–54,54–56] which open up new interesting possibilities in terms of using various interpolation spaces for different variables, leading to enhanced type of formulations [42,103–108]. A Finite Element implementation of these new variational principles has been presented in Reference [75], summarised in Chapter 6.

Moreover, some simple strategies (denoted as convexification or stabilisation strategies) to create convex multi-variable energy functionals by incorporating minor modifications to a priori non-convex multi-variable functionals are also presented in this Chapter. Finally, under a characteristic experimental set up in dielectric elastomers, the behaviour of a convex multi-variable constitutive model capturing some intrinsic nonlinear effects such as electrostriction, is numerically studied.

This Chapter is organised as follows. Section 5.2 revises the fundamental concepts of large strain kinematics with the help of the tensor cross product notation re-introduced by Bonet et al. [44]. Section 5.3 presents the extension of the concept of polyconvexity to nonlinear electro-elasticity, replaced by the technically more convenient term multi-variable convexity. An extended set of electro-kinematic variables and its work conjugate counterpart are presented for the first time. Moreover, different energy functionals are derived via appropriate application of the Legendre transform over the convex multi-variable internal energy functional. Section 5.4 presents new interesting Hu-Washizu type of mixed variational principles. Section 5.5 presents simple (stabilisation) strategies which permit to create convex multi-variable electromechanical invariants by adding simple modifications to a priori non-convex multi-variable ones. A simple convex multi-variable constitutive model able to capture nonlinear constitutive features inherent to Dielectric Elastomers, namely, electrostriction and electric saturation, is presented in Section 5.6. The material parameters of the proposed constitutive model are adjusted to reproduce the electrostrictive behaviour reported by Zhao et al [109] in DE films. Moreover, the effect of electrostriction and saturation on the behaviour of the DE films subjected to a specific experimental set up is investigated numerically. Section 5.7 provides some concluding remarks and a summary of the key contributions of this Chapter.

5.2 Motion and deformation

Let us consider the motion of an electro active polymer which in its initial or material configuration is defined by a domain V of boundary ∂V with outward unit normal $\boldsymbol{N}$, which is embedded within a truncated continuum V_∞ with inner boundary ∂V (with outward unit normal $-\boldsymbol{N}$) and outer boundary $\partial_\infty V_\infty$. Let $\partial_\infty V_\infty$ be ideally located in a region infinitely far from the electro active polymer such that the deformation can be assumed to vanish. After the motion, the electro active polymer occupies a spatial configuration defined by a domain v of boundary ∂v with

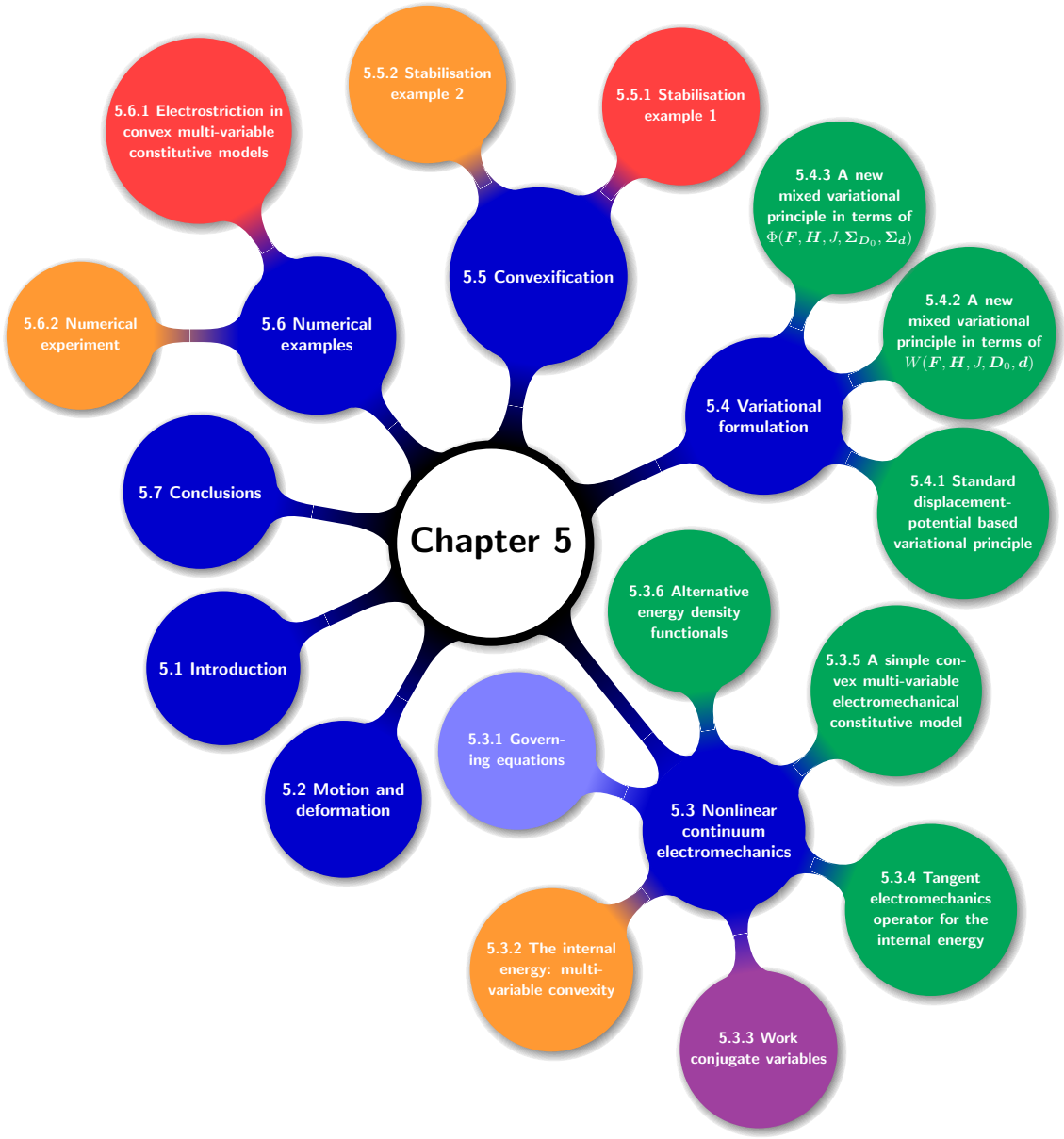

Figure 5.1: Chapter layout.

outward unit normal $\boldsymbol{n}$, whilst the deformed truncated continuum is defined by v_∞ with boundaries ∂v (with outward unit normal $-\boldsymbol{n}$) and $\partial_\infty v_\infty \equiv \partial_\infty V_\infty$ (refer to Figure 5.2).

The motion of the electro active polymer V (extended to also include that of the surrounding truncated continuum V_∞) is defined by a pseudo-time t dependent mapping field $\boldsymbol{\phi}$ which links a material particle from material configuration $\boldsymbol{X}$ to spatial configuration $\boldsymbol{x}$ according to $\boldsymbol{x} = \boldsymbol{\phi}(\boldsymbol{X}, t)$, where displacement boundary conditions can be defined as $\boldsymbol{x} = (\boldsymbol{\phi})_{\partial_u V}$ on the boundary $\partial_u V \subset \partial V$, where the notation $(\bullet)_{\partial_u V}$ is used to indicate the *given* value of a variable $\bullet$ on the boundary $\partial_u V$.

The three strain measures defined in Section 2.2, namely the deformation gradient tensor $\boldsymbol{F}$ or fibre map, its co-factor $\boldsymbol{H}$ or area map and its Jacobian or volume map are recalled for completeness,

$$\boldsymbol{F} = \boldsymbol{\nabla}_0 \boldsymbol{x}; \qquad \boldsymbol{H} = \frac{1}{2}\boldsymbol{F} \times \boldsymbol{F}; \qquad J = \frac{1}{3}\boldsymbol{H} : \boldsymbol{F}, \tag{5.1}$$

where the more convenient representation of the co-factor $\boldsymbol{H}$ in terms of the algebraically useful tensor cross product operation introduced in Chapter 2 has been used in above equation (5.1). Figure 5.2 depicts the deformation process as well the three kinematic maps, that is, $\boldsymbol{F}$, $\boldsymbol{H}$ and J for the described electro active material. Moreover, both the deformation gradient tensor $\boldsymbol{H}$ and the co-factor are subjected to the *curl-free* and *divergence-free* involutions in equations (2.36) and (4.1), namely

$$\mathrm{CURL}\boldsymbol{F} = \boldsymbol{0}; \qquad \mathrm{DIV}\boldsymbol{H} = \boldsymbol{0}. \tag{5.2}$$

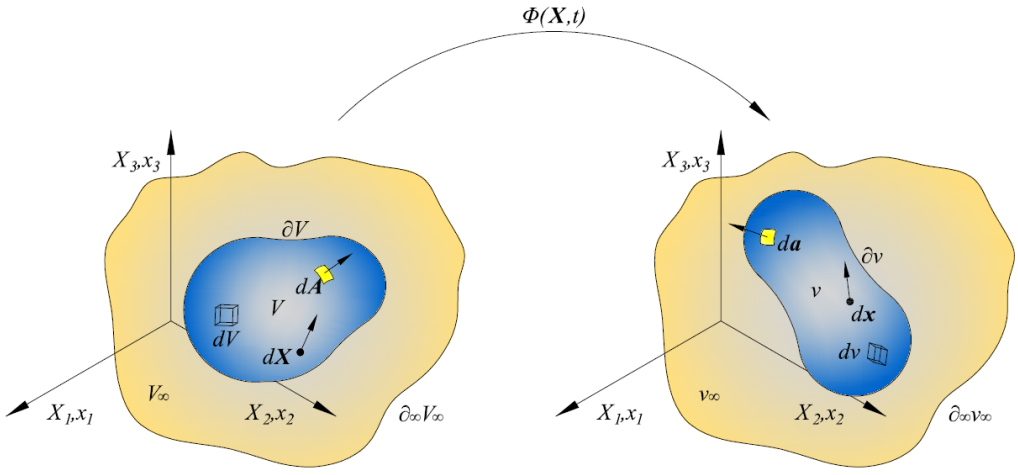

Figure 5.2: Electro active polymer and surrounding truncated domain in initial (undeformed) and final (deformed) configurations.

In general, it is possible to consider a subdivision of the domain V so that $V = \cup_{i=1}^{i=n} V_i$, with interfaces $\partial V_i \cap \partial V_j, i \neq j$. The deformation mapping $\boldsymbol{\phi}$ is

considered to be sufficiently regular in every subdomain V_i and in the surrounding truncated domain V_∞ but not necessarily smooth across interfaces. In this case, equations (5.2) apply to V_i and V_∞, whilst suitable boundary and jump conditions can be introduced as follows

$$\boldsymbol{\phi} = (\boldsymbol{\phi})_{\partial_u V} \qquad \text{on } \partial_u V; \tag{5.3a}$$

$$\boldsymbol{\phi} = \boldsymbol{0} \qquad \text{on } \partial_\infty V_\infty; \tag{5.3b}$$

$$[\![\boldsymbol{\phi}]\!] = \boldsymbol{0} \qquad \text{on } (\partial V_i \cap \partial V_j) \cup \partial V; \tag{5.3c}$$

$$\boldsymbol{F} \times \boldsymbol{N} = (\boldsymbol{F} \times \boldsymbol{N})_{\partial_u V} \qquad \text{on } \partial_u V; \tag{5.3d}$$

$$[\![\boldsymbol{F}]\!] \times \boldsymbol{N}|_{\partial V_i} = \boldsymbol{0} \qquad \text{on } (\partial V_i \cap \partial V_j) \cup \partial V; \tag{5.3e}$$

$$\boldsymbol{H}\boldsymbol{N} = (\boldsymbol{H}\boldsymbol{N})_{\partial_u V} \qquad \text{on } \partial_u V; \tag{5.3f}$$

$$[\![\boldsymbol{H}]\!]\, \boldsymbol{N}|_{\partial V_i} = \boldsymbol{0} \qquad \text{on } (\partial V_i \cap \partial V_j) \cup \partial V, \tag{5.3g}$$

where $[\![\varphi]\!] = (\varphi^i - \varphi^j)$ denotes the jump of a variable φ across an interface $\partial V_i \cap \partial V_j$ with associated unit outward normal $\boldsymbol{N}|_{\partial V_i}$.

Let us define $\delta\boldsymbol{u}$ and $\boldsymbol{u}$ as virtual and incremental variations of $\boldsymbol{x}$, respectively, where it will be assumed that $\delta\boldsymbol{u}$ and $\boldsymbol{u}$ satisfy compatible homogeneous displacement based boundary conditions that vanishes on $\partial_u V$ and $\partial_\infty V_\infty$.

5.3 Nonlinear continuum electromechanics

5.3.1 Governing equations in nonlinear electromechanics

In this section, the entire set of governing equations in nonlinear electromechanics is presented. First, the Faraday and Gauss laws are introduced in a global and local manner. Then, the translational and rotational equilibrium equations are revisited. Moreover, the internal energy (the analogous to the strain energy in elasticity) and the concept of multi-variable convexity in the context of nonlinear electromechanics are introduced in this section.

Faraday and Gauss laws

Maxwell's equations, when neglecting time dependent effects and in the absence of magnetic fields and electric currents, can be used to describe the behaviour of electrostatic fields. Let us recall the electro active polymer introduced in Section **??** surrounded by a medium which, without loss of generality in the present manuscript, will be the vacuum or free space. Moreover, let ρ_0^e denote an applied electric charge per unit of undeformed volume. The electric charge per unit of undeformed volume V_∞ is typically neglected in the particular case in which V_∞ corresponds to the vacuum. Let ω_0^e be an electric charge per unit of undeformed area applied on $\partial_\omega V \subset \partial V$. The local version of the Gauss law and its associated boundary and jump

conditions can be written in a Lagrangian setting as

$$\begin{aligned}
\mathrm{DIV}\boldsymbol{D}_0 &= \rho_0 && \text{in } V_i,\ i = 1\dots n; && (5.4a)\\
\mathrm{DIV}\boldsymbol{D}_0 &= 0 && \text{in } V_\infty; && (5.4b)\\
[\![\boldsymbol{D}_0]\!]\cdot\boldsymbol{N} &= \omega_0 && \text{on } \partial_\omega V; && (5.4c)\\
[\![\boldsymbol{D}_0]\!]\cdot\boldsymbol{N} &= 0 && \text{on } \partial_\varphi V; && (5.4d)\\
[\![\boldsymbol{D}_0]\!]\cdot\boldsymbol{N}|_{\partial V_i} &= 0 && \text{on } \partial V_i\cap\partial V_j && (5.4e)
\end{aligned}$$

where $\boldsymbol{D}_0$ is the Lagrangian electric displacement field [61,62]. Notice that equations (5.4a) and (5.4b) represent the local Gauss law in the dielectric and the vacuum, respectively. In addition, in the case of equations (5.4c)-(5.4d), the term $[\![\boldsymbol{D}_0]\!]$ represents the jump of electric displacement between the domain defined by the dielectric V and the surrounding vacuum V_∞. Equations (5.4) could alternatively be presented in a spatial description in terms of the Eulerian electric displacement $\boldsymbol{D}$ field[2], which is related to its Lagrangian counterpart $\boldsymbol{D}_0$ through the standard Piola (area) transformation as $\boldsymbol{D}_0 = \boldsymbol{H}^T\boldsymbol{D}$ [61,62].

Analogously, the local version the Faraday law and the associated boundary and jump conditions can be expressed in a Lagrangian setting as

$$\begin{aligned}
\boldsymbol{E}_0 &= -\boldsymbol{\nabla}_0\varphi && \text{in } V_i,\ i = 1\dots n; && (5.5a)\\
\boldsymbol{E}_0 &= -\boldsymbol{\nabla}_0\varphi && \text{in } V_\infty; && (5.5b)\\
\varphi &= (\varphi)_{\partial_\varphi V} && \text{on } \partial_\varphi V; && (5.5c)\\
\varphi &= 0 && \text{on } \partial_\infty V_\infty; && (5.5d)\\
[\![\boldsymbol{E}_0]\!]\times\boldsymbol{N} &= \boldsymbol{0} && \text{on } \partial_\omega V; && (5.5e)\\
[\![\boldsymbol{E}_0]\!]\times\boldsymbol{N}|_{\partial V_i} &= \boldsymbol{0} && \text{on } \partial V_i\cap\partial V_j, && (5.5f)
\end{aligned}$$

where $\boldsymbol{E}_0$ is the Lagrangian electric field and φ an electric potential field that can be introduced in the case of a contractible domain[3]. Typically, the origin of electric potential field is defined on $\partial_\infty V_\infty$. This is mathematically stated in equation (5.5d). In equation (5.5c), $\partial_\varphi V \subset \partial V$ represents the part of the boundary subjected to electric potential boundary conditions, such that $\partial_\omega V\cup\partial_\varphi V = \partial V$ and $\partial_\omega V\cap\partial_\varphi V = \emptyset$. As above equations (5.4), equations (5.5) could alternatively be presented in a spatial description in terms of the Eulerian electric field $\boldsymbol{E}$, which is related to its Lagrangian counterpart $\boldsymbol{E}_0$ through the standard fibre transformation $\boldsymbol{E}_0 = \boldsymbol{F}^T\boldsymbol{E}$ [61,62].

[2]Note that the computation of the Eulerian electric displacement $\boldsymbol{D}$ is also important at a post-processing stage when computing or visualising final results.

[3]Alternatively, equation (5.5a) could be replaced by the more general condition $\mathrm{CURL}\boldsymbol{E}_0 = \boldsymbol{0}$ and equation (5.5c) by $\boldsymbol{E}_0\times\boldsymbol{N} = (\boldsymbol{E}_0\times\boldsymbol{N})_{\partial_\varphi V}$.

Translational and rotational equilibrium

The local version of conservation of linear momentum (refer to equation (4.9) in the context of elasticity) can be expressed in a Lagrangian setting as

$$\mathrm{DIV}\boldsymbol{P} + \boldsymbol{f}_0 = \boldsymbol{0} \qquad \text{in } V_i,\ i = 1 \dots n; \tag{5.6a}$$

$$\mathrm{DIV}\boldsymbol{P} = \boldsymbol{0} \qquad \text{in } V_\infty; \tag{5.6b}$$

$$[\![\boldsymbol{P}]\!]\boldsymbol{N} = \boldsymbol{t}_0 \qquad \text{on } \partial_t V; \tag{5.6c}$$

$$[\![\boldsymbol{P}]\!]\boldsymbol{N} = \boldsymbol{0} \qquad \text{on } \partial_u V; \tag{5.6d}$$

$$[\![\boldsymbol{P}]\!]\,\boldsymbol{N}|_{\partial V_i} = \boldsymbol{0} \qquad \text{on } \partial V_i \cap \partial V_j, \tag{5.6e}$$

with $\boldsymbol{f}_0$ and $\boldsymbol{t}_0$ forces per unit undeformed volume and surface, respectively, as described in Section 2.2.1.

Notice that equations (5.6a) and (5.6b) represent the local translational equilibrium in the dielectric and the vacuum, respectively. Moreover, in the case of equations (5.6c)-(5.6d), $[\![\boldsymbol{P}]\!]$ represents the jump in the first Piola-Kirchhoff stress tensor between that of the domain defined by the dielectric V and that of the surrounding vacuum, the latter known as Maxwell stress tensor [63, 68, 77].

It is possible to highlight the differences for the local translational equilibrium equation and its associated jump condition (equations (5.6a) and (5.6b)) in both pure elasticity and in the more general context hereby considered, namely electroelasticity. Refer to Section 4.2.3 in the context of nonlinear elasticity, where the jump condition is replaced with the simpler one $\boldsymbol{P}\boldsymbol{N} = \boldsymbol{t}_0$. Moreover, in the electromechanical case considered, the stress tensor $\boldsymbol{P}$ includes now both deformation and electrical components. As pointed out in [63], as there are no experiments that can separate the mechanical from the electrical contributions in $\boldsymbol{P}$, it is preferred to work with the overall coupled stress tensor and not with its individual (deformation and electrical) components.

Once again, satisfaction of rotational equilibrium leads to the condition $\boldsymbol{P}\boldsymbol{F}^T = \boldsymbol{F}\boldsymbol{P}^T$ imposed on the coupled electromechanical stress tensor [61], and not on its individual deformation and electrical contributions.

Remark 5.1. When the surrounding truncated medium corresponds to vacuum, a distribution of stress (typically known as the Maxwell stress) due to the surrounding electric field arises. The Maxwell stress is divergence free and hence, we can conclude that $\boldsymbol{f}_0 = \boldsymbol{0}$ in V_∞, which is stated in equation (5.6b).

5.3.2 The internal energy in nonlinear electro-elasticity: multi-variable convexity

For the closure of the system of equations defined by (5.3), (5.4), (5.5), (5.6) and (5.10), an additional constitutive law is needed relating deformation and electric

displacement with stresses and electric field in the domain defined by the dielectric. In the case of reversible electro-elasticity, where thermal effects and any other possible state variables (i.e. accumulated plastic deformation or electrical relaxation) are disregarded, the internal energy density e (this would be the analogous to the strain energy $\Psi(\boldsymbol{\nabla}_0\boldsymbol{x})$ (2.39) for elasticity) per unit of undeformed volume can be defined in terms of the deformation and the electric displacement, namely $e = e(\boldsymbol{\nabla}_0\boldsymbol{x}, \boldsymbol{D}_0)$. In addition, let us consider $\delta\boldsymbol{D}_0$ and $\Delta\boldsymbol{D}_0$ to denote virtual and incremental variations of $\boldsymbol{D}_0$, respectively, satisfying compatible homogeneous electric displacement based boundary conditions on $\partial_\omega V$. In this case, combination of (5.4) and (5.6) and the first law of thermodynamics yields

$$De[\delta\boldsymbol{u}, \delta\boldsymbol{D}_0] = \boldsymbol{P} : \boldsymbol{\nabla}_0\delta\boldsymbol{u} + \boldsymbol{E}_0 \cdot \delta\boldsymbol{D}_0, \tag{5.7}$$

or alternatively,

$$\boldsymbol{P} = \left.\frac{\partial e(\boldsymbol{F}, \boldsymbol{D}_0)}{\partial \boldsymbol{F}}\right|_{\boldsymbol{F}=\boldsymbol{\nabla}_0\boldsymbol{x}}; \qquad \boldsymbol{E}_0 = \left.\frac{\partial e(\boldsymbol{F}, \boldsymbol{D}_0)}{\partial \boldsymbol{D_0}}\right|_{\boldsymbol{F}=\boldsymbol{\nabla}_0\boldsymbol{x}}. \tag{5.8}$$

As an example, the internal energy functional of a very popular material is that of an ideal isotropic dielectric elastomer, which is defined based on the additive decomposition of a purely mechanical component $e_m(\boldsymbol{\nabla}_0\boldsymbol{x})$ and an electromechanical component which is proportional to the internal energy of the vacuum e_0, namely

$$\begin{aligned} e_{\text{ideal}}(\boldsymbol{\nabla}_0\boldsymbol{x}, \boldsymbol{D}_0) &= e_m(\boldsymbol{\nabla}_0\boldsymbol{x}) + \frac{1}{\varepsilon_r} e_0(\boldsymbol{\nabla}_0\boldsymbol{x}, \boldsymbol{D}_0); \\ e_0(\boldsymbol{\nabla}_0\boldsymbol{x}, \boldsymbol{D}_0) &= \frac{1}{2\varepsilon_0 J} II_{\boldsymbol{d}}; \qquad \boldsymbol{d} = \boldsymbol{F}\boldsymbol{D}_0 = J\boldsymbol{D}; \qquad II_{\boldsymbol{d}} = \boldsymbol{d}\cdot\boldsymbol{d}; \end{aligned} \tag{5.9}$$

where ε_r is a dimensionless constant representing the relative permittivity of the dielectric and ε_0, the electric permittivity of the vacuum, with $\varepsilon_0 \approx 8.854\times10^{-12} A^2 s^4 kg^{-1} m^{-3}$. For the particular case of the vacuum, equation (5.8) enables to obtain the Maxwell stress tensor and the relationship between the electric field and the electric displacement field based on the internal energy $W_0(\boldsymbol{x}, \boldsymbol{D}_0)$ defined in equation (5.9) as

$$\begin{aligned} \boldsymbol{P} &= \frac{1}{\varepsilon_0 J}\boldsymbol{d}\otimes\boldsymbol{D}_0 - \frac{1}{2\varepsilon_0 J^2} II_{\boldsymbol{d}}\boldsymbol{H} && \text{in } V_\infty; \\ \boldsymbol{E}_0 &= \frac{1}{\varepsilon_0 J}\boldsymbol{F}^T\boldsymbol{d} && \text{in } V_\infty. \end{aligned} \tag{5.10}$$

These expressions can be pushed forward to the Eulerian configuration using the standard Piola transformation $\boldsymbol{\sigma} = J^{-1}\boldsymbol{P}\boldsymbol{F}^T$ and $\boldsymbol{E} = \boldsymbol{F}^{-T}\boldsymbol{E}_0$ to give after simple algebra the Cauchy stress tensor in the vacuum and the corresponding electric field as

$$\begin{aligned} \boldsymbol{\sigma} &= \frac{1}{\varepsilon_0}\boldsymbol{D}\otimes\boldsymbol{D} - \frac{1}{2\varepsilon_0} II_{\boldsymbol{D}}\boldsymbol{I} && \text{in } V_\infty; \\ \boldsymbol{E} &= \frac{1}{\varepsilon_0}\boldsymbol{D} && \text{in } V_\infty. \end{aligned} \tag{5.11}$$

In this paper, a generalisation of of equation (2.39) for the internal energy density functional e including electromechanical contributions is postulated as

$$e\left(\boldsymbol{\nabla}_0\boldsymbol{x}, \boldsymbol{D}_0\right) = W\left(\boldsymbol{F}, \boldsymbol{H}, J, \boldsymbol{D}_0, \boldsymbol{d}\right), \tag{5.12}$$

where W represents a convex muti-variable functional in terms of its extended set of arguments $\mathcal{V} = \{\boldsymbol{F}, \boldsymbol{H}, J, \boldsymbol{D}_0, \boldsymbol{d}\}$ and with $\boldsymbol{d}$ defined in equation (5.9). Refer to Figure 5.3 for a comparison of the above definition of multi-variable convexity with that in the context of elasticity. Objectivity or material frame indifference implies that $W(\boldsymbol{F}, \boldsymbol{H}, J, \boldsymbol{D}_0, \boldsymbol{F}\boldsymbol{D}_0)$ must be independent of the rotational components of $\boldsymbol{F}$ and $\boldsymbol{H}$ via symmetric tensors such as the right Cauchy-Green strain tensor $\boldsymbol{C} = \boldsymbol{F}^T\boldsymbol{F}$ or $\boldsymbol{G} = \boldsymbol{H}^T\boldsymbol{H}$.

Remark 5.2. It would be tempting to postulate W as a convex function of $\{\boldsymbol{F}, \boldsymbol{H}, J, \boldsymbol{D}_0\}$ [83], excluding the additional variable $\boldsymbol{d}$. However, it is easy to show that this leads to a non-convex representation of the energy function describing the vacuum (5.9) and hence, that for a ideal dielectric elastomer. In other words, as the invariant $\boldsymbol{F}\boldsymbol{D}_0 \cdot \boldsymbol{F}\boldsymbol{D}_0$ is not convex with respect to arguments $\{\boldsymbol{F}, \boldsymbol{D}_0\}$, this would preclude its use in the sense of material stability. However, as this invariant is convex with respect to $\boldsymbol{d}$, its use can still be incorporated into our framework, hence including the electro-mechanical energy of both vacuum and ideal dielectric elastomers as a valid degenerate case of our formulation.

5.3.3 Work conjugate variables

The definition of multi-variable convexity in equation (5.12) enables the introduction of a set of work conjugate variables $\Sigma_{\mathcal{V}} = \{\boldsymbol{\Sigma}_{\boldsymbol{F}}, \boldsymbol{\Sigma}_{\boldsymbol{H}}, \Sigma_J, \boldsymbol{\Sigma}_{\boldsymbol{D}_0}, \boldsymbol{\Sigma}_{\boldsymbol{d}}\}$ to those in the set $\mathcal{V}$ defined as

$$\boldsymbol{\Sigma}_{\boldsymbol{F}} = \frac{\partial W}{\partial \boldsymbol{F}}; \quad \boldsymbol{\Sigma}_{\boldsymbol{H}} = \frac{\partial W}{\partial \boldsymbol{H}}; \quad \Sigma_J = \frac{\partial W}{\partial J}; \quad \boldsymbol{\Sigma}_{\boldsymbol{D}_0} = \frac{\partial W}{\partial \boldsymbol{D}_0}; \quad \boldsymbol{\Sigma}_{\boldsymbol{d}} = \frac{\partial W}{\partial \boldsymbol{d}}. \tag{5.13}$$

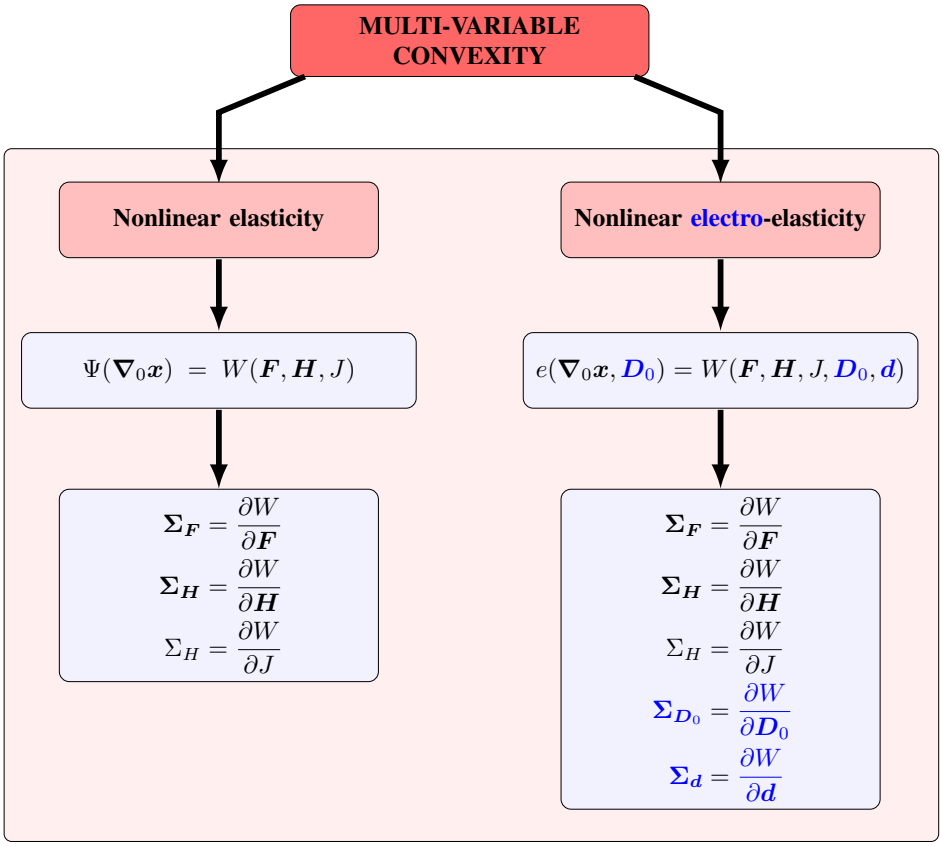

Figure 5.3: Extension of multi-variable convexity from nonlinear elasticity to nonlinear electro-elasticity. Definition of work conjugates. Electrical variables highlighted in blue.

Refer to Figure 5.3 for a comparison of the different work conjugates in convex multi-variable electro-elasticity and convex multi-variable elasticity (polyconvex elasticity). For notational convenience, for sets containing mechanical and electrical variables, namely $\mathcal{V}^m$, $\Sigma^m_{\mathcal{V}}$, $\mathcal{V}^e$ and $\Sigma^e_{\mathcal{V}}$, used in subsequent sections are defined as,

$$\begin{aligned} \mathcal{V}^m &= \{\boldsymbol{F},\boldsymbol{H},J\}; & \Sigma^m_{\mathcal{V}} &= \{\boldsymbol{\Sigma}_{\boldsymbol{F}},\boldsymbol{\Sigma}_{\boldsymbol{H}},\Sigma_J\}; \\ \mathcal{V}^e &= \{\boldsymbol{D}_0,\boldsymbol{d}\}; & \Sigma^e_{\mathcal{V}} &= \{\boldsymbol{\Sigma}_{\boldsymbol{D}_0},\boldsymbol{\Sigma}_{\boldsymbol{d}}\}. \end{aligned} \tag{5.14}$$

Following a similar procedure to that of equation (2.52), the directional derivative of the internal energy e with respect to virtual changes in the geometry is obtained as

$$\begin{aligned} De\left[\delta\boldsymbol{u}\right] &= DW\left[D\boldsymbol{F}\left[\delta\boldsymbol{u}\right], D\boldsymbol{H}\left[\delta\boldsymbol{u}\right], DJ\left[\delta\boldsymbol{u}\right], D\boldsymbol{d}\left[\delta\boldsymbol{u}\right]\right] \\ &= \boldsymbol{\Sigma}_{\boldsymbol{F}} : D\boldsymbol{F}\left[\delta\boldsymbol{u}\right] + \boldsymbol{\Sigma}_{\boldsymbol{H}} : D\boldsymbol{H}\left[\delta\boldsymbol{u}\right] + \Sigma_J DJ\left[\delta\boldsymbol{u}\right] + \boldsymbol{\Sigma}_{\boldsymbol{d}} \cdot D\boldsymbol{d}\left[\delta\boldsymbol{u}\right] \\ &= \boldsymbol{\Sigma}_{\boldsymbol{F}} : \boldsymbol{\nabla}_0\delta\boldsymbol{u} + \boldsymbol{\Sigma}_{\boldsymbol{H}} : (\boldsymbol{F} \times \boldsymbol{\nabla}_0\delta\boldsymbol{u}) + \Sigma_J\left(\boldsymbol{H} : \boldsymbol{\nabla}_0\delta\boldsymbol{u}\right) + (\boldsymbol{\Sigma}_{\boldsymbol{d}} \otimes \boldsymbol{D}_0) : \boldsymbol{\nabla}_0\delta\boldsymbol{u} \\ &= (\boldsymbol{\Sigma}_{\boldsymbol{F}} + \boldsymbol{\Sigma}_{\boldsymbol{H}} \times \boldsymbol{F} + \Sigma_J\boldsymbol{H} + \boldsymbol{\Sigma}_{\boldsymbol{d}} \otimes \boldsymbol{D}_0) : \boldsymbol{\nabla}_0\delta\boldsymbol{u}, \end{aligned} \tag{5.15}$$

where the relationship $D\boldsymbol{d}[\delta\boldsymbol{u}] = (\boldsymbol{\nabla}_0\delta\boldsymbol{u})\boldsymbol{D}_0$ emanating from the relationship $\boldsymbol{d} = \boldsymbol{F}\boldsymbol{D}_0$ has been used. Similarly, the first directional derivative of the internal energy with respect to virtual variations of the electric displacement field is obtained as

$$\begin{aligned} De\left[\delta\boldsymbol{D}_0\right] &= DW\left[\delta\boldsymbol{D}_0, \boldsymbol{F}\delta\boldsymbol{D}_0\right] = \boldsymbol{\Sigma}_{\boldsymbol{D}_0}\cdot\delta\boldsymbol{D}_0 + \boldsymbol{\Sigma}_{\boldsymbol{d}}\cdot\boldsymbol{F}\delta\boldsymbol{D}_0 \\ &= \left(\boldsymbol{\Sigma}_{\boldsymbol{D}_0} + \boldsymbol{F}^T\boldsymbol{\Sigma}_{\boldsymbol{d}}\right)\cdot\delta\boldsymbol{D}_0. \end{aligned} \tag{5.16}$$

Comparison of equations (5.15) and (5.16) against (5.7), enables the first Piola-Kirchhoff stress tensor and the material electric displacement field to be expressed in terms of the elements of both sets $\mathcal{V}$ and $\Sigma_{\mathcal{V}}$ as

$$\boldsymbol{P} = \boldsymbol{\Sigma}_{\boldsymbol{F}} + \boldsymbol{\Sigma}_{\boldsymbol{H}} \boldsymbol{\times} \boldsymbol{F} + \Sigma_J\boldsymbol{H} + \boldsymbol{\Sigma}_{\boldsymbol{d}}\otimes\boldsymbol{D}_0; \quad \boldsymbol{E}_0 = \boldsymbol{\Sigma}_{\boldsymbol{D}_0} + \boldsymbol{F}^T\boldsymbol{\Sigma}_{\boldsymbol{d}}. \tag{5.17}$$

An expression for the Kirchhoff stress tensor [44] and the spatial electric field emerges based upon the relations $\boldsymbol{\tau} = \boldsymbol{P}\boldsymbol{F}^T$ and $\boldsymbol{E} = \boldsymbol{F}^{-T}\boldsymbol{E}_0$ as

$$\begin{aligned} \boldsymbol{\tau} &= \boldsymbol{\Sigma}_{\boldsymbol{F}}\boldsymbol{F}^T + \left(\boldsymbol{\Sigma}_{\boldsymbol{H}}\boldsymbol{H}^T\right)\boldsymbol{\times}\boldsymbol{I} + J\Sigma_J\boldsymbol{I} + \boldsymbol{\Sigma}_{\boldsymbol{d}}\otimes\boldsymbol{d}; \\ \boldsymbol{E} &= \boldsymbol{F}^{-T}\left(\boldsymbol{\Sigma}_{\boldsymbol{D}_0} + \boldsymbol{F}^T\boldsymbol{\Sigma}_{\boldsymbol{d}}\right) = \boldsymbol{F}^{-T}\boldsymbol{\Sigma}_{\boldsymbol{D}_0} + \boldsymbol{\Sigma}_{\boldsymbol{d}}. \end{aligned} \tag{5.18}$$

5.3.4 Tangent electromechanics operator for the internal energy

With a Newton-Raphson type of solution process in mind, the internal energy $e = e(\boldsymbol{\nabla}_0\boldsymbol{x}, \boldsymbol{D}_0)$ can be further linearised leading to a tangent operator defined as follows

$$D^2e\left[\delta\boldsymbol{u}, \delta\boldsymbol{D}_0; \boldsymbol{u}, \Delta\boldsymbol{D}_0\right] = \left[\begin{array}{cc} \boldsymbol{\nabla}_0\delta\boldsymbol{u}: & \delta\boldsymbol{D}_0\cdot \end{array}\right] \left[\begin{array}{cc} \boldsymbol{\mathcal{C}} & \boldsymbol{\mathcal{Q}}^T \\ \boldsymbol{\mathcal{Q}} & \boldsymbol{\theta} \end{array}\right] \left[\begin{array}{c} :\boldsymbol{\nabla}_0\boldsymbol{u} \\ \Delta\boldsymbol{D}_0 \end{array}\right], \tag{5.19}$$

with the fourth order tensor $\boldsymbol{\mathcal{C}}$, the third order tensor $\boldsymbol{\mathcal{Q}}$ and the second order tensor $\boldsymbol{\theta}$ defined as

$$\boldsymbol{\mathcal{C}} = \left.\frac{\partial^2 e(\boldsymbol{F}, \boldsymbol{D}_0)}{\partial\boldsymbol{F}\partial\boldsymbol{F}}\right|_{\boldsymbol{F}=\boldsymbol{\nabla}_0\boldsymbol{x}}; \; \boldsymbol{\mathcal{Q}} = \left.\frac{\partial^2 e(\boldsymbol{F}, \boldsymbol{D}_0)}{\partial\boldsymbol{D}_0\partial\boldsymbol{F}}\right|_{\boldsymbol{F}=\boldsymbol{\nabla}_0\boldsymbol{x}}; \; \boldsymbol{\theta} = \left.\frac{\partial^2 e(\boldsymbol{F}, \boldsymbol{D}_0)}{\partial\boldsymbol{D}_0\partial\boldsymbol{D}_0}\right|_{\boldsymbol{F}=\boldsymbol{\nabla}_0\boldsymbol{x}}. \tag{5.20}$$

Following a similar procedure to that presented in Section 2.3.5, with the additional relationships $D^2\boldsymbol{d}[\delta\boldsymbol{u}, \Delta\boldsymbol{D}_0] = (\boldsymbol{\nabla}_0\delta\boldsymbol{u})\Delta\boldsymbol{D}_0$ and $D^2\boldsymbol{d}[\delta\boldsymbol{D}_0, \boldsymbol{u}] = (\boldsymbol{\nabla}_0\boldsymbol{u})\delta\boldsymbol{D}_0$, a more physically insightful representation of the tangent operator (5.19) is

$$\begin{aligned} D^2e\left[\delta\boldsymbol{u}, \delta\boldsymbol{D}_0; \boldsymbol{u}, \Delta\boldsymbol{D}_0\right] = \left[\mathbb{S}_\delta\right]^T\left[\mathbb{H}_W\right]\left[\mathbb{S}_\Delta\right] + (\boldsymbol{\Sigma}_{\boldsymbol{H}} + \Sigma_J\boldsymbol{F}) : (\boldsymbol{\nabla}_0\delta\boldsymbol{u}\boldsymbol{\times}\boldsymbol{\nabla}_0\boldsymbol{u}) \\ + \boldsymbol{\Sigma}_{\boldsymbol{d}}\cdot\left((\boldsymbol{\nabla}_0\delta\boldsymbol{u})\Delta\boldsymbol{D}_0 + (\boldsymbol{\nabla}_0\boldsymbol{u})\delta\boldsymbol{D}_0\right), \end{aligned} \tag{5.21}$$

where

$$\begin{aligned} \left[\mathbb{S}_\delta\right]^T &= \left[(\boldsymbol{\nabla}_0\delta\boldsymbol{u}): \quad (\boldsymbol{\nabla}_0\delta\boldsymbol{u}\boldsymbol{\times}\boldsymbol{F}): \quad (\boldsymbol{\nabla}_0\delta\boldsymbol{u} : \boldsymbol{H}) \quad \delta\boldsymbol{D}_0\cdot \quad ((\boldsymbol{\nabla}_0\delta\boldsymbol{u})\boldsymbol{D}_0 + \boldsymbol{F}\delta\boldsymbol{D}_0)\cdot\right]; \\ \left[\mathbb{S}_\Delta\right] &= \left[\begin{array}{c} :(\boldsymbol{\nabla}_0\boldsymbol{u}) \\ :(\boldsymbol{F}\boldsymbol{\times}\boldsymbol{\nabla}_0\boldsymbol{u}) \\ (\boldsymbol{H} : \boldsymbol{\nabla}_0\boldsymbol{u}) \\ \Delta\boldsymbol{D}_0 \\ (\boldsymbol{\nabla}_0\boldsymbol{u})\boldsymbol{D}_0 + \boldsymbol{F}\Delta\boldsymbol{D}_0 \end{array}\right], \end{aligned} \tag{5.22}$$

and with the extended Hessian operator $[\mathbb{H}_W]$ denoting the symmetric positive definite operator containing the second derivatives of $W(\boldsymbol{F}, \boldsymbol{H}, J, \boldsymbol{D}_0, \boldsymbol{d})$ as

$$[\mathbb{H}_W] = \begin{bmatrix} W_{\boldsymbol{FF}} & W_{\boldsymbol{FH}} & W_{\boldsymbol{F}J} & W_{\boldsymbol{FD}_0} & W_{\boldsymbol{Fd}} \\ W_{\boldsymbol{HF}} & W_{\boldsymbol{HH}} & W_{\boldsymbol{H}J} & W_{\boldsymbol{HD}_0} & W_{\boldsymbol{Hd}} \\ W_{J\boldsymbol{F}} & W_{J\boldsymbol{H}} & W_{JJ} & W_{J\boldsymbol{D}_0} & W_{J\boldsymbol{d}} \\ W_{\boldsymbol{D}_0\boldsymbol{F}} & W_{\boldsymbol{D}_0\boldsymbol{H}} & W_{\boldsymbol{D}_0J} & W_{\boldsymbol{D}_0\boldsymbol{D}_0} & W_{\boldsymbol{D}_0\boldsymbol{d}} \\ W_{\boldsymbol{dF}} & W_{\boldsymbol{dH}} & W_{\boldsymbol{d}J} & W_{\boldsymbol{dD}_0} & W_{\boldsymbol{dd}} \end{bmatrix}. \tag{5.23}$$

It is important to emphasise that this additive decomposition of the tangent operator is not merely technical but, extremely useful, as the multi-physics of the problem is completely captured in the first term on the right hand side of equation (5.38), whilst geometrically nonlinear terms are collected on the second and third terms.

Multi-variable convexity dictates that the first term on the right hand side of equation (5.38) is necessarily positive for virtual fields $\{\delta\boldsymbol{u}, \delta\boldsymbol{D}_0\}$ satisfying $\{\delta\boldsymbol{u} = \boldsymbol{u}, \delta\boldsymbol{D}_0 = \Delta\boldsymbol{D}_0\}$ and thus, buckling can only be induced by the second and third (geometrically-based) terms.

Remark 5.3. Equation (5.38) makes it possible to highlight the relationship between multi-variable convexity and ellipticity in the case of electromechanics. Taking rank-one equal virtual and incremental displacement gradient tensors $\boldsymbol{\nabla}_0\delta\boldsymbol{u} = \boldsymbol{\nabla}_0\boldsymbol{u} = \boldsymbol{v} \otimes \boldsymbol{V}$ and $\Delta\boldsymbol{D}_0 = \delta\boldsymbol{D}_0 = \boldsymbol{V}_\perp$ (where $\boldsymbol{V}_\perp$ represents any orthogonal vector to $\boldsymbol{V}$) [74] in equation (5.38) makes the initial stress term vanish since,

$$\begin{aligned} &\boldsymbol{\nabla}_0\delta\boldsymbol{u} \times \boldsymbol{\nabla}_0\boldsymbol{u} = (\boldsymbol{v} \otimes \boldsymbol{V}) \times (\boldsymbol{v} \otimes \boldsymbol{V}) = (\boldsymbol{v} \times \boldsymbol{v}) \otimes (\boldsymbol{V} \times \boldsymbol{V}) = \boldsymbol{0}; \\ &\boldsymbol{\Sigma}_{\boldsymbol{d}} \cdot ((\boldsymbol{\nabla}_0\delta\boldsymbol{u})\Delta\boldsymbol{D}_0 + (\boldsymbol{\nabla}_0\boldsymbol{u})\delta\boldsymbol{D}_0) = 2\,(\boldsymbol{v} \cdot \boldsymbol{\Sigma}_{\boldsymbol{d}})\,(\boldsymbol{V} \cdot \boldsymbol{V}_\perp) = 0. \end{aligned} \tag{5.24}$$

This leaves only the contribution from the first positive definite term in equation (5.38), leading to (refer to equation (5.19)),

$$\left[\ \boldsymbol{u} \otimes \boldsymbol{V} : \quad \boldsymbol{V}_\perp \cdot\ \right] \begin{bmatrix} \boldsymbol{\mathcal{C}} & \boldsymbol{\mathcal{Q}}^T \\ \boldsymbol{\mathcal{Q}} & \boldsymbol{\theta} \end{bmatrix} \begin{bmatrix} : \boldsymbol{u} \otimes \boldsymbol{V} \\ \boldsymbol{V}_\perp \end{bmatrix} > 0. \tag{5.25}$$

Equation (5.25) is a generalisation of the concept of ellipticity to the case of electromechanics[4].

---

[4]In the context of elasticity, ellipticity is equivalent to rank-one convexity and requires that the double contraction of the elasticity tensor by an arbitrary rank-one tensor $\boldsymbol{v} \otimes \boldsymbol{V}$ should be positive.

5.3.5 A simple convex multi-variable electromechanical constitutive model

As an example, a simple internal energy functional which complies with the definition of multi-variable in (5.12) can be defined as

$$W_1 = \mu_1 II_{\boldsymbol{F}} + \mu_2 II_{\boldsymbol{H}} + f(J) + \frac{1}{2\varepsilon_1 J} II_{\boldsymbol{d}} + \frac{1}{2\varepsilon_2} II_{\boldsymbol{D}_0}, \tag{5.26}$$

where a possible definition of the function $f(J)$ in equation (5.26) could be

$$f(J) = -2\left(\mu_1 + 2\mu_2\right) \ln J + \frac{\kappa}{2}\left(J-1\right)^2. \tag{5.27}$$

The work conjugates in (5.13) for the internal energy functional in (5.26) are obtained as

$$\boldsymbol{\Sigma}_{\boldsymbol{F}} = 2\mu_1 \boldsymbol{F}; \quad \boldsymbol{\Sigma}_{\boldsymbol{H}} = 2\mu_2 \boldsymbol{H}; \quad \Sigma_J = f'(J) - \frac{1}{2\varepsilon_1 J^2} II_{\boldsymbol{d}}; \quad \boldsymbol{\Sigma}_{\boldsymbol{D}_0} = \frac{1}{\varepsilon_2}\boldsymbol{D}_0; \quad \boldsymbol{\Sigma}_{\boldsymbol{d}} = \frac{1}{\varepsilon_1 J}\boldsymbol{d}. \tag{5.28}$$

For the particular constitutive model defined in equation (5.26), the first Piola-Kirchhoff stress tensor and the material electric field are obtained according to equation (5.17) as

$$\begin{aligned} \boldsymbol{P} =& 2\mu_1 \boldsymbol{F} + 2\mu_2 \boldsymbol{H} \times \boldsymbol{F} + \left(f'(J) - \frac{1}{2\varepsilon_1 J^2} II_{\boldsymbol{d}} \right) \boldsymbol{H} + \frac{1}{\varepsilon_1 J} \boldsymbol{d} \otimes \boldsymbol{D}_0; \\ \boldsymbol{E}_0 =& \frac{1}{\varepsilon_2}\boldsymbol{D}_0 + \frac{1}{\varepsilon_1 J}\boldsymbol{F}^T \boldsymbol{d}. \end{aligned} \tag{5.29}$$

Substitution of the relationship $\boldsymbol{d} = \boldsymbol{F}\boldsymbol{D}_0$ enables the last equation to be re-written as

$$\boldsymbol{E}_0 = \left(\frac{1}{\varepsilon_2}\boldsymbol{I} + \frac{1}{\varepsilon_1}\boldsymbol{C} \right) \boldsymbol{D}_0. \tag{5.30}$$

For the particular constitutive model defined in equation (5.26), the Hessian operator becomes

$$[\mathbb{H}_W] = \begin{bmatrix} 2\mu_1 \boldsymbol{\mathcal{I}} & \boldsymbol{0} & \boldsymbol{0} & \boldsymbol{0} & \boldsymbol{0} \\ \boldsymbol{0} & 2\mu_2 \boldsymbol{\mathcal{I}} & \boldsymbol{0} & \boldsymbol{0} & \boldsymbol{0} \\ \boldsymbol{0} & \boldsymbol{0} & f''(J) + \frac{1}{\varepsilon_1 J^3} II_{\boldsymbol{d}} & \boldsymbol{0} & -\frac{1}{\varepsilon_1 J^2}\boldsymbol{d} \\ \boldsymbol{0} & \boldsymbol{0} & \boldsymbol{0} & \frac{1}{\varepsilon_2}\boldsymbol{I} & \boldsymbol{0} \\ \boldsymbol{0} & \boldsymbol{0} & -\frac{1}{\varepsilon_1 J^2}\boldsymbol{d} & \boldsymbol{0} & \frac{1}{\varepsilon_1 J}\boldsymbol{I} \end{bmatrix}. \tag{5.31}$$

It is interesting to observe the positive definite nature of the above Hessian operator provided that the constants μ_1, μ_2, ε_1 and ε_2 are positive and that the function $f(J)$ is convex.

Remark 5.4. Similarly to *Remark 1* in the case of nonlinear elasticity, the degenerate case $\varepsilon_2 = \infty$ results in the ideal dielectric model in equation (5.9), which is convex in $\{\boldsymbol{F}, \boldsymbol{H}, J, \boldsymbol{d}\}$ alone without the need to introduce $\boldsymbol{D}_0$ as a separate independent variable. Moreover, for $\mu_1 = \mu_2 = 0$ and $f(J) = 0$, the energy of the vacuum is retrieved, which is convex in the reduced set $\{J, \boldsymbol{d}\}$.

It is important to emphasise that the energy of an ideal dielectric (vacuum) cannot be expressed as a multivalued convex function of $\{\boldsymbol{F}, \boldsymbol{H}, J, \boldsymbol{D}_0\}$ ($\{J, \boldsymbol{D}_0\}$). That is the reason behind the definition of the extended set $\mathcal{V}$ including the spatial vector $\boldsymbol{d}$ among its variables. Crucially, this enables to consider the vacuum as a degenerate case of the formulation presented in this work.

5.3.6 Alternative energy density functionals

Multi-variable convexity of the internal energy guarantees that the relationship between both sets of variables $\mathcal{V}$ and $\Sigma_{\mathcal{V}}$ is one to one and invertible. This enables the definition of alternative energy functionals established via appropriate Legendre transforms applied to the internal energy $W(\mathcal{V})$ as

$$\Upsilon\left(\Sigma_{\mathcal{V}}\right) = \sup_{\mathcal{V}} \left\{T^m + T^e - W\left(\mathcal{V}\right)\right\}; \tag{5.32a}$$

$$\Psi\left(\Sigma^m_{\mathcal{V}}, \mathcal{V}^e\right) = \sup_{\mathcal{V}^m} \left\{T^m - W\left(\mathcal{V}\right)\right\}; \tag{5.32b}$$

$$\Phi\left(\mathcal{V}^m, \Sigma^e_{\mathcal{V}}\right) = -\sup_{\mathcal{V}^e} \left\{T^e - W\left(\mathcal{V}\right)\right\}, \tag{5.32c}$$

with the sets $\mathcal{V}^m$, $\mathcal{V}^e$, $\Sigma^m_{\mathcal{V}}$ and $\Sigma^e_{\mathcal{V}}$ defined in equations (5.14) and with

$$T^m = \boldsymbol{\Sigma}_{\boldsymbol{F}} : \boldsymbol{F} + \boldsymbol{\Sigma}_{\boldsymbol{H}} : \boldsymbol{H} + \Sigma_J J; \qquad T^e = \boldsymbol{\Sigma}_{\boldsymbol{D_0}} \cdot \boldsymbol{D}_0 + \boldsymbol{\Sigma}_{\boldsymbol{d}} \cdot \boldsymbol{d}. \tag{5.33}$$

In equation (5.32), $\Upsilon\left(\Sigma_{\mathcal{V}}\right)$ represents an extended Gibbs' energy density, $\Psi\left(\Sigma^m_{\mathcal{V}}, \mathcal{V}^e\right)$, an extended enthalpy energy density and $\Phi\left(\mathcal{V}, \Sigma^e_{\mathcal{V}}\right)$, an extended Helmholtz's energy density[5]. Expressions relating strain, stress and electric fields, in terms of the different energy densities, follow naturally as in Table 5.1.

Figure 5.4 summarises the set of arguments (denoted as $\mathcal{R}$) for the different extended energy functionals defined, namely the internal, Gibbs's, Enthalpy and Helmtholz's energy functionals and their respective set of work conjugates (denoted as $\Sigma_{\mathcal{R}}$).

Remark 5.5. Notice that the definition of multi-variable convexity in (5.12) ensures a one to one relationship between the pairs $\{\boldsymbol{D}_0, \boldsymbol{d}\}$ and $\{\boldsymbol{\Sigma}_{\boldsymbol{D}_0}, \boldsymbol{\Sigma}_{\boldsymbol{d}}\}$, respectively. Moreover, consideration of the definition of the spatial vector $\boldsymbol{d} = \boldsymbol{\nabla}_0 \boldsymbol{x} \boldsymbol{D}_0$ and

[5]The terminology adopted here matches that of classical Thermodynamics, where the electric displacement (electric field) plays the same role as the entropy (temperature) of the system.

$\boldsymbol{F} = \frac{\partial \Upsilon}{\partial \boldsymbol{\Sigma}_{\boldsymbol{F}}}$	$\boldsymbol{H} = \frac{\partial \Upsilon}{\partial \boldsymbol{\Sigma}_{\boldsymbol{H}}}$	$J = \frac{\partial \Upsilon}{\partial \Sigma_J}$	$\boldsymbol{D}_0 = \frac{\partial \Upsilon}{\partial \boldsymbol{\Sigma}_{\boldsymbol{D}_0}}$	$\boldsymbol{d} = \frac{\partial \Upsilon}{\partial \boldsymbol{\Sigma}_{\boldsymbol{d}}}$
$\boldsymbol{F} = \frac{\partial \Psi}{\partial \boldsymbol{\Sigma}_{\boldsymbol{F}}}$	$\boldsymbol{H} = \frac{\partial \Psi}{\partial \boldsymbol{\Sigma}_{\boldsymbol{H}}}$	$J = \frac{\partial \Psi}{\partial \Sigma_J}$	$\boldsymbol{\Sigma}_{\boldsymbol{D}_0} = -\frac{\partial \Psi}{\partial \boldsymbol{D}_0}$	$\boldsymbol{\Sigma}_{\boldsymbol{d}} = -\frac{\partial \Psi}{\partial \boldsymbol{d}}$
$\boldsymbol{\Sigma}_{\boldsymbol{F}} = \frac{\partial \Phi}{\partial \boldsymbol{F}}$	$\boldsymbol{\Sigma}_{\boldsymbol{H}} = \frac{\partial \Phi}{\partial \boldsymbol{H}}$	$\Sigma_J = \frac{\partial \Phi}{\partial J}$	$\boldsymbol{D}_0 = -\frac{\partial \Phi}{\partial \boldsymbol{\Sigma}_{\boldsymbol{D}_0}}$	$\boldsymbol{d} = -\frac{\partial \Phi}{\partial \boldsymbol{\Sigma}_{\boldsymbol{d}}}$

Table 5.1: Expressions relating strain, stress, and electric variables for the energy functionals Υ (5.32a), Ψ (5.32b) and Φ (5.32c).

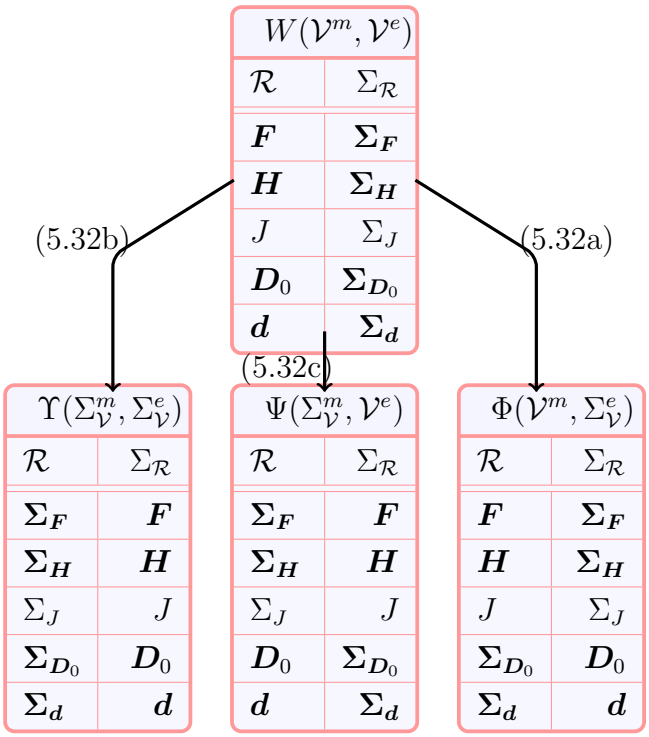

Figure 5.4: The arguments ($\mathcal{R}$) of the internal $W(\mathcal{V})$ (5.12), Gibbs's $\Upsilon\,(\Sigma_{\mathcal{V}})$ (5.32a), Enthalpy $\Psi\,(\Sigma^m_{\mathcal{V}}, \mathcal{V}^e)$ (5.32b) and Helmtholz's $\Phi\,(\mathcal{V}^m, \Sigma^e_{\mathcal{V}})$ (5.32c) energy functionals and their respective set of work conjugates ($\Sigma_{\mathcal{R}}$). Relation between $W(\mathcal{V})$ and the remaining energy functionals according to the Legendre transforms defined in equation (5.32).

the definition of the material electric field $-\boldsymbol{\nabla}_0\varphi$ in terms of the work conjugates $\{\boldsymbol{\Sigma}_{\boldsymbol{D}_0}, \boldsymbol{\Sigma}_{\boldsymbol{d}}\}$ in (5.17), results in turn in a one to one relationship between the variables $\boldsymbol{D}_0$ and $-\boldsymbol{\nabla}_0\varphi$.

In this case, it is possible to define an alternative energy functional to $e = e(\boldsymbol{\nabla}_0\boldsymbol{x}, \boldsymbol{D}_0)$ by making use of the Legendre transform. This might be a computationally convenient approach in the case of pursuing a standard semi-discrete variational implementation via the Finite Element Method, where the scalar electric potential is preferred as an unknown over the electric displacement field vector. For instance, the Helmholtz's energy density $\Phi = \Phi(\boldsymbol{\nabla}_0\boldsymbol{x}, -\boldsymbol{\nabla}_0\varphi)$ can be defined as[6]

$$\Phi\left(\boldsymbol{\nabla}_0\boldsymbol{x}, -\boldsymbol{\nabla}_0\varphi\right) = -\sup_{\boldsymbol{D}_0}\left\{-\boldsymbol{\nabla}_0\varphi\cdot\boldsymbol{D}_0 - e\left(\boldsymbol{\nabla}_0\boldsymbol{x}, \boldsymbol{D}_0\right)\right\}, \tag{5.34}$$

leading to an alternative definition to that of (5.8) for the stress and electric fields as

$$\boldsymbol{P} = \left.\frac{\partial\Phi(\boldsymbol{F}, \boldsymbol{E}_0)}{\partial\boldsymbol{F}}\right|_{\substack{\boldsymbol{F}=\boldsymbol{\nabla}_0\boldsymbol{x}\\ \boldsymbol{E}_0=-\boldsymbol{\nabla}_0\varphi}}; \qquad \boldsymbol{D}_0 = -\left.\frac{\partial\Phi(\boldsymbol{F}, \boldsymbol{E}_0)}{\partial\boldsymbol{E}_0}\right|_{\substack{\boldsymbol{F}=\boldsymbol{\nabla}_0\boldsymbol{x}\\ \boldsymbol{E}_0=-\boldsymbol{\nabla}_0\varphi}}. \tag{5.35}$$

Tangent operators for the Helmholtz's and extended Helmholtz's energy functionals

The tangent operator for the Helmholtz's energy density $\Phi = \Phi(\boldsymbol{\nabla}_0\boldsymbol{x}, -\boldsymbol{\nabla}_0\varphi)$ defined in (5.34) is computed as

$$D^2\Phi\left[\delta\boldsymbol{u}, \delta\varphi; \boldsymbol{u}, \Delta\varphi\right] = \left[\begin{array}{cc} \boldsymbol{\nabla}_0\delta\boldsymbol{u}: & -\boldsymbol{\nabla}_0\delta\varphi\cdot \end{array}\right]\left[\begin{array}{cc} \boldsymbol{\mathcal{C}}^* & -\boldsymbol{\mathcal{P}}^T \\ -\boldsymbol{\mathcal{P}} & -\boldsymbol{\varepsilon} \end{array}\right]\left[\begin{array}{c} :\boldsymbol{\nabla}_0\boldsymbol{u} \\ -\boldsymbol{\nabla}_0\Delta\varphi \end{array}\right], \tag{5.36}$$

with the fourth order elastic tensor $\boldsymbol{\mathcal{C}}^*$, the third order piezoelectric tensor $\boldsymbol{\mathcal{P}}$ and the second order dielectric tensor $\boldsymbol{\varepsilon}$ defined as

$$\boldsymbol{\mathcal{C}}^* = \left.\frac{\partial^2\Phi(\boldsymbol{F}, \boldsymbol{E}_0)}{\partial\boldsymbol{F}\partial\boldsymbol{F}}\right|_{\substack{\boldsymbol{F}=\boldsymbol{\nabla}_0\boldsymbol{x}\\ \boldsymbol{E}_0=-\boldsymbol{\nabla}_0\varphi}}; \ \boldsymbol{\mathcal{P}} = -\left.\frac{\partial^2\Phi(\boldsymbol{F}, \boldsymbol{E}_0)}{\partial\boldsymbol{F}\partial\boldsymbol{E}_0}\right|_{\substack{\boldsymbol{F}=\boldsymbol{\nabla}_0\boldsymbol{x}\\ \boldsymbol{E}_0=-\boldsymbol{\nabla}_0\varphi}}; \ \boldsymbol{\varepsilon} = -\left.\frac{\partial^2\Phi(\boldsymbol{F}, \boldsymbol{E}_0)}{\partial\boldsymbol{E}_0\partial\boldsymbol{E}_0}\right|_{\substack{\boldsymbol{F}=\boldsymbol{\nabla}_0\boldsymbol{x}\\ \boldsymbol{E}_0=-\boldsymbol{\nabla}_0\varphi}}. \tag{5.37}$$

As shown in Appendix C, it is possible to relate the constitutive tensors $\boldsymbol{\mathcal{C}}^\star$, $\boldsymbol{\mathcal{P}}$ and $\boldsymbol{\varepsilon}$ in (5.37) to those emerging from the tangent operator of the internal energy, namely $\boldsymbol{\mathcal{C}}$, $\boldsymbol{\mathcal{Q}}$ and $\boldsymbol{\theta}$ in (5.20).

Following a similar procedure to that of equation (5.38) and in preparation for a new mixed variational principle presented in the following Section 6.2.3, a possible tangent operator for the extended Helmholtz's energy functional $\Phi(\mathcal{V}^m, \Sigma^e_{\mathcal{V}})$ defined in equation (5.32c) is obtained as

$$D^2\Phi\left[\delta\boldsymbol{u}, \delta\boldsymbol{\Sigma}_{\boldsymbol{D}_0}, \delta\boldsymbol{\Sigma}_{\boldsymbol{d}}; \boldsymbol{u}, \Delta\boldsymbol{\Sigma}_{\boldsymbol{D}_0}, \Delta\boldsymbol{\Sigma}_{\boldsymbol{d}}\right] = \left[\mathbb{S}^\star_\delta\right]^T\left[\mathbb{H}_\Phi\right]\left[\mathbb{S}^\star_\Delta\right] + \left(\boldsymbol{\Sigma}_{\boldsymbol{H}} + \Sigma_J\boldsymbol{F}\right) : \left(\boldsymbol{\nabla}_0\delta\boldsymbol{u}\times\boldsymbol{\nabla}_0\boldsymbol{u}\right), \tag{5.38}$$

[6]Alternatively, an equivalent definition of the Legendre transform in equation (5.34) can be defined as $\Phi\left(\boldsymbol{\nabla}_0\boldsymbol{x}, -\boldsymbol{\nabla}_0\varphi\right) = \inf_{\boldsymbol{D}_0}\left\{\boldsymbol{\nabla}_0\varphi\cdot\boldsymbol{D}_0 + e\left(\boldsymbol{\nabla}_0\boldsymbol{x}, \boldsymbol{D}_0\right)\right\}$

where

$$\begin{aligned}\left[\mathbb{S}^{\star}_{\delta}\right]^{T} &= \left[(\boldsymbol{\nabla}_0\delta\boldsymbol{u}): \quad (\boldsymbol{\nabla}_0\delta\boldsymbol{u}\times\boldsymbol{F}): \quad (\boldsymbol{\nabla}_0\delta\boldsymbol{u}:\boldsymbol{H}) \quad \delta\boldsymbol{\Sigma}_{\boldsymbol{D}_0}\cdot \quad \delta\boldsymbol{\Sigma}_{\boldsymbol{d}}\cdot\right];\\ \left[\mathbb{S}^{\star}_{\Delta}\right] &= \begin{bmatrix} :(\boldsymbol{\nabla}_0\boldsymbol{u}) \\ :(\boldsymbol{F}\times\boldsymbol{\nabla}_0\boldsymbol{u}) \\ (\boldsymbol{H}:\boldsymbol{\nabla}_0\boldsymbol{u}) \\ \Delta\boldsymbol{\Sigma}_{\boldsymbol{D}_0} \\ \Delta\boldsymbol{\Sigma}_{\boldsymbol{d}} \end{bmatrix},\end{aligned} \tag{5.39}$$

and with the extended Hessian operator $[\mathbb{H}_{\Phi}]$ denoting the operator containing the second derivatives of $\Phi\left(\boldsymbol{F},\boldsymbol{H},J,\boldsymbol{\Sigma}_{\boldsymbol{D}_0},\boldsymbol{\Sigma}_{\boldsymbol{d}}\right)$ as

$$[\mathbb{H}_{\Phi}] = \begin{bmatrix} \Phi_{\boldsymbol{FF}} & \Phi_{\boldsymbol{FH}} & \Phi_{\boldsymbol{F}J} & \Phi_{\boldsymbol{F}\boldsymbol{\Sigma}_{\boldsymbol{D}_0}} & \Phi_{\boldsymbol{F}\boldsymbol{\Sigma}_{\boldsymbol{d}}} \\ \Phi_{\boldsymbol{HF}} & \Phi_{\boldsymbol{HH}} & \Phi_{\boldsymbol{H}J} & \Phi_{\boldsymbol{H}\boldsymbol{\Sigma}_{\boldsymbol{D}_0}} & \Phi_{\boldsymbol{H}\boldsymbol{\Sigma}_{\boldsymbol{d}}} \\ \Phi_{J\boldsymbol{F}} & \Phi_{J\boldsymbol{H}} & \Phi_{JJ} & \Phi_{J\boldsymbol{\Sigma}_{\boldsymbol{D}_0}} & \Phi_{J\boldsymbol{\Sigma}_{\boldsymbol{d}}} \\ \Phi_{\boldsymbol{\Sigma}_{\boldsymbol{D}_0}\boldsymbol{F}} & \Phi_{\boldsymbol{\Sigma}_{\boldsymbol{D}_0}\boldsymbol{F}} & \Phi_{\boldsymbol{\Sigma}_{\boldsymbol{D}_0}J} & \Phi_{\boldsymbol{\Sigma}_{\boldsymbol{D}_0}\boldsymbol{\Sigma}_{\boldsymbol{D}_0}} & \Phi_{\boldsymbol{\Sigma}_{\boldsymbol{D}_0}\boldsymbol{\Sigma}_{\boldsymbol{d}}} \\ \Phi_{\boldsymbol{\Sigma}_{\boldsymbol{d}}\boldsymbol{F}} & \Phi_{\boldsymbol{\Sigma}_{\boldsymbol{d}}\boldsymbol{F}} & \Phi_{\boldsymbol{\Sigma}_{\boldsymbol{d}}J} & \Phi_{\boldsymbol{\Sigma}_{\boldsymbol{d}}\boldsymbol{\Sigma}_{\boldsymbol{D}_0}} & \Phi_{\boldsymbol{\Sigma}_{\boldsymbol{d}}\boldsymbol{\Sigma}_{\boldsymbol{d}}} \end{bmatrix}. \tag{5.40}$$

Notice that the definition of multi-variable convexity in equation (5.12) enables to relate each of the components of the above Hessian operator $[\mathbb{H}_{\Phi}]$ (5.40) with the components of the Hessian operator $[\mathbb{H}_{W}]$ (5.23), as shown in Appendix C.

5.4 Variational formulations

This section presents several possible variational principles in nonlinear electro-elasticity. Initially, a revision of the standard displacement and electric potential based variational principle [63, 110] is presented for completeness. Exploiting the convex multi-variable properties of the internal energy $e(\boldsymbol{\nabla}_0\boldsymbol{x},\boldsymbol{D}_0)$, new interesting mixed variational principles in terms of the extended energy functionals $W(\mathcal{V})$ (5.12), $\Phi(\mathcal{V}^m,\Sigma^e_{\mathcal{V}})$ (5.32c), $\Psi(\Sigma^m_{\mathcal{V}},\mathcal{V}^e)$ (5.32b) and $\Upsilon(\Sigma_{\mathcal{V}})$ (5.32a) emerge. In particular, two new mixed variational principles based upon the extended energy functionals $W(\mathcal{V})$ (5.12) and $\Phi(\mathcal{V}^m,\Sigma^e_{\mathcal{V}})$ (5.32c) are presented in Sections 5.4.2 and 5.4.3 respectively, for the first time in the context of nonlinear electro-elasticity.

These new mixed variational principles belong to the general class of Fraeijs-de-Veubeke-Hu-Washizu (FdVHW) type variational principles, which were developed with the purpose of enhancing the numerical solution obtained though Finite Element based variational principles. Finite element implementation of the two mixed variational principles presented will be presented in Chapter 5 based on the work carried out in Reference [75].

5.4.1 Standard displacement and electric potential based variational principle

A first variational principle can be established by the total energy minimisation defined in terms of the internal energy of the system $e(\boldsymbol{\nabla}_0\boldsymbol{x}, \boldsymbol{D}_0)$. The principle applies to the space occupied by both the electro active polymer and the surrounding truncated domain, namely $V \cup V_\infty$, as [63]

$$\begin{aligned} \hat{\Pi}_e(\boldsymbol{x}^*, \boldsymbol{D}_0^*) = \inf_{\boldsymbol{x}, \boldsymbol{D}_0} \left\{ \int_{V \cup V_\infty} e(\boldsymbol{\nabla}_0\boldsymbol{x}, \boldsymbol{D}_0) dV - \Pi_{ext}^m(\boldsymbol{x}) \right\}; \\ \text{s.t.} \begin{cases} \mathbf{DIV}\boldsymbol{D}_0 = \rho_0^e & \text{in } V \cup V_\infty \\ [\![\boldsymbol{D}_0]\!] \cdot \boldsymbol{N} = \omega_0^e & \text{on } \partial_\omega V \end{cases}; \end{aligned} \tag{5.41}$$

where $\{\boldsymbol{x}^*, \boldsymbol{D}_0^*\}$ denotes the exact solution and

$$\Pi_{ext}^m(\boldsymbol{x}) = \int_V \boldsymbol{f}_0 \cdot \boldsymbol{x} dV + \int_{\partial_t V} \boldsymbol{t}_0 \cdot \boldsymbol{x} dA, \tag{5.42}$$

represents the total external work due to the action of external mechanical forces. Using a standard Lagrange multiplier approach to enforce the constraints defined by the Gauss' law, a new variational principle defined by a new energy potential $\Pi_e(\boldsymbol{x}^*, \varphi^*, \boldsymbol{D}_0^*)$ emerges as

$$\begin{aligned} \Pi_e(\boldsymbol{x}^*, \varphi^*, \boldsymbol{D}_0^*) = \inf_{\boldsymbol{x}, \boldsymbol{D}_0} \sup_{\varphi} \left\{ \int_{V \cup V_\infty} e(\boldsymbol{\nabla}_0\boldsymbol{x}, \boldsymbol{D}_0) dV - \Pi_{ext}^m(\boldsymbol{x}) \right. \\ \left. + \int_{V \cup V_\infty} \varphi \left(\rho_0^e - \mathbf{DIV}\boldsymbol{D}_0 \right) dV + \int_{\partial_\omega V} \varphi \left(\omega_0^e - [\![\boldsymbol{D}_0]\!] \cdot \boldsymbol{N} \right) dA \right\}, \end{aligned} \tag{5.43}$$

where the electric potential φ acts as the Lagrange multiplier needed to enforce the constraints. Application of the Gauss divergence theorem to above equation (5.43) yields an alternative representation of the variational principle as

$$\Pi_e(\boldsymbol{x}^*, \varphi^*, \boldsymbol{D}_0^*) = \inf_{\boldsymbol{x}, \boldsymbol{D}_0} \sup_{\varphi} \left\{ \int_{V \cup V_\infty} e(\boldsymbol{\nabla}_0\boldsymbol{x}, \boldsymbol{D}_0) dV + \int_{V \cup V_\infty} \boldsymbol{\nabla}_0\varphi \cdot \boldsymbol{D}_0 dV - \Pi_{ext}(\boldsymbol{x}, \varphi) \right\}, \tag{5.44}$$

with

$$\Pi_{ext}(\boldsymbol{x}, \varphi) = \Pi_{ext}^m(\boldsymbol{x}) + \Pi_{ext}^e(\varphi); \qquad \Pi_{ext}^e(\varphi) = -\int_V \rho_0^e \varphi dV - \int_{\partial_\omega V} \omega_0^e \varphi dA, \tag{5.45}$$

where a new external work contribution, that is $\Pi_{ext}^e(\varphi)$, appears due to electrical effects. Provided that a one to one relationship between $\boldsymbol{D}_0$ and $-\boldsymbol{\nabla}_0\varphi$ exists (refer

to Remark 5), application of the Legendre transform (5.34) enables above variational principle (5.44) to be reformulated as

$$\Pi_{\Phi}(\boldsymbol{x}^*, \varphi^*) = \inf_{\boldsymbol{x}} \sup_{\varphi} \left\{ \int_{V \cup V_\infty} \Phi(\boldsymbol{\nabla}_0 \boldsymbol{x}, -\boldsymbol{\nabla}_0 \varphi) dV - \Pi_{ext}(\boldsymbol{x}, \varphi) \right\}. \tag{5.46}$$

Traditional Finite Element based implementations resort to this variational principle, where the geometry and the electrical potential are the only unknowns of the problem [77,110]. The stationary condition of this functional with respect to changes in the geometry leads to the principle of virtual work (or power), written as

$$D\Pi_{\Phi}[\delta \boldsymbol{u}] = \int_{V \cup V_\infty} \boldsymbol{P}_{\boldsymbol{x}} : \boldsymbol{\nabla}_0 \delta \boldsymbol{u} dV - D\Pi_{ext}[\delta \boldsymbol{v}], \tag{5.47}$$

where the term $\boldsymbol{P}_{\boldsymbol{x}}$ represents the first Piola-Kirchhoff stress tensor evaluated in the standard fashion (2.53) in terms of the gradient of the geometry and the electric potential, namely, by using $\{\boldsymbol{F}_{\boldsymbol{x}}, \boldsymbol{H}_{\boldsymbol{x}}, J_{\boldsymbol{x}}, -\boldsymbol{\nabla}_0 \varphi\}$, where

$$\boldsymbol{F}_{\boldsymbol{x}} = \boldsymbol{\nabla}_0 \boldsymbol{x}; \qquad \boldsymbol{H}_{\boldsymbol{x}} = \frac{1}{2} \boldsymbol{\nabla}_0 \boldsymbol{x} \times \boldsymbol{\nabla}_0 \boldsymbol{x}; \qquad J_{\boldsymbol{x}} = \det \boldsymbol{\nabla}_0 \boldsymbol{x}. \tag{5.48}$$

Explicitly, the computation can be carried out from equation $(5.35)_a$. Analogously, the stationary point with respect to changes in the electric potential leads to the variational statement for the Gauss' law as

$$D\Pi_{\Phi}[\delta \varphi] = \int_{V \cup V_\infty} \boldsymbol{D}_{0,\varphi} \cdot \boldsymbol{\nabla}_0 \delta \varphi dV - D\Pi_{ext}[\delta \varphi], \tag{5.49}$$

where the term $\boldsymbol{D}_{0,\varphi}$ represents the electric displacement evaluated from $(5.35)_b$ by using $\{\boldsymbol{F}_{\boldsymbol{x}}, \boldsymbol{H}_{\boldsymbol{x}}, J_{\boldsymbol{x}}, -\boldsymbol{\nabla}_0 \varphi\}$.

5.4.2 A new mixed variational principle in terms of the extended internal energy functional W

In the case of an electromechanical convex multi-variable energy functional, an equivalent representation of the total variational principle Π_e in equation (5.44) is

$$\begin{aligned} \Pi_e(\boldsymbol{x}^*, \varphi^*, \boldsymbol{D}_0^*) = \inf_{\boldsymbol{x}, \boldsymbol{D}_0} \sup_{\varphi} \left\{ \int_{V \cup V_\infty} W(\mathcal{V})\, dV + \int_{V \cup V_\infty} \boldsymbol{D}_0 \cdot \boldsymbol{\nabla}_0 \varphi\, dV - \Pi_{ext}(\boldsymbol{x}, \varphi) \right\}; \\ \text{s.t. } \left\{ \boldsymbol{F} = \boldsymbol{F}_{\boldsymbol{x}}; \quad \boldsymbol{H} = \boldsymbol{H}_{\boldsymbol{x}}; \quad J = J_{\boldsymbol{x}}; \quad \boldsymbol{d} = \boldsymbol{F}_x \boldsymbol{D}_0 \quad \text{in } V \cup V_\infty \right. \end{aligned} \tag{5.50}$$

Using a standard Lagrange multiplier approach to enforce the compatibility constraints in (5.50) yields a new variational principle which can be represented as

$$\begin{aligned}
&\Pi_W(\boldsymbol{x}^*, \boldsymbol{F}^*, \boldsymbol{H}^*, J^*, \boldsymbol{\Sigma}_{\boldsymbol{F}}^*, \boldsymbol{\Sigma}_{\boldsymbol{H}}^*, \Sigma_J^*, \varphi^*, \boldsymbol{D}_0^*, \boldsymbol{d}^*, \boldsymbol{\Sigma}_{\boldsymbol{d}}^*) \\
&= \inf_{\boldsymbol{x},\boldsymbol{F},\boldsymbol{H},J,\boldsymbol{D}_0,\boldsymbol{d}} \sup_{\boldsymbol{\Sigma}_{\boldsymbol{F}},\boldsymbol{\Sigma}_{\boldsymbol{H}},\Sigma_J,\varphi,\boldsymbol{\Sigma}_{\boldsymbol{d}}} \left\{ \int_{V\cup V_\infty} W(\mathcal{V})\, dV + \int_{V\cup V_\infty} \boldsymbol{D}_0 \cdot \boldsymbol{\nabla}_0 \varphi \, dV \right. \\
&+ \int_{V\cup V_\infty} [\boldsymbol{\Sigma}_{\boldsymbol{F}} : (\boldsymbol{F}_{\boldsymbol{x}} - \boldsymbol{F}) + \boldsymbol{\Sigma}_{\boldsymbol{H}} : (\boldsymbol{H}_{\boldsymbol{x}} - \boldsymbol{H}) + \Sigma_J (J_{\boldsymbol{x}} - J) \\
&\left. + \boldsymbol{\Sigma}_{\boldsymbol{d}} \cdot (\boldsymbol{F}_{\boldsymbol{x}} \boldsymbol{D}_0 - \boldsymbol{d})]\, dV - \Pi_{ext}(\boldsymbol{x}, \varphi) \right\}.
\end{aligned} \tag{5.51}$$

For notational convenience, the following sets of variables are introduced

$$\mathcal{Y} = \{\boldsymbol{F}, \boldsymbol{H}, J, \boldsymbol{d}\}; \qquad \Sigma_{\mathcal{Y}} = \{\boldsymbol{\Sigma}_{\boldsymbol{F}}, \boldsymbol{\Sigma}_{\boldsymbol{H}}, \Sigma_J, \boldsymbol{\Sigma}_{\boldsymbol{d}}\}. \tag{5.52}$$

Virtual and incremental variations of the elements in the sets $\mathcal{Y}$ and $\Sigma_{\mathcal{Y}}$ in above equation (5.52) are denoted as

$$\begin{aligned}
\delta\mathcal{Y} &= \{\delta\boldsymbol{F}, \delta\boldsymbol{H}, \delta J, \delta\boldsymbol{\Sigma}_{\boldsymbol{D}_0}\}; & \delta\Sigma_{\mathcal{Y}} &= \{\delta\boldsymbol{\Sigma}_{\boldsymbol{F}}, \delta\boldsymbol{\Sigma}_{\boldsymbol{H}}, \delta\Sigma_J, \delta\boldsymbol{\Sigma}_{\boldsymbol{d}}\}; \\
\Delta\mathcal{Y} &= \{\Delta\boldsymbol{F}, \Delta\boldsymbol{H}, \Delta J, \Delta\boldsymbol{\Sigma}_{\boldsymbol{d}}\}; & \Delta\Sigma_{\mathcal{Y}} &= \{\Delta\boldsymbol{\Sigma}_{\boldsymbol{F}}, \Delta\boldsymbol{\Sigma}_{\boldsymbol{H}}, \Delta\Sigma_J, \Delta\boldsymbol{\Sigma}_{\boldsymbol{d}}\}.
\end{aligned} \tag{5.53}$$

The stationary point of the above variational principle (5.60) with respect to virtual changes of the geometry leads to the principle of virtual work as

$$D_1\Pi_W[\delta\boldsymbol{u}] = \int_{V\cup V_\infty} \boldsymbol{P}_W : \boldsymbol{\nabla}_0 \delta\boldsymbol{u}\, dV - D\Pi_{ext}[\delta\boldsymbol{v}], \tag{5.54}$$

where the first Piola-Kirchoff stress tensor is now evaluated as

$$\boldsymbol{P}_W = \boldsymbol{\Sigma}_{\boldsymbol{F}} + \boldsymbol{\Sigma}_{\boldsymbol{H}} \times \boldsymbol{F}_{\boldsymbol{x}} + \Sigma_J \boldsymbol{H}_{\boldsymbol{x}} + \boldsymbol{\Sigma}_{\boldsymbol{d}} \otimes \boldsymbol{D}_0. \tag{5.55}$$

Similarly, the stationary point of (5.60) with respect to the electric potential yields

$$D_8\Pi_W[\delta\varphi] = \int_{V\cup V_\infty} \boldsymbol{D}_0 \cdot \boldsymbol{\nabla}_0 \delta\varphi\, dV - D\Pi_{ext}[\delta\varphi]. \tag{5.56}$$

The directional derivative with respect to the elements in the set $\mathcal{Y}$ (5.52) and with respect to the electric displacement field results in the constitutive relationships formulated in a weak (variational) sense

$$\begin{aligned}
D_{2,3,4,9,10}\Pi_W[\delta\mathcal{Y}, \delta\boldsymbol{D}_0] &= \int_{V\cup V_\infty} \left(\frac{\partial W}{\partial \boldsymbol{F}} - \boldsymbol{\Sigma}_{\boldsymbol{F}} \right) : \delta\boldsymbol{F}\, dV + \int_{V\cup V_\infty} \left(\frac{\partial W}{\partial \boldsymbol{H}} - \boldsymbol{\Sigma}_{\boldsymbol{H}} \right) : \delta\boldsymbol{H}\, dV \\
&+ \int_{V\cup V_\infty} \left(\frac{\partial W}{\partial J} - \Sigma_J \right) \delta J\, dV + \int_{V\cup V_\infty} \left(\frac{\partial W}{\partial \boldsymbol{d}} - \boldsymbol{\Sigma}_{\boldsymbol{d}} \right) \cdot \delta\boldsymbol{d}\, dV \\
&+ \int_{V\cup V_\infty} \left(\frac{\partial W}{\partial \boldsymbol{D}_0} + \boldsymbol{\nabla}_0 \varphi + \boldsymbol{F}_{\boldsymbol{x}}{}^T \boldsymbol{\Sigma}_{\boldsymbol{d}} \right) \cdot \delta\boldsymbol{D}_0\, dV.
\end{aligned} \tag{5.57}$$

The directional derivative with respect to the elements of the set $\Sigma_{\mathcal{Y}}$ (5.52) results in the electro-kinematic constraints as follows

$$D_{5,6,7,11}\Pi_W[\delta\Sigma_{\mathcal{Y}}] = \int_{V\cup V_\infty} (\boldsymbol{F}_{\boldsymbol{x}} - \boldsymbol{F}) : \delta\boldsymbol{\Sigma}_{\boldsymbol{F}}\, dV + \int_{V\cup V_\infty} (\boldsymbol{H}_{\boldsymbol{x}} - \boldsymbol{H}) : \delta\boldsymbol{\Sigma}_{\boldsymbol{H}}\, dV + \int_{V\cup V_\infty} (J_{\boldsymbol{x}} - J)\, \delta\Sigma_J\, dV + \int_{V\cup V_\infty} (\boldsymbol{F}_{\boldsymbol{x}}\boldsymbol{D}_0 - \boldsymbol{d}) \cdot \delta\boldsymbol{\Sigma}_{\boldsymbol{d}}\, dV. \tag{5.58}$$

5.4.3 A new mixed variational principle in terms of the extended Helmholtz' energy functional Φ

In order to derive a variational principle in terms of the extended Helmholtz's energy (5.32c), recall first the mixed variational principle Π_W in (5.51) with a different ordering of terms and where addition of subtraction of the term $\boldsymbol{\Sigma}_{\boldsymbol{D}_0} \cdot \boldsymbol{D}_0$ has been carried out, namely

$$\begin{aligned}
&\Pi_W(\boldsymbol{x}^*, \boldsymbol{F}^*, \boldsymbol{H}^*, J^*, \boldsymbol{\Sigma}_{\boldsymbol{F}}^*, \boldsymbol{\Sigma}_{\boldsymbol{H}}^*, \Sigma_J^*, \varphi^*, \boldsymbol{D}_0^*, \boldsymbol{d}^*, \boldsymbol{\Sigma}_{\boldsymbol{d}}^*) \\
&= -\inf_{\boldsymbol{x},\boldsymbol{F},\boldsymbol{H},J,\boldsymbol{D}_0,\boldsymbol{d}} \sup_{\boldsymbol{\Sigma}_{\boldsymbol{F}},\boldsymbol{\Sigma}_{\boldsymbol{H}},\Sigma_J,\varphi,\boldsymbol{\Sigma}_{\boldsymbol{d}}} \left\{ \int_{V\cup V_\infty} [T^e - W(\mathcal{V})]\, dV + \int_{V\cup V_\infty} \boldsymbol{D}_0 \cdot \boldsymbol{\nabla}_0\varphi\, dV \right. \\
&+ \int_{V\cup V_\infty} [\boldsymbol{\Sigma}_{\boldsymbol{F}} : (\boldsymbol{F}_{\boldsymbol{x}} - \boldsymbol{F}) + \boldsymbol{\Sigma}_{\boldsymbol{H}} : (\boldsymbol{H}_{\boldsymbol{x}} - \boldsymbol{H}) + \Sigma_J(J_{\boldsymbol{x}} - J) \\
&\left. + \boldsymbol{\Sigma}_{\boldsymbol{d}} \cdot \boldsymbol{F}_{\boldsymbol{x}}\boldsymbol{D}_0 + \boldsymbol{\Sigma}_{\boldsymbol{D}_0} \cdot \boldsymbol{D}_0]\, dV - \Pi_{ext}(\boldsymbol{x}, \varphi) \right\}.
\end{aligned} \tag{5.59}$$

where T^e has been defined in equation (5.33). Comparing the term in brackets in the first integral in above equation with the definition of the extended Helmholtz's energy functional in (5.32c) enables to obtain an equivalent representation of the above variational principle as

$$\begin{aligned}
&\Pi_\Phi(\boldsymbol{x}^*, \boldsymbol{F}^*, \boldsymbol{H}^*, J^*, \boldsymbol{\Sigma}_{\boldsymbol{F}}^*, \boldsymbol{\Sigma}_{\boldsymbol{H}}^*, \Sigma_J^*, \varphi^*, \boldsymbol{D}_0^*, \boldsymbol{\Sigma}_{\boldsymbol{D}_0}^*, \boldsymbol{\Sigma}_{\boldsymbol{d}}{}^*) \\
&= \inf_{\boldsymbol{x},\boldsymbol{F},\boldsymbol{H},J,\boldsymbol{D}_0} \sup_{\boldsymbol{\Sigma}_{\boldsymbol{F}},\boldsymbol{\Sigma}_{\boldsymbol{H}},\Sigma_J,\varphi,\boldsymbol{\Sigma}_{\boldsymbol{D}_0},\boldsymbol{\Sigma}_{\boldsymbol{d}}} \left\{ \int_{V\cup V_\infty} \Phi(\mathcal{V}^m, \Sigma_{\mathcal{V}}^e) dV \right. \\
&+ \int_{V\cup V_\infty} [\boldsymbol{\Sigma}_{\boldsymbol{F}} : (\boldsymbol{F}_{\boldsymbol{x}} - \boldsymbol{F}) + \boldsymbol{\Sigma}_{\boldsymbol{H}} : (\boldsymbol{H}_{\boldsymbol{x}} - \boldsymbol{H}) + \Sigma_J(J_{\boldsymbol{x}} - J) \\
&\left. + \boldsymbol{D}_0 \cdot (\boldsymbol{\Sigma}_{\boldsymbol{D}_0} + \boldsymbol{\nabla}_0\varphi) + \boldsymbol{\Sigma}_{\boldsymbol{d}} \cdot \boldsymbol{F}_{\boldsymbol{x}}\boldsymbol{D}_0]\, dV - \Pi_{ext}(\boldsymbol{x}, \varphi) \right\}.
\end{aligned} \tag{5.60}$$

For notational convenience, the following sets are introduced,

$$\mathcal{D} = \{\boldsymbol{F}, \boldsymbol{H}, J, \boldsymbol{\Sigma}_{\boldsymbol{D}_0}\}; \qquad \Sigma_{\mathcal{D}} = \{\boldsymbol{\Sigma}_{\boldsymbol{F}}, \boldsymbol{\Sigma}_{\boldsymbol{H}}, \Sigma_J, \boldsymbol{D}_0\}. \tag{5.61}$$

Virtual and incremental variations of the elements in the sets $\mathcal{D}$ and $\Sigma_{\mathcal{D}}$ in above equation (5.61) are denoted as

$$\begin{aligned}
\delta\mathcal{D} &= \{\delta\boldsymbol{F}, \delta\boldsymbol{H}, \delta J, \delta\boldsymbol{\Sigma}_{\boldsymbol{D}_0}\}; & \delta\Sigma_{\mathcal{D}} &= \{\delta\boldsymbol{\Sigma}_{\boldsymbol{F}}, \delta\boldsymbol{\Sigma}_{\boldsymbol{H}}, \delta\Sigma_J, \delta\boldsymbol{D}_0\}; \\
\Delta\mathcal{D} &= \{\Delta\boldsymbol{F}, \Delta\boldsymbol{H}, \Delta J, \Delta\boldsymbol{\Sigma}_{\boldsymbol{D}_0}\}; & \Delta\Sigma_{\mathcal{D}} &= \{\Delta\boldsymbol{\Sigma}_{\boldsymbol{F}}, \Delta\boldsymbol{\Sigma}_{\boldsymbol{H}}, \Delta\Sigma_J, \Delta\boldsymbol{D}_0\}.
\end{aligned} \tag{5.62}$$

The directional derivative of above variational principle in (5.51) with respect to virtual changes of the geometry and electrical potential leads to identical expressions to those for Π_Φ in (5.54) and (5.56) as

$$D_1\Pi_\Phi[\delta\boldsymbol{u}] = D_1\Pi_W[\delta\boldsymbol{u}]; \qquad D_8\Pi_\Phi[\delta\varphi] = D_8\Pi_W[\delta\varphi]. \tag{5.63}$$

The stationary conditions with respect to the elements in the set $\mathcal{D}$ (5.61) and $\boldsymbol{\Sigma_d}$ results in the constitutive relationships formulated in a weak (variational) sense as

$$\begin{aligned} D_{2,3,4,10,11}\Pi_\Phi[\delta\mathcal{D}, \delta\boldsymbol{\Sigma_d}] = &\int_{V\cup V_\infty} \left(\frac{\partial\Phi}{\partial\boldsymbol{F}} - \boldsymbol{\Sigma_F}\right) : \delta\boldsymbol{F}\, dV + \int_{V\cup V_\infty} \left(\frac{\partial\Phi}{\partial\boldsymbol{H}} - \boldsymbol{\Sigma_H}\right) : \delta\boldsymbol{H}\, dV \\ &+ \int_{V\cup V_\infty} \left(\frac{\partial\Phi}{\partial J} - \Sigma_J\right) \delta J\, dV + \int_{V\cup V_\infty} \left(\frac{\partial\Phi}{\partial\boldsymbol{\Sigma}_{\boldsymbol{D}_0}} + \boldsymbol{D}_0\right) \cdot \delta\boldsymbol{\Sigma}_{\boldsymbol{D}_0}\, dV \\ &+ \int_{V\cup V_\infty} \left(\frac{\partial\Phi}{\partial\boldsymbol{\Sigma_d}} + \boldsymbol{F_x}\boldsymbol{D}_0\right) \cdot \delta\boldsymbol{\Sigma_d}\, dV. \end{aligned} \tag{5.64}$$

The stationary conditions with respect to the elements of the set $\Sigma_\mathcal{D}$ (5.61) results in the kinematic constraints and Faraday's law as follows

$$\begin{aligned} D_{5,6,7,9}\Pi_\Phi[\delta\Sigma_\mathcal{D}] = &\int_{V\cup V_\infty} (\boldsymbol{F_x} - \boldsymbol{F}) : \delta\boldsymbol{\Sigma_F}\, dV + \int_{V\cup V_\infty} (\boldsymbol{H_x} - \boldsymbol{H}) : \delta\boldsymbol{\Sigma_H}\, dV \\ &+ \int_{V\cup V_\infty} (J_{\boldsymbol{x}} - J)\, \delta\Sigma_J\, dV + \int_{V\cup V_\infty} \left(\boldsymbol{\Sigma}_{\boldsymbol{D}_0} + \boldsymbol{F_x}^T\boldsymbol{\Sigma_d} + \boldsymbol{\nabla}_0\varphi\right) \cdot \delta\boldsymbol{D}_0\, dV. \end{aligned} \tag{5.65}$$

5.5 Convexification (stabilisation) of materially unstable invariants

For isotropic materials, the internal energy e is typically represented [61, 62, 65] as

$$e(\boldsymbol{\nabla}_0\boldsymbol{x}, \boldsymbol{D}_0) = \hat{e}(II_{\boldsymbol{F}}, II_{\boldsymbol{H}}, J, II_{\boldsymbol{D}_0}, II_{\boldsymbol{d}}, II_{\boldsymbol{h}}), \tag{5.66}$$

where $\boldsymbol{h} = \boldsymbol{H}\boldsymbol{D}_0$. Unfortunately, since $\boldsymbol{h}$ is not included in the extended set $\mathcal{V}$, the invariant $II_{\boldsymbol{h}}$ is not convex multi-variable itself. Furthermore, not every possible combination of the remaining convex multi-variable invariants in (5.66), namely $II_{\boldsymbol{F}}$, $II_{\boldsymbol{H}}$, J, $II_{\boldsymbol{D}_0}$ and $II_{\boldsymbol{d}}$ will result in a convex multi-variable energy functional according to (5.12) [7].

Nevertheless, appropriate modifications of a non-convex multi-variable invariant can yield an invariant convex multi-variable according to (5.12). The obtention

[7] For instance, the purely mechanical invariant Ψ_m defined as $\Psi_m(\boldsymbol{F}, \boldsymbol{H}) = II_{\boldsymbol{F}} II_{\boldsymbol{H}}$ is not convex in its arguments, i.e, $\boldsymbol{F}$ and $\boldsymbol{H}$.

of convex multi-variable invariants through suitable modifications of non-convex multi-variable invariants is denoted in the present manuscript as convexification or stabilisation. In particular, two simple examples of stabilisation of a priori non-convex multi-variable invariants will be shown.

5.5.1 Stabilisation example 1

In this section, the following non-convex multi-variable invariants will be considered

$$W_1 = II_{\boldsymbol{F}} II_{\boldsymbol{D_0}}; \qquad W_2 = II_{\boldsymbol{H}} II_{\boldsymbol{D_0}}. \tag{5.67}$$

The one-dimensional representation of the invariant W_1 in above equation (5.67) is expressed in terms of the stretch λ and the sole component of the electric displacement D_0 as $W_1(\lambda, D_0) = \lambda^2 D_0^2$. The Hessian of $W_1(\lambda, D_0)$ is simply obtained as

$$[\mathbb{H}_{W_1}] = \begin{bmatrix} \frac{\partial^2 W}{\partial \lambda \partial \lambda} & \frac{\partial^2 W}{\partial \lambda \partial D_0} \\ \\ \frac{\partial^2 W}{\partial D_0 \partial \lambda} & \frac{\partial^2 W}{\partial D_0 \partial D_0} \end{bmatrix} = \begin{bmatrix} 2D_0^2 & 4\lambda D_0 \\ \\ 4\lambda D_0 & 2\lambda^2 \end{bmatrix}. \tag{5.68}$$

Clearly, the one dimensional representation of the invariant W_1 and hence, its three-dimensional counterpart, is not convex multi-variable as $\det[\mathbb{H}_{W_1}] \leq 0$. Alternatively, the invariant $W_1(\lambda, D_0)$ could be stabilised by adding two convex functions of λ and D_0 as

$$W_{1,mod}(\lambda, D_0) = (\lambda^2 + D_0^2)^2 = 2W_1(\lambda, D_0) + \lambda^4 + D_0^4. \tag{5.69}$$

The Hessian of the resulting invariant $W_{1,mod}(\lambda, D_0)$ in above equation (5.69) is obtained as

$$\left[\mathbb{H}_{W_{1,mod}}\right] = \begin{bmatrix} \frac{\partial^2 W_{1,mod}}{\partial \lambda \partial \lambda} & \frac{\partial^2 W_{1,mod}}{\partial \lambda \partial D_0} \\ \\ \frac{\partial^2 W_{1,mod}}{\partial D_0 \partial \lambda} & \frac{\partial^2 W_{1,mod}}{\partial D_0 \partial D_0} \end{bmatrix} = \begin{bmatrix} 12\lambda^2 + 4D_0^2 & 8\lambda D_0 \\ \\ 8\lambda D_0 & 12D_0^2 + 4\lambda^2 \end{bmatrix}. \tag{5.70}$$

Clearly, $W_{1,mod}(\lambda, D_0)$ is convex in its arguments $\{\lambda, D_0\}$ since $\det[\mathbb{H}_{W1,mod}] \geq 0$. Based on the stabilisation procedure in equation (5.69) for the one-dimensional representations of $W_1(\lambda, D_0)$, a convex multi-variable three-dimensional energy functional including the stabilised version of the non-convex multi-variable invariants $W_1(\boldsymbol{F}, \boldsymbol{D}_0)$ and $W_2(\boldsymbol{H}, \boldsymbol{D}_0)$ in (5.67) could be defined as

$$W(\boldsymbol{F}, \boldsymbol{H}, J, \boldsymbol{D}_0, \boldsymbol{d}) = \alpha \underbrace{\left(II_{\boldsymbol{F}} + \gamma^2 II_{\boldsymbol{D_0}}\right)^2}_{W_{\boldsymbol{F}\boldsymbol{D}_0}(\boldsymbol{F}, \boldsymbol{D}_0)} + \beta \underbrace{\left(II_{\boldsymbol{H}} + \gamma^2 II_{\boldsymbol{D_0}}\right)^2}_{W_{\boldsymbol{H}\boldsymbol{D}_0}(\boldsymbol{H}, \boldsymbol{D}_0)} + f(\boldsymbol{F}, \boldsymbol{H}, J, \boldsymbol{D}_0, \boldsymbol{d}), \tag{5.71}$$

with α, β and γ[8] positive material parameters and $f(\boldsymbol{F}, \boldsymbol{H}, J, \boldsymbol{D}_0, \boldsymbol{d})$, a convex function of the elements of the extended set $\mathcal{V}$. Appropriate values for α, β and γ

[8]The material parameter γ is employed for re-scaling purposes.

and suitable functions f must be such that, at the initial configuration, the stress vanishes, the Hessian operator (5.23) is positive definite and material characterisation can be carried out against available data. Since f is convex multi-variable and α and β are positive material parameters, sufficient conditions to ensure the multi-variable convexity of the functional (5.71) are the convexity of the energy contributions $W_{\boldsymbol{FD}_0}$ with respect to its arguments $\{\boldsymbol{F}, \boldsymbol{D}_0\}$ and $W_{\boldsymbol{HD}_0}$ with respect to its arguments $\{\boldsymbol{H}, \boldsymbol{D}_0\}$ (refer to equation (5.71)). Proof of convexity of $W_{\boldsymbol{FD}_0}$ with respect to $\{\boldsymbol{F}, \boldsymbol{D}_0\}$ can be found in Appendix A.1. Similar procedure can be applied to prove convexity of $W_{\boldsymbol{HD}_0}$ with respect to $\{\boldsymbol{H}, \boldsymbol{D}_0\}$.

5.5.2 Stabilisation example 2

Following a similar stabilisation procedure to that presented in Section 5.5.1 for invariants W_1 and W_2 (5.67), an energy functional including the stabilised version of the non-convex multi-variable invariant $II_{\boldsymbol{h}}$ could be defined as

$$W(\boldsymbol{F}, \boldsymbol{H}, J, \boldsymbol{D}_0, \boldsymbol{d}) = \alpha \underbrace{\left[II_{\boldsymbol{H}}^2 + \gamma^2 II_{\boldsymbol{h}} + \gamma^4 II_{\boldsymbol{D_0}}^2\right]}_{\hat{W}_{\boldsymbol{HD}_0}(\boldsymbol{H}, \boldsymbol{D}_0)}, + f(\boldsymbol{F}, \boldsymbol{H}, J, \boldsymbol{D}_0, \boldsymbol{d}), \tag{5.72}$$

with α, β and γ[9] positive material parameters and f a convex multi-variable function. Therefore, a sufficient condition to ensure the multi-variable convexity of the functional (5.72) is the convexity of the energy contribution $\hat{W}_{\boldsymbol{HD}_0}$ with respect to its arguments $\{\boldsymbol{H}, \boldsymbol{D}_0\}$ (refer to equation (5.72)). Proof of convexity of $\hat{W}_{\boldsymbol{HD}_0}$ with respect to $\{\boldsymbol{H}, \boldsymbol{D}_0\}$ can be found in Appendix A.2.

5.6 Numerical examples

The objective of this section is to present well posed constitutive models via definition of internal energy density functionals $e(\boldsymbol{\nabla}_0 \boldsymbol{x}, \boldsymbol{D}_0)$ complying with the multi-variable convexity condition in equation (5.12). Without loss of generality, multi-variable convexity internal energy functionals suitable for a reliable description of the constitutive behaviour of isotropic dielectric elastomers will be presented.

Two examples will be presented. The objective of the first example, in Section 5.6.1, is to present a convex multi-variable constitutive model which captures the electrostrictive behaviour of dielectric elastomers measured typically for a small value of the electric field, which can be considered in practice as zero. The objective of the second example, in Section 5.6.2, is to study the effect of two additional material parameters necessary for the stabilisation of the constitutive model. These material parameters do not intervene in the characterisation of electrostriction at low values of the electric field. However, modification of these parameters might alter significantly the response of the material, showing an additional nonlinearity

[9]The material parameter γ is employed for re-scaling purposes.

which manifests in dielectric elastomers, namely electric saturation, which manifests at high values of the electric field.

5.6.1 Incorporation of electrostriction in convex multi-variable constitutive models for dielectric elastomers

It is customary to define the internal energy for ideal dielectric elastomers (recall the definition of the internal energy $e_{\text{ideal}}(\boldsymbol{\nabla}_0\boldsymbol{x}, \boldsymbol{D}_0)$ in equation (5.9)) via an additive decomposition of a purely mechanical component and an additional contribution proportional to the internal energy of the vacuum, as

$$\begin{aligned} W_{\text{ideal}} &= W_m(\boldsymbol{F}, \boldsymbol{H}, J) + \frac{1}{\varepsilon_r} W_0(J, \boldsymbol{d}); \qquad W_0(J, \boldsymbol{d}) = \frac{1}{2\varepsilon_0 J} II_{\boldsymbol{d}}; \\ W_m(\boldsymbol{F}, \boldsymbol{H}, J) &= \mu_{1,0} II_{\boldsymbol{F}} + \mu_{2,0} II_{\boldsymbol{H}} + f(J), \end{aligned} \tag{5.73}$$

where $f(J)$ is defined as in equation (5.27) by replacing the constants μ_1, μ_2 and κ with $\mu_{1,0}$, $\mu_{2,0}$ and κ_0, respectively. In addition, the elastic parameters $\mu_{1,0}$, $\mu_{2,0}$ and κ_0 and the relative electric permittivity ε_r in (5.73) match the material properties of the dielectric elastomer in the reference configuration, namely the shear modulus μ, the first Lamé parameter $\hat{\lambda}$ and the electric permittivity ϵ if the following relationships are imposed

$$\mu = 2\mu_{1,0} + 2\mu_{2,0}; \qquad \hat{\lambda} = \kappa_0 + 4\mu_{2,0}; \qquad \varepsilon = \varepsilon_r \varepsilon_0. \tag{5.74}$$

A constitutive model defined as in equation (5.73) is termed ideal because it neglects physical nonlinearities which are inherent to dielectric elastomers. In particular, electrostriction [109] and saturation [111] are not captured in a model like that in (5.73). It has been reported in the experimental literature [5, 109] that the spatial electric permittivity of dielectric elastomers, namely ε, is a function of the deformation gradient tensor. This phenomenon is called electrostrictive effect [109]. Moreover, the spatial electric permittivity exhibits a nonlinear dependence with respect to the electric field. In general, as the electric field increases, the value of ε decreases until a stagnation scenario is reached. In this situation, the electric displacement field would not exhibit any further variation irrespectively of the increment in the applied electric field. This asymptotic behaviour is denoted as saturation [111].

For the particular constitutive model in equation (5.73), tensor $\boldsymbol{\theta}$ in equation (5.19) (inverse of the dielectric tensor) can be obtained by using equation (B.8), leading to the following expression

$$\boldsymbol{\theta} = \frac{1}{\varepsilon J} \boldsymbol{F}^T \boldsymbol{F}. \tag{5.75}$$

Equation (5.75) and the push forward relation $\boldsymbol{\varepsilon}^{-1} = J\boldsymbol{F}^{-T}\boldsymbol{\theta}\boldsymbol{F}^{-1}$ between the tensor $\boldsymbol{\theta}$ and its spatial counterpart $\boldsymbol{\varepsilon}^{-1}$ enables the following expression for the spatial dielectric tensor $\boldsymbol{\varepsilon}$ to be obtained as

$$\boldsymbol{\varepsilon} = \varepsilon \boldsymbol{I}. \tag{5.76}$$

Since the electric permittivity tensor $\boldsymbol{\varepsilon}$ in equation (5.76) is constant, electrostriction and saturation cannot be incorporated using a constitutive model defined as that defined in equation (5.73).

The authors in Reference [109] have proposed constitutive models for dielectric elastomers incorporating the electrostrictive behaviour based on experimental observations. These authors focused on the particular experimental set up depicted in Figure 5.5. In this set up, a thin film of an incompressible dielectric elastomer is subjected to an electric field applied across its thickness, namely, in direction OX_3. Consequently, a uniform deformation in the plane of the film (perpendicular to the axis OX_3) characterised by the stretch λ, is observed. Moreover, the incompressibility constraint enables the deformation gradient in the film to be expressed as

$$\boldsymbol{F} = \begin{bmatrix} \lambda & 0 & 0 \\ 0 & \lambda & 0 \\ 0 & 0 & 1/\lambda^2 \end{bmatrix}. \tag{5.77}$$

Under this particular experimental set up, the internal electromechanical energy of the vacuum, namely W_0 (5.73) can be expressed in terms of the stretch λ and the only component of the material electric displacement field D_0 as

$$W_0(\lambda, D_0) = \frac{D_0^2}{2\varepsilon_r \varepsilon_0 \lambda^4}. \tag{5.78}$$

The authors in Reference [109] incorporate the electrostrictive effect by modifying the internal energy in equation (5.73) as

$$W_{\text{Zhao}} = W_m(\lambda) + \frac{1}{\varepsilon_{r,\text{Zhao}}(\lambda)} W_0(\lambda, D_0), \tag{5.79}$$

with $W_0(\lambda, D_0)$ defined in (5.78). For different levels of pre-stretch λ, the spatial electric permittivity was measured as a function of the stretch (at a fixed value of the electric field). Then, Zhao et al. propose an expression for $\varepsilon_{r,\text{Zhao}}(\lambda)$ as

$$\varepsilon_{r,\text{Zhao}}(\lambda) = 4.68\left(1 - 0.106(\lambda - 1)\right). \tag{5.80}$$

The spatial electric permittivity in the reference configuration, namely ε, of the dielectric elastomer studied by Zhao et al is $\varepsilon = \varepsilon_{r,\text{Zhao}}|_{\lambda=1}\, \varepsilon_0 = 4.68\varepsilon_0$. Notice that the electric permittivity associated to the constitutive model proposed by Zhao et al. [109] in equations (5.79) and (5.80) does not depend on the electric displacement, and hence, on the electric field. Therefore, this model cannot capture the saturation effect. Alternatively, a generalised three-dimensional[10] convex multi-variable constitutive model incorporating electrostriction and, moreover, saturation, can be

[10]The proposed constitutive model can be applied to more general scenarios than that for the experimental set up depicted in Figure 7.6.

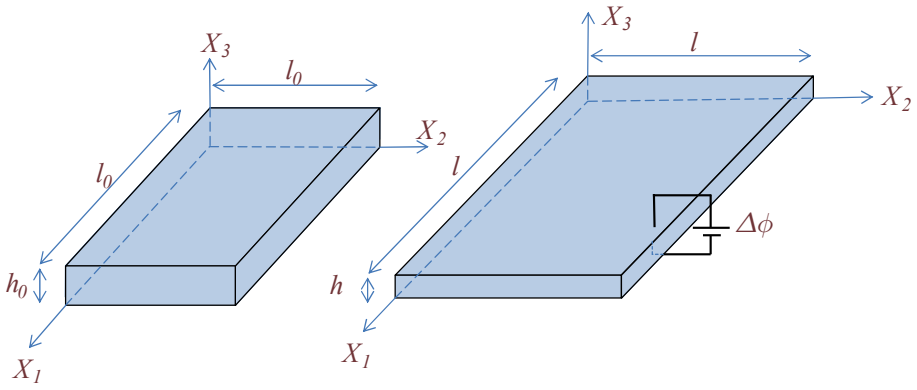

Figure 5.5: Experimental set up. The application of a uniform electric potential gradient across the thickness of the incompressible dielectric elastomer film (parallel to the axis OX_3) of initial length and thickness l_0 and h_0 respectively, leads to a uniform biaxial expansion of the film with final length $l = \lambda l_0$ and final thickness $h = 1/\lambda^2 h_0$, with λ the stretch in the dielectric elastomer.

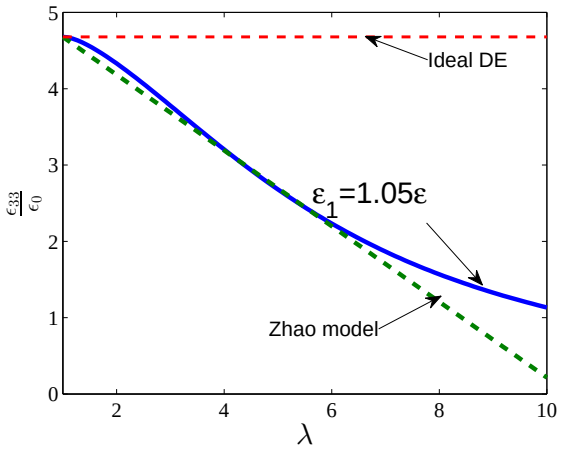

Figure 5.6: Prediction of electrostrictive effect in a dielectric elastomer film subjected to different levels of pre-stretch and at a fixed value of the electric field of $E = 0$. The green dashed line corresponds to the constitutive model proposed by Zhao et al. (5.80). The blue line corresponds to the convex multi-variable constitutive model in equation (5.81) with $\mu_1 = 0.45\mu$, $\mu_e = 0.1\mu$, $\varepsilon_2 = \infty$ and $\varepsilon_1 = 1.05\varepsilon$, consistent with $\varepsilon_r = 4.68$, $\mu = 1.55 \times 10^5\, N/m^2$ and $\lambda = 10^6\, N/m^2$ in the reference configuration.

defined through and extended convex multi-variable function as follows

$$W_{el,1} = \mu_1 II_{\boldsymbol{F}} + \mu_2 II_{\boldsymbol{H}} + \frac{1}{2J\varepsilon_1} II_{\boldsymbol{d}} + \mu_e \underbrace{\left(II_{\boldsymbol{F}}^2 + \frac{2}{\mu_e \varepsilon_e} II_{\boldsymbol{F}} II_{\boldsymbol{d}} + \frac{1}{\mu_e^2 \varepsilon_e^2} II_{\boldsymbol{d}}^2 \right)}_{\text{Stabilised electrostrictive invariant } W_{\boldsymbol{Fd}}(\boldsymbol{F},\boldsymbol{d})} + \frac{1}{2\varepsilon_2} II_{\boldsymbol{D}_0} - (2\mu_1 + 4\mu_2 + 12\mu_2) \ln J + \frac{\kappa}{2}(J-1)^2. \tag{5.81}$$

Material characterisation in the reference configuration enables the material parameters μ_1, μ_2, μ_e, ε_1, ε_2 and ε_e in above (5.81) to be expressed in terms of the material properties in the reference configuration, namely μ, $\hat{\lambda}$ and ε as

$$\mu = 2\mu_1 + 2\mu_2 + 12\mu_e; \qquad \hat{\lambda} = \kappa + 8\mu_e + 4\mu_2; \qquad \frac{1}{\varepsilon} = \frac{1}{\varepsilon_1} + \frac{1}{\varepsilon_2} + \frac{12}{\varepsilon_e}. \tag{5.82}$$

The amount of electrostriction in the constitutive model $W_{el,1}$ (5.81) is controlled by an additional electrostrictive parameter f_e, defined as

$$\varepsilon_1 = f_e \varepsilon, \tag{5.83}$$

where $f_e \geq 1$ in order to ensure positiveness of ε_2 and ε_e. High values of the parameter f_e are associated to highly electrostrictive materials (for a constant value of ε_2) leading to a high value of $\frac{12}{\varepsilon_e}$ in detriment of $\frac{1}{\varepsilon_1}$ (5.82). An additional stiffening parameter can be introduced for the convex multi-variable constitutive model $W_{el,1}$ (5.81), defined as

$$12\mu_e = f_s \mu. \tag{5.84}$$

High values of the stiffening parameter f_s lead to mechanically stiffer constitutive models. Notice that the energy functional $W_{el,1}$ in above equation (5.81) contains the invariant $W_{\boldsymbol{Fd}}$. This invariant results after stabilising the non-convex multi-variable invariant $II_{\boldsymbol{F}} II_{\boldsymbol{d}}$, where the same stabilisation procedure as that for $W_{\boldsymbol{FD}_0}$ and $W_{\boldsymbol{HD}_0}$ in equation (5.71) has been utilised (refer to Section 5.5). Following the same procedure as that for the constitutive model in (5.73), the spatial dielectric tensor is obtained as

$$\begin{aligned} \boldsymbol{\varepsilon}(\boldsymbol{F},\boldsymbol{d}) &= \left(\frac{1}{\varepsilon_1}\boldsymbol{I} + \frac{4J}{\varepsilon_e} II_{\boldsymbol{F}} \boldsymbol{I} + \hat{\boldsymbol{\varepsilon}}^{-1}(J,\boldsymbol{F},\boldsymbol{d}) \right)^{-1}; \\ \hat{\boldsymbol{\varepsilon}}^{-1}(\boldsymbol{F},\boldsymbol{d}) &= \frac{4J}{\varepsilon_e^2 \mu_e} II_{\boldsymbol{d}} \boldsymbol{b}^{-1} + \frac{8J}{\varepsilon_e^2 \mu_e} \boldsymbol{d} \otimes \boldsymbol{d} + \frac{J\boldsymbol{b}^{-1}}{\varepsilon_2}, \end{aligned} \tag{5.85}$$

where $\boldsymbol{b}$ is the left Cauchy-Green deformation tensor, defined as $\boldsymbol{b} = \boldsymbol{F}\boldsymbol{F}^T$. Evaluation of the expression for $\boldsymbol{\varepsilon}$ in above (5.85) for a vanishing electric displacement field, namely $\boldsymbol{D}_0 = \boldsymbol{0}$ leads to the following expression for $\boldsymbol{\varepsilon}(\boldsymbol{F},\boldsymbol{0})$

$$\boldsymbol{\varepsilon}(\boldsymbol{F},\boldsymbol{0}) = \left(\frac{1}{\varepsilon_1}\boldsymbol{I} + \frac{4J}{\varepsilon_e} II_{\boldsymbol{F}} \boldsymbol{I} + \frac{J}{\varepsilon_2}\boldsymbol{b}^{-1} \right)^{-1}. \tag{5.86}$$

Particularisation of the kinematical restrictions of the experimental set up described in equation (5.77) enables a diagonal representation of the above electric permittivity tensor as

$$\boldsymbol{\varepsilon} = \begin{bmatrix} \varepsilon_{11} & 0 & 0 \\ 0 & \varepsilon_{11} & 0 \\ 0 & 0 & \varepsilon_{33} \end{bmatrix}, \tag{5.87}$$

where an expression for the component ε_{33} can be obtained in terms of the stretch λ as

$$\varepsilon_{33}(\lambda, 0) = \left(\frac{1}{\varepsilon_1} + \frac{4}{\varepsilon_e} f(\lambda) + \frac{1}{\varepsilon_2} \lambda^4 \right)^{-1}; \qquad f(\lambda) = 2\lambda^2 + \frac{1}{\lambda^4}. \tag{5.88}$$

For the shake of simplicity, the material parameter ε_2 is prescribed as $\varepsilon_2 = \infty$. Notice that the resulting energy functional would be convex in a reduced set $\{\boldsymbol{F}, \boldsymbol{H}, J, \boldsymbol{d}\} \subset \mathcal{V}$. Choosing the extreme values of the deformation in the experiment considered in reference [109], namely $\lambda_1 = 1$ and $\lambda_2 = 6$, the following system of equations is obtained

$$\left(\frac{1}{\varepsilon_1} + \frac{1}{\varepsilon_e} f(\lambda_1) \right)^{-1} = \varepsilon_{r,\text{Zhao}}(\lambda_1)\varepsilon_0; \qquad \left(\frac{1}{\varepsilon_1} + \frac{1}{\varepsilon_e} f(\lambda_2) \right)^{-1} = \varepsilon_{r,\text{Zhao}}(\lambda_2)\varepsilon_0 \tag{5.89}$$

The above system of equations in (5.89) enables ε_1 and ε_e to be determined as

$$\varepsilon_1 = 1.05\varepsilon \Rightarrow f_e = 1.05; \qquad \varepsilon_e = 252\varepsilon. \tag{5.90}$$

Figure 5.6 shows the good agreement between the predicted spatial permittivity for the constitutive model proposed by Zhao et al. [109] and for the convex multi-variable (with electric material parameters chosen as in (5.90)) constitutive models in equations (5.81), for the range of deformations considered in the experiment, i.e $1 \leq \lambda \leq 6$ and for the particular scenario for which $\boldsymbol{D}_0 = \boldsymbol{0}$. Notice that in the material characterisation carried out to predict the electrostrictive behaviour of the constitutive model in equation (5.81), the elastic parameter μ_e did not have any influence. This characterisation was performed at the specific scenario for which $\boldsymbol{D}_0 = \boldsymbol{0}$. In the more general case, i.e. $\boldsymbol{D}_0 \neq \boldsymbol{0}$, the parameter μ_e introduces a further nonlinear dependence of the spatial electric permittivity upon the material electric displacement field which, for extreme values of the electric field, resembles the physical behaviour known as electric saturation. This nonlinear effect will be appreciated in the following section.

5.6.2 Numerical experiment

In this section, in addition to the constitutive models W_{ideal} and $W_{el,1}$ in equations (5.73) and (5.81), respectively, a non-convex multi-variable internal energy functional very similar to the convex multi-variable model in (5.81) containing the

invariant $II_{\boldsymbol{F}}II_{\boldsymbol{d}}$ without the additional stabilising invariants will be defined as

$$\begin{aligned} W_{el,2} =& \hat{\mu}_1 II_{\boldsymbol{F}} + \hat{\mu}_2 II_{\boldsymbol{H}} + \frac{1}{2J\hat{\varepsilon}_1} II_{\boldsymbol{d}} + \underbrace{\frac{2}{\hat{\varepsilon}_e} II_{\boldsymbol{F}} II_{\boldsymbol{d}}}_{\text{Non-convex multi-variable invariant}} \\ &+ \frac{1}{2\hat{\varepsilon}_2} II_{\boldsymbol{D}_0} - (2\hat{\mu}_1 + 4\hat{\mu}_2)\ln J + \frac{\hat{\kappa}}{2}(J-1)^2. \end{aligned} \tag{5.91}$$

Equivalence in the reference configuration between the convex multi-variable constitutive model in equation (5.81)-(5.82) and the non-convex multi-variable model in above (5.91) is guaranteed if the parameters $\hat{\mu_1}$, $\hat{\mu_2}$, $\hat{\varepsilon}_e$, $\hat{\varepsilon}_2$ and $\hat{\kappa}$ are related to the material properties of the material in the reference configuration, namely μ, κ and ε as

$$\mu = 2\hat{\mu}_1 + 2\hat{\mu}_2; \qquad \hat{\lambda} = \hat{\kappa} + 4\hat{\mu}_2; \qquad \frac{1}{\varepsilon} = \frac{1}{\hat{\varepsilon}_1} + \frac{1}{\hat{\varepsilon}_2} + \frac{12}{\hat{\varepsilon}_e} \tag{5.92}$$

An electrostrictive parameter similar to that in equation (5.83) can be defined for the constitutive model in above equation (5.91) as

$$\hat{\varepsilon}_1 = \hat{f}_e \varepsilon. \tag{5.93}$$

Notice that the following choice of material parameters, i.e,

$$\hat{\varepsilon}_1 = 1.05\varepsilon \Rightarrow \hat{f}_e = 1.05; \qquad \hat{\varepsilon}_e = 252\varepsilon, \tag{5.94}$$

would replicate the electrostrictive behaviour (variation of the spatial electric permittivity with the deformation for $\boldsymbol{D}_0 = \boldsymbol{0}$) of the model in (5.81) with the particular choice of electric material parameters ε_1, c_1 and c_2 in equation (5.94).

The objective of this section is to study the behaviour of the convex multi-variable and non-convex multi-variable constitutive models in equations (5.81) and (5.91) respectively, for the experimental set up depicted in Figure 5.5 under a more general scenario where $\boldsymbol{D}_0 \neq \boldsymbol{0}$. For a given value of the only component of the material electric field, i.e, E_0, the stretch λ and the only component of the material electric displacement field, namely D_0 are obtained via minimisation of an energy functional per unit undeformed volume $\pi(\lambda, D_0)$ defined as

$$\pi(\lambda, D_0) = \min_{\lambda, D_0} \left\{ W(\boldsymbol{F}(\lambda), \boldsymbol{D}_0(D_0)) - E_0 D_0 \right\}. \tag{5.95}$$

The stationary conditions of the energy functional $\pi(\lambda, D_0)$ in above (5.95) are obtained as

$$\begin{aligned} D\pi(\lambda, D_0)[\delta\lambda] &= \frac{\partial W}{\partial \boldsymbol{F}} : \frac{\partial \boldsymbol{F}}{\partial \lambda}\delta\lambda = 0; \\ D\pi(\lambda, D_0)[\delta D_0] &= \left(\frac{\partial W}{\partial \boldsymbol{D}_0} \cdot \frac{\partial \boldsymbol{D}_0}{\partial D_0} - E_0 \right) \delta D_0 = 0. \end{aligned} \tag{5.96}$$

Since equation (5.96) must hold for any arbitrary virtual variations $\{\delta\lambda, \delta D_0\}$, the final system of nonlinear equations is obtained

$$\boldsymbol{\mathcal{R}}(\lambda, D_0) = \boldsymbol{0}; \qquad \boldsymbol{\mathcal{R}}(\lambda, D_0) = \begin{bmatrix} \mathcal{R}_\lambda(\lambda, D_0) \\ \mathcal{R}_{D_0}(\lambda, D_0) \end{bmatrix}, \tag{5.97}$$

with

$$\mathcal{R}_\lambda(\lambda, D_0) = \frac{\partial W}{\partial \boldsymbol{F}} : \frac{\partial \boldsymbol{F}}{\partial \lambda}; \qquad \mathcal{R}_{D_0}(\lambda, D_0) = \frac{\partial W}{\partial \boldsymbol{D}_0} \cdot \frac{\partial \boldsymbol{D}_0}{\partial D_0} - E_0. \tag{5.98}$$

For the particular experimental set up described in Section 5.6.1, where the deformation gradient tensor $\boldsymbol{F}$ is defined as in equation (5.77) and where the material electric displacement field is defined as $\boldsymbol{D}_0 = \begin{bmatrix} 0 & 0 & D_0 \end{bmatrix}^T$, the derivatives $\frac{\partial \boldsymbol{F}}{\partial \lambda}$ and $\frac{\partial \boldsymbol{D}_0}{\partial D_0}$ featuring in equations (5.96) and (5.98) are obtained as

$$\frac{\partial \boldsymbol{F}}{\partial \lambda} = \begin{bmatrix} 1 & 0 & 0 \\ 0 & 1 & 0 \\ 0 & 0 & -2\lambda^{-3} \end{bmatrix}; \qquad \frac{\partial \boldsymbol{D}_0}{\partial D_0} = \begin{bmatrix} 0 & 0 & 1 \end{bmatrix}^T. \tag{5.99}$$

A combined Newton-Raphson/arc length algorithm has been applied to solve the above system of nonlinear equations in (5.97)-(5.98). Figure 5.7 shows the result of the nonlinear equations (5.97) replicating the experimental set up in Figure 5.5. The predicted behaviour of the dielectric elastomer film considering the convex multi-variable constitutive model in equation (5.81) (where different values of the material parameter μ_e have been considered), the non-convex multi-variable constitutive model in (5.91) and the ideal dielectric elastomer model in (5.73) has been studied. The three models considered have identical material properties in the reference configuration, namely μ, $\hat{\lambda}$ and ε. As it can observed from Figure 5.7(b), a constitutive model with a low value of the material parameter μ_e is more prone to develop electric saturation. In other words, a highly nonlinear behaviour of the curve relating $\boldsymbol{E}$ and $\boldsymbol{D}$ occurs, which in the ideal case, would tend to a stagnation scenario.

Additionally, Figure 5.8 studies the influence of the electrostrictive electric parameter f_e on the convex multi-variable constitutive model in equation (5.81). Notice that in this case, unlike that one depicted in Figure 5.7 (for which the stiffening parameter f_s is changed), the electrostrictive behaviour of the convex multi-variable constitutive model for $\boldsymbol{D}_0 = \boldsymbol{0}$ is not the same for different values of f_e, since f_e (refer to equation (5.90)) takes place in the definition of electrostriction for $\boldsymbol{D}_0 = \boldsymbol{0}$, as shown in equation (5.88). A comparison of the response of the convex multi-variable constitutive model in equation (5.81) for different values of the electrostrictive parameter f_e for a fixed value of f_s is carried out against that of the non-convex multi-variable constitutive model in equation (5.91) (with $\hat{f}_e$ chosen according to equation (5.94)) and the ideal dielectric elastomer model in equation (5.73). As it can be observed from Figure 5.8(b), a constitutive model with a high value of the electrostrictive parameter f_e is also more prone to develop electric saturation.

Finally, Figure 5.9 shows the graphical visualisation of the inverse of the Lagrangian dielectric tensor $\boldsymbol{\theta}$, the piezoelectric tensor $\boldsymbol{\mathcal{Q}}^T$, and the Lagrangian electrostrictive tensor $\boldsymbol{\mathcal{B}}$ computed according to equations (B.8), (B.5) and (B.10), respectively, for the convex multi-variable constitutive model in equation (5.81), the

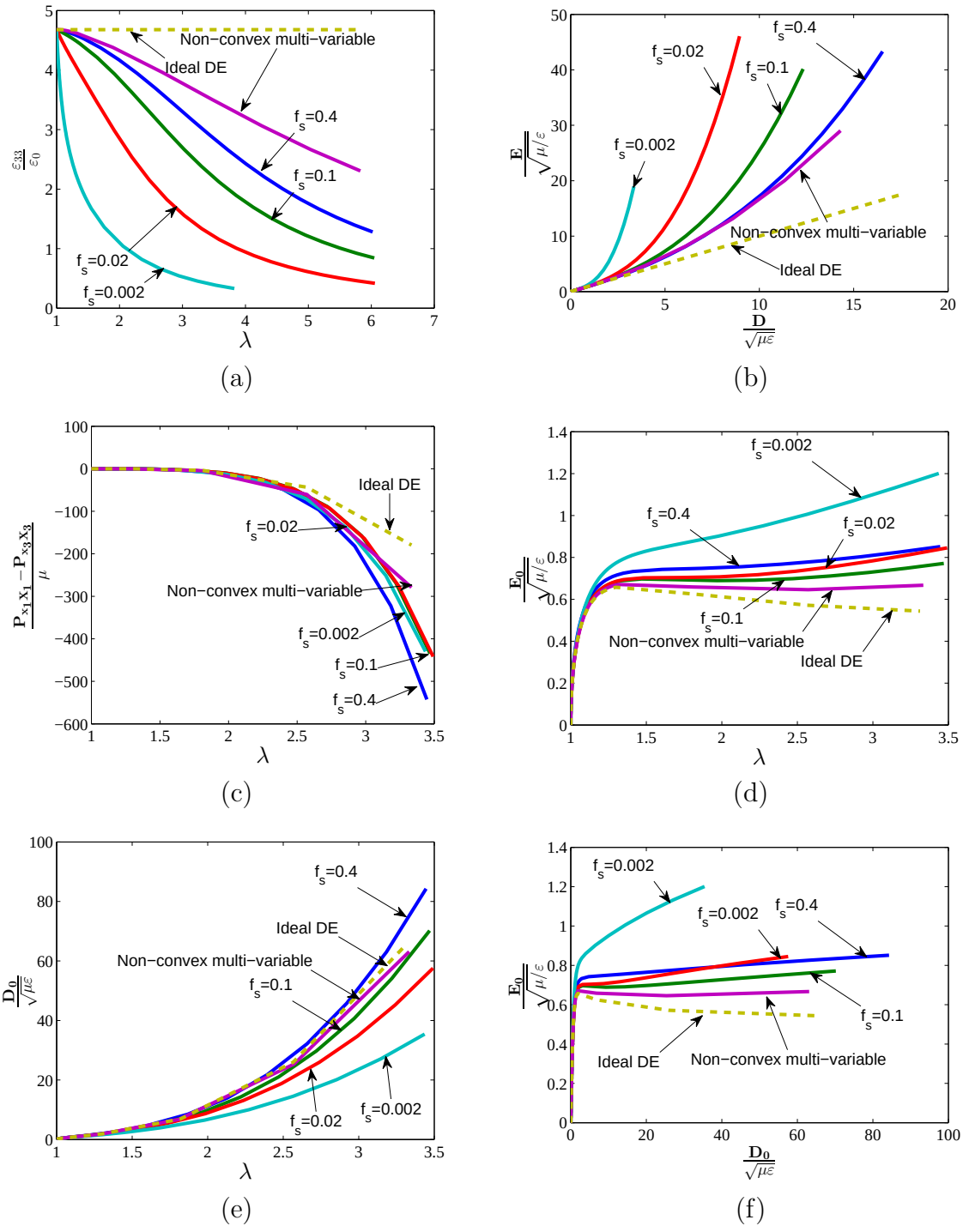

Figure 5.7: Relation between (a) ε_3 and λ, (b) E and D, (c) $\boldsymbol{P}_{x_1X_1} - \boldsymbol{P}_{x_3X_3}$ and λ, (d) E_0 and λ, (e) D_0 and λ and (f) E_0 and D_0 for the convex multi-variable model in equation (5.91) (for different values of the elastic constant μ_e), the non-convex multi-variable model in (5.91) and an ideal dielectric elastomer (5.73). Material parameters: $\varepsilon_1 = 1.05\varepsilon$, $\varepsilon_2 = \infty$ and $\mu_1 = 2\mu_2$ for the convex multi-variable model and with $\hat{\varepsilon}_1 = 1.05\varepsilon$, $\hat{\varepsilon}_2 = \infty$ and $\hat{\mu}_1 = 2\hat{\mu}_2$ for the non-convex multi-variable model. $\varepsilon_r = 4.68$, $\mu = 10^5\ N/m^2$ and $\lambda = 10^6\ N/m^2$.

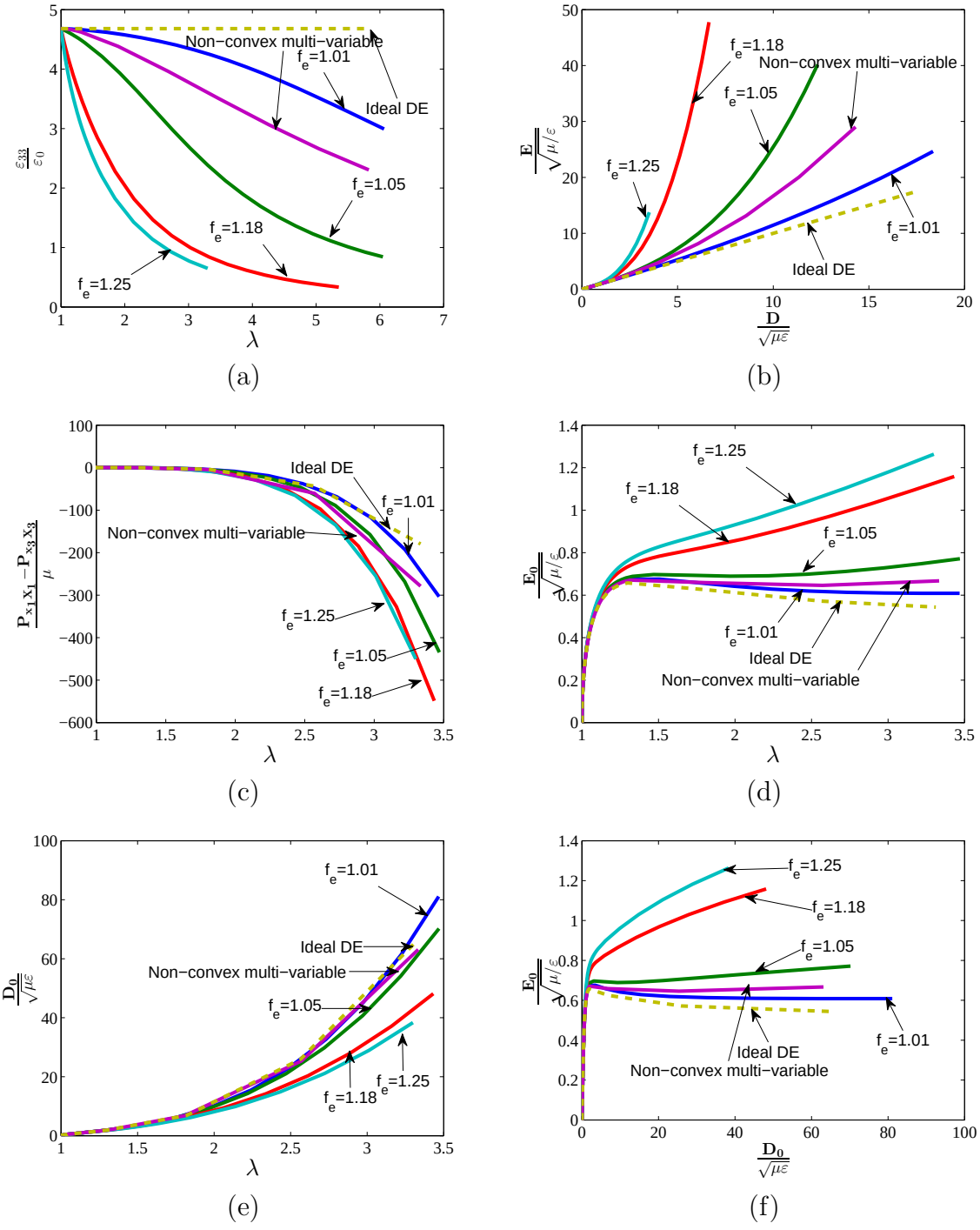

Figure 5.8: Relations between (a) ε_3 and λ, (b) E and D, (c) $\boldsymbol{P}_{x_1X_1} - \boldsymbol{P}_{x_3X_3}$ and λ, (d) E_0 and λ, (e) D_0 and λ and (f) E_0 and D_0 for the convex multi-variable model in equation (5.81) (for different values of ε_e), the non-convex multi-variable model in (5.91) and an ideal dielectric elastomer (5.73). Material parameters: $\varepsilon_2 = \infty$, $\mu_e = 0.1\mu$ and $\mu_1 = 2\mu_2$ for the convex multi-variable model and with $\hat{\varepsilon}_2 = \infty$ and $\hat{\mu}_1 = 2\hat{\mu}_2$ for the non-convex multi-variable mode. $\varepsilon_r = 4.68$, $\mu = 10^5\, N/m^2$ and $\lambda = 10^6\, N/m^2$.

non-convex multi-variable constitutive model in (5.91) and the ideal dielectric elastomer model (5.73), having the three models the same material properties in the reference configuration, namely, μ, $\hat{\lambda}$ and ε. For the visualisation of these tensors, their associated moduli $\frac{1}{\widetilde{\varepsilon}}$, $\widetilde{\mathcal{Q}}$, and $\widetilde{\mathcal{B}}_\mu$ are defined via a spherical parametrisation of the arbitrary direction $\boldsymbol{n}$ as in [112][11]:

$$\frac{1}{\widetilde{\varepsilon}} = \boldsymbol{n}\cdot\boldsymbol{\theta}\boldsymbol{n}; \qquad \widetilde{\mathcal{Q}} = \boldsymbol{\mathcal{Q}} : (\boldsymbol{n}\otimes\boldsymbol{n}\otimes\boldsymbol{n}) ; \qquad \widetilde{\mathcal{B}}_\mu = (\boldsymbol{n}\otimes\boldsymbol{n}) : \boldsymbol{\mathcal{B}} : (\boldsymbol{n}\otimes\boldsymbol{n}) . \quad (5.100)$$

As predicted from Figures 5.7 and 5.8, for increasing values of the dimensionless electric field $\boldsymbol{E}/\sqrt{\mu/\varepsilon}$, the differences in the three constitutive tensors between the three constitutive models involved increase.

5.7 Concluding remarks

This Chapter has proposed a new variational framework to formulate large strain/large electric field electro-elasticity. This work extends for the first time the ideas presented by Bonet et al. [44] in the field of polyconvex elasticity to nonlinear electro-elasticity [76]. With that in mind, a new internal energy density functional has been introduced in the form of a convex multi-variable function with respect to an extended set of electromechanical variables $\mathcal{V} = \{\boldsymbol{F}, \boldsymbol{H}, J, \boldsymbol{D}_0, \boldsymbol{d}\}$, which enables the ellipticity condition and hence, material stability to be satisfied for the entire range of deformations and electric fields. Notice that the focus of this work is on material stability and not on the existence minimisers. The latter would also require the study of the sequentially weak lower semicontinuity and the coercivity of the energy functional.

The introduction of the spatial vector $\boldsymbol{d}$ as an element of the set $\mathcal{V}$ proves to be extremely relevant since it permits the electromechanical energy of the vacuum and hence, that of ideal dielectric elastomers, to be considered as a degenerate case of a convex multi-variable functional. Furthermore, the authors show simple techniques, denoted as stabilisation, which enable to create convex multi-variable electromechanical invariants by modifying a priori non-convex multi-variable invariants.

An additional set of variables $\Sigma_{\mathcal{V}} = \{\boldsymbol{\Sigma}_{\boldsymbol{F}}, \boldsymbol{\Sigma}_{\boldsymbol{H}}, \Sigma_J, \boldsymbol{\Sigma}_{\boldsymbol{D}_0}, \boldsymbol{\Sigma}_{\boldsymbol{d}}\}$, dual (work conjugate) to those in $\mathcal{V}$ is presented for the first time in the context of nonlinear electro-elasticity. Very remarkably, the one to one relationship between both sets $\mathcal{V}$ and $\Sigma_{\mathcal{V}}$, enable the definition of new interesting extended Hu-Washizu type of mixed variational principles which are presented. The use of a tensor cross product [1, 44, 82] operation and its associated algebra, greatly facilitates the algebraic manipulations of expressions involving the adjoint of the deformation gradient and its derivatives.

[11] An additional modulus can be associated to the forth order tensor $\boldsymbol{\mathcal{B}}$, namely $\widetilde{\mathcal{B}}_\kappa = \frac{1}{3}\boldsymbol{I} : \boldsymbol{\mathcal{B}} : \boldsymbol{n}\otimes\boldsymbol{n}.$, resembling both $\widetilde{\mathcal{B}}_\mu$ and $\widetilde{\mathcal{B}}_\kappa$ the shear $\widetilde{\mathcal{C}}_\mu$ an volumetric $\widetilde{\mathcal{C}}_\kappa$ counterparts of the elasticity tensor $\boldsymbol{\mathcal{C}}$ (B.2).

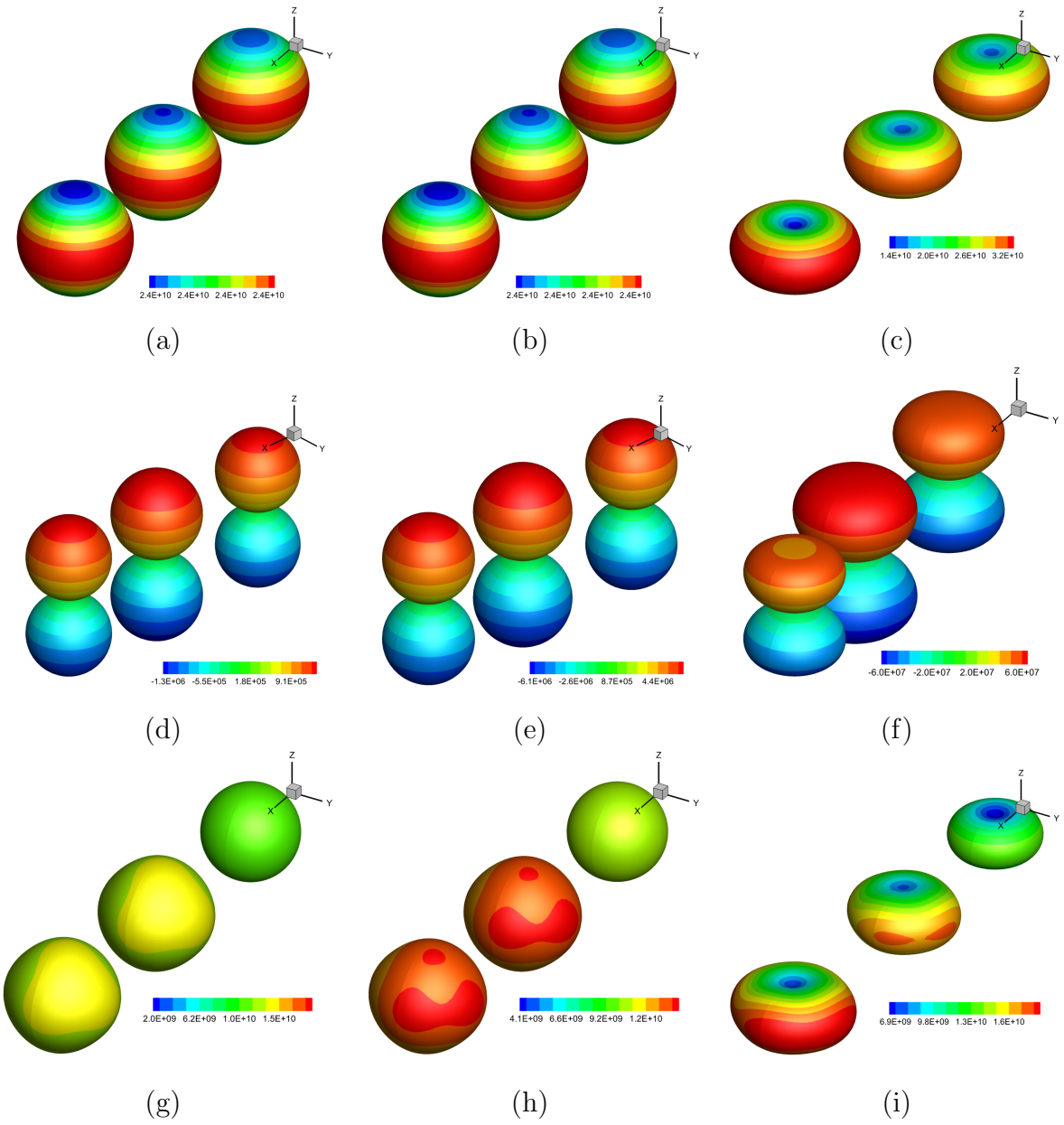

Figure 5.9: Numerical experiment for the experimental set up in Figure 7.6. From left to right: convex multi-variable constitutive model in equation (5.81); non-convex multi-variable constitutive model in (5.91); ideal dielectric elastomer (5.73). Graphical representation of $1/\widetilde{\varepsilon}$ $(5.100)_a$ for (a) $E/\sqrt{\mu/\varepsilon} = 0.028$, (b) $E/\sqrt{\mu/\varepsilon} = 0.14$ and (c) $E/\sqrt{\mu/\varepsilon} = 2.35$. Graphical representation of $\widetilde{\mathcal{Q}}$ $(5.100)_b$ for (d) $E/\sqrt{\mu/\varepsilon} = 0.028$, (e) $E/\sqrt{\mu/\varepsilon} = 0.14$ and (f) $E/\sqrt{\mu/\varepsilon} = 2.35$. Graphical representation of $\widetilde{\mathcal{B}}_\mu$ $(5.100)_c$ for (g) $E/\sqrt{\mu/\varepsilon} = 0.028$, (h) $E/\sqrt{\mu/\varepsilon} = 0.14$ and (i) $E/\sqrt{\mu/\varepsilon} = 2.35$. Material parameters: $\varepsilon_1 = 1.05\varepsilon$, $\varepsilon_2 = \infty$ and $\mu_1 = 2\mu_2$ for the convex multi-variable model in (6.47) and $\hat{\varepsilon}_1 = 1.05\varepsilon$, $\hat{\varepsilon}_2 = \infty$ and $\hat{\mu}_1 = 2\hat{\mu}_2$ for the non-convex multi-variable model in (5.91). $\varepsilon_r = 4.68$, $\mu = 10^5\, N/m^2$ and $\lambda = 10^6\, N/m^2$.

Chapter 6

Computational framework in convex multi-variable electromechanics

6.1 Introduction

This Chapter presents the Finite Element computational framework tailor–made for the simulation of Electro Active Polymers (EAPs) [4–8, 109] in applications where very large deformations and electric fields are involved, developed by Gil and Ortigosa [76].

Chapter 5, based on the work published in Reference [76], has presented the concept of multi-variable convexity in the context of electromechanics. This mathematical condition enables the most accepted constitutive inequality, namely ellipticity (rank-one convexity) [11], to be fulfilled for the entire range of deformations and electric fields. Moreover, taking advantage of a new tensor cross product operation [44, 82], tedious algebra is remarkably simplified yielding insightful representations of otherwise complex expressions (i.e. electro-mechanical tangent operators).

The consideration of convex multi-variable energy functionals brings additional benefits, including the solution to the well known shortcomings of classical displacement-potential based formulations [60, 77–79, 110]. More specifically, a new family of extended Hu-Washizu type of variational principles [40, 47, 51, 53–55, 80] has been presented in Chapter 5. The development of these new mixed variational principles [76] is a robust alternative to resolve the spurious (non-physical) mechanisms associated to the more classical displacement-potential approach. This Chapter presents the Finite Element implementation of these new mixed variational principles.

This Chapter is organised as follows. Section 6.2 is focussed on the Finite Element discretisation and implementation of the variational principles presented in Section 5.4. Section 6.3 includes a wide spectrum of challenging numerical examples in order to demonstrate the robustness and applicability of the proposed enhanced mixed formulations, ranging from simpler isotropic to more complex anisotropic polyconvex models. Finally, Section 6.4 provides some concluding remarks and a summary of the key contributions of this Chapter.

6.2 Finite Element discretisation

In this Section, the Finite Element implementation of the variational principles presented in Section 5.4, suitable for large strain and large electric field scenarios, where electro active materials can be typically encountered, is carried out.

6.2.1 General remarks

The implementation of the variational principles in Section 5.4 is based on a finite element partition (tesselation) of the domain V (representing an electro active polymer in its initial configuration) into a set of elements. Inside each element the

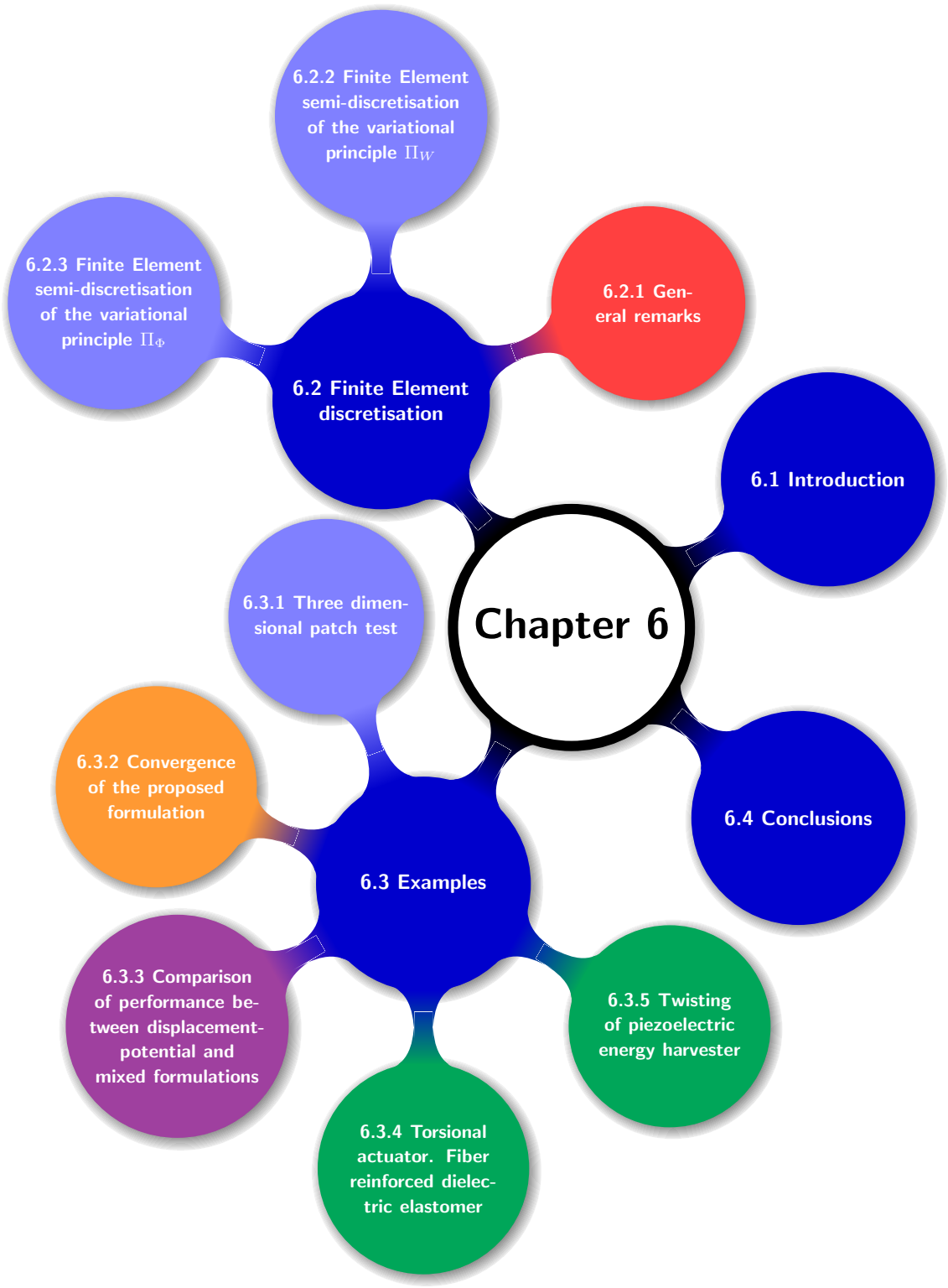

Figure 6.1: Chapter layout.

problem variables can be interpolated in terms of a set of nodal shape functions as,

$$\boldsymbol{x} = \sum_{a=1}^{n_{\boldsymbol{x}}} \boldsymbol{x}_a N_a^{\boldsymbol{x}}; \quad \boldsymbol{F} = \sum_{a=1}^{n_{\boldsymbol{F}}} \boldsymbol{F}_a N_a^{\boldsymbol{F}}; \quad ...; \quad \boldsymbol{D}_0 = \sum_{a=1}^{n_{\boldsymbol{D}_0}} \boldsymbol{D}_{0a} N_a^{\boldsymbol{D}_0}; \quad ... \tag{6.1}$$

where a denotes the nodes used in the interpolation of the above variables and $n_{(\bullet)}$ denotes the number of nodes associated to the variable $(\bullet)$. In general, different interpolations are used to describe different variables. The same interpolation space is used for work conjugate pairs; that is, $N_a^{\boldsymbol{F}} = N_a^{\boldsymbol{\Sigma}_{\boldsymbol{F}}}$, $N_a^{\boldsymbol{D}_0} = N_a^{\boldsymbol{\Sigma}_{\boldsymbol{D}0}}$ etc. All the variables and their virtual and incremental variations $\{\boldsymbol{x}, \delta\boldsymbol{u}, \boldsymbol{u}\}$, $\{\boldsymbol{F}, \delta\boldsymbol{F}, \Delta\boldsymbol{F}\}$, $\{\boldsymbol{D}_0, \delta\boldsymbol{D}_0, \Delta\boldsymbol{D}_0\}$ etc. are interpolated using the same interpolation spaces (Galerkin-type discretisation).

The variational framework associated to the variational principles Π_W and Π_Φ in (5.51) and (5.60), respectively, can be implemented using a variety of finite element spaces. Of course, not all choices will lead to effective or valid finite element formulations. In particular, the LBB [94, 95] condition must be satisfied. Alternatively, the LBB condition can be circumvented via stabilised formulations [43, 84, 96, 97].

Mixed formulations might result in expensive computations due to the large number of additional variables involved. However, careful analysis of the continuity required for each of the variables, shows that only displacements and electric potential need to be continuous across elements. Stress, strain and electric variables can actually be discretised independently on each element of the mesh. Crucially, a static condensation procedure (as that carried out for the Hu-Washizu and Hellinger-Reissner mixed variational principles in Sections 2.6.2 and 2.6.3 in the context of nonlinear elasticity) of the residuals and stiffness matrices associated to those variables for which continuity across elements is not required leads to a computationally comparable cost with respect to displacement potential formulations [44].

A plausible choice [40, 44] for the interpolation functions of the different variables involved in the variational principle Π_W (5.51) considers a quadratic tetrahedron element for the geometry and electric potential discretisation, piecewise linear element by element interpolations for $\{\boldsymbol{F}, \boldsymbol{\Sigma}_{\boldsymbol{F}}\}$, $\{\boldsymbol{H}, \boldsymbol{\Sigma}_{\boldsymbol{H}}\}$, $\{\boldsymbol{d}, \boldsymbol{\Sigma}_{\boldsymbol{d}}\}$ and $\boldsymbol{D}_0$ and piecewise constant interpolation for $\{J, \Sigma_J\}$.

Similarly, a quadratic tetrahedron element for the geometry and electric potential discretisation, piecewise linear interpolations for $\boldsymbol{\{F, \Sigma_F\}}$, $\{\boldsymbol{H}, \boldsymbol{\Sigma}_{\boldsymbol{H}}\}$, $\{\boldsymbol{D}_0, \boldsymbol{\Sigma}_{\boldsymbol{D}_0}\}$ and $\boldsymbol{d}$ and a piecewise constant interpolation for $\{J, \Sigma_J\}$ is used for the formulation associated to the variational principle Π_Φ (5.60).

In what follows, for a variational principle $\Pi_{\boldsymbol{\mathcal{U}}}$ formulated in terms of the variables $\boldsymbol{\mathcal{U}}$, for which virtual and incremental variations are denoted as $\delta\boldsymbol{\mathcal{U}}$ and $\Delta\boldsymbol{\mathcal{U}}$, respectively, a $k-$iterative Newton-Raphson process is usually established by solving a linearised system of equations for the increment $\Delta\boldsymbol{\mathcal{U}}$ as

$$D^2\Pi_{\boldsymbol{\mathcal{U}}}(\boldsymbol{\mathcal{U}}_k)[\delta\boldsymbol{\mathcal{U}}; \Delta\boldsymbol{\mathcal{U}}] = -D\Pi_{\boldsymbol{\mathcal{U}}}(\boldsymbol{\mathcal{U}}_k)[\delta\boldsymbol{\mathcal{U}}]; \qquad \boldsymbol{\mathcal{U}}_{k+1} = \boldsymbol{\mathcal{U}}_k + \Delta\boldsymbol{\mathcal{U}}. \tag{6.2}$$

Finite element discretisation of above system (6.2) results in the well known residual vector $\boldsymbol{R}_{\boldsymbol{\mathcal{U}}}$ and tangent stiffness matrix $\boldsymbol{K}_{\boldsymbol{\mathcal{U}}\boldsymbol{\mathcal{U}}}$.

6.2.2 Finite Element semi-discretisation of the variational principle Π_W

Let us consider the mixed variational principle Π_W in equation (5.51). For notational convenience, the following set q of variables is introduced

$$q = \{\boldsymbol{x}, \varphi, \mathcal{Y}, \Sigma_{\mathcal{Y}}, \boldsymbol{D}_0\}, \tag{6.3}$$

where the sets $\mathcal{Y}$ and $\Sigma_{\mathcal{Y}}$ defined in equation (5.52). The discrete stationary conditions of the variational principle Π_W (5.51) with respect to virtual changes in the geometry and in the electric potential (i.e. equilibrium and Gauss law) are

$$\begin{aligned} D\Pi_W[\delta\boldsymbol{u}] &= \sum_{a=1}^{n_{\boldsymbol{x}}} \boldsymbol{R}^a_{\boldsymbol{x}} \cdot \delta\boldsymbol{u}^a; \quad \boldsymbol{R}^a_{\boldsymbol{x}} = \int_V \boldsymbol{P}_W \boldsymbol{\nabla}_0 N^{\boldsymbol{x}}_a \, dV - \int_V \boldsymbol{f}_0 N^{\boldsymbol{x}}_a \, dV - \int_{\partial_t V} \boldsymbol{t}_0 N^{\boldsymbol{x}}_a \, dA; \\ D\Pi_W[\delta\varphi] &= \sum_{a=1}^{n_\varphi} R^a_\varphi \cdot \delta\varphi^a; \quad R^a_\varphi = \int_V \boldsymbol{D}_0 \cdot \boldsymbol{\nabla}_0 N^\varphi_a \, dV - \int_V \rho_0 N^\varphi_a \, dV - \int_{\partial_\omega V} \omega_0 N^\varphi_a \, dA, \end{aligned} \tag{6.4}$$

where the first Piola-Kirchhoff stress tensor $\boldsymbol{P}_W$ is evaluated as

$$\boldsymbol{P}_W = \boldsymbol{\Sigma}_{\boldsymbol{F}} + \boldsymbol{\Sigma}_{\boldsymbol{H}} \times \boldsymbol{F}_{\boldsymbol{x}} + \Sigma_J \boldsymbol{H}_{\boldsymbol{x}} + \boldsymbol{\Sigma}_{\boldsymbol{d}} \otimes \boldsymbol{D}_0. \tag{6.5}$$

The discrete stationary conditions of the variational principle Π_W (5.51) with respect to virtual changes of the elements of the set $\mathcal{Y}$ (5.52) and $\boldsymbol{D}_0$ (i.e. constitutive and Faraday laws) is

$$\begin{aligned} D\Pi_W[\delta\mathcal{Y}, \delta\boldsymbol{D}_0] = &\sum_{a=1}^{n_{\boldsymbol{F}}} \boldsymbol{R}^a_{\boldsymbol{F}} : \delta\boldsymbol{F}^a + \sum_{a=1}^{n_{\boldsymbol{H}}} \boldsymbol{R}^a_{\boldsymbol{H}} : \delta\boldsymbol{H}^a + \sum_{a=1}^{n_J} R^a_J \delta J^a \\ &+ \sum_{a=1}^{n_{\boldsymbol{d}}} \boldsymbol{R}^a_{\boldsymbol{d}} \cdot \delta\boldsymbol{d}^a + \sum_{a=1}^{n_{\boldsymbol{D}_0}} \boldsymbol{R}^a_{\boldsymbol{D}_0} \cdot \delta\boldsymbol{D}^a_0, \end{aligned} \tag{6.6}$$

where the different residuals emerging in above equation (6.6) are

$$\begin{aligned} \boldsymbol{R}^a_{\boldsymbol{F}} &= \int_V \left(\frac{\partial W}{\partial \boldsymbol{F}} - \boldsymbol{\Sigma}_{\boldsymbol{F}} \right) N^{\boldsymbol{F}}_a \, dV; & \boldsymbol{R}^a_{\boldsymbol{H}} &= \int_V \left(\frac{\partial W}{\partial \boldsymbol{H}} - \boldsymbol{\Sigma}_{\boldsymbol{H}} \right) N^{\boldsymbol{H}}_a \, dV; \\ R^a_J &= \int_V \left(\frac{\partial W}{\partial J} - \Sigma_J \right) N^J_a \, dV; & \boldsymbol{R}^a_{\boldsymbol{d}} &= \int_V \left(\frac{\partial W}{\partial \boldsymbol{d}} - \boldsymbol{\Sigma}_{\boldsymbol{d}} \right) N^{\boldsymbol{d}}_a \, dV; \\ \boldsymbol{R}^a_{\boldsymbol{D}_0} &= \int_V \left(\frac{\partial W}{\partial \boldsymbol{D}_0} + \boldsymbol{\nabla}_0 \varphi + \boldsymbol{F}_{\boldsymbol{x}}{}^T \boldsymbol{\Sigma}_{\boldsymbol{d}} \right) N^{\boldsymbol{d}}_a \, dV. \end{aligned} \tag{6.7}$$

The discrete stationary conditions with respect to the elements of the set $\Sigma_{\mathcal{Y}}$

(5.52) (i.e. compatibility) yields

$$D\Pi_W[\delta\Sigma_{\mathcal{Y}}] = \sum_{a=1}^{n_{\boldsymbol{\Sigma_F}}} \boldsymbol{R}^a_{\boldsymbol{\Sigma_F}} : \delta\boldsymbol{\Sigma_F}^a + \sum_{a=1}^{n_{\boldsymbol{\Sigma_H}}} \boldsymbol{R}^a_{\boldsymbol{\Sigma_H}} : \delta\boldsymbol{\Sigma_H}^a + \sum_{a=1}^{n_{\Sigma_J}} R^a_{\Sigma_J}\delta\Sigma^a_J + \sum_{a=1}^{n_{\boldsymbol{\Sigma_d}}} \boldsymbol{R}^a_{\boldsymbol{\Sigma_d}} \cdot \delta\boldsymbol{\Sigma_d}^a, \tag{6.8}$$

where the residuals in above equation (6.8) are

$$\begin{aligned} \boldsymbol{R}^a_{\boldsymbol{\Sigma_F}} &= \int_V (\boldsymbol{F_x} - \boldsymbol{F})\, N^{\boldsymbol{F}}_a\, dV; & \boldsymbol{R}^a_{\boldsymbol{\Sigma_H}} &= \int_V (\boldsymbol{H_x} - \boldsymbol{H})\, N^{\boldsymbol{H}}_a\, dV; \\ R^a_{\Sigma_J} &= \int_V (J_{\boldsymbol{x}} - J)\, N^J_a\, dV; & \boldsymbol{R}^a_{\boldsymbol{\Sigma_d}} &= \int_V (\boldsymbol{F_x D}_0 - \boldsymbol{d})\, N^{\boldsymbol{d}}_a\, dV. \end{aligned} \tag{6.9}$$

The stiffness matrices arising from the variational principle Π_W (5.51) (before static condensation is carried out) emerge as

$$D^2\Pi_W\left[\delta q; \Delta q\right] = \begin{bmatrix} \delta\mathbf{u} \\ \delta\boldsymbol{\phi} \\ \delta\boldsymbol{\mathcal{Y}} \\ \delta\boldsymbol{\Sigma}_{\mathcal{Y}} \\ \delta\mathbf{D}_0 \end{bmatrix}^T \begin{bmatrix} \boldsymbol{K}_{\boldsymbol{xx}} & \mathbf{0} & \mathbf{0} & \boldsymbol{K}_{\boldsymbol{x}\Sigma_{\mathcal{Y}}} & \boldsymbol{K}_{\boldsymbol{x}\boldsymbol{D}_0} \\ \mathbf{0} & \mathbf{0} & \mathbf{0} & \mathbf{0} & \boldsymbol{K}_{\varphi\boldsymbol{D}_0} \\ \mathbf{0} & \mathbf{0} & \boldsymbol{K}_{\mathcal{Y}\mathcal{Y}} & \boldsymbol{K}_{\mathcal{Y}\Sigma_{\mathcal{Y}}} & \boldsymbol{K}_{\mathcal{Y}\boldsymbol{D}_0} \\ \boldsymbol{K}_{\Sigma_{\mathcal{Y}}\boldsymbol{x}} & \mathbf{0} & \boldsymbol{K}_{\Sigma_{\mathcal{Y}}\mathcal{Y}} & \mathbf{0} & \boldsymbol{K}_{\Sigma_{\mathcal{Y}}\boldsymbol{D}_0} \\ \boldsymbol{K}_{\boldsymbol{D}_0\boldsymbol{x}} & \boldsymbol{K}_{\boldsymbol{D}_0\varphi} & \boldsymbol{K}_{\boldsymbol{D}_0\mathcal{Y}} & \boldsymbol{K}_{\boldsymbol{D}_0\Sigma_{\mathcal{Y}}} & \boldsymbol{K}_{\boldsymbol{D}_0\boldsymbol{D}_0} \end{bmatrix} \begin{bmatrix} \mathbf{u} \\ \Delta\boldsymbol{\phi} \\ \Delta\boldsymbol{\mathcal{Y}} \\ \Delta\boldsymbol{\Sigma}_{\mathcal{Y}} \\ \Delta\mathbf{D}_0 \end{bmatrix}. \tag{6.10}$$

Notice that since the above formulation emerges from a variational principle, namely Π_W in (5.51), the resulting global stiffness matrix is symmetric. Hence, the following relations will be satisfied: $\boldsymbol{K}_{\Sigma_{\mathcal{Y}}\boldsymbol{x}} = \boldsymbol{K}^T_{\boldsymbol{x}\Sigma_{\mathcal{Y}}}$, $\boldsymbol{K}_{\boldsymbol{\Sigma}_{\boldsymbol{D}_0}\boldsymbol{x}} = \boldsymbol{K}^T_{\boldsymbol{x}\boldsymbol{\Sigma}_{\boldsymbol{D}_0}}$, etc. The expressions for the non-zero blocks in the stiffness matrix defined in equation (6.10) are presented below.

The procedure to obtain the stiffness matrix contribution $\boldsymbol{K}^{ab}_{\boldsymbol{xx}}$ has been already presented in Reference [44] and in Section 4.2.2 in the context of nonlinear elasticity, yielding

$$\left[\boldsymbol{K}^{ab}_{\boldsymbol{xx}}\right]_{ij} = \mathcal{E}_{ijk}\left[\boldsymbol{k}^{ab}_{\boldsymbol{xx}}\right]_k; \qquad \boldsymbol{k}^{ab}_{\boldsymbol{xx}} = \int_V (\boldsymbol{\Sigma_H} + \Sigma_J \boldsymbol{F_x})\,(\boldsymbol{\nabla}_0 N^{\boldsymbol{x}}_a \times \boldsymbol{\nabla}_0 N^{\boldsymbol{x}}_b)\, dV. \tag{6.11}$$

The stiffness matrix contribution $\boldsymbol{K}^{ab}_{\boldsymbol{x}\Sigma_{\mathcal{Y}}}$ arising from the linearisation of $\boldsymbol{R}^a_{\boldsymbol{x}}$ with respect to incremental changes of the elements in the set $\Sigma^{ab}_{\mathcal{Y}}$ is defined as

$$\boldsymbol{K}^{ab}_{\boldsymbol{x}\Sigma_{\mathcal{Y}}} = \begin{bmatrix} \boldsymbol{K}^{ab}_{\boldsymbol{x}\boldsymbol{\Sigma_F}} & \boldsymbol{K}^{ab}_{\boldsymbol{x}\boldsymbol{\Sigma_H}} & \boldsymbol{K}^{ab}_{\boldsymbol{x}\Sigma_J} & \boldsymbol{K}^{ab}_{\boldsymbol{x}\boldsymbol{\Sigma_d}} \end{bmatrix}, \tag{6.12}$$

where the individual stiffness matrices in (6.12) are defined as

$$\begin{aligned} \boldsymbol{K}^{ab}_{\boldsymbol{x}\boldsymbol{\Sigma_F}} &= \int_V (\boldsymbol{I} \otimes \boldsymbol{\nabla}_0 N^{\boldsymbol{x}}_a)\, N^{\boldsymbol{F}}_b\, dV; & \left[\boldsymbol{K}^{ab}_{\boldsymbol{x}\boldsymbol{\Sigma_H}}\right]_{ijI} &= \mathcal{E}_{ijk}\left[\int_V (\boldsymbol{F_x} \boldsymbol{\times} \boldsymbol{\nabla}_0 N^{\boldsymbol{x}}_a)\, N^{\boldsymbol{H}}_b\, dV\right]_{kI}; \\ \boldsymbol{K}^{ab}_{\boldsymbol{x}\Sigma_J} &= \int_V N^J_b \boldsymbol{H_x} \boldsymbol{\nabla}_0 N^{\boldsymbol{x}}_a\, dV; & \boldsymbol{K}^{ab}_{\boldsymbol{x}\boldsymbol{\Sigma_d}} &= \int_V (\boldsymbol{D}_0 \cdot \boldsymbol{\nabla}_0 N^{\boldsymbol{x}}_a)\, N^{\boldsymbol{d}}_b \boldsymbol{I}\, dV. \end{aligned} \tag{6.13}$$

The stiffness matrix contribution $\boldsymbol{K}^{ab}_{\boldsymbol{x}\boldsymbol{D}_0}$ is obtained as

$$\boldsymbol{K}^{ab}_{\boldsymbol{x}\boldsymbol{D}_0} = \int_V (\boldsymbol{\Sigma}_{\boldsymbol{d}} \otimes \boldsymbol{\nabla}_0 N^{\boldsymbol{x}}_a)\, N^{\boldsymbol{D}_0}_b \, dV. \tag{6.14}$$

The only stiffness matrix contribution emerging from the linearisation of the residual $\boldsymbol{R}^a_{\varphi}$, namely $\boldsymbol{K}^{ab}_{\varphi\boldsymbol{D}_0}$ is obtained as

$$\boldsymbol{K}^{ab}_{\varphi\boldsymbol{D}_0} = \int_V N^{\varphi}_a N^{\boldsymbol{D}_0}_b \boldsymbol{I}\, dV. \tag{6.15}$$

The stiffness matrix contribution of the diagonal block $\boldsymbol{K}_{\mathcal{Y}\mathcal{Y}}$ adopts the following expression

$$\boldsymbol{K}^{ab}_{\mathcal{Y}\mathcal{Y}} = \int_V \begin{bmatrix} N^{\boldsymbol{F}}_a N^{\boldsymbol{F}}_b W_{\boldsymbol{F}\boldsymbol{F}} & N^{\boldsymbol{F}}_a N^{\boldsymbol{H}}_b W_{\boldsymbol{F}\boldsymbol{H}} & N^{\boldsymbol{F}}_a N^{J}_b W_{\boldsymbol{F}J} & N^{\boldsymbol{F}}_a N^{\boldsymbol{d}}_b W_{\boldsymbol{F}\boldsymbol{d}} \\ N^{\boldsymbol{H}}_a N^{\boldsymbol{F}}_b W_{\boldsymbol{H}\boldsymbol{F}} & N^{\boldsymbol{H}}_a N^{\boldsymbol{H}}_b W_{\boldsymbol{H}\boldsymbol{H}} & N^{\boldsymbol{H}}_a N^{J}_b W_{\boldsymbol{H}J} & N^{\boldsymbol{H}}_a N^{\boldsymbol{d}}_b W_{\boldsymbol{H}\boldsymbol{d}} \\ N^{J}_a N^{\boldsymbol{F}}_b W_{J\boldsymbol{F}} & N^{J}_a N^{\boldsymbol{H}}_b W_{J\boldsymbol{H}} & N^{J}_a N^{J}_b W_{JJ} & N^{J}_a N^{\boldsymbol{d}}_b W_{J\boldsymbol{d}} \\ N^{\boldsymbol{d}}_a N^{\boldsymbol{F}}_b W_{\boldsymbol{d}\boldsymbol{F}} & N^{\boldsymbol{d}}_a N^{\boldsymbol{H}}_b W_{\boldsymbol{d}\boldsymbol{H}} & N^{\boldsymbol{d}}_a N^{J}_b W_{\boldsymbol{d}J} & N^{\boldsymbol{d}}_a N^{\boldsymbol{d}}_b W_{\boldsymbol{d}\boldsymbol{d}} \end{bmatrix} dV, \tag{6.16}$$

where the Hessian operator $[\mathbb{H}_W]$ has been defined in equation (5.23). The stiffness matrix contribution $\boldsymbol{K}^{ab}_{\mathcal{Y}\Sigma_{\mathcal{Y}}}$ emerging from the linearisation of the residual $\boldsymbol{R}^a_{\mathcal{Y}}$ with respect to incremental changes in the elements of the set $\Sigma_{\mathcal{Y}}$ is

$$\boldsymbol{K}^{ab}_{\mathcal{Y}\Sigma_{\mathcal{Y}}} = -\int_V \begin{bmatrix} N^{\boldsymbol{F}}_a N^{\boldsymbol{F}}_b \boldsymbol{\mathcal{I}} & \boldsymbol{0} & \boldsymbol{0} & \boldsymbol{0} \\ \boldsymbol{0} & N^{\boldsymbol{H}}_a N^{\boldsymbol{H}}_b \boldsymbol{\mathcal{I}} & \boldsymbol{0} & \boldsymbol{0} \\ \boldsymbol{0} & \boldsymbol{0} & N^{J}_a N^{J}_b & \boldsymbol{0} \\ \boldsymbol{0} & \boldsymbol{0} & \boldsymbol{0} & N^{\boldsymbol{d}}_a N^{\boldsymbol{d}}_b \boldsymbol{I} \end{bmatrix} dV, \tag{6.17}$$

The stiffness matrix contribution associated to the residual $\boldsymbol{R}^a_{\mathcal{Y}}$, namely $\boldsymbol{K}^{ab}_{\mathcal{Y}\boldsymbol{D}_0}$ is defined as

$$\boldsymbol{K}^{ab}_{\mathcal{Y}\boldsymbol{D}_0} = \int_V \begin{bmatrix} N^{\boldsymbol{F}}_a N^{\boldsymbol{D}_0}_b W_{\boldsymbol{F}\boldsymbol{D}_0} & N^{\boldsymbol{H}}_a N^{\boldsymbol{D}_0}_b W_{\boldsymbol{H}\boldsymbol{D}_0} & N^{J}_a N^{\boldsymbol{D}_0}_b W_{J\boldsymbol{D}_0} & N^{\boldsymbol{d}}_a N^{\boldsymbol{D}_0}_b W_{\boldsymbol{d}\boldsymbol{D}_0} \end{bmatrix} dV. \tag{6.18}$$

The stiffness matrix contribution $\boldsymbol{K}^{ab}_{\Sigma_{\mathcal{Y}}\boldsymbol{D}_0}$ resulting from the linearisation of the residual $\boldsymbol{R}^a_{\Sigma_{\mathcal{Y}}}$ with respect to incremental changes in $\boldsymbol{D}_0$ is defined as

$$\boldsymbol{K}^{ab}_{\Sigma_{\mathcal{Y}}\boldsymbol{D}_0} = \begin{bmatrix} \boldsymbol{0} & \boldsymbol{0} & \boldsymbol{0} & \boldsymbol{K}^{ab}_{\boldsymbol{\Sigma}_{\boldsymbol{d}}\boldsymbol{D}_0} \end{bmatrix}, \qquad \boldsymbol{K}^{ab}_{\boldsymbol{\Sigma}_{\boldsymbol{d}}\boldsymbol{D}_0} = \int_V N^{\boldsymbol{d}}_a N^{\boldsymbol{D}_0}_b \boldsymbol{F}_{\boldsymbol{x}}\, dV. \tag{6.19}$$

Finally, the block $\boldsymbol{K}^{ab}_{\boldsymbol{D}_0\boldsymbol{D}_0}$ is obtained from

$$\boldsymbol{K}^{ab}_{\boldsymbol{D}_0\boldsymbol{D}_0} = \int_V N^{\boldsymbol{D}_0}_a N^{\boldsymbol{D}_0}_b W_{\boldsymbol{D}_0\boldsymbol{D}_0}\, dV. \tag{6.20}$$

Static condensation

This process will be illustrated for the particular formulation associated to the variational principle Π_W (5.51). Similar procedure can be applied to the formulation associated to the variational principle Π_Φ (5.60). The algebraic system of equations obtained locally at a particular element e (see equation (6.10)) is written as

$$\boldsymbol{K}^e_{\text{local}} \Delta q^e = \tilde{\boldsymbol{R}}_{\text{local}}, \tag{6.21}$$

with

$$\tilde{\boldsymbol{R}}_{\text{local}} = \begin{bmatrix} \boldsymbol{R}^e_{\boldsymbol{x}} & \boldsymbol{R}^e_{\varphi} & \boldsymbol{R}^e_{\mathcal{Y}} & \boldsymbol{R}^e_{\Sigma_{\mathcal{Y}}} & \boldsymbol{R}^e_{\boldsymbol{D}_0} \end{bmatrix}^T; \qquad \Delta q^e = \begin{bmatrix} \mathbf{u}^e & \Delta\boldsymbol{\varphi}^e & \Delta\boldsymbol{\mathcal{Y}}^e & \Delta\boldsymbol{\Sigma}^e_{\mathcal{Y}} & \Delta\mathbf{D}^e_0 \end{bmatrix}^T, \tag{6.22}$$

and where the local stiffness matrix $\boldsymbol{K}^e_{\text{local}}$ is defined as,

$$\boldsymbol{K}^e_{\text{local}} = \begin{bmatrix} \boldsymbol{K}^e_{\boldsymbol{x}\boldsymbol{x}} & \mathbf{0} & \mathbf{0} & \boldsymbol{K}^e_{\boldsymbol{x}\Sigma_{\mathcal{Y}}} & \boldsymbol{K}^e_{\boldsymbol{x}\boldsymbol{D}_0} \\ \mathbf{0} & \mathbf{0} & \mathbf{0} & \mathbf{0} & \boldsymbol{K}^e_{\varphi\boldsymbol{D}_0} \\ \mathbf{0} & \mathbf{0} & \boldsymbol{K}^e_{\mathcal{Y}\mathcal{Y}} & \boldsymbol{K}^e_{\mathcal{Y}\Sigma_{\mathcal{Y}}} & \boldsymbol{K}^e_{\mathcal{Y}\boldsymbol{D}_0} \\ \boldsymbol{K}^e_{\Sigma_{\mathcal{Y}}\boldsymbol{x}} & \mathbf{0} & \boldsymbol{K}^e_{\Sigma_{\mathcal{Y}}\mathcal{Y}} & \mathbf{0} & \boldsymbol{K}^e_{\Sigma_{\mathcal{Y}}\boldsymbol{D}_0} \\ \boldsymbol{K}^e_{\boldsymbol{D}_0\boldsymbol{x}} & \boldsymbol{K}^e_{\boldsymbol{D}_0\varphi} & \boldsymbol{K}^e_{\boldsymbol{D}_0\mathcal{Y}} & \boldsymbol{K}^e_{\boldsymbol{D}_0\Sigma_{\mathcal{Y}}} & \boldsymbol{K}^e_{\boldsymbol{D}_0\boldsymbol{D}_0} \end{bmatrix}. \tag{6.23}$$

Notice that the superscript e in equations (6.21) and (6.23) has been used to denote the local (element) character of the variables involved. The fourth, fifth and third (in this order) equations (forth, fifth and third rows) in above (6.21) enables the local variables $\Delta\boldsymbol{\mathcal{Y}}^e$, $\Delta\mathbf{D}^e_0$ and $\Delta\boldsymbol{\Sigma}^e_{\mathcal{Y}}$ to be expressed as

$$\Delta\boldsymbol{\mathcal{Y}}^e = -\left[\boldsymbol{K}^e_{\Sigma_{\mathcal{Y}}\mathcal{Y}}\right]^{-1}\left(\boldsymbol{R}^e_{\Sigma_{\mathcal{Y}}} + \boldsymbol{K}^e_{\Sigma_{\mathcal{Y}}\boldsymbol{x}}\mathbf{u}^e + \boldsymbol{K}^e_{\Sigma_{\mathcal{Y}}\boldsymbol{D}_0}\Delta\mathbf{D}^e_0\right); \tag{6.24a}$$

$$\Delta\mathbf{D}^e_0 = -\left[\boldsymbol{K}^e_{\boldsymbol{D}_0\boldsymbol{D}_0}\right]^{-1}\left(\boldsymbol{R}^e_{\boldsymbol{D}_0} + \boldsymbol{K}^e_{\boldsymbol{D}_0\boldsymbol{x}}\mathbf{u}^e + \boldsymbol{K}^e_{\boldsymbol{D}_0\varphi}\Delta\boldsymbol{\varphi}^e + \boldsymbol{K}^e_{\boldsymbol{D}_0\mathcal{Y}}\Delta\boldsymbol{\mathcal{Y}}^e + \boldsymbol{K}^e_{\boldsymbol{D}_0\Sigma_{\mathcal{Y}}}\Delta\boldsymbol{\Sigma}^e_{\mathcal{Y}}\right); \tag{6.24b}$$

$$\Delta\boldsymbol{\Sigma}^e_{\mathcal{Y}} = -\left[\boldsymbol{K}^e_{\mathcal{Y}\Sigma_{\mathcal{Y}}}\right]^{-1}\left(\boldsymbol{R}^e_{\mathcal{Y}} + \boldsymbol{K}^e_{\mathcal{Y}\mathcal{Y}}\Delta\boldsymbol{\mathcal{Y}}^e + \boldsymbol{K}^e_{\mathcal{Y}\boldsymbol{D}_0}\Delta\mathbf{D}^e_0\right). \tag{6.24c}$$

Substitution of $\Delta\boldsymbol{\mathcal{Y}}^e$ (6.24a) into the expression for $\Delta\mathbf{D}^e_0$ in (6.24b) and subsequent substitution of these two into the expression for $\Delta\boldsymbol{\Sigma}^e_{\mathcal{Y}}$ in (6.24c) enables the local variable $\Delta\boldsymbol{\Sigma}^e_{\mathcal{Y}}$ to be expressed in terms of the geometry and electric potential as

$$\Delta\boldsymbol{\Sigma}^e_{\mathcal{Y}} = \bar{\boldsymbol{R}}^e_{\Sigma_{\mathcal{Y}}} + \boldsymbol{M}^e_{\Sigma_{\mathcal{Y}}\boldsymbol{x}}\mathbf{u}^e + \boldsymbol{M}^e_{\Sigma_{\mathcal{Y}}\varphi}\Delta\boldsymbol{\phi}^e, \tag{6.25}$$

where $\bar{\boldsymbol{R}}^e_{\Sigma_{\mathcal{Y}}}$, $\boldsymbol{M}^e_{\Sigma_{\mathcal{Y}}\boldsymbol{x}}$ and $\boldsymbol{M}^e_{\Sigma_{\mathcal{Y}}\varphi}$ will be defined in equation (D.1). Using this expression for $\Delta\boldsymbol{\Sigma}^e_{\mathcal{Y}}$, the fifth equation in (6.21) enables the local variable $\Delta\mathbf{D}^e_0$ to be expressed as

$$\Delta\mathbf{D}^e_0 = \bar{\boldsymbol{R}}^e_{\boldsymbol{D}_0} + \bar{\boldsymbol{M}}^e_{\boldsymbol{D}_0\boldsymbol{x}}\mathbf{u}^e + \bar{\boldsymbol{M}}^e_{\boldsymbol{D}_0\varphi}\Delta\boldsymbol{\phi}^e, \tag{6.26}$$

where the auxiliary residuals and matrices $\bar{\boldsymbol{R}}^e_{\boldsymbol{D}_0}$, $\bar{\boldsymbol{M}}^e_{\boldsymbol{D}_0\boldsymbol{x}}$ and $\bar{\boldsymbol{M}}^e_{\boldsymbol{D}_0\varphi}$ will be defined in equation (D.1). Finally, the third equation in (6.21) enables the local variable $\Delta\boldsymbol{\mathcal{Y}}^e$ to be expressed as

$$\Delta\boldsymbol{\mathcal{Y}}^e = \bar{\boldsymbol{R}}^e_{\mathcal{Y}} + \bar{\boldsymbol{M}}^e_{\mathcal{Y}\boldsymbol{x}}\mathbf{u}^e + \bar{\boldsymbol{M}}^e_{\mathcal{Y}\varphi}\Delta\boldsymbol{\phi}^e, \tag{6.27}$$

where the auxiliary residuals and matrices $\bar{\boldsymbol{R}}^e_{\mathcal{Y}}$, $\bar{\boldsymbol{M}}^e_{\mathcal{Y}\boldsymbol{x}}$ and $\bar{\boldsymbol{M}}^e_{\mathcal{Y}\varphi}$ will be defined in equation (D.1). All in all, the new expressions for the incremental local variables $\Delta\boldsymbol{\Sigma}^e_{\mathcal{Y}}$, $\Delta\mathbf{D}^e_0$ and $\Delta\boldsymbol{\mathcal{Y}}^e$ in terms $\mathbf{u}^e$ and $\Delta\boldsymbol{\phi}^e$ enable the local algebraic system of equations in (6.21) to be formulated exclusively in terms of the unknowns $\mathbf{u}^e$ and $\Delta\boldsymbol{\phi}^e$ as

$$\begin{bmatrix} \bar{\boldsymbol{K}}^e_{\boldsymbol{x}\boldsymbol{x}} & \bar{\boldsymbol{K}}^e_{\boldsymbol{x}\varphi} \\ \bar{\boldsymbol{K}}^e_{\varphi\boldsymbol{x}} & \bar{\boldsymbol{K}}^e_{\varphi\varphi} \end{bmatrix} \begin{bmatrix} \mathbf{u}^e \\ \Delta\boldsymbol{\phi}^e \end{bmatrix} = \begin{bmatrix} \bar{\boldsymbol{R}}^e_{\boldsymbol{x}} \\ \bar{\boldsymbol{R}}^e_{\varphi} \end{bmatrix}, \tag{6.28}$$

where the modified residuals (6.28) are expressed as

$$\bar{\boldsymbol{R}}^e_{\boldsymbol{x}} = \boldsymbol{R}_{\boldsymbol{x}}{}^e + \boldsymbol{K}^e_{\boldsymbol{x}\Sigma_{\mathcal{Y}}}\bar{\boldsymbol{R}}^e_{\Sigma_{\mathcal{Y}}} + \boldsymbol{K}^e_{\boldsymbol{x}\boldsymbol{D}_0}\bar{\bar{\boldsymbol{R}}}^e_{\boldsymbol{D}_0}; \qquad \bar{\boldsymbol{R}}^e_{\varphi} = \boldsymbol{R}^e_{\varphi} + \boldsymbol{K}^e_{\varphi\boldsymbol{D}_0}\bar{\bar{\boldsymbol{R}}}^e_{\boldsymbol{D}_0}. \tag{6.29}$$

Finally, the modified stiffness matrices in (6.28) are expressed as

$$\begin{aligned} \bar{\boldsymbol{K}}^e_{\boldsymbol{x}\boldsymbol{x}} &= \boldsymbol{K}^e_{\boldsymbol{x}\boldsymbol{x}} + \boldsymbol{K}^e_{\boldsymbol{x}\Sigma_{\mathcal{Y}}}\boldsymbol{M}^e_{\Sigma_{\mathcal{Y}}\boldsymbol{x}} + \boldsymbol{K}^e_{\boldsymbol{x}\boldsymbol{D}_0}\bar{\boldsymbol{M}}^e_{\boldsymbol{D}_0\boldsymbol{x}}; \\ \bar{\boldsymbol{K}}^e_{\boldsymbol{x}\varphi} &= \boldsymbol{K}^e_{\boldsymbol{x}\Sigma_{\mathcal{Y}}}\boldsymbol{M}^e_{\Sigma_{\mathcal{Y}}\varphi} + \boldsymbol{K}^e_{\boldsymbol{x}\boldsymbol{D}_0}\bar{\boldsymbol{M}}_{\boldsymbol{D}_0\varphi}; \\ \bar{\boldsymbol{K}}^e_{\varphi\varphi} &= \boldsymbol{K}^e_{\varphi\boldsymbol{D}_0}\bar{\boldsymbol{M}}^e_{\boldsymbol{D}_0\varphi}. \end{aligned} \tag{6.30}$$

The expressions for all the auxiliary residuals and stiffness matrices in equations (6.29) and (6.30) are presented in Appendix (D.1).

6.2.3 Finite Element semi-discretisation of the variational principle Π_Φ

Let us now consider the mixed variational principle Π_Φ in equation (5.60). For notational convenience, the following set of variables p is introduced

$$p = \{\boldsymbol{x}, \varphi, \mathcal{D}, \Sigma_{\mathcal{D}}, \boldsymbol{\Sigma}_{\boldsymbol{d}}\}, \tag{6.31}$$

with the sets $\mathcal{D}$ and $\Sigma_{\mathcal{D}}$ defined in equation (5.61). The discrete stationary conditions of the variational principle Π_Φ in (5.60) with respect to virtual changes of the geometry and with respect to virtual changes of the electric potential are

$$D\Pi_\Phi\left[\delta\boldsymbol{u}\right] = \sum_a \boldsymbol{R}^a_{\boldsymbol{x}} \cdot \delta\boldsymbol{u}^a; \qquad D\Pi_\Phi\left[\delta\varphi\right] = \sum_a R^a_{\varphi} \cdot \delta\varphi^a, \tag{6.32}$$

where the expressions for $\boldsymbol{R}^a_{\boldsymbol{x}}$ and R^a_{φ} in (6.32) are identical for those in (6.4). The discrete stationary conditions with respect to the elements in the set $\mathcal{D}$ (5.61) and $\boldsymbol{\Sigma}_{\boldsymbol{d}}$ (i.e. constitutive laws) are

$$\begin{aligned} D\Pi_\Phi[\delta\mathcal{D}, \delta\boldsymbol{\Sigma}_{\boldsymbol{d}}] = &\sum_{a=1}^{n_{\boldsymbol{F}}} \boldsymbol{R}^a_{\boldsymbol{F}} : \delta\boldsymbol{F}^a + \sum_{a=1}^{n_{\boldsymbol{H}}} \boldsymbol{R}^a_{\boldsymbol{H}} : \delta\boldsymbol{H}^a + \sum_{a=1}^{n_J} \boldsymbol{R}^a_J \delta J^a \\ &+ \sum_{a=1}^{n_{\boldsymbol{\Sigma}_{\boldsymbol{D}_0}}} \boldsymbol{R}^a_{\boldsymbol{\Sigma}_{\boldsymbol{D}_0}} \cdot \delta\boldsymbol{\Sigma}^a_{\boldsymbol{D}_0} + \sum_{a=1}^{n_{\boldsymbol{\Sigma}_{\boldsymbol{d}}}} \boldsymbol{R}^a_{\boldsymbol{\Sigma}_{\boldsymbol{d}}} \cdot \delta\boldsymbol{\Sigma}^a_{\boldsymbol{d}}, \end{aligned} \tag{6.33}$$

where the residuals in above equation (6.33) are

$$\begin{aligned}
\boldsymbol{R}^a_{\boldsymbol{F}} &= \int_V \left(\frac{\partial \Phi}{\partial \boldsymbol{F}} - \boldsymbol{\Sigma}_{\boldsymbol{F}}\right) N^{\boldsymbol{F}}_a \, dV; & \boldsymbol{R}^a_{\boldsymbol{H}} &= \int_V \left(\frac{\partial \Phi}{\partial \boldsymbol{H}} - \boldsymbol{\Sigma}_{\boldsymbol{H}}\right) N^{\boldsymbol{H}}_a \, dV; \\
R^a_J &= \int_V \left(\frac{\partial \Phi}{\partial J} - \Sigma_J\right) N^J_a \, dV; & \boldsymbol{R}^a_{\boldsymbol{\Sigma}_{\boldsymbol{D}0}} &= \int_V \left(\frac{\partial \Phi}{\partial \boldsymbol{\Sigma}_{\boldsymbol{D}0}} + \boldsymbol{D}_0\right) N^{\boldsymbol{D}_0}_a \, dV; \\
\boldsymbol{R}^a_{\boldsymbol{\Sigma}_{\boldsymbol{d}}} &= \int_V \left(\frac{\partial \Phi}{\partial \boldsymbol{\Sigma}_{\boldsymbol{d}}} - \boldsymbol{F}_{\boldsymbol{x}} \boldsymbol{D}_0\right) N^{\boldsymbol{d}}_a \, dV.
\end{aligned} \tag{6.34}$$

The discrete stationary conditions with respect to the elements of the set $\Sigma_{\mathcal{D}}$ (5.61) yield (i.e. compatibility and Faraday laws)

$$\begin{aligned}
D\Pi_\Phi[\delta\Sigma_{\mathcal{D}}] = &\sum_{a=1}^{n_{\boldsymbol{\Sigma}_{\boldsymbol{F}}}} \boldsymbol{R}^a_{\boldsymbol{\Sigma}_{\boldsymbol{F}}} : \delta\boldsymbol{\Sigma}_{\boldsymbol{F}}{}^a + \sum_{a=1}^{n_{\boldsymbol{\Sigma}_{\boldsymbol{H}}}} \boldsymbol{R}^a_{\boldsymbol{\Sigma}_{\boldsymbol{H}}} : \delta\boldsymbol{\Sigma}_{\boldsymbol{H}}{}^a + \sum_{a=1}^{n_{\Sigma_J}} R^a_{\Sigma_J} \delta\Sigma^a_J \\
&+ \sum_{a=1}^{n_{\boldsymbol{D}_0}} \boldsymbol{R}^a_{\boldsymbol{D}_0} \cdot \delta\boldsymbol{D}^a_0,
\end{aligned} \tag{6.35}$$

where the residuals in above equation (6.35) are

$$\begin{aligned}
\boldsymbol{R}^a_{\boldsymbol{\Sigma}_{\boldsymbol{F}}} &= \int_V (\boldsymbol{F}_{\boldsymbol{x}} - \boldsymbol{F}) \, N^{\boldsymbol{F}}_a \, dV; & \boldsymbol{R}^a_{\boldsymbol{\Sigma}_{\boldsymbol{H}}} &= \int_V (\boldsymbol{H}_{\boldsymbol{x}} - \boldsymbol{H}) \, N^{\boldsymbol{H}}_a \, dV; \\
R^a_{\Sigma_J} &= \int_V (J_{\boldsymbol{x}} - J) \, N^J_a \, dV; & \boldsymbol{R}^a_{\boldsymbol{D}_0} &= \int_V \left(\boldsymbol{\Sigma}_{\boldsymbol{D}_0} + \boldsymbol{F}^{\boldsymbol{T}}_{\boldsymbol{x}} \boldsymbol{\Sigma}_{\boldsymbol{d}} + \boldsymbol{\nabla}_{\mathbf{0}} \boldsymbol{\varphi}\right) N^{\boldsymbol{D}_0}_a \, dV.
\end{aligned} \tag{6.36}$$

The stiffness matrix contribution arising for the variational principle Π_Φ (5.60) before static condensation is carried out emerge as

$$D^2\Pi_\Phi\left[\delta p; \Delta p\right] = \begin{bmatrix} \delta\mathbf{u} \\ \delta\boldsymbol{\phi} \\ \delta\boldsymbol{\mathcal{D}} \\ \delta\boldsymbol{\Sigma}_{\mathcal{D}} \\ \delta\boldsymbol{\Sigma}_{\boldsymbol{d}} \end{bmatrix}^T \begin{bmatrix} \boldsymbol{K}_{\boldsymbol{xx}} & \mathbf{0} & \mathbf{0} & \boldsymbol{K}_{\boldsymbol{x}\Sigma_{\mathcal{D}}} & \boldsymbol{K}_{\boldsymbol{x}\boldsymbol{\Sigma}_{\boldsymbol{d}}} \\ \mathbf{0} & \mathbf{0} & \boldsymbol{K}_{\varphi\mathcal{D}} & \mathbf{0} & \mathbf{0} \\ \mathbf{0} & \boldsymbol{K}_{\mathcal{D}\varphi} & \boldsymbol{K}_{\mathcal{D}\mathcal{D}} & \boldsymbol{K}_{\mathcal{D}\Sigma_{\mathcal{D}}} & \boldsymbol{K}_{\mathcal{D}\boldsymbol{\Sigma}_{\boldsymbol{d}}} \\ \boldsymbol{K}_{\Sigma_{\mathcal{D}}\boldsymbol{x}} & \mathbf{0} & \boldsymbol{K}_{\Sigma_{\mathcal{D}}\mathcal{D}} & \mathbf{0} & \boldsymbol{K}_{\Sigma_{\mathcal{D}}\boldsymbol{\Sigma}_{\boldsymbol{d}}} \\ \boldsymbol{K}_{\boldsymbol{\Sigma}_{\boldsymbol{d}}\boldsymbol{x}} & \mathbf{0} & \boldsymbol{K}_{\boldsymbol{\Sigma}_{\boldsymbol{d}}\mathcal{D}} & \boldsymbol{K}_{\boldsymbol{\Sigma}_{\boldsymbol{d}}\Sigma_{\mathcal{D}}} & \boldsymbol{K}_{\boldsymbol{\Sigma}_{\boldsymbol{d}}\boldsymbol{\Sigma}_{\boldsymbol{d}}} \end{bmatrix} \begin{bmatrix} \mathbf{u} \\ \Delta\boldsymbol{\phi} \\ \Delta\boldsymbol{\mathcal{D}} \\ \Delta\boldsymbol{\Sigma}_{\mathcal{D}} \\ \Delta\boldsymbol{\Sigma}_{\boldsymbol{d}} \end{bmatrix}. \tag{6.37}$$

The objective of the following derivations is to present the expressions for non-zero blocks of the stiffness matrix in above equation (6.37). The stiffness matrix contribution $\boldsymbol{K}^{ab}_{\boldsymbol{xx}}$ is obtained exactly as in equation (6.11). The stiffness matrix contribution $\boldsymbol{K}^{ab}_{\boldsymbol{x}\Sigma_{\mathcal{D}}}$, emerging from the linearisation of $\boldsymbol{R}^a_{\boldsymbol{x}}$ with respect to incremental changes in the set $\Sigma_{\mathcal{D}}$, can be further decomposed into each of the contributions of the elements of the set $\Sigma_{\mathcal{D}}$ as

$$\boldsymbol{K}^{ab}_{\boldsymbol{x}\Sigma_{\mathcal{D}}} = \begin{bmatrix} \boldsymbol{K}^{ab}_{\boldsymbol{x}\boldsymbol{\Sigma}_{\boldsymbol{F}}} & \boldsymbol{K}^{ab}_{\boldsymbol{x}\boldsymbol{\Sigma}_{\boldsymbol{H}}} & \boldsymbol{K}^{ab}_{\boldsymbol{x}\Sigma_J} & \boldsymbol{K}^{ab}_{\boldsymbol{x}\boldsymbol{D}_0} \end{bmatrix}, \tag{6.38}$$

where each of the individual contribution in (6.38) is obtained as

$$\begin{aligned}
&\boldsymbol{K}^{ab}_{\boldsymbol{x}\boldsymbol{\Sigma}_{\boldsymbol{F}}} = \int_V (\boldsymbol{I}\otimes\boldsymbol{\nabla}_0 N^{\boldsymbol{x}}_a)\, N^{\boldsymbol{F}}_b\, dV; \qquad \left[\boldsymbol{K}^{ab}_{\boldsymbol{x}\boldsymbol{\Sigma}_{\boldsymbol{H}}}\right]_{ijI} = \mathcal{E}_{ijk}\left[\int_V (\boldsymbol{F}_{\boldsymbol{x}}\times\boldsymbol{\nabla}_0 N^{\boldsymbol{x}}_a)\, N^{\boldsymbol{H}}_b\, dV\right]_{kI};\\
&\boldsymbol{K}^{ab}_{\boldsymbol{x}\Sigma_J} = \int_V N^J_b\, \boldsymbol{H}_{\boldsymbol{x}}\boldsymbol{\nabla}_0 N^{\boldsymbol{x}}_a\, dV; \qquad\qquad \boldsymbol{K}^{ab}_{\boldsymbol{x}\boldsymbol{D}_0} = \int_V (\boldsymbol{\Sigma}_{\boldsymbol{d}}\otimes\boldsymbol{\nabla}_0 N^{\boldsymbol{x}}_a)\, N^{\boldsymbol{D}_0}_b\, dV.
\end{aligned} \tag{6.39}$$

The stiffness matrix contribution $\boldsymbol{K}^{ab}_{\boldsymbol{x}\boldsymbol{\Sigma}_{\boldsymbol{d}}}$ yields

$$\boldsymbol{K}^{ab}_{\boldsymbol{x}\boldsymbol{\Sigma}_{\boldsymbol{d}}} = \int_V (\boldsymbol{D}_0\cdot\boldsymbol{\nabla}_0 N^{\boldsymbol{x}}_a)\, N^{\boldsymbol{d}}_b \boldsymbol{I}\, dV. \tag{6.40}$$

The stiffness matrix contribution obtained from the linearisation of $\boldsymbol{R}^a_\varphi$ with respect to incremental changes in the elements of the set $\mathcal{D}$ is

$$\boldsymbol{K}^{ab}_{\varphi\mathcal{D}} = \begin{bmatrix}\boldsymbol{0} & \boldsymbol{0} & 0 & \boldsymbol{K}^{ab}_{\varphi\boldsymbol{D}_0}\end{bmatrix}; \qquad \boldsymbol{K}^{ab}_{\varphi\boldsymbol{D}_0} = \int_V N^\varphi_a N^{\boldsymbol{D}_0}_b \boldsymbol{I}\, dV. \tag{6.41}$$

The stiffness matrix contribution of the diagonal block $\boldsymbol{K}^{ab}_{\mathcal{D}\mathcal{D}}$ results in

$$\boldsymbol{K}^{ab}_{\mathcal{D}\mathcal{D}} = \int_V \begin{bmatrix} N^{\boldsymbol{F}}_a N^{\boldsymbol{F}}_b \Phi_{\boldsymbol{F}\boldsymbol{F}} & N^{\boldsymbol{F}}_a N^{\boldsymbol{H}}_b \Phi_{\boldsymbol{F}\boldsymbol{H}} & N^{\boldsymbol{F}}_a N^J_b \Phi_{\boldsymbol{F}J} & N^{\boldsymbol{F}}_a N^{\boldsymbol{D}_0}_b \Phi_{\boldsymbol{F}\boldsymbol{\Sigma}_{\boldsymbol{D}_0}} \\ N^{\boldsymbol{H}}_a N^{\boldsymbol{F}}_b \Phi_{\boldsymbol{H}\boldsymbol{F}} & N^{\boldsymbol{H}}_a N^{\boldsymbol{H}}_b \Phi_{\boldsymbol{H}\boldsymbol{H}} & N^{\boldsymbol{H}}_a N^J_b \Phi_{\boldsymbol{H}J} & N^{\boldsymbol{H}}_a N^{\boldsymbol{D}_0}_b \Phi_{\boldsymbol{H}\boldsymbol{\Sigma}_{\boldsymbol{D}_0}} \\ N^J_a N^{\boldsymbol{F}}_b \Phi_{J\boldsymbol{F}} & N^J_a N^{\boldsymbol{H}}_b \Phi_{J\boldsymbol{H}} & N^J_a N^J_b \Phi_{JJ} & N^J_a N^{\boldsymbol{D}_0}_b \Phi_{J\boldsymbol{\Sigma}_{\boldsymbol{D}_0}} \\ N^{\boldsymbol{D}_0}_a N^{\boldsymbol{F}}_b \Phi_{\boldsymbol{\Sigma}_{\boldsymbol{D}_0}\boldsymbol{F}} & N^{\boldsymbol{D}_0}_a N^{\boldsymbol{H}}_b \Phi_{\boldsymbol{\Sigma}_{\boldsymbol{D}_0}\boldsymbol{H}} & N^{\boldsymbol{D}_0}_a N^J_b \Phi_{\boldsymbol{\Sigma}_{\boldsymbol{D}_0}J} & N^{\boldsymbol{D}_0}_a N^{\boldsymbol{D}_0}_b \Phi_{\boldsymbol{\Sigma}_{\boldsymbol{D}_0}\boldsymbol{\Sigma}_{\boldsymbol{D}_0}} \end{bmatrix} dV, \tag{6.42}$$

In the case in which an explicit representation of the extended Helmholtz's energy functional $\Phi(\boldsymbol{F},\boldsymbol{H},J,\boldsymbol{\Sigma}_{\boldsymbol{D}_0},\boldsymbol{\Sigma}_{\boldsymbol{d}})$ is not available, Appendix C shows the relationship between the components of the Hessian operator $[\mathbb{H}_\Phi]$ in terms of the components of the Hessian operator $[\mathbb{H}_W]$. The stiffness matrix contribution $\boldsymbol{K}^{ab}_{\mathcal{D}\Sigma_{\mathcal{D}}}$ arising from the linearisation of $\boldsymbol{R}^a_{\mathcal{D}}$ with respect to incremental changes in the elements of the set $\Sigma_{\mathcal{D}}$ is defined as

$$\boldsymbol{K}^{ab}_{\mathcal{D}\Sigma_{\mathcal{D}}} = -\int_V \begin{bmatrix} N^{\boldsymbol{F}}_a N^{\boldsymbol{F}}_b \boldsymbol{\mathcal{I}} & \boldsymbol{0} & \boldsymbol{0} & \boldsymbol{0} \\ \boldsymbol{0} & N^{\boldsymbol{H}}_a N^{\boldsymbol{H}}_b \boldsymbol{\mathcal{I}} & \boldsymbol{0} & \boldsymbol{0} \\ \boldsymbol{0} & \boldsymbol{0} & N^J_a N^J_b & \boldsymbol{0} \\ \boldsymbol{0} & \boldsymbol{0} & \boldsymbol{0} & -N^{\boldsymbol{D}_0}_a N^{\boldsymbol{D}_0}_b \boldsymbol{I} \end{bmatrix} dV. \tag{6.43}$$

Finally, the expression for the matrix $\boldsymbol{K}^{ab}_{\mathcal{D}\boldsymbol{\Sigma}_{\boldsymbol{d}}}$ emerges as

$$\boldsymbol{K}^{ab}_{\mathcal{D}\boldsymbol{\Sigma}_{\boldsymbol{d}}} = \int_V \begin{bmatrix} N^{\boldsymbol{F}}_a N^{\boldsymbol{d}}_b \Phi_{\boldsymbol{F}\boldsymbol{\Sigma}_{\boldsymbol{d}}} & N^{\boldsymbol{H}}_a N^{\boldsymbol{d}}_b \Phi_{\boldsymbol{H}\boldsymbol{\Sigma}_{\boldsymbol{d}}} & N^J_a N^{\boldsymbol{d}}_b \Phi_{J\boldsymbol{\Sigma}_{\boldsymbol{d}}} & N^{\boldsymbol{D}_0}_a N^{\boldsymbol{d}}_b \Phi_{\boldsymbol{\Sigma}_{\boldsymbol{D}_0}\boldsymbol{\Sigma}_{\boldsymbol{d}}} \end{bmatrix} dV. \tag{6.44}$$

The stiffness matrix contribution $\boldsymbol{K}^{ab}_{\Sigma_{\mathcal{D}}\boldsymbol{\Sigma}_{\boldsymbol{d}}}$ yields

$$\boldsymbol{K}^{ab}_{\Sigma_{\mathcal{D}}\boldsymbol{\Sigma}_{\boldsymbol{d}}} = \begin{bmatrix}\boldsymbol{0} & \boldsymbol{0} & \boldsymbol{0} & \boldsymbol{K}^{ab}_{\boldsymbol{D}_0\boldsymbol{\Sigma}_{\boldsymbol{d}}}\end{bmatrix}; \qquad \boldsymbol{K}^{ab}_{\boldsymbol{D}_0\boldsymbol{\Sigma}_{\boldsymbol{d}}} = \int_V N^{\boldsymbol{D}_0}_a N^{\boldsymbol{d}}_b \boldsymbol{F}^T_{\boldsymbol{x}}\, dV. \tag{6.45}$$

The last stiffness matrix involved in the variational principle Π_Φ (5.60), namely, $\boldsymbol{K}^{ab}_{\boldsymbol{\Sigma_d}\boldsymbol{\Sigma_d}}$ is obtained as

$$\boldsymbol{K}^{ab}_{\boldsymbol{\Sigma_d}\boldsymbol{\Sigma_d}} = \int_V N_a^{\boldsymbol{D}_0} N_b^{\boldsymbol{\Sigma_d}} \Phi_{\boldsymbol{\Sigma_d}\boldsymbol{\Sigma_d}}\, dV. \tag{6.46}$$

6.3 Examples

The objective of this section is to present a series of numerical examples in order to prove the robustness, accuracy and applicability of the computational framework presented above. Numerical results dealing with both displacement-potential based and mixed formulations will be displayed.

Three formulations have been compared, corresponding to: i) displacement-potential based formulation, hereby denoted as **DPF** [110]; ii) an eleven field $\{p, \mathcal{D}, \Sigma_\mathcal{D}, \boldsymbol{\Sigma_d}\}$ (6.31)-(5.61) formulation associated to the variational principle Π_Φ (5.60) and described in Section (6.2.3), hereby denoted as **MΦF** and iii), an eleven field $\{q, \mathcal{W}, \Sigma_\mathcal{W}, \boldsymbol{D}_0\}$ (6.3)-(5.52) formulation associated to the variational principle Π_W (5.51) and described in Section (6.2.2), hereby denoted as **MWF**.

All of the numerical results in which mixed formulations have been used correspond to the following selection of functional spaces: continuous quadratic interpolation of the displacement field (geometry) $\boldsymbol{x}$ and the electric potential field ϕ, piecewise linear interpolation of the conjugate pairs $\{\boldsymbol{F}, \boldsymbol{\Sigma_F}\}$, $\{\boldsymbol{H}, \boldsymbol{\Sigma_H}\}$, $\{\boldsymbol{D}_0, \boldsymbol{\Sigma}_{\boldsymbol{D}_0}\}$ and $\{\boldsymbol{d}, \boldsymbol{\Sigma_d}\}$, and piecewise constant interpolation of the Jacobian J and its associated stress conjugate Σ_J. With these functional spaces, the two mixed formulations **MΦF** and **MWF** will render identical results.

6.3.1 Three dimensional patch test

This first numerical example includes a standard three dimensional patch test in order to asses the correctness of the computational implementation. This problem has already been presented in References [40, 44] in the context of elasticity. The constitutive model used in this case is that in equation (5.81), hereby recalled for the sake of clarity, that is

$$\begin{aligned} W_{el} =& \mu_1 II_{\boldsymbol{F}} + \mu_2 II_{\boldsymbol{H}} + \frac{1}{2J\varepsilon_1} II_{\boldsymbol{d}} + \mu_e \left(II^2_{\boldsymbol{F}} + \frac{2}{\mu_e \varepsilon_e} II_{\boldsymbol{F}} II_{\boldsymbol{d}} + \frac{1}{\mu_e^2 \varepsilon_e^2} II^2_{\boldsymbol{d}} \right) \\ &+ \frac{1}{2\varepsilon_2} II_{\boldsymbol{D}_0} - 2(\mu_1 + 2\mu_2 + 6\mu_e) \ln J + \frac{\lambda}{2}(J-1)^2, \end{aligned} \tag{6.47}$$

The material properties in the reference configuration are chosen as $\mu = 10^5\,(Pa)$, $\hat{\lambda} = 1.094 \times 10^6\,(Pa)$ and $\varepsilon = 4.68\varepsilon 0$, which are compatible with a Poisson ratio of $\nu = 0.4582$ in the reference configuration. The material parameters, corresponding with this definition in the reference configuration, can thus be obtained and are presented in Table 6.1.

$\mu_1\,(Pa)$	$\mu_2\,(Pa)$	$\lambda\,(Pa)$	$\varepsilon_1\,(N/V^2)$	$(\varepsilon_2)^{-1}\,(V^2/N)$	f_e	f_s
0.225μ	$0.5\mu_1$	10^6	$4.68\varepsilon_0$	0	1.0515	0.0996

Table 6.1: Material properties for example 6.3.1. Parameters f_e and f_s defined in equations (5.83) and (5.84), respectively.

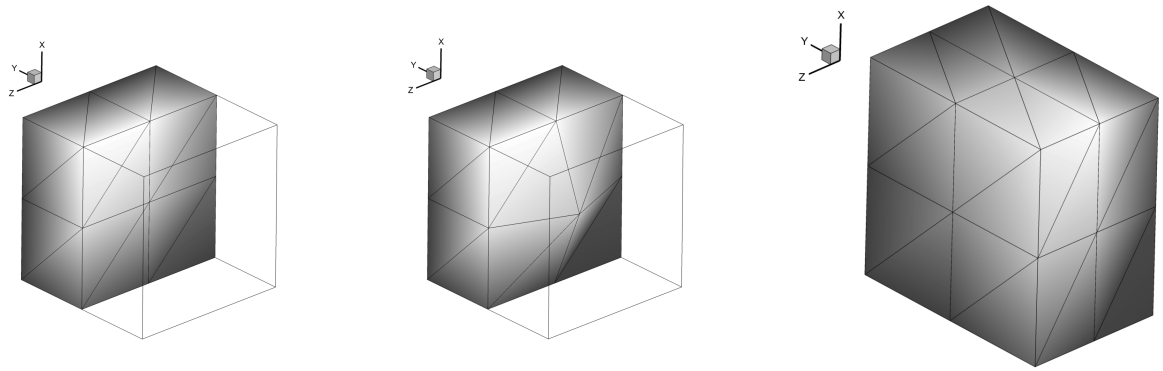

(a) (b) (c)

Figure 6.2: Three dimensional patch test. (a) View of half undistorted mesh in the reference configuration. (b) View of half distorted mesh in the reference configuration. (c) Example of deformed geometry after applying a voltage difference of $\Delta\varphi = 30\,MV$ in the OX_3 direction for the constitutive model defined in (6.47). Parameters f_e and f_s defined in equations (5.83) and (5.84).

A homogeneous electric field is defined in the OX_3 direction, applied to a cubic shape domain of side L, as depicted in Figure 6.2. To achieve this distribution of electric field, non-zero normal (electric) Dirichlet boundary conditions are applied on the boundary faces perpendicular to the OX_3 axis and zero (electric) Neumann boundary conditions are defined everywhere else. Moreover, zero (mechanical) normal Dirichlet boundary conditions are defined on three faces perpendicular to the OX_1, OX_2 and OX_3 directions and zero (mechanical) Neumann boundary conditions are applied everywhere else.

The domain is discretised using two different meshes of $(2\times2\times2)\times6$ tetrahedral elements. First, a structured mesh is shown in Figure 6.2(a) and second, a distorted mesh is shown in Figure 6.2(b), where the interior node is displaced randomly. The objective of this example is to demonstrate that the same homogeneous solution is obtained for both meshes. As expected, hence passing the patch test, for the two mixed formulations defined, namely **MWF** and **MΦF**, the results are identical for both meshes. A homogeneous deformation gradient tensor and a Lagrangian electric field for both meshes is obtained as

$$\boldsymbol{F} = \begin{bmatrix} 1.15598 & 0 & 0 \\ 0 & 1.15598 & 0 \\ 0 & 0 & 0.749559 \end{bmatrix}; \qquad \boldsymbol{E}_0 = \begin{bmatrix} 0 \\ 0 \\ 30 \end{bmatrix} (MV/m). \tag{6.48}$$

For completeness, the quadratic convergence of the Newton-Raphson algorithm is displayed in Figure 6.3.

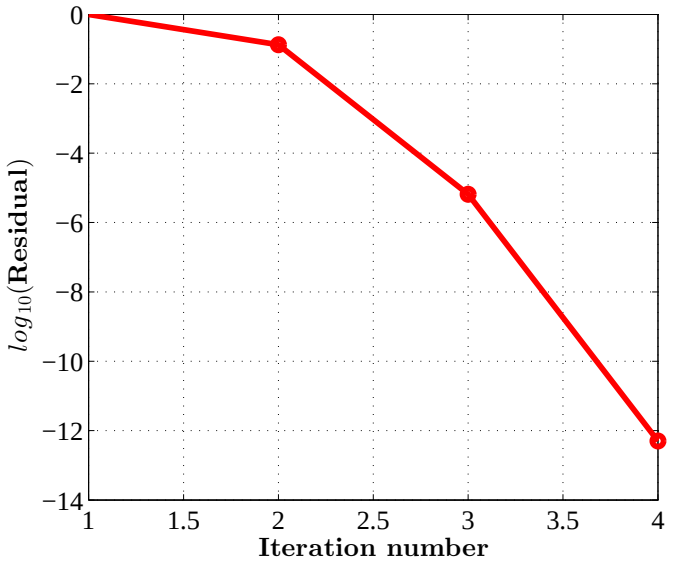

Figure 6.3: Three dimensional patch test: quadratic convergence of the Newton-Raphson linearisation procedure.

6.3.2 Convergence of the proposed formulation

The objective of this example is to demonstrate the p-order of accuracy of the different mixed formulations, as a function of the chosen finite element approximation spaces. The constitutive model considered is based on the following convex multi-variable expansion

$$W_{simple} = \mu_1 II_{\boldsymbol{F}} + \mu_2 II_{\boldsymbol{H}} - 2(\mu_1 + 2\mu_2)\ln J + \frac{\lambda}{2}(J-1)^2 + \frac{1}{2\varepsilon_1} II_{\boldsymbol{d}} + \frac{1}{2\varepsilon_2} II_{\boldsymbol{D}_0}. \quad (6.49)$$

The material parameters in (6.49) are presented in Table 6.2. In order to study

$\mu_1\,(Pa)$	$\mu_2\,(Pa)$	$\lambda\,(Pa)$	$\varepsilon_1\,(N/V^2)$	$\varepsilon_2\,(N/V^2)$
1	$\frac{1}{2}$	1	4	4

Table 6.2: Material properties for example 6.3.2. Parameters f_e and f_s defined in equations (5.83) and (5.84), respectively.

the p-order of convergence of the new mixed Finite Element formulations, the analysis of an ad-hoc test problem is carried out. The problem is constructed so that smoothness of the solution is guaranteed. For that purpose, the following simple exact fields associated to the deformed or Eulerian configuration $\boldsymbol{x}$ and the electric potential φ are considered

$$\boldsymbol{x}^{\text{exact}} = \boldsymbol{X} + \begin{bmatrix} AX_1^3 \\ BX_1^3 \\ CX_1^3 \end{bmatrix}; \qquad \varphi^{\text{exact}} = \varphi_0 X_1^3, \quad (6.50)$$

where the superscript in (6.50) is used to emphasise the exact smooth solution with $A = 0.1$, $B = 0.2$, $C = 0.3$ and $\varphi_0 = 10^4$. The deformation gradient tensor and the Lagrangian electric field are obtained via equations (2.1) and (5.5a), respectively, leading to

$$\boldsymbol{F}^{\text{exact}} = \begin{bmatrix} 1+3AX_1^2 & 0 & 0 \\ 0 & 1+3BX_2^2 & 0 \\ 0 & 0 & 1+3CX_3^2 \end{bmatrix}; \qquad \boldsymbol{E}_0^{\text{exact}} = -\begin{bmatrix} 3\varphi_0 X_1^2 \\ 0 \\ 0 \end{bmatrix}. \quad (6.51)$$

The remaining variables defining multi-variable convexity, namely $\{\boldsymbol{H}, J, \boldsymbol{D}_0, \boldsymbol{d}\}$ need to be obtained for the smooth displacement and electric potential fields in equation (6.50). Particularisation of equation (2.26) for the smooth fields in equations (6.50) enables $\boldsymbol{H}^{\text{exact}}$ and J^{exact} to be obtained as

$$\boldsymbol{H}^{\text{exact}} = \frac{1}{2}\boldsymbol{F}^{\text{exact}} \boldsymbol{\times} \boldsymbol{F}^{\text{exact}}; \qquad J^{\text{exact}} = \frac{1}{3}\boldsymbol{H}^{\text{exact}} : \boldsymbol{F}^{\text{exact}}. \quad (6.52)$$

Particularisation of equation (5.17) to the constitutive model in equation (6.49) leads to

$$\frac{1}{\varepsilon_2}\boldsymbol{D}_0^{\text{exact}} + \frac{1}{\varepsilon_1}\left(\boldsymbol{F}^{\text{exact}}\right)^T \boldsymbol{d}^{\text{exact}} = \boldsymbol{E}_0^{\text{exact}}. \quad (6.53)$$

Making use of the relationship $\boldsymbol{d}^{\text{exact}} = \boldsymbol{F}^{\text{exact}}\boldsymbol{D}_0^{\text{exact}}$ in (6.53) results in the final expression of the Lagrangian electric displacement field $\boldsymbol{D}_0^{\text{exact}}$ as

$$\left(\frac{1}{\varepsilon_2}\boldsymbol{I} + \frac{1}{\varepsilon_1}\boldsymbol{C}^{\text{exact}}\right)\boldsymbol{D}_0^{\text{exact}} = \boldsymbol{E}_0^{\text{exact}} \Rightarrow \boldsymbol{D}_0^{\text{exact}} = \left(\frac{1}{\varepsilon_2}\boldsymbol{I} + \frac{1}{\varepsilon_1}\boldsymbol{C}^{\text{exact}}\right)^{-1}\boldsymbol{E}_0^{\text{exact}}. \tag{6.54}$$

where $\boldsymbol{C}^{\text{exact}}$ is the right Cauchy-Green tensor. Once all the elements of the set $\mathcal{V}^{\text{exact}}$ have been determined, it is possible to obtain the set of exact work conjugates $\Sigma_{\mathcal{V}}^{\text{exact}}$ via equation (5.13). Finally, the associated volumetric force and electric charge in mechanical and electrical equilibrium with the exact first Piola-Kirchhoff stress tensor $\boldsymbol{P}^{\text{exact}}$ and exact Lagrangian electric displacement field $\boldsymbol{D}_0^{\text{exact}}$ are determined from equations (5.6a) and (5.4a), respectively as

$$\boldsymbol{f}_0(\boldsymbol{x}^{\text{exact}}, \varphi^{\text{exact}}) = -\text{DIV}\boldsymbol{P}^{\text{exact}}; \qquad \rho_0(\boldsymbol{x}^{\text{exact}}, \varphi^{\text{exact}}) = \text{DIV}\boldsymbol{D}_0^{\text{exact}}, \tag{6.55}$$

where $\boldsymbol{D}_0^{\text{exact}}$ has been obtained in (6.54) and where $\boldsymbol{P}^{\text{exact}}$ can be obtained after application of equation (5.17).

It is then that the rate of convergence of the different variables $\{\boldsymbol{x}, \varphi, \mathcal{V}, \Sigma_{\mathcal{V}}\}$ to their analytical counterparts, namely $\{\boldsymbol{x}^{\text{exact}}, \varphi^{\text{exact}}, \mathcal{V}^{\text{exact}}, \Sigma_{\mathcal{V}}^{\text{exact}}\}$ can be studied. For that purpose, the same geometry as that presented in Section 6.3.2 is considered and initially discretised with $(2 \times 2 \times 2) \times 6$ tetrahedral elements and, subsequently, h-refinement is carried out generating a total of three discretisations.

The L^1 norm of the error for a particular component of the different variables involved, namely $\boldsymbol{x}$, $\boldsymbol{F}$, $\boldsymbol{H}$, J, $\boldsymbol{D}_0$, $\boldsymbol{d}$, $\boldsymbol{\Sigma}_{\boldsymbol{F}}$, $\boldsymbol{\Sigma}_{\boldsymbol{H}}$, Σ_J, $\boldsymbol{\Sigma}_{\boldsymbol{D}_0}$ and $\boldsymbol{\Sigma}_{\boldsymbol{d}}$ is investigated for two different choices of interpolation spaces, leading to the definition of two different Finite Element types. The first element, called "Element 1", corresponds to the choice of interpolation spaces described at the beginning of Section 5.6, namely, continuous quadratic interpolation of the displacement field (geometry) $\boldsymbol{x}$ and the electric potential field ϕ, piecewise linear interpolation of the conjugate pairs $\{\boldsymbol{F}, \boldsymbol{\Sigma}_{\boldsymbol{F}}\}$, $\{\boldsymbol{H}, \boldsymbol{\Sigma}_{\boldsymbol{H}}\}$, $\{\boldsymbol{D}_0, \boldsymbol{\Sigma}_{\boldsymbol{D}_0}\}$ and $\{\boldsymbol{d}, \boldsymbol{\Sigma}_{\boldsymbol{d}}\}$ and piecewise constant interpolation of the Jacobian J and its associated stress conjugate Σ_J. Alternatively, "Element 2" is characterised by the same choice of interpolation spaces for the electric potential (continuous quadratic interpolation) and for the pairs $\{\boldsymbol{F}, \boldsymbol{\Sigma}_{\boldsymbol{F}}\}$, $\{\boldsymbol{H}, \boldsymbol{\Sigma}_{\boldsymbol{H}}\}$, $\{\boldsymbol{D}_0, \boldsymbol{\Sigma}_{\boldsymbol{D}_0}\}$ and $\{\boldsymbol{d}, \boldsymbol{\Sigma}_{\boldsymbol{d}}\}$ (piecewise linear interpolation). The Jacobian and its work conjugate, namely J, Σ_J are interpolated using piecewise linear interpolation. Four cubic bubble functions are added at the barycentre of each face of the tetrahedron and a quartic bubble function is added at the barycentre of the tetrahedron itself, in analogy with the classical $P2^+ - P1$ Crouzeix-Raviart element [45], typically used in $u - p$ formulations for incompressible and nearly incompressible elasticity.

Figure 6.4 shows the order of accuracy of the different unknown variables for the mixed formulations (all yielding identical convergence pattern). Figure 6.4(a) displays the convergence of the variables $\{\boldsymbol{x}, \boldsymbol{F}, \boldsymbol{H}, J, \boldsymbol{D}_0, \boldsymbol{d}\}$ whereas Figure 6.4(c) displays the convergence of the variables $\{\boldsymbol{\Sigma}_{\boldsymbol{F}}, \boldsymbol{\Sigma}_{\boldsymbol{H}}, \Sigma_J, \boldsymbol{\Sigma}_{\boldsymbol{D}_0}, \boldsymbol{\Sigma}_{\boldsymbol{d}}\}$ for "Element 1". As expected, the constant interpolation of the Jacobian J and its work conjugate Σ_J affects the optimal convergence of the different variables, specially those

purely mechanical and the pair $\{\boldsymbol{d}, \boldsymbol{\Sigma_d}\}$, for which a decrease of one is observed in the order of convergence. Figure 6.4(b) displays the convergence of the variables $\{\boldsymbol{x}, \boldsymbol{F}, \boldsymbol{H}, J, \boldsymbol{D}_0, \boldsymbol{d}\}$ whereas Figure 6.4(d) displays the convergence of the variables $\{\boldsymbol{\Sigma_F}, \boldsymbol{\Sigma_H}, \Sigma_J, \boldsymbol{\Sigma_{D_0}}, \boldsymbol{\Sigma_d}\}$ for "Element 2". As expected, the convergence observed is $p+1$ in all the variables, since the convergence is optimal for this element.

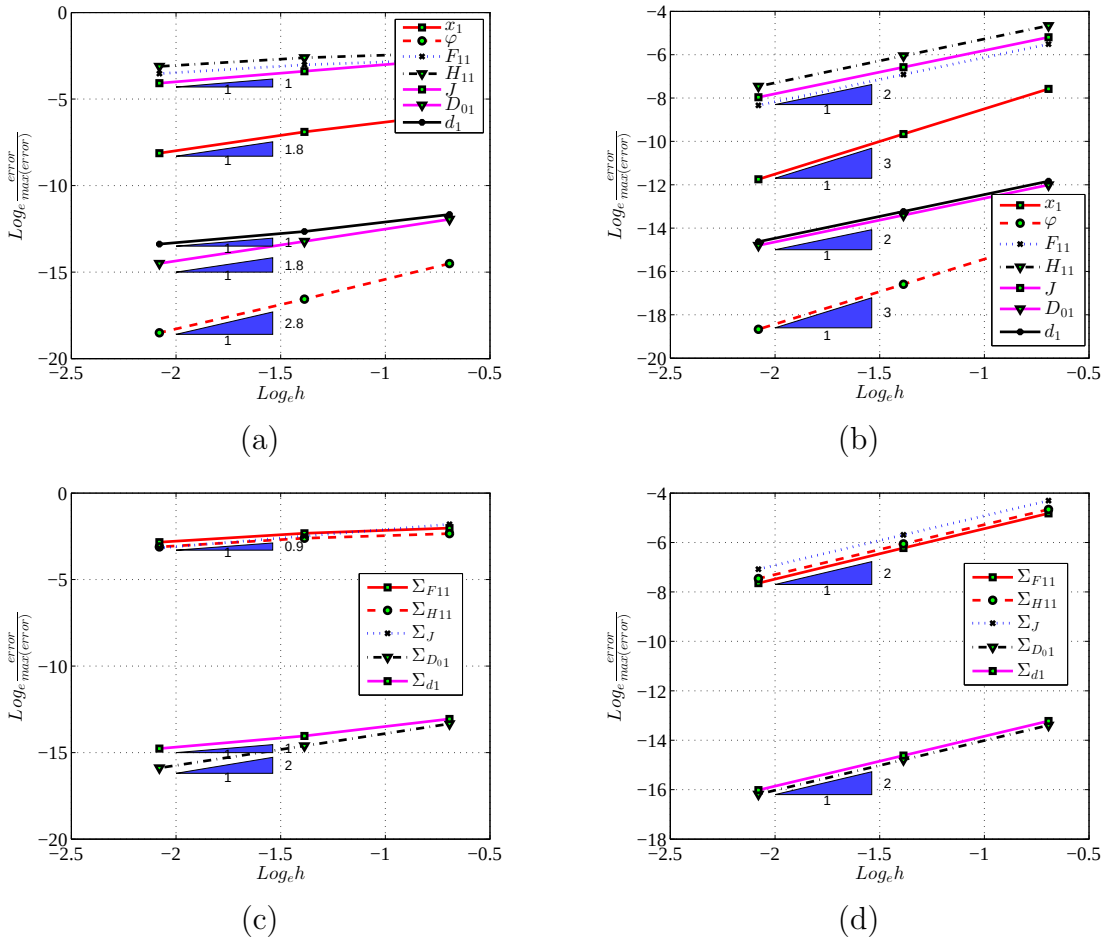

Figure 6.4: Convergence of the proposed formulation: order of accuracy of different strain, stress and electric magnitudes for the mixed formulations. Order of accuracy of the kinematic variables $\boldsymbol{x}$, $\boldsymbol{F}$, $\boldsymbol{H}$ and J and electric variables φ, $\boldsymbol{\Sigma_{D_0}}$ and $\boldsymbol{\Sigma_d}$ for (a) Element 1 and (b) Element 2. Order of accuracy of the kinetic variables $\boldsymbol{\Sigma_F}$, $\boldsymbol{\Sigma_H}$ and Σ_J and electric variables $\boldsymbol{D}_0$ and $\boldsymbol{d}$ (c) Element 1 and (d) Element 2. Constitutive model defined in (6.47). Results obtained with the **MΦF** formulation.

6.3.3 Comparison of performance between displacement-potential and mixed formulations

The objective of this example is to compare the solution obtained with the displacement-potential based formulation **DPF** against those obtained with the mixed formula-

tions **MΦF** and **MWF** in a bending dominated scenario and near the verge of incompressibility. A standard benchmark problem typically used in the computational mechanics community to test formulations under those specific conditions is the Cook's membrane problem [40, 44].

The geometry and boundary conditions of the membrane are depicted in Figure 6.5. The application of an electric potential in the electrodes leads to an out of plane bending-type deformation. In fact, although in more realistic geometrical configurations (the purpose of this example is exclusively to test the mixed formulations proposed), this type of potential Dirichlet boundary conditions are used in practical applications where dielectric elastomers and piezoelectric polymers are utilised as bending actuators.

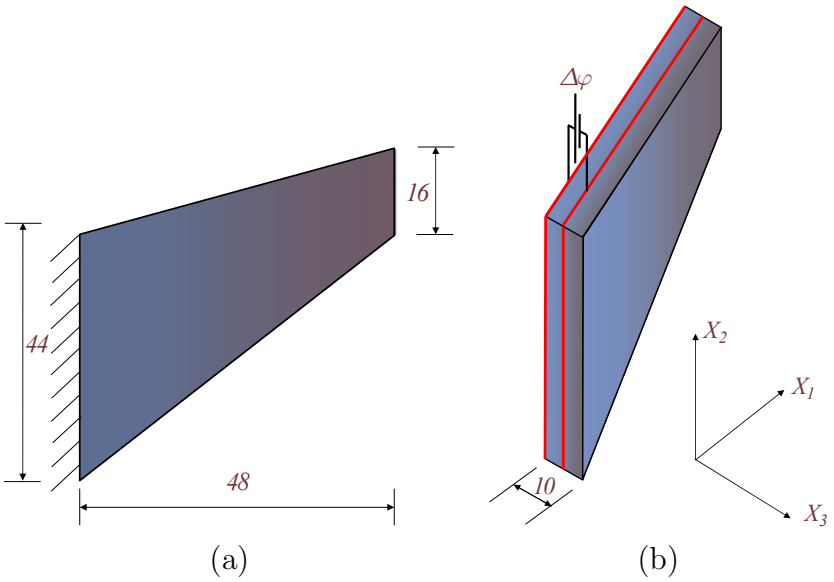

Figure 6.5: Comparison of performance between **DPF** and **MWF** formulations. Geometry and boundary conditions.

The constitutive model used is identical to that described in Section 6.3.1 in equation (6.47). The material properties in the reference configuration are chosen as $\mu = 10^5\,(Pa)$, $\hat{\lambda} = 4.99 \times 10^7\,(Pa)$ and $\varepsilon = 4.68\varepsilon 0$, which are compatible with a Poisson ratio of $\nu = 0.499$ in the reference configuration. The material parameters of the model, compatible with this definition in the reference configuration (as explained in Section 6.3.1), are chosen according to Table 6.3.

Figures 6.6(a)-(b) show the contour plot for the hydrostatic pressure p and for the stress variable $\boldsymbol{\Sigma}_{\boldsymbol{F}23}$ obtained with the **MWF** formulation. Finally, Figures 6.6(c)-(d) display the contour plot for the Eulerian electric field component $\boldsymbol{E}_1$ and the Eulerian displacement field component $\boldsymbol{D}_2$ obtained with the **MWF** formulation.

A detailed comparison between the results provided by the **DPF** and the mixed formulations is established in Table 6.5 for different meshes. For completeness, Table 6.4 displays the discretisation details for each of the meshes employed. Results are

$\mu_1\,(Pa)$	$\mu_2\,(Pa)$	$\lambda\,(Pa)$	$\varepsilon_1\,(N/V^2)$	$(\varepsilon_2)^{-1}\,(V^2/N)$	f_e	f_s
0.225μ	$0.5\mu_1$	4.99×10^7	$4.68\varepsilon_0$	0	1.0515	0.0996

Table 6.3: Material properties for example 6.3.3. Parameters f_e and f_s defined in equations (5.83) and (5.84), respectively.

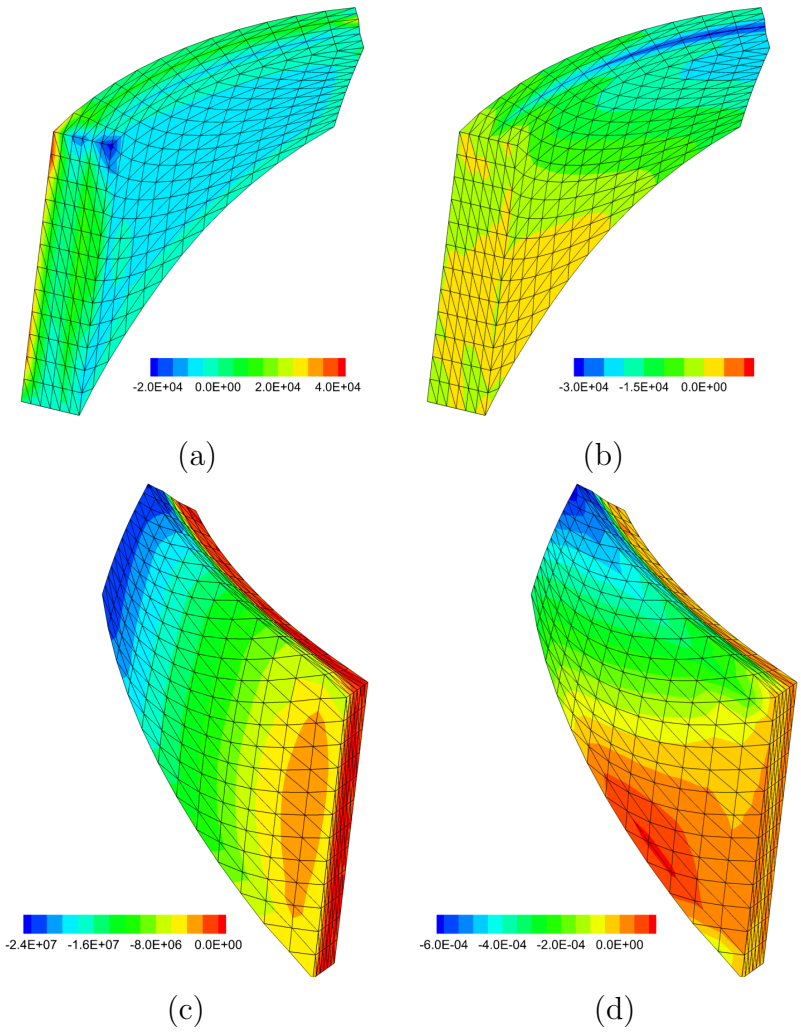

Figure 6.6: Contour plot of (a) the hydrostatic pressure (N/m^2), (b) stress conjugate variable $\boldsymbol{\Sigma}_{\boldsymbol{F}23}$ (N/m^2), (c) the electric field component $\boldsymbol{E}_1$ and (d) the electric displacement complement $\boldsymbol{D}_2$ for the **MWF** formulation. Polyconvex constitutive model in equation (6.47), with material parameters defined in Table 6.3. Electric potential difference $\Delta\varphi$ applied between electrodes of $140.49\,MV$. Results shown for a discretisation of $(12 \times 12 \times 4) \times 6$ tetrahedral elements ($8,125 \times 3$ and $8,125$ degrees of freedom associated to the spatial coordinates $\boldsymbol{x}$ and the electric potential, respectively).

Mesh	Elems.	Dofs. $\boldsymbol{x}$	Dofs. φ	Dofs. $\mathcal{U}$	Dofs. J, Σ_J
1	1,470	$2,475 \times 3$	2,475	$1,470 \times 4 \times 9$	$1,470 \times 1$
2	3,600	$5,730 \times 3$	5,730	$3,600 \times 4 \times 9$	$3,600 \times 1$
3	5,880	$9,251 \times 3$	9,251	$5,880 \times 4 \times 9$	$5,880 \times 1$

Table 6.4: Comparison of performance between **DPF** and **MWF** formulations. Mesh discretisation details. Column 2: number of tetrahedral elements (Elems.). Column 3: number of degrees of freedom (Dofs.) associated to the spatial coordinates $\boldsymbol{x}$. Columnn 4: number of degrees of freedom (Dofs.) associated to the electric potential. Column 5: number of degrees of freedom (Dofs.) associated to the fields $\mathcal{U} \equiv \{\boldsymbol{F}, \boldsymbol{H}, \boldsymbol{D}_0, \boldsymbol{\Sigma}_{\boldsymbol{F}}, \boldsymbol{\Sigma}_{\boldsymbol{H}}, \boldsymbol{\Sigma}_{\boldsymbol{D}_0}, \boldsymbol{\Sigma}_{\boldsymbol{d}}\}$. Column 6: number of degrees of freedom (Dofs.) associated to the strain/stress fields $\{J, \Sigma_J\}$.

presented for stresses, electric displacements and displacements sampled at points A, B and C ($\mathbf{X}_A = [24 \;\; 52 \;\; -2]^T$; $\mathbf{X}_B = [24 \;\; 22 \;\; -2]^T$; $\mathbf{X}_C = [48 \;\; 60 \;\; -2]^T$). As can be noticed, the **DPF** implementation underestimates the displacements obtained with respect to those for the alternative mixed formulations. As expected, regarding the stresses, the differences are very significant between both formulations. Whereas the results for the mixed formulations show a defined convergence pattern, the results of the **DPF** do not seem to converge, with clear pressure oscillations (even with incoherent changes in sign as mesh refinement is carried out).

6.3.4 Torsional actuator. Fibre reinforced dielectric elastomer

The objective of this example is to observe how the behaviour of a dielectric elastomer matrix can be modified when fibres are introduced in a specific direction characterised by the unit normal vector $\boldsymbol{N}$. The geometry and boundary conditions for this example are depicted in Figure 6.7(a), where the dimensions a, b and c are set to $a = 1$, $b = 2$ and $c = 10$. The actuator is completely fixed at the position $X_3 = 0$ ($0 \leq X_3 \leq 10$) and a pair of electrodes is located in $X_1 = -0.5$ and $X_1 = 0$, where $-0.5 \leq X_1 \leq 1$. Moreover, the dielectric elastomer matrix is reinforced with fibres oriented as in Figure 6.7(b). For clarity, the vector $\boldsymbol{N}$ in the direction of the fibres has been parametrised spherically in terms of the angles θ and ψ (refer to Figure 6.7(b)). In order to produce intricate deformation patterns, different arrangements of the fibres are used in the areas defined by the constraint $X_2 > 0$ and $X_2 < 0$, where $-1 \leq X_2 \leq 1$.

In order to account for the fibres in the constitutive model, an additive decomposition of the internal energy in terms of a purely isotropic component (associated to the dielectric elastomer matrix) and an anisotropic component (associated to the

	DPF formulation			**MWF** formulation		
	Coarse	Medium	Fine	Coarse	Medium	Fine
σ_{xx}^{A}	1192.87	333.04	118.32	520.28	494.75	412.81
σ_{xx}^{B}	1542.95	1033.10	739.31	415.80	325.46	233.81
σ_{yy}^{A}	1064.70	112.11	-123.94	132.35	157.46	155.31
σ_{yy}^{B}	1569.10	1046.26	734.48	260.29	159.92	87.60
σ_{zz}^{A}	1506.68	821.84	693.71	1199.33	1021.09	874.46
σ_{zz}^{B}	2169.36	1836.70	1570.01	1009.44	778.38	674.34
${D_{0z}}^{A}(\times 10^{-4})$	5.447	5.440	5.438	5.432	5.436	5.439
${D_{0z}}^{B}(\times 10^{-4})$	5.439	5.435	5.434	5.424	5.433	5.438
u_{x}^{C}	0.455	0.456	0.456	0.455	0.456	0.456
u_{y}^{C}	0.495	0.498	0.499	0.502	0.503	0.503
u_{z}^{C}	3.708	3.802	3.843	3.897	3.933	3.948

Table 6.5: Comparison of performance between **DPF** and **MWF** formulations. Stress components (kPa), electric displacement components ($10^{-4}N/mV$) and displacements (m) at points A, B and C. Results obtained using the **DPF** formulation (columns 2 to 4) and mixed formulations (columns 5 to 7). Prescribed potential difference $\Delta\varphi = 62.5\,MV/m$. Coarse, medium and fine discretisations of $(8 \times 8 \times 6) \times 6$, $(12 \times 12 \times 6) \times 6$ and $(16 \times 16 \times 6) \times 6$ tetrahedral elements, respectively.

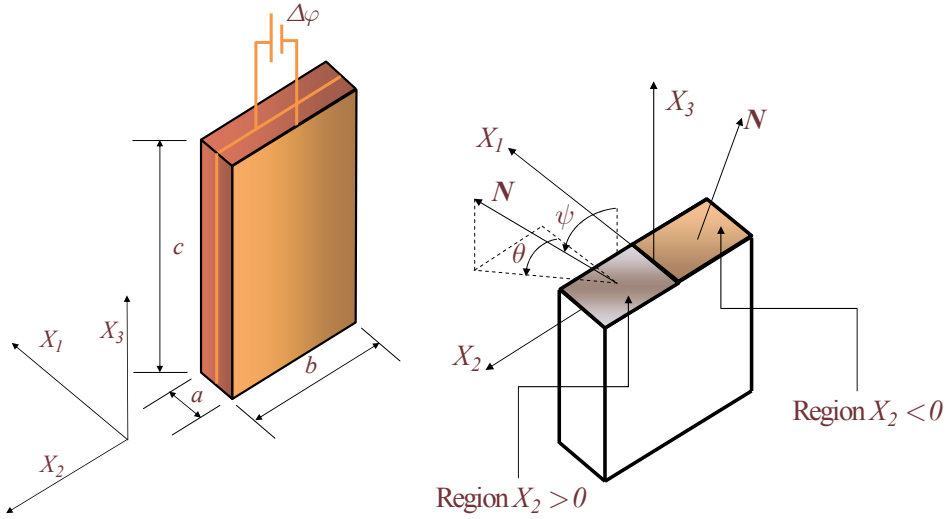

(a) (b)

Figure 6.7: Torsional actuator. Fibre reinforced dielectric elastomer. (a) Geometry and boundary conditions. (b) Arrangement of the fibres within the isotropic matrix. Illustration of spherical parametrisation of the vector $\boldsymbol{N}$ in the region characterised by $X_2 > 0$.

fibres) is followed as

$$W_{fibre} = W_{el} + W_{ani}(\boldsymbol{F}, \boldsymbol{H}, J, \boldsymbol{N}), \tag{6.56}$$

where the convex multi-variable isotropic component W_{el} has been defined in equation (6.47) and with $W_{ani}(\boldsymbol{F}, \boldsymbol{H}, J, \boldsymbol{N})$ defined as,

$$W_{ani}(\boldsymbol{F}, \boldsymbol{H}, J, \boldsymbol{N}) = \mu_3 II_{\boldsymbol{FN}} + \mu_3 II_{\boldsymbol{HN}} - 2\mu_3 \ln J. \tag{6.57}$$

Notice that the above additive decomposition of the internal energy W_{fibre} in (6.56) into its isotropic and anisotropic contributions, namely W_{el} and W_{ani} guarantees that the stress and the electric displacement field vanish in the reference configuration. Moreover, provided that μ_3 is positive, the anisotropic component W_{ani} in (6.57) is convex multi-variable itself. Hence, the resulting energy functional is convex multi-variable. The following choice of material parameters is used

$\mu_1\,(Pa)$	$\mu_2\,(Pa)$	$\mu_3\,(Pa)$	$\lambda\,(Pa)$	$\varepsilon_1\,(N/V^2)$	$(\varepsilon_2)^{-1}\,(V^2/N)$	f_e	f_s
$\frac{1}{20}\mu$	$\frac{1}{40}\mu$	$\frac{1}{2.63}\mu$	10^5	$4.68\varepsilon_0$	0	1.15	0.04

Table 6.6: Material properties for example 6.3.4. Parameters f_e and f_s defined in equations (5.83) and (5.84), respectively.

Figure 6.8 shows, for the same value of the applied electric potential, the deformed shape and the contour plots for the stress conjugate $\boldsymbol{\Sigma}_{\boldsymbol{F}11}$ and the Eulerian electric field component $\boldsymbol{E}_1$ corresponding to different orientations of the angles θ and ψ parametrising the unit vector $\boldsymbol{N}$ (see Figure 6.7(b)). Finally, Figure 6.9 shows the contour plot of the hydrostatic pressure p for different stages of the deformation corresponding to different values of the prescribed voltage in the electrodes for the particular arrangement of fibres described in Figure 6.8(b).

6.3.5 Twisting of piezoelectric energy harvester

This example includes the twisting of a piezoelectric material whose geometry is characterised by a length $L = 6m$ and a squared cross sectional area of side $a = 1m$. The energy harvester is clamped at its left end and subjected to a torsion on its right end. The electric potential is fixed to zero at the plane defined by the constraint $X_1 = 0$. This example is included to demonstrate the robustness of the mixed formulations in extreme deformation scenarios. The torsion at the right end is generated through Dirichlet boundary conditions as follows

$$(\boldsymbol{I} - \boldsymbol{E}_Y \otimes \boldsymbol{E}_Y)\,\boldsymbol{x} = \theta \boldsymbol{E}_Y \times \boldsymbol{X}, \tag{6.58}$$

where $\boldsymbol{E}_Y$ is the unit vector normal to the cross section in the reference configuration, $\boldsymbol{X}$ are the initial coordinates, θ is the angle of rotation and $\boldsymbol{x}$ are the final coordinates. As can be observed, the section is not restricted to in-plane torsion

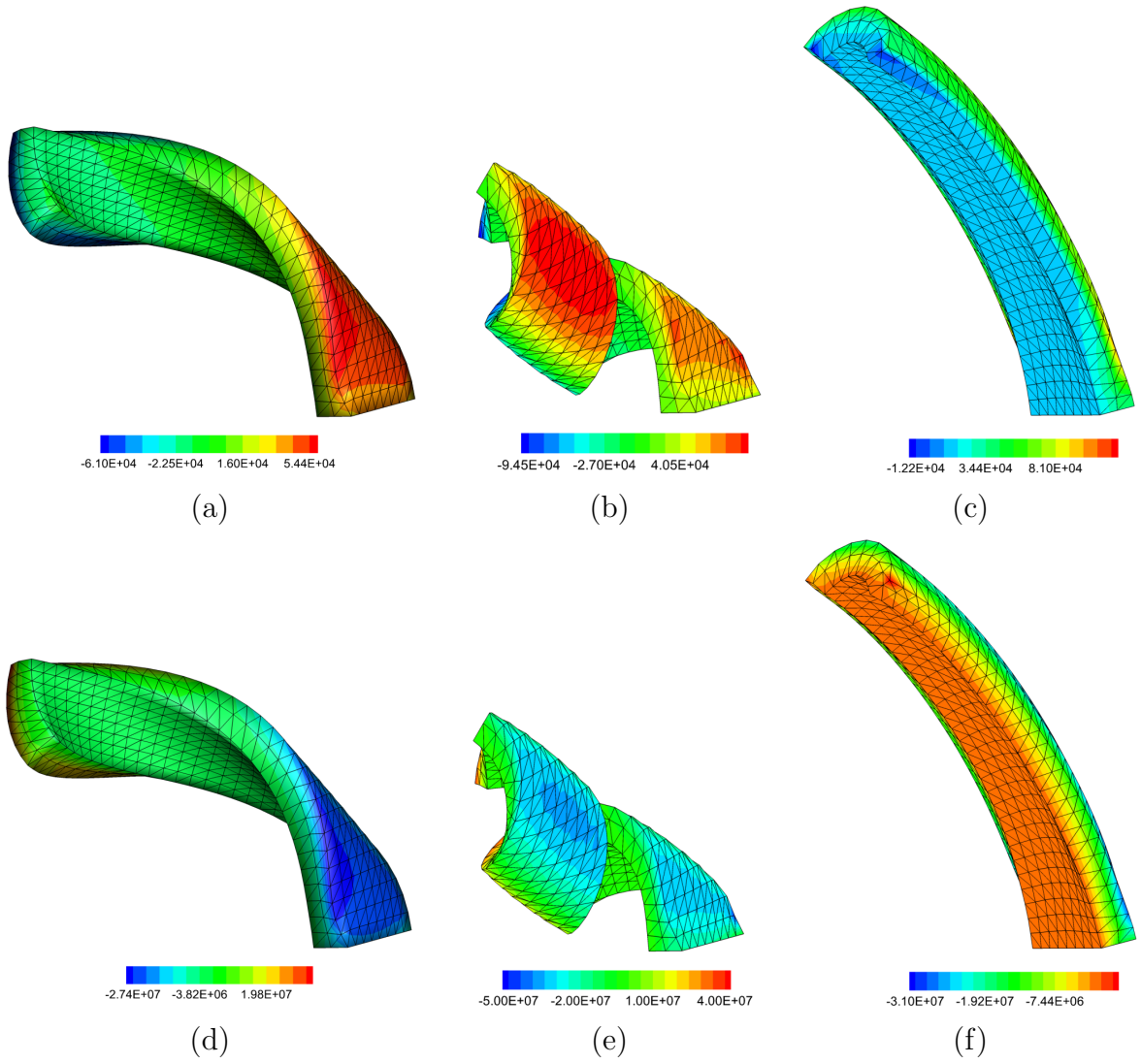

Figure 6.8: Torsional actuator. Fibre reinforced dielectric elastomer. Contour plot of hydrostatic pressure p and Eulerian electric field $\boldsymbol{E}_1$ for the following spherical parametrisation of the vector $\boldsymbol{N}$ in the direction of the fibres: (a) p and (d) $\boldsymbol{E}_1$ for $\theta = \pi/2$ and $\psi = \pi/4$ in $X_2 > 0$ and $\theta = -\pi/2$ and $\psi = \pi/4$ in $X_2 < 0$, (b) p and (e) $\boldsymbol{E}_1$ for $\theta = \psi = \pi/4$ in $X_2 > 0$ and $\theta = 5\pi/4$ and $\psi = \pi/4$ in $X_2 < 0$ and (c) p and (f) $\boldsymbol{E}_1$ for $\theta = \psi = 0$. Results obtained with the **MWF** formulation for $\Delta\varphi = 11.53\, MV/m$. Constitutive model defined in (6.56) and (6.57) with material parameters given in Table 6.6. Results shown for a discretisation of $(2 \times 8 \times 30) \times 6$ tetrahedral elements ($5,185 \times 3$ and $5,185$ degrees of freedom associated to the spatial coordinates $\boldsymbol{x}$ and electric potential, respectively).

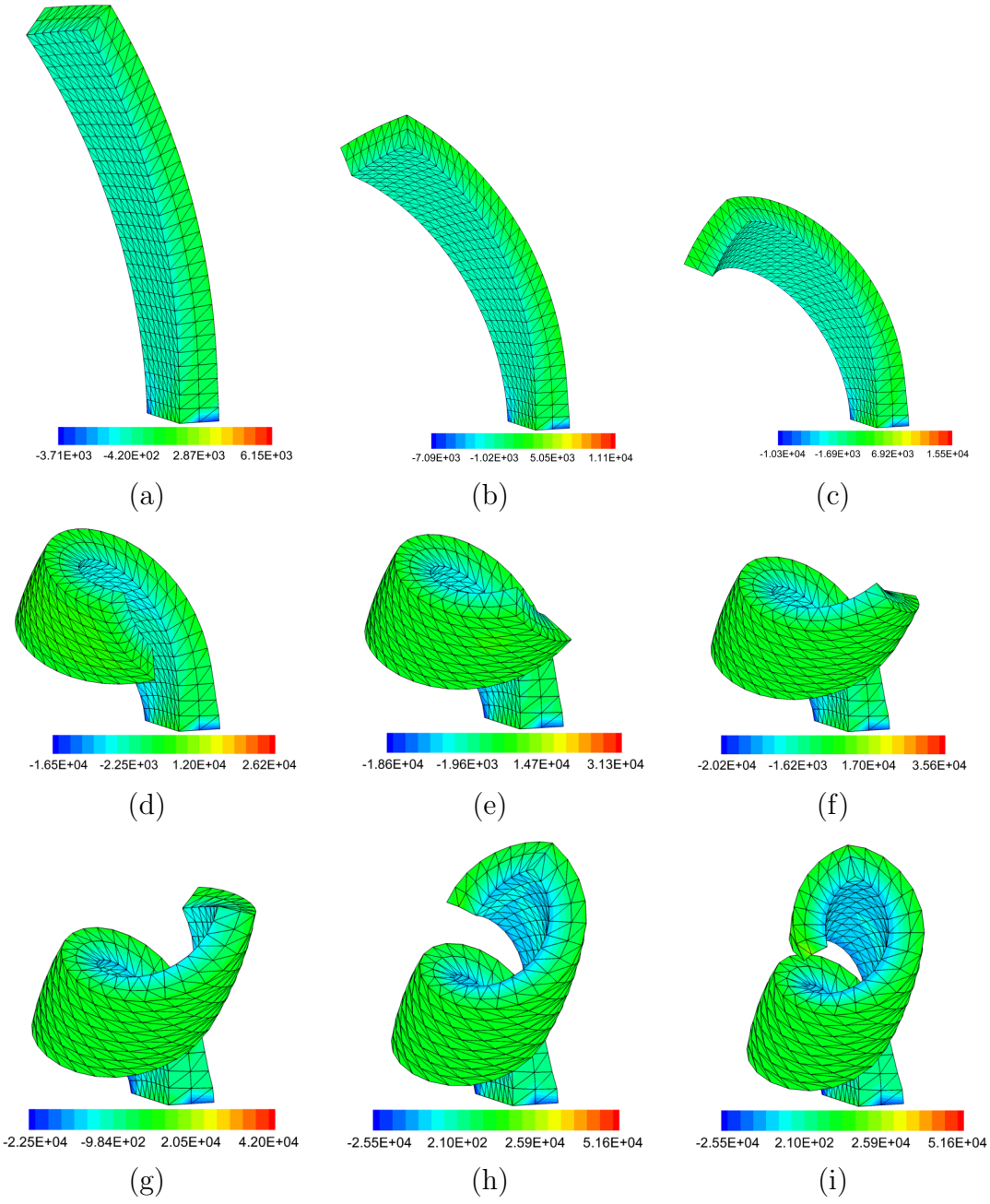

Figure 6.9: Torsional actuator. Fibre reinforced dielectric elastomer. Contour plot of the hydrostatic pressure p for (a) $\Delta\varphi = 5.49\,MV$, (b) $\Delta\varphi = 7.27\,MV$, (c) $\Delta\varphi = 8.43\,MV$, (d) $\Delta\varphi = 10.01\,MV$, (e) $\Delta\varphi = 10.43\,MV$, (f) $\Delta\varphi = 10.71\,MV$, (g) $\Delta\varphi = 11.07\,MV$, (h) $\Delta\varphi = 11.48\,MV$ and (i) $\Delta\varphi = 11.67\,MV$. Fibres arrangement: $\theta = \psi = \pi/4$ in $X_2 > 0$ and $\theta = 5\pi/4$ and $\psi = \pi/4$ in $X_2 < 0$. Results obtained with the mixed formulations. Constitutive model defined in (6.56) and (6.57) with material parameters given in Table 6.6. Results shown for a discretisation of $(2 \times 8 \times 30) \times 6$ tetrahedral elements ($5,185 \times 3$ and $5,185$ degrees of freedom associated to the spatial coordinates $\boldsymbol{x}$ and electric potential, respectively).

and zero Neumann boundary conditions are imposed normal to the cross sectional area. The same example in the context of pure elasticity has been presented by the authors in Reference [44].

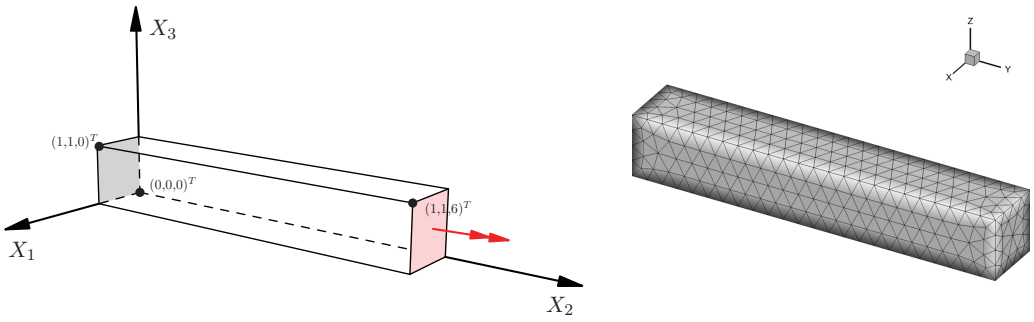

(a) (b)

Figure 6.10: Twisting of piezoelectric energy harvester. (a) Boundary conditions: clamped left end and twisting rotation applied at the right end. $\varphi = 0$ in plane $X_1 = 0$. Axes OX_1, OX_2 and OX_3 coincide with ox, oy and oz in (b), respectively. (b) Example of finite element discretisation: $(4 \times 4 \times 24) \times 6$ tetrahedral elements ($3,969 \times 3$ and $3,969$ degrees of freedom associated to the spatial coordinates $\boldsymbol{x}$ and electric potential, respectively).

The geometry and boundary conditions for the problem are depicted in Figure 6.10(a). In this example, a simple convex multi-variable constitutive model able to generate the direct piezoelectric effect is proposed. In particular, a transversely isotropic material characterised by a preferred direction $\boldsymbol{N}$ parallel to the axis OX_2 is considered. Notice that the aim of this example is not to fully characterise this specific material symmetry class. A simple convex multi-variable constitutive law for transverse isotropy incorporating piezoelectricity is proposed as,

$$W_p = \mu_1 II_{\boldsymbol{F}} + \mu_2 II_{\boldsymbol{H}} + \frac{1}{2J\varepsilon_1} II_{\boldsymbol{d}} + \frac{1}{2\varepsilon_2} II_{\boldsymbol{D}_0} + \mu_3 II_{\boldsymbol{v}} + g(J, \boldsymbol{D}_0, \boldsymbol{N}), \tag{6.59}$$

where the vector $\boldsymbol{v}$ in above equation (6.59) is defined as,

$$\boldsymbol{v} = \frac{\boldsymbol{d}}{\sqrt{\mu_3 \varepsilon_3}} + \boldsymbol{F}\boldsymbol{N}, \tag{6.60}$$

where μ_3 has units of stress, namely (Pa) and ε_3 of electric permittivity, namely (N/V^2) . The convex function g in above equation (6.59) has been introduced to guarantee that both the stress and the electric field in the reference configuration vanish. A possible choice of g which satisfies that condition is,

$$g(J, \boldsymbol{D}_0, \boldsymbol{N}) = -\left(2\mu_1 + 4\mu_2 + 2\mu_3\right) \ln J + \frac{\lambda}{2}\left(J-1\right)^2 - 2\sqrt{\frac{\mu_3}{\varepsilon_3}} \boldsymbol{D}_0 \cdot \boldsymbol{N}. \tag{6.61}$$

$\mu_1\,(GPa)$	$\mu_2\,(GPa)$	$\mu_3\,(GPa)$	$\lambda\,(GPa)$	$\varepsilon_1\,(N/V^2)$	$\varepsilon_2\,(N/V^2)$	$\varepsilon_3\,(N/V^2)$
1	$\frac{1}{2}$	$\frac{1}{2}$	495	$4.68\varepsilon_0$	$10^6\varepsilon_1$	$10^3\varepsilon_1$

Table 6.7: Material properties for example 6.3.5.

Notice that the proposed constitutive law defined in equations (6.59) and (6.61) is convex multi-variable. The material parameters in above equation (6.59) has been chosen according to Table 6.7.

Notice that now the material parameters in Table 6.7 are more consistent with those of piezoelectric polymers. Figures 6.11(a)-(d) display the contour plot of the stress component $\boldsymbol{\sigma}_{12}$, the stress conjugate $\boldsymbol{\Sigma}_{\boldsymbol{F}32}$, and the components of the Eulerian electric displacement field $\boldsymbol{D}_1$ and $\boldsymbol{D}_3$, respectively.

6.4 Concluding remarks

This Chapter encompasses the work in Reference [75], where a new computational framework tailor–made for the numerical simulation of electro active polymers subjected to extreme deformations and/or electric fields was developed. In this Reference (and in Chapter 5) Gil and Ortigosa proposed an extension of the concept of polyconvexity to the field of nonlinear electro-elasticity, via a convex multi-variable definition the internal energy with respect to the deformation gradient $\boldsymbol{F}$, its cofactor $\boldsymbol{H}$, its Jacobian J, the Lagrangian electric displacement field $\boldsymbol{D}_0$ and an additional spatial or Eulerian vector $\boldsymbol{d}$ computed as the product between the deformation gradient tensor and the Lagrangian electric displacement field.

The new definition of multi-variable convexity electro-elasticity has enabled a new family of new mixed variational principles to be defined for the first time (refer to Section 5.4). This Chapter has focussed on the Finite Element discretisation of two of those types of mixed variational principles. These types of Finite Element enhanced methodologies are necessary in scenarios in which the simpler displacement potential based formulation yields non-physical results, such as volumetric locking, bending and shear locking, pressure oscillations and electro-mechanical locking, to name but a few. The applicability, accuracy and robustness of the new formulation are demonstrated via a series of challenging numerical examples, including both isotropic and anisotropic convex multi-variable constitutive models.

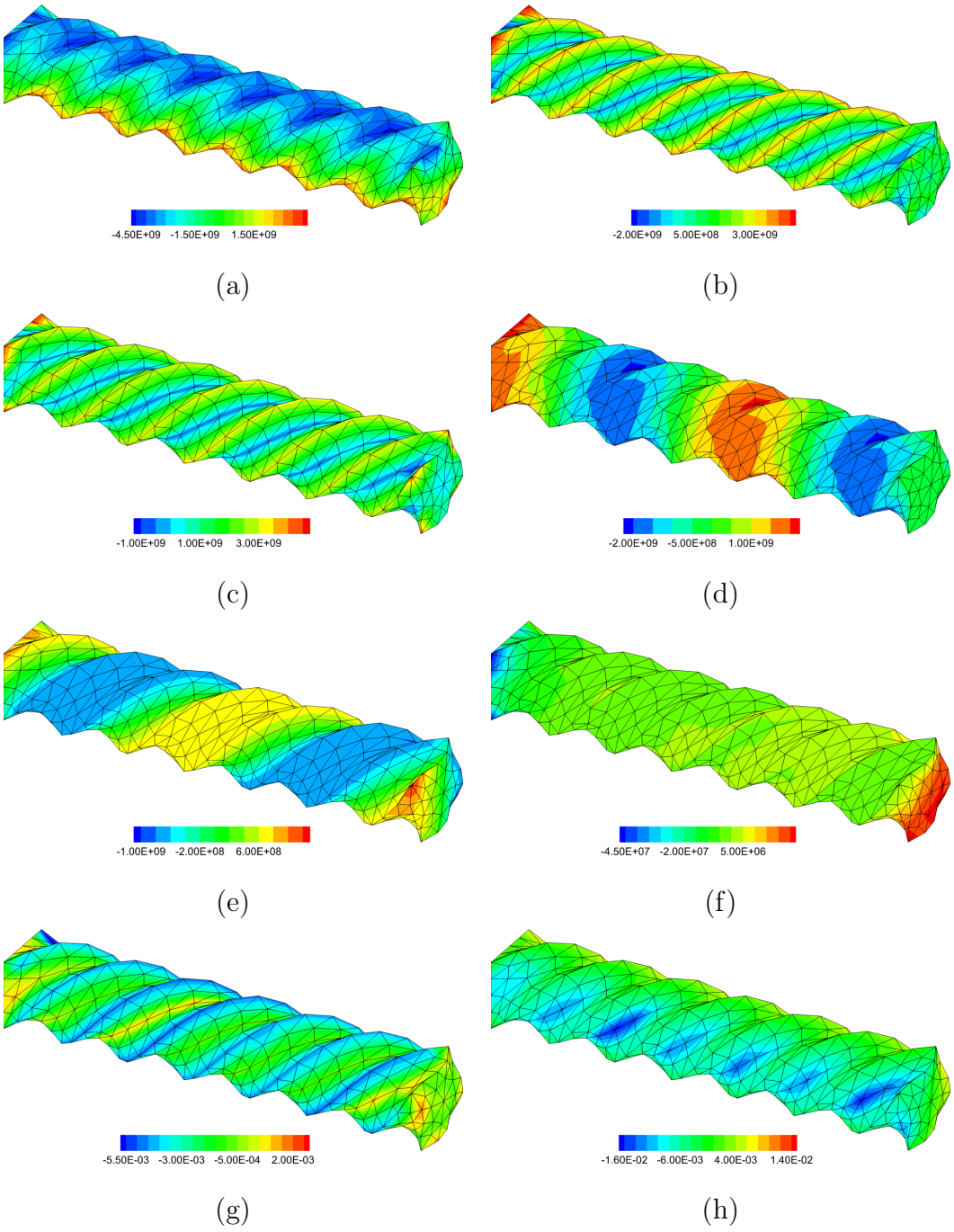

Figure 6.11: Twisting of piezoelectric energy harvester. Contour plots corresponding to (a) $\boldsymbol{\sigma}_{12}$, (b) $\boldsymbol{\sigma}_{22}$, (c) p, (d) $\boldsymbol{\Sigma}_{\boldsymbol{F}11}$, (e) $\boldsymbol{\Sigma}_{\boldsymbol{H}21}$, (f) φ, (g) $\boldsymbol{D}_2$ and (h) $\boldsymbol{D}_3$. Results obtained with the new mixed formulations. Constitutive model defined in (6.59) and (6.61) with material parameters given Table 6.7. Results shown for a discretisation of $(4 \times 4 \times 24) \times 6$ tetrahedral elements ($3,969 \times 3$ and $3,969$ degrees of freedom associated to the spatial coordinates $\boldsymbol{x}$ and electric potential, respectively).

Chapter 7

First order hyperbolic framework for convex multi-variable electro-magneto-mechanics

7.1 Introduction

In this Chapter, unlike the two preceding Chapters, where only electromechanical interactions were considered, a more general scenario characterised by the coexistence of both electromechanical and magnetomechanical interactions will be analysed. Notice that this more general situation, characterised by a more complex physical coupling, is deliberately considered as it enables to particularise the resulting hyperbolic framework to more specific scenarios suitable for either electroactive materials (characterised by the existence of electromechanical interactions) or magnetoactive materials (characterised by the existence of magnetomechanical interactions).

Starting with the same rationale as in Chapter 5, an extension of the new concept of multi-variable convexity is proposed in this Chapter for the more general scenario of nonlinear electro-magneto-mechanics. The extended set of variables which define multi-variable convexity is now enriched with two additional variables accounting for the magnetic nature of the problem, namely the Lagrangian magnetic induction and a spatial or Eulerian magnetomechanical variables $\boldsymbol{b}$ analogous to $\boldsymbol{d}$ in the context of electroelasticity (refer to equation (5.9)). The resulting extended set, i.e, $\mathcal{V} = \{\boldsymbol{F}, \boldsymbol{H}, J, \boldsymbol{D}_0, \boldsymbol{B}_0, \boldsymbol{d}, \boldsymbol{b}\}$ enables to extend concept of ellipticity to the entire range of deformations, electric and magnetic fields hence, guaranteeing the material stability of the constitutive equations.

Conservation laws for each of the arguments of the extended set $\mathcal{V}$ will be presented in this Chapter. Conservation laws for the purely geometrical arguments of $\mathcal{V}$, namely $\boldsymbol{F}$, $\boldsymbol{H}$ and J have been presented in Chapter 4. Moreover, the Maxwell equations represent first order hyperbolic conservation laws for $\boldsymbol{D}_0$ and $\boldsymbol{B}_0$. However, two completely new conservation laws for the electromehcanical and magnetomechanical variables $\boldsymbol{d}$ and $\boldsymbol{b}$, respectively are presented in this Chapter.

The extended set of variables, namely $\{\boldsymbol{F}, \boldsymbol{H}, J, \boldsymbol{D}_0, \boldsymbol{B}_0, \boldsymbol{d}, \boldsymbol{b}\}$ enables a new set of entropy conjugate variables $\{\boldsymbol{\Sigma}_{\boldsymbol{F}}, \boldsymbol{\Sigma}_{\boldsymbol{H}}, \Sigma_J, \boldsymbol{\Sigma}_{\boldsymbol{D}_0}, \boldsymbol{\Sigma}_{\boldsymbol{B}_0}, \boldsymbol{\Sigma}_{\boldsymbol{d}}, \boldsymbol{\Sigma}_{\boldsymbol{b}}\}$ [84] to be introduced. Multi-variable convexity of the internal energy guarantees that the relationship between both sets of variables is one to one and invertible. Crucially, and in line with the pioneering work of Hughes *et al.* [2] in the context of Computational Fluid Dynamics and later Bonet *et al.* [43] in the context of nonlinear Computational Solid Dynamics (recapitulated in Chapter 4), the new definition of multi-variable enables a generalised convex entropy function to be defined in the context of nonlinear electro-magneto-mechanics.

The existence of the generalised entropy function enables the transformation of the system of conservation laws in electro-magneto-mechanics into a symmetric set of hyperbolic equations when expressed in terms of the entropy conjugates of the conservation variables, as shown in Chapter 4 in the context of nonlinear elasticity. Furthermore, the eigenvalue structure [30] of the full new set of hyperbolic equations is studied in this Chapter.

This Chapter is organised as follows. Section 7.2 extends the new definition of multi-variable convexity introduced in Reference [76] and presented in Chapter

5 for nonlinear electro-magneto-mechanics. A completely new set of first order hyperbolic conservation laws is presented in this scenario. Section 7.3 presents the eigenvalue structure associated the set of first order hyperbolic equations in nonlinear electro-magneto-mechanics. Section 7.4 defines the generalised convex entropy function and its associated flux for the context of nonlinear electro-magneto-mechanics and presents the symmetric set of conservation laws expressed in terms of the new set of extended entropy variables. Finally, Section 7.5 focuses mainly on the analysis of material stability of convex multi-variable and non-convex multi-variable constitutive models suitable for the description of electrostrictive dielectric elastomers [5–8].

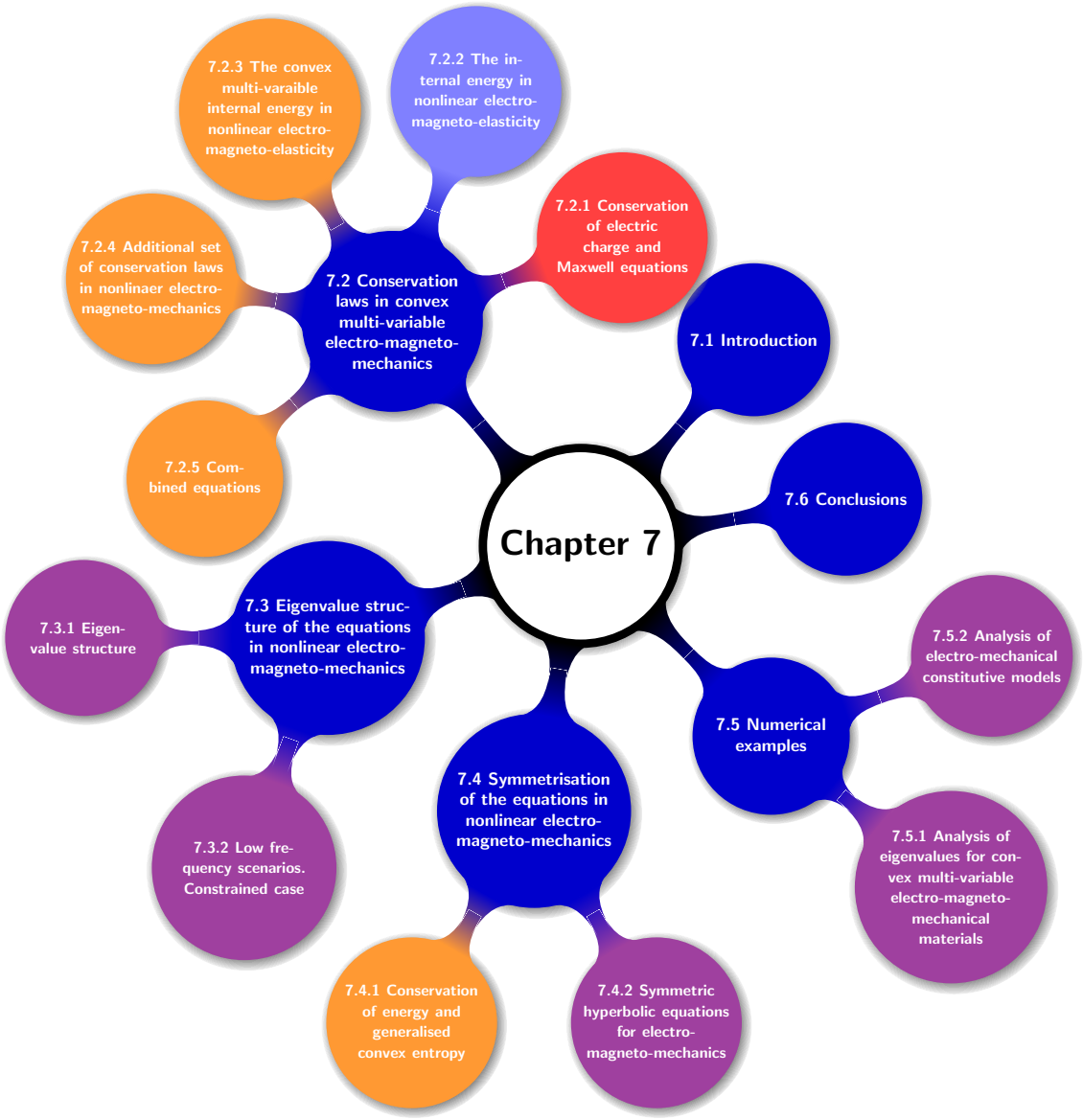

Figure 7.1: Chapter layout.

7.2 Conservation laws in convex multi-variable non-linear electro-magneto-mechanics

Let us consider the solid body described in Section 5.2. Let us assume that this material responds mechanically when magnetically excited [3]. Moreover, let us consider that electromechanical and magnetomechanical interactios are not exclusive. Starting with this material with a very highly coupled electro-magneto-mechanical response and following the rationale and notation as those in Chapter 4 (for the particular case of nonlinear elasticity), the objective of this Chapter is to present a first order hyperbolic framework for the more general case of electro-magneto-mechanics. Notice that we have deliberately avoided focussing on electro active materials (which do not exhibit magnetomechanical interactions) or magneto active materials (which do not exhibit electromechanical interactions). Following this more generic approach, it is possible to particularise the hyperbolic framework hereby developed to those more specific scenarios.

7.2.1 Conservation of mass and momentum

For the sake of completeness, we include in this Chapter both equations for the conservation of mass and linear momentum mathematically stated in Section 4.2.3 for the more specific case of pure elasticity. Let us recall (refer to equation (7.4)) that the conservation of mass for a Lagrangian setting can be written in terms of the Lagrangian (and therefore constant) density of the material ρ_0 as

$$\frac{d}{dt}\int_V \rho_0^e \, dV = 0, \tag{7.1}$$

which enables to not to incorporate the density within the vector of unknowns $\boldsymbol{\mathcal{U}}$ (refer to equation (4.2)). The global form of the conservation of linear momentum (refer to equation (4.8)) in a Lagrangian setting is hereby included for completeness too

$$\frac{d}{dt}\int_V \boldsymbol{p} \, dV = \int_{\partial V} \boldsymbol{t}_0 \, dA + \int_V \boldsymbol{f}_0 \, dV, \tag{7.2}$$

with its associated local form and jump conditions (refer to (4.9)), both in a Lagrangian setting expressed as

$$\frac{\partial \boldsymbol{p}}{\partial t} - \mathbf{DIV}\boldsymbol{P} = \boldsymbol{f}_0; \qquad U\left[\!\left[\boldsymbol{p}\right]\!\right] = -\left[\!\left[\boldsymbol{P}\right]\!\right]\boldsymbol{N}, \tag{7.3}$$

where the assumption of negligible vacuum effects has been made in above equations (7.2) and (7.3), hence leading to the relationship $\boldsymbol{PN} = \boldsymbol{t}_0$ in the boundary of the solid.

7.2.2 Conservation of electric charge and Maxwell equations

In a Lagrangian setting, conservation of electric charge is simply stated as

$$\frac{d}{dt}\int_V \rho_0^e \, dV = 0, \tag{7.4}$$

Analogously to the equation of conservation of mass in (7.1), equation (7.4) implies that the initial electric density charge of the material ρ_0^e is constant and therefore does not need to be considered as part of the vector of problem unknowns $\boldsymbol{\mathcal{U}}$. The Faraday and Ampère laws for an arbitrary Lagrangian volume can be established as

$$\frac{d}{dt}\int_V \boldsymbol{B}_0 \, dV = -\int_V \mathrm{CURL}\boldsymbol{E}_0 \, dV; \tag{7.5a}$$

$$\frac{d}{dt}\int_V \boldsymbol{D}_0 \, dV = \int_V \mathrm{CURL}\boldsymbol{H}_0 \, dV + \int_V \boldsymbol{J}_0 \, dV, \tag{7.5b}$$

where $\boldsymbol{D}_0$ and $\boldsymbol{B}_0$ denote the material form of the electric displacement field and the magnetic inductions, $\boldsymbol{E}_0$ and $\boldsymbol{H}_0$, the electric and magnetic fields, respectively and $\boldsymbol{J}_0$, a surface current density in the reference or material configuration. Application of the divergence theorem on both equations (7.5a) and (7.5b) results in the associated global conservation laws as

$$\frac{d}{dt}\int_V \boldsymbol{B}_0 \, dV = \int_{\partial V} \boldsymbol{E}_0 \times d\boldsymbol{A}; \tag{7.6a}$$

$$\frac{d}{dt}\int_V \boldsymbol{D}_0 \, dV = -\int_{\partial V} \boldsymbol{H}_0 \times d\boldsymbol{A} + \int_V \boldsymbol{J}_0 \, dV. \tag{7.6b}$$

Finally, the equivalent local differential equations and jump conditions are

$$\frac{\partial \boldsymbol{B}_0}{\partial t} + \mathrm{CURL}\boldsymbol{E}_0 = \boldsymbol{0}; \qquad U\left[\!\left[\boldsymbol{B}_0\right]\!\right] = -\left[\!\left[\boldsymbol{E}_0\right]\!\right] \times \boldsymbol{N}; \tag{7.7a}$$

$$\frac{\partial \boldsymbol{D}_0}{\partial t} - \mathrm{CURL}\boldsymbol{H}_0 = \boldsymbol{J}_0; \qquad U\left[\!\left[\boldsymbol{D}_0\right]\!\right] = \left[\!\left[\boldsymbol{H}_0\right]\!\right] \times \boldsymbol{N}; \tag{7.7b}$$

The Maxwell equations include two more differential equations: the Gauss law and the Gauss law for magnetism, which can be expressed as

$$\mathrm{DIV}\boldsymbol{D}_0 = \rho_0^e; \qquad \mathrm{DIV}\boldsymbol{B}_0 = 0. \tag{7.8}$$

There exists a clear similitude between equation (7.8) and equation (5.2). In fact, both Gauss laws in equation (7.8) can be seen as an additional set of (electromagnetic) involutions [113] to those described in equation (5.2) for the fibre and area maps which need to be satisfied by the conservation variables. Figure 7.2 illustrates the evolution of a continuum from the reference configuration to two different configurations at different time stages satisfying the mechanical and electromagnetic involutions in equations (5.2) and (7.8), respectively.

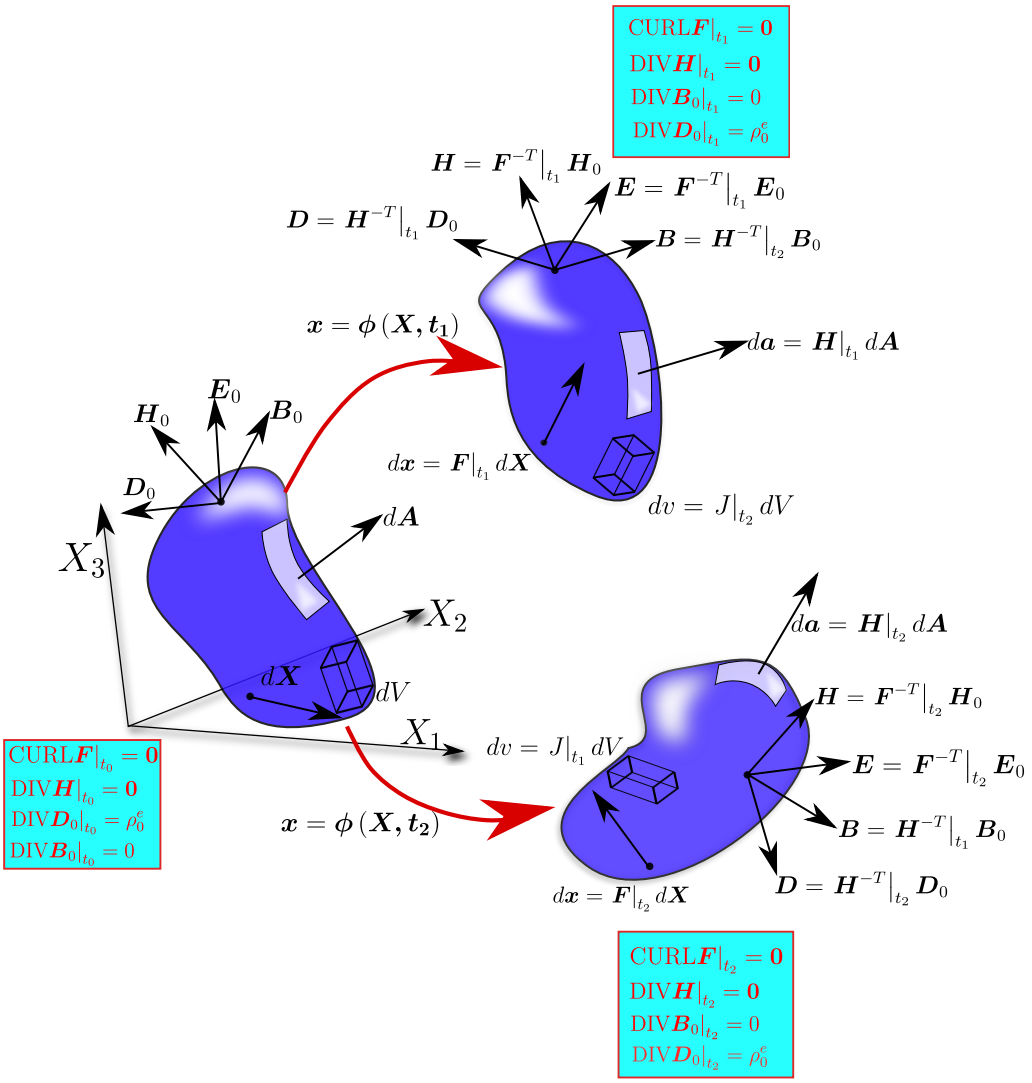

Figure 7.2: Evolution of the continuum from its reference configuration ($t = t_0$) to two different instants $t = t_1$ and $t = t_2$. Satisfaction of the associated involutions at every instant of the deformation. Evolution of the infinitesimal fibre, area and volume elements and of the Eulerian fields $\{\boldsymbol{E}, \boldsymbol{D}, \boldsymbol{H}, \boldsymbol{B}\}$.

7.2.3 The internal energy in nonlinear electro-magneto-elasticity

Equations (7.2), (7.5a) and (7.5b) establish a balance between the evolution of the conservation variables $\boldsymbol{p}$, $\boldsymbol{B}_0$ and $\boldsymbol{D}_0$ and their associated fluxes. These fluxes depend on the first Piola-Kirchhoff stress tensor $\boldsymbol{P}$ and the material form of the electric and magnetic fields, namely $\boldsymbol{E}_0$ and $\boldsymbol{H}_0$ respectively, which are determined based upon an appropriate constitutive law.

In the case of reversible electro-magneto-mechanics, where thermal effects and any other possible state variables (i.e. accumulated plastic deformation or electrical relaxation) are disregarded, constitutive laws can be derived from the internal energy density e per unit of undeformed volume, defined as

$$e = e(\boldsymbol{\nabla}_0 \boldsymbol{x}, \boldsymbol{D}_0, \boldsymbol{B}_0). \tag{7.9}$$

Notice that in the more specific scenario of electromechanics, the internal energy e is a function of the deformation gradient tensor and the electric displacement field, namely $e(\boldsymbol{\nabla}_0 \boldsymbol{x}, \boldsymbol{D}_0)$ (refer to equation (5.8) in Section 5.3.2). For the more general case considered now, the first principle of thermodynamics (under the assumption of no dissipative effects) yields the following expression for the time derivative of the internal energy $e(\boldsymbol{\nabla}_0 \boldsymbol{x}, \boldsymbol{D}_0, \boldsymbol{B}_0)$

$$\dot{e} = \boldsymbol{P} : \boldsymbol{\nabla}_0 \boldsymbol{v} + \boldsymbol{E}_0 \cdot \dot{\boldsymbol{D}}_0 + \boldsymbol{H}_0 \cdot \dot{\boldsymbol{B}}_0. \tag{7.10}$$

Combination of equations (7.9) and (7.10), establishes the necessary constitutive relationships from which the first Piola-Kirchhoff stress tensor $\boldsymbol{P}$ and the material form of the electric and magnetic fields, namely $\boldsymbol{E}_0$ and $\boldsymbol{H}_0$ respectively, can be defined as

$$\boldsymbol{P} = \left.\frac{\partial e(\boldsymbol{F}, \boldsymbol{D}_0, \boldsymbol{B}_0)}{\partial \boldsymbol{F}}\right|_{\boldsymbol{F}=\boldsymbol{\nabla}_0 \boldsymbol{x}}; \quad \boldsymbol{E}_0 = \left.\frac{\partial e(\boldsymbol{F}, \boldsymbol{D}_0, \boldsymbol{B}_0)}{\partial \boldsymbol{D_0}}\right|_{\boldsymbol{F}=\boldsymbol{\nabla}_0 \boldsymbol{x}}; \quad \boldsymbol{H}_0 = \left.\frac{\partial e(\boldsymbol{F}, \boldsymbol{D}_0, \boldsymbol{B}_0)}{\partial \boldsymbol{D_0}}\right|_{\boldsymbol{F}=\boldsymbol{\nabla}_0 \boldsymbol{x}}. \tag{7.11}$$

7.2.4 The convex multi-variable internal energy in nonlinear electro-magneto-elasticity

Following the same rationale as in Section 5.3.2 in the context of electromechanics, it is possible to extended the concept of ellipticity to the entire range for deformations, electric fields and magnetic fields, via a convex multi-variable definition of the internal energy $e(\boldsymbol{\nabla}_0 \boldsymbol{x}, \boldsymbol{D}_0, \boldsymbol{B}_0)$ (7.9) as [74, 75]

$$e\left(\boldsymbol{\nabla}_0 \boldsymbol{x}, \boldsymbol{D}_0, \boldsymbol{B}_0\right) = W\left(\boldsymbol{F}, \boldsymbol{H}, J, \boldsymbol{D}_0, \boldsymbol{B}_0, \boldsymbol{d}, \boldsymbol{b}\right), \tag{7.12}$$

where W represents a convex multi-variable functional in terms of its extended set of arguments $\mathcal{V}$, defined as

$$\mathcal{V} = \{\boldsymbol{F}, \boldsymbol{H}, J, \boldsymbol{D}_0, \boldsymbol{B}_0, \boldsymbol{d}, \boldsymbol{b}\}, \tag{7.13}$$

with the electromechanical variable $\boldsymbol{d}$ defined as $\boldsymbol{F}\boldsymbol{D}_0$ (refer to equation (5.9)) and with the new magnetomechanical variable $\boldsymbol{b}$ defined as

$$\boldsymbol{b} = \boldsymbol{F}\boldsymbol{B}_0. \tag{7.14}$$

Work conjugate variables in convex multi-variable electro-magneto-mechanics

The definition of multi-variable convexity in equation (7.12) enables the introduction of a set of work conjugate variables $\Sigma_{\mathcal{V}} = \{\boldsymbol{\Sigma}_{\boldsymbol{F}}, \boldsymbol{\Sigma}_{\boldsymbol{H}}, \Sigma_J, \boldsymbol{\Sigma}_{\boldsymbol{D}_0}, \boldsymbol{\Sigma}_{\boldsymbol{B}_0}, \boldsymbol{\Sigma}_{\boldsymbol{d}}, \boldsymbol{\Sigma}_{\boldsymbol{b}}\}$ to those in the set $\mathcal{V}$ (7.13) defined as

$$\begin{aligned} \boldsymbol{\Sigma}_{\boldsymbol{F}} &= \frac{\partial W}{\partial \boldsymbol{F}}; \quad \boldsymbol{\Sigma}_{\boldsymbol{H}} = \frac{\partial W}{\partial \boldsymbol{H}}; \quad \Sigma_J = \frac{\partial W}{\partial J}; \\ \boldsymbol{\Sigma}_{\boldsymbol{D}_0} &= \frac{\partial W}{\partial \boldsymbol{D}_0}; \quad \boldsymbol{\Sigma}_{\boldsymbol{B}_0} = \frac{\partial W}{\partial \boldsymbol{B}_0}; \\ \boldsymbol{\Sigma}_{\boldsymbol{d}} &= \frac{\partial W}{\partial \boldsymbol{d}}; \quad \boldsymbol{\Sigma}_{\boldsymbol{b}} = \frac{\partial W}{\partial \boldsymbol{b}}. \end{aligned} \tag{7.15}$$

Using the properties of the tensor cross product in Reference [43,44], it is possible to obtain the time derivative of the internal energy e (7.9) now expressed in terms of $\mathcal{V}$ (7.13) as

$$\begin{aligned} \dot{e}(\boldsymbol{F}, \boldsymbol{D}_0, \boldsymbol{B}_0) &= \dot{W}(\boldsymbol{F}, \boldsymbol{H}, J, \boldsymbol{D}_0, \boldsymbol{d}, \boldsymbol{B}_0, \boldsymbol{b}) \\ &= \boldsymbol{\Sigma}_{\boldsymbol{F}} : \dot{\boldsymbol{F}} + \boldsymbol{\Sigma}_{\boldsymbol{H}} : \dot{\boldsymbol{H}} + \Sigma_J \dot{J} \\ &+ \boldsymbol{\Sigma}_{\boldsymbol{D}_0} \cdot \dot{\boldsymbol{D}}_0 + \boldsymbol{\Sigma}_{\boldsymbol{B}_0} \cdot \dot{\boldsymbol{B}}_0 \\ &+ \boldsymbol{\Sigma}_{\boldsymbol{d}} \cdot \dot{\boldsymbol{d}} + \boldsymbol{\Sigma}_{\boldsymbol{b}} \cdot \dot{\boldsymbol{b}} \\ &= (\boldsymbol{\Sigma}_{\boldsymbol{F}} + \boldsymbol{\Sigma}_{\boldsymbol{H}} \times \boldsymbol{F} + \Sigma_J \boldsymbol{H} + \boldsymbol{\Sigma}_{\boldsymbol{d}} \otimes \boldsymbol{D}_0 + \boldsymbol{\Sigma}_{\boldsymbol{b}} \otimes \boldsymbol{B}_0) : \boldsymbol{\nabla}_0 \boldsymbol{v} \\ &+ \left(\boldsymbol{\Sigma}_{\boldsymbol{D}_0} + \boldsymbol{F}^T \boldsymbol{\Sigma}_{\boldsymbol{d}}\right) \cdot \dot{\boldsymbol{D}}_0 + \left(\boldsymbol{\Sigma}_{\boldsymbol{B}_0} + \boldsymbol{F}^T \boldsymbol{\Sigma}_{\boldsymbol{b}}\right) \cdot \dot{\boldsymbol{B}}_0. \end{aligned} \tag{7.16}$$

Comparison of equations (7.16) against (7.10), enables the first Piola-Kirchhoff stress tensor $\boldsymbol{P}$ and the material form of the electric and magnetic fields, namely $\boldsymbol{E}_0$ and $\boldsymbol{H}_0$ respectively, to be expressed in terms of the elements of both sets $\mathcal{V}$ and $\Sigma_{\mathcal{V}}$ as

$$\boldsymbol{P} = \boldsymbol{\Sigma}_{\boldsymbol{F}} + \boldsymbol{\Sigma}_{\boldsymbol{H}} \times \boldsymbol{F} + \Sigma_J \boldsymbol{H} + \boldsymbol{\Sigma}_{\boldsymbol{d}} \otimes \boldsymbol{D}_0 + \boldsymbol{\Sigma}_{\boldsymbol{b}} \otimes \boldsymbol{B}_0; \tag{7.17a}$$

$$\boldsymbol{E}_0 = \boldsymbol{\Sigma}_{\boldsymbol{D}_0} + \boldsymbol{F}^T \boldsymbol{\Sigma}_{\boldsymbol{d}}; \tag{7.17b}$$

$$\boldsymbol{H}_0 = \boldsymbol{\Sigma}_{\boldsymbol{B}_0} + \boldsymbol{F}^T \boldsymbol{\Sigma}_{\boldsymbol{b}}. \tag{7.17c}$$

Finally, a convex multi-variable representation of the internal energy as that in equation (7.12) ensures that the extended Hessian operator of the extended internal

energy, namely $[\mathbb{H}_W]$ (7.12) is positive definite, with $[\mathbb{H}_W]$ defined as

$$[\mathbb{H}_W] = \begin{bmatrix} W_{\boldsymbol{FF}} & W_{\boldsymbol{FH}} & W_{\boldsymbol{F}J} & W_{\boldsymbol{F}\boldsymbol{D}_0} & W_{\boldsymbol{Fd}} & W_{\boldsymbol{F}\boldsymbol{B}_0} & W_{\boldsymbol{Fb}} \\ W_{\boldsymbol{HF}} & W_{\boldsymbol{HH}} & W_{\boldsymbol{H}J} & W_{\boldsymbol{H}\boldsymbol{D}_0} & W_{\boldsymbol{Hd}} & W_{\boldsymbol{H}\boldsymbol{B}_0} & W_{\boldsymbol{Hb}} \\ W_{J\boldsymbol{F}} & W_{J\boldsymbol{H}} & W_{JJ} & W_{J\boldsymbol{D}_0} & W_{J\boldsymbol{d}} & W_{J\boldsymbol{B}_0} & W_{J\boldsymbol{b}} \\ W_{\boldsymbol{D}_0\boldsymbol{F}} & W_{\boldsymbol{D}_0\boldsymbol{H}} & W_{\boldsymbol{D}_0J} & W_{\boldsymbol{D}_0\boldsymbol{D}_0} & W_{\boldsymbol{D}_0\boldsymbol{d}} & W_{\boldsymbol{D}_0\boldsymbol{B}_0} & W_{\boldsymbol{D}_0\boldsymbol{b}} \\ W_{\boldsymbol{dF}} & W_{\boldsymbol{dH}} & W_{\boldsymbol{d}J} & W_{\boldsymbol{d}\boldsymbol{D}_0} & W_{\boldsymbol{dd}} & W_{\boldsymbol{d}\boldsymbol{B}_0} & W_{\boldsymbol{db}} \\ W_{\boldsymbol{B}_0\boldsymbol{F}} & W_{\boldsymbol{B}_0\boldsymbol{H}} & W_{\boldsymbol{B}_0J} & W_{\boldsymbol{B}_0\boldsymbol{D}_0} & W_{\boldsymbol{B}_0\boldsymbol{d}} & W_{\boldsymbol{B}_0\boldsymbol{B}_0} & W_{\boldsymbol{B}_0\boldsymbol{b}} \\ W_{\boldsymbol{bF}} & W_{\boldsymbol{bH}} & W_{\boldsymbol{b}J} & W_{\boldsymbol{b}\boldsymbol{D}_0} & W_{\boldsymbol{bd}} & W_{\boldsymbol{b}\boldsymbol{B}_0} & W_{\boldsymbol{bb}} \end{bmatrix}. \tag{7.18}$$

A simple convex multi-variable electro-magneto-mechanical constitutive model

As an example, a simple internal energy functional which complies with the definition of multi-variable convexity in (7.12) can be defined as

$$W_1 = \mu_1 II_{\boldsymbol{F}} + \mu_2 II_{\boldsymbol{H}} + f(J) + \frac{1}{2\varepsilon_1} II_{\boldsymbol{D}_0} + \frac{1}{2\varepsilon_2} II_{\boldsymbol{d}} + \frac{1}{2\hat{\mu}_1} II_{\boldsymbol{B}_0} + \frac{1}{2\hat{\mu}_2} II_{\boldsymbol{b}}. \tag{7.19}$$

A possible definition of the function $f(J)$ in equation (7.19) could be [44]

$$f(J) = -2\left(\mu_1 + 2\mu_2\right) \ln J + \frac{\kappa}{2}\left(J-1\right)^2. \tag{7.20}$$

Moreover, multi-variable convexity is subject to positiveness of all the constants in above equation (7.19). Among those, μ_1, μ_2 and κ have unit of stress, namely N/m^2, ε_1 and ε_2 units of electric permittivity, namely N/V^2 and $\hat{\mu}_1$ and $\hat{\mu}_2$ units of magnetic permeability, namely N/A^2 , where A denote the Ampère units in the international system. These material parameters relate to the shear modulus μ, first Lamé parameter $\hat{\lambda}$, relative electric permittivity ε_r and relative magnetic permeability $\hat{\mu}_r$ of the material in the reference configuration as

$$\mu = 2\mu_1 + 2\mu_2; \qquad \hat{\lambda} = \kappa + 4\mu_2; \qquad \frac{1}{\varepsilon_1} + \frac{1}{\varepsilon_2} = \frac{1}{\varepsilon_r \varepsilon_0}; \qquad \frac{1}{\hat{\mu}_1} + \frac{1}{\hat{\mu}_2} = \frac{1}{\hat{\mu}_r \hat{\mu}_0}, \tag{7.21}$$

where ε_0 and $\hat{\mu}_0$ denote the electric permittivity and magnetic permeability of the vacuum, respectively, of value $\varepsilon_0 = 8.854 \times 10^{-12}\, N/V^2$ and $\hat{\mu}_0 = 1.256 \times 10^{-6}\, N/A^2$.

The work conjugates in (7.15) for the internal energy functional in (7.19) are

obtained as

$$\begin{aligned}
&\boldsymbol{\Sigma}_{\boldsymbol{F}} = 2\mu_1 \boldsymbol{F}; \quad \boldsymbol{\Sigma}_{\boldsymbol{H}} = 2\mu_2 \boldsymbol{H}; \quad \Sigma_J = f'(J) - \frac{1}{2\varepsilon_1 J^2} II_{\boldsymbol{d}}; \\
&\boldsymbol{\Sigma}_{\boldsymbol{D}_0} = \frac{1}{\varepsilon_2}\boldsymbol{D}_0; \quad \boldsymbol{\Sigma}_{\boldsymbol{d}} = \frac{1}{\varepsilon_1}\boldsymbol{d}; \\
&\boldsymbol{\Sigma}_{\boldsymbol{B}_0} = \frac{1}{\varepsilon_2}\boldsymbol{B}_0; \quad \boldsymbol{\Sigma}_{\boldsymbol{b}} = \frac{1}{\hat{\mu}_2}\boldsymbol{b}.
\end{aligned} \tag{7.22}$$

For the particular constitutive model defined in equation (7.19), the first Piola-Kirchhoff stress tensor and the material electric field are obtained according to equation (7.17) as

$$\begin{aligned}
\boldsymbol{P} =& 2\mu_1 \boldsymbol{F} + 2\mu_2 \boldsymbol{H} \times \boldsymbol{F} + f'(J)\boldsymbol{H} + \frac{1}{\varepsilon_2}\boldsymbol{d} \otimes \boldsymbol{D}_0 + \frac{1}{\hat{\mu}_2}\boldsymbol{b} \otimes \boldsymbol{B}_0; \\
\boldsymbol{E}_0 =& \frac{1}{\varepsilon_1}\boldsymbol{D}_0 + \frac{1}{\varepsilon_2}\boldsymbol{F}^T\boldsymbol{d}; \qquad \boldsymbol{H}_0 = \frac{1}{\hat{\mu}_1}\boldsymbol{B}_0 + \frac{1}{\hat{\mu}_2}\boldsymbol{F}^T\boldsymbol{b}.
\end{aligned} \tag{7.23}$$

Finally, the Hessian operator $[\mathbb{H}_W]$ in above equation (7.18) adopts the following diagonal positive definite representation,

$$[\mathbb{H}_W] = \begin{bmatrix}
2\mu_1\boldsymbol{\mathcal{I}} & \boldsymbol{0} & \boldsymbol{0} & \boldsymbol{0} & \boldsymbol{0} & \boldsymbol{0} & \boldsymbol{0} \\
\boldsymbol{0} & 2\mu_2\boldsymbol{\mathcal{I}} & \boldsymbol{0} & \boldsymbol{0} & \boldsymbol{0} & \boldsymbol{0} & \boldsymbol{0} \\
\boldsymbol{0} & \boldsymbol{0} & f''(J) & \boldsymbol{0} & \boldsymbol{0} & \boldsymbol{0} & \boldsymbol{0} \\
\boldsymbol{0} & \boldsymbol{0} & \boldsymbol{0} & \frac{1}{\varepsilon_1}\boldsymbol{I} & \boldsymbol{0} & \boldsymbol{0} & \boldsymbol{0} \\
\boldsymbol{0} & \boldsymbol{0} & \boldsymbol{0} & \boldsymbol{0} & \frac{1}{\varepsilon_2}\boldsymbol{I} & \boldsymbol{0} & \boldsymbol{0} \\
\boldsymbol{0} & \boldsymbol{0} & \boldsymbol{0} & \boldsymbol{0} & \boldsymbol{0} & \frac{1}{\hat{\mu}_1}\boldsymbol{I} & \boldsymbol{0} \\
\boldsymbol{0} & \boldsymbol{0} & \boldsymbol{0} & \boldsymbol{0} & \boldsymbol{0} & \boldsymbol{0} & \frac{1}{\hat{\mu}_2}\boldsymbol{I}
\end{bmatrix}. \tag{7.24}$$

7.2.5 Additional set of conservation laws in nonlinear electro-magneto-mechanics

The definition of multi-variable convexity in equation (7.12) represents a suitable relaxation of the convexity criteria on the internal energy $e(\boldsymbol{\nabla}_0\boldsymbol{x}, \boldsymbol{D}_0, \boldsymbol{B}_0)$ which is compatible with the Legendre-Hadamard condition (refer to Reference [76]) and which does not preclude buckling. This relaxation relies on the definition of the internal energy in terms of the extended set of variables $\mathcal{V}$ (7.13). Remarkably, each of the elements of the extended set $\mathcal{V}$ can be expressed as a first order conservation law, which enables to identify all the variables in $\mathcal{V}$ as conservation variables. For instance, equations (7.7a) and (7.7b) represent a set of conservation laws in terms of the conservation variables $\boldsymbol{D}_0$ and $\boldsymbol{B}_0$. Moreover, Section 4.2.4, following the work of References [42, 43, 57, 58, 99, 104, 105] has presented the conservation laws associated to the purely kinematic entities of the set $\mathcal{V}$ (7.13), namely $\{\boldsymbol{F}, \boldsymbol{H}, J\}$. The objective of this section is to briefly recall the conservation laws for $\{\boldsymbol{F}, \boldsymbol{H}, J\}$ and then, to present two completely new conservation laws for the remaining variables in $\mathcal{V}$ (7.13), namely $\boldsymbol{d}$ and $\boldsymbol{b}$.

Conservation line, area and volume maps

The global form of the set of conservation laws associated to the purely kinematic arguments of the set $\mathcal{V}$ (7.13), namely $\{\boldsymbol{F}, \boldsymbol{H}, J\}$ have been presented in equations (4.11), (4.15) and (4.19), respectively. For the sake of completeness, we recall this equations hereby as,

$$\frac{d}{dt}\int_V \boldsymbol{F}\, dV = \int_{\partial V} \frac{1}{\rho_0}\boldsymbol{p} \otimes\, d\boldsymbol{A}; \tag{7.25a}$$

$$\frac{d}{dt}\int_V \boldsymbol{H}\, dV = \int_{\partial V} \boldsymbol{F} \boldsymbol{\times} \left(\frac{1}{\rho_0}\boldsymbol{p} \otimes d\boldsymbol{A}\right); \tag{7.25b}$$

$$\frac{d}{dt}\int_V J\, dV = \int_{\partial V} \boldsymbol{H} : \left(\frac{1}{\rho_0}\boldsymbol{p} \otimes d\boldsymbol{A}\right). \tag{7.25c}$$

The corresponding local differential equations and jump conditions to those in equation (7.25) have been presented in equations (4.12), (4.16) and (4.20), respectively, which are hereby included for the sake of completeness, that is

$$\frac{\partial \boldsymbol{F}}{\partial t} - \mathrm{DIV}\left(\frac{1}{\rho_0}\boldsymbol{p} \otimes \boldsymbol{I}\right) = \boldsymbol{0}; \qquad U\left[\!\left[\boldsymbol{F}\right]\!\right] = -\left[\!\left[\frac{1}{\rho_0}\boldsymbol{p}\right]\!\right] \otimes \boldsymbol{N}; \tag{7.26a}$$

$$\frac{\partial \boldsymbol{H}}{\partial t} - \mathrm{CURL}\left(\frac{1}{\rho_0}\boldsymbol{p} \boldsymbol{\times} \boldsymbol{F}\right) = \boldsymbol{0}; \qquad U\left[\!\left[\boldsymbol{H}\right]\!\right] = -\boldsymbol{F} \boldsymbol{\times} \left[\!\left[\frac{1}{\rho_0}\boldsymbol{p}\right]\!\right] \otimes \boldsymbol{N}; \tag{7.26b}$$

$$\frac{\partial J}{\partial t} - \mathrm{DIV}\left(\frac{1}{\rho_0}\boldsymbol{H}^T\boldsymbol{p}\right) = 0; \qquad U\left[\!\left[J\right]\!\right] = -\boldsymbol{H} : \left(\left[\!\left[\frac{1}{\rho_0}\boldsymbol{p}\right]\!\right] \otimes \boldsymbol{N}\right). \tag{7.26c}$$

Conservation of $\boldsymbol{d}$

In order to evaluate global and local conservation laws for the electromechanical variable $\boldsymbol{d}$ $(7.14)_a$, let us recall its definition $\boldsymbol{d} = \boldsymbol{F}\boldsymbol{D}_0$. In the regions of the domain V where the fields are smooth, it is possible to obtain

$$\begin{aligned}\frac{\partial \boldsymbol{d}}{\partial t} = \frac{\partial \boldsymbol{F}}{\partial t}\boldsymbol{D}_0 + \boldsymbol{F}\frac{\partial \boldsymbol{D}_0}{\partial t} &= \boldsymbol{\nabla}_0\left(\frac{1}{\rho_0}\boldsymbol{p}\right)\boldsymbol{D}_0 + \boldsymbol{F}\left(\mathrm{CURL}\boldsymbol{H}_0 - \boldsymbol{J}_0\right) \\ &= \mathrm{DIV}\left(\frac{1}{\rho_0}\boldsymbol{p} \otimes \boldsymbol{D}_0\right) - \left(\mathrm{DIV}\boldsymbol{D}_0\right)\left(\frac{1}{\rho_0}\boldsymbol{p}\right) + \boldsymbol{F}\left(\mathrm{CURL}\boldsymbol{H}_0 - \boldsymbol{J}_0\right),\end{aligned} \tag{7.27}$$

where the local conservations laws for $\boldsymbol{F}$ and $\boldsymbol{D}_0$ in equations (7.26a) and (7.7b), respectively, have been conveniently substituted in above (7.27). Use of the involution equation for $\boldsymbol{D}_0$ $(7.8)_a$ into above equation (7.27) yields

$$\frac{\partial \boldsymbol{d}}{\partial t} = \mathrm{DIV}\left(\boldsymbol{v} \otimes \boldsymbol{D}_0\right) - \frac{\rho_0^e}{\rho_0}\boldsymbol{p} + \boldsymbol{F}\left(\mathrm{CURL}\boldsymbol{H}_0 - \boldsymbol{J}_0\right). \tag{7.28}$$

Let us now focus on the term $\boldsymbol{F}\mathrm{CURL}\boldsymbol{H}_0$ in above equation (7.28). Consideration of the *curl-free* involution equation for $\boldsymbol{F}$ in (4.1) enables us to re-write this term as

$$\left(\boldsymbol{F}\mathrm{CURL}\boldsymbol{H}_0\right)_i = F_{iI}\mathcal{E}_{IJK}\frac{\partial\left(\boldsymbol{H}_0\right)_K}{\partial X_J} = -\frac{\partial}{\partial X_J}\left(\mathcal{E}_{JIK}F_{iI}\left(\boldsymbol{H}_0\right)_K\right), \tag{7.29}$$

and hence,

$$\boldsymbol{F}\mathrm{CURL}\boldsymbol{H}_0 = -\mathrm{DIV}\left(\boldsymbol{F}\times\boldsymbol{H}_0\right). \tag{7.30}$$

Substitution of the above expression (7.30) into equation (7.28) finally yields the local conservation law for the variable $\boldsymbol{d}$ as

$$\frac{\partial \boldsymbol{d}}{\partial t} - \mathrm{DIV}\left(\frac{1}{\rho_0}\boldsymbol{p}\otimes\boldsymbol{D}_0 - \boldsymbol{F}\times\boldsymbol{H}_0\right) = -\boldsymbol{F}\boldsymbol{J}_0 - \frac{\rho_0^e}{\rho_0}\boldsymbol{p}. \tag{7.31}$$

With the purpose of deriving the correct jump conditions for the variable $\boldsymbol{d}$ across a discontinuity surface with unit normal $\boldsymbol{N}$ and moving with velocity U, let us note first that the jump of any product operation $(\bullet)$ of two conservation variables $\boldsymbol{a}$ and $\boldsymbol{b}$ across the discontinuity can be obtained as

$$\left[\!\left[\boldsymbol{a}\bullet\boldsymbol{b}\right]\!\right] = \bar{\boldsymbol{a}}\bullet\left[\!\left[\boldsymbol{b}\right]\!\right] + \left[\!\left[\boldsymbol{a}\right]\!\right]\bullet\bar{\boldsymbol{b}}, \tag{7.32}$$

where $\bar{\boldsymbol{a}}$ and $\bar{\boldsymbol{b}}$ denote the average values of both variables at both sides of the discontinuity, i.e, $\bar{\boldsymbol{a}} = \frac{1}{2}\left(\boldsymbol{a}^+ + \boldsymbol{a}^-\right)$. Hence, above equation (7.32) can be applied in order to compute the jump of the variable $\boldsymbol{d}$ as

$$\left[\!\left[\boldsymbol{d}\right]\!\right] = \left[\!\left[\boldsymbol{F}\boldsymbol{D}_0\right]\!\right] = \bar{\boldsymbol{F}}\left[\!\left[\boldsymbol{D}_0\right]\!\right] + \left[\!\left[\boldsymbol{F}\right]\!\right]\bar{\boldsymbol{D}}_0. \tag{7.33}$$

Introduction of the jump conditions for both $\boldsymbol{D}_0$ (7.7b) and $\boldsymbol{F}$ (7.26a) into (7.33) gives

$$U\left[\!\left[\boldsymbol{d}\right]\!\right] = \bar{\boldsymbol{F}}\left(\left[\!\left[\boldsymbol{H}_0\right]\!\right]\times\boldsymbol{N}\right) - \left(\left[\!\left[\frac{1}{\rho_0}\boldsymbol{p}\right]\!\right]\otimes\boldsymbol{N}\right)\bar{\boldsymbol{D}}_0. \tag{7.34}$$

Moreover, note that the second term of the right hand side of above equation (7.34) can be alternatively written as

$$\begin{aligned}
\left(\left[\!\left[\frac{1}{\rho_0}\boldsymbol{p}\right]\!\right]\otimes\boldsymbol{N}\right)\bar{\boldsymbol{D}}_0 &= \left[\!\left[\left(\frac{1}{\rho_0}\boldsymbol{p}\right)\left(\boldsymbol{D}_0\cdot\boldsymbol{N}\right)\right]\!\right] - \left(\frac{1}{\rho_0}\bar{\boldsymbol{p}}\right)\left[\!\left[\boldsymbol{D}_0\cdot\boldsymbol{N}\right]\!\right] \\
&= \left[\!\left[\frac{1}{\rho_0}\boldsymbol{p}\otimes\boldsymbol{D}_0\right]\!\right]\boldsymbol{N} - \left(\frac{1}{\rho_0}\bar{\boldsymbol{p}}\right)\left(\left[\!\left[\boldsymbol{D}_0\right]\!\right]\cdot\boldsymbol{N}\right) \\
&= \left[\!\left[\frac{1}{\rho_0}\boldsymbol{p}\otimes\boldsymbol{D}_0\right]\!\right]\boldsymbol{N} - \underbrace{\left(\frac{1}{U\rho_0}\bar{\boldsymbol{p}}\right)\left(\left[\!\left[\boldsymbol{H}_0\right]\!\right]\times\boldsymbol{N}\right)\cdot\boldsymbol{N}}_{=\boldsymbol{0}} \\
&= \left[\!\left[\frac{1}{\rho_0}\boldsymbol{p}\otimes\boldsymbol{D}_0\right]\!\right]\boldsymbol{N}.
\end{aligned} \tag{7.35}$$

Similarly, the first term on the right hand side of above equation (7.34) can be alternatively written as

$$\begin{aligned}\bar{\boldsymbol{F}}\left(\left[\!\left[\boldsymbol{H}_0\right]\!\right]\times\boldsymbol{N}\right) &= -\left(\bar{\boldsymbol{F}}\times\boldsymbol{N}\right)\left[\!\left[\boldsymbol{H}_0\right]\!\right]\\ &= -\left[\!\left[\left(\boldsymbol{F}\times\boldsymbol{N}\right)\boldsymbol{H}_0\right]\!\right]+\left[\!\left[\boldsymbol{F}\times\boldsymbol{N}\right]\!\right]\bar{\boldsymbol{H}}_0\\ &= \left[\!\left[\boldsymbol{F}\times\boldsymbol{H}_0\right]\!\right]\boldsymbol{N}-\frac{1}{U\rho_0}\left(\left(\left[\!\left[\boldsymbol{p}\right]\!\right]\otimes\boldsymbol{N}\right)\times\boldsymbol{N}\right)\bar{\boldsymbol{H}}_0\\ &= \left[\!\left[\boldsymbol{F}\times\boldsymbol{H}_0\right]\!\right]\boldsymbol{N}-\underbrace{\frac{1}{U\rho_0}\left(\left[\!\left[\boldsymbol{p}\right]\!\right]\otimes\left(\boldsymbol{N}\times\boldsymbol{N}\right)\right)\bar{\boldsymbol{H}}_0}_{=\boldsymbol{0}}\\ &= \left[\!\left[\boldsymbol{F}\times\boldsymbol{H}_0\right]\!\right]\boldsymbol{N}.\end{aligned}\tag{7.36}$$

Introduction of both equations (7.35) and (7.36) into equation (7.34) finally yields the jump condition for $\boldsymbol{d}$

$$U\left[\!\left[\boldsymbol{d}\right]\!\right]=-\left(\left[\!\left[\frac{1}{\rho_0}\boldsymbol{p}\otimes\boldsymbol{D}_0\right]\!\right]-\left[\!\left[\boldsymbol{F}\times\boldsymbol{H}_0\right]\!\right]\right)\boldsymbol{N}.\tag{7.37}$$

Combination of the local conservation law for $\boldsymbol{d}$ in (7.31) and the jump conditions in (7.37) finally gives the global conservation law for this variable as

$$\frac{d}{dt}\int_V\boldsymbol{d}\,dV=\int_V\boldsymbol{\nabla}_0\left(\frac{1}{\rho_0}\boldsymbol{p}\right)\boldsymbol{D}_0\,dV+\int_V\boldsymbol{F}\left(\mathrm{CURL}\boldsymbol{H}_0-\boldsymbol{J}_0\right)\,dV.\tag{7.38}$$

Conservation of $\boldsymbol{b}$

Following a similar approach to that in the preceding Section, it is possible to derive the local form of the conservation law for the variable $\boldsymbol{b}$ $(7.14)_b$ and its associated jump conditions as

$$\frac{\partial\boldsymbol{b}}{\partial t}-\mathrm{DIV}\left(\frac{1}{\rho_0}\boldsymbol{p}\otimes\boldsymbol{B}_0+\boldsymbol{F}\times\boldsymbol{E}_0\right)=\boldsymbol{0};\quad U\left[\!\left[\boldsymbol{b}\right]\!\right]=-\left(\left[\!\left[\frac{1}{\rho_0}\boldsymbol{p}\otimes\boldsymbol{B}_0\right]\!\right]+\left[\!\left[\boldsymbol{F}\times\boldsymbol{E}_0\right]\!\right]\right)\boldsymbol{N}.\tag{7.39}$$

Combination of the local conservation law for $\boldsymbol{b}$ and its associated jump condition in above equation (7.39) enables to obtain the global conservation law for $\boldsymbol{b}$ as

$$\frac{d}{dt}\int_V\boldsymbol{b}\,dV=\int_{\partial V}\left(\frac{1}{\rho_0}\boldsymbol{p}\otimes\boldsymbol{B}_0\right)\,d\boldsymbol{A}+\int_{\partial V}\left(\boldsymbol{F}\times\boldsymbol{E}_0\right)\,d\boldsymbol{A}.\tag{7.40a}$$

7.2.6 Combined equations

Combining the results of the Sections above, a full set of first order conservation laws (4.3) can be established with vector of variables $\boldsymbol{\mathcal{U}}$, vector of fluxes $\boldsymbol{\mathcal{F}}_I$ and vector of source terms $\boldsymbol{\mathcal{S}}$ defined as

$$\boldsymbol{\mathcal{U}} = \begin{bmatrix} \boldsymbol{p} \\ \boldsymbol{F} \\ \boldsymbol{H} \\ J \\ \boldsymbol{D}_0 \\ \boldsymbol{B}_0 \\ \boldsymbol{d} \\ \boldsymbol{b} \end{bmatrix}; \qquad \boldsymbol{\mathcal{F}}_I = \begin{bmatrix} \boldsymbol{\mathcal{F}}_I^{\boldsymbol{p}} \\ \boldsymbol{\mathcal{F}}_I^{\boldsymbol{F}} \\ \boldsymbol{\mathcal{F}}_I^{\boldsymbol{H}} \\ \boldsymbol{\mathcal{F}}_I^{J} \\ \boldsymbol{\mathcal{F}}_I^{\boldsymbol{D}_0} \\ \boldsymbol{\mathcal{F}}_I^{\boldsymbol{B}_0} \\ \boldsymbol{\mathcal{F}}_I^{\boldsymbol{d}} \\ \boldsymbol{\mathcal{F}}_I^{\boldsymbol{b}} \end{bmatrix}; \qquad \boldsymbol{\mathcal{S}} = \begin{bmatrix} \boldsymbol{f}_0 \\ \boldsymbol{0} \\ \boldsymbol{0} \\ 0 \\ -\boldsymbol{J}_0 \\ \boldsymbol{0} \\ -\boldsymbol{F}\boldsymbol{J}_0 - \frac{\rho_0^e}{\rho_0}\boldsymbol{p} \\ \boldsymbol{0} \end{bmatrix}, \tag{7.41}$$

where the components of the flux vector $\boldsymbol{\mathcal{F}}_I$ are defined as

$$\begin{aligned}
&\boldsymbol{\mathcal{F}}_I^{\boldsymbol{p}} = -\boldsymbol{P}\boldsymbol{E}_I; && \boldsymbol{\mathcal{F}}_I^{\boldsymbol{F}} = -\frac{1}{\rho_0}\boldsymbol{p}\otimes\boldsymbol{E}_I; \\
&\boldsymbol{\mathcal{F}}_I^{\boldsymbol{H}} = -\boldsymbol{F}\times\left(\frac{1}{\rho_0}\boldsymbol{p}\otimes\boldsymbol{E}_I\right); && \boldsymbol{\mathcal{F}}_I^{J} = -\boldsymbol{H}:\left(\frac{1}{\rho_0}\boldsymbol{p}\otimes\boldsymbol{E}_I\right); \\
&\boldsymbol{\mathcal{F}}_I^{\boldsymbol{D}_0} = \boldsymbol{H}_0\times\boldsymbol{E}_I; && \boldsymbol{\mathcal{F}}_I^{\boldsymbol{B}_0} = -\boldsymbol{E}_0\times\boldsymbol{E}_I; \\
&\boldsymbol{\mathcal{F}}_I^{\boldsymbol{d}} = -\frac{1}{\rho_0}\boldsymbol{p}(\boldsymbol{D}_0\cdot\boldsymbol{E}_I) + (\boldsymbol{F}\times\boldsymbol{H}_0)\,\boldsymbol{E}_I; && \boldsymbol{\mathcal{F}}_I^{\boldsymbol{b}} = -\frac{1}{\rho_0}\boldsymbol{p}(\boldsymbol{B}_0\cdot\boldsymbol{E}_I) - (\boldsymbol{F}\times\boldsymbol{E}_0)\,\boldsymbol{E}_I,
\end{aligned} \tag{7.42}$$

where $\boldsymbol{P}$, $\boldsymbol{E}_0$ and $\boldsymbol{H}_0$ are defined in terms of the extended sets $\mathcal{V}$ and $\Sigma_{\mathcal{V}}$ as in equations (7.17a), (7.17b) and (7.17c), respectively. Let us recall the quasilinear form for the system of hyperbolic equations with vector of variables $\boldsymbol{\mathcal{U}}$, vector of fluxes $\boldsymbol{\mathcal{F}}_I$ and vector of source terms $\boldsymbol{\mathcal{S}}$ in (7.41), that is

$$\frac{\partial\boldsymbol{\mathcal{U}}}{\partial t} + \underbrace{\boldsymbol{\mathcal{A}}_I\frac{\partial\boldsymbol{\mathcal{U}}}{\partial X_I}}_{\alpha^\star} = \boldsymbol{\mathcal{S}}, \tag{7.43}$$

where the 'non-trivial' second term on the left-hand side of above equation (7.43), namely $\alpha^\star$ can be expressed as

$$\alpha^\star = -\underbrace{\left[\begin{array}{c:c} \boldsymbol{0}_{3\times3} & \\ \frac{\partial\boldsymbol{\mathcal{F}}_I^{\boldsymbol{F}}}{\partial\boldsymbol{p}} & \\ \frac{\partial\boldsymbol{\mathcal{F}}_I^{\boldsymbol{H}}}{\partial\boldsymbol{p}} & \widetilde{\boldsymbol{W}}_I^{\star\star} \\ \frac{\partial\boldsymbol{\mathcal{F}}_I^{J}}{\partial\boldsymbol{p}} & \\ \hdashline \boldsymbol{0}_{3\times3} & \\ \boldsymbol{0}_{3\times3} & \\ \frac{\partial\boldsymbol{\mathcal{F}}_I^{\boldsymbol{d}}}{\partial\boldsymbol{p}} & \widetilde{\boldsymbol{W}}_I^{\star} \\ \frac{\partial\boldsymbol{\mathcal{F}}_I^{\boldsymbol{b}}}{\partial\boldsymbol{p}} & \end{array}\right]}_{\boldsymbol{\mathcal{A}}_I} \frac{\partial}{\partial X_I}\begin{bmatrix} \cdot\boldsymbol{p} \\ :\boldsymbol{F} \\ :\boldsymbol{H} \\ J \\ \cdot\boldsymbol{D}_0 \\ \cdot\boldsymbol{B}_0 \\ \cdot\boldsymbol{d} \\ \cdot\boldsymbol{b} \end{bmatrix}, \tag{7.44}$$

where the entries in the first column of above matrix $\boldsymbol{\mathcal{A}}_I$ can be written in indicial notation as

$$\left[\frac{\partial \boldsymbol{\mathcal{F}}_I^{\boldsymbol{F}}}{\partial \boldsymbol{p}}\right]_{iKk} = \frac{1}{\rho_0}\delta_{ik}\delta_{IK}; \qquad \left[\frac{\partial \boldsymbol{\mathcal{F}}_I^{\boldsymbol{H}}}{\partial \boldsymbol{p}}\right]_{iKk} = \frac{1}{\rho_0}\mathcal{E}_{imk}\mathcal{E}_{KMI}F_{mM}; \qquad \left[\frac{\partial \boldsymbol{\mathcal{F}}_I^{J}}{\partial \boldsymbol{p}}\right]_{i} = \frac{1}{\rho_0}H_{iI};$$
$$\left[\frac{\partial \boldsymbol{\mathcal{F}}_I^{\boldsymbol{d}}}{\partial \boldsymbol{p}}\right]_{ik} = \frac{1}{\rho_0}\delta_{ik}\left(\boldsymbol{D}_0 \cdot \boldsymbol{E}_I\right); \qquad \left[\frac{\partial \boldsymbol{\mathcal{F}}_I^{\boldsymbol{b}}}{\partial \boldsymbol{p}}\right]_{ik} = \frac{1}{\rho_0}\delta_{ik}\left(\boldsymbol{B}_0 \cdot \boldsymbol{E}_I\right). \tag{7.45}$$

In addition, the inner products $(\cdot)$ and $(:)$ appearing in the vector of conservation variables in (7.44) represent standard contraction of repeated indices. For simplicity, the expressions for both matrices $\widetilde{\boldsymbol{W}_I}^{\star\star}$ and $\widetilde{\boldsymbol{W}_I}^{\star}$ (7.44) have been carried out in Appendix E (see equations (E.1) and (E.4), respectively).

7.3 Eigenvalue structure of the equations in non-linear electro-magneto-mechanics

The objective of this Section is to analyse the eigenvalue structure of the combined set of conservation laws for electro-magneto-mechanics presented in equation (7.41) and demonstrate its hyperbolicity. Two scenarios will be considered: firstly, that defined by the system of conservation laws (7.41) and, second, a simplified case for low frequency scenarios.

7.3.1 Eigenvalue structure

The eigenvalues or wave speeds and the corresponding eigenvectors of the system of conservation laws in equation (7.41) can be determined by identifying possible plane wave solutions (in the absence of source terms) of the type

$$\boldsymbol{\mathcal{U}} = \phi(\boldsymbol{X}\cdot\boldsymbol{N} - c_\alpha t)\bar{\boldsymbol{\mathcal{U}}}_\alpha = \phi(\boldsymbol{X}\cdot\boldsymbol{N} - c_\alpha t)\begin{bmatrix} \bar{\boldsymbol{p}}_\alpha \\ \bar{\boldsymbol{F}}_\alpha \\ \bar{\boldsymbol{H}}_\alpha \\ \bar{J}_\alpha \\ \bar{\boldsymbol{D}}_{0\alpha} \\ \bar{\boldsymbol{B}}_{0\alpha} \\ \bar{\boldsymbol{d}}_\alpha \\ \bar{\boldsymbol{b}}_\alpha \end{bmatrix}, \tag{7.46}$$

where c_α are the wave speeds corresponding to the eigenmode $\bar{\boldsymbol{\mathcal{U}}}_\alpha$ and $\boldsymbol{N}$, the normalised direction of propagation. The above expression in (7.46) for the set of conservation variables $\boldsymbol{\mathcal{U}}$ leads to an eigenvalue problem (refer to equation (4.5)) given by

$$\boldsymbol{\mathcal{A}}_{\boldsymbol{N}}\bar{\boldsymbol{\mathcal{U}}}_\alpha = c_\alpha\bar{\boldsymbol{\mathcal{U}}}_\alpha; \qquad \boldsymbol{\mathcal{A}}_{\boldsymbol{N}} = \boldsymbol{\mathcal{A}}_I N_I, \tag{7.47}$$

with the flux Jacobian matrix $\boldsymbol{\mathcal{A}}_I$ defined in equation (7.44). Particularisation of the involution equations for $\boldsymbol{D}_0$ and $\boldsymbol{B}_0$ in equations (7.8) (for the case in which $\rho_0^e = 0$) to plane wave solutions of the type described in equation (7.46) yields

$$(\bar{\boldsymbol{D}}_{0\alpha} \cdot \boldsymbol{N})\phi' = 0; \qquad (\bar{\boldsymbol{B}}_{0\alpha} \cdot \boldsymbol{N})\phi' = 0. \tag{7.48}$$

For non trivial solutions $\phi' \neq 0$, equation (7.48) leads to (refer to Figure 7.3)

$$(\bar{\boldsymbol{D}}_{0\alpha} \cdot \boldsymbol{N}) = 0; \qquad (\bar{\boldsymbol{B}}_{0\alpha} \cdot \boldsymbol{N}) = 0, \tag{7.49}$$

which enables to re-define $\bar{\boldsymbol{\mathcal{U}}}_\alpha$ (4.28) as

$$\bar{\boldsymbol{\mathcal{U}}}_\alpha = \begin{bmatrix} \bar{\boldsymbol{p}}_\alpha \\ \bar{\boldsymbol{F}}_\alpha \\ \bar{\boldsymbol{H}}_\alpha \\ \bar{J}_\alpha \\ \boldsymbol{I_{NN}}\bar{\boldsymbol{D}}_{0\alpha} \\ \boldsymbol{I_{NN}}\bar{\boldsymbol{B}}_{0\alpha} \\ \bar{\boldsymbol{d}}_\alpha \\ \bar{\boldsymbol{b}}_\alpha \end{bmatrix}, \tag{7.50}$$

with the projection operator $\boldsymbol{I_{NN}}$ defined as

$$\boldsymbol{I_{NN}} = \boldsymbol{I} - \boldsymbol{N} \otimes \boldsymbol{N}. \tag{7.51}$$

Particularisation of the local conservation equation for the deformation gradient tensor $\boldsymbol{F}$ (7.26a) to plane wave solutions of the type described in equation (7.46) yields (refer to Figure 7.3)

$$-c_\alpha \bar{\boldsymbol{F}}_\alpha \phi' - \frac{1}{\rho_0}\bar{\boldsymbol{p}}_\alpha \otimes \boldsymbol{N}\phi' = \boldsymbol{0} \Rightarrow \bar{\boldsymbol{F}}_\alpha = \bar{\boldsymbol{f}}_\alpha \otimes \boldsymbol{N}, \tag{7.52}$$

where $\bar{\boldsymbol{f}}_\alpha = -\frac{1}{c_\alpha \rho_0}\bar{\boldsymbol{p}}_\alpha$. Moreover, substitution of the above plane wave-like solutions (7.46) in conjunction with (7.52) into equations (7.26b), (7.26c) and (7.31), (7.39) yields

$$\begin{aligned} \bar{\boldsymbol{H}}_\alpha &= \boldsymbol{F} \times \left(\bar{\boldsymbol{f}}_\alpha \otimes \boldsymbol{N}\right); & \bar{J}_\alpha &= \boldsymbol{H} : \left(\bar{\boldsymbol{f}}_\alpha \otimes \boldsymbol{N}\right); \\ \bar{\boldsymbol{d}}_\alpha &= \bar{\boldsymbol{f}}_\alpha \left(\boldsymbol{D}_0 \cdot \boldsymbol{N}\right) + \boldsymbol{F}\left(\boldsymbol{I_{NN}}\bar{\boldsymbol{D}}_{0_\alpha}\right); & \bar{\boldsymbol{b}}_\alpha &= \bar{\boldsymbol{f}}_\alpha \left(\boldsymbol{B}_0 \cdot \boldsymbol{N}\right) + \boldsymbol{F}\left(\boldsymbol{I_{NN}}\bar{\boldsymbol{B}}_{0_\alpha}\right). \end{aligned} \tag{7.53}$$

The expressions in above equations (7.52)-(7.53), where the eigenmodes $\bar{\boldsymbol{F}}_\alpha$, $\bar{\boldsymbol{H}}_\alpha$, $\bar{J}_\alpha$, $\bar{\boldsymbol{d}}_\alpha$ and $\bar{\boldsymbol{b}}_\alpha$ have been expressed in terms of a reduced set of eigenmodes $\{\bar{\boldsymbol{f}}_\alpha, \boldsymbol{I_{NN}}\bar{\boldsymbol{D}}_{0_\alpha}, \boldsymbol{I_{NN}}\bar{\boldsymbol{B}}_{0_\alpha}\}$, enable to re-write and reduce the eigenvalue problem in (7.47) (with $\boldsymbol{\mathcal{A}_I}$ defined as in equation (7.44)) to

$$c_\alpha \bar{\boldsymbol{\mathcal{U}}}^\star_\alpha = \boldsymbol{\mathcal{A}}^\star_{\boldsymbol{N}} \bar{\boldsymbol{\mathcal{U}}}^\star_\alpha, \tag{7.54}$$

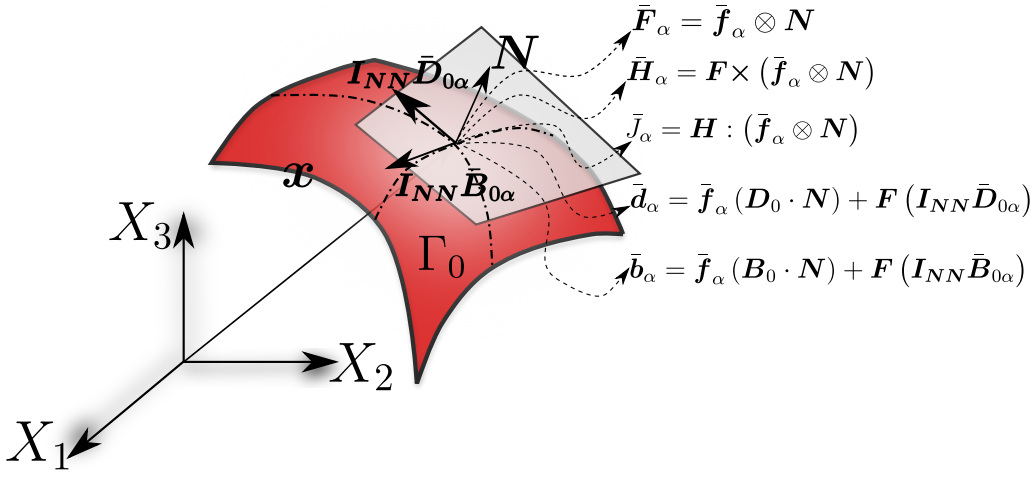

Figure 7.3: Eigenmodes $\bar{\boldsymbol{F}}_\alpha$, $\bar{\boldsymbol{H}}_\alpha$, $\bar{J}_\alpha$, $\boldsymbol{I}_{\boldsymbol{NN}} \bar{\boldsymbol{D}}_{0_\alpha}$, $\boldsymbol{I}_{\boldsymbol{NN}} \bar{\boldsymbol{B}}_{0_\alpha}$, $\bar{\boldsymbol{d}}_\alpha$ and $\bar{\boldsymbol{b}}_\alpha$ at a discontinuity surface Γ_0. The eigenmodes $\bar{\boldsymbol{D}}_{0_\alpha}$, $\bar{\boldsymbol{B}}_{0_\alpha}$ are perpendicular to the vector of propagation $\boldsymbol{N}$, thus complying with the involution equations (7.49).

in terms of the reduced set of eigenvectors $\bar{\boldsymbol{\mathcal{U}}}^\star_\alpha$ and of the reduced Jacobian matrix $\boldsymbol{\mathcal{A}}^\star_{\boldsymbol{N}}$ defined as

$$\bar{\boldsymbol{\mathcal{U}}}^\star_\alpha = \begin{bmatrix} \bar{\boldsymbol{p}}_\alpha \\ \bar{\boldsymbol{f}}_\alpha \\ \boldsymbol{I}_{\boldsymbol{NN}} \bar{\boldsymbol{D}}_{0\alpha} \\ \boldsymbol{I}_{\boldsymbol{NN}} \bar{\boldsymbol{B}}_{0\alpha} \end{bmatrix}; \quad \boldsymbol{\mathcal{A}}^\star_{\boldsymbol{N}} = - \begin{bmatrix} \boldsymbol{0} & \boldsymbol{\mathcal{C}}_{\boldsymbol{NN}} & \boldsymbol{\mathcal{Q}}_{\boldsymbol{N}}{}^T & \boldsymbol{\mathcal{T}}_{\boldsymbol{N}}{}^T \\ \frac{1}{\rho_0}\boldsymbol{I} & \boldsymbol{0} & \boldsymbol{0} & \boldsymbol{0} \\ \boldsymbol{0} & -\boldsymbol{W}\boldsymbol{\mathcal{T}}_{\boldsymbol{N}} & -\boldsymbol{W}\boldsymbol{R}^T & -\boldsymbol{W}\boldsymbol{\vartheta} \\ \boldsymbol{0} & \boldsymbol{W}\boldsymbol{\mathcal{Q}}_{\boldsymbol{N}} & \boldsymbol{W}\boldsymbol{\theta} & \boldsymbol{W}\boldsymbol{R} \end{bmatrix}, \tag{7.55}$$

where the second order tensor $\boldsymbol{W}$ in above equation (7.55) is defined as $W_{IJ} = \mathcal{E}_{IJK} N_K$. Moreover, the second order tensors $\boldsymbol{\mathcal{C}}_{\boldsymbol{NN}}$, $\boldsymbol{\mathcal{Q}}_{\boldsymbol{N}}$ and $\boldsymbol{\mathcal{T}}_{\boldsymbol{N}}$ in (7.55) are defined as

$$(\mathcal{C}_{NN})_{ij} = \mathcal{C}_{iIjJ} N_I N_J; \qquad (\mathcal{Q}_N)_{Ij} = \mathcal{Q}_{IjJ} N_J; \qquad (\mathcal{T}_N)_{Ij} = \mathcal{T}_{IjJ} N_J, \tag{7.56}$$

and with the different constitutive tensors $\boldsymbol{\mathcal{C}}$ (fourth order elasticity tensor), $\boldsymbol{\mathcal{Q}}$ (third order piezoelectric tensor), $\boldsymbol{\mathcal{T}}$ (third order piezomagnetic tensor), $\boldsymbol{\theta}$ (second order dielectric tensor), $\boldsymbol{R}$ (second order magnetoelectric tensor) and $\boldsymbol{\vartheta}$ (second order permeability tensor) featuring in equations (7.55) and (7.56) defined in equations (G.2), (G.5), (G.8), (G.11), (G.14) and (G.13), respectively, in terms of the components of the Hessian operator $[\mathbb{H}_W]$ (7.18).

Careful analysis of the matrix $\boldsymbol{\mathcal{A}}^\star_{\boldsymbol{N}}$ in (7.55) enables to identify the following multiplicative decomposition of $\boldsymbol{\mathcal{A}}^\star_{\boldsymbol{N}}$ as

$$\boldsymbol{\mathcal{A}}^\star_{\boldsymbol{N}} = -\boldsymbol{S}\boldsymbol{U}, \tag{7.57}$$

where the second order tensors $\boldsymbol{S}$ and $\boldsymbol{U}$ are defined as

$$\boldsymbol{S} = \begin{bmatrix} \boldsymbol{0} & \boldsymbol{I} & \boldsymbol{0} & \boldsymbol{0} \\ \boldsymbol{I} & \boldsymbol{0} & \boldsymbol{0} & \boldsymbol{0} \\ \boldsymbol{0} & \boldsymbol{0} & \boldsymbol{0} & -\boldsymbol{W} \\ \boldsymbol{0} & \boldsymbol{0} & \boldsymbol{W} & \boldsymbol{0} \end{bmatrix}; \qquad \boldsymbol{U} = \begin{bmatrix} \frac{1}{\rho_0}\boldsymbol{I} & \boldsymbol{0}_{9\times 9} \\ \boldsymbol{0}_{9\times 9} & \boldsymbol{Q} \end{bmatrix}, \tag{7.58}$$

with $\boldsymbol{Q}$ the so-called electro-magneto-mechanical acoustic tensor, defined as

$$\boldsymbol{Q} = \begin{bmatrix} \boldsymbol{\mathcal{C}_{NN}} & \boldsymbol{\mathcal{Q}_N}^T & \boldsymbol{\mathcal{T}_N}^T \\ \boldsymbol{\mathcal{Q}_N} & \boldsymbol{\theta} & \boldsymbol{R} \\ \boldsymbol{\mathcal{T}_N} & \boldsymbol{R}^T & \boldsymbol{\vartheta} \end{bmatrix}. \tag{7.59}$$

Following a fundamental theorem in the theory of hyperbolic equations [2], summarised in F for completeness, given the symmetric nature of $\boldsymbol{S}$ $(7.58)_a$, a sufficient condition for the existence of real eigenvalues for the above Jacobian matrix $\boldsymbol{\mathcal{A}^\star_N}$ (refer to (7.55) and (7.57)) would be the symmetric positive definiteness of $\boldsymbol{U}$ $(7.58)_b$ and hence, of $\boldsymbol{Q}$ (7.59). Moreover, positive definiteness of the electro-magneto-mechanical acoustic tensor $\boldsymbol{Q}$ can be shown by noticing the following relationship between $\boldsymbol{Q}$ and the Hessian operator $[\mathbb{H}_W]$, namely

$$\begin{bmatrix} \bar{\boldsymbol{f}}_\alpha \\ \boldsymbol{I_{NN}}\bar{\boldsymbol{D}}_{0\alpha} \\ \boldsymbol{I_{NN}}\bar{\boldsymbol{B}}_{0\alpha} \end{bmatrix}^T \boldsymbol{Q} \begin{bmatrix} \bar{\boldsymbol{f}}_\alpha \\ \boldsymbol{I_{NN}}\bar{\boldsymbol{D}}_{0\alpha} \\ \boldsymbol{I_{NN}}\bar{\boldsymbol{B}}_{0\alpha} \end{bmatrix} = \begin{bmatrix} \bar{\boldsymbol{F}}_\alpha \\ \bar{\boldsymbol{H}}_\alpha \\ \bar{J}_\alpha \\ \boldsymbol{I_{NN}}\bar{\boldsymbol{D}}_{0\alpha} \\ \boldsymbol{I_{NN}}\bar{\boldsymbol{B}}_{0\alpha} \\ \bar{\boldsymbol{d}}_\alpha \\ \bar{\boldsymbol{b}}_\alpha \end{bmatrix}^T [\mathbb{H}_W] \begin{bmatrix} \bar{\boldsymbol{F}}_\alpha \\ \bar{\boldsymbol{H}}_\alpha \\ \bar{J}_\alpha \\ \boldsymbol{I_{NN}}\bar{\boldsymbol{D}}_{0\alpha} \\ \boldsymbol{I_{NN}}\bar{\boldsymbol{B}}_{0\alpha} \\ \bar{\boldsymbol{d}}_\alpha \\ \bar{\boldsymbol{b}}_\alpha \end{bmatrix} > 0. \tag{7.60}$$

As can be seen, the positive definiteness of the electro-magneto-mechanical acoustic tensor $\boldsymbol{Q}$ is implied by the positive definiteness of the extended Hessian operator $[\mathbb{H}_W]$, always satisfied by convex multi-variable energy functionals (7.12). Results in this Section enable the extension of the multi-variable convexity concepts presented in [76] to more general 'dynamic' and 'electro-magneto-mechanics' scenarios.

Remark 7.1. Equation (7.60) makes it possible to highlight the relationship between multi-variable convexity, ellipticity (rank-one convexity) and the Legendre-Hadamard condition (existence of real wave speeds). Notice first that it is possible to re-write the first term on the left hand side of (7.60) as

$$\begin{bmatrix} \bar{\boldsymbol{f}}_\alpha \otimes \boldsymbol{N} : & \boldsymbol{N}_{\perp,1} \cdot & \boldsymbol{N}_{\perp,2} \cdot \end{bmatrix} \begin{bmatrix} \boldsymbol{\mathcal{C}} & \boldsymbol{\mathcal{Q}}^T & \boldsymbol{\mathcal{T}}^T \\ \boldsymbol{\mathcal{Q}} & \boldsymbol{\theta} & \boldsymbol{R} \\ \boldsymbol{\mathcal{T}} & \boldsymbol{R}^T & \boldsymbol{\vartheta} \end{bmatrix} \begin{bmatrix} : \bar{\boldsymbol{f}}_\alpha \otimes \boldsymbol{N} \\ \boldsymbol{N}_{\perp,1} \\ \boldsymbol{N}_{\perp,2} \end{bmatrix} > 0, \tag{7.61}$$

where $\boldsymbol{N}_{\perp,1}$ and $\boldsymbol{N}_{\perp,2}$ represent two arbitrary vectors orthogonal to $\boldsymbol{N}$. Above expression (7.61) is a generalisation of the concept of ellipticity [11] to the case of electro-magneto-mechanics. Moreover, this equation, in conjunction with (7.60) links this property to the satisfaction of multi-variable convexity and, as a result of Appendix F, to the Legendre-Hadamard condition.

Finally, notice that expression (7.61) is nothing more than the generalisation to electro-magneto-mechanical scenarios of the simpler electro-mechanical condition

$$\begin{bmatrix} \bar{\boldsymbol{f}}_\alpha \otimes \boldsymbol{N} : & \boldsymbol{N}_{\perp,1} \cdot \end{bmatrix} \begin{bmatrix} \boldsymbol{\mathcal{C}} & \boldsymbol{\mathcal{Q}}^T \\ \boldsymbol{\mathcal{Q}} & \boldsymbol{\theta} \end{bmatrix} \begin{bmatrix} : \bar{\boldsymbol{f}}_\alpha \otimes \boldsymbol{N} \\ \boldsymbol{N}_{\perp,1} \end{bmatrix} > 0. \tag{7.62}$$

Above equation (7.62) is identical to Remark 4 in Reference [76], which establishes the relationship between multi-variable convexity and ellipticity.

7.3.2 Low frequency scenarios. Constrained case

In this Section, a particular scenario, interesting from the point of view of possible engineering applications characterised by the absence of current and electric charge densities ($\boldsymbol{J}_0 = \boldsymbol{0}$ ad $\rho_0^e = 0$) and by low frequency electro-magnetic waves is analysed. This scenario enables the analysis of the system of conservation laws presented in equation (7.41) to be dramatically simplified. Specifically, the Maxwell equations (refer to both (7.7a) and (7.7b)) are now treated as constraints[1], as shown in Reference [114]. The resulting system of hyperbolic equations is then

$$\boldsymbol{\mathcal{U}} = \begin{bmatrix} \boldsymbol{p} \\ \boldsymbol{F} \\ \boldsymbol{H} \\ J \\ \boldsymbol{d} \\ \boldsymbol{b} \end{bmatrix}; \qquad \boldsymbol{\mathcal{F}}_I = - \begin{bmatrix} \boldsymbol{P}\boldsymbol{E}_I \\ \frac{1}{\rho_0}\boldsymbol{p} \otimes \boldsymbol{E}_I \\ \boldsymbol{F} \times \left(\frac{1}{\rho_0}\boldsymbol{p} \otimes \boldsymbol{E}_I \right) \\ \boldsymbol{H} : \left(\frac{1}{\rho_0}\boldsymbol{p} \otimes \boldsymbol{E}_I \right) \\ \frac{1}{\rho_0}\boldsymbol{p}(\boldsymbol{D}_0 \cdot \boldsymbol{E}_I) \\ \frac{1}{\rho_0}\boldsymbol{p}(\boldsymbol{B}_0 \cdot \boldsymbol{E}_I) \end{bmatrix}; \qquad \boldsymbol{\mathcal{S}} = \begin{bmatrix} \boldsymbol{f}_0 \\ \boldsymbol{0} \\ \boldsymbol{0} \\ 0 \\ \boldsymbol{0} \\ \boldsymbol{0} \end{bmatrix}, \tag{7.63}$$

subjected to the following constraints (different to the concept of involutions [113])

$$\mathrm{CURL}\boldsymbol{E}_0 = \boldsymbol{0}; \qquad \mathrm{CURL}\boldsymbol{H}_0 = \boldsymbol{0}. \tag{7.64}$$

For the constrained set of first hyperbolic equations in equation (7.63), the associated eigenvalue problem can be obtained following a similar procedure to that presented in Section (7.3.1) for the unconstrained case, yielding a similar expression for the eigenvalue problem as that presented in equation (7.55), now subjected to the constraints in equation (7.64), that is

$$c_\alpha \begin{bmatrix} \bar{\boldsymbol{p}}_\alpha \\ \bar{\boldsymbol{f}}_\alpha \\ \boldsymbol{0} \\ \boldsymbol{0} \end{bmatrix} + \begin{bmatrix} \boldsymbol{0} & \boldsymbol{\mathcal{C}}_{\boldsymbol{NN}} & \boldsymbol{\mathcal{Q}}_{\boldsymbol{N}}{}^T & \boldsymbol{\mathcal{T}}_{\boldsymbol{N}}{}^T \\ \frac{1}{\rho_0}\boldsymbol{I} & \boldsymbol{0} & \boldsymbol{0} & \boldsymbol{0} \\ \boldsymbol{0} & -\boldsymbol{W}\boldsymbol{\mathcal{T}}_{\boldsymbol{N}} & -\boldsymbol{W}\boldsymbol{R}^T & -\boldsymbol{W}\boldsymbol{\vartheta} \\ \boldsymbol{0} & \boldsymbol{W}\boldsymbol{\mathcal{Q}}_{\boldsymbol{N}} & \boldsymbol{W}\boldsymbol{\theta} & \boldsymbol{W}\boldsymbol{R} \end{bmatrix} \begin{bmatrix} \bar{\boldsymbol{p}}_\alpha \\ \bar{\boldsymbol{f}}_\alpha \\ \bar{\boldsymbol{D}}_{0\alpha} \\ \bar{\boldsymbol{B}}_{0\alpha} \end{bmatrix} = \boldsymbol{0}. \tag{7.65}$$

Notice that the last two rows in above equation (7.65) are in fact constraints imposed on the eigenmodes $\bar{\boldsymbol{D}}_{0\alpha}$ and $\bar{\boldsymbol{B}}_{0\alpha}$. These two rows can alternatively be written in terms of the auxiliary scalar parameters $\lambda_{\boldsymbol{D}_0}$ and $\lambda_{\boldsymbol{B}_0}$ as

$$\begin{aligned} \boldsymbol{\mathcal{T}}_{\boldsymbol{N}}\bar{\boldsymbol{f}}_\alpha + \boldsymbol{R}^T\bar{\boldsymbol{D}}_{0\alpha} + \boldsymbol{\vartheta}\bar{\boldsymbol{B}}_{0\alpha} &= \lambda_{\boldsymbol{B}_0}\boldsymbol{N}; \\ \boldsymbol{\mathcal{Q}}_{\boldsymbol{N}}\bar{\boldsymbol{f}}_\alpha + \boldsymbol{\theta}\bar{\boldsymbol{D}}_{0\alpha} + \boldsymbol{R}\bar{\boldsymbol{B}}_{0\alpha} &= \lambda_{\boldsymbol{D}_0}\boldsymbol{N}. \end{aligned} \tag{7.66}$$

[1] For low frequency scenarios, it is customary to adopt the simplification $\frac{\partial \boldsymbol{D}_0}{\partial t} \approx \boldsymbol{0}$ and $\frac{\partial \boldsymbol{B}_0}{\partial t} \approx \boldsymbol{0}$.

Notice that the scalar parameters $\lambda_{\boldsymbol{D}_0}$ and $\lambda_{\boldsymbol{B}_0}$ in above equation (7.66) are used to indicate the collinear nature between the vector $\boldsymbol{N}$ and the vectors $\boldsymbol{\mathcal{Q}_N}\bar{\boldsymbol{f}}_\alpha + \boldsymbol{\theta}\bar{\boldsymbol{D}}_{0\alpha} + \boldsymbol{R}\bar{\boldsymbol{B}}_{0\alpha}$ and $\boldsymbol{\mathcal{T}_N}\bar{\boldsymbol{f}}_\alpha + \boldsymbol{R}^T\bar{\boldsymbol{D}}_{0\alpha} + \boldsymbol{\vartheta}\bar{\boldsymbol{B}}_{0\alpha}$, respectively. From equation (7.66), it is possible to obtain both $\bar{\boldsymbol{B}}_{0\alpha}$ and $\bar{\boldsymbol{D}}_{0\alpha}$ as

$$\begin{aligned}\bar{\boldsymbol{B}}_{0\alpha} &= \boldsymbol{\vartheta}^{-1}\left(\lambda_{\boldsymbol{B}_0}\boldsymbol{N} - \boldsymbol{\mathcal{T}_N}\bar{\boldsymbol{f}}_\alpha - \boldsymbol{R}^T\bar{\boldsymbol{D}}_{0\alpha}\right);\\ \bar{\boldsymbol{D}}_{0\alpha} &= \boldsymbol{\theta}^{-1}\left(\lambda_{\boldsymbol{D}_0}\boldsymbol{N} - \boldsymbol{\mathcal{Q}_N}\bar{\boldsymbol{f}}_\alpha - \boldsymbol{R}\bar{\boldsymbol{B}}_{0\alpha}\right).\end{aligned} \tag{7.67}$$

Consideration of the involutions in equation (7.49) (namely $\bar{\boldsymbol{D}}_{0_\alpha}\cdot\boldsymbol{N} = \bar{\boldsymbol{B}}_{0_\alpha}\cdot\boldsymbol{N} = 0$) yields an expression for the two scalar parameters $\lambda_{\boldsymbol{B}_0}$ and $\lambda_{\boldsymbol{D}_0}$ as

$$\lambda_{\boldsymbol{B}_0} = \frac{\boldsymbol{N}\cdot\boldsymbol{\vartheta}^{-1}\left(\boldsymbol{\mathcal{T}_N}\bar{\boldsymbol{f}}_{\boldsymbol{\alpha}} + \boldsymbol{R}^T\bar{\boldsymbol{D}}_{0\alpha}\right)}{\boldsymbol{N}\cdot\boldsymbol{\vartheta}^{-1}\boldsymbol{N}}; \qquad \lambda_{\boldsymbol{D}_0} = \frac{\boldsymbol{N}\cdot\boldsymbol{\theta}^{-1}\left(\boldsymbol{\mathcal{Q}_N}\bar{\boldsymbol{f}}_{\boldsymbol{\alpha}} + \boldsymbol{R}\bar{\boldsymbol{B}}_{0\alpha}\right)}{\boldsymbol{N}\cdot\boldsymbol{\theta}^{-1}\boldsymbol{N}}. \tag{7.68}$$

Substitution of equation (7.68) into equation (7.67) enables both eigenmodes $\bar{\boldsymbol{B}}_{0\alpha}$ and $\bar{\boldsymbol{D}}_{0\alpha}$ to be expressed in terms of the eigenmodes $\bar{\boldsymbol{f}}_\alpha$ as

$$\begin{aligned}\bar{\boldsymbol{B}}_{0\alpha} &= -\left[\boldsymbol{\vartheta} - \boldsymbol{B}\boldsymbol{R}^T\boldsymbol{\theta}^{-1}\boldsymbol{C}\boldsymbol{R}\right]^{-1}\left(\boldsymbol{\mathcal{T}_N}^\star - \boldsymbol{B}\boldsymbol{R}^T\boldsymbol{\theta}^{-1}\boldsymbol{\mathcal{Q}_N}\right)\bar{\boldsymbol{f}}_\alpha;\\ \bar{\boldsymbol{D}}_{0\alpha} &= -\left[\boldsymbol{\theta} - \boldsymbol{C}\boldsymbol{R}\boldsymbol{\vartheta}^{-1}\boldsymbol{B}\boldsymbol{R}^T\right]^{-1}\left(\boldsymbol{\mathcal{Q}_N}^\star - \boldsymbol{C}\boldsymbol{R}\boldsymbol{\vartheta}^{-1}\boldsymbol{\mathcal{T}_N}\right)\bar{\boldsymbol{f}}_\alpha,\end{aligned} \tag{7.69}$$

where the modified (coupled) matrices $\boldsymbol{\mathcal{Q}_N}^\star$, $\boldsymbol{\mathcal{T}_N}^\star$, $\boldsymbol{R}^\star_{\boldsymbol{\theta}}$ and $\boldsymbol{R}^\star_{\boldsymbol{\vartheta}}$ are defined as

$$\begin{aligned}\boldsymbol{\mathcal{Q}_N}^\star &= \left[\boldsymbol{I} - \frac{\left(\boldsymbol{N}\otimes\boldsymbol{\theta}^{-1}\boldsymbol{N}\right)}{\boldsymbol{N}\cdot\boldsymbol{\theta}^{-1}\boldsymbol{N}}\right]\boldsymbol{\mathcal{Q}_N}; \qquad \boldsymbol{\mathcal{T}_N}^\star = \left[\boldsymbol{I} - \frac{\left(\boldsymbol{N}\otimes\boldsymbol{\vartheta}^{-1}\boldsymbol{N}\right)}{\boldsymbol{N}\cdot\boldsymbol{\vartheta}^{-1}\boldsymbol{N}}\right]\boldsymbol{\mathcal{T}_N};\\ \boldsymbol{B} &= \left[\boldsymbol{I} - \frac{\left(\boldsymbol{N}\otimes\boldsymbol{\vartheta}^{-1}\boldsymbol{N}\right)}{\boldsymbol{N}\cdot\boldsymbol{\vartheta}^{-1}\boldsymbol{N}}\right]; \qquad \boldsymbol{C} = \left[\boldsymbol{I} - \frac{\left(\boldsymbol{N}\otimes\boldsymbol{\theta}^{-1}\boldsymbol{N}\right)}{\boldsymbol{N}\cdot\boldsymbol{\theta}^{-1}\boldsymbol{N}}\right]; \qquad .\end{aligned} \tag{7.70}$$

Finally, the first two equations (rows) in above equation (7.65) can be written as

$$c_\alpha\begin{bmatrix}\bar{\boldsymbol{p}}_\alpha\\ \bar{\boldsymbol{f}}_\alpha\end{bmatrix} + \begin{bmatrix}\boldsymbol{0} & \boldsymbol{\mathcal{C}_{NN}} & \boldsymbol{\mathcal{Q}_N}^T & \boldsymbol{\mathcal{T}_N}^T\\ \frac{1}{\rho_0}\boldsymbol{I} & \boldsymbol{0} & \boldsymbol{0} & \boldsymbol{0}\end{bmatrix}\begin{bmatrix}\bar{\boldsymbol{p}}_\alpha\\ \bar{\boldsymbol{f}}_\alpha\\ \bar{\boldsymbol{D}}_{0\alpha}\\ \bar{\boldsymbol{B}}_{0\alpha}\end{bmatrix} = \boldsymbol{0}, \tag{7.71}$$

with $\bar{\boldsymbol{D}}_{0\alpha}$ and $\bar{\boldsymbol{B}}_{0\alpha}$ defined in terms of $\bar{\boldsymbol{f}}_\alpha$ in equation (7.69). Finally, substitution of the second row into the first row in above equation (7.71) and consideration of the expressions for both $\bar{\boldsymbol{D}}_{0\alpha}$ and $\bar{\boldsymbol{B}}_{0\alpha}$ in terms of $\bar{\boldsymbol{f}}_\alpha$ (refer to equation (7.69)) yields the following eigenvalue problem

$$\left(\rho_0 c_\alpha^2\boldsymbol{I} - \boldsymbol{Q}^\star\right)\bar{\boldsymbol{p}}_\alpha = \boldsymbol{0}, \tag{7.72}$$

where the generalised electro-magneto-mechanical acoustic tensor $\boldsymbol{Q}^\star$ in above equation (7.72) is defined as

$$\begin{aligned}\boldsymbol{Q}^\star = \underbrace{\boldsymbol{\mathcal{C}_{NN}}}_{\text{Classical acoustic tensor}} &\underbrace{-\boldsymbol{\mathcal{Q}_N}^T\left[\boldsymbol{\theta} - \boldsymbol{C}\boldsymbol{R}\boldsymbol{\vartheta}^{-1}\boldsymbol{B}\boldsymbol{R}^T\right]^{-1}\left(\boldsymbol{\mathcal{Q}_N}^\star - \boldsymbol{C}\boldsymbol{R}\boldsymbol{\vartheta}^{-1}\boldsymbol{\mathcal{T}_N}\right)}_{\text{Electric contribution to the acoustic tensor}}\\ &\underbrace{-\boldsymbol{\mathcal{T}_N}^T\left[\boldsymbol{\vartheta} - \boldsymbol{B}\boldsymbol{R}^T\boldsymbol{\theta}^{-1}\boldsymbol{C}\boldsymbol{R}\right]^{-1}\left(\boldsymbol{\mathcal{T}_N}^\star - \boldsymbol{B}\boldsymbol{R}^T\boldsymbol{\theta}^{-1}\boldsymbol{\mathcal{Q}_N}\right)}_{\text{Magnetic contribution to the acoustic tensor}}.\end{aligned} \tag{7.73}$$

Remark 7.2. Particularisation of the expression for the generalised electro-magneto-mechanical acoustic tensor $\boldsymbol{Q}^{\star}$ in equation (7.73) to the field of electromechanics yields the following expression for the generalised electromechanical acoustic tensor, also derived in Reference [30], as

$$\boldsymbol{Q}^{\star} = \boldsymbol{\mathcal{C}}_{\boldsymbol{NN}} - \boldsymbol{\mathcal{Q}}_{\boldsymbol{N}}{}^{T}\boldsymbol{\theta}^{-1}\left[\boldsymbol{I} - \frac{\left(\boldsymbol{N}\otimes\boldsymbol{\theta}^{-1}\boldsymbol{N}\right)}{\boldsymbol{N}\cdot\boldsymbol{\theta}^{-1}\boldsymbol{N}}\right]\boldsymbol{\mathcal{Q}}_{\boldsymbol{N}}. \tag{7.74}$$

Similarly, the expression for the generalised magnetomechanical acoustic tensor can be obtained as

$$\boldsymbol{Q}^{\star} = \boldsymbol{\mathcal{C}}_{\boldsymbol{NN}} - \boldsymbol{\mathcal{T}}_{\boldsymbol{N}}{}^{T}\boldsymbol{\vartheta}^{-1}\left[\boldsymbol{I} - \frac{\left(\boldsymbol{N}\otimes\boldsymbol{\vartheta}^{-1}\boldsymbol{N}\right)}{\boldsymbol{N}\cdot\boldsymbol{\vartheta}^{-1}\boldsymbol{N}}\right]\boldsymbol{\mathcal{T}}_{\boldsymbol{N}}. \tag{7.75}$$

7.4 Symmetrisation of the equations in nonlinear electro-magneto-mechanics

For completeness, the objective of this Section is to show that multi-variable convexity of the internal energy enables the introduction of a generalised convex entropy function which, in turn, guarantees symmetrisation of the system of conservation laws [2,102] presented in equation (7.41). This symmetrisation confirms (see Section 7.3.1) existence of travelling waves in the material, as shown by Hughes *et al.* [2] in the context of Computational Fluid Dynamics and in Section 4.4.3 in the context of Computational Solid Dynamics.

7.4.1 Conservation of energy and generalised convex entropy

In order to derive the suitable generalised entropy and entropy flux functions for electro-magneto-mechanics, let us consider the following convex entropy function defined as

$$S(\boldsymbol{p},\boldsymbol{F},\boldsymbol{H},J,\boldsymbol{D}_0,\boldsymbol{B}_0,\boldsymbol{d},\boldsymbol{b}) = \frac{1}{2\rho_0}\boldsymbol{p}\cdot\boldsymbol{p} + W(\boldsymbol{F},\boldsymbol{H},J,\boldsymbol{D}_0,\boldsymbol{B}_0,\boldsymbol{d},\boldsymbol{b}), \tag{7.76}$$

which clearly represents the kinetic and internal energy per unit undeformed volume. The corresponding flux vector is defined as

$$\boldsymbol{\Lambda} = -\frac{1}{\rho_0}\boldsymbol{P}^{T}\boldsymbol{p} + \boldsymbol{S}_0; \qquad \boldsymbol{S}_0 = \boldsymbol{E}_0\times\boldsymbol{H}_0, \tag{7.77}$$

where $\boldsymbol{S}_0$ in above equation (7.77) is the Poynting vector in the Lagrangian or material configuration. Having defined the entropy S of the system, note first that the conjugate entropy variables are given by the derivatives of S as,

$$\boldsymbol{\mathcal{V}} = \frac{\partial S}{\partial \boldsymbol{\mathcal{U}}} = \begin{bmatrix} \boldsymbol{v} \\ \boldsymbol{\Sigma_F} \\ \boldsymbol{\Sigma_H} \\ \Sigma_J \\ \boldsymbol{\Sigma_{D_0}} \\ \boldsymbol{\Sigma_{B_0}} \\ \boldsymbol{\Sigma_d} \\ \boldsymbol{\Sigma_b} \end{bmatrix}. \tag{7.78}$$

Multiplication of each of the conservation laws in equation (7.41) by the corresponding conjugate variables (7.78), with the use of the involution equations (5.2) for the deformation gradient and its co-factor and (7.8) for $\boldsymbol{D}_0$ and $\boldsymbol{B}_0$ yields

$$\begin{aligned} \dot{S} &= \boldsymbol{v} \cdot \dot{\boldsymbol{p}} + \boldsymbol{\Sigma_F} : \dot{\boldsymbol{F}} + \boldsymbol{\Sigma_H} : \dot{\boldsymbol{H}} + \Sigma_J \dot{J} \\ &\quad + \boldsymbol{\Sigma_{D_0}} \cdot \dot{\boldsymbol{D}}_0 + \boldsymbol{\Sigma_{B_0}} \cdot \dot{\boldsymbol{B}}_0 + \boldsymbol{\Sigma_d} \cdot \dot{\boldsymbol{d}} + \boldsymbol{\Sigma_b} \cdot \dot{\boldsymbol{b}} \\ &= \boldsymbol{v} \cdot \mathrm{DIV}\boldsymbol{P} + \boldsymbol{v} \cdot \boldsymbol{f}_0 + \boldsymbol{\Sigma_F} : \boldsymbol{\nabla}_0 \boldsymbol{v} + \boldsymbol{\Sigma_H} : \mathrm{CURL}\,(\boldsymbol{v} \times \boldsymbol{F}) + \Sigma_J \mathrm{DIV}\left(\boldsymbol{H}^T \boldsymbol{v}\right) \\ &\quad + \boldsymbol{\Sigma_{D_0}} \cdot \dot{\boldsymbol{D}}_0 + \boldsymbol{\Sigma_{B_0}} \cdot \dot{\boldsymbol{B}}_0 + \boldsymbol{\Sigma_d} \cdot (\boldsymbol{\nabla}_0 \boldsymbol{v} \boldsymbol{D}_0 + \boldsymbol{F} \dot{\boldsymbol{D}}_0) + \boldsymbol{\Sigma_b} \cdot (\boldsymbol{\nabla}_0 \boldsymbol{v} \boldsymbol{B}_0 + \boldsymbol{F} \dot{\boldsymbol{B}}_0). \end{aligned} \tag{7.79}$$

Introduction of the expressions for $\boldsymbol{P}$, $\boldsymbol{E}_0$ and $\boldsymbol{H}_0$ in equations (7.17a), (7.17b) and (7.17c) into above equation (7.79) yields

$$\dot{S} = \boldsymbol{v} \cdot \mathrm{DIV}\boldsymbol{P} + \boldsymbol{v} \cdot \boldsymbol{f}_0 + \boldsymbol{P} : \boldsymbol{\nabla}_0 \boldsymbol{v} + \boldsymbol{E}_0 \cdot \dot{\boldsymbol{D}}_0 + \boldsymbol{H}_0 \cdot \dot{\boldsymbol{B}}_0. \tag{7.80}$$

Finally, use of equations (7.7a)-(7.7b) enable to re-write above equation (7.80) as

$$\dot{S} = \mathrm{DIV}\left(\boldsymbol{P}^T \boldsymbol{v} - \boldsymbol{S}_0\right) + \boldsymbol{v} \cdot \boldsymbol{f}_0 - \boldsymbol{E}_0 \cdot \boldsymbol{J}_0, \tag{7.81}$$

with $\boldsymbol{S}_0$ defined in (7.77). Notice that use of the property

$$\boldsymbol{E}_0 \cdot \mathrm{CURL}\boldsymbol{H}_0 - \boldsymbol{H}_0 \cdot \mathrm{CURL}\boldsymbol{E}_0 = -\mathrm{DIV}\,(\boldsymbol{E}_0 \times \boldsymbol{H}_0) \tag{7.82}$$

has been made in above equation (7.81). The statement in equation (7.79) is in fact a simplified version of the energy conservation law, or first law of thermodynamics, which, in the absence of the heat sources and heat flow is globally stated as

$$\frac{d}{dt}\int_V E\, dV = \int_{\partial V} \boldsymbol{t}_0 \cdot \boldsymbol{v}\, dA + \int_V \boldsymbol{f}_0 \cdot \boldsymbol{v}\, dV - \int_{\partial V} \boldsymbol{S}_0 \cdot\, d\boldsymbol{A} - \int_V \boldsymbol{E}_0 \cdot \boldsymbol{J}_0\, dV, \tag{7.83}$$

where E denotes the total energy per unit undeformed volume. The local version of this equation gives,

$$\frac{\partial E}{\partial t} - \mathrm{DIV}\left(\boldsymbol{P}^T \boldsymbol{v} - \boldsymbol{S}_0\right) = \boldsymbol{f}_0 \cdot \boldsymbol{v} - \boldsymbol{E}_0 \cdot \boldsymbol{J}_0. \tag{7.84}$$

From the comparison of both equations (7.81) and (7.84), it is therefore clear that for the reversible scenarios and under consideration of smooth solutions (i.e. in the absence of physical shocks), the generalised entropy can be simply identified as the total energy per unit undeformed volume, that is, $S = E$, coinciding with the notion of Hamiltonian per unit of undeformed volume.

7.4.2 Symmetric hyperbolic equations for elastodynamics

With the definition of the conjugate entropy variables given above (7.78), it is now possible to derive a symmetric quasi-linear system for these variables. Consideration of the involution equations for $\boldsymbol{F}$ and $\boldsymbol{H}$ in (5.2) and those for $\boldsymbol{D}_0$ and $\boldsymbol{B}_0$ in (7.8), enables us to re-write the local form of the conservation law for linear momentum $\boldsymbol{p}$ (refer to equation (7.3) where first Piola-Kirchhoff stress tensor $\boldsymbol{P}$ is substituted by its equivalent representation in (7.17a)), the deformation gradient tensor $\boldsymbol{F}$ (refer to equation (7.26a)), the Co-factor $\boldsymbol{H}$ (refer to (7.26b)), the Jacobian J (refer to (7.26c)), $\boldsymbol{D}_0$ (refer to (7.7b) where $\boldsymbol{H}_0$ is substituted by its equivalent representation (7.17c)), $\boldsymbol{B}_0$ (refer to (7.7a) where $\boldsymbol{E}_0$ is substituted by its equivalent representation (7.17b)), $\boldsymbol{d}$ (refer to (7.31) where $\boldsymbol{H}_0$ is substituted by its equivalent representation (7.17c)) and $\boldsymbol{b}$ (refer to (7.39) where $\boldsymbol{E}_0$ is substituted by its equivalent representation (7.17b)) as

$$\rho_0 \frac{\partial \boldsymbol{v}}{\partial t} - \mathrm{DIV}\boldsymbol{\Sigma}_{\boldsymbol{F}} + \boldsymbol{F}_{\boldsymbol{\Sigma}} \times \mathrm{CURL}\boldsymbol{\Sigma}_{\boldsymbol{H}} - \boldsymbol{H}_{\boldsymbol{\Sigma}} \boldsymbol{\nabla}_0 \Sigma_J - \boldsymbol{\nabla}_0 \boldsymbol{\Sigma}_{\boldsymbol{d}} \boldsymbol{D}_{0\boldsymbol{\Sigma}} - \boldsymbol{\nabla}_0 \boldsymbol{\Sigma}_{\boldsymbol{b}} \boldsymbol{B}_{0\boldsymbol{\Sigma}} = \boldsymbol{f}_0 - \rho_0^e \boldsymbol{\Sigma}_{\boldsymbol{d}}, \tag{7.85}$$

which represents the conservation of linear momentum and

$$[\mathbb{H}_W]^{-1} \frac{\partial}{\partial t} \begin{bmatrix} \boldsymbol{\Sigma}_{\boldsymbol{F}} \\ \boldsymbol{\Sigma}_{\boldsymbol{H}} \\ \Sigma_J \\ \boldsymbol{\Sigma}_{\boldsymbol{D}_0} \\ \boldsymbol{\Sigma}_{\boldsymbol{B}_0} \\ \boldsymbol{\Sigma}_{\boldsymbol{d}} \\ \boldsymbol{\Sigma}_{\boldsymbol{b}} \end{bmatrix} - \begin{bmatrix} \boldsymbol{\nabla}_0 \boldsymbol{v} \\ \boldsymbol{F}_\Sigma \boldsymbol{\times} \boldsymbol{\nabla}_0 \boldsymbol{v} \\ \boldsymbol{H}_{\boldsymbol{\Sigma}} : \boldsymbol{\nabla}_0 \boldsymbol{v} \\ \mathrm{CURL}\boldsymbol{\Sigma}_{\boldsymbol{B}_0} + \boldsymbol{F}_{\boldsymbol{\Sigma}}{}^T \times \boldsymbol{\nabla}_0 \boldsymbol{\Sigma}_{\boldsymbol{b}}{}^T \\ -\mathrm{CURL}\boldsymbol{\Sigma}_{\boldsymbol{D}_0} - \boldsymbol{F}_{\boldsymbol{\Sigma}}{}^T \times \boldsymbol{\nabla}_0 \boldsymbol{\Sigma}_{\boldsymbol{d}}{}^T \\ \boldsymbol{\nabla}_0 \boldsymbol{v} \otimes \boldsymbol{D}_0 - \boldsymbol{F}_{\boldsymbol{\Sigma}} \left(\mathrm{CURL}\boldsymbol{\Sigma}_{\boldsymbol{B}_0} + \boldsymbol{F}_{\boldsymbol{\Sigma}}{}^T \times \boldsymbol{\nabla}_0 \boldsymbol{\Sigma}_{\boldsymbol{b}}{}^T \right) \\ \boldsymbol{\nabla}_0 \boldsymbol{v} \otimes \boldsymbol{B}_0 + \boldsymbol{F}_{\boldsymbol{\Sigma}} \left(\mathrm{CURL}\boldsymbol{\Sigma}_{\boldsymbol{D}_0} + \boldsymbol{F}_{\boldsymbol{\Sigma}}{}^T \times \boldsymbol{\nabla}_0 \boldsymbol{\Sigma}_{\boldsymbol{d}}{}^T \right) \end{bmatrix} = \begin{bmatrix} \boldsymbol{0} \\ \boldsymbol{0} \\ 0 \\ \boldsymbol{J}_0 \\ \boldsymbol{0} \\ \boldsymbol{F}_\Sigma \boldsymbol{J}_0 \\ \boldsymbol{0} \end{bmatrix}, \tag{7.86}$$

which represents the remaining set of conservation laws. Notice in above equation (7.86) that the notations $\boldsymbol{F}_{\boldsymbol{\Sigma}}$, $\boldsymbol{H}_{\boldsymbol{\Sigma}}$, $\boldsymbol{D}_{0\boldsymbol{\Sigma}}$ and $\boldsymbol{B}_{0\boldsymbol{\Sigma}}$ have been used here to explicitly indicate that these variables are now being evaluated from the conjugate variables in (7.78) using the reverse constitutive relationships, namely

$$\begin{aligned} \boldsymbol{F}_{\boldsymbol{\Sigma}} &= \boldsymbol{F}(\boldsymbol{\Sigma}_{\boldsymbol{F}}, \boldsymbol{\Sigma}_{\boldsymbol{H}}, \Sigma_J, \boldsymbol{\Sigma}_{\boldsymbol{D}_0}, \boldsymbol{\Sigma}_{\boldsymbol{B}_0}, \boldsymbol{\Sigma}_{\boldsymbol{d}}, \boldsymbol{\Sigma}_{\boldsymbol{b}}); \\ \boldsymbol{H}_{\boldsymbol{\Sigma}} &= \boldsymbol{H}(\boldsymbol{\Sigma}_{\boldsymbol{F}}, \boldsymbol{\Sigma}_{\boldsymbol{H}}, \Sigma_J, \boldsymbol{\Sigma}_{\boldsymbol{D}_0}, \boldsymbol{\Sigma}_{\boldsymbol{B}_0}, \boldsymbol{\Sigma}_{\boldsymbol{d}}, \boldsymbol{\Sigma}_{\boldsymbol{b}}); \\ \boldsymbol{D}_{0\boldsymbol{\Sigma}} &= \boldsymbol{D}_0(\boldsymbol{\Sigma}_{\boldsymbol{F}}, \boldsymbol{\Sigma}_{\boldsymbol{H}}, \Sigma_J, \boldsymbol{\Sigma}_{\boldsymbol{D}_0}, \boldsymbol{\Sigma}_{\boldsymbol{B}_0}, \boldsymbol{\Sigma}_{\boldsymbol{d}}, \boldsymbol{\Sigma}_{\boldsymbol{b}}); \\ \boldsymbol{B}_{0\boldsymbol{\Sigma}} &= \boldsymbol{B}_0(\boldsymbol{\Sigma}_{\boldsymbol{F}}, \boldsymbol{\Sigma}_{\boldsymbol{H}}, \Sigma_J, \boldsymbol{\Sigma}_{\boldsymbol{D}_0}, \boldsymbol{\Sigma}_{\boldsymbol{B}_0}, \boldsymbol{\Sigma}_{\boldsymbol{d}}, \boldsymbol{\Sigma}_{\boldsymbol{b}}). \end{aligned} \tag{7.87}$$

The symmetric nature of this system is more easily appreciated combining the above set of equations (7.85) and (7.86) to give

$$\boldsymbol{\mathcal{A}}_0 \frac{\partial \boldsymbol{\mathcal{V}}}{\partial t} + \underbrace{\tilde{\boldsymbol{\mathcal{A}}}_I \frac{\partial \boldsymbol{\mathcal{V}}}{\partial X_I}}_{\beta^\star} = \boldsymbol{\mathcal{S}}, \tag{7.88}$$

where matrix $\boldsymbol{\mathcal{A}}_0$ in above equation (7.88) is defined as

$$\boldsymbol{\mathcal{A}}_0 = \begin{bmatrix} \rho_0 \boldsymbol{I} & \boldsymbol{0} \\ \boldsymbol{0} & [\mathbb{H}_W]^{-1} \end{bmatrix}, \tag{7.89}$$

with $[\mathbb{H}_W]$ defined in equation (7.18). It is therefore certain that the matrix $\boldsymbol{\mathcal{A}}_0$ is symmetric positive definite provided that the internal energy e (7.9) is convex multi-variable in the sense described in equation (7.12). Finally, the second term on the left-hand side of (7.88), namely $\beta^\star$ can be expanded in indicial notation as

$$\beta^\star = - \underbrace{\begin{bmatrix} \boldsymbol{0} & \delta_{ik}\delta_{KI} & \mathcal{E}_{ijk}\mathcal{E}_{IJK}F_{jJ} & H_{iI} & \boldsymbol{0} & \boldsymbol{0} & \delta_{ik}D_{0I} & \delta_{ik}B_{0I} \\ & \boldsymbol{0} & \boldsymbol{0} & \boldsymbol{0} & \boldsymbol{0} & \boldsymbol{0} & \boldsymbol{0} & \boldsymbol{0} \\ & & \boldsymbol{0} & \boldsymbol{0} & \boldsymbol{0} & \boldsymbol{0} & \boldsymbol{0} & \boldsymbol{0} \\ & & & 0 & \boldsymbol{0} & \boldsymbol{0} & \boldsymbol{0} & \boldsymbol{0} \\ & & & & \boldsymbol{0} & \mathcal{E}_{JIK} & \boldsymbol{0} & \mathcal{E}_{JIK}F_{kK} \\ & & & & & \boldsymbol{0} & \mathcal{E}_{JKI}F_{kK} & \boldsymbol{0} \\ & & \text{sym} & & & & \boldsymbol{0} & \mathcal{E}_{JIK}F_{iJ}F_{kK} \\ & & & & & & & \boldsymbol{0} \end{bmatrix}}_{\tilde{\boldsymbol{\mathcal{A}}}_I} \frac{\partial}{\partial X_I} \begin{bmatrix} v_k \\ [\boldsymbol{\Sigma}_{\boldsymbol{F}}]_{kK} \\ [\boldsymbol{\Sigma}_{\boldsymbol{H}}]_{kK} \\ \Sigma_J \\ \Sigma_{D_0 K} \\ \Sigma_{B_0 K} \\ \Sigma_{dk} \\ \Sigma_{bk} \end{bmatrix}. \tag{7.90}$$

7.5 Numerical examples

The objective of this section is to analyse the behaviour of convex multi-variable constitutive laws in different scenarios. First, the convex multi-variable electro-magneto-mechanical constitutive law in equation (7.19) will be analysed. In particular, the speed of propagation of acoustic and electro-mechanical waves for this material will be studied for a particular experimental set up. Additionally, an interesting and more detailed study of convex multi-variable constitutive models for the particular case of electro-mechanics will be carried out in this section.

7.5.1 Analysis of eigenvalues (wave speeds) for polyconvex electro-magneto-mechanical materials

Let us consider the constitutive model presented in equation (7.19), suitable for the description of the behaviour of electro-magnetrostrictive materials in the large deformation and large electric and magnetic fields regime. For this specific simple

convex multi-variable constitutive law, the non-zero components of the matrix $\boldsymbol{\mathcal{A}}^{\star}_{\boldsymbol{N}}$ in equation (7.55) can be written as

$$\begin{aligned}
\boldsymbol{\mathcal{C}}_{\boldsymbol{NN}} &= 2\mu_1\boldsymbol{I} + 2\mu_2\left[(\boldsymbol{FN}\otimes\boldsymbol{FN}) - (\boldsymbol{FN}\cdot\boldsymbol{FN})\boldsymbol{I} - \boldsymbol{FF}^T + (\boldsymbol{F}:\boldsymbol{F})\boldsymbol{I}\right] \\
&\quad + f''(J)(\boldsymbol{HN}\otimes\boldsymbol{HN}) + \frac{1}{\varepsilon_2}\boldsymbol{D}^2_{0\boldsymbol{N}}\boldsymbol{I} + \frac{1}{\hat{\mu}_2}\boldsymbol{B}^2_{0\boldsymbol{N}}\boldsymbol{I}; \\
\boldsymbol{\mathcal{Q}}_{\boldsymbol{N}}{}^T &= \frac{1}{\varepsilon_2}\left(\boldsymbol{d}\otimes\boldsymbol{N} + \boldsymbol{F}\left(\boldsymbol{D}_0\cdot\boldsymbol{N}\right)\right); \\
\boldsymbol{\mathcal{T}}_{\boldsymbol{N}}{}^T &= \frac{1}{\hat{\mu}_2}\left(\boldsymbol{b}\otimes\boldsymbol{N} + \boldsymbol{F}\left(\boldsymbol{B}_0\cdot\boldsymbol{N}\right)\right); \\
\boldsymbol{\theta} &= \frac{1}{\varepsilon_1}\boldsymbol{I} + \frac{1}{\varepsilon_2}\boldsymbol{F}^T\boldsymbol{F}; \\
\boldsymbol{\vartheta} &= \frac{1}{\hat{\mu}_1}\boldsymbol{I} + \frac{1}{\hat{\mu}_2}\boldsymbol{F}^T\boldsymbol{F}.
\end{aligned} \tag{7.91}$$

In the reference configuration, where $\boldsymbol{\nabla}_0\boldsymbol{x} = \boldsymbol{I}$, $\boldsymbol{D}_0 = \boldsymbol{0}$ and $\boldsymbol{B}_0 = \boldsymbol{0}$, an explicit expression for the the eigenvalues of the matrix $\boldsymbol{\mathcal{A}}^{\star}_{\boldsymbol{N}}$ can be obtained (e.g. by using a standard symbolic algebra computer package) as

$$\begin{aligned}
c_1 = c_2 &= 0; \\
c_l = c_3 = c_4 = -c_5 = -c_6 &= \sqrt{\frac{(\hat{\mu}_2+\hat{\mu}_1)(\varepsilon_2+\varepsilon_1)}{\varepsilon_2\varepsilon_1\hat{\mu}_2\hat{\mu}_2}} = c_0 c_r; \\
c_s = c_7 = c_8 = -c_9 = -c_{10} &= \sqrt{\frac{2\left(\mu_1+\mu_2\right)}{\rho_0}} = \sqrt{\frac{\mu}{\rho_0}}; \\
c_p = c_{11} = c_{12} &= \sqrt{\frac{2\left(\mu_1+\mu_2\right)+\lambda}{\rho_0}} = \sqrt{\frac{\mu+\lambda}{\rho_0}}.
\end{aligned} \tag{7.92}$$

The set of eigenvalues denoted as c_l represents the speed of light in the material. Therefore, c_0 and c_r in above equation (7.92) represent the speed of light in vacuum and the relative speed of light in the material. The set of eigenvalues denoted as c_s corresponds to the speed of propagation of shear waves [42]. Finally, the set of eigenvalues c_p corresponds to the speed of propagation of pressure waves [42] in the material. For a Young's modulus $E = 10^5\,Pa$, Poisson ratio $\nu = 0.48$[2], relative permittivity $\varepsilon_r = 4$, relative permeability $\hat{\mu}_r = 4$ and a density of $720\,kg/m^3$, all of them in the reference configuration, the speed of propagation for shear, pressure and electromagnetic (speed of light) waves is

$$c_s = 6.85\,m/s; \qquad c_p = 34.25\,m/s; \qquad c_l = 7.49\times10^7\,m/s. \tag{7.94}$$

[2]Given the Young's modulus E and the Poisson ratio ν, the shear modulus μ and the first Lamé parameter λ are obtained as

$$\mu = \frac{E}{2\left(1+\nu\right)}; \qquad \lambda = \frac{E\nu}{\left(1+\nu\right)\left(1-2\nu\right)}. \tag{7.93}$$

Let us now consider a different configuration characterised by a purely volumetric deformation gradient tensor defined in terms of the uniform stretch λ as $\boldsymbol{F} = \lambda \boldsymbol{I}$. Moreover, let the electric displacement and magnetic induction be defined in terms of their dimensionless modulus, $\tilde{D}_0$ and $\tilde{B}_0$ respectively, as $\boldsymbol{D}_0 = \sqrt{\mu\varepsilon}\tilde{D}_0\boldsymbol{E}_2$ and $\boldsymbol{B}_0 = \sqrt{\mu\hat{\mu}}\tilde{B}_0\boldsymbol{E}_3$, with the unit vectors $\boldsymbol{E}_2$ and $\boldsymbol{E}_3$ defined in equation (4.6). For this specific configuration, Figure 7.4 shows the speed of propagation of the pressure waves for different values of $\{\lambda, \tilde{D}_0, \tilde{B}_0\}$ and for different orientations of the propagation vector $\boldsymbol{N}$, spherically characterised in terms of the angles $0 \leq \alpha \leq 2\pi$ and $0 \leq \beta \leq \pi$ as

$$\boldsymbol{N} = \begin{bmatrix} \sin\beta\cos\alpha & \sin\beta\sin\alpha & \cos\beta \end{bmatrix}^T . \tag{7.95}$$

Similarly, Figure 7.5 displays the evolution of the speed of propagation of shear waves for different values of $\{\lambda, \tilde{D}_0, \tilde{B}_0\}$ and for different orientations of the propagation vector $\boldsymbol{N}$. The speed of light in the material c_l remains practically unaltered throughout the entire range of deformations. This confirms that the speed of propagation of acoustic waves are dramatically changed in the presence of an electric field and/or magnetic field. However, the speed of propagation of electromagnetic waves is almost unaffected by the deformation in the material and hence, not displayed.

7.5.2 Analysis of electro-mechanical constitutive models

In this section, an analysis of the behaviour of electro-active materials described via polyconvex and non polyconvex constitutive models is carried out.

Analytical derivation of wave speeds in simple polyconvex constitutive models for dielectric elastomers

The aim of this section is to obtain the explicit representation of the speed of propagation of the acoustic waves for the particular scenario of electro-mechanics, where magnetic effects can be neglected and for the case of a simple convex multi-variable constitutive model. From the eigenvalue problem in equation (7.72), the wave speeds can be obtained as the square root of the quotient between the eigenvalues of the generalised electro-mechanical acoustic tensor $\boldsymbol{Q}^\star$ (7.74) and the density ρ_0. The convex multi-variable constitutive model in equation (7.19) is considered (where magnetic effects are neglected). For this particular constitutive model, the expression for $\boldsymbol{Q}^\star$ yields

$$\begin{aligned} \boldsymbol{Q}^\star = {} & 2\mu_1\boldsymbol{I} + 2\mu_2\left[(\boldsymbol{F}\boldsymbol{N}\otimes\boldsymbol{F}\boldsymbol{N}) - (\boldsymbol{F}\boldsymbol{N}\cdot\boldsymbol{F}\boldsymbol{N})\boldsymbol{I} - \boldsymbol{F}\boldsymbol{F}^T + (\boldsymbol{F}:\boldsymbol{F})\boldsymbol{I}\right] + f''(J)\,(\boldsymbol{H}\boldsymbol{N}\otimes\boldsymbol{H}\boldsymbol{N}) \\ & + \varepsilon_2\left(\frac{\boldsymbol{D}_0\cdot\boldsymbol{N}}{\varepsilon_2}\right)^2 - \left(\frac{\boldsymbol{D}_0\cdot\boldsymbol{N}}{\varepsilon_2}\right)^2 \underbrace{\boldsymbol{F}\boldsymbol{I}_{\boldsymbol{N}\boldsymbol{N}}\boldsymbol{\theta}^{-1}\left[\boldsymbol{I} - \frac{\left(\boldsymbol{N}\otimes\boldsymbol{\theta}^{-1}\boldsymbol{N}\right)}{\boldsymbol{N}\cdot\boldsymbol{\theta}^{-1}\boldsymbol{N}}\right]\boldsymbol{F}^T}_{\boldsymbol{c}_{\boldsymbol{D}}} . \end{aligned} \tag{7.96}$$

The eigenvalues of the generalised electro-mechanical acoustic tensor $\boldsymbol{Q}^\star$ in above equation (7.96) depend on the propagation vector $\boldsymbol{N}$. We restrict our analysis to

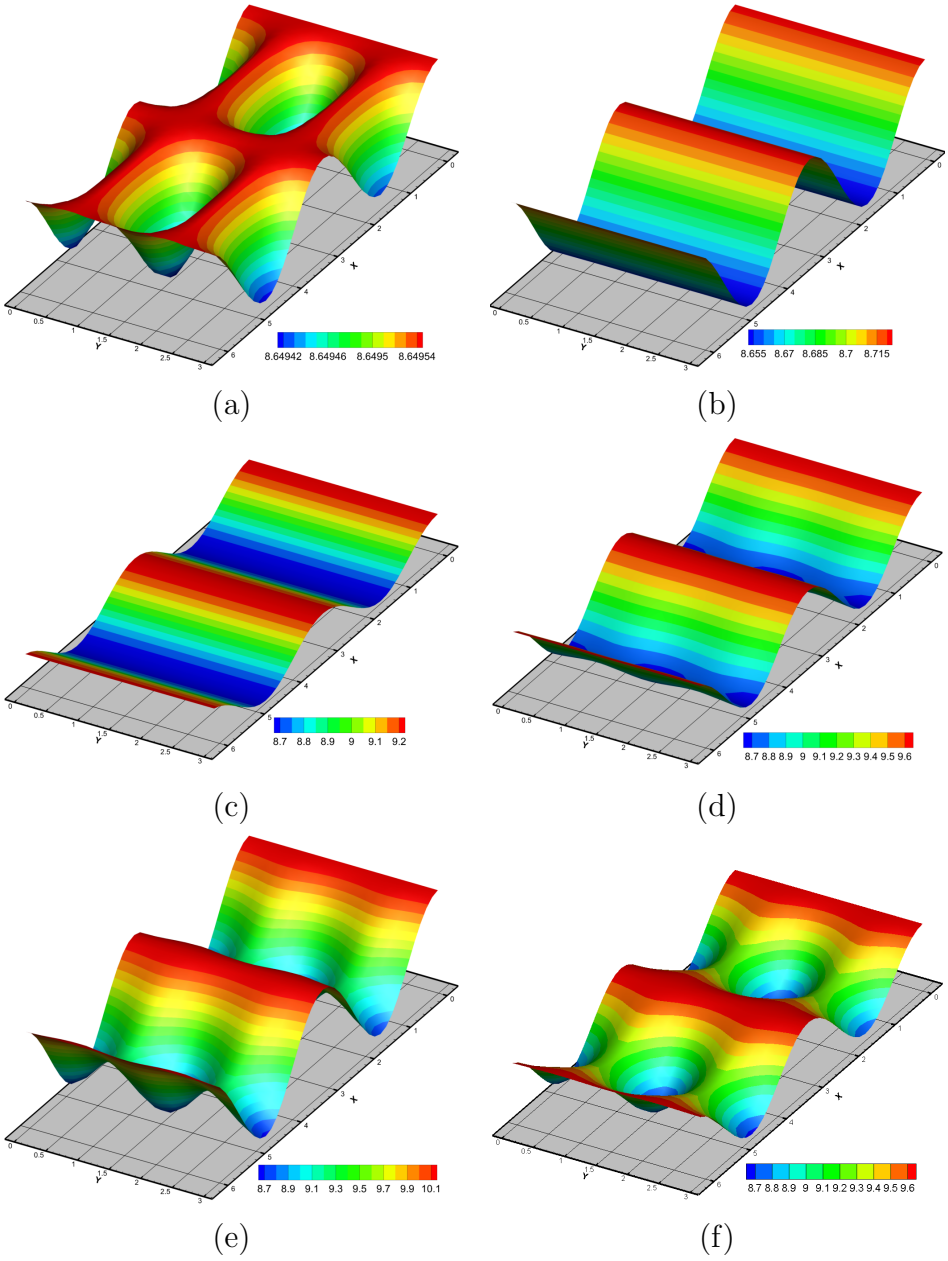

Figure 7.4: Representation of the pressure waves for the convex multi-variable constitutive model in equation (7.19) for different orientations of the propagation vector $\boldsymbol{N}$, spherically parametrised as in equation (7.95). The values for the set $\{\lambda, \tilde{D}_0, \tilde{B}_0\}$ are a) $\{0.54, 0.01, 1\}$; b) $\{0.58, 0.1, 1\}$; c) $\{0.62, 0.2, 1\}$; d) $\{1, 0.2, 1\}$; e) $\{1.4, 0.2, 1\}$ and f) $\{1.14, 0.3, 1\}$.

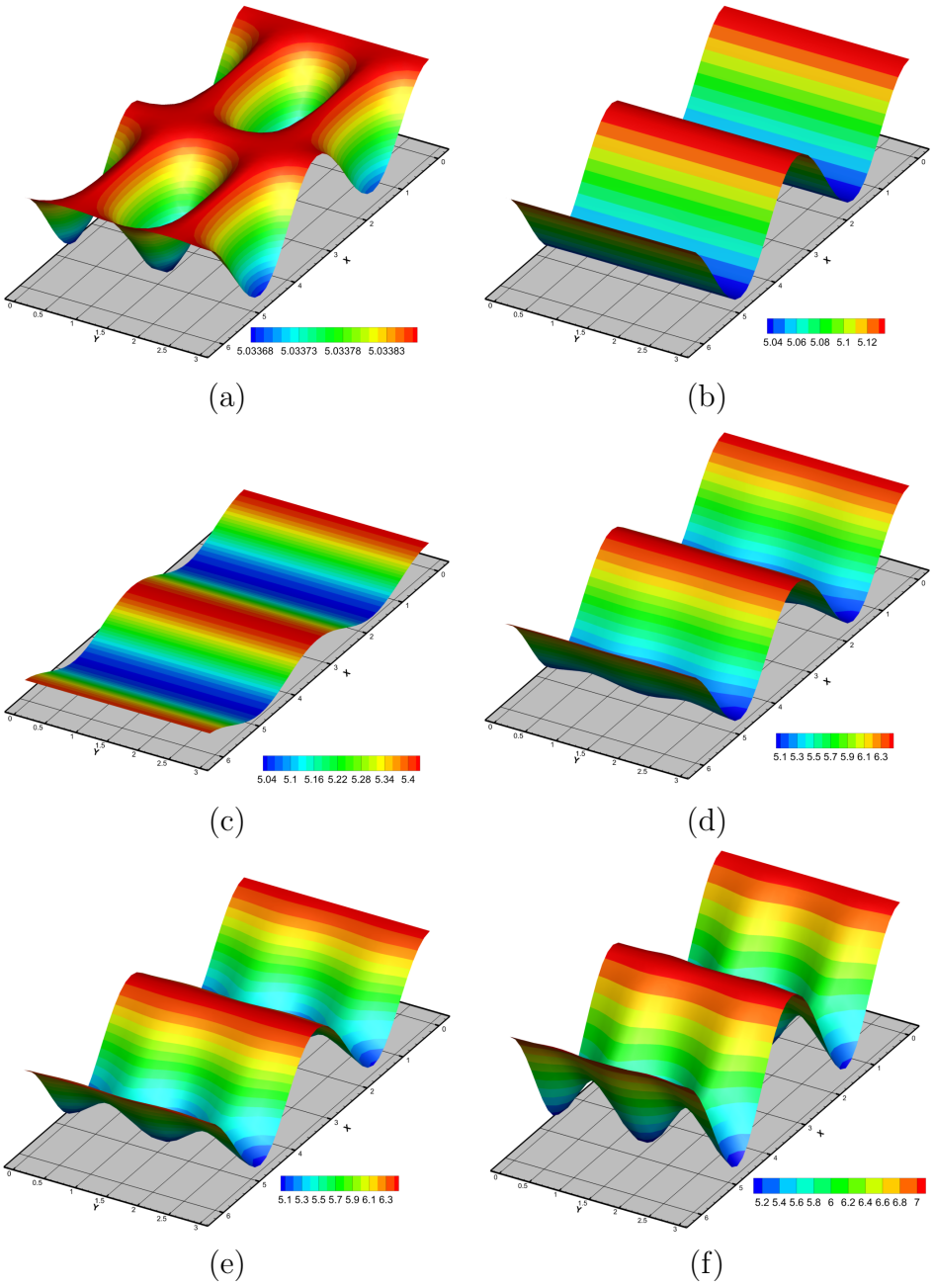

Figure 7.5: Representation of the shear waves for the convex multi-variable constitutive model in equation (7.19) for different orientations of the propagation vector $\boldsymbol{N}$, spherically parametrised as in equation (7.95). The values for the set $\{\lambda, \tilde{D}_0, \tilde{B}_0\}$ are a) $\{0.54, 0.01, 1\}$; b) $\{0.58, 0.1, 1\}$; c) $\{0.62, 0.2, 1\}$; d) $\{1, 0.2, 1\}$; e) $\{1.4, 0.2, 1\}$ and f) $\{1.14, 0.3, 1\}$.

the case where the propagation vector is a principal direction of the deformation. In this case, let the eigenvalues of the deformation $\{\lambda_1, \lambda_2, \lambda_3\}$ be associated to the (unitary) principal directions in the deformed and undeformed configurations, denoted as $\{\boldsymbol{t}_1, \boldsymbol{t}_2, \boldsymbol{n}\}$ and $\{\boldsymbol{T}_1, \boldsymbol{T}_2, \boldsymbol{N}\}$, as in Section 4.6.1. In that case, introduction of the different identities in equation (4.68) into equation (7.96) for the specialised scenario considered yields the following expression for the generalised electro-mechanical acoustic tensor $\boldsymbol{Q}^*$

$$\begin{aligned}\boldsymbol{Q}^\star = 2\mu_1\boldsymbol{I} + 2\mu_2\left(\left(\lambda_1^2+\lambda_2^2\right)\boldsymbol{I} - \boldsymbol{\Lambda}_T\right) + f''(J)\left(\frac{J}{\lambda_3}\right)^2 \boldsymbol{n}\otimes\boldsymbol{n} \\ + \varepsilon_2\left(\frac{\boldsymbol{D}_0\cdot\boldsymbol{N}}{\varepsilon_2}\right)^2 - \left(\frac{\boldsymbol{D}_0\cdot\boldsymbol{N}}{\varepsilon_2}\right)^2 \underbrace{\boldsymbol{F}\boldsymbol{I}_{\boldsymbol{NN}}\boldsymbol{\theta}^{-1}\left[\boldsymbol{I} - \frac{\left(\boldsymbol{N}\otimes\boldsymbol{\theta}^{-1}\boldsymbol{N}\right)}{\boldsymbol{N}\cdot\boldsymbol{\theta}^{-1}\boldsymbol{N}}\right]\boldsymbol{F}^T}_{\boldsymbol{\mathcal{C}_D}}.\end{aligned} \tag{7.97}$$

where the rank two tensor $\boldsymbol{\Lambda}_T$ in above equation (7.97) is defined as

$$\boldsymbol{\Lambda}_T = \lambda_1^2\boldsymbol{t}_1\otimes\boldsymbol{t}_1 + \lambda_2^2\boldsymbol{t}\otimes\boldsymbol{t}_2. \tag{7.98}$$

The wave speeds then can be obtained by solving the following equation (refer to equation (7.72))

$$\rho_0 c_\alpha^2 = \bar{\boldsymbol{p}}_\alpha\cdot\boldsymbol{Q}^\star\bar{\boldsymbol{p}}_\alpha. \tag{7.99}$$

Combination of equation (7.99) and the expression for $\boldsymbol{Q}^\star$ in (7.97) finally yields

$$\begin{aligned}\rho_0 c_\alpha^2 = 2\mu_1 + 2\mu_2\left(\left(\lambda_1^2+\lambda_2^2\right) - \bar{\boldsymbol{p}}_\alpha\cdot\boldsymbol{\Lambda}_T\bar{\boldsymbol{p}}_\alpha\right) + f''(J)\left(\frac{J}{\lambda_3}\right)^2(\bar{\boldsymbol{p}}_\alpha\cdot\boldsymbol{n})^2 \\ + \left(\frac{D_{0N}}{\varepsilon_2}\right)^2\left(1 - \underbrace{\left(\sum_{\alpha=1}^{2}\lambda_\alpha\boldsymbol{t}_\alpha\cdot\bar{\boldsymbol{p}}_\alpha\right)\left(\left(\boldsymbol{F}^T\bar{\boldsymbol{p}}_\alpha\cdot\boldsymbol{\theta}^{-1}\boldsymbol{T}_\alpha\right) - \frac{\left(\boldsymbol{T}_\alpha\cdot\boldsymbol{\theta}^{-1}\boldsymbol{N}\right)\left(\boldsymbol{\theta}^{-1}\boldsymbol{N}\cdot\boldsymbol{F}^T\bar{\boldsymbol{p}}_\alpha\right)}{\boldsymbol{N}\cdot\boldsymbol{\theta}^{-1}\boldsymbol{N}}\right)}_{\bar{\boldsymbol{p}}_\alpha\cdot\boldsymbol{\mathcal{C}_D}\bar{\boldsymbol{p}}_\alpha}\right).\end{aligned} \tag{7.100}$$

where $D_{0N} = \boldsymbol{D}_0\cdot\boldsymbol{N}$ and where the expression for $\bar{\boldsymbol{p}}_\alpha\cdot\boldsymbol{\mathcal{C}_D}\bar{\boldsymbol{p}}_\alpha$ in above equation (7.100) has been obtained in equation (H.11). The first set of eigenvalues corresponding to $p-$waves is obtained by taking $\bar{\boldsymbol{p}}_\alpha = \boldsymbol{n}$ to give

$$c_{1,2} = \pm\sqrt{\frac{\mu_1 + \mu_2\left(\lambda_1^2+\lambda_2^2\right) + f''(J)\left(\frac{J}{\lambda_3}\right)^2 + \frac{D_{0N}^2}{\varepsilon_2}}{\rho_0}}. \tag{7.101}$$

The next four eigenvalues correspond to shear waves where the vibration takes place on the propagation plane. The corresponding velocity vectors are orthogonal to $\boldsymbol{n}$ and in the directions of the unit eigenvectors $\{\boldsymbol{t}_1, \boldsymbol{t}_2\}$ of the rank-two tensor $\boldsymbol{\Lambda}_T$. Particularisation of the expression for $\boldsymbol{\mathcal{C}_D}$ in equation (H.11) to the case of

shear waves gives

$$c_{3,4} = \pm\sqrt{\frac{\mu_1 + \mu_2\lambda_2^2 + f''(J)\left(\frac{J}{\lambda_3}\right)^2 + \left(\frac{D_{0N}}{\varepsilon_2}\right)^2\left(\varepsilon_2 - \lambda_1\left(\alpha_1 + \alpha_2\lambda_1^2 + \alpha_3\left(\frac{J}{\lambda_1}\right)^2\right)\right)}{\rho_0}};$$
$$c_{5,6} = \pm\sqrt{\frac{\mu_1 + \mu_2\lambda_1^2 + f''(J)\left(\frac{J}{\lambda_3}\right)^2 + \left(\frac{D_{0N}}{\varepsilon_2}\right)^2\left(\varepsilon_2 - \lambda_2\left(\alpha_1 + \alpha_2\lambda_1^2 + \alpha_3\left(\frac{J}{\lambda_2}\right)^2\right)\right)}{\rho_0}}, \tag{7.102}$$

where the expression for the coefficients $\{\alpha_1, \alpha_2, \alpha_3\}$ in above equation (7.102) has been determined in equation (H.7). Polyconvexity of the constitutive model considered entails that the six eigenvalues in equations (7.101) and (7.102) must be real.

For more complex convex multi-variable constitutive models, the same procedure as that followed in the current section can be followed in order to derive an explicit representation of the wave speeds for a specific direction of propagation coinciding with a principal direction of the deformation. However, the complexity of the model, associated to possible nonlinear effects such as electrostriction [109] or electric saturation [109] could lead to cumbersome algebraic manipulations.

Analysis of material stability in dielectric elastomers

The Legendre-Hadamard condition is strongly related to the material stability of the constitutive equations [86]. The objective of this Section is to analyse the material stability of some relevant convex and non-convex multi-variable constitutive models suitable for the description of isotropic electrostrictive [109] dielectric elastomers.

In particular, we focus on dielectric elastomers subjected to a specific experimental set up which has been presented in Reference [75] and which is depicted in Figure 7.6. In this set up, a thin film of an incompressible dielectric elastomer is subjected to an electric field applied across its thickness, namely, in direction OX_3. Consequently, a uniform deformation in the plane of the film (perpendicular to the axis OX_3) characterised by the stretch λ, is observed. However, a slightly different scenario to that in Reference [75] is analysed in the present section, in which the deformation in the OX_2 is completely constrained. Therefore, the deformation gradient tensor (accounting for the incompressibility constraint) can be expressed as

$$\boldsymbol{F} = \begin{bmatrix} \lambda & 0 & 0 \\ 0 & 1 & 0 \\ 0 & 0 & 1/\lambda \end{bmatrix}. \tag{7.103}$$

The behaviour of two constitutive models is studied in this section. First, the following convex multi-variable constitutive model (slightly different to the convex multi-variable electrostrictive constitutive model presented in equation (5.81)) is

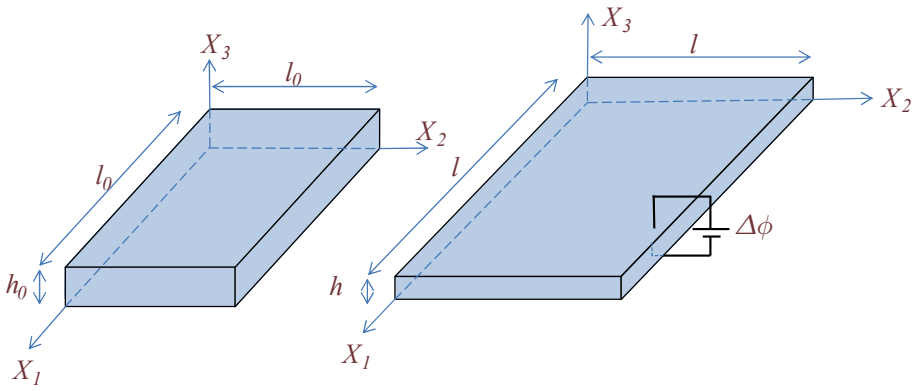

Figure 7.6: Experimental set up. The application of a uniform electric potential gradient across the thickness of the incompressible dielectric elastomer film (parallel to the axis OX_3) of initial length and thickness l_0 and h_0 respectively, leads to a uniform axial expansion in the OX_1 direction and final thickness $h = 1/\lambda h_0$, with λ the stretch in the dielectric elastomer.

defined as

$$W_{el,1} = \mu_1 II_{\boldsymbol{F}} + \mu_2 II_{\boldsymbol{H}} + \frac{1}{2\varepsilon_1} II_{\boldsymbol{d}} + \mu_e \underbrace{\left(II_{\boldsymbol{F}}^2 + \frac{2}{\mu_e \varepsilon_e} II_{\boldsymbol{F}} II_{\boldsymbol{d}} + \frac{1}{\mu_e^2 \varepsilon_e^2} II_{\boldsymbol{d}} \right)}_{\text{Stabilised electrostrictive invariant}} + \frac{1}{2\varepsilon_2} II_{\boldsymbol{D}_0} - \mu \ln J + \frac{\kappa}{2} (J-1)^2 . \tag{7.104}$$

An alternative non-convex multi-variable constitutive model(slightly different to the non-convex multi-variable electrostrictive constitutive model presented in equation (5.91)) is defined as

$$W_{el,2} = \tilde{\mu}_1 II_{\boldsymbol{F}} + \tilde{\mu}_2 II_{\boldsymbol{H}} + \frac{1}{2\tilde{\varepsilon}_1} II_{\boldsymbol{d}} + \underbrace{\frac{2}{\tilde{\varepsilon}_e} II_{\boldsymbol{F}} II_{\boldsymbol{d}}}_{\text{Non polyconvex invariant}} + \frac{1}{2\tilde{\varepsilon}_2} II_{\boldsymbol{D}_0} - \mu \ln J + \frac{\tilde{\kappa}}{2} (J-1)^2 . \tag{7.105}$$

Auxiliary material parameters f_e and f_s, defined exactly as in equations (5.83) and (5.84) for the convex multi-variable model in (5.81) and $\hat{f}_e$, defined as in equation (5.93) for the non-convex multi-variable model in (5.91) can be introduced to control the level of electrostriction and electrical saturation of the model.

Notice that more severe mechanical stiffening can be achieved via introduction of invariants of the form $II_{\boldsymbol{F}}^m$, with $m \geq 2$ as in the purely mechanical Arruda-Boyce constitutive model [77]. An alternative constitutive model, suitable for rubber-like materials with stiffening behaviour and hence, for dielectric elastomers, is the Gent constitutive model [81]. This two alternative constitutive models can always be written as a convex combination of some of the strictly mechanical entities in the set $\mathcal{V}$ (7.13), namely $\{\boldsymbol{F}, \boldsymbol{H}, J\}$.

Determination of the value of the variables $\{f_e, f_s\}$ for the constitutive model $W_{el,1}$ in (7.104) which minimises the error in the variables $\{\boldsymbol{P}, \lambda, \tilde{D}, \tilde{E}\}$ between both constitutive models $W_{el,1}$ in (7.104) and $W_{el,2}$ in (7.105) for the entire experimental set up has been carried out. Figure 7.8 shows the qualitatively accurate agreement in the response for both convex multi-variable and non-multi-variable convex constitutive models in equations (7.104) and (7.105), respectively, for a particular value of the electrostrictive parameter of $\hat{f}_e = 1.5$ (moderate electrostriction), which corresponds (after minimisation) to a value of the parameters $\{f_e, f_s\}$ of $f_e = 1.195$ and $f_s = 0.163$[3].

Certainly, this minimisation procedure entails a qualitative similarity of the different constitutive tensors relevant in electro-mechanics, namely $\boldsymbol{\mathcal{C}}$, $\boldsymbol{\mathcal{Q}}$ and $\boldsymbol{\theta}$ in equation (5.20) for the entire experimental set up for both multi-variable convex $W_{el,1}$ and non-multi-variable convex $W_{el,2}$ constitutive models. Figure 7.9 shows the graphical visualisation of these tensors for both constitutive models in equation (7.104) and (7.105) for different stages of the experimental set up for a value of the electrostrictive parameter for the non-multi-variable convex model $W_{el,2}$ of $\hat{f}_e = 1.5$ $\hat{f}_e = 1.5$ (moderate electrostriction), which corresponds (after minimisation) to a value of the parameters $\{f_e, f_s\}$ of $f_e = 1.195$ and $f_s = 0.163$. Based on Reference [112] and [76], a spherical parametrisation of a vector $\boldsymbol{n}$ permits to define the moduli $\tilde{\mu}$, $\tilde{\mathcal{Q}}$ and $\tilde{\varepsilon}$ in Figure (7.9) as

$$\tilde{\mu} = (\boldsymbol{n} \otimes \boldsymbol{n}) : \boldsymbol{\mathcal{C}} : (\boldsymbol{n} \otimes \boldsymbol{n})\,; \qquad \tilde{\mathcal{Q}} = \boldsymbol{\mathcal{Q}} : (\boldsymbol{n} \otimes \boldsymbol{n} \otimes \boldsymbol{n})\,; \qquad \frac{1}{\tilde{\varepsilon}} = \boldsymbol{n}\boldsymbol{\theta}\boldsymbol{n}. \tag{7.106}$$

Figures 7.10 and 7.11 study the possible loss of material stability for the non-multi-variable convex constitutive law $W_{el,2}$ (7.105) and the multi-variable convex constitutive model $W_{el,1}$ (7.104)[4] for the current experimental set up considered, depicted in Figure 7.6. Loss of material stability is associated to the loss of positive definiteness of the generalised electro-mechanical acoustic tensor $\boldsymbol{Q}^\star$ in equation (7.74) [86]. Therefore, a sufficient condition for material instability (refer to equation (4.76)) is

$$\begin{aligned} q &= \min\left(q_1, q_2, q_3\right) \leq 0; \qquad & q_1 &= Q^\star_{11}; \\ q_2 &= Q^\star_{11}Q^\star_{22} - Q^\star_{12}Q^\star_{21}; \qquad & q_3 &= \det \boldsymbol{Q}^\star. \end{aligned} \tag{7.107}$$

The evolution of the variable q in (7.107) for all the possible orientations of the propagation vector $\boldsymbol{N}$ for both constitutive models $W_{el,1}$ (7.104) and $W_{el,2}$ (7.105) is depicted in Figures 7.10 and 7.11, respectively. The same highly electrostrictive material as in Figure 7.9 is considered. It can be observed in Figure 7.10 that at a certain stage of the experimental set up, the variable q becomes zero (negative values of the variable q (7.107) have been set to zero in order to facilitate the

[3]For the remaining values of $\tilde{f}_e$ (5.93) used in Figure 7.7, namely $\{1.05, 10, 100\}$, the associated value of the parameters f_e (5.83) and f_s (5.84) resulting after minimisation are $\{1.024, 1.701, 1.833\}$ and $\{0.019, 0.887, 0.999\}$, respectively.

[4]Convex multi-variable constitutive models in the sense described in equation (5.12) are always materially stable.

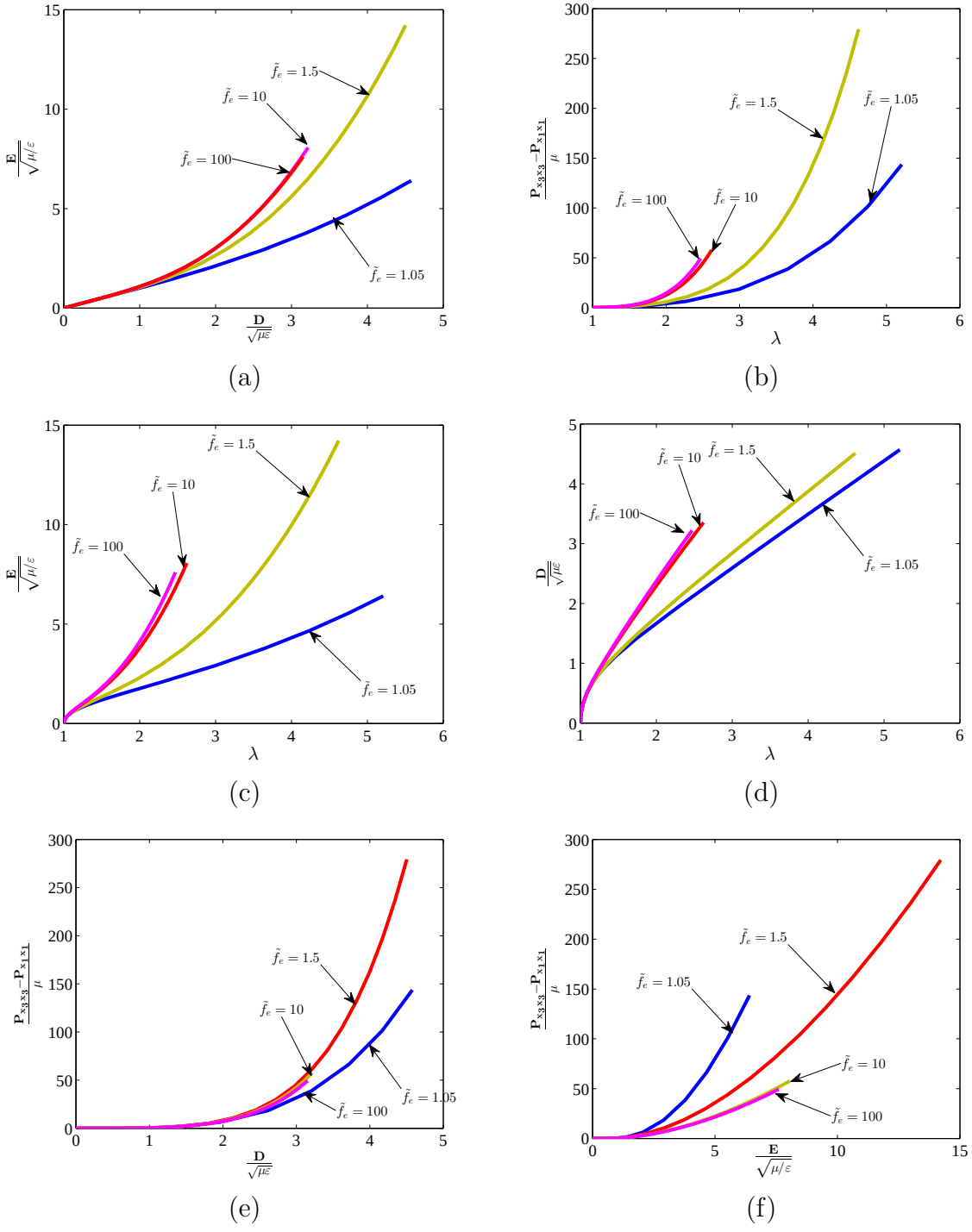

Figure 7.7: Numerical experiment reproducing the experimental set up in Figure 7.6. Response of the non-multi-variable convex constitutive model $W_{el,2}$ in (7.105) for different values of the electrostrictive parameter $\hat{f}_e$ in equation (5.93) for material parameters $E = 10^5\, N/m^2$, $\nu = 0.48$ and $\varepsilon_r = 4$. The following choice of material parameters was used: $\tilde{\mu}_1 = 2\tilde{\mu}_2$, $\varepsilon_2 = \infty$. Representation of the relation between (a) E vs D, (b) $\boldsymbol{P}_{\boldsymbol{x}_1\boldsymbol{x}_1} - \boldsymbol{P}_{\boldsymbol{x}_3\boldsymbol{x}_3}$ vs λ, (c) E vs λ, (d) D vs λ, (d) $\boldsymbol{P}_{\boldsymbol{x}_1\boldsymbol{x}_1} - \boldsymbol{P}_{\boldsymbol{x}_3\boldsymbol{x}_3}$ vs D and (d) $\boldsymbol{P}_{\boldsymbol{x}_1\boldsymbol{x}_1} - \boldsymbol{P}_{\boldsymbol{x}_3\boldsymbol{x}_3}$ vs E.

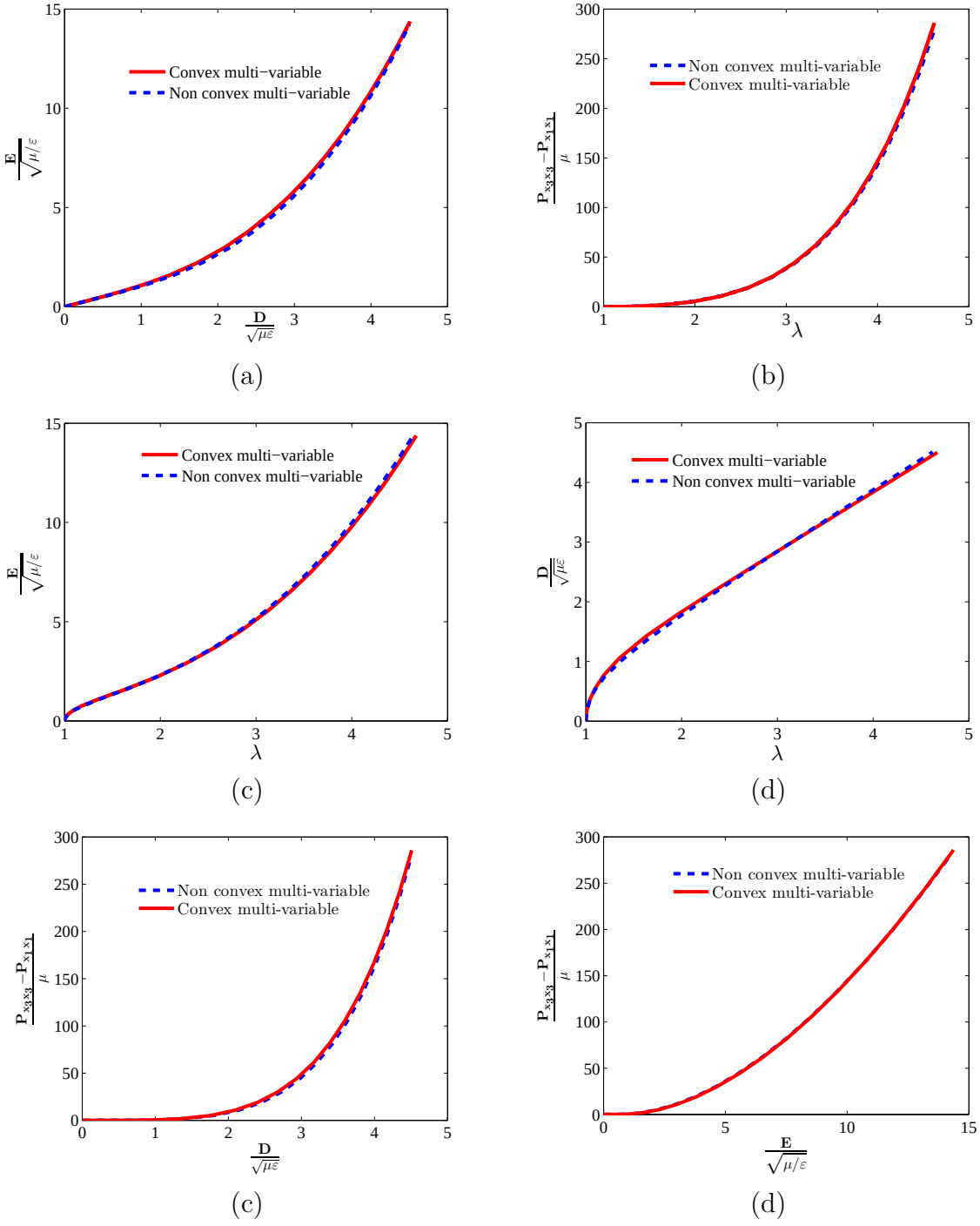

Figure 7.8: Numerical experiment reproducing the experimental set up in Figure 7.6. Response of the non-multi-variable convex constitutive model $W_{el,2}$ in (7.105) for $\hat{f}_e = 1.5$ (5.93) and multi-variable convex model $W_{el,1}$ in (7.104) for $f_e = 1.195$ (5.83) and $f_s = 0.163$ (5.84). The following choice of material parameters was used: $\tilde{\mu}_1 = 2\tilde{\mu}_2$, $\varepsilon_2 = \infty$. Representation of the relation between (a) E vs D, (b) $\boldsymbol{P}_{\boldsymbol{x}_1\boldsymbol{x}_1} - \boldsymbol{P}_{\boldsymbol{x}_3\boldsymbol{x}_3}$ vs λ, (c) E vs λ, (d) D vs λ, (d) $\boldsymbol{P}_{\boldsymbol{x}_1\boldsymbol{x}_1} - \boldsymbol{P}_{\boldsymbol{x}_3\boldsymbol{x}_3}$ vs D and (d) $\boldsymbol{P}_{\boldsymbol{x}_1\boldsymbol{x}_1} - \boldsymbol{P}_{\boldsymbol{x}_3\boldsymbol{x}_3}$ vs E.

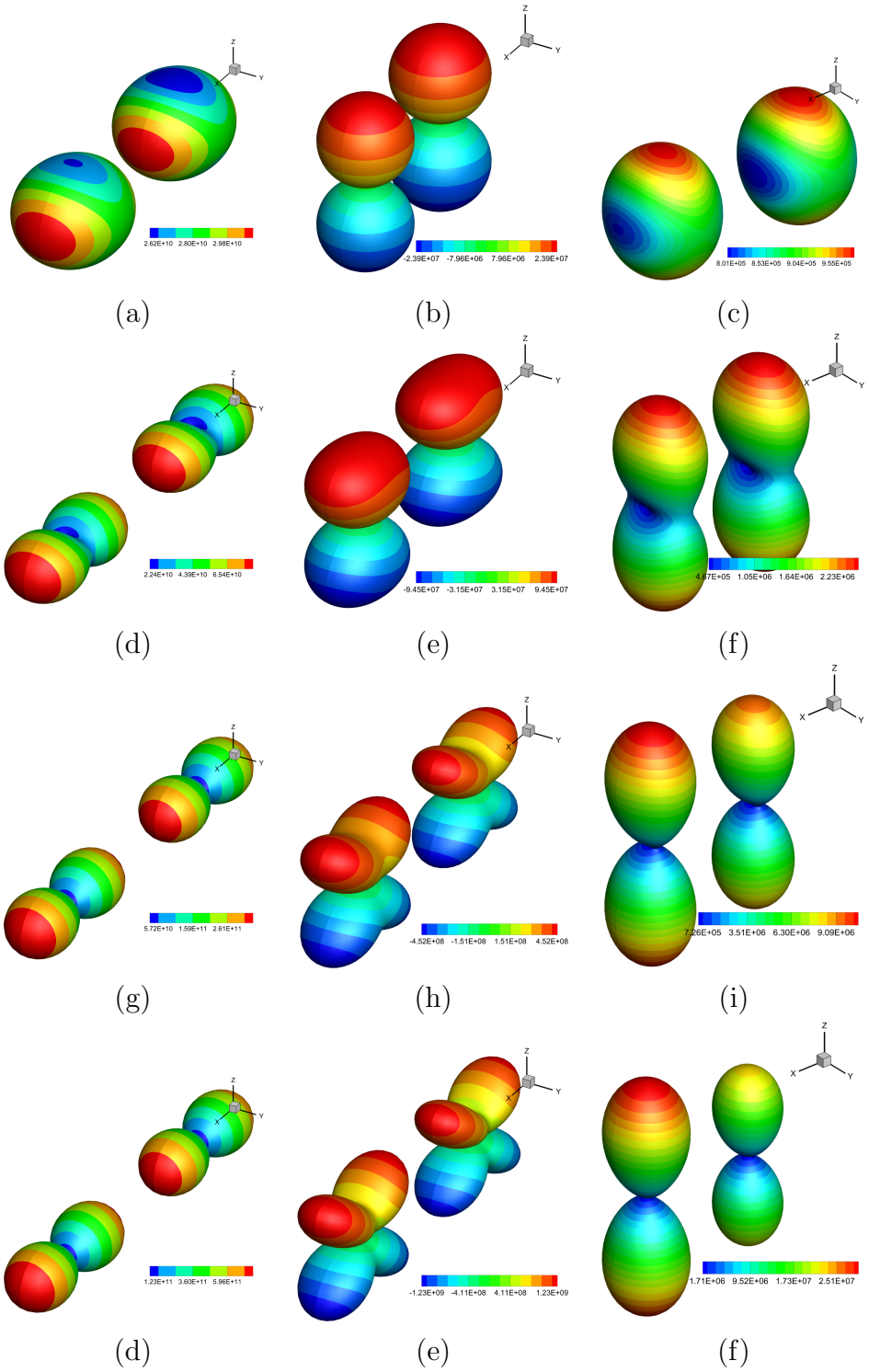

Figure 7.9: Numerical experiment reproducing the experimental set up in Figure 7.6. Evolution of $\frac{1}{\tilde{\varepsilon}}$ (7.106) (left column), $\tilde{\mathcal{Q}}$ (7.106) (center column) and $\tilde{\mu}$ (7.106) (right column) for the non-multi-variable convex constitutive model $W_{el,2}$ in (7.105) for $\hat{f}_e = 1.5$ (5.93) and multi-variable convex model $W_{el,1}$ in (7.104) for $f_e = 1.195$ (5.83) and $f_s = 0.163$ (5.84). The following choice of material parameters was used: $\tilde{\mu}_1 = 2\tilde{\mu}_2$, $\varepsilon_2 = \infty$. Results obtained for an electrically induced strain (actuated strain) of (a)-(b)-(c) $\lambda = 1.053$, (d)-(e)-(f) $\lambda = 1.631$, (g)-(h)-(i) $\lambda = 3.081$ and (j)-(k)-l $\lambda = 3.081$

identification of material instability) for the non-multi-variable convex model $W_{el,2}$ (7.105). Obviously, it is impossible to obtain negative values of q (7.107) for the multi-variable convex model $W_{el,1}$ (7.104) (refer to Figure 7.11).

7.6 Concluding remarks

This Chapter, based on the work presented in Reference [74] completes the new convex multi-variable variational and computational framework for the analysis of Electro Active Polymers (EAP) developed by Gil and Ortigosa in References [75,76] and described in Chapters 6 and 5. The approach presented in this paper allows also for a simple extension of the proposed framework to the field of Magneto Active Polymers.

One of the main contributions of this paper resides in the extension of the convex multi-variable definition of the electromechanical internal energy, postulated in [76], to the field of nonlinear electro-magneto-elasticity. This paper shows that the extended set of variables defining multi-variable convexity can be presented in the form of a system of first order conservation laws. In particular, two completely new conservation equations for the spatial vectors $\boldsymbol{d}$ and $\boldsymbol{b}$ (7.14) have been presented in this work. The proposed convex multi-variable definition of the internal energy in terms of conservation variables automatically leads to the fulfilment of the Legendre-Hadamard condition in the context of nonlinear electro-magneto-mechanics or, in other words, the positive definiteness nature of the electro-magneto-mechanical acoustic tensor.

The one-to-one and invertible relationship between the extended set of variables defining multi-variable convexity in the context of electro-magneto-elasticity and its associated set of entropy variables allows to define a generalised convex entropy function and its associated flux. Following the work of [44] in the context of nonlinear Solid Dynamics, a symmetrisation of the hyperbolic equations has been carried out for the first time in the context of nonlinear electro-magneto-mechanics.

Finally, a series of challenging numerical examples have been presented in order to demonstrate the validity of the approach. Specifically, computation of wave speeds has been carried out for a series of sophisticated constitutive models and a comparison between convex and non-convex multi-variable energy functionals has also been presented.

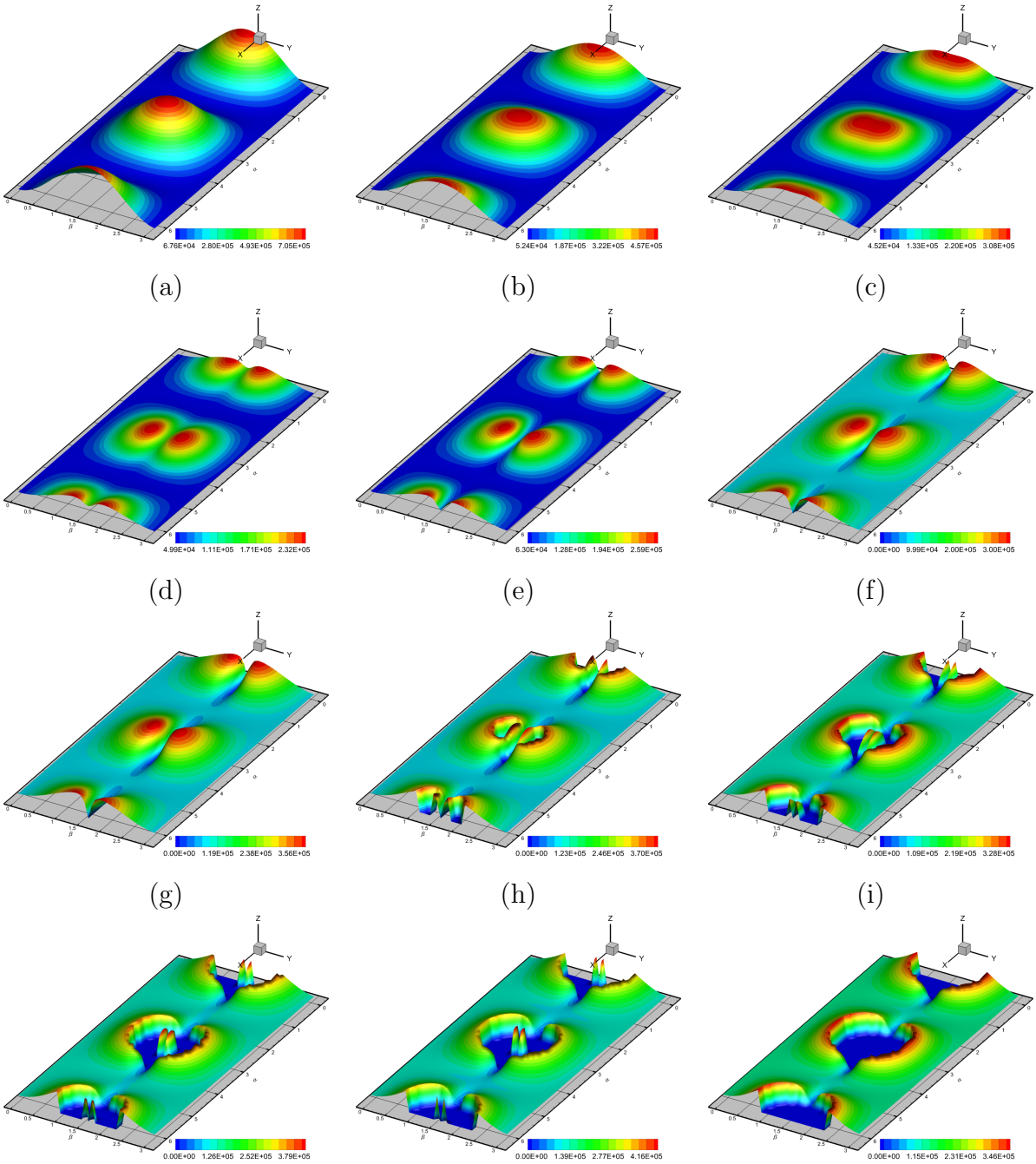

Figure 7.10: Numerical experiment reproducing the experimental set up in Figure 7.6. Evolution of the variable q (7.107) (a value of zero of this variable would indicate material instability) for the non-multi-variable convex constitutive model $W_{el,2}$ in (7.105) for $\hat{f}_e = 1.5$ (5.93). The following choice of material parameters was used: $\tilde{\mu}_1 = 2\tilde{\mu}_2$, $\varepsilon_2 = \infty$. Results obtained for an electrically induced strain (actuated strain) of (a) $\lambda = 1.053$, (b) $\lambda = 1.311$, (c) $\lambda = 1.631$, (d) $\lambda = 2.428$, (e) $\lambda = 3.081$, (f) $\lambda = 3.621$, (g) $\lambda = 4.089$, (h) $\lambda = 4.304$, (i) $\lambda = 4.508$, (j) $\lambda = 4.891$, (k) $\lambda = 5.07$ and (l) $\lambda = 5.246$.

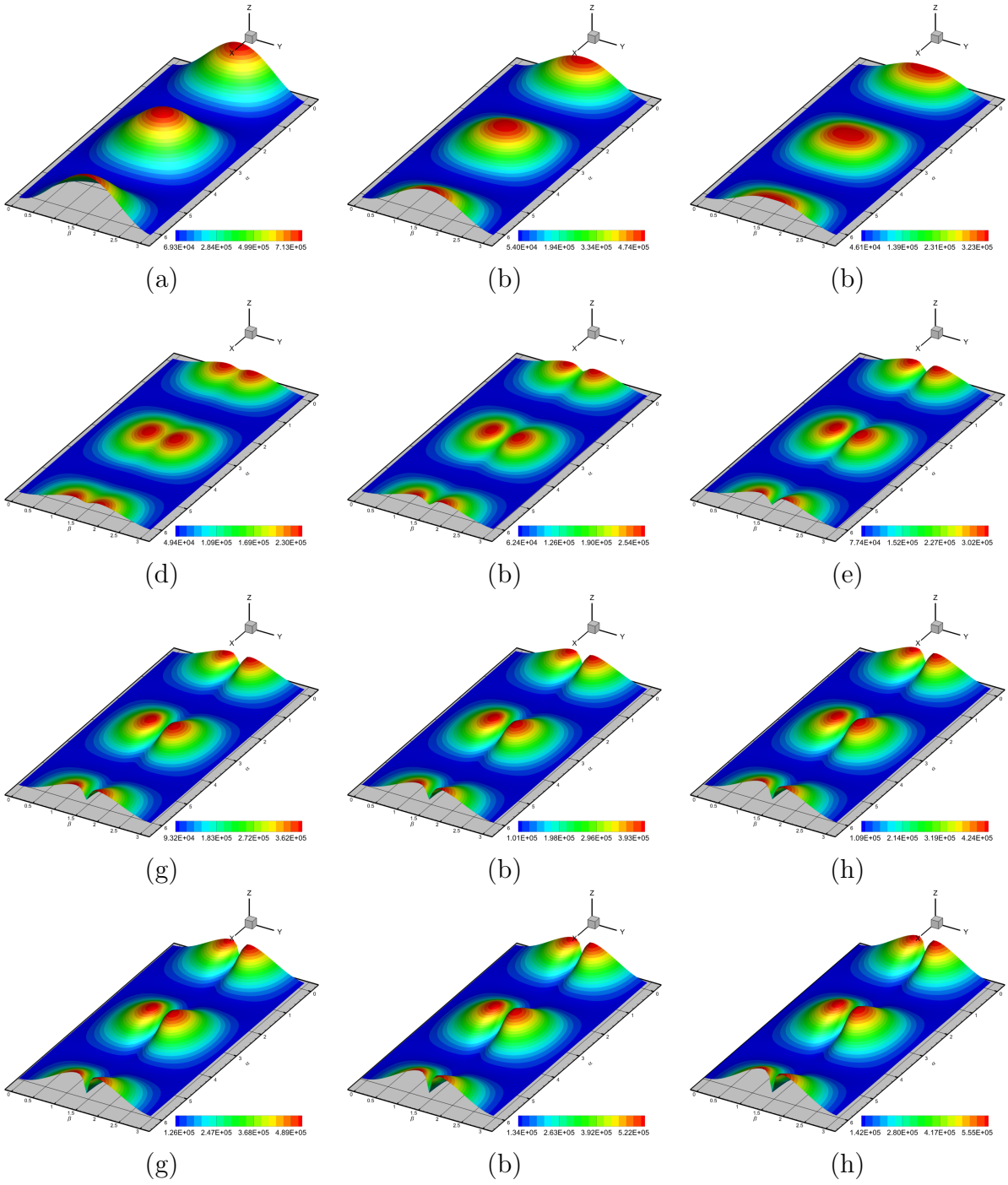

Figure 7.11: Numerical experiment reproducing the experimental set up in Figure 7.6. Evolution of the variable q (7.107) (a value of zero of this variable would indicate material instability) for the multi-variable convex constitutive model $W_{el,1}$ in (7.104) for $f_e = 1.195$ (5.83) and f_s (5.84) and $f_s = 0.163$. The following choice of material parameters was used: $\tilde{\mu}_1 = 2\tilde{\mu}_2$, $\varepsilon_2 = \infty$. Results obtained for an electrically induced strain (actuated strain) of (a) $\lambda = 1.053$, (b) $\lambda = 1.311$, (c) $\lambda = 1.631$, (d) $\lambda = 2.428$, (e) $\lambda = 3.081$, (f) $\lambda = 3.621$, (g) $\lambda = 4.089$, (h) $\lambda = 4.304$, (i) $\lambda = 4.508$, (j) $\lambda = 4.891$, (k) $\lambda = 5.07$ and (l) $\lambda = 5.246$.

Part IV

Conclusions

Chapter 8

Concluding remarks

8.1 Conclusions

The main objective of this thesis is the development of materially stable constitutive laws for nonlinear electro-elasticity in scenarios characterised by extreme electrically induced deformations in the presence of high electric fields. Starting with the most well-accepted convexity restriction which complies with the ellipticity condition, namely multi-variable convexity, tantamount to the concept of polyconvexity in the context of nonlinear elasticity, this work proposes an extension of the concept of multi-variable convexity to the field of nonlinear electro-elasticity.

8.1.1 Polyconvex nonlinear elasticity

The key contributions of these thesis in the context of convex multi-variable (polyconvex) elasticity are:

- Application of a tensor cross product operation initially introduced by de Boer [82] and recently rediscovered in [44], for the first time in the context of nonlinear continuum mechanics. The algebra associated to this tensor cross product has been exploited in this work, greatly facilitating the manipulations of the co-factor and the Jacobian of the deformation gradient as well as its derivatives.

- The definition of a new set of variables, conjugate to those defining multi-variable convexity (polyconvexity), namely the deformation gradient tensor, its co-factor and its Jacobian. The consideration of polyconvex energy functionals enables a one to one and invertible relationship between these two sets of variables, leading to the definition of a complementary energy for the first time in the context of polyconvex elasticity.

- The definition of new Hu-Washizu and Hellinger-Reissner type of mixed variational principles in the context of polyconvex elasticity, where the new tensor cross product operation introduced features heavily.

- The Finite Element implementation of the new Hu-Washizu and Hellinger-Reissner mixed variational principles. A static condensation procedure has been presented for the Hellinger-Reissner mixed variational principle, where a particular choice of functional spaces for the different variables satisfying the Ladyzenskaja-Babuška-Brezzi condition has been utilised, the resulting formulation having a comparable computational cost to those of displacement based formulations. Linear continuous interpolation using tetrahedral elements for both displacement and pressure and stabilised via a PetrovGalerkin technique for fully incompressible scenarios has been presented.

- This thesis endows multi-variable convexity (polyconvexity) with a physical and insightful interpretation. Exploration of the connections between the

Legendre-Hadamard condition and the hyperbolicity of the equations for Solid Dynamics enables to conclude that the time derivative of each of arguments of the convex multi-variable set must be written as first order conservation laws. A set of first order conservation laws is presented in this thesis for polyconvex elasticity. Exploiting the one to one and invertible relationship between these arguments and their associated work conjugates, a symmetrisation of the system of conservation laws in terms of the entropy conjugates has been carried out in this thesis.

8.1.2 Convex multi-variable nonlinear electro-elasticity

The most relevant novelties of this thesis in the context of convex multi-variable nonlinear electro-elasticity are:

- The extension of the definition of multi-variable convexity to the field of nonlinear electro-elasticity, whereby the convex nature of the internal energy is enriched with additional electromechanical variables to those in the purely mechanical context. The new definition of multi-variable convexity ensures the material stability of the constitutive equations and hence, the ellipticity condition for the entire range of deformations and electric fields.

- The definition of a new extended set of variables work conjugate to those in the convex multi-variable set in electro-mechanics.

- The definition of a new family of Hu-Washizu type of mixed variational principles in the context of nonlinear electro-elasticity heavily relying in the use of the newly introduced tensor cross product operation.

- The Finite Element implementation of the new Hu-Washizu mixed variational principles. A series of challenging numerical examples have been included in order to prove the superiority of the proposed mixed formulations with respect to classical potential-displacement formulations.

- The definition of a new set of first order hyperbolic equations for nonlinear electro-magneto-elasticity. Moreover, exploiting the one to one and invertible relationship between the convex multi-variable set and its work conjugate set, it has been possible to define a novel generalised convex entropy functional in the context of nonlinear electro-magneto-elasticity, permitting a symmetrisation of the conservation laws in terms of the work (entropy) conjugates.

8.2 Recommendations for further research

- **Fluid Structure Interaction.** Dielectric elastomers have a promising future in biomedical applications, where they have already been suggested as reliable

actuators capable of pumping blood and hence, act as an artificial heart. Immersed or boundary fitted methodologies are reliable numerical techniques for the simulation of these fluid structure interaction scenarios.

- **Continuum enriched Cosserat description.** Flexoelectric materials exhibit an spontaneous polarisation when subjected to a change in the gradient of the strains. A proper Cosserat theory extended to the context of electro-elasticity and scenarios where large deformations might occur is probably the most plausible approach for this new type of interesting materials.

- **Incorporation of dissipative effects.** Dielectric elastomers exhibit visco-electro-elasticity. The consideration of dissipative phenomena is one of the few remaining ingredients for an extensive material characterisation of electro active materials.

- **Electrically induced fracture.** One of the main failure modes of dielectric elastomers is electric breakdown, a threshold value for the electric field beyond which fracture of the material can occur. The numerical simulation of electrically induced fracture at finite strains is an interesting and challenging area of research

Appendices

Appendix A

Proof of convexity of stabilised invariants

The objective of this Appendix is to prove the convexity of the stabilised family of invariants proposed in Section 5.5 with respect to its arguments, proving that the resulting estabilised invariant complies with the definition of multi-variable convexity given in equation (5.12).

A.1 Stabilisation strategy 1 in Section 5.5.1

Convexity of invariant $W_{\boldsymbol{F}\boldsymbol{D}_0}(\boldsymbol{F}, \boldsymbol{D}_0)$ in equation (5.71) is subject to positiveness of the variable $\mathcal{F}$ defined as

$$\mathcal{F} = \left[\begin{array}{cc} \delta\boldsymbol{F} : & \delta\boldsymbol{D}_0 \cdot \end{array} \right] \left[\begin{array}{cc} \frac{\partial^2 W_{\boldsymbol{F}\boldsymbol{D}_0}}{\partial \boldsymbol{F} \partial \boldsymbol{F}} & \frac{\partial^2 W_{\boldsymbol{F}\boldsymbol{D}_0}}{\partial \boldsymbol{F} \partial \boldsymbol{D}_0} \\ \\ \frac{\partial^2 W_{\boldsymbol{F}\boldsymbol{D}_0}}{\partial \boldsymbol{D}_0 \partial \boldsymbol{F}} & \frac{\partial^2 W_{\boldsymbol{F}\boldsymbol{D}_0}}{\partial \boldsymbol{D}_0 \partial \boldsymbol{D}_0} \end{array} \right] \left[\begin{array}{c} : \delta\boldsymbol{F} \\ \delta\boldsymbol{D}_0 \end{array} \right] \geq 0, \tag{A.1}$$

where each of the terms featuring in the Hessian of $W_{\boldsymbol{F}\boldsymbol{D}_0}$ in (A.1) are obtained as

$$\begin{aligned} \frac{\partial^2 W_{\boldsymbol{F}\boldsymbol{D}_0}}{\partial \boldsymbol{F} \partial \boldsymbol{F}} &= 8\boldsymbol{F} \otimes \boldsymbol{F} + 4(II_{\boldsymbol{F}} + \gamma^2 II_{\boldsymbol{D}_0})\boldsymbol{\mathcal{I}}; \\ \frac{\partial^2 W_{\boldsymbol{F}\boldsymbol{D}_0}}{\partial \boldsymbol{F} \partial \boldsymbol{D}_0} &= 8\gamma^2 \boldsymbol{F} \otimes \boldsymbol{D}_0; \\ \frac{\partial^2 W_{\boldsymbol{F}\boldsymbol{D}_0}}{\partial \boldsymbol{D}_0 \partial \boldsymbol{D}_0} &= 8\gamma^4 \boldsymbol{D}_0 \otimes \boldsymbol{D}_0 + 4\gamma^2(II_{\boldsymbol{F}} + \gamma^2 II_{\boldsymbol{D}_0})\boldsymbol{I}. \end{aligned} \tag{A.2}$$

Introduction of above equation (A.2) into (A.1) yields

$$\begin{aligned} \mathcal{F} = & \underbrace{8(\delta\boldsymbol{F} : \boldsymbol{F})^2 + 4II_{\boldsymbol{F}} II_{\delta\boldsymbol{F}}}_{\mathcal{F}_1} + \underbrace{4\gamma^2 II_{\boldsymbol{D}_0} II_{\delta\boldsymbol{F}}}_{\mathcal{F}_3} \\ & + \underbrace{8\gamma^4(\delta\boldsymbol{D}_0 \cdot \boldsymbol{D}_0)^2 + 4\gamma^4 II_{\boldsymbol{D}_0} II_{\delta\boldsymbol{D}_0}}_{\mathcal{F}_2} + \underbrace{4\gamma^2 II_{\boldsymbol{F}} II_{\delta\boldsymbol{D}_0}}_{\mathcal{F}_4} \\ & + \underbrace{16\gamma^2(\delta\boldsymbol{F} : \boldsymbol{F})(\delta\boldsymbol{D}_0 \cdot \boldsymbol{D}_0)}_{\mathcal{F}_5}. \end{aligned} \tag{A.3}$$

Application of the Cauchy-Schwarz inequality to the tensors $\boldsymbol{F}$ and $\delta\boldsymbol{F}$ and to the vectors $\boldsymbol{D}_0$ and $\delta\boldsymbol{D}_0$ reads as,

$$II_{\boldsymbol{F}}II_{\delta\boldsymbol{F}} \geq (\delta\boldsymbol{F} : \boldsymbol{F})^2\,; \quad II_{\boldsymbol{D}_0}II_{\delta\boldsymbol{D}_0} \geq (\delta\boldsymbol{D}_0 \cdot \boldsymbol{D}_0)^2\,. \tag{A.4}$$

Equation (A.4) enables a set of inequalities for $\mathcal{F}_1$ and $\mathcal{F}_2$ in (A.3) to be written as,

$$\begin{aligned} \mathcal{F}_1 &= 8(\delta\boldsymbol{F} : \boldsymbol{F})^2 + 4II_{\boldsymbol{F}}II_{\delta\boldsymbol{F}} \geq 12(\delta\boldsymbol{F} : \boldsymbol{F})^2; \\ \mathcal{F}_2 &= 8\gamma^4(\delta\boldsymbol{D}_0 \cdot \boldsymbol{D}_0)^2 + 4\gamma^4 II_{\boldsymbol{D}_0}II_{\delta\boldsymbol{D}_0} \geq 12\gamma^4(\delta\boldsymbol{D}_0 \cdot \boldsymbol{D}_0)^2. \end{aligned} \tag{A.5}$$

Introduction of the inequalities for $\mathcal{F}_1$ and $\mathcal{F}_2$ in (A.5) into equation (A.3) yields the following inequality

$$\begin{aligned} \mathcal{F} \geq\ & \underbrace{12(\delta\boldsymbol{F} : \boldsymbol{F})^2}_{\mathcal{F}_1^*} + \underbrace{4\gamma^2 II_{\boldsymbol{D}_0}II_{\delta\boldsymbol{F}}}_{\mathcal{F}_3} + \underbrace{12\gamma^4(\delta\boldsymbol{D}_0 \cdot \boldsymbol{D}_0)^2}_{\mathcal{F}_2^*} \\ & + \underbrace{4\gamma^4 II_{\boldsymbol{F}}II_{\delta\boldsymbol{D}_0}}_{\mathcal{F}_4} + \underbrace{16\gamma^2(\delta\boldsymbol{F} : \boldsymbol{F})(\delta\boldsymbol{D}_0 \cdot \boldsymbol{D}_0)}_{\mathcal{F}_5}. \end{aligned} \tag{A.6}$$

Notice in above (A.6) that $\mathcal{F}_3 \geq 0$ and $\mathcal{F}_4 \geq 0$. Therefore, inequality (A.6) can be further modifed as

$$\mathcal{F} \geq \mathcal{F}^*; \qquad \mathcal{F}^* = \mathcal{F}_1^* + \mathcal{F}_2^* + \mathcal{F}_5. \tag{A.7}$$

Introduction of equation (A.6) into equation $(\text{A.7})_b$ enables the intermediate variable $\mathcal{F}^*$ in (A.7) to be written as

$$\mathcal{F}^* = \mathcal{F}_1^* + \mathcal{F}_2^* + \mathcal{F}_5 = 12\underbrace{(\delta\boldsymbol{F} : \boldsymbol{F})^2}_{a^2} + 12\underbrace{\gamma^4(\delta\boldsymbol{D}_0 \cdot \boldsymbol{D}_0)^2}_{b^2} + 16\underbrace{\gamma^2(\delta\boldsymbol{F} : \boldsymbol{F})(\delta\boldsymbol{D}_0 \cdot \boldsymbol{D}_0)}_{ab}. \tag{A.8}$$

Notice from equation (A.8) that $\mathcal{F}^*$ can be re-written in a more compact and clearer form in terms of a and b (A.8) as

$$\mathcal{F}^* = 12a^2 + 12b^2 + 16ab = 4(a^2 + b^2 + 2(a+b)^2) \geq 0. \tag{A.9}$$

Positiveness of $\mathcal{F}^*$ in above (A.9) yields positiveness of $\mathcal{F}$ in (A.6) (inferred from $(\text{A.7})_a$). Hence, the invariant $W_{\boldsymbol{F}\boldsymbol{D}_0}(\boldsymbol{F}, \boldsymbol{D}_0)$ in equation (5.71) is convex with respect to its arguments, namely $\{\boldsymbol{F}, \boldsymbol{D}_0\}$.

A.2 Stabilisation strategy 1 in Section 5.5.2

Convexity of invariant $\hat{W}_{\boldsymbol{H}\boldsymbol{D}_0}$ in equation (5.72) is subject to positiveness of the variable $\mathcal{G}$ defined as

$$\mathcal{G} = \left[\ \delta\boldsymbol{H} :\ \ \delta\boldsymbol{D}_0 \cdot\ \right] \begin{bmatrix} \frac{\partial^2 \hat{W}_{\boldsymbol{H}\boldsymbol{D}_0}}{\partial \boldsymbol{H}\partial \boldsymbol{H}} & \frac{\partial^2 \hat{W}_{\boldsymbol{H}\boldsymbol{D}_0}}{\partial \boldsymbol{H}\partial \boldsymbol{D}_0} \\ \\ \frac{\partial^2 \hat{W}_{\boldsymbol{H}\boldsymbol{D}_0}}{\partial \boldsymbol{D}_0\partial \boldsymbol{H}} & \frac{\partial^2 \hat{W}_{\boldsymbol{H}\boldsymbol{D}_0}}{\partial \boldsymbol{D}_0\partial \boldsymbol{D}_0} \end{bmatrix} \begin{bmatrix} :\delta\boldsymbol{H} \\ \delta\boldsymbol{D}_0 \end{bmatrix} \geq 0, \tag{A.10}$$

where each of the terms featuring in the Hessian of $\hat{W}_{\boldsymbol{HD}_0}$ in (A.10) are obtained as

$$\begin{aligned}
\frac{\partial^2 \hat{W}_{\boldsymbol{HD}_0}}{\partial \boldsymbol{H} \partial \boldsymbol{H}} &= 8\boldsymbol{H} \otimes \boldsymbol{H} + 4II_{\boldsymbol{H}} + 2\gamma^2 \boldsymbol{\mathcal{T}}; \\
\frac{\partial^2 \hat{W}_{\boldsymbol{HD}_0}}{\partial \boldsymbol{H} \partial \boldsymbol{D}_0} &= 2\gamma^2 \boldsymbol{\mathcal{S}}; \\
\frac{\partial^2 \hat{W}_{\boldsymbol{HD}_0}}{\partial \boldsymbol{D}_0 \partial \boldsymbol{D}_0} &= 8\gamma^4 \boldsymbol{D}_0 \otimes \boldsymbol{D}_0 + 2\gamma^2 (\boldsymbol{H}^T \boldsymbol{H} + 2\gamma^2 II_{\boldsymbol{D}_0} \boldsymbol{I}) \boldsymbol{I}.
\end{aligned} \tag{A.11}$$

with $\mathcal{T}_{iIjJ} = \delta_{ij} D_{0_I} D_{0_J}$ and $\mathcal{S}_{iIJ} = H_{iJ} D_{0I} + (\boldsymbol{H}\boldsymbol{D}_0)_i \, \delta_{IJ}$. Introduction of above equation (A.11) into (A.10) enables $\mathcal{G}$ in (A.10) to be re-written as

$$\begin{aligned}
\mathcal{G} = &\underbrace{4II_{\boldsymbol{H}} II_{\delta \boldsymbol{H}}}_{\mathcal{G}_1} + \underbrace{4\gamma^4 II_{\boldsymbol{D}_0} II_{\delta \boldsymbol{D}_0}}_{\mathcal{G}_2} + \underbrace{4\gamma^2 \left(\delta \boldsymbol{H} \boldsymbol{D}_0 \cdot \boldsymbol{H} \delta \boldsymbol{D}_0 + \boldsymbol{H} \boldsymbol{D}_0 \cdot \delta \boldsymbol{H} \delta \boldsymbol{D}_0\right)}_{\mathcal{F}_3} \\
&+ \underbrace{8 \left(\delta \boldsymbol{H} : \boldsymbol{H}\right)^2 + 8\gamma^4 \left(\boldsymbol{D}_0 \cdot \delta \boldsymbol{D}_0\right)^2 + 2\gamma^2 II_{\delta \boldsymbol{H} \boldsymbol{D}_0} + 2\gamma^2 II_{\boldsymbol{H} \delta \boldsymbol{D}_0}}_{\mathcal{G}_4}.
\end{aligned} \tag{A.12}$$

Application of the Cauchy-Schwarz inequality to the term $\mathcal{G}_1$ in above (A.12) yields the following inequality

$$\mathcal{G}_1 = 4II_{\boldsymbol{H}} II_{\delta \boldsymbol{H}} \geq 4\mathrm{tr}\left(\boldsymbol{H}^T \boldsymbol{H} \delta \boldsymbol{H}^T \delta \boldsymbol{H}\right) = 4\mathrm{tr}\left(\boldsymbol{H}^T \delta \boldsymbol{H} \delta \boldsymbol{H}^T \boldsymbol{H}\right). \tag{A.13}$$

Introduction of inequality (A.13) for $\mathcal{G}_1$ into equation (A.12) renders the following inequality for $\mathcal{G}$ (A.12)

$$\begin{aligned}
\mathcal{G} \geq &\underbrace{4\mathrm{tr}\left(\boldsymbol{H}^T \delta \boldsymbol{H} \delta \boldsymbol{H}^T \delta \boldsymbol{H}\right)}_{\mathcal{G}_1^*} + \underbrace{4\gamma^4 II_{\boldsymbol{D}_0} II_{\delta \boldsymbol{D}_0}}_{\mathcal{G}_2} + \underbrace{4\gamma^2 \left(\delta \boldsymbol{H} \boldsymbol{D}_0 \cdot \boldsymbol{H} \delta \boldsymbol{D}_0 + \boldsymbol{H} \boldsymbol{D}_0 \cdot \delta \boldsymbol{H} \delta \boldsymbol{D}_0\right)}_{\mathcal{G}_3} \\
&+ \underbrace{8 \left(\delta \boldsymbol{H} : \boldsymbol{H}\right)^2 + 8\gamma^4 \left(\boldsymbol{D}_0 \cdot \delta \boldsymbol{D}_0\right)^2 + 2\gamma^2 II_{\delta \boldsymbol{H} \boldsymbol{D}_0} + 2\gamma^2 II_{\boldsymbol{H} \delta \boldsymbol{D}_0}}_{\mathcal{G}_4}.
\end{aligned} \tag{A.14}$$

Notice in above equation (A.14) that $\mathcal{G}_4 \geq 0$. Therefore, inequality (A.14) can be further modified as

$$\mathcal{G} \geq \mathcal{G}^*; \qquad \mathcal{G}^* = \mathcal{G}_1^* + \mathcal{G}_2 + \mathcal{G}_3. \tag{A.15}$$

Introduction of equation (A.14) into $(\text{A.15})_b$ enables the intermediate variable $\mathcal{G}^\star$ to be written as

$$\mathcal{G}^\star = \mathcal{G}_1^* + \mathcal{G}_2 + \mathcal{G}_3 = 4\mathrm{tr}\left(\boldsymbol{B}^T \boldsymbol{B}\right); \quad \boldsymbol{B} = \delta \boldsymbol{H}^T \boldsymbol{H} + \gamma^2 \delta \boldsymbol{D}_0 \otimes \boldsymbol{D}_0. \tag{A.16}$$

Finally, positive definiteness of the tensor $\boldsymbol{B}^T \boldsymbol{B}$ in above equation (A.16) implies positiveness of $\mathcal{G}^\star$ and hence, positiveness of $\mathcal{G}$ (inferred from equation $(\text{A.15})_a$). Therefore, convexity of invariant $\hat{W}_{\boldsymbol{HD}_0}$ in (5.72) with respect to its arguments, namely $\{\boldsymbol{H}, \boldsymbol{D}_0\}$ is proved.

Appendix B

Relationship between the constitutive tensors of the internal energy in terms of its reduced and extended representations. Electro-elasticity

The objective of this section is to express the physically meaningful constitutive tensors introduced in equation (5.20), namely $\boldsymbol{\mathcal{C}}$, $\boldsymbol{\mathcal{Q}}$ and $\boldsymbol{\theta}$, emanating from the Hessian operator of the internal energy e (5.12), in terms of the components of the Hessian operator of the extended representation of the internal energy, namely $[\mathbb{H}_W]$ (5.23).

B.1 Elasticity tensor

From equation (5.19), the second directional derivative of the internal energy e with respect to changes of the geometry can be obtained as

$$D^2 e\left[\delta\boldsymbol{u};\boldsymbol{u}\right] = \boldsymbol{\nabla}_0\delta\boldsymbol{u} : \boldsymbol{\mathcal{C}} : \boldsymbol{\nabla}_0\boldsymbol{u}. \tag{B.1}$$

Comparison of equations (B.1) and (5.38) enables the elasticity tensor $\boldsymbol{\mathcal{C}}$ to be alternatively re-written in terms of the derivatives of the electro-kinematic variable set $\mathcal{V}$ as

$$\begin{aligned}\boldsymbol{\mathcal{C}} = {} & W_{\boldsymbol{FF}} + \boldsymbol{F}\bigtimes(W_{\boldsymbol{HH}}\bigtimes\boldsymbol{F}) + W_{JJ}\boldsymbol{H}\otimes\boldsymbol{H} + \boldsymbol{\mathcal{C}}_1 \\ & + 2(W_{\boldsymbol{FH}}\bigtimes\boldsymbol{F})^{\text{sym}} + 2(W_{\boldsymbol{F}J}\otimes\boldsymbol{H})^{\text{sym}} + 2(W_{\boldsymbol{Fd}}\otimes\boldsymbol{D}_0)^{\text{sym}} \\ & + 2((\boldsymbol{F}\bigtimes W_{\boldsymbol{H}J})\otimes\boldsymbol{H})^{\text{sym}} + 2((\boldsymbol{F}\bigtimes W_{\boldsymbol{Hd}})\otimes\boldsymbol{D}_0)^{\text{sym}} \\ & + 2(\boldsymbol{H}\otimes(W_{J\boldsymbol{d}}\otimes\boldsymbol{D}_0))^{\text{sym}} + \boldsymbol{\mathcal{A}},\end{aligned} \tag{B.2}$$

where

$$\mathcal{A}_{iIjJ} = \mathcal{E}_{ijp}\mathcal{E}_{IJP}\left(\boldsymbol{\Sigma}_{\boldsymbol{H}} + \Sigma_J\boldsymbol{\Sigma}_{\boldsymbol{H}}\right)_{pP}; \quad \mathcal{C}_{1,iIjJ} = \left(W_{\boldsymbol{dd}}\right)_{ij} D_{0I}D_{0J}. \tag{B.3}$$

B.2 Piezoelectric tensor

From equation (5.19), the second directional derivative of the internal energy e with respect to changes in geometry and electric displacement field leads to the following expression

$$D^2 e\left[\delta \boldsymbol{u}; \Delta \boldsymbol{D}_0\right] = \left(\boldsymbol{\nabla}_0 \delta \boldsymbol{u} : \boldsymbol{\mathcal{Q}}^T\right) \cdot \Delta \boldsymbol{D}_0. \tag{B.4}$$

Comparison of equations (B.4) and (5.38) allows to re-express the piezoelectric tensor $\boldsymbol{\mathcal{Q}}^T$ in terms of the elements of the set $\mathcal{V}$ as

$$\begin{aligned} \boldsymbol{\mathcal{Q}}^T = & W_{\boldsymbol{F}\boldsymbol{D}_0} + \boldsymbol{F} \times W_{\boldsymbol{H}\boldsymbol{D}_0} + \boldsymbol{H} \otimes W_{J\boldsymbol{D}_0} + \boldsymbol{\mathcal{Q}}_1^T \\ & + \boldsymbol{\mathcal{Q}}_2^T + \boldsymbol{\mathcal{Q}}_3^T + \boldsymbol{\mathcal{Q}}_4^T + \boldsymbol{\mathcal{Q}}_5^T + \boldsymbol{\Sigma}_{\boldsymbol{d}} \otimes \boldsymbol{I}. \end{aligned} \tag{B.5}$$

where the expressions for the tensors $\boldsymbol{\mathcal{Q}}_i^T$ in above equation (B.5) are given as

$$\left(\boldsymbol{\mathcal{Q}}_1^T\right)_{iIJ} = \left(W_{\boldsymbol{d}\boldsymbol{D}_0}\right)_{iJ} D_{0I}; \tag{B.6a}$$

$$\left(\boldsymbol{\mathcal{Q}}_2^T\right)_{iIJ} = \left(W_{\boldsymbol{F}\boldsymbol{d}iIj}\right) F_{jJ}; \tag{B.6b}$$

$$\left(\boldsymbol{\mathcal{Q}}_3^T\right)_{iIJ} = (\boldsymbol{F} \times W_{\boldsymbol{H}\boldsymbol{d}})_{iIj} F_{jJ}; \tag{B.6c}$$

$$\left(\boldsymbol{\mathcal{Q}}_4^T\right)_{iIJ} = (\boldsymbol{H} \otimes W_{J\boldsymbol{d}})_{iIj} F_{jJ}; \tag{B.6d}$$

$$\left(\boldsymbol{\mathcal{Q}}_5^T\right)_{iIJ} = \left(W_{\boldsymbol{d}\boldsymbol{d}}\right)_{ij} F_{jJ} D_{0I}. \tag{B.6e}$$

B.3 Dielectric tensor

The second directional derivative of the internal energy e with respect to changes in the electric displacement field can be identified from equation (5.19) as

$$D^2 e\left[\delta \boldsymbol{D}_0; \Delta \boldsymbol{D}_0\right] = \delta \boldsymbol{D}_0 \cdot \boldsymbol{\theta} \Delta \boldsymbol{D}_0. \tag{B.7}$$

Comparison of equations (B.7) and (5.38) enables the inverse of the dielectric tensor $\boldsymbol{\theta}$ to be re-expressed in terms of the elements of the set $\mathcal{V}$ as

$$\boldsymbol{\theta} = W_{\boldsymbol{D}_0\boldsymbol{D}_0} + \left(W_{\boldsymbol{D}_0\boldsymbol{d}}\boldsymbol{F} + \boldsymbol{F}^T W_{\boldsymbol{d}\boldsymbol{D}_0}\right) + \boldsymbol{F}^T W_{\boldsymbol{d}\boldsymbol{d}} \boldsymbol{F}. \tag{B.8}$$

B.4 Electrostrictive tensor

A very important constitutive tensor described as a second order effect (it does not appear in the tangent operator of the internal energy $e\left(\boldsymbol{\nabla}_0 \boldsymbol{x}, \boldsymbol{D}_0\right)$ in (5.19)) is the electrostrictive tensor, defined as

$$\boldsymbol{\mathcal{B}}\big|_{\boldsymbol{F}=\boldsymbol{\nabla}_0 \boldsymbol{x}} = \frac{\partial \boldsymbol{\mathcal{Q}}^T}{\partial \boldsymbol{D}_0}. \tag{B.9}$$

Introduction of equation (B.5) into (B.9) enables $\boldsymbol{\mathcal{B}}$ to be expressed in terms of the elements of the set $\mathcal{V}$ as

$$\begin{aligned}\left(\boldsymbol{\mathcal{B}}|_{\boldsymbol{F}=\boldsymbol{\nabla}_0\boldsymbol{x}}\right)_{iIJK} &= (W_{\boldsymbol{F}\boldsymbol{D}_0\boldsymbol{D}_0})_{iIJK} + (W_{\boldsymbol{F}\boldsymbol{D}_0\boldsymbol{d}})_{iIJm}\, F_{mK} \\ &+ (\boldsymbol{F}\times W_{\boldsymbol{H}\boldsymbol{D}_0\boldsymbol{D}_0})_{iIJK} + (\boldsymbol{F}\times W_{\boldsymbol{H}\boldsymbol{D}_0\boldsymbol{d}})_{iIJm}\, F_{mK} \\ &+ (\boldsymbol{H}\otimes W_{J\boldsymbol{D}_0\boldsymbol{D}_0})_{iIJK} + (\boldsymbol{H}\otimes W_{J\boldsymbol{D}_0\boldsymbol{d}})_{iIJm}\, F_{mK} \\ &+ (\boldsymbol{\mathcal{B}}_1+\boldsymbol{\mathcal{B}}_2+\boldsymbol{\mathcal{B}}_3+\boldsymbol{\mathcal{B}}_4+\boldsymbol{\mathcal{B}}_5)_{iIJK} + (W_{\boldsymbol{d}\boldsymbol{D}_0})_{iK}\,\delta_{IJ} + (W_{\boldsymbol{d}\boldsymbol{d}})_{im}\,F_{mK}\delta_{IJ},\end{aligned} \tag{B.10}$$

where $W_{\boldsymbol{A}\boldsymbol{B}\boldsymbol{C}} = \frac{\partial^3 W}{\partial \boldsymbol{A}\partial \boldsymbol{B}\partial \boldsymbol{C}}$ and with

$$(\boldsymbol{\mathcal{B}}_1)_{iIJK} = (W_{\boldsymbol{d}\boldsymbol{D}_0\boldsymbol{D}_0})_{iJk}\, D_{0I} + (W_{\boldsymbol{d}\boldsymbol{D}_0\boldsymbol{d}})_{iJm}\, F_{mK} D_{0I} + (W_{\boldsymbol{d}\boldsymbol{D}_0})_{iJ}\,\delta_{IK}; \tag{B.11a}$$

$$(\boldsymbol{\mathcal{B}}_2)_{iIJK} = (W_{\boldsymbol{F}\boldsymbol{d}\boldsymbol{D}_0})_{iIjK}\, F_{jJ} + (W_{\boldsymbol{F}\boldsymbol{d}\boldsymbol{d}})_{iIjk}\, F_{jJ}F_{kK}; \tag{B.11b}$$

$$(\boldsymbol{\mathcal{B}}_3)_{iIJK} = (\boldsymbol{F}\times W_{\boldsymbol{H}\boldsymbol{d}\boldsymbol{D}_0})_{iIjK}\, F_{jJ} + (\boldsymbol{F}\times W_{\boldsymbol{H}\boldsymbol{d}\boldsymbol{d}})_{iIjk}\, F_{jJ}F_{kK}; \tag{B.11c}$$

$$(\boldsymbol{\mathcal{B}}_4)_{iIJK} = (\boldsymbol{H}\otimes W_{J\boldsymbol{d}\boldsymbol{D}_0})_{iIjK}\, F_{jJ} + (\boldsymbol{H}\otimes W_{J\boldsymbol{d}\boldsymbol{d}})_{iIjk}\, F_{jJ}F_{kK}; \tag{B.11d}$$

$$(\boldsymbol{\mathcal{B}}_5)_{iIJK} = (W_{\boldsymbol{d}\boldsymbol{d}\boldsymbol{D}_0})_{ijK}\, F_{jJ}D_{0I} + (W_{\boldsymbol{d}\boldsymbol{d}\boldsymbol{d}})_{ijk}\, F_{jJ}F_{kK}D_{0I} + (W_{\boldsymbol{d}\boldsymbol{d}})_{ij}\, F_{jJ}\delta_{IK}. \tag{B.11e}$$

Appendix C

Relationships between the Hessian operator of the Helmholtz's energy functional and that for the internal energy

When an explicit representation of the Helmholtz's and extended Helmholtz's energy functionals, namely $\Phi(\boldsymbol{\nabla}_0\boldsymbol{x}, -\boldsymbol{\nabla}_0\varphi)$ (5.34) and $\Phi(\boldsymbol{F}, \boldsymbol{H}, J, \boldsymbol{\Sigma}_{\boldsymbol{D}_0}, \boldsymbol{\Sigma}_{\boldsymbol{d}})$ (5.32c) is not available, their associated Hessian operators need to be obtained in terms of the components of the Hessian operators associated to the internal energy function $e(\boldsymbol{\nabla}_0\boldsymbol{x}, \boldsymbol{D}_0)$ and its extended representation $W(\boldsymbol{F}, \boldsymbol{H}, J, \boldsymbol{D}_0, \boldsymbol{d})$ respectively, by exploiting the partial Legendre transforms presented in equations (5.34) and (5.32c), respectively.

Starting with a generic partial Legendre transform between two generic energy functionals, this section shows how to relate the Hessian operators of $\Phi(\boldsymbol{\nabla}_0\boldsymbol{x}, -\boldsymbol{\nabla}_0\varphi)$ and $\Phi(\boldsymbol{F}, \boldsymbol{H}, J, \boldsymbol{\Sigma}_{\boldsymbol{D}_0}, \boldsymbol{\Sigma}_{\boldsymbol{d}})$ to those for $e(\boldsymbol{\nabla}_0\boldsymbol{x}, \boldsymbol{D}_0)$ and its extended representation $W(\boldsymbol{F}, \boldsymbol{H}, J, \boldsymbol{D}_0, \boldsymbol{d})$.

C.1 Generic transformation between Hessian operators

Let $\mathcal{F}(\mathcal{A}, \mathcal{B})$ be an energy functional convex in the sets of variables $\{\mathcal{A}, \mathcal{B}\}$. Convexity of the energy functional enables a new energy functional $\mathcal{L}(\mathcal{A}, \Sigma_{\mathcal{B}})$ depending upon the set of variables $\mathcal{A}$ and a set of variables $\Sigma_{\mathcal{B}}$ (work conjugate to those contained in the set $\mathcal{B}$) to be defined via the following partial Legendre transformation,

$$\mathcal{L}(\mathcal{A}, \Sigma_{\mathcal{B}}) = -\max_{\mathcal{B}} \left\{ \Sigma_{\mathcal{B}} : \mathcal{B} - \mathcal{F}(\mathcal{A}, \mathcal{B}) \right\}. \tag{C.1}$$

Let the first derivatives of the energy functional $\mathcal{L}(\mathcal{A}, \Sigma_{\mathcal{B}})$ and the sets of variables

$\Sigma_{\mathcal{A}}$ and $\Sigma_{\mathcal{B}}$ be related as

$$\frac{\partial \mathcal{F}}{\partial \mathcal{A}} = \Sigma_{\mathcal{A}}; \qquad \frac{\partial \mathcal{F}}{\partial \mathcal{B}} = \Sigma_{\mathcal{B}}. \tag{C.2}$$

Combination of equations (C.1) and (C.2) enables the first derivatives of the energy functional $\mathcal{L}(\mathcal{A}, \Sigma_{\mathcal{B}})$ to be obtained as,

$$\frac{\partial \mathcal{L}}{\partial \mathcal{A}} = \Sigma_{\mathcal{A}}; \qquad \frac{\partial \mathcal{L}}{\partial \Sigma_{\mathcal{B}}} = -\mathcal{B}. \tag{C.3}$$

Let the Hessian operators of both energy functionals $\mathcal{F}(\mathcal{A}, \mathcal{B})$ and $\mathcal{F}(\mathcal{A}, \mathcal{B})$ be represented as,

$$[\mathbb{H}_{\mathcal{L}}] = \begin{bmatrix} \mathcal{L}_{\mathcal{A}\mathcal{A}} & \mathcal{L}_{\mathcal{A}\Sigma_{\mathcal{B}}} \\ \mathcal{L}_{\Sigma_{\mathcal{B}}\mathcal{A}} & \mathcal{L}_{\Sigma_{\mathcal{B}}\Sigma_{\mathcal{B}}} \end{bmatrix}; \qquad [\mathbb{H}_{\mathcal{F}}] = \begin{bmatrix} \mathcal{F}_{\mathcal{A}\mathcal{A}} & \mathcal{F}_{\mathcal{A}\mathcal{B}} \\ \mathcal{F}_{\mathcal{B}\mathcal{A}} & \mathcal{F}_{\mathcal{B}\mathcal{B}} \end{bmatrix}, \tag{C.4}$$

with $\mathcal{L}_{\mathcal{C}\mathcal{D}} = \frac{\partial^2 \mathcal{L}}{\partial \mathcal{C} \partial \mathcal{D}}$. The components of the Hessian operator $[\mathbb{H}_{\mathcal{F}}]$ can obtained in terms of the components of the Hessian operator $[\mathbb{H}_{\mathcal{L}}]$ in a standard manner as

$$\mathcal{L}_{\Sigma_{\mathcal{B}}\Sigma_{\mathcal{B}}} = -\left[\mathcal{F}_{\mathcal{B}\mathcal{B}}\right]^{-1}; \tag{C.5a}$$

$$\mathcal{L}_{\mathcal{A}\Sigma_{\mathcal{B}}} = -\mathcal{F}_{\mathcal{A}\mathcal{B}}\mathcal{L}_{\Sigma_{\mathcal{B}}\Sigma_{\mathcal{B}}}; \tag{C.5b}$$

$$\mathcal{L}_{\mathcal{A}\mathcal{A}} = \mathcal{F}_{\mathcal{A}\mathcal{A}} - \mathcal{F}_{\mathcal{A}\mathcal{B}}\mathcal{L}_{\Sigma_{\mathcal{B}}\mathcal{A}};, \tag{C.5c}$$

where $\mathcal{L}_{\mathcal{A}\Sigma_{\mathcal{B}}} = \left[\mathcal{L}_{\Sigma_{\mathcal{B}}\mathcal{A}}\right]^T$.

C.2 Relation between the Hessian operator of the Helmholtz's energy $\Phi(\boldsymbol{\nabla}_0 \boldsymbol{x}, \boldsymbol{\nabla}_0 \varphi)$ and the Hessian operator of the internal energy $e(\boldsymbol{\nabla}_0 \boldsymbol{x}, \boldsymbol{D}_0)$

Let the set of variables $\mathcal{A}$, $\mathcal{B}$, $\Sigma_{\mathcal{A}}$ and $\Sigma_{\mathcal{B}}$ (C.1) be defined as,

$$\begin{aligned} \mathcal{A} &= \boldsymbol{\nabla}_0 \boldsymbol{x}; & \mathcal{B} &= \boldsymbol{D}_0; \\ \Sigma_{\mathcal{A}} &= \boldsymbol{P}; & \Sigma_{\mathcal{B}} &= -\boldsymbol{\nabla}_0 \varphi. \end{aligned} \tag{C.6}$$

For this particular case, the energy functions $\mathcal{L}(\mathcal{A}, \Sigma_{\mathcal{B}})$ and $\mathcal{F}(\mathcal{A}, \mathcal{B})$ coincide with the Helmholtz's energy functional $\Phi(\boldsymbol{\nabla}_0 \boldsymbol{x}, -\boldsymbol{\nabla}_0 \varphi)$ and the internal energy $e(\boldsymbol{\nabla}_0 \boldsymbol{x}, \boldsymbol{D}_0)$, respectively, namely

$$\mathcal{L}(\mathcal{A}, \Sigma_{\mathcal{B}}) = \Phi(\boldsymbol{\nabla}_0 \boldsymbol{x}, -\boldsymbol{\nabla}_0 \varphi); \qquad \mathcal{F}(\mathcal{A}, \mathcal{B}) = e(\boldsymbol{\nabla}_0 \boldsymbol{x}, \boldsymbol{D}_0). \tag{C.7}$$

For these two energy functionals, the equivalent expression to that in (C.5a), relating electrical components of the Hessian operators of $\Phi(\boldsymbol{\nabla}_0 \boldsymbol{x}, -\boldsymbol{\nabla}_0 \varphi)$ and $e(\boldsymbol{\nabla}_0 \boldsymbol{x}, \boldsymbol{D}_0)$, namely $\boldsymbol{\varepsilon}$ (5.37) and $\boldsymbol{\theta}$ (5.20), respectively is

$$\boldsymbol{\varepsilon} = \boldsymbol{\theta}^{-1}. \tag{C.8}$$

The equivalent expression to equation (C.5b), relating the coupled contributions of both Hessian operators, namely $\boldsymbol{\mathcal{P}}$ (5.37) and $\boldsymbol{\mathcal{Q}}$ (5.20), yields

$$-\boldsymbol{\mathcal{P}}^T = \boldsymbol{\mathcal{Q}}^T \bullet \boldsymbol{\varepsilon}, \tag{C.9}$$

where the operation $\bullet$ in above (C.9) indicates the contraction of the last and first components of the tensors on the left and right hand sides of the operation symbol $\bullet$, respectively. Finally, the mechanical component of the Hessian operator of the Helmholtz energy, namely $\boldsymbol{\mathcal{C}}^\star$ (5.20) emerges after applying equation (C.5a), yielding

$$\boldsymbol{\mathcal{C}}^\star = \boldsymbol{\mathcal{C}} + \boldsymbol{\mathcal{Q}} \bullet \boldsymbol{\mathcal{P}}, \tag{C.10}$$

with $\boldsymbol{\mathcal{C}}$ defined in (5.20).

C.3 Relation between the Hessian operator $[\mathbb{H}_\Phi]$ and the Hessian operator $[\mathbb{H}_W]$

Let the set of variables $\mathcal{A}$, $\mathcal{B}$, $\Sigma_\mathcal{A}$ and $\Sigma_\mathcal{B}$ (C.1) be defined as,

$$\begin{aligned} \mathcal{A} &= \{\boldsymbol{F}, \boldsymbol{H}, J\}; & \mathcal{B} &= \{\boldsymbol{D}_0, \boldsymbol{d}\}; \\ \Sigma_\mathcal{A} &= \{\boldsymbol{\Sigma}_{\boldsymbol{F}}, \boldsymbol{\Sigma}_{\boldsymbol{H}}, \Sigma_J\}; & \Sigma_\mathcal{B} &= \{\Sigma_{\boldsymbol{D}_0}, \Sigma_{\boldsymbol{d}}\}. \end{aligned} \tag{C.11}$$

For this particular case, the energy functions $\mathcal{L}(\mathcal{A}, \Sigma_\mathcal{B})$ and $\mathcal{F}(\mathcal{A}, \mathcal{B})$ coincide with the extended Helmholtz's energy $\Phi(\boldsymbol{F}, \boldsymbol{H}, J, \boldsymbol{\Sigma}_{\boldsymbol{D}_0}, \boldsymbol{\Sigma}_{\boldsymbol{d}})$ and the internal energy $W(\boldsymbol{F}, \boldsymbol{H}, J, \boldsymbol{D}_0, \boldsymbol{d})$, respectively, namely

$$\mathcal{L}(\mathcal{A}, \Sigma_\mathcal{B}) = \Phi(\boldsymbol{F}, \boldsymbol{H}, J, \boldsymbol{\Sigma}_{\boldsymbol{D}_0}, \boldsymbol{\Sigma}_{\boldsymbol{d}}); \qquad \mathcal{F}(\mathcal{A}, \mathcal{B}) = W(\boldsymbol{F}, \boldsymbol{H}, J, \boldsymbol{D}_0, \boldsymbol{d}). \tag{C.12}$$

For these two energy functionals, the equivalent expression to that in (C.5a), relating some of the components of the Hessian operators $[\mathbb{H}_\Phi]$ and $[\mathbb{H}_W]$ reads as

$$\begin{bmatrix} \Phi_{\boldsymbol{\Sigma}_{\boldsymbol{D}_0}\boldsymbol{\Sigma}_{\boldsymbol{D}_0}} & \Phi_{\boldsymbol{\Sigma}_{\boldsymbol{D}_0}\boldsymbol{\Sigma}_{\boldsymbol{d}}} \\ \Phi_{\boldsymbol{\Sigma}_{\boldsymbol{d}}\boldsymbol{\Sigma}_{\boldsymbol{D}_0}} & \Phi_{\boldsymbol{\Sigma}_{\boldsymbol{d}}\boldsymbol{\Sigma}_{\boldsymbol{d}}} \end{bmatrix} = - \begin{bmatrix} W_{\boldsymbol{D}_0\boldsymbol{D}_0} & W_{\boldsymbol{D}_0\boldsymbol{d}} \\ W_{\boldsymbol{d}\boldsymbol{D}_0} & W_{\boldsymbol{d}\boldsymbol{d}} \end{bmatrix}^{-1}. \tag{C.13}$$

Analogously, the equivalent expression to equation (C.5b) yields

$$\begin{bmatrix} \Phi_{\boldsymbol{F}\boldsymbol{\Sigma}_{\boldsymbol{D}_0}} \\ \Phi_{\boldsymbol{H}\boldsymbol{\Sigma}_{\boldsymbol{D}_0}} \\ \Phi_{J\boldsymbol{\Sigma}_{\boldsymbol{D}_0}} \end{bmatrix} = - \begin{bmatrix} W_{\boldsymbol{F}\boldsymbol{D}_0} \\ W_{\boldsymbol{H}\boldsymbol{D}_0} \\ W_{J\boldsymbol{D}_0} \end{bmatrix} \left[\Phi_{\boldsymbol{\Sigma}_{\boldsymbol{D}_0}\boldsymbol{\Sigma}_{\boldsymbol{D}_0}}\right]; \quad \begin{bmatrix} \Phi_{\boldsymbol{F}\boldsymbol{\Sigma}_{\boldsymbol{d}}} \\ \Phi_{\boldsymbol{H}\boldsymbol{\Sigma}_{\boldsymbol{d}}} \\ \Phi_{J\boldsymbol{\Sigma}_{\boldsymbol{d}}} \end{bmatrix} = - \begin{bmatrix} W_{\boldsymbol{F}\boldsymbol{V}} \\ W_{\boldsymbol{H}\boldsymbol{V}} \\ W_{J\boldsymbol{d}} \end{bmatrix} \left[\Phi_{\boldsymbol{\Sigma}_{\boldsymbol{d}}\boldsymbol{\Sigma}_{\boldsymbol{d}}}\right]. \tag{C.14}$$

Finally, the remaining components of the Hessian operator $[\mathbb{H}_\Phi]$ emerge after

applying equation (C.5a), yielding

$$\Phi_{\boldsymbol{FF}} = W_{\boldsymbol{FF}} - \begin{bmatrix} W_{\boldsymbol{FD}_0} & W_{\boldsymbol{Fd}} \end{bmatrix} \begin{bmatrix} \Phi_{\boldsymbol{\Sigma}_{D_0}\boldsymbol{F}} \\ \Phi_{\boldsymbol{\Sigma}_{\boldsymbol{d}}\boldsymbol{F}} \end{bmatrix}; \tag{C.15a}$$

$$\Phi_{\boldsymbol{FH}} = W_{\boldsymbol{FH}} - \begin{bmatrix} W_{\boldsymbol{FD}_0} & W_{\boldsymbol{Fd}} \end{bmatrix} \begin{bmatrix} \Phi_{\boldsymbol{\Sigma}_{D_0}\boldsymbol{H}} \\ \Phi_{\boldsymbol{\Sigma}_{\boldsymbol{d}}\boldsymbol{H}} \end{bmatrix}; \tag{C.15b}$$

$$\Phi_{\boldsymbol{F}J} = W_{\boldsymbol{F}J} - \begin{bmatrix} W_{\boldsymbol{FD}_0} & W_{\boldsymbol{Fd}} \end{bmatrix} \begin{bmatrix} \Phi_{\boldsymbol{\Sigma}_{D_0}J} \\ \Phi_{\boldsymbol{\Sigma}_{\boldsymbol{d}}J} \end{bmatrix}; \tag{C.15c}$$

$$\Phi_{\boldsymbol{HH}} = W_{\boldsymbol{HH}} - \begin{bmatrix} W_{\boldsymbol{HD}_0} & W_{\boldsymbol{Hd}} \end{bmatrix} \begin{bmatrix} \Phi_{\boldsymbol{\Sigma}_{D_0}\boldsymbol{H}} \\ \Phi_{\boldsymbol{\Sigma}_{\boldsymbol{d}}\boldsymbol{H}} \end{bmatrix}; \tag{C.15d}$$

$$\Phi_{\boldsymbol{H}J} = W_{\boldsymbol{H}J} - \begin{bmatrix} W_{\boldsymbol{HD}_0} & W_{\boldsymbol{Hd}} \end{bmatrix} \begin{bmatrix} \Phi_{\boldsymbol{\Sigma}_{D_0}J} \\ \Phi_{\boldsymbol{\Sigma}_{\boldsymbol{d}}J} \end{bmatrix}; \tag{C.15e}$$

$$\Phi_{JJ} = W_{JJ} - \begin{bmatrix} W_{J\boldsymbol{D}_0} & W_{J\boldsymbol{d}} \end{bmatrix} \begin{bmatrix} \Phi_{\boldsymbol{\Sigma}_{D_0}J} \\ \Phi_{\boldsymbol{\Sigma}_{\boldsymbol{d}}J} \end{bmatrix}. \tag{C.15f}$$

Appendix D

Auxiliary residuals and stiffness matrices associated to static condensation procedure

The auxiliary residuals and stiffness matrices arising in the static condensation procedure for the variational principle Π_W (5.42) (see equations (6.25), (6.26), (6.27),

(6.29) and (6.30)) are

$$\bar{\boldsymbol{R}}^e_{\Sigma_\mathcal{Y}} = -[\boldsymbol{M}^e_3]^{-1}\left(\boldsymbol{R}^e_\mathcal{Y} + \boldsymbol{K}^e_{\mathcal{Y}\mathcal{Y}}\bar{\boldsymbol{R}}^e_\mathcal{Y} - \boldsymbol{M}^e_2\boldsymbol{M}^e_1\left(\boldsymbol{R}^e_{\boldsymbol{D}_0} + \boldsymbol{K}^e_{\boldsymbol{D}_0\mathcal{Y}}\bar{\boldsymbol{R}}^e_\mathcal{Y}\right)\right); \tag{D.1a}$$

$$\bar{\bar{\boldsymbol{R}}}^e_{\boldsymbol{D}_0} = -\boldsymbol{M}^e_1\left(\boldsymbol{R}^e_{\boldsymbol{D}_0} + \boldsymbol{K}^e_{\boldsymbol{D}_0\mathcal{Y}}\bar{\boldsymbol{R}}^e_\mathcal{Y} + \boldsymbol{K}^e_{\boldsymbol{D}_0\Sigma_\mathcal{Y}}\bar{\boldsymbol{R}}^e_{\Sigma_\mathcal{Y}}\right); \tag{D.1b}$$

$$\bar{\boldsymbol{R}}^e_\mathcal{Y} = -[\boldsymbol{K}^e_{\Sigma_\mathcal{Y}\mathcal{Y}}]^{-1}\boldsymbol{R}^e_{\Sigma_\mathcal{Y}}; \tag{D.1c}$$

$$\boldsymbol{M}^e_1 = [\boldsymbol{K}^e_{\boldsymbol{D}_0\boldsymbol{D}_0} - \boldsymbol{K}^e_{\boldsymbol{D}_0\mathcal{Y}}\left([\boldsymbol{K}^e_{\Sigma_\mathcal{Y}\mathcal{Y}}]^{-1}\boldsymbol{K}^e_{\Sigma_\mathcal{Y}\boldsymbol{D}_0}\right)]^{-1}; \tag{D.1d}$$

$$\boldsymbol{M}^e_2 = [\boldsymbol{K}^e_{\mathcal{Y}\boldsymbol{D}_0} - \boldsymbol{K}^e_{\mathcal{Y}\mathcal{Y}}\left([\boldsymbol{K}^e_{\Sigma_\mathcal{Y}\mathcal{Y}}]^{-1}\boldsymbol{K}^e_{\Sigma_\mathcal{Y}\boldsymbol{D}_0}\right)]^{-1}; \tag{D.1e}$$

$$\boldsymbol{M}^e_3 = [\boldsymbol{K}^e_{\mathcal{Y}\Sigma_\mathcal{Y}} - \boldsymbol{M}^e_2\boldsymbol{M}^e_1\boldsymbol{K}^e_{\boldsymbol{D}_0\Sigma_\mathcal{Y}}]^{-1}; \tag{D.1f}$$

$$\boldsymbol{M}^e_{\mathcal{Y}\boldsymbol{x}} = -[\boldsymbol{K}^e_{\Sigma_\mathcal{Y}\mathcal{Y}}]^{-1}\boldsymbol{K}^e_{\Sigma_\mathcal{Y}\boldsymbol{x}}; \tag{D.1g}$$

$$\boldsymbol{M}^e_{\Sigma_\mathcal{Y}\boldsymbol{x}} = -\boldsymbol{M}^e_3\left(\boldsymbol{K}^e_{\mathcal{Y}\mathcal{Y}}\boldsymbol{M}^e_{\mathcal{Y}\boldsymbol{x}} - \boldsymbol{M}^e_2\boldsymbol{M}^e_1\left(\boldsymbol{K}^e_{\boldsymbol{D}_0\boldsymbol{x}} + \boldsymbol{K}^e_{\boldsymbol{D}_0\mathcal{Y}}\boldsymbol{M}^e_{\mathcal{Y}\boldsymbol{x}}\right)\right); \tag{D.1h}$$

$$\boldsymbol{M}^e_{\Sigma_\mathcal{Y}\varphi} = \boldsymbol{M}^e_3\boldsymbol{M}^e_2\boldsymbol{M}^e_1\boldsymbol{K}^e_{\boldsymbol{D}_0\varphi}; \tag{D.1i}$$

$$\bar{\boldsymbol{M}}^e_{\boldsymbol{D}_0\boldsymbol{x}} = -\boldsymbol{M}^e_1\left(\boldsymbol{K}^e_{\boldsymbol{D}_0\Sigma_\mathcal{Y}}\boldsymbol{M}^e_{\Sigma_\mathcal{Y}\boldsymbol{x}} + \boldsymbol{K}^e_{\boldsymbol{D}_0\boldsymbol{x}} + \boldsymbol{K}^e_{\boldsymbol{D}_0\mathcal{Y}}\boldsymbol{M}^e_{\mathcal{Y}\boldsymbol{x}}\right); \tag{D.1j}$$

$$\bar{\boldsymbol{M}}^e_{\boldsymbol{D}_0\varphi} = -\boldsymbol{M}^e_1\left(\boldsymbol{K}^e_{\boldsymbol{D}_0\Sigma_\mathcal{Y}}\boldsymbol{M}^e_{\Sigma_\mathcal{Y}\varphi} + \boldsymbol{K}^e_{\boldsymbol{D}_0\varphi}\right); \tag{D.1k}$$

$$\bar{\boldsymbol{M}}^e_{\mathcal{Y}\boldsymbol{x}} = \boldsymbol{M}^e_{\mathcal{Y}\boldsymbol{x}} - [\boldsymbol{K}^e_{\Sigma_\mathcal{Y}\mathcal{Y}}]^{-1}\boldsymbol{K}^e_{\Sigma_\mathcal{Y}\boldsymbol{D}_0}\bar{\boldsymbol{M}}^e_{\boldsymbol{D}_0\boldsymbol{x}}; \tag{D.1l}$$

$$\bar{\boldsymbol{M}}^e_{\mathcal{Y}\varphi} = -[\boldsymbol{K}^e_{\Sigma_\mathcal{Y}\mathcal{Y}}]^{-1}\boldsymbol{K}^e_{\Sigma_\mathcal{Y}\boldsymbol{D}_0}\bar{\boldsymbol{M}}^e_{\boldsymbol{D}_0\varphi}. \tag{D.1m}$$

Appendix E

Components of the Jacobian matrix for the full system of hyperbolic equations in convex multi-variable electro-magneto-elasticity

The objective of this Section is to present the expressions for the tensors emerging in the derivation of the Jacobian matrix $\boldsymbol{\mathcal{A}}_I$ in equation (7.44). This matrix is needed for the study of the eigenvalue structure of the quasilinear form of the hyperbolic equations in electro-magneto-elasticity presented in Section 4.3.

Matrix $\widetilde{\boldsymbol{W}_I}^{\star\star}$ in equation (7.44) adopts the following expression

$$\widetilde{\boldsymbol{W}_I}^{\star\star} = \begin{bmatrix} \widetilde{\boldsymbol{P_F}}\boldsymbol{E}_I & \widetilde{\boldsymbol{P_H}}\boldsymbol{E}_I & \widetilde{\boldsymbol{P}}_J\boldsymbol{E}_I & \widetilde{\boldsymbol{P_{D_0}}}\boldsymbol{E}_I & \widetilde{\boldsymbol{P_{B_0}}}\boldsymbol{E}_I & \widetilde{\boldsymbol{P_d}}\boldsymbol{E}_I & \widetilde{\boldsymbol{P_b}}\boldsymbol{E}_I \\ \boldsymbol{0}_{3\times3\times3\times3} & \boldsymbol{0}_{3\times3\times3\times3} & \boldsymbol{0}_{3\times3} & \boldsymbol{0}_{3\times3\times3} & \boldsymbol{0}_{3\times3\times3} & \boldsymbol{0}_{3\times3\times3} & \boldsymbol{0}_{3\times3\times3} \\ \boldsymbol{0}_{3\times3\times3\times3} & \boldsymbol{0}_{3\times3\times3\times3} & \boldsymbol{0}_{3\times3} & \boldsymbol{0}_{3\times3\times3} & \boldsymbol{0}_{3\times3\times3} & \boldsymbol{0}_{3\times3\times3} & \boldsymbol{0}_{3\times3\times3} \\ \boldsymbol{0}_{3\times3} & \boldsymbol{0}_{3\times3} & 0 & \boldsymbol{0}_{3\times1} & \boldsymbol{0}_{3\times1} & \boldsymbol{0}_{3\times1} & \boldsymbol{0}_{3\times1} \end{bmatrix}, \tag{E.1}$$

with

$$\begin{aligned}
\widetilde{\boldsymbol{P_F}} &= W_{\boldsymbol{FF}} + \boldsymbol{F}\times W_{\boldsymbol{HF}} + \boldsymbol{H}\otimes W_{J\boldsymbol{F}} + W_{\boldsymbol{dF}}\diamond\boldsymbol{D}_0 + W_{\boldsymbol{bF}}\diamond\boldsymbol{B}_0;\\
\widetilde{\boldsymbol{P_H}} &= W_{\boldsymbol{FH}} + \boldsymbol{F}\times W_{\boldsymbol{HH}} + \boldsymbol{H}\otimes W_{J\boldsymbol{H}} + W_{\boldsymbol{dH}}\diamond\boldsymbol{D}_0 + W_{\boldsymbol{bH}}\diamond\boldsymbol{B}_0;\\
\widetilde{\boldsymbol{P}}_J &= W_{\boldsymbol{F}J} + \boldsymbol{F}\times W_{\boldsymbol{H}J} + \boldsymbol{H}W_{JJ} + W_{\boldsymbol{d}J}\otimes\boldsymbol{D}_0 + W_{\boldsymbol{b}J}\otimes\boldsymbol{B}_0;\\
\widetilde{\boldsymbol{P_{D_0}}} &= W_{\boldsymbol{FD}_0} + \boldsymbol{F}\times W_{\boldsymbol{HD}_0} + \boldsymbol{H}\otimes W_{J\boldsymbol{D}_0} + W_{\boldsymbol{dD}_0}\diamond\boldsymbol{D}_0 + W_{\boldsymbol{bD}_0}\diamond\boldsymbol{B}_0;\\
\widetilde{\boldsymbol{P_{B_0}}} &= W_{\boldsymbol{FB}_0} + \boldsymbol{F}\times W_{\boldsymbol{HB}_0} + \boldsymbol{H}\otimes W_{J\boldsymbol{B}_0} + W_{\boldsymbol{dB}_0}\diamond\boldsymbol{D}_0 + W_{\boldsymbol{bB}_0}\diamond\boldsymbol{B}_0;\\
\widetilde{\boldsymbol{P_d}} &= W_{\boldsymbol{Fd}} + \boldsymbol{F}\times W_{\boldsymbol{Hd}} + \boldsymbol{H}\otimes W_{J\boldsymbol{d}} + W_{\boldsymbol{dD}_0}\diamond\boldsymbol{D}_0 + W_{\boldsymbol{bD}_0}\diamond\boldsymbol{B}_0;\\
\widetilde{\boldsymbol{P_b}} &= W_{\boldsymbol{Fb}} + \boldsymbol{F}\times W_{\boldsymbol{Hb}} + \boldsymbol{H}\otimes W_{J\boldsymbol{b}} + W_{\boldsymbol{db}}\diamond\boldsymbol{D}_0 + W_{\boldsymbol{bb}}\diamond\boldsymbol{B}_0,
\end{aligned} \tag{E.2}$$

where the tensor operation $(\bullet)\diamond(\bullet)$ between a third or second order tensors, $\boldsymbol{\mathcal{A}}$ and

$\boldsymbol{A}$ respectively, and a vector $\boldsymbol{V}$ yields

$$(\boldsymbol{\mathcal{A}} \diamond \boldsymbol{V})_{iImM} = \mathcal{A}_{imM} V_I; \qquad (\boldsymbol{A} \diamond \boldsymbol{V})_{iIM} = A_{iM} V_I. \tag{E.3}$$

The matrix $\widetilde{\boldsymbol{W}_I}^{\star}$ (featuring in the definition of the Jacobian matrix $\boldsymbol{\mathcal{A}}_I$ (7.44)) is defined so that $\widetilde{\boldsymbol{W}}^{\star}_{\boldsymbol{N}} = \widetilde{\boldsymbol{W}}^{\star}_I N_I$, with $\widetilde{\boldsymbol{W}}^{\star}_{\boldsymbol{N}}$ defined as

$$\widetilde{W}^{\star}_{\boldsymbol{N}} = \begin{bmatrix} -\left(\boldsymbol{W}\widetilde{\boldsymbol{H}_{0\boldsymbol{F}}}\right) & -\left(\boldsymbol{W}\widetilde{\boldsymbol{H}_{0\boldsymbol{H}}}\right) & -\left(\boldsymbol{W}\widetilde{\boldsymbol{H}_{0J}}\right) & -\left(\boldsymbol{W}\widetilde{\boldsymbol{H}_{0\boldsymbol{D}_0}}\right) & -\left(\boldsymbol{W}\widetilde{\boldsymbol{H}_{0\boldsymbol{B}_0}}\right) & -\left(\boldsymbol{W}\widetilde{\boldsymbol{H}_{0\boldsymbol{d}}}\right) & -\left(\boldsymbol{W}\widetilde{\boldsymbol{H}_{0\boldsymbol{b}}}\right) \\ \left(\boldsymbol{W}\widetilde{\boldsymbol{E}_{0\boldsymbol{F}}}\right) & \left(\boldsymbol{W}\widetilde{\boldsymbol{E}_{0\boldsymbol{H}}}\right) & \left(\boldsymbol{W}\widetilde{\boldsymbol{E}_{0J}}\right) & \left(\boldsymbol{W}\widetilde{\boldsymbol{E}_{0\boldsymbol{D}_0}}\right) & \left(\boldsymbol{W}\widetilde{\boldsymbol{E}_{0\boldsymbol{B}_0}}\right) & \left(\boldsymbol{W}\widetilde{\boldsymbol{E}_{0\boldsymbol{d}}}\right) & \left(\boldsymbol{W}\widetilde{\boldsymbol{E}_{0\boldsymbol{b}}}\right) \\ -\left(\boldsymbol{F}\boldsymbol{W}\widetilde{\boldsymbol{H}_{0\boldsymbol{F}}}\right) & -\left(\boldsymbol{F}\boldsymbol{W}\widetilde{\boldsymbol{H}_{0\boldsymbol{H}}}\right) & -\left(\boldsymbol{F}\boldsymbol{W}\widetilde{\boldsymbol{H}_{0J}}\right) & -\left(\boldsymbol{F}\boldsymbol{W}\widetilde{\boldsymbol{H}_{0\boldsymbol{D}_0}}\right) & -\left(\boldsymbol{F}\boldsymbol{W}\widetilde{\boldsymbol{H}_{0\boldsymbol{B}_0}}\right) & -\left(\boldsymbol{F}\boldsymbol{W}\widetilde{\boldsymbol{H}_{0\boldsymbol{d}}}\right) & -\left(\boldsymbol{F}\boldsymbol{W}\widetilde{\boldsymbol{H}_{0\boldsymbol{b}}}\right) \\ \left(\boldsymbol{F}\boldsymbol{W}\widetilde{\boldsymbol{E}_{0\boldsymbol{F}}}\right) & \left(\boldsymbol{F}\boldsymbol{W}\widetilde{\boldsymbol{E}_{0\boldsymbol{H}}}\right) & \left(\boldsymbol{F}\boldsymbol{W}\widetilde{\boldsymbol{E}_{0J}}\right) & \left(\boldsymbol{F}\boldsymbol{W}\widetilde{\boldsymbol{E}_{0\boldsymbol{D}_0}}\right) & \left(\boldsymbol{F}\boldsymbol{W}\widetilde{\boldsymbol{E}_{0\boldsymbol{B}_0}}\right) & \left(\boldsymbol{F}\boldsymbol{W}\widetilde{\boldsymbol{E}_{0\boldsymbol{d}}}\right) & \left(\boldsymbol{F}\boldsymbol{W}\widetilde{\boldsymbol{E}_{0\boldsymbol{b}}}\right) \end{bmatrix}. \tag{E.4}$$

Notice that the second order tensor $\boldsymbol{W}$ is defined as $W_{IJ} = \mathcal{E}_{IJK} N_K$ and that the terms $\widetilde{\boldsymbol{E}_{0\boldsymbol{F}}}$, $\widetilde{\boldsymbol{E}_{0\boldsymbol{H}}}$, etc. in above equation (E.4) are defined as

$$\begin{aligned} \widetilde{\boldsymbol{E}_{0\boldsymbol{F}}} &= W_{\boldsymbol{D}_0\boldsymbol{F}} + \boldsymbol{F}^T W_{\boldsymbol{d}\boldsymbol{F}}; & \widetilde{\boldsymbol{E}_{0\boldsymbol{H}}} &= W_{\boldsymbol{D}_0\boldsymbol{H}} + \boldsymbol{F}^T W_{\boldsymbol{d}\boldsymbol{H}}; \\ \widetilde{\boldsymbol{E}_{0J}} &= W_{\boldsymbol{D}_0 J} + \boldsymbol{F}^T W_{\boldsymbol{d}J}; & \widetilde{\boldsymbol{E}_{0\boldsymbol{D}_0}} &= W_{\boldsymbol{D}_0\boldsymbol{D}_0} + \boldsymbol{F}^T W_{\boldsymbol{d}\boldsymbol{D}_0}; \\ \widetilde{\boldsymbol{E}_{0\boldsymbol{D}_0}} &= W_{\boldsymbol{D}_0\boldsymbol{B}_0} + \boldsymbol{F}^T W_{\boldsymbol{d}\boldsymbol{B}_0}; & \widetilde{\boldsymbol{E}_{0\boldsymbol{d}}} &= W_{\boldsymbol{D}_0\boldsymbol{d}} + \boldsymbol{F}^T W_{\boldsymbol{d}\boldsymbol{d}}; \\ \widetilde{\boldsymbol{E}_{0\boldsymbol{b}}} &= W_{\boldsymbol{D}_0\boldsymbol{b}} + \boldsymbol{F}^T W_{\boldsymbol{d}\boldsymbol{b}}. \end{aligned} \tag{E.5}$$

Finally, the terms $\widetilde{\boldsymbol{H}_{0\boldsymbol{F}}}$, $\widetilde{\boldsymbol{H}_{0\boldsymbol{H}}}$, etc. in above equation (E.4) are defined as

$$\begin{aligned} \widetilde{\boldsymbol{H}_{0\boldsymbol{F}}} &= W_{\boldsymbol{B}_0\boldsymbol{F}} + \boldsymbol{F}^T W_{\boldsymbol{b}\boldsymbol{F}}; & \widetilde{\boldsymbol{H}_{0\boldsymbol{H}}} &= W_{\boldsymbol{B}_0\boldsymbol{H}} + \boldsymbol{F}^T W_{\boldsymbol{b}\boldsymbol{H}}; \\ \widetilde{\boldsymbol{H}_{0J}} &= W_{\boldsymbol{B}_0 J} + \boldsymbol{F}^T W_{\boldsymbol{b}J}; & \widetilde{\boldsymbol{H}_{0\boldsymbol{D}_0}} &= W_{\boldsymbol{B}_0\boldsymbol{D}_0} + \boldsymbol{F}^T W_{\boldsymbol{b}\boldsymbol{D}_0}; \\ \widetilde{\boldsymbol{H}_{0\boldsymbol{D}_0}} &= W_{\boldsymbol{B}_0\boldsymbol{B}_0} + \boldsymbol{F}^T W_{\boldsymbol{b}\boldsymbol{B}_0}; & \widetilde{\boldsymbol{H}_{0\boldsymbol{d}}} &= W_{\boldsymbol{B}_0\boldsymbol{d}} + \boldsymbol{F}^T W_{\boldsymbol{b}\boldsymbol{d}}; \\ \widetilde{\boldsymbol{H}_{0\boldsymbol{b}}} &= W_{\boldsymbol{B}_0\boldsymbol{b}} + \boldsymbol{F}^T W_{\boldsymbol{b}\boldsymbol{b}}. \end{aligned} \tag{E.6}$$

Appendix F

Theorem relevant to the hyperbolicity of the eigenvalue problem for both elasticity and nonlinear electro-magneto-elasticity

The objective of this section is to prove that, as stated in Sections (4.3.1) and (7.3.1), a second order tensor $\boldsymbol{\mathcal{A}}_{\boldsymbol{N}}^{\star}$, defined via the multiplicative decomposition in equations (4.35) and (7.57) (for the respective cases of nonlinear elasticity and nonlinear electro-magneto-elasticity) in terms of a symmetric and a symmetric positive definite second order tensor admits only real eigenvalues. This can be stated in the following theorem

Theorem F.0.1 *Let $\boldsymbol{A} \in \mathbb{R}^{n\times n}$ and $\boldsymbol{B} \in \mathbb{R}^{n\times n}$ be symmetric and symmetric positive definite matrices for any arbitrary dimension specification n. Let $\boldsymbol{C}$ be defined in terms of the following multiplicative decomposition as*

$$\boldsymbol{C} = \boldsymbol{A}\boldsymbol{B}. \tag{F.1}$$

Then, the matrix $\boldsymbol{C}$ defined as in equation (F.1) *has real eigenvalues.*

Proof. The eigenvalue problem associated to matrix $\boldsymbol{C}$ introduced in Theorem F.0.1 is defined as

$$(c_\alpha \boldsymbol{I} - \boldsymbol{A}\boldsymbol{B})\,\bar{\boldsymbol{m}}_\alpha = \boldsymbol{0}, \tag{F.2}$$

where $\bar{\boldsymbol{m}}_\alpha$ are the eigenvectors of $\boldsymbol{C}$. Note that $\boldsymbol{B}$ admits the following non-unique multiplicative decomposition, $\boldsymbol{B} = \boldsymbol{L}\boldsymbol{L}^T$. A possible choice for $\boldsymbol{L}$ could be the symmetric matrix $\boldsymbol{L} = \sqrt{\boldsymbol{B}}$[1]. This particular choice of $\boldsymbol{L}$ enables to re-write equation

[1]Since $\boldsymbol{B}$ is a positive definite matrix, it admits the following decomposition in terms of its eigenvalues $c_{\alpha_{\boldsymbol{B}}}$ and eigenvectors $\bar{\boldsymbol{m}}_{\alpha_{\boldsymbol{B}}}$, namely $\boldsymbol{B} = c_{\alpha_{\boldsymbol{B}}}\bar{\boldsymbol{m}}_{\alpha_{\boldsymbol{B}}} \otimes \bar{\boldsymbol{m}}_{\alpha_{\boldsymbol{B}}}$.The symmetric matrix $\sqrt{\boldsymbol{B}}$ can be defined as $\sqrt{\boldsymbol{B}} = \sqrt{c_{\alpha_{\boldsymbol{B}}}}\bar{\boldsymbol{m}}_{\alpha_{\boldsymbol{B}}} \otimes \bar{\boldsymbol{m}}_{\alpha_{\boldsymbol{B}}}$.

(F.2) as

$$\left(c_\alpha \boldsymbol{I} - \boldsymbol{A}\sqrt{\boldsymbol{B}}\sqrt{\boldsymbol{B}}\right)\bar{\boldsymbol{m}}_\alpha = \boldsymbol{0} \tag{F.3}$$

The identification of the eigenvalues c_α in above (F.3) is equivalent to the solution of the following polynomial equation, namely $\det\boldsymbol{D} = 0$, where $\boldsymbol{D} = c_\alpha \boldsymbol{I} - \boldsymbol{A}\sqrt{\boldsymbol{B}}\sqrt{\boldsymbol{B}}$. Pre- and post-multiplication by $\sqrt{\boldsymbol{B}}\ \sqrt{\boldsymbol{B}}^{-1}$ does not alter the solution to the polynomial equation (F.3), namely $\det(\boldsymbol{D}) = \det(\sqrt{\boldsymbol{B}}\boldsymbol{D}\sqrt{\boldsymbol{B}}^{-1})$. Therefore, the roots (the eigenvalues of $\boldsymbol{C}$) can be equivalently obtained as

$$\det\left(c_\alpha \boldsymbol{I} - \sqrt{\boldsymbol{B}}\boldsymbol{A}\sqrt{\boldsymbol{B}}\right) = 0. \tag{F.4}$$

Equation (F.4) proves that the eigenvalues of the matrix $\boldsymbol{C}$ defined in Theorem F.0.1 are the same as those for the matrix defined as $\sqrt{\boldsymbol{B}}\boldsymbol{A}\sqrt{\boldsymbol{B}}$ (the same cannot be said regarding the eigenvectors). Symmetry of this new matrix $\sqrt{\boldsymbol{B}}\boldsymbol{A}\sqrt{\boldsymbol{B}}$ (it is obvious to verify symmetry of this matrix) guarantees therefore that its eigenvalues, and therefore those for matrix $\boldsymbol{C}$ are real.

Appendix G

Relationship between the constitutive tensors of the internal energy in terms of its reduced and extended representations for electro-magneto-mechanics

The objective of this section is to express the physically meaningful constitutive tensors in electro-magneto-elasticity in Section 7.3.1, namely $\boldsymbol{\mathcal{C}}$, $\boldsymbol{\mathcal{Q}}$, $\boldsymbol{\mathcal{T}}$, $\boldsymbol{R}$, $\boldsymbol{\theta}$ and $\boldsymbol{\vartheta}$, emanating from the Hessian operator of the internal energy e, in terms of the components of the Hessian operator of the extended representation of the internal energy, namely $[\mathbb{H}_W]$ (7.18).

G.1 Elasticity tensor

The fourth order elasticity tensor $\boldsymbol{\mathcal{C}}$ emanates from the second directional derivative of the internal energy e with respect to changes of the geometry as

$$D^2 e\left[\delta\boldsymbol{u};\boldsymbol{u}\right] = \boldsymbol{\nabla}_0\delta\boldsymbol{u} : \boldsymbol{\mathcal{C}} : \boldsymbol{\nabla}_0\boldsymbol{u} \Rightarrow \boldsymbol{\mathcal{C}} = \frac{\partial^2 e}{\partial\boldsymbol{\nabla}_0\boldsymbol{x}\boldsymbol{\nabla}_0\boldsymbol{x}}. \tag{G.1}$$

Alternatively, $\boldsymbol{\mathcal{C}}$ can be re-written in terms of the derivatives of the electro-kinematic variable set $\mathcal{V}$ as

$$\begin{aligned}\boldsymbol{\mathcal{C}} = {} & W_{\boldsymbol{FF}} + \boldsymbol{F}\boldsymbol{\times}(W_{\boldsymbol{HH}}\boldsymbol{\times}\boldsymbol{F}) + W_{JJ}\boldsymbol{H}\otimes\boldsymbol{H} + \boldsymbol{\mathcal{C}}_1 + \boldsymbol{\mathcal{C}}_2 \\ & + 2(W_{\boldsymbol{FH}}\boldsymbol{\times}\boldsymbol{F})^{\mathrm{sym}} + 2(W_{\boldsymbol{F}J}\otimes\boldsymbol{H})^{\mathrm{sym}} + 2(W_{\boldsymbol{Fd}}\otimes\boldsymbol{D}_0)^{\mathrm{sym}} + 2(W_{\boldsymbol{Fb}}\otimes\boldsymbol{B}_0)^{\mathrm{sym}} \\ & + 2((\boldsymbol{F}\boldsymbol{\times}W_{\boldsymbol{H}J})\otimes\boldsymbol{H})^{\mathrm{sym}} + 2((\boldsymbol{F}\boldsymbol{\times}W_{\boldsymbol{Hd}})\otimes\boldsymbol{D}_0)^{\mathrm{sym}} + 2((\boldsymbol{F}\boldsymbol{\times}W_{\boldsymbol{Hb}})\otimes\boldsymbol{B}_0)^{\mathrm{sym}} \\ & + 2(\boldsymbol{H}\otimes(W_{J\boldsymbol{d}}\otimes\boldsymbol{D}_0))^{\mathrm{sym}} + 2(\boldsymbol{H}\otimes(W_{J\boldsymbol{b}}\otimes\boldsymbol{B}_0))^{\mathrm{sym}} + \boldsymbol{\mathcal{A}},\end{aligned} \tag{G.2}$$

with

$$\mathcal{A}_{iIjJ} = \mathcal{E}_{ijp}\mathcal{E}_{IJP}\left(\boldsymbol{\Sigma}_{\boldsymbol{H}} + \Sigma_J \boldsymbol{\Sigma}_{\boldsymbol{H}}\right)_{pP}; \quad \mathcal{C}_{1,iIjJ} = \left(W_{\boldsymbol{dd}}\right)_{ij} D_{0I} D_{0J}; \quad \mathcal{C}_{2,iIjJ} = \left(W_{\boldsymbol{bb}}\right)_{ij} B_{0I} B_{0J}. \tag{G.3}$$

G.2 Piezoelectric tensor

The third order piezoelectric tensor $\boldsymbol{\mathcal{Q}}$ emanates from the second directional derivative of the internal energy e with respect to changes in geometry and electric displacement field as

$$D^2 e\left[\delta\boldsymbol{u}; \Delta\boldsymbol{D}_0\right] = \left(\boldsymbol{\nabla}_0 \delta\boldsymbol{u} : \boldsymbol{\mathcal{Q}}^T\right) \cdot \Delta\boldsymbol{D}_0 \Rightarrow \boldsymbol{\mathcal{Q}} = \frac{\partial^2 e}{\partial \boldsymbol{\nabla}_0 \boldsymbol{x} \partial \boldsymbol{D}_0}. \tag{G.4}$$

Alternatively, the piezoelectric tensor $\boldsymbol{\mathcal{Q}}^T$ can be re-expresses in terms of the elements of the set $\mathcal{V}$ as

$$\begin{aligned} \boldsymbol{\mathcal{Q}}^T = & W_{\boldsymbol{F}\boldsymbol{D}_0} + \boldsymbol{F} \boldsymbol{\times} W_{\boldsymbol{H}\boldsymbol{D}_0} + \boldsymbol{H} \otimes W_{J\boldsymbol{D}_0} + \boldsymbol{\mathcal{Q}}_1^T \\ & + \boldsymbol{\mathcal{Q}}_2^T + \boldsymbol{\mathcal{Q}}_3^T + \boldsymbol{\mathcal{Q}}_4^T + \boldsymbol{\mathcal{Q}}_5^T + \boldsymbol{\mathcal{Q}}_6^T + \boldsymbol{\mathcal{Q}}_7^T + \boldsymbol{\Sigma}_{\boldsymbol{d}} \otimes \boldsymbol{I}. \end{aligned} \tag{G.5}$$

where the expressions for the tensors $\boldsymbol{\mathcal{Q}}_i^T$ in above equation (G.5) are given as

$$\left(\boldsymbol{\mathcal{Q}}_1^T\right)_{iIJ} = \left(W_{\boldsymbol{d}\boldsymbol{D}_0}\right)_{iJ} D_{0I}; \tag{G.6a}$$

$$\left(\boldsymbol{\mathcal{Q}}_2^T\right)_{iIJ} = \left(W_{\boldsymbol{F}\boldsymbol{d}iIj}\right) F_{jJ}; \tag{G.6b}$$

$$\left(\boldsymbol{\mathcal{Q}}_3^T\right)_{iIJ} = (\boldsymbol{F} \boldsymbol{\times} W_{\boldsymbol{H}\boldsymbol{d}})_{iIj} F_{jJ}; \tag{G.6c}$$

$$\left(\boldsymbol{\mathcal{Q}}_4^T\right)_{iIJ} = (\boldsymbol{H} \otimes W_{J\boldsymbol{d}})_{iIj} F_{jJ}; \tag{G.6d}$$

$$\left(\boldsymbol{\mathcal{Q}}_5^T\right)_{iIJ} = \left(W_{\boldsymbol{d}\boldsymbol{d}}\right)_{ij} F_{jJ} D_{0I}; \tag{G.6e}$$

$$\left(\boldsymbol{\mathcal{Q}}_6^T\right)_{iIJ} = \left(W_{\boldsymbol{b}\boldsymbol{D}_0}\right)_{iJ} B_{0I}; \tag{G.6f}$$

$$\left(\boldsymbol{\mathcal{Q}}_7^T\right)_{iIJ} = \left(W_{\boldsymbol{b}\boldsymbol{d}}\right)_{ij} F_{jJ} B_{0I}. \tag{G.6g}$$

G.3 Piezomagnetic tensor

The third order piezomagnetic tensor $\boldsymbol{\mathcal{T}}$ emanates from the second directional derivative of the internal energy e with respect to changes in geometry and magnetic inductions field as

$$D^2 e\left[\delta\boldsymbol{u}; \Delta\boldsymbol{B}_0\right] = \left(\boldsymbol{\nabla}_0 \delta\boldsymbol{u} : \boldsymbol{\mathcal{T}}^T\right) \cdot \Delta\boldsymbol{B}_0 \Rightarrow \boldsymbol{\mathcal{T}} = \frac{\partial^2 e}{\partial \boldsymbol{\nabla}_0 \boldsymbol{x} \partial \boldsymbol{B}_0}. \tag{G.7}$$

The piezomagnetic tensor $\boldsymbol{\mathcal{T}}^T$ can be re-expressed in terms of the elements of the set $\mathcal{V}$ as

$$\begin{aligned} \boldsymbol{\mathcal{T}}^T = & W_{\boldsymbol{F}\boldsymbol{B}_0} + \boldsymbol{F} \boldsymbol{\times} W_{\boldsymbol{H}\boldsymbol{B}_0} + \boldsymbol{H} \otimes W_{J\boldsymbol{B}_0} + \boldsymbol{\mathcal{T}}_1^T \\ & + \boldsymbol{\mathcal{T}}_2^T + \boldsymbol{\mathcal{T}}_3^T + \boldsymbol{\mathcal{T}}_4^T + \boldsymbol{\mathcal{T}}_5^T + \boldsymbol{\mathcal{T}}_6^T + \boldsymbol{\mathcal{T}}_7^T + \boldsymbol{\Sigma}_{\boldsymbol{b}} \otimes \boldsymbol{I}. \end{aligned} \tag{G.8}$$

with

$$\left(\boldsymbol{\mathcal{T}}_1^T\right)_{iIJ} = \left(W_{\boldsymbol{dB}_0}\right)_{iJ} B_{0I}; \tag{G.9a}$$
$$\left(\boldsymbol{\mathcal{T}}_2^T\right)_{iIJ} = \left(W_{\boldsymbol{Fb}iIj}\right) F_{jJ}; \tag{G.9b}$$
$$\left(\boldsymbol{\mathcal{T}}_3^T\right)_{iIJ} = (\boldsymbol{F} \times W_{\boldsymbol{Hb}})_{iIj} F_{jJ}; \tag{G.9c}$$
$$\left(\boldsymbol{\mathcal{T}}_4^T\right)_{iIJ} = (\boldsymbol{H} \otimes W_{J\boldsymbol{b}})_{iIj} F_{jJ}; \tag{G.9d}$$
$$\left(\boldsymbol{\mathcal{T}}_5^T\right)_{iIJ} = \left(W_{\boldsymbol{bb}}\right)_{ij} F_{jJ} B_{0I}.; \tag{G.9e}$$
$$\left(\boldsymbol{\mathcal{T}}_6^T\right)_{iIJ} = \left(W_{\boldsymbol{dB}_0}\right)_{iJ} D_{0I}; \tag{G.9f}$$
$$\left(\boldsymbol{\mathcal{T}}_7^T\right)_{iIJ} = \left(W_{\boldsymbol{db}}\right)_{ij} F_{jJ} D_{0I}. \tag{G.9g}$$

G.4 Dielectric tensor

The second order dielectric tensor $\boldsymbol{\theta}$ emanates from the second directional derivative of the internal energy e with respect to changes in the electric displacement field as

$$D^2 e\left[\delta \boldsymbol{D}_0; \Delta \boldsymbol{D}_0\right] = \delta \boldsymbol{D}_0 \cdot \boldsymbol{\theta} \Delta \boldsymbol{D}_0 \Rightarrow \boldsymbol{\theta} = \frac{\partial^2 e}{\partial \boldsymbol{D}_0 \partial \boldsymbol{D}_0}. \tag{G.10}$$

Alternatively, the inverse of the dielectric tensor $\boldsymbol{\theta}$ can be re-expressed in terms of the elements of the set $\mathcal{V}$ as

$$\boldsymbol{\theta} = W_{\boldsymbol{D}_0\boldsymbol{D}_0} + \left(W_{\boldsymbol{D}_0\boldsymbol{d}}\boldsymbol{F} + \boldsymbol{F}^T W_{\boldsymbol{d}\boldsymbol{D}_0}\right) + \boldsymbol{F}^T W_{\boldsymbol{dd}} \boldsymbol{F}. \tag{G.11}$$

G.5 Permeability tensor

The second order permeability tensor $\boldsymbol{\vartheta}$ emanates from the second directional derivative of the internal energy e with respect to changes in the magnetic induction field as

$$D^2 e\left[\delta \boldsymbol{B}_0; \Delta \boldsymbol{B}_0\right] = \delta \boldsymbol{B}_0 \cdot \boldsymbol{\vartheta} \Delta \boldsymbol{B}_0 \Rightarrow \boldsymbol{\vartheta} = \frac{\partial^2 e}{\partial \boldsymbol{B}_0 \partial \boldsymbol{B}_0}. \tag{G.12}$$

Alternatively, the inverse of the permeability tensor $\boldsymbol{\vartheta}$ can be re-expressed in terms of the elements of the set $\mathcal{V}$ as

$$\boldsymbol{\vartheta} = W_{\boldsymbol{B}_0\boldsymbol{B}_0} + \left(W_{\boldsymbol{B}_0\boldsymbol{b}}\boldsymbol{F} + \boldsymbol{F}^T W_{\boldsymbol{b}\boldsymbol{B}_0}\right) + \boldsymbol{F}^T W_{\boldsymbol{bb}} \boldsymbol{F}. \tag{G.13}$$

G.6 Magnetoelectric tensor

The second order magnetoelectric tensor $\boldsymbol{R}$ emanates from the second directional derivative of the internal energy e with respect to changes in the electric displacement field and magnetic induction field as

$$D^2 e\left[\delta \boldsymbol{D}_0; \Delta \boldsymbol{B}_0\right] = \delta \boldsymbol{D}_0 \cdot \boldsymbol{R} \cdot \Delta \boldsymbol{B}_0 \Rightarrow \boldsymbol{R} = \frac{\partial^2 e}{\partial \boldsymbol{D}_0 \partial \boldsymbol{B}_0}. \tag{G.14}$$

Alternatively, the magnetoelectric tensor $\boldsymbol{R}$ can be re-expressed in terms of the elements of the set $\mathcal{V}$ as

$$\boldsymbol{R} = W_{\boldsymbol{D}_0\boldsymbol{B}_0} + W_{\boldsymbol{D}_0\boldsymbol{b}}\boldsymbol{F} + \boldsymbol{F}^T W_{\boldsymbol{d}\boldsymbol{B}_0} + \boldsymbol{F}^T W_{\boldsymbol{d}\boldsymbol{b}}\boldsymbol{F}. \tag{G.15}$$

Appendix H

Algebraic manipulations for the explicit representation of acoustic waves in dielectric elastomers

The objective of this section is to obtain a simple expression for the second order tensor $\boldsymbol{\mathcal{C}_D}$ in equation (7.96) which would allow to obtain a simple explicit representation for the speed of propagation of acoustic waves for the polyconvex constitutive model in equation (7.19), particularised to the case of electro-mechanics. This tensor involves computing the inverse of the constitutive tensor $\boldsymbol{\theta}$ (5.20), which is defined as

$$\boldsymbol{\theta} = \frac{1}{\varepsilon_1}\boldsymbol{I} + \frac{1}{\varepsilon_2}\boldsymbol{C}, \tag{H.1}$$

where $\boldsymbol{C} = \boldsymbol{F}^T\boldsymbol{F}$ is the right Cauchy-Green deformation tensor. The inverse of every symemtric positive definite second order tensor (still a symmetric positive definite second order tensor), and in particular $\boldsymbol{\theta}^{-1}$ admits the following additive decomposition

$$\boldsymbol{\theta}^{-1} = \alpha_1\boldsymbol{I} + \alpha_2\boldsymbol{C} + \alpha_3\boldsymbol{G}, \tag{H.2}$$

where $\boldsymbol{G}$ is the co-factor of $\boldsymbol{C}$. Noting that $\boldsymbol{\theta}\boldsymbol{\theta}^{-1} = \boldsymbol{I}$ and $\boldsymbol{C}\boldsymbol{G} = J^2$ and considering equations (H.1) and (H.2) gives

$$\begin{aligned}\boldsymbol{\theta}\boldsymbol{\theta}^{-1} &= \left(\frac{1}{\varepsilon_1}\boldsymbol{I} + \frac{1}{\varepsilon_2}\boldsymbol{C}\right)(\alpha_1\boldsymbol{I} + \alpha_2\boldsymbol{C} + \alpha_3\boldsymbol{G}) \\ &= \left(\frac{\alpha_1}{\varepsilon_1} + \frac{\alpha_3 J^2}{\varepsilon_2}\right)\boldsymbol{I} + \left(\frac{\alpha_2}{\varepsilon_1} + \frac{\alpha_1}{\varepsilon_2}\right)\boldsymbol{C} + \frac{\alpha_2}{\varepsilon_2}\boldsymbol{C}^2 + \frac{\alpha_3}{\varepsilon_1}\boldsymbol{G}.\end{aligned} \tag{H.3}$$

As shown in [32], the co-factor of a symmetric positive definite tensor, and in particular $\boldsymbol{G}$, can be alternatively expressed as

$$\boldsymbol{G} = \boldsymbol{C}^2 - I_{1\boldsymbol{C}}\boldsymbol{C} + I_{2\boldsymbol{C}}\boldsymbol{I}. \tag{H.4}$$

Introduction of the expression for $\boldsymbol{G}$ in (H.4) into equation (H.3) yields,

$$\boldsymbol{\theta}\boldsymbol{\theta}^{-1} = \left(\frac{\alpha_1}{\varepsilon_1} + \frac{\alpha_3 J^2}{\varepsilon_2} + \frac{\alpha_3 I_{2\boldsymbol{C}}}{\varepsilon_1}\right)\boldsymbol{I} + \left(\frac{\alpha_2}{\varepsilon_1} + \frac{\alpha_1}{\varepsilon_2} - \frac{\alpha_3 I_{1\boldsymbol{C}}}{\varepsilon_1}\right)\boldsymbol{C} + \left(\frac{\alpha_2}{\varepsilon_2} + \frac{\alpha_3}{\varepsilon_1}\right)\boldsymbol{C}^2 = \boldsymbol{I}. \tag{H.5}$$

Identification of the coefficients $\{\alpha_1, \alpha_2, \alpha_3\}$ in above equation (H.5) can be obtained by solving the following system of linear equations

$$\begin{aligned} \frac{\alpha_1}{\varepsilon_1} + \frac{\alpha_3 J^2}{\varepsilon_2} + \frac{\alpha_3 I_{2\boldsymbol{C}}}{\varepsilon_1} &= 1; \\ \frac{\alpha_2}{\varepsilon_1} + \frac{\alpha_1}{\varepsilon_2} - \frac{\alpha_3 I_{1\boldsymbol{C}}}{\varepsilon_1} &= 0; \\ \frac{\alpha_2}{\varepsilon_2} + \frac{\alpha_3}{\varepsilon_1} &= 0. \end{aligned} \tag{H.6}$$

Solution of the above system of equations results in

$$\alpha_1 = \frac{\theta_1^2 + \theta_1\theta_2 I_{1\boldsymbol{C}}}{g}; \qquad \alpha_2 = -\frac{\theta_1\theta_2}{g}; \qquad \alpha_3 = \frac{\theta_2^2}{g}. \tag{H.7}$$

where $\theta_i = \frac{1}{\varepsilon_i}$, $i = \{1, 2\}$ and with

$$g = \theta_1^3 + \theta_1^2\theta_2 I_{1\boldsymbol{C}} + \theta_1\theta_2^2 I_{2\boldsymbol{C}} + \theta_2^2 J^2. \tag{H.8}$$

With the help of the result in equations (H.1) and (H.7), it is now possible to evaluate the second order $\boldsymbol{\mathcal{C}_D}$ in equation (7.96) and re-express it in a more convenient manner which would enable to obtain an explicit representation of the speed of propagation of acoustic waves for the polyconvex constitutive model considered, and defined in equation (7.19). This tensor can be additively decomposed into two tensor $\boldsymbol{\mathcal{C}_{D1}}$ and $\boldsymbol{\mathcal{C}_{D2}}$ as $\boldsymbol{\mathcal{C}_D} = \boldsymbol{\mathcal{C}_{D1}} - \boldsymbol{\mathcal{C}_{D2}}$, defined as

$$\begin{aligned} \boldsymbol{\mathcal{C}_{D1}} &= \boldsymbol{F}\left(\boldsymbol{I} - \boldsymbol{N}\otimes\boldsymbol{N}\right)\boldsymbol{\theta}^{-1}\boldsymbol{F}^T; \\ \boldsymbol{\mathcal{C}_{D2}} &= \boldsymbol{F}\left(\boldsymbol{I} - \boldsymbol{N}\otimes\boldsymbol{N}\right)\frac{\boldsymbol{\theta}^{-1}\boldsymbol{N}\otimes\boldsymbol{\theta}^{-1}\boldsymbol{N}}{\boldsymbol{N}\cdot\boldsymbol{\theta}^{-1}\boldsymbol{N}}\boldsymbol{F}^T. \end{aligned} \tag{H.9}$$

Proper re-arrangement of the expressions for $\boldsymbol{\mathcal{C}_{D1}}$ and $\boldsymbol{\mathcal{C}_{D2}}$ in above equation (H.9) yields

$$\boldsymbol{\mathcal{C}_{D1}} = \left(\sum_{\alpha=1}^{2}\lambda_\alpha \boldsymbol{t}_\alpha\otimes\boldsymbol{T}_\alpha\right)\boldsymbol{\theta}^{-1}\boldsymbol{F}^T; \tag{H.10a}$$

$$\boldsymbol{\mathcal{C}_{D2}} = \left(\sum_{\alpha=1}^{2}\lambda_\alpha \boldsymbol{t}_\alpha\otimes\boldsymbol{T}_\alpha\right)\frac{\boldsymbol{\theta}^{-1}\boldsymbol{N}\otimes\boldsymbol{\theta}^{-1}\boldsymbol{N}}{\boldsymbol{N}\cdot\boldsymbol{\theta}^{-1}\boldsymbol{N}}\boldsymbol{F}^T. \tag{H.10b}$$

Analytical derivations of the wave speeds requires pre- and post-multiplication of the above second order tensor $\boldsymbol{\mathcal{C}_{D1}}$ and $\boldsymbol{\mathcal{C}_{D2}}$ by the eigenmodes $\bar{\boldsymbol{p}}_\alpha$, yielding

$$\begin{aligned} \bar{\boldsymbol{p}}_\alpha\cdot\boldsymbol{\mathcal{C}_{D1}}\bar{\boldsymbol{p}}_\alpha &= \left(\sum_{\alpha=1}^{2}\lambda_\alpha \boldsymbol{t}_\alpha\cdot\bar{\boldsymbol{p}}_\alpha\right)\left(\boldsymbol{F}^T\bar{\boldsymbol{p}}_\alpha\cdot\boldsymbol{\theta}^{-1}\boldsymbol{T}_\alpha\right); \\ \bar{\boldsymbol{p}}_\alpha\cdot\boldsymbol{\mathcal{C}_{D2}}\bar{\boldsymbol{p}}_\alpha &= \frac{\left(\sum_{\alpha=1}^{2}\lambda_\alpha \boldsymbol{t}_\alpha\cdot\bar{\boldsymbol{p}}_\alpha\right)\left(\boldsymbol{T}_\alpha\cdot\boldsymbol{\theta}^{-1}\boldsymbol{N}\right)\left(\boldsymbol{\theta}^{-1}\boldsymbol{N}\cdot\boldsymbol{F}^T\bar{\boldsymbol{p}}_\alpha\right)}{\boldsymbol{N}\cdot\boldsymbol{\theta}^{-1}\boldsymbol{N}}, \end{aligned}$$

which enables $\bar{\boldsymbol{p}}_\alpha \cdot \boldsymbol{\mathcal{C}_D} \bar{\boldsymbol{p}}_\alpha$ to be finally obtained as

$$\bar{\boldsymbol{p}}_\alpha \cdot \boldsymbol{\mathcal{C}_D} \bar{\boldsymbol{p}}_\alpha = \left(\sum_{\alpha=1}^{2} \lambda_\alpha \boldsymbol{t}_\alpha \cdot \bar{\boldsymbol{p}}_\alpha \right) \left(\left(\boldsymbol{F}^T \bar{\boldsymbol{p}}_\alpha \cdot \boldsymbol{\theta}^{-1} \boldsymbol{T}_\alpha \right) - \frac{\left(\boldsymbol{T}_\alpha \cdot \boldsymbol{\theta}^{-1} \boldsymbol{N} \right) \left(\boldsymbol{\theta}^{-1} \boldsymbol{N} \cdot \boldsymbol{F}^T \bar{\boldsymbol{p}}_\alpha \right)}{\boldsymbol{N} \cdot \boldsymbol{\theta}^{-1} \boldsymbol{N}} \right) \tag{H.11}$$

where $\boldsymbol{\theta}^{-1} \boldsymbol{T}_\alpha$ and $\boldsymbol{\theta}^{-1} \boldsymbol{N}$ in above equation (H.11) can be written by making use of the identities in equation (4.68) and of equation (H.2) for the inverse of the second order tensor $\boldsymbol{\theta}$ defined in equation (H.1) as

$$\begin{aligned} \boldsymbol{\theta}^{-1} \boldsymbol{T}_\alpha &= \left(\alpha_1 + \alpha_2 \lambda_\alpha^2 + \alpha_3 \left(\frac{J}{\lambda_\alpha} \right)^2 \right) \boldsymbol{T}_\alpha; \\ \boldsymbol{\theta}^{-1} \boldsymbol{N} &= \left(\alpha_1 + \alpha_2 \lambda_3^2 + \alpha_3 \left(\frac{J}{\lambda_3} \right)^2 \right) \boldsymbol{N}. \end{aligned} \tag{H.12}$$

From equation (H.12), it is easy to notice that

$$\boldsymbol{T}_\alpha \cdot \boldsymbol{\theta}^{-1} \boldsymbol{N} = 0. \tag{H.13}$$

Therefore, equation (H.11) can be further simplified as

$$\bar{\boldsymbol{p}}_\alpha \cdot \boldsymbol{\mathcal{C}_D} \bar{\boldsymbol{p}}_\alpha = \left(\sum_{\alpha=1}^{2} \lambda_\alpha \boldsymbol{t}_\alpha \cdot \bar{\boldsymbol{p}}_\alpha \right) \left(\boldsymbol{F}^T \bar{\boldsymbol{p}}_\alpha \cdot \boldsymbol{\theta}^{-1} \boldsymbol{T}_\alpha \right) \tag{H.14}$$

For pressure waves, characterised by $\bar{\boldsymbol{p}}_\alpha = \boldsymbol{n}$, it is easy to see that $\boldsymbol{n} \cdot \boldsymbol{\mathcal{C}_D} \boldsymbol{n} = 0$. For shear waves, where $\bar{\boldsymbol{p}}_\alpha = \boldsymbol{t}_\alpha$ (with $\{\boldsymbol{t}_1, \boldsymbol{t}_2\}$ two orthonormal vectors to $\boldsymbol{n}$), the expression for $\bar{\boldsymbol{p}}_\alpha \cdot \boldsymbol{\mathcal{C}_D} \bar{\boldsymbol{p}}_\alpha$ in (H.14) becomes

$$\boldsymbol{t}_\alpha \cdot \boldsymbol{\mathcal{C}_D} \boldsymbol{t}_\alpha = \lambda_\alpha \left(\boldsymbol{F}^T \boldsymbol{t}_\alpha \cdot \boldsymbol{\theta}^{-1} \boldsymbol{T}_\alpha \right). \tag{H.15}$$

Finally, use of equations $(4.68)_b$ and $(\text{H.12})_b$ enables $\boldsymbol{t}_\alpha \cdot \boldsymbol{\mathcal{C}_D} \boldsymbol{t}_\alpha$ to be written as

$$\boldsymbol{t}_\alpha \cdot \boldsymbol{\mathcal{C}_D} \boldsymbol{t}_\alpha = \lambda_\alpha \left(\boldsymbol{F}^T \boldsymbol{t}_\alpha \cdot \boldsymbol{\theta}^{-1} \boldsymbol{T}_\alpha \right) = \lambda_\alpha \left(\alpha_1 + \alpha_2 \lambda_3^2 + \alpha_3 \left(\frac{J}{\lambda_3} \right)^2 \right). \tag{H.16}$$

Part V

References

Bibliography

[1] J. Bonet, A. J. Gil, and R. Ortigosa, "On a tensor cross product based formulation of large strain solid mechanics," *International Journal of Solids and Structures*, vol. 84, pp. 49–63, 2016.

[2] T. J. R. Hughes, L. P. Franca, and M. Mallet, "A new finite element formulation for computational fluid dynamics: I. Symmetric forms of the compressible Euler and Navier-Stokes equations and the second law of thermodynamics," *Computer Methods in Applied Mechanics and Engineering*, vol. 54, pp. 223–234, 1986.

[3] P. Saxena, J. Pelteret, and P. Steinmann, "Modelling of iron-filled magneto-active polymers with a dispersed chain-like microstructure," *European Journal of Mechanics - A/Solids*, vol. 50, pp. 132–151, 2015.

[4] A. O'Halloran, F. O'Malley, and P. McHugh, "A review on dielectric elastomer actuators, technology, applications, and challenges," *Journal of Applied Physics*, vol. 104, no. 7, 2008.

[5] R. E. Pelrine, R. D. Kornbluh, and J. P. Joseph, "Electrostriction of polymer dielectrics with compliant electrodes as a means of actuation," *Sensors and Actuators A: Physical*, vol. 64, no. 1, pp. 77–85, 1998.

[6] R. Pelrine, R. Kornbluh, Q. Pei, and J. Joseph, "High-speed electrically actuated elastomers with strain greater than 100 %," *Science*, vol. 287, no. 5454, pp. 836–839, 2000.

[7] G. Kofod, P. Sommer-Larsen, R. Kornbluh, and R. Pelrine, "Actuation response of polyacrylate dielectric elastomers," *Journal of Intelligent Material Systems and Structures*, vol. 14, no. 12, pp. 787–793, 2003.

[8] R. Pelrine, R. D. Kornbluh, Q. Pei, S. Stanford, S. Oh, J. Eckerle, R. J. Full, M. A. Rosenthal, and K. Meijer, "Dielectric elastomer artificial muscle actuators: toward biomimetic motion," 2002.

[9] T. Li, C. Keplinger, R. Baumgartner, S. Bauer, W. Yang, and Z. Suo, "Giant voltage-induced deformation in dielectric elastomers near the verge of snap-through instability," *Journal of the Mechanics and Physics of Solids*, vol. 61, no. 2, pp. 611–628, 2013.

[10] B. D. Coleman and W. Noll, "On the thermostatics of continuous media," *Archive for Rational Mechanics and Analysis*, vol. 4, pp. 97–128, 1959.

[11] J. E. Marsden and T. J. R. Hughes, *Mathematical foundations of elasticity*. 1994.

[12] J. Bonet and R. D. Wood, *Nonlinear Continuum Mechanics for Finite Element Analysis*. Cambridge University Press, second ed., 2008.

[13] E. de Souza Neto, D. Períc, and D. Owen, *Computational Methods for Plasticity. Theory and Applications*. 2008.

[14] T. J. R. Hughes, *The finite element method: Linear static and dynamic finite element analysis*. Dover Publications, 2000.

[15] T. Belytschko, W. K. Liu, and B. Moran, *Nonlinear finite elements for continua and structures*. John Wiley and Sons, 2000.

[16] J. Bonet, A. J. Gil, R. D. Wood, R. Said, and R. V. Curtis, "Simulating superplastic forming," *Computer Methods in Applied Mechanics and Engineering*, vol. 195, no. 48-49, pp. 6580–6603, 2006.

[17] A. J. Gil, R. V. Curtis, J. Bonet, and T. Coward, "Finite element superplastic forming (FE-SPF) of patient-specific maxillofacial prostheses," *International Journal for Numerical Methods in Biomedical Engineering*, vol. 26, no. 1, pp. 139–155, 2010.

[18] O. C. Zienkiewicz, J. Rojek, R. L. Taylor, and M. Pastor, "Triangles and tetrahedra in explicit dynamic codes for solids," *International Journal for Numerical Methods in Engineering*, vol. 43, pp. 565–583, 1998.

[19] M. W. Gee, C. R. Dohrmann, S. W. Key, and W. A. Wall, "A uniform nodal strain tetrahedron with isochoric stabilization," *International Journal for Numerical Methods in Engineering*, vol. 78, pp. 429–443, 2009.

[20] A. J. Gil, "Structural analysis of prestressed Saint Venant-Kirchhoff hyperelastic membranes subjected to moderate strains," *Computers & Structures*, vol. 84, no. 15-16, pp. 1012–1028, 2006.

[21] A. J. Gil and J. Bonet, "Finite element analysis of partly wrinkled reinforced prestressed membranes," *Computational Mechanics*, vol. 40, no. 3, pp. 595–615, 2007.

[22] A. J. Gil and J. Bonet, "Finite element analysis of prestressed structural membranes," *Finite Elements in Analysis and Design*, vol. 42, no. 8-9, pp. 683–697, 2006.

[23] J. Bonet, "Large strain viscoelastic constitutive models," *International Journal of Solids and Structures*, vol. 38, no. 17, pp. 2953–2968, 2001.

[24] R. Hill, "On uniqueness and stability in the theory of finite elastic strain," *Journal of the Mechanics and Physics of Solids*, vol. 5, pp. 229–241, 1957.

[25] P. G. Ciarlet, *Mathematical Elasticity. Volume 1: Three Dimensional Elasticity*. 1988.

[26] O. Gonzalez and A. M. Stuart, *A first course in Continuum Mechanics*. Cambridge University Press, 2008.

[27] J. M. Ball, "Convexity conditions and existence theorems in nonlinear elasticity," *Archive for Rational Mechanics and Analysis*, vol. 63, no. 4, pp. 337–403, 1976.

[28] J. M. Ball, *Geometry, Mechanics and Dynamics*, ch. Some open problems in Elasticity, pp. 3–59. Springer, 2002.

[29] J. M. Ball and F. Murat, "$W^{1,p}$-quasiconvexity and variational problems for multiple integrals," *Journal of Functional Analysis*, vol. 58, no. 3, pp. 225–253, 1984.

[30] A. Dorfmann and R. W. Ogden, "Electroelastic waves in a finitely deformed electroactive material," *IMA Journal of Applied Mathematics*, vol. 75, no. 4, pp. 603–636, 2010.

[31] C. B. Morrey, "Quasiconvexity and the lower semicontinuity of multiple integrals.," *Pacific Journal of Mathematics*, vol. 2, pp. 25–53, 1952.

[32] J. Schröder, "Anisotropic Polyconvex Energies," in *Poly-, quasi- and rank-one convexity in Applied Mechanics* (J. Schröder and P. Neff, eds.), vol. 516 of CISM Courses and Lectures, pp. 53–105, Springer-Verlag, 2010.

[33] J. M. Ball, "Energy-minimising configurations in nonlinear elasticity," in *Proceedings of the International Congress of Mathematicians, Warsaw*, 1983.

[34] K. Zhang, "A construction of quasiconvex functions with linear growth at infinity," *Annali della Scuola Normale Superiore di Pisa, Classe di Scienze*, vol. 97, no. 4, pp. 313–326, 1992.

[35] B. Dacorogna, *Direct Methods in the Calculus of Variations*. Springer, 2008.

[36] P. Ciarlet, "Existence theorems in intrinsic nonlinear elasticity," *Journal des mathématiques pures et appliqués*, vol. 94, pp. 229–243, 2010.

[37] J. Schröder and P. Neff, "Invariant formulation of hyperelastic transverse isotropy based on polyconvex free energy functions," *International Journal of Solids and Structures*, vol. 40, pp. 401–445, 2003.

[38] J. Schröder, P. Neff, and V. Ebbing, "Anisotropic polyconvex energies on the basis of crystallographic motived structural tensors," *Journal of Mechanics and Physics of Solids*, vol. 56, pp. 3486–3506, 2008.

[39] J. Schröder, P. Neff, and V. Ebbing, "Polyconvex energies for trigonal, tetragonal and cubic symmetry groups," in *IUTAM-Symposium on variational concepts with applications to the mechanics of materials: Proceedings of the IUTAM-Syposium*, 2010.

[40] J. Schröder, P. Wriggers, and D. Balzani, "A new mixed finite element based on different approximations of the minors of deformation tensors," *Com-*

puter Methods in Applied Mechanics and Engineering, vol. 200, no. 49-52, pp. 3583–3600, 2011.

[41] N. Kambouchev, R. Radovitzky, and J. Fernández, "Anisotropic materials which can be modeled by polyconvex strain energy functions," in *47th AIAA/ASME/ASCE/AHS/ASC Structures, Structural Dynamics, and Materials Conference*, vol. AIAA 2006-2250, 2006.

[42] A. J. Gil, C. H. Lee, J. Bonet, and M. Aguirre, "A stabilised Petrov-Galerkin formulation for linear tetrahedral elements in compressible, nearly incompressible and truly incompressible fast dynamics," *Computer Methods in Applied Mechanics and Engineering*, vol. 276, pp. 659–690, 2014.

[43] J. Bonet, A. J. Gil, C. H. Lee, M. Aguirre, and R. Ortigosa, "A first order hyperbolic framework for large strain computational solid dynamics - Part I: Total Lagrangian isothermal elasticity," *Computer Methods in Applied Mechanics and Engineering*, vol. 283, pp. 689–732, 2015.

[44] J. Bonet, A. J. Gil, and R. Ortigosa, "A computational framework for polyconvex large strain elasticity," *Computer Methods in Applied Mechanics and Engineering*, vol. 283, pp. 1061–1094, 2015.

[45] K. J. Bathe, *Finite Element Procedures*. Prentice Hall, 1996.

[46] D. P. Flanagan and T. Belytschko, "A uniform strain hexahedron and quadrilateral with orthogonal hourglass control," *International Journal for Numerical Methods in Engineering*, vol. 17, pp. 679–706, 1981.

[47] R. Stenberg, "A family of mixed finite elements for elasticity problems," *Numerische Mathematik*, vol. 48, pp. 513–538, 1988.

[48] J. C. Simo and F. Armero, "Geometrically non-linear enhanced strain mixed methods and the method of incompatible modes," *International Journal for Numerical Methods in Engineering*, vol. 33, pp. 1413–1449, 1992.

[49] J. C. Simo, F. Armero, and R. Taylor, "Improved versions of assumed enhanced strain tri-linear elements for 3D finite deformation problems," *Computational Methods for Applied Mechanical Engineering*, vol. 110, pp. 359–386, 1993.

[50] M. A. Puso, "A highly efficient enhanced assumed strain physically stabilized hexahedral element," *International Journal for Numerical Methods in Engineering*, vol. 49, pp. 1029–1064, 2000.

[51] F. Auricchio, L. B. de Veiga, C. Lovadina, and A. Reali, "A stability study of some mixed finite elements for large deformation elasticity problems," *Computational Methods for Applied Mechanical Engineering*, vol. 194, pp. 1075–1092, 2005.

[52] F. Auricchio, L. B. de Veiga, C. Lovadina, and A. Reali, "The importance of the exact satisfaction of the incompressibility constraint in nonlinear

elasticity: mixed fems versus nurbs-based approximations," *Computational Methods for Applied Mechanical Engineering*, vol. 199, pp. 314–323, 2008.

[53] R. L. Taylor, "A mixed-enhanced formulation for tetrahedral finite elements," *International Journal for Numerical Methods in Engineering*, vol. 47, pp. 205–227, 2000.

[54] J. C. Simo, F. Armero, and K. S. Pister, "Variational and projection methods for the volume constraint in finite deformation elasto-plasticity," *Computational Methods for Applied Mechanical Engineering*, vol. 51, pp. 177–208, 1985.

[55] Q. Tiehu, "Symmetrizing nonlinear elastodynamic system," *Journal of Elasticity*, vol. 50, no. 3, pp. 245–252, 1998.

[56] D. H. Wagner, "Symmetric-hyperbolic equations of motion for a hyperelastic material," *Journal of Hyperbolic Differential Equations*, vol. 06, no. 03, pp. 615–630, 2009.

[57] A. J. Gil, C. H. Lee, J. Bonet, and R. Ortigosa, "A first order hyperbolic framework for large strain computational solid dynamics - Part II: Total Lagrangian compressible, nearly incompressible and truly incompressible elasticity," *Computer Methods in Applied Mechanics and Engineering*, Under review.

[58] C. H. Lee, A. J. Gil, and J. Bonet, "Development of a stabilised Petrov-Galerkin formulation for conservation laws in Lagrangian fast solid dynamics," *Computer Methods in Applied Mechanics and Engineering*, vol. 268, pp. 40–64.

[59] S. Chiba, M. Waki, T. Wada, Y. Hirakawa, K. Masuda, and T. Ikoma, "Consistent ocean wave energy harvesting using electroactive polymer (dielectric elastomer) artificial muscle generators," *Applied Energy*, vol. 104, no. 0, pp. 497–502, 2013.

[60] S. Skatulla, C. Sansour, and A. Arockiarajan, "A multiplicative approach for nonlinear electro-elasticity," *Computer Methods in Applied Mechanics and Engineering*, vol. 245-246, pp. 243–255, 2012.

[61] A. Dorfmann and R. W. Ogden, "Nonlinear electroelasticity," *Acta Mechanica*, vol. 174, no. 3-4, pp. 167–183, 2005.

[62] A. Dorfmann and R. Ogden, "Nonlinear electroelastic deformations," *Journal of Elasticity*, vol. 82, no. 2, pp. 99–127, 2006.

[63] R. Bustamante, A. Dorfmann, and R. Ogden, "Nonlinear electroelastostatics: a variational framework," *Zeitschrift für angewandte Mathematik und Physik*, vol. 60, no. 1, pp. 154–177, 2009.

[64] R. Bustamante, A. Dorfmann, and R. Ogden, "On electric body forces and Maxwell stresses in nonlinearly electroelastic solids," *International Journal of Engineering Science*, vol. 47, no. 11-12, pp. 1131–1141, 2009.

[65] R. Bustamante, "Transversely isotropic non-linear electro-active elastomers," *Acta Mechanica*, vol. 206, no. 3-4, pp. 237–259, 2009.

[66] R. Bustamante and J. Merodio, "Constitutive structure in coupled non-linear electro-elasticity: Invariant descriptions and constitutive restrictions," *International Journal of Non-Linear Mechanics*, vol. 46, no. 10, pp. 1315–1323, 2011.

[67] A. W. Richards and G. M. Odegard, "Constitutive modeling of electrostrictive polymers using a hyperelasticity-based approach," *Journal of Applied Mechanics*, vol. 77, no. 1, 2009.

[68] R. M. McMeeking and C. M. Landis, "Electrostatic forces and stored energy for deformable dielectric materials," *Journal of Applied Mechanics*, vol. 72, no. 4, pp. 581–590, 2008.

[69] Z. Suo, X. Zhao, and W. H. Greene, "A nonlinear field theory of deformable dielectrics," *Journal of the Mechanics and Physics of Solids*, vol. 56, no. 2, pp. 467–486, 2008.

[70] R. Bustamante and J. Merodio, "On simple constitutive restrictions for transversely isotropic nonlinearly elastic materials and isotropic magneto-sensitive elastomers," *Journal of Engineering Mathematics*, vol. 68, no. 1, pp. 15–26, 2010.

[71] M. H. Siboni and P. P. Castañeda, "Fiber-constrained, dielectric-elastomer composites: Finite-strain response and stability analysis," *Journal of the Mechanics and Physics of Solids*, vol. 68, pp. 211–238, 2014.

[72] M. H. Siboni, R. Avazmohammadi, and P. P. Castañeda, "Electromechanical instabilities in fiber-constrained, dielectric-elastomer composites subjected to all-around dead-loading," *Mathematics and Mechanics of Solids*, 2014.

[73] C. Miehe, D. Vallicotti, and D. Zäh, "Computational structural and material stability analysis in finite electro-elasto-statics of electro-active materials," *International Journal for Numerical Methods in Engineering*, vol. 102, no. 10, pp. 1605–1637, 2015. nme.4855.

[74] R. Ortigosa and A. J. Gil, "A new framework for large strain electromechancis based on convex multi-variable strain energies: conservation laws and hyperbolicity," *Computer Methods in Applied Mechanics and Engineering*, 2016, submitted for publication.

[75] R. Ortigosa and A. J. Gil, "A new framework for large strain electromechancis based on convex multi-variable strain energies: Finite Element discretisation and computational implementation," *Computer Methods in Applied Mechanics and Engineering*, vol. 302, pp. 329–360, 2016.

[76] A. J. Gil and R. Ortigosa, "A new framework for large strain electromechancis based on convex multi-variable strain energies: variational formulation and

material characterisation," *Computer Methods in Applied Mechanics and Engineering*, vol. 302, pp. 293–328, 2016.

[77] J. Zhou, W. Hong, X. Zhao, Z. Zhang, and Z. Suo, "Propagation of instability in dielectric elastomers," *International Journal of Solids and Structures*, vol. 45, no. 13, pp. 3739–3750, 2008.

[78] D. Vu and P. Steinmann, "On 3-D coupled BEM-FEM simulation of nonlinear electro-elastostatics," *Computer Methods in Applied Mechanics and Engineering*, vol. 201-204, pp. 82–90, 2012.

[79] D. Vu and P. Steinmann, "A 2-D coupled BEM-FEM simulation of electro-elastostatics at large strain," *Computer Methods in Applied Mechanics and Engineering*, vol. 199, no. 17-20, pp. 1124–1133, 2010.

[80] F. Vogel, R. Bustamante, and P. Steinmann, "On some mixed variational principles in electro-elastostatics," *International Journal of Non-Linear Mechanics*, vol. 47, no. 2, pp. 341–354, 2012. Nonlinear Continuum Theories.

[81] M. Itskov and A. E. Ehret, "A generalised polyconvex hyperelastic model for anisotropic solids," in *Proceedings of the 2nd IASME/WSEAS International Conference on Continuum Mechanics*, 2007.

[82] R. de Boer, *Vektor- und Tensorrechnung für Ingenieure*. Springer-Verlag, 1982.

[83] M. Itskov and V. N. Khiêm, "A polyconvex anisotropic free energy function for electro- and magneto-rheological elastomers," *Mathematics and Mechanics of Solids*, pp. 1–12, 2014.

[84] A. N. Brooks and T. J. R. Hughes, "Streamline upwind/Petrov-Galerkin formulations for convection dominated flows with particular emphasis on the incompressible Navier-Stokes equations," *Computer Methods in Applied Mechanics and Engineering*, vol. 32, pp. 199–259, 1982.

[85] J. M. Ball, "Energy-minimising configurations in nonlinear elasticity," *Archive for Rational Mechanics and Analysis*, vol. 63, no. 4, pp. 337–403, 1976.

[86] J. Schröder, P. Neff, and D. Balzani, "A variational approach for materially stable anisotropic hyperelasticity," *International Journal of Solids and Structures*, vol. 42, pp. 4352–4371, 2005.

[87] R. Ogden, *Non-linear Elastic Deformations*. Dover Civil and Mechanical Engineering Series, Dover Publications, 1997.

[88] D. Gao, *Duality Principles in Nonconvex Systems: Theory, Methods and Applications*. Nonconvex Optimization and Its Applications, Springer, 2000.

[89] S. Timoshenko, *Theory of Elasticity*. Engineering societies monographs, McGraw-Hill, 1934.

[90] C. Sansour, "On the physical assumptions underlying the volumetric-isochoric split and the case of anisotropy," *European Journal of Mechanics - A/Solids*, vol. 27, pp. 28–39, 2008.

[91] D. Balzani, P. Neff, J. Schröder, and G. Holzapfel, "A polyconvex framework for soft biological tissues. Adjustment to experimental data," *International Journal of Solids and Structures*, vol. 43, no. 20, pp. 6052–6070, 2006.

[92] J. Bonet and A. Burton, "A simple orthotropic, transversely isotropic hyperelastic constitutive equation for large strain computations," *Computer Methods in Applied Mechanics and Engineering*, vol. 162, no. 1-4, pp. 151–164, 1998.

[93] K. Washizu, *Variational methods in elasticity and plasticity*. Pergamon Press, Oxford, 1975.

[94] I. Babuška, "The finite element method with lagrangian multipliers," *Numerische Mathematik*, vol. 20, no. 3, pp. 179–192, 1973.

[95] F. Brezzi and M. Fortin, *Mixed and Hybrid Finite Element Methods*. New York, NY, USA: Springer-Verlag New York, Inc., 1991.

[96] J. Donea and A. Huerta, *Finite Element Methods for Flow Problems*. John Wiley and Sons, 2003.

[97] A. J. Gil, C. H. Lee, J. Bonet, and M. Aguirre, "A stabilised Petrov-Galerkin formulation for linear tetrahedral elements in compressible, nearly incompressible and truly incompressible fast dynamics," *Computer Methods in Applied Mechanics and Engineering*, 2014.

[98] T. J. R. Hughes, L. P. Franca, and M. Balestra, "A new finite element formulation for computational fluid dynamics: V. Circumventing the Babuška-Brezzi condition: a stable Petrov-Galerkin formulation of the Stokes problem accommodating equal-order interpolations," *Computer Methods in Applied Mechanics and Engineering*, vol. 59, pp. 85–99, 1986.

[99] C. H. Lee, A. J. Gil, and J. Bonet, "Development of a cell centred upwind finite volume algorithm for a new conservation law formulation in structural dynamics," *Computers and Structures*, vol. 118, pp. 13–38, 2013.

[100] G. H. Miller, "An iterative Riemann solver for systems of hyperbolic conservation laws, with application to hyperelastic solid mechanics," *Journal of Computational Physics*, vol. 193, pp. 198–225, 2003.

[101] R. Abedi and R. B. Haber, "Riemann solutions and spacetime discontinuous Galerkin method for linear elastodynamic contact," *Computer Methods in Applied Mechanics and Engineering*, vol. 270, pp. 150–177, 2014.

[102] M. Mock, "Systems of conservation laws of mixed type," *Journal of Differential Equations*, vol. 37, no. 1, pp. 70–88, 1980.

[103] C. H. Lee, A. J. Gil, and J. Bonet, "Development of a stabilised PetrovGalerkin formulation for conservation laws in lagrangian fast solid dynamics," *Computer Methods in Applied Mechanics and Engineering*, vol. 268, pp. 40–64, 2014.

[104] M. Aguirre, A. J. Gil, J. Bonet, and A. A. Carreño, "A vertex centred finite volume Jameson-Schmidt-Turkel (JST) algorithm for a mixed conservation formulation in solid dynamics," *Journal of Computational Physics*, vol. 259, pp. 672–699, 2014.

[105] M. Aguirre, A. J. Gil, J. Bonet, and C. H. Lee, "A vertex centred upwind finite volume method for solid dynamics," *Journal of Computational Physics*, vol. 300, pp. 387–422, 2015.

[106] I. A. Karim, C. H. Lee, A. J. Gil, and J. Bonet, "A two-step Taylor-Galerkin formulation for fast dynamics," *Engineering Computations*, vol. 31, no. 3, pp. 366–387, 2014.

[107] G. Scovazzi, B. Carnes, and X. Zeng, "A simple, stable and accurate tetrahedral finite element for transient, nearly incompressible, linear and nonlinear elasticity: A dynamic variational multiscale approach," *International Journal for Numerical Methods in Engineering*, 2015. Under review.

[108] C. H. Lee, A. J. Gil, and J. Bonet, "Development of a cell centred upwind finite volume algorithm for a new conservation law formulation in structural dynamics," *Computers & Structures*, vol. 118, pp. 13–38, 2013.

[109] X. Zhao and Z. Suo, "Electrostriction in elastic dielectrics undergoing large deformation," *Journal of Applied Physics*, vol. 104, no. 12, p. 123530, 2008.

[110] D. K. Vu, P. Steinmann, and G. Possart, "Numerical modelling of non-linear electroelasticity," *International Journal for Numerical Methods in Engineering*, vol. 70, no. 6, pp. 685–704, 2007.

[111] B. Li, L. Liu, and Z. Suo, "Extension limit, polarization saturation, and snap-through instability of dielectric elastomers," *International Journal of Smart and Nano Materials*, vol. 2, no. 2, pp. 59–67, 2011.

[112] C. B. T. Böhlke, "Graphical representation of the generalised Hooke's law," *Technische Mechanik*, vol. 21, pp. 145–158, 2001.

[113] T. Barth, "On the Role of Involutions in the Discontinuous Galerkin Discretization of Maxwell and Magnetohydrodynamic Systems," in *Compatible Spatial Discretizations* (D. Arnold, P. Bochev, R. Lehoucq, R. Nicolaides, and M. Shashkov, eds.), vol. 142 of *The IMA Volumes in Mathematics and its Applications*, pp. 69–88, Springer New York, 2006.

[114] J. Pérez-Aparicio, R. Palma, and R. Taylor, "Multiphysics and Thermodynamic Formulations for Equilibrium and Non-equilibrium Interactions: Non-linear Finite Elements Applied to Multi-coupled Active Materials," *Archives of Computational Methods in Engineering*, pp. 1–49, 2015.